Université Fédérale
Toulouse Midi-Pyrénées

THÈSE

En vue de l'obtention du

DOCTORAT DE L'UNIVERSITÉ DE TOULOUSE

Délivré par : *l'Université Toulouse 3 Paul Sabatier (UT3 Paul Sabatier)*

Présentée et soutenue le *06/10/2016* **par :**

Juan SANZ GARCÍA

Theoretical Study of New Nitrosyl Ruthenium Complexes: Mechanisms of Photoisomerization and Photorelease of NO

JURY

ASSFELD Xavier	Professeur (Rapporteur)	Université de Lorraine
CARISSAN Yannick	Maître de Conférence (Rapporteur)	Aix-Marseille Université
LE GUENNIC Boris	Chargé de Recherche (Examinateur)	Université de Rennes 1
ROYAL Guy	Professeur (Examinateur)	Université de Grenoble Alpes
MALFANT Isabelle	Professeur (Examinateur)	UT3 Paul Sabatier
POTEAU Romuald	Professeur (Examinateur)	UT3 Paul Sabatier
HEULLY Jean-Louis	Directeur de Recherche	UT3 Paul Sabatier
BOGGIO-PASQUA Martial	Chargé de Recherche	UT3 Paul Sabatier

École doctorale et spécialité :
SDM : Physicochimie théorique - COP 01
Unité de Recherche :
Laboratoire de Chimie et Physique Quantiques (UMR 5626)
Directeur(s) de Thèse :
Jean-Louis HEULLY et *Martial BOGGIO-PASQUA*
Rapporteurs :
Xavier ASSFELD et *Yannick CARISSAN*

Para Ofelia

Remerciements

La décision de faire une thèse de doctorat n'est pas une chose qu'il faut prendre à la légère. Il est important d'avoir de fortes convictions et surtout une soif insatiable de nouvelles connaissances. Personnellement, il y a trois ans, je n'ai pas pris cette décision à la légère. Au contraire, la recherche scientifique a toujours été pour moi une véritable vocation. Cependant, il ne faut pas croire que ces trois ans ont été faciles ; cette thèse s'est avérée être une des plus importantes épreuves auxquelles j'ai dû me confronter. C'est avec beaucoup de patience et de persévérance que j'ai pu mener à bien ce projet. Toutefois, ce n'est pas seul que j'ai pu réaliser cette œuvre, mais grâce à l'aide de nombreuses personnes, qui directement ou indirectement, ont contribué au bon déroulement de ce travail.

Tout d'abord, je tiens à remercier Fabienne Alary, qui m'a beaucoup aidé à réaliser ce travail de recherche. Je ne serai jamais capable d'exprimer en quelques mots toute ma gratitude. Merci infiniment pour tout ce que tu as fait pour moi, et surtout, merci d'avoir pris le temps de m'écouter et de m'encourager dans les moments plus difficiles. Il y a encore une liste de choses considérable pour lesquelles je voudrais exprimer ma reconnaissance et te dire un grand merci, mais quelques lignes ne suffiraient à y rendre hommage.

Je voudrais également remercier mes deux directeurs de thèse Jean-Louis Heully et Martial Boggio-Pasqua. Merci à tous les deux pour toute votre aide et tous vos précieux conseils ; vous m'avez appris énormément de choses. Merci Jean-Louis de m'avoir fait découvrir de nombreux aspects et curiosités de la chimie théorique que je ne connaissais pas. Merci de m'avoir fait découvrir autant de logiciels puissants et gratuits de calculs de structures électroniques ainsi que de traitement des résultats. Merci Martial de m'avoir transmis ton savoir-faire et ton expertise. J'apprécie énormément ton goût pour les choses bien faites et ton attention aux détails. Merci de m'avoir fait découvrir le vaste monde de la photochimie. Et surtout un grand merci pour ton soutien dans les moments très dures et difficiles, merci beaucoup Martial !

Je ne pourrais pas finir le tour de mon équipe sans exprimer ma gratitude à Isabelle Dixon. Merci beaucoup pour ta gentillesse, tes conseils, les nombreuses discussions scientifiques et surtout un grand merci pour tout le temps que tu as consacré à m'aider avec

mes problèmes scientifiques, pratiques et même '*spirituels*'. Merci beaucoup Isabelle pour ton soutien et tes encouragements, ainsi que pour ta bonne humeur.

Je tiens également à remercier Isabelle Malfant et son équipe de recherche. Merci pour toutes les discussions et échanges scientifiques au cours de cette thèse qui ont permis de clarifier certains points ainsi que d'établir un vrai dialogue expérience/théorie.

Je voudrais aussi remercier les membres du jury d'avoir pris le temps d'examiner ce manuscrit de thèse : les rapporteurs Xavier Assfeld et Yannick Carissan, ainsi que les examinateurs Boris Le Guennic, Guy Royal, Isabelle Malfant et Romuald Poteau.

Je tiens à remercier aussi tous mes amis qui sont vénus à Toulouse pour la soutenance de ma thèse : Juanma, Josep, David, Burcu, Thomas, Riccardo, Anna, Ursula et Laia, un grand merci à vous tous, ça m'a fait énormément plaisir de vous voir tous réunis pour cet événement si important pour moi.

Je tiens à remercier Ria Broer et Remco Havenith qui m'ont chaleureusement accueilli à Groningen pendant quelque mois. Merci beaucoup à tous les deux pour votre gentillesse et vos conseils. Je voudrais aussi remercier Remco pour ces 'petits' codes FORTRAN et surtout de m'avoir encouragé à programmer moi-même un petit code Hartree-Fock. C'est justement grâce à la programmation de ce code que j'ai pu comprendre beaucoup mieux certains points de la méthode SCF qui n'étaient pas clairs avant.

Je voudrais également remercier tout l'équipe d'informaticiens Eric, David et Anthony pour avoir toujours assuré le bon fonctionnement de tous les clusters du labo, passerelle, imprimantes, ainsi que de tout le matériel informatique. Je profite aussi pour remercier les secrétaires du labo, Fanny et Patricia pour leur bonne humeur et gentillesse, ça fait toujours plaisir de voir des personnes joyeuses et souriantes au labo. Merci beaucoup Patricia pour avoir toujours assuré la disponibilité des salles et pour la papeterie.

Je remercie le centre du calcul de Midi-Pyrénées, CALMIP, pour les allocations d'heures de calculs du projet 1133 qui m'ont permis de réaliser la plupart des calculs présentés dans ce travail. Je voudrais également remercier le Ministère de l'Enseignement Supérieur et de la Recherche pour le financement de cette thèse.

Forcément, je vois cette thèse comme une réaction photochimique complexe. Pour transformer l'idée de départ (réactif) en un projet abouti (produit), il y a eu des grandes barrières énergétiques le long de la SEP de l'état fondamental. Heureusement, j'étais rarement dans un état « tranquille » (fondamental), mais la plupart du temps j'étais plutôt dans un état excité. J'ai tout de même réussi à trouver des points de croisement qui m'ont permis de me relaxer vers l'état fondamental et ainsi continuer les différentes étapes de ce travail. Merci surtout à Giuseppe, Florian et Cyril de m'avoir toujours aidé à relativiser et de m'avoir permis de me relaxer dans un état un peu plus calme et tranquille. Le long du chemin de cette thèse en photochimie, il y a eu plusieurs étapes qui ont nécessité l'absorption d'un photon. Merci beaucoup Maria Francesca d'avoir été la lumière qui m'a permis de photolibérer ce travail et de clôturer ce parcours photochimique complexe.

Je voudrais aussi avoir un petit mot pour toutes ces personnes que je n'ai pas mentionnées encore et qui ont laissé quand-même une empreinte sur moi le long de ces trois ans de thèse. Merci beaucoup Stefano Evangelisti et Thierry Leininger pour votre soutien moral et vos encouragements le long de la thèse ainsi que le long du Master. Vous avez été parmi les premières personnes que j'ai rencontrées quand je suis arrivé à Toulouse et je garde de très bons souvenirs de cette époque. Ça a toujours été très agréable de vous rencontrer et discuter avec vous au labo. Merci beaucoup aussi à Nathalie Guihéry et Nicolas Suaud. Vous avez été mes professeurs pendant le Master, et ça fait toujours plaisir de vous croiser au labo et discuter avec vous. Un grand merci aussi à Michel Caffarel pour son soutien, sa disponibilité, et tous les renseignements lorsque je postulais pour obtenir une bourse de thèse et même plus tard quand il n'était plus le directeur de l'école doctorale. Merci aussi à la secrétaire de l'école doctorale Soraya Berkouk pour tous les renseignements et sa disponibilité. Merci Jérôme pour ta bonne humeur ainsi que pour ton humour. On est arrivé en même temps au laboratoire, à l'époque j'étais encore un étudiant en M1 et tu venais d'avoir ton poste. J'ai vu ta progression au labo au cours de ces années et c'est quand-même impressionnant, maintenant tu fais même partie du bureau de l'école doctorale. Bravo, je suis sûr que tu arriveras très loin dans ta carrière. D'ailleurs, merci de t'être occupé de mon dossier de soutenance. Merci beaucoup Hélène de t'être intéressé à mon code pour tracer les spectres, ça me fait énormément plaisir que mes codes soit utiles pour d'autres personnes que moi. Merci beaucoup Malika pour ta gentillesse, ta bonne humeur, et surtout je voudrais exprimer ma gratitude pour ton soutien, tes encouragements et aussi pour m'avoir tenu compagnie tous ces long week-ends au cours de ma thèse. Et aussi un grand merci général à tous les

doctorants et permanents du labo qui m'ont soutenu pendant toutes ces années, merci beaucoup à vous tous.

Je ne pourrais pas finir ces remerciements sans dédier quelques mots à ma petite chère famille Italo-turque-mexico-palestinienne. Quel bonheur d'habiter avec vous mes chères et chers '*Sciapecotti*', cette période que j'ai pu passer avec vous a été une des plus belles de ma vie, merci beaucoup Burcu, Cecilia, Alessandra et Ahmad, on a passé de très bons moments ensemble. Merci Ahmad pour toutes ces parties de Jenga les samedis matin avec Manu Chao comme musique de fond. Merci Burcu pour tes pancakes du samedi matin et tes gâteaux et aussi merci Cecilia pour les Chilaquiles et les piments farcis ; tous étaient vraiment délicieux. Merci Alessandra pour tous ces dimanches après-midi autour d'un bon repas italien, j'ai adoré les tagliatelles fait maison.

Ofelia merci beaucoup d'avoir toujours été là pour moi.

Table of Contents

Avant-Propos 3

Chapter I. General Background 5

1.1 Introducing Photochemistry 7

1.2 Overview on Modern Computational Photochemistry 10

1.3 Relevant Chemical Aspects and Historical Facts about NO 12

1.4 Nitric Oxide Photorelease in the Ru−NO Complexes Studied 16

1.5 Photoisomerization of Metal-Nitrosyl Complexes 17

1.6 References 20

Chapter II. Methodology and Analysis Tools 27

2.1 Theoretical Background 29

2.1.1 Born-Oppenheimer Approximation 30

2.1.2 Origins of the Wave Function Methods: the Hartree-Fock Theory 31

a) The Hartree Product 32

b) The Variational Principle 32

c) Self-Consistent Field Method 33

d) Slater Determinant as the Antisymmetric Wave Function: Hartree-Fock Theory 35

2.1.3 Density Functional Theory 36

a) The Hohenberg-Kohn Theorems 37

b) The Kohn-Sham Method 39

c) The Exchange-Correlation Energy 39

d) Spin Densities, Spin Symmetry and Spin Contamination 40

e) Different Approximations of the Density Functional 41

f) Description of Strong Correlation 41

2.1.4 Time-Dependent Density Functional Theory 42

2.2 Exploring Potential Energy Surfaces 43
2.2.1 Standard Approach to the MEP Problem 44
a) Optimization of the Minima 45
b) Generating a Good Educated Guess for the TS Optimization 56
c) TS Optimization 61
d) Characterization of the Stationary Points Optimized: Frequency Calculations 62
e) Minimum Energy Path Calculations: Intrinsic Reaction Coordinate vs. Steepest Descent 65
2.2.2 Alternative Approach to the MEP Problem: The Nudged Elastic Band Method 66
2.2.3 Minimum Energy Crossing Points 69
2.3 Dispersion Effects 71
2.4 Solvation Models 72
2.5 Analysis of the Triplet State Nature: Natural Orbitals 78
2.6 Thermochemistry 83
2.7 References 86

Chapter III. Photoinduced Linkage Isomerization of the *trans*-$[RuClNO(py)_4]^{2+}$ Complex 91
3.1 Motivation 93
3.2 Exploring the Singlet and Triplet Potential Energy Surfaces of the *trans*-$[RuClNO(py)_4]^{2+}$ Complex 95
3.2.2 Singlet Potential Energy Surface 95
3.2.2 Lowest Triplet Potential Energy Surface 98
3.3 Absorption Spectra of GS, MS1 and MS2 100
3.4 Singlet-Triplet Minimum Energy Crossing Points 102
3.5 Forward and Reverse Photoisomerization Mechanisms 103

3.5.1 Mechanism for the Forward Isomerization (**GS ⇄ MS1**)..... 104

a) Step1: **GS ⇄ MS2** 104

b) Step2: **MS2 ⇄ MS1** 105

e) Different Approximations of the Density Functional 41

f) Description of Strong Correlation 41

2.1.4 Time-Dependent Density Functional Theory..... 42

c) Pitfalls along the **GS ▾▾ MS1** Path 105
3.5.2 Mechanism for the Reverse Isomerization (**MS1 ▾▾ GS**) 106
a) Red-Light Excitation 106
b) Infrared Light Excitation 107
3.6 Conclusions 109
3.7 Comparing Ru−NO with Ru−SO Complexes 110
3.8 References 112
Résumé : Chapitre III 117

Chapter IV. Photorelease *vs*. Photoisomerization in Ruthenium Nitrosyl Complexes 125
4.1 Motivation 127
4.2 Characteristics of the Ru−NO Complexes Studied 130
4.3 Absorption Spectra of the GS, MS1 and MS2 Isomers of all Complexes 131
4.4 Thermal Isomerization and Photoisomerization Pathways 135
4.4.1 Thermal Isomerization Pathway 136
4.4.2 Triplet State Adiabatic Pathway 136
4.4.3 Non adiabatic Pathway 136
4.5 Capability of NO Photorelease from the Three Different Triplet States, ^{3}GS, ^{3}MS2 and ^{3}MS1 137
4.6 Discussion: Photorelease *vs*. Photoisomerization 139
4.7 Conclusions 141
4.8 References 141
Résumé : Chapitre IV 143

Chapitre V. Conclusion Générale et Perspectives 149
5.1 Conclusions 151
5.2 Perspectives 157
5.3 Références 160

Appendix A: Supporting Information for Chapter III AA1

Appendix B: Photochromic Response of Various Ru−NO Complexes AB1

Appendix C: Supporting Information for Chapter IV AC1

Résumé .....

Abstract .....

Avant-Propos

Le travail présenté dans ce manuscrit comporte les principaux résultats obtenus issus des études théoriques menées au cours de cette thèse. Ces études mécanistiques s'inscrivent dans le cadre général de la photochimie computationnelle, plus concrètement, dans le cadre de la photoréactivité de complexes polypyridyles de ruthénium à ligand nitrosyle. Depuis des années, ces complexes ont attiré l'attention de la communauté pharmaceutique par leur capacité à libérer NO sous irradiation, propriété très intéressante dans le traitement par photothérapie dynamique de plusieurs maladies dont le cancer. De plus, grâce à leur remarquable réponse photochromique, ces complexes de ruthénium sont également attractifs pour la confection de dispositifs optiques de stockage massif. Le changement de couleur est dû à la photoisomérisation d'enchaînement du ligand nitrosyle (Ru−NO ⁚⁚ Ru−ON). Afin d'éclaircir la relation entre photolibération et photoisomérisation, des études mécanistiques de ces réactions photochimiques ont été réalisées au cours de cette thèse.

La stratégie utilisée pour mener ces études est basée sur une approche statique : La modélisation des mécanismes étudiés, photolibération et photoisomérisation du ligand nitrosyle, repose sur l'exploration exhaustive des surfaces d´énergie potentielle de l'état fondamental ainsi que de l'état excité triplet de plus basse énergie. Cette modélisation a permis d'identifier et d'établir les chemins réactionnels suivis par les complexes depuis l'absorption initiale d'un photon jusqu'à la formation du photoproduit. Les résultats théoriques ont permis d'interpréter et de rationaliser des observations expérimentales cruciales concernant le comportement photochimique de ces systèmes.

Ce manuscrit, rédigé principalement en anglais, est divisé en cinq chapitres et articulé comme suit : dans un premier temps, le chapitre I introduit de manière générale la photochimie, l'état de l'art de la photochimie computationnelle, une introduction sur le monoxyde d'azote (NO), ainsi que les principales propriétés photoréactives des complexes de ruthénium à ligand nitrosyle. Le deuxième chapitre donne un bref aperçu du contexte théorique et une brève présentation des grandes lignes de la Théorie de la Fonctionnelle de la Densité et de sa version dépendante du temps. Dans ce chapitre, les stratégies méthodologiques et outils employés au cours de ce travail sont également introduits, avec une attention particulière sur les méthodes d'exploration de surfaces d'énergie potentielle. Dans le chapitre III, le complexe *trans*-$[RuCl(NO)(py)_4]^{2+}$ a été étudié pour explorer et rationaliser les

différents mécanismes de photoisomérisation d'aller-retour du ligand nitrosyle. Ce chapitre est basé sur les résultats présentés dans un article publié dans '*Inorganic Chemistry*'. Un bref résumé rédigé en français est fourni à fin de ce chapitre. Les informations supplémentaires concernant ce travail sont données en annexe (Appendix A). Suite à cette étude, la tendance des rendements de photoconversion observée expérimentalement dans une série de trois complexes a pu être rationalisée. Les résultats sont présentés sous forme d'annexe (Appendix B). Le chapitre IV présente le mécanisme de photolibération de NO ainsi que sa relation directe avec le mécanisme de photoisomérisation à partir de la comparaison de la photoréactivité de cinq complexes différents. Ce travail a fait l'objet d'un article publié dans '*Journal of Molecular Modeling*'. Les informations supplémentaires de cette étude sont données en annexe (Appendix C). Finalement, le dernier chapitre clôture l'ensemble de ce travail de thèse avec une conclusion générale, ainsi que des perspectives sur la suite à donner à ce travail.

Chapter I

General Background

1.1 Introducing Photochemistry

The experimental evidence of the photoelectric effect validated the very foundations of Quantum Mechanics (QM). Indeed, comprehension of the interaction phenomenon between light (photons) and matter (electrons) helped very much in the development of the Quantum theory, which is the basis of Quantum Chemistry (QM applied to chemistry). Furthermore, in photochemistry (branch of chemistry dealing with the interaction between light and molecules) most of the theoretical tools employed in the study of photochemical reactions come from the development of modern Quantum Chemistry.

Photochemistry, being a branch of photophysics, could be defined as the study of the physical and subsequent chemical phenomena induced by the interaction of light with molecules. Indeed, since the beginning of phototrophic life, molecular photochemistry has been present and it is of capital importance for many living organisms. These organisms, ranging from the simplest cyanobacteria to the more complex and evolved trees, need to capture the energy from light to transform it into chemical energy by the well-known process called photosynthesis. Energy from light (photons) is 'captured' (absorbed) by the natural pigments (biomolecules) present in these organisms. Chlorophylls are the most important pigments involved in the light absorption mechanism of photosynthesis. Light-based vision as we know it today, is another good example of an intricate chain of complex biochemical reactions triggered by photons.[1]

The interest of photochemistry resides in its wide scope of varied applications in medicine, science and industry. For instance, already in the early sixties Toyo Rayon industries developed its own photosynthetic process to produce tons of ε-caprolactam (Nylon 6 monomer) per day.[2] Interestingly, this process starts with the nitrosyl photocleavage from the nitrosonium chloride (ClNO), to yield, after a cascade of reactions, the desired ε-caprolactam (Reaction 1.1).

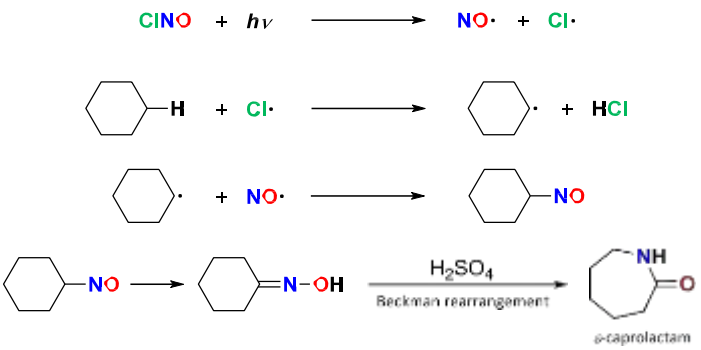

(1.1)

One part of this manuscript will focus on the description of the photo-induced nitrosyl cleavage as well. The nitric oxide delivering agents studied in this PhD thesis are various ruthenium nitrosyl complexes (Figure 1.5).

In general terms, the chronology of a photochemical reaction can be explained in mainly three steps: i) the initial interaction of a photon with the electrons of the photoactive molecule (the so-called absorption) promoting the system in an (or a superposition of) electronic excited state(s), ii) the following relaxation processes, happening in these electronic excited states, (certain chemical reactions can only happen through these states), and iii) the final decay to the electronic ground state. This decay can occur either *via* radiative or non-radiative processes. In the first case, the system decays by fluorescence or phosphorescence phenomena. Kasha's rule states that, if a molecule is fluorescent, it rapidly relaxes by radiationless decay to the lower excited state, from which it subsequently deactivates by radiative decay to the ground state. One of the differences between fluorescence and phosphorescence is that, generally speaking, fluorescence emission is much faster than phosphorescence. The main reason is that fluorescence is the emission from the lowest excited state to the ground state (GS) (both having the same spin multiplicity), while the phosphorescence is the emission from the lowest excited state (with a different spin multiplicity from the ground state) to the ground state, thus, in the phosphorescence process light emission must 'wait' until one electron undergoes a spin-flip to go back to the ground state. Another important reason why phosphorescence processes are slower than fluorescence processes is that the non-radiative relaxation pathway to reach the lower state with the same multiplicity as the GS is 'shorter' than the pathway to reach the lower state with different multiplicity to the GS. In addition to or alongside these radiative decay processes, the system may decay to the ground state non-radiatively. This can happen either through internal conversion (IC) when the radiationless transitions occur between electronic states of same spin multiplicity or through intersystem crossing (ISC) when the radiationless transitions occur

between electronic states of different spin multiplicity. IC and ISC take place on a much shorter timescale than the corresponding radiative processes (*i.e.*, fluorescence and phosphorescence), thus providing effective ways to return to the ground electronic state.

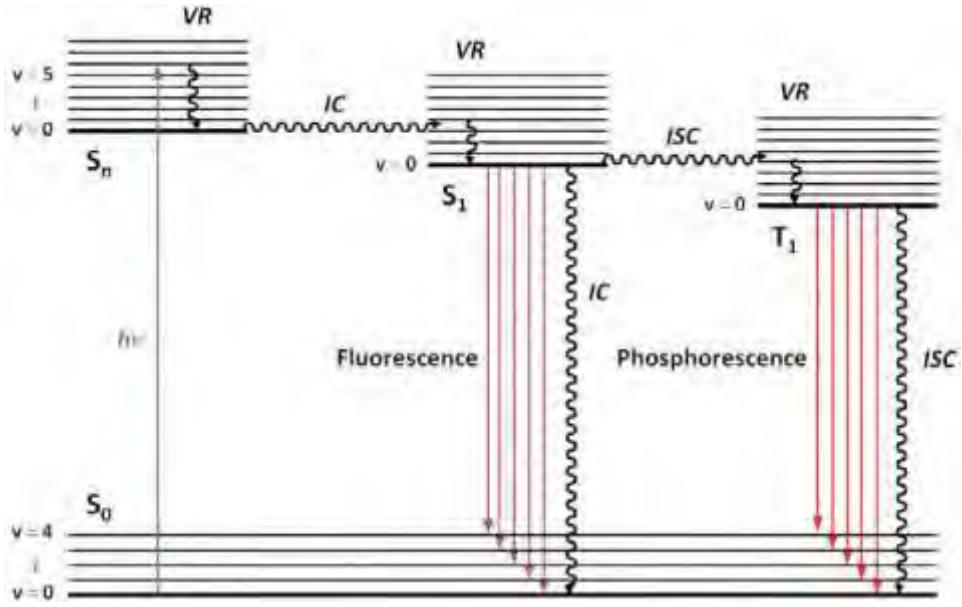

Figure 1.1: Jablonski-Perrin diagram. Wavy lines represent non-radiative processes; *IC*: Internal Conversion, *ISC*: Intersystem Crossing and *VR*: Vibrational Relaxation, while straight lines represent radiative processes; initial absorption (in blue), fluorescence (in dark red) and phosphorescence (in red).

In a Jablonski-Perrin diagram, the most important radiative and non-radiative processes that can undergo a system are represented. The wavy lines represent non-radiative processes, while the straight lines represent the radiative ones. In the given example (Figure 1.1), after photon absorption, the system relaxes to the lower excited state S_1 by IC, from where it may fluoresce (Kasha's rule) or decay non-radiatively to S_0 by IC. The molecule may also undergo ISC from S_1 to produce the lowest triplet state T_1 (if spin-orbit coupling is non-negligible). Eventually, the system can deactivate to the ground state radiatively via phosphorescence or non-radiatively by ISC. This type of diagram, while useful, does not provide any information on the photochemical reaction itself. It simply represents the main photophysical processes occurring in the system, but includes no information about nuclear relaxation coordinates, excited-state intermediates and activation energies involved in the formation of eventual photoproducts. All these information can be obtained from quantum chemical calculations, which can thus provide very useful mechanistic information on the photophysical and photochemical behaviour of molecular systems. The following section gives a very short overview on modern computational photochemistry, a discipline that has been

applied throughout this PhD in the challenging context of studying the complex photochemistry of ruthenium nitrosyl complexes.

1.2 Overview on Modern Computational Photochemistry

In the past three decades or so, computational photochemistry has gained considerable credit as a tool to investigate photochemical reaction mechanisms in organic, inorganic and even biological molecules.[3,4] This reputation has been gained thanks to the concomitant growing of computational power and theoretical developments in the field of quantum chemistry, and to the fact that experimental photochemical studies with modern spectroscopies are notoriously hard to interpret without the insight provided by the complementary theoretical description at the molecular level. Modern computational photochemistry allows peering beyond the traditional interpretations focused on vertical excitations at the Franck–Condon geometry. Indeed, to understand the fate of a molecular system after photoexcitation, it is not only necessary to understand the excited-state properties of the molecule but also to determine how the system will evolve chemically in terms of bond making and bond breaking in these excited states. Thus, it is crucial to understand the reaction pathway describing the passage from the ground-state reactants to the final photoproducts evolving along the potential energy surfaces (PESs) of the photochemically relevant electronic states. This reaction path is called *photochemical reaction path* or *photochemical pathway*. The photochemical pathway is determined by following the detailed relaxation and reaction paths of the molecule along the relevant potential energy surfaces from the Franck-Condon point (*i.e.*, vertically excited geometry) to the ground state. Static calculations are performed to investigate the topology of the PESs. It requires finding all the relevant critical structures (minima, saddle points, barriers, surface crossings – see Chapter II for a description of the methods used to do locate these structures) involved along the reaction path and understanding how all these critical points are interconnected on the PESs. This interconnection is often determined by minimum energy path (MEP) calculations (see Chapter II for details on how to compute MEP). Once the potential energy landscape for all the relevant electronic states is understood, very detailed mechanistic information can be derived on the photochemistry of the system. These static calculations of PESs and characterization of the photochemical pathway are often complemented by dynamics simulations to gain a more complete understanding of the molecular photochemistry.

While standard state-of-the-art quantum chemical methods are already capable of providing a complete description of what happens at the molecular level during bond-breaking and bond-forming processes in thermal reactions, the task is much more challenging when contemplating photochemical reactions. First, the description of the electronic structures in the electronic excited states is more challenging because of their usual multiconfigurational character. Second, the reaction path cannot be described on a single PES, but rather two branches at least are required: one located on an excited state (reactant side) and the other located on the ground-state (product side). Finally, the Born-Oppenheimer approximation (see Chapter II) breaks down in the 'funnel' region where the excited-state deactivates non-radiatively (*i.e.*, by IC or ISC) to the ground state. Thus, appropriate quantum chemical methods need to be used to describe consistently the electronic structures of all the electronic states involved along the entire photochemical path. Critical structures such as crossings between electronic states (*i.e.*, conical intersections) that provide funnels[5–8] for efficient radiationless electronic transitions need to be located and characterized. Non-adiabatic effects resulting from the break-down of the Born-Oppenheimer approximation around these funnel need to be taken into account.[9] For all these reasons, carrying out a computational study of any photochemical reaction is everything but simple. This is probably the reasons why most computational photochemical studies are performed by leading experts in the field (c.f. works by the groups of M. Robb in the U.K., K. Morokuma in Japan, W. Thiel and W. Domcke in Germany, M. Olivucci and M. Persico in Italy, D. Yarkony, D. Truhlar, T. Martínez, S. Matsika in the U.S., to cite just a few). Due to the inherent difficulties to perform such studies, most of the studied systems involve relatively small organic chromophores (up to a few tens of atoms). For such systems, computational investigations of photochemical processes such as photoisomerization, photoinduced electron transfer, photosensitization and photodissociation have become a standard practice (see references[10–18] for relevant review articles). Note that these photochemical studies can be extended to large biological systems as long as the organic chromophore responsible for light absorption remains relatively small.[19,20]

However, the computational studies of photochemical pathways in transition metal complexes are complicated due to the high density of electronic states involved in these systems and to the difficulty to describe accurately their electronic structures. Unsurprisingly, very few computational studies can be found regarding the mechanistic description of photoisomerization or photodissociation processes involving directly the metal center.[21–26] In all these computational studies involving a ruthenium center, the main assumption is that,

after light absorption, the singlet excited states initially populated rapidly deactivate to the lowest triplet state by non-radiative decays (ISC and IC). Then, the photochemical pathway is computed on the lowest triplet PES using density functional theory (DFT; see Chapter II). To account for possible non-radiative decay back to the singlet ground state from the lowest triplet state by ISC, singlet/triplet crossings are determined as they provide efficient funnels for deactivation. Discussion on the adiabatic and nonadiabatic mechanisms can then be developed on the basis of the static information provided by the PESs topology. This PhD project follows a similar computational strategy to study the competing NO photorelease and photoisomerization mechanisms in ruthenium nitrosyl complexes. The following section describes the importance of the nitric oxide NO radical. Then, the two photochemical processes (*i.e.*, photorelease and photoisomerization) are introduced in the next sections.

1.3 Relevant Chemical Aspects and Historical Facts about NO

Nitric oxide, NO, is a simple yet fascinating heteronuclear diatomic molecule. It is a paramagnetic colorless gas at standard conditions (25° C, 1 bar). Its neutral form has in total fifteen electrons, eleven of them being valence electrons. The molecular orbital (MO) diagram of this diatomic molecule can easily be constructed using the linear combination of atomic orbitals (LCAO) approach Figure (1.2), affording as a result the following electronic structure $(1\sigma)^2(2\sigma*)^2(3\sigma)^2(4\sigma*)^2(1\pi)^4(5\sigma)^2(2\pi*)^1$. The radical nature of the nitric oxide (doublet in its neutral ground state) explains its high reactivity and toxicity. It can be prepared industrially oxidizing ammoniac (reaction 1.2)[27] or in the laboratory reducing the nitrate anion with a metallic cation, e.g. iron (II) (reaction 1.3).[27]

$$4NH_3 + 5O_2 \rightleftharpoons 4NO + 6H_2O \quad (1.2)$$

$$NO_3^- + 3Fe^{2+} + 4H^+ \rightleftharpoons NO + 3Fe^{3+} + 2H_2O \quad (1.3)$$

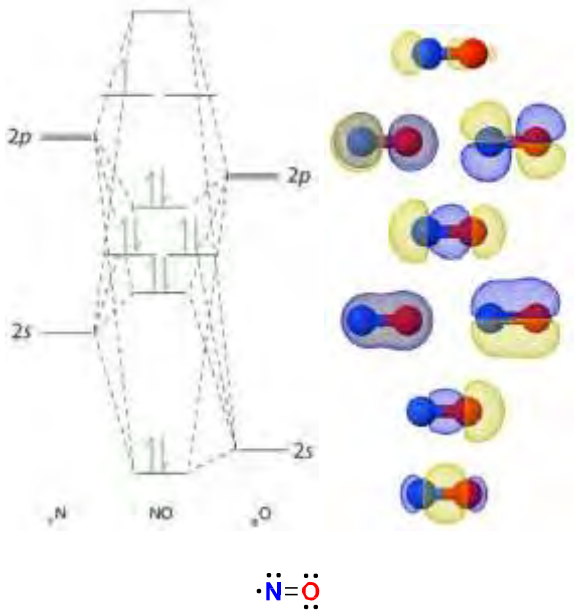

Figure 1.2: Schematic representation of the MO of the NO radical (and Lewis structure).

Nitric oxide is one of the common tropospheric pollutant gases of the family known as NO_x (nitrogen oxides). The positive value of its standard enthalpy of formation, $\Delta_f H°$ (NO) = 90.25 kJ/mol,[28] means that at high temperatures its formation from atmospheric nitrogen and oxygen gases is favored. This is the reason why the artificial increase of this gas in the atmosphere over the last century is directly link to the human activity. During combustion of vehicle fuels and large industrial activities, nitric oxide among other nitrogen oxides is formed. It can also be generated naturally in the vicinities of a lightning bolt strike. The over expression of nitric oxide in the air has drastic effects not only in the environment, but in the formation of large smogs over cities as well. It is also known to be one of the gases responsible for the acid rain, since it easily becomes nitric acid after its quick oxidation process in the air.

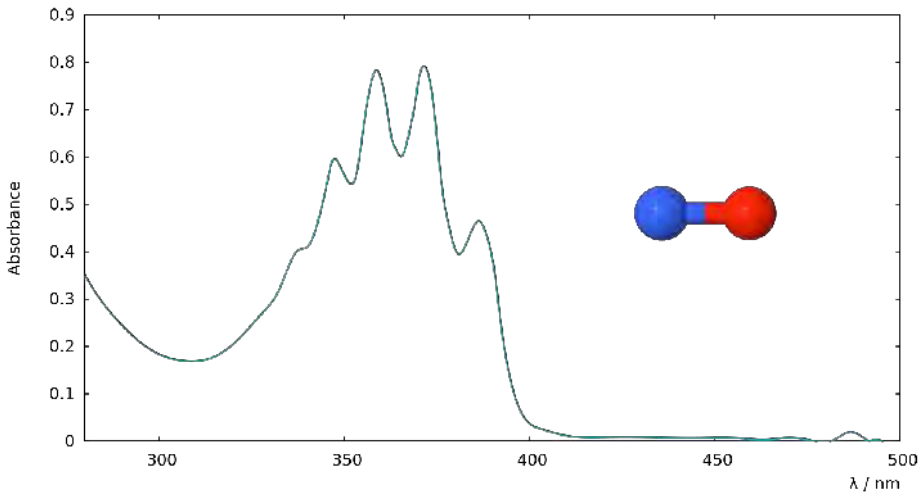

Figure 1.3: Nitric oxide absorption spectra. Data extracted from ref. 29.

Experimentally, it can be quite useful to know the absorption spectra of nitric oxide to determine its concentration in a solution where release of NO has been photo-induced. NO presents several bands,[29] centered at 372 nm for the most intense one (Figure 1.3). If other molecules in solution do not absorb or absorb moderately with respect to NO in the spectral range of 350-400 nm, the band centered at 372 nm could be used for measuring the concentration of NO in a specific solution. Unfortunately, in practice many secondary species issue of a NO photorelease reaction present quite intense bands in this region, which make difficult or even impossible to determine the NO concentration in the solution with a bare analysis of the UV-visible absorption spectra.

It is a curious historical fact that Alfred Nobel was prescribed nitroglycerin as a remedy for his heart disease (nitroglycerin is the main component in dynamite). Since 1867 nitroglycerin has been used in the treatment of *angina pectoris* disease relieving the associated chest pain, but the physiological mechanism remained unknown until the discoveries of three American pharmacologists.[30–32] Thanks to their findings, it is now known that nitroglycerin acts as a NO delivering agent which is indeed a vasodilator.

In the late 70's the Medicinae Doctor and pharmacologist Ferid Murad discovered that the nitrates like nitroglycerin,[30] used in the treatment for *angina pectoris* disease, and other related vasodilating compounds release nitric oxide by the action of the mitochondrial aldehyde dehydrogenase.[33] Though the release mechanism of NO remained unclear until many years later, for the first time NO was discovered to be an important signal molecule in biological systems. In 1980, the American pharmacologist R. F. Furchgott elucidated the paradox of acetylcholine (ACh) being a vasodilator *in vivo*, while being a vasoconstrictor *in vitro*.[31] In fact, ACh produces contractions in the vascular smooth muscle; while at the same time stimulates the surrounding cells of the blood vessels (endothelial cells) to release an unknown agent which relaxes the vascular smooth muscle. In full normally working biological systems, if the dose is not too high to override the relaxation effect of the unknown agent, the net effect of the ACh drug is vasodilatation. On the contrary, if in the system the endothelium is absent or malfunctioning (no relaxing agent expression in blood vessels) the net effect of ACh is vasoconstriction. Furchgott's findings rapidly inspired a quest to identify the unknown relaxing agent, later famously known as the 'endothelium-derived relaxing factor' (EDRF). Few years later, Louis J. Ignarro, another American pharmacologist, after a series of analyses concluded together with and independently of Furchgott that the mysterious EDRF was, indeed nitric oxide.[32] All these discoveries marked a new chapter in the evolution of medicine

and pharmacology, and NO being a simple diatomic gas, drew more than ever the attention of the chemical and biological scientific communities, inspiring an exponentially growing plethora of research until these days. In 1992 *Science* dubbed nitric oxide as 'Molecule of the year', and the ever growing, intense and extensive research dealing with it made possible in February 1997 the birth of a completely new journal called '*NITRIC OXIDE: Biology and Chemistry*' which deals mainly with the NO biological roles in human beings and other living organisms. One year later, the Nobel Prize in Physiology or Medicine (1998) was awarded jointly to F. Murad, R. F. Furchgott, and L. J. Ignarro for their contributions and discoveries concerning nitric oxide as a signaling molecule in the cardiovascular system.

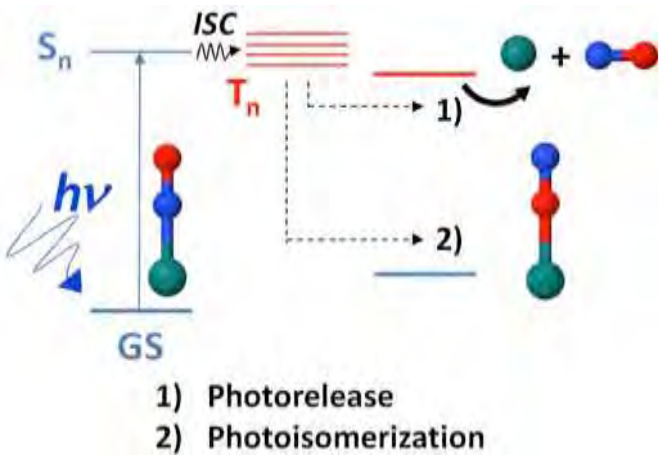

Figure 1.4: Scheme of the possible photoreactions pathways that ruthenium-nitrosyl complexes may undergo after irradiation.

After all these events, the sudden growth of general interest for NO becomes totally understandable. Not surprisingly, many researchers have gone back to re-explore the traditional coordination chemistry of transition metal nitrosyl compounds.[34,35] Some transition metal complexes containing at least one nitrosyl ligand are known to be able to release NO upon light irradiation with the appropriate wavelength,[36] which makes them perfect candidates for photo-dynamic cancer therapy (PDT). This is one of the topics that would be dealt with in the following section (§1.4) and in Chapter IV, where various potential ruthenium nitrosyl NO delivering agents will be analyzed in detail. Depending on the concentration of nitric oxide in a cell, apoptosis or cellular growth can be induced. This is the reason why a perfect control of the dosage is needed in the chemotherapeutic cancer treatment and this can be regulated by an external signal, namely light irradiation. The transition metal nitrosyl complexes can undergo not only photorelease of the NO radical, but photo-induced linkage isomerism as well (Figure 1.4).[37] This phenomenon can be interesting for the design of high capacity optical storage devices. This is another topic that would be dealt with in section (§1.5)

and in Chapter III, where photoisomerization of a ruthenium mononitrosyl complex will be analyzed in detail.

1.4 Nitric Oxide Photorelease in the Ru−NO Complexes Studied

Long before the discovery of the antitumor activity of cisplatin (*cis*-diamminedichloridoplatinum (II), *cis*-$[Pt^{II}(NH_3)_2Cl_2]$ in the mid 60's,[38] metal-based drugs have been used in the treatment of many diseases since the early days of civilization.[39] Chemists, biologists, pharmacologists and many other scientists work together in the quest of developing new efficient drugs to reduce the side effects and drug resistance of cisplatin and many other existing metallopharmaceuticals.

In vivo sodium nitroprusside (SNP), $Na_2[Fe(NO)(CN)_5]$, is a vasodilator drug which acts as nitroglycerin does, delivering nitric oxide by reduction. Its use in clinical subjects presents few drawbacks like the release of cyanide among others.[40] In the same *d*-block metallic group of Iron (group 8) two other easily accessible metals worth to explore exist. Osmium compounds are quite difficult to synthetize and highly toxic.[41] On the other hand, ruthenium complexes are less toxic and much easier to handle and synthetize. In the last few decades, the development of new metallo drugs based in ruthenium nitrosyl (NO as a ligand) complexes has been intensively active. Many of these ruthenium nitrosyl complexes are able to release NO not only by reduction, but by light irradiation as well. Though nitric oxide photorelease have uncountable therapeutic applications ranging from cardiovascular problems to cancer, tuberculosis to drug addiction, anorexia to sunburn, with a list that can go on indefinitely, the best known and most developed research efforts focus on the light-induced delivery of nitric oxide and especially in the PDT treatment of cancer.

In the treatment of cancer, ruthenium complexes present an important advantage over platinum complexes, their kinetic behavior being similar (*i.e.* adequate for the timescale of cellular processes as for platinum compounds), but their secondary effects much lower. Ruthenium can also mimic iron binding to some biomolecules like albumin and protein transferrin. Thus, ruthenium nitrosyl complexes are promising candidates for medical purposes. Under suitable conditions, a number of these complexes have been shown to photorelease NO in solution with different quantum yields (Figure 1.5).[42,43] In such systems,

the NO photorelease is ultimately related to electronic transitions having a strong charge transfer character to the nitrosyl fragment. Therefore, the use of terpyridines bearing donor substituents seems especially appealing to enhance the Ru •• NO charge transfer, and hence the NO release capabilities. The complexes shown in Figure 1.5 will be investigated in detail in Chapter IV.

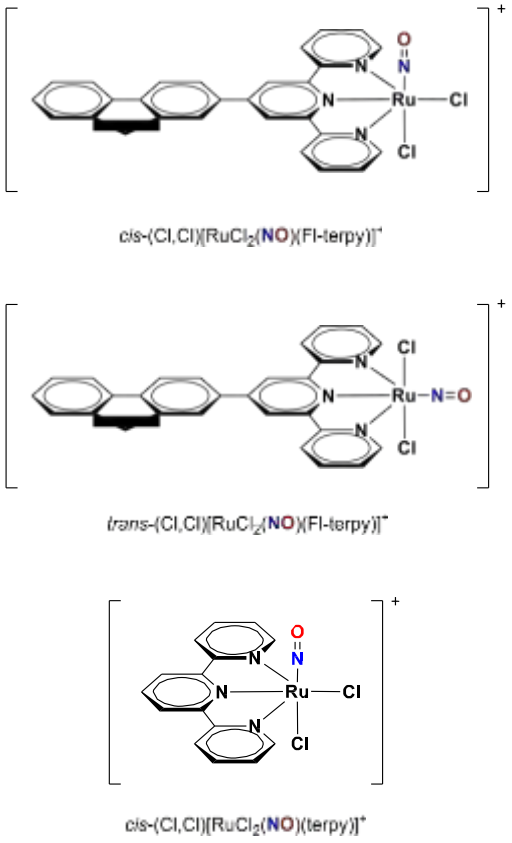

Figure 1.5: Examples of ruthenium nitrosyl complexes undergoing NO photorelease.[42,43]

1.5 Photoisomerization of Metal-Nitrosyl Complexes

The ever-growing need to increase the performance of electronic digital devices has inspired, for many years, the research and development of new high-efficient materials able to overcome the limitations imposed by the present technological barriers. In this context, the light induced molecular switches are of special interest.[44,45] Generally speaking, light driven molecular switches offer a wide range of technological applications not only in the design of new optical high capacity storage devices,[46–48] or logic gates,[49–51] but also in the development of miniaturized photomechanical gadgets[52–57] or even in advanced pharmaceutical therapy.[58,59] In particular, reversible photochromic switches, in which spectroscopic properties differ

between light induced species, have been largely studied over the years, ranging from the most emblematic system, *i.e.* rhodopsin protein,[1] responsible for the vision process, to the newest hybrid materials.[60]

The development of new materials based on transition metal complexes showing a phototriggered linkage isomerism has become quite popular over the past few decades. Of special importance are the systems based on ruthenium polypyridyl sulfoxides[61–68] studied by Rack. The widely studied transition metal nitrosyl complexes are another important example of compounds which present an outstanding photochromic behavior. With respect to the latter complexes, the first light-induced changes in iron based nitrosyl complexes were discovered accidentally in 1977,[69,70] while Mössbauer spectroscopy studies were performed using SNP as environment for the experiments. New low-temperature-stable species of SNP were observed and later differential scanning calorimetry (DSC) studies allowed the determination of the energy difference between the so-called **GS** and two meta-stable species.[71] Further work showed[72] that both species, dubbed as meta-stable states **MS1** and **MS2**, are diamagnetic, meaning that they are singlet electronic states having all the electrons paired. The nature of these 'states' remained unclear until 1994 when Prof. Coppens *et al.* conducted photocrystallographic studies showing that an atomic rearrangement was involved in this photo-induced process.[73] Similar results were also obtained for the crystalline structure of $K_2[RuNO(NO_2)_4OH]$.[74] Further analyses showed that the new species detected in the photo-excited crystals were, indeed, photo-induced linkage isomers.[75] Since the first characterization of photoisomerism in SNP crystals, extensive research on metallic nitrosyl complexes have revealed many other species with similar photochemical behavior.[76–84]

Photochemical linkage isomerism of M−NO complexes has also been reviewed several times.[37,85–87] This photo-isomerization phenomenon is due to a change in the bonding nature of the nitrosyl ligand with the metal center. The so-called 'ground state' (**GS**) is characterized by the commonly known N-bound form of the nitrosyl to the metallic center. Upon adequate irradiation the **GS** turns into two different conformations: the metastable state 1 (**MS1**) O-bound form (isonitrosyl) and the sideways bound, metastable state 2 (**MS2**). In this regard, pyridyl ruthenium nitrosyl complexes are very promising, yielding important transformation rates (Figure 1.6).[88–91]

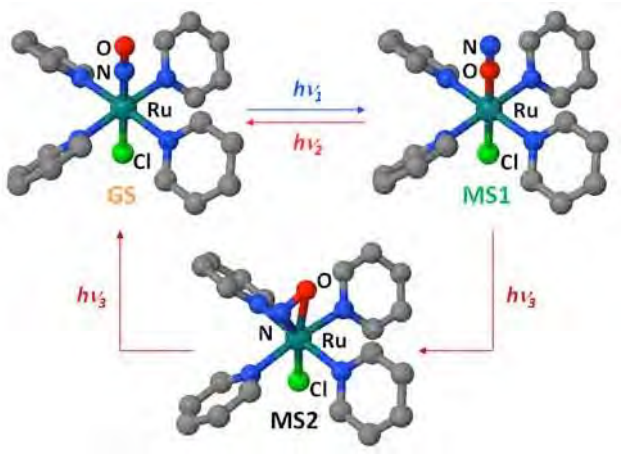

Figure 1.6: Schematic representations of the linkage isomers of the *trans*-[RuCl(NO)(py)$_4$]$^{2+}$ complex in its ground state (GS), metastable states (MS1 and MS2) and experimental irradiation conditions (blue, 473 nm; red 782 nm; dark red, 980 nm).[88–91]

Thanks to the high computing power available today, electronic structure calculations have become an essential complement in the design of new efficient nitrosyl photoisomers. In particular, the density functional theory (DFT) and its time-dependent formalism (TDDFT) have proven to be adequate for the reproducibility of the qualitative UV-Vis absorption spectra of metal nitrosyl complexes.[92–94]

Regarding the SNP and other Fe nitrosyl derivates, theoretical studies and experimental time resolved experiences have been performed in order to shed some light to the linkage isomerization mechanism. In many of these studies, only the ground state potential energy surfaces, as well as few minima lying on excited singlet electronic states have been characterized, no complete potential energy surface (PES) of any excited electronic state have been yet reported (no characterization of any transition state connecting the minima, affording a complete description of an adiabatic pathway in an excited electronic state). Similar studies have been performed to gain some insight on the family of ruthenium nitrosyl complexes containing heme-like, pyridyl, polypiridyl and other auxiliary ligands. Full characterization of the ground state PES, as well as the minima on the lowest excited triplet states has been reported, in general, for many ruthenium nitrosyl complexes with a detailed description of the nature of the Ru−NO bond, and in particular, for few pyridyl or polypiridyl ruthenium complexes. Yet many fundamental questions concerning the nature of the photo-isomerism remain unclear, for instance, a whole picture of the full mechanism is not yet successfully explained.

The first theoretical study of a photochromic polypyridyl ruthenium system showing photo-induced linkage isomerism dates back to 2003, where DFT proved to be an appropriate electronic structure method in the study of such complexes.[21] Three years later, another work from the same group was published, where it was shown once more that DFT and TDDFT methods where appropriate to described the complex photochemical and photophysical behavior of polypyridyl ruthenium (II) and osmium (II) complexes.[95] Few years later, the complete characterization of the lowest triplet excited state PES of a photochromic polypyridyl ruthenium mono-sulfoxide complexe allowed a complete description of the adiabatic pathway through the triplet state PES.[22] Thanks to this study, the importance of metal centered (MC) states for a satisfactory description of the photoisomerism was put in evidence. A more recent study following the same DFT approach allowed shedding some light in the photo-triggered isomerism of polypyridyl ruthenium di-sulfoxide species.[24] Similar DFT studies on ruthenium (II) phosphinidene oxide complexes gave important insight in the key points of the light induced switching between two linkage phosphinidine oxide isomers.[23]

In Chapter III, a plausible explanation for the experimental observations made on the photochromic Ru−NO system, *trans*-$[RuCl(NO)py_4]^{2+}$,[88–91] will be presented. The outstanding photochromic behavior of the system studied was reported few years ago.[88,89] When the **GS** crystallised form (orange translucent crystal) of this salt is irradiated with blue light, λ = 476,5 nm, it turns into the **MS1** crystalline form (green translucent crystal). Subsequent irradiation with red light, λ = 980 nm, generates the **MS2** crystal (black crystal) which upon continuous irradiation, eventually becomes the starting linkage isomer **GS** (Figure 1.6).

1.6 References

(1) Baylor, D. *Proc. Natl. Acad. Sci.* **1996**, *93* (2), 560–565.

(2) Cowan, D. O.; Drisko, R. L. In *Elements of Organic Photochemistry*; Plenum Press: New York, 1976; pp 1–18.

(3) Kutateladze, A. G. *Computational Methods in Photochemistry*; CRC Press, 2005.

(4) Olivucci, M. *Computational Photochemistry*; Elsevier, 2005.

(5) Zimmerman, H. E. *J. Am. Chem. Soc.* **1966**, *88* (7), 1564–1565.

(6) Zimmerman, H. E. *J. Am. Chem. Soc.* **1966**, *88* (7), 1566–1567.

(7) Teller, E. *Isr. J. Chem.* **1969**, *7* (2), 227–235.

(8) Michl, J. *Mol. Photochem.* **1972**, *4*, 243–255.

(9) Baer, M. In *Beyond Born-Oppenheimer: Electronic Nonadiabatic Coupling Terms and Conical Intersections*; Wiley: New York, 2006; pp 1–234.

(10) Bernardi, F.; Olivucci, M.; Robb, M. A. *Chem. Soc. Rev.* **1996**, *25* (5), 321–328.

(11) Robb, M. A.; Garavelli, M.; Olivucci, M.; Bernardi, F. *Rev. Comput. Chem.* **2000**, *15*, 87–146.

(12) Bearpark, M. J.; Robb, M. A. In *Reviews of reactive intermediate chemistry*; Wiley: New Jersey, 2007; pp 379–414.

(13) Garavelli, M. *Theor. Chem. Acc.* **2006**, *116* (1–3), 87–105.

(14) Levine, B. G.; Martínez, T. J. *Annu. Rev. Phys. Chem.* **2007**, *58* (1), 613–634.

(15) Matsika, S.; Krause, P. *Annu. Rev. Phys. Chem.* **2011**, *62* (1), 621–643.

(16) Domcke, W.; Yarkony, D. R. *Annu. Rev. Phys. Chem.* **2012**, *63* (1), 325–352.

(17) Blancafort, L. *ChemPhysChem* **2014**, *15* (15), 3166–3181.

(18) Improta, R.; Santoro, F.; Blancafort, L. *Chem. Rev.* **2016**, *116* (6), 3540–3593.

(19) Sinicropi, A.; Andruniow, T.; De Vico, L.; Ferré, N.; Olivucci, M. *Pure Appl. Chem.* **2005**, *77* (6), 977–993.

(20) Boggio-Pasqua, M.; Burmeister, C. F.; Robb, M. A.; Groenhof, G. *Phys. Chem. Chem. Phys.* **2012**, *14* (22), 7912–7928.

(21) Ciofini, I.; Daul, C. A.; Adamo, C. *J. Phys. Chem. A* **2003**, *107* (50), 11182–11190.

(22) Göttle, A. J.; Dixon, I. M.; Alary, F.; Heully, J.-L.; Boggio-Pasqua, M. *J. Am. Chem. Soc.* **2011**, *133* (24), 9172–9174.

(23) Vieuxmaire, O. P. J.; Piau, R. E.; Alary, F.; Heully, J.-L.; Sutra, P.; Igau, A.; Boggio-Pasqua, M. *J. Phys. Chem. A* **2013**, *117* (48), 12821–12830.

(24) Göttle, A. J.; Alary, F.; Dixon, I. M.; Heully, J.-L.; Boggio-Pasqua, M. *Inorg. Chem.* **2014**, *53* (13), 6752–6760.

(25) Ding, L.; Chung, L. W.; Morokuma, K. *J. Chem. Theory Comput.* **2014**, *10* (2), 668–675.

(26) Göttle, A. J.; Alary, F.; Boggio-Pasqua, M.; Dixon, I. M.; Heully, J.-L.; Bahreman, A.; Askes, S. H. C.; Bonnet, S. *Inorg. Chem.* **2016**, *55* (9), 4448–4456.

(27) Housecroft, C. E.; Sharpe, A. G. In *Inorganic Chemistry*; Pearson Education Limited: Harlow, 2005; pp 385–431.

(28) Chase, M. W. *J. Phys. Chem. Ref. Data, Monograph 9* **1998**, 1–1951.

(29) Gabor, G. *Microchem. J.* **1997**, *56* (2), 171–176.

(30) Arnold, W. P.; Mittal, C. K.; Katsuki, S.; Murad, F. *Proc. Natl. Acad. Sci. U. S. A.* **1977**, *74* (8), 3203–3207.

(31) Furchgott, R. F.; Zawadzki, J. V. *Nature* **1980**, *288* (5789), 373–376.

(32) Ignarro, L. J.; Buga, G. M.; Wood, K. S.; Byrns, R. E.; Chaudhuri, G. *Proc. Natl. Acad. Sci. U. S. A.* **1987**, *84* (24), 9265–9269.

(33) Chen, Z.; Foster, M. W.; Zhang, J.; Mao, L.; Rockman, H. A.; Kawamoto, T.; Kitagawa, K.; Nakayama, K. I.; Hess, D. T.; Stamler, J. S. *Proc. Natl. Acad. Sci. U. S. A.* **2005**, *102* (34), 12159–12164.

(34) Richter-Addo, G. B.; Legzdins, P.; Burstyn, J. *Chem. Rev.* **2002**, *102* (4), 857–860.

(35) Hayton, T. W.; Legzdins, P.; Sharp, W. B. *Chem. Rev.* **2002**, *102* (4), 935–992. (36)

Ford, P. C. *Nitric Oxide* **2013**, *34*, 56–64.

(37) Coppens, P.; Novozhilova, I.; Kovalevsky, A. *Chem. Rev.* **2002**, *102* (4), 861–884.

(38) Rosenberg, B.; Van Camp, L.; Krigas, T. *Nature* **1965**, *205* (4972), 698–699.

(39) Sadler, P. J. In *Advances in Inorganic Chemistry*; Sykes, A. G., Ed.; Academic Press, 1991; Vol. 36, pp 1–48.

(40) Bates, J. N.; Baker, M. T.; Guerra Jr., R.; Harrison, D. G. *Biochem. Pharmacol.* **1991**, *42*, *Supplement 1*, S157–S165.

(41) Peacock, A. F. A.; Habtemariam, A.; Fernández, R.; Walland, V.; Fabbiani, F. P. A.; Parsons, S.; Aird, R. E.; Jodrell, D. I.; Sadler, P. J. *J. Am. Chem. Soc.* **2006**, *128* (5), 1739–1748.

(42) Karidi, K.; Garoufis, A.; Tsipis, A.; Hadjiliadis, N.; Dulk, H. den; Reedijk, J. *Dalton Trans.* **2005**, No. 7, 1176–1187.

(43) Akl, J.; Sasaki, I.; Lacroix, P. G.; Malfant, I.; Mallet-Ladeira, S.; Vicendo, P.; Farfán, N.; Santillan, R. *Dalton Trans.* **2014**, *43* (33), 12721–12733.

(44) Feringa, B. L.; van Delden, R. A.; Koumura, N.; Geertsema, E. M. *Chem. Rev.* **2000**, *100* (5), 1789–1816.

(45) Altoè, P.; Bernardi, F.; Conti, I.; Garavelli, M.; Negri, F.; Orlandi, G. *Theor. Chem. Acc.* **2007**, *117* (5–6), 1041–1059.

(46) Jiang, G.; Song, Y.; Guo, X.; Zhang, D.; Zhu, D. *Adv. Mater.* **2008**, *20* (15), 2888–2898.

(47) Liu, W.; Li, Z.; Hu, F.; Yin, J.; Yu, G.-A.; Liu, S. H. *Photochem. Photobiol. Sci.* **2014**, *13* (12), 1773–1780.

(48) Redeckas, K.; Voiciuk, V.; Steponavičiūtė, R.; Martynaitis, V.; Šačkus, A.; Vengris, M. *J. Phys. Chem. A* **2014**, *118* (30), 5642–5651.

(49) Straight, S. D.; Andréasson, J.; Kodis, G.; Bandyopadhyay, S.; Mitchell, R. H.; Moore, T. A.; Moore, A. L.; Gust, D. *J. Am. Chem. Soc.* **2005**, *127* (26), 9403–9409.

(50) Straight, S. D.; Andréasson, J.; Kodis, G.; Moore, A. L.; Moore, T. A.; Gust, D. *J. Am. Chem. Soc.* **2005**, *127* (8), 2717–2724.

(51) Bonnet, S.; Collin, J.-P.; Sauvage, J.-P. *Inorg. Chem.* **2006**, *45* (10), 4024–4034.

(52) Feringa, B. L. *Acc. Chem. Res.* **2001**, *34* (6), 504–513.

(53) Feringa, B. L.; Koumura, N.; Delden, R. A. van; Wiel, M. K. J. ter. *Appl. Phys. A* **2002**, *75* (2), 301–308.

(54) Eelkema, R.; Pollard, M. M.; Vicario, J.; Katsonis, N.; Ramon, B. S.; Bastiaansen, C. W. M.; Broer, D. J.; Feringa, B. L. *Nature* **2006**, *440* (7081), 163–163.

(55) Schäfer, L. V.; Müller, E. M.; Gaub, H. E.; Grubmüller, H. *Angew. Chem. Int. Ed.* **2007**, *46* (13), 2232–2237.

(56) Natansohn, A.; Rochon, P. *Chem. Rev.* **2002**, *102* (11), 4139–4176.

(57) Hugel, T.; Holland, N. B.; Cattani, A.; Moroder, L.; Seitz, M.; Gaub, H. E. *Science* **2002**, *296* (5570), 1103–1106.

(58) Al-Atar, U.; Fernandes, R.; Johnsen, B.; Baillie, D.; Branda, N. R. *J. Am. Chem. Soc.* **2009**, *131* (44), 15966–15967.

(59) Gorostiza, P.; Isacoff, E. Y. *Science* **2008**, *322* (5900), 395–399.

(60) Fihey, A.; Maurel, F.; Perrier, A. *Phys. Chem. Chem. Phys.* **2014**, *16* (47), 26240–26251.

(61) Rack, J. J.; Winkler, J. R.; Gray, H. B. *J. Am. Chem. Soc.* **2001**, *123* (10), 2432–2433.

(62) Rack, J. J.; Mockus, N. V. *Inorg. Chem.* **2003**, *42* (19), 5792–5794.

(63) Lutterman, D. A.; Rachford, A. A.; Rack, J. J.; Turro, C. *J. Phys. Chem. Lett.* **2010**, *1* (23), 3371–3375.

(64) McClure, B. A.; Abrams, E. R.; Rack, J. J. *J. Am. Chem. Soc.* **2010**, *132* (15), 5428–5436.

(65) McClure, B. A.; Rack, J. J. *Inorg. Chem.* **2011**, *50* (16), 7586–7590.

(66) Porter, B. L.; McClure, B. A.; Abrams, E. R.; Engle, J. T.; Ziegler, C. J.; Rack, J. J. *J. Photochem. Photobiol. Chem.* **2011**, *217* (2–3), 341–346.

(67) Jin, Y.; Rack, J. J. *Isr. J. Chem.* **2013**, *53* (5), 280–287.

(68) King, A. W.; Jin, Y.; Engle, J. T.; Ziegler, C. J.; Rack, J. J. *Inorg. Chem.* **2013**, *52* (4), 2086–2093.

(69) Hauser, U.; Oestreich, V.; Rohrweck, H. D. Z. *Phys. A* **1977**, *280*, 17.

(70) Hauser, U.; Oestreich, V.; Rohrweck, H. D. Z. *Phys. A* **1977**, *280*, 125.

(71) Zöllner, H.; Woike, T.; Krasser, W.; Haussühl, S. *Z. Für Krist. - Cryst. Mater.* **1989**, *188* (1–4), 139–154.

(72) Woike, T.; Kirchner, W.; Kim, H.; Haussühl, S.; Rusanov, V.; Angelov, V.; Ormandjiev, S.; Bonchev, T.; Schroeder, A. N. F. *Hyperfine Interact.* **1993**, *77* (1), 265–275.

(73) Pressprich, M. R.; White, M. A.; Vekhter, Y.; Coppens, P. *J. Am. Chem. Soc.* **1994**, *116* (12), 5233–5238.

(74) Fomitchev, D. V.; Coppens, P. *Inorg. Chem.* **1996**, *35* (24), 7021–7026.

(75) Carducci, M. D.; Pressprich, M. R.; Coppens, P. *J. Am. Chem. Soc.* **1997**, *119* (11), 2669–2678.

(76) Woike, T.; Zöllner, H.; Krasser, W.; Haussühl, S. *Solid State Commun.* **1990**, *73* (2), 149–152.

(77) Woike, T.; Haussühl, S. *Solid State Commun.* **1993**, *86* (5), 333–337.

(78) Gueida, J. A.; Piro, O. E.; Aymonino, P. J. *Inorg. Chem.* **1995**, *34* (16), 4113–4116.

(79) Fomitchev, D. V.; Coppens, P.; Li, T.; Bagley, K. A.; Chen, L.; Richter-Addo, G. B. *Chem. Commun.* **1999**, No. 19, 2013–2014.

(80) Da Silva, S. C.; Franco, D. W. *Spectrochim. Acta. A. Mol. Biomol. Spectrosc.* **1999**, *55* (7–8), 1515–1525.

(81) Schaniel, D.; Woike, T.; Boskovic, C.; Güdel, H.-U. *Chem. Phys. Lett.* **2004**, *390* (4–6), 347–351.

(82) Schaniel, D.; Woike, T.; Delley, B.; Biner, D.; Krämer, K. W.; Güdel, H.-U. *Phys. Chem. Chem. Phys.* **2007**, *9* (37), 5149–5157.

(83) Bitterwolf, T. E. *Inorg. Chem. Commun.* **2008**, *11* (7), 772–773.

(84) Schaniel, D.; Woike, T.; Behrnd, N.-R.; Hauser, J.; Krämer, K. W.; Todorova, T.; Delley, B. *Inorg. Chem.* **2009**, *48* (23), 11399–11406.

(85) Gütlich, P.; Garcia, Y.; Woike, T. *Coord. Chem. Rev.* **2001**, *250* (9–10), 839–879.

(86) Ford, P. C.; Wecksler, S. *Coord. Chem. Rev.* **2005**, *249* (13–14), 1382–1395.

(87) Bitterwolf, T. E. *Coord. Chem. Rev.* **2006**, *250* (9–10), 1196–1207.

(88) Schaniel, D.; Cormary, B.; Malfant, I.; Valade, L.; Woike, T.; Delley, B.; Krämer, K. W.; Güdel, H.-U. *Phys. Chem. Chem. Phys.* **2007**, *9* (28), 3717–3724.

(89) Cormary, B.; Malfant, I.; Buron-Le Cointe, M.; Toupet, L.; Delley, B.; Schaniel, D.; Mockus, N.; Woike, T.; Fejfarová, K.; Petříček, V.; Dušek, M. *Acta Crystallogr. B* **2009**, *65* (6), 612–623.

(90) Cormary, B.; Ladeira, S.; Jacob, K.; Lacroix, P. G.; Woike, T.; Schaniel, D.; Malfant, I. *Inorg. Chem.* **2012**, *51* (14), 7492–7501.

(91) Khadeeva, L.; Kaszub, W.; Lorenc, M.; Malfant, I.; Buron-Le Cointe, M. *Inorg. Chem.* **2016**, *55* (9), 4117–4123.

(92) De Candia, A. G.; Marcolongo, J. P.; Etchenique, R.; Slep, L. D. *Inorg. Chem.* **2010**, *49* (15), 6925–6930.

(93) Merkle, A. C.; Fry, N. L.; Mascharak, P. K.; Lehnert, N. *Inorg. Chem.* **2011**, *50* (23), 12192–12203.

(94) Fry, N. L.; Mascharak, P. K. *Dalton Trans.* **2012**, *41* (16), 4726.

(95) Ciofini, I.; Lainé, P. P.; Bedioui, F.; Daul, C. A.; Adamo, C. *Comptes Rendus Chim.* **2006**, *9* (2), 226–239.

Chapter II

Methodology and Analysis Tools

This chapter pretends to give a brief overview on the theoretical background and fundamentals of the Density Functional Theory (DFT) used in this PhD. Throughout this chapter, a brief explanation of the methods and analysis tools used is presented as well.

2.1 Theoretical Background

The main goal of quantum chemistry is to solve the Schrödinger equation to predict atomic and molecular properties and to solve chemical problems.

$$\hat{H}\Psi(\boldsymbol{r}) = E\Psi(\boldsymbol{r}) \tag{2.1}$$

The Austrian physicist Erwin Schrödinger postulated, in 1926, his famous equation which is as important in modern quantum physics as the Newton's second law in classical physics. Knowing all the initial forces, position and velocity of a classical particle (knowing its state), its future position can be exactly determined. However, the Heisenberg principle shows that the position and the velocity of a microscopic particle cannot be determined at the same time without an important incertitude, $\Delta\boldsymbol{r}\cdot\Delta\boldsymbol{p} \geq h$. Thus, a different way of determining the properties of a system had to be found. The wave-function in the Schrödinger equation (eq. (2.1)), $\Psi(\boldsymbol{r})$, contains all the necessary information to fully describe a microscopic system. $\hat{H}$ represents the Hamiltonian quantum mechanical operator, equivalent to the classical Hamiltonian function in a conservative system. This quantum operator applied to the wave-function gives the total energy of the system. For a one-particle system in a stationary state, eq. (2.1) becomes:

$$\hat{H} = \hat{T} + \hat{V} = -\frac{\hbar^2}{2m}\nabla^2\Psi(\boldsymbol{r}) + \hat{V}(\boldsymbol{r})\Psi(\boldsymbol{r}) = E\Psi(\boldsymbol{r}) \tag{2.2}$$

where $\hat{T} = -\frac{\hbar^2}{2m}\nabla^2$ and $\hat{V} = \hat{V}(\boldsymbol{r})$ are the kinetic and potential quantum operators, respectively. For one electron under the potential created by an atomic nucleus with charge, Z, the analytical solution for equation (2.2) is well known. In the case of molecules (polyelectronic systems), the form of the Hamiltonian becomes more complex with two kinetic terms, one for the electrons, $\hat{T}_e$, and the other for the nuclei, $\hat{T}_n$, and three potential energy components, one for the Coulomb attraction, $\hat{V}_{en}$, another for the Nuclei repulsion, $\hat{V}_{nn}$ and the last one for

the electronic repulsion energy term, $\hat{V}_{ee}$. This Hamiltonian (without any relativistic effect) takes the following mathematical form (in atomic units):

$$\hat{H} = \hat{T}_n + \hat{T}_e + \hat{V}_{en} + \hat{V}_{nn} + \hat{V}_{ee} = -\frac{1}{2}\sum_A \frac{1}{M_A}\nabla_A^2 - \frac{1}{2}\sum_i \nabla_i^2 - \sum_i \sum_A \frac{Z_A}{d_{iA}} + \\ + \sum_A \sum_{B>A} \frac{Z_A Z_B}{d_{AB}} + \sum_i \sum_{j>i} \frac{1}{d_{ij}} \tag{2.3}$$

where *A, B* are the indices for the nuclei and *i, j* are the indices for the electrons, *d* is the distance between two particles and *Z* is the charge, which represent the atomic number of the nuclei. In this kind of systems, the wave-function contains information about all the nuclei and electrons, thus it is a function of 3*N* variables (in Cartesian coordinates), where *N* represents the total number of particles. Unfortunately, the exact solution for such many-body systems (with two or more electrons) remains unknown. One of the main priorities of Quantum Chemistry is to overcome this obstacle and find appropriate approximations to solve the Schrödinger equation for a many-body system. In the case of polyelectronic atoms and molecules, electronic structure theory (within the Born-Oppenheimer Approximation in most cases) uses mainly two different approaches to solve the Schrödinger equation for stationary systems: the wave-function based methods (wave-function theory (WFT) like Hartree-Fock and post-Hartree-Fock methods) and the electronic density based methods, namely Density Functional Theory (DFT) (see §2.1.3).

2.1.1 Born-Oppenheimer Approximation

One of the most important approximations done in electronic structure calculations is the so-called Born-Oppenheimer approximation, also known as the adiabatic approximation. Fortunately, nuclei are much heavier than electrons; this allows treating their movement separately, simplifying the problem of solving the Schrödinger equation. Electrons move orders of magnitude more rapidly than the massive nuclei, relaxing and rearranging themselves instantaneously in response to the movement of the nuclei. This is the main motivation of the B-O approximation, rather than solving simultaneously the Schrödinger equation for all coordinates, it can be solved by considering only the movement of the electrons in the field generated by the fixed charges of the static nuclei.

The Hamiltonian and molecular wave-function used in the electronic structure theory calculations in the context of the B-O approximation are obtained as follows:

1) The nuclei are treated as stationary classical point charges (they are much heavier than the electrons). The kinetic and potential energy terms corresponding to the nuclei (in eq. (2.3) first and fourth terms respectively) are removed from the Hamiltonian operator of the Schrödinger equation.

2) Then, for a fixed position of all the nuclei, $\boldsymbol{q}$, the electronic Schrödinger equation is solved:

$$\left[-\frac{1}{2}\sum_i \nabla_i^2 - \sum_i \sum_A \frac{Z_A}{d_{iA}} + \sum_i \sum_{j>i} \frac{1}{d_{ij}}\right] \psi_{elec}(\boldsymbol{r};\boldsymbol{q}) = E_{elec}(\boldsymbol{q}) \psi_{elec}(\boldsymbol{r};\boldsymbol{q}) \tag{2.4}$$

The electronic energy and wave function depend parametrically on the nuclear coordinates, *i.e.* the positions of the nuclei are fixed thus, the nuclear coordinates are constant parameters. This nuclear position dependency means that a unique electronic wave function exists for each possible nuclear arrangement (molecular geometry).

3) Finally, the constant nuclear repulsion energy V_{nn} is added to the electronic energy in order to compute the total potential energy of the system (for a fixed nuclear configuration):

$$U = E_{elec}(\boldsymbol{q}) + \sum_A \sum_{B>A} \frac{Z_A}{d_{AB}} \tag{2.5}$$

Note that within the framework of the B-O approximation it is quite common to represent the total potential energy of a molecule U, as $E(\boldsymbol{q})$ or simply E.

2.1.2 Origins of the Wave Function Methods: the Hartree-Fock Theory

The solution for the electronic Schrödinger equation of a system with more than two electrons is not known analytically because of the last term in the Hamiltonian of eq. (2.3), $\sum_i \sum_{j>i} \frac{1}{d_{ij}}$.

a) The Hartree Product

One of the first attempts to solve the electronic Schrödinger equation (within the B-O approximation) for many-electrons systems was proposed in 1928 by the English mathematician and physicist Douglas Rayner Hartree.[1] The main idea behind the Hartree method was to transform the *N*-electron unsolvable problem into *N*-monoelectronic solvable problems. He proposed, as an initial approach, to represent the electronic wave function as the product of monoelectronic wave functions (spin orbitals):

$$\Psi(\boldsymbol{x}_1,\boldsymbol{x}_2,\boldsymbol{x}_3,\ldots,\boldsymbol{x}_N)=\chi_1(\boldsymbol{x}_1)\cdot\chi_2(\boldsymbol{x}_2)\cdot\chi_3(\boldsymbol{x}_3)\ldots\chi_N(\boldsymbol{x}_N) \tag{2.6}$$

where $\chi_i(\boldsymbol{x}_i)$ are the spin orbitals $\chi(\boldsymbol{x})=\varphi_{n,l,m_l}(\boldsymbol{r})\cdot\sigma_{m_s}(\omega)$ and $\boldsymbol{x}_i$ is the vector containing the spatial and spin coordinates of the electron ($\boldsymbol{x}$ = {$\boldsymbol{r}$,ω} ; where ω can be α or β). Equation (2.6) is known as the Hartree Product and arises from the assumption of electrons moving independently of one another; within this assumption the Hamiltonian becomes separable (can be expressed as the sum of *N*-monoeletronic Hamiltonians, eq. (2.7)), since the term $\sum_i\sum_{j>i}\frac{1}{d_{ij}}$ is neglected, and thus coordinates of different electrons are independent.

$$\hat{H}=\sum_i^N h_i^0 \tag{2.7}$$

Once a trial function is defined for every spin orbital, they can be optimized using the variational principle with the help of a powerful mathematical method called Self-Consistent Field. (Note: In order to solve the *N*-electron problems, Hartree redefined a new monoelectronic Hamiltonian including an effective potential, taking into account somehow the missing interelectronic repulsion (see §2.1.2.c)).

b) The Variational Principle

The variational principle is a cornerstone theorem in Quantum Chemistry. Assuming the stationary ground state of a system, where its normalized wave function Ψ_0 and energy E_0 satisfy the Schrödinger equation (eq. (2.1)), the expectation value of the energy should be equal to E_0:

$$\langle E\rangle=\frac{\int\Psi_0^*\hat{H}\Psi_0 d\tau}{\int\Psi_0^*\Psi_0 d\tau}=\int\Psi_0^*E_0\Psi_0 d\tau=E_0\int\Psi_0^*\Psi_0 d\tau=E_0 \tag{2.8}$$

If the wave function of this system is substituted by a trial wave function χ which satisfies all the limit conditions of the problem and it is well-behaved, the expectation value computed with that trial wave function eq. (2.9) will always be equal or greater than the exact energy E_0, *i.e.* $E \geq E_0$.

$$\left.\begin{array}{c} \hat{H}\chi \neq E\chi \\ \langle\chi|\chi\rangle = \int \chi^* \chi d\tau = 1 \end{array}\right\} E = \langle E\rangle = \frac{\int \chi^* \hat{H} \chi d\tau}{\int \chi^* \chi d\tau} \neq \int \chi^* \hat{H} \chi d\tau \qquad (2.9)$$

This variational principle allows computing an upper limit to the energy E_0 using the trial wave function χ. In general, the trial wave function is a function of some parameters known as variational parameters. Obviously, the energy is also a function of these variational paramenters. In order to find the closest value to the exact energy, the computed energy needs to be minimized with respect to the variational parameters. In the Hartree method, the exponents of the Gaussians used as a trial functions to model the atomic orbitals of polyelectronic atoms are variational parameters. Hence, the Gaussian exponents which minimize the energy of the system are variationally determined.

c) Self-Consistent Field Method

In his method, Hartree used the 'cloud of charge' model for the atomic orbital (density of charge eq. (2.10)), *i.e.* the electron described by a space orbital φ_j behaves as a charge distribution defined by the probability of finding that electron in the space.

$$\rho_j = \int \varphi_j^*(\boldsymbol{r}) \varphi_j(\boldsymbol{r}) d\tau \qquad (2.10)$$

Thus, an electron moving in the mean field created by many electrons would feel an effective potential defined as:

$$V_i^{effect} = \sum_{j \neq i}^{N} \int \frac{\varphi_j^*(\boldsymbol{r}) \varphi_j(\boldsymbol{r})}{d_{ij}} d\tau \qquad (2.11)$$

In Hartree's method, in order to include the effective potential, the definition of the monoelectronic Hamiltonian is modified as follows:

$$\hat{H}^H = \sum_i^N h_i \quad ; \quad h_i = h_i^0 + V_i^{effect} \quad ; \quad h_i^0 = -\frac{1}{2} \nabla_i^2 - \sum_A \frac{Z_A}{d_{iA}} \qquad (2.12)$$

which is not the real Hamiltonian of the system, but at least includes in a mean-field sense the interelectronic repulsion term.

Another clever idea introduced by Hartree was the way of solving the variational problem. Starting from an initial guess of the spin orbitals, an iterative minimization procedure is performed in order to find the best ensemble of orbitals which minimize the energy of the system (variational principle). The iterative minimization used is a mathematical procedure known under the name of Self-Consistent Field (SCF). This iterative procedure finishes when the following conditions are satisfied:

$$\chi_i^{k+1} \cong \chi_i^{k} \text{ and } \varepsilon_i^{k+1} \cong \varepsilon_i^{k} \tag{2.13}$$

where χ_i^{k+1} and ε_i^{k+1} correspond to the computed spin orbital and its energy, respectively, in the (*k + 1*) step of the minimization iterative process and χ_i^{k} and ε_i^{k} are to the spin orbital and its energy of the previous step. The conditions above (eq. (2.13)) mean that the spin orbitals and their energies do not change any more in the iterative procedure and thus, they are converged. In simple terms, the idea behind the SCF procedure consists on computing the averaged field seen by each electron, using the initial guess of spin orbitals, in order to find a new set of orbitals which minimize the energy. Then, with the new set of orbitals, the averaged field is recomputed, new orbitals are found, and the procedure is repeated until self-consistency is reached (the field computed is self-consistent and the spin orbitals do not change).

The Hartree method presents two main drawbacks:

1) The most important problem is the well-known missing electronic correlation energy. It rises due to the fact that in this method the interelectronic interaction is introduced as a mean-field. The electronic repulsion is computed as an average field hence, two electrons have still a slight probability to be in the same position, which is unphysical. This problem can be partially solved using post-Hartree-Fock methods WFT (which will not be discussed in this PhD manuscript) or by using the Density Functional Theory (see §2.1.3).

2) The second drawback is directly linked with the wave function defined as the Hartree Product. Using the Hartree wave function, the *i*th electron is defined by the *i*th spin orbital χ_i, but the electrons are indistinguishable and thus, any electron can be defined by any spin orbital. A direct consequence of the indistinguishability of electrons is the well-known *exclusion principle* enunciated by Wolfgang Pauli in

1925.[2,3] The solution to the problem of the Hartree wave function was introduced in 1930 by the Russian physicist Vladimir Aleksandrovich Fock[4] and the American physicist John Clarke Slater.[5] It consists on using as a wave function a Slater determinant instead of the Hartree Product, in which case the electrons are indistinguishable.

d) Slater Determinant as the Antisymmetric Electronic Wave Function: Hartree-Fock Theory

Pauli's exclusion principle implies that a wave function describing an ensemble of fermions must be antisymmetric with respect to the interchange of any two of them. This requirement is not satisfy by the Hartree Product wave function. This problem can be solved by taking advantage of the mathematical properties offered by determinants. Interchanging any column or row in a determinant changes its sign. Moreover, if two columns or two rows are identical the determinant is zero. Using these characteristic properties of determinants, Slater introduced a new formulation for the wave function:

$$\Psi(\boldsymbol{x}_1, \boldsymbol{x}_2, \boldsymbol{x}_3, \ldots, \boldsymbol{x}_N) = \frac{1}{\sqrt{N!}} \begin{vmatrix} \chi_1(\boldsymbol{x}_1) & \chi_2(\boldsymbol{x}_1) & \cdots & \chi_N(\boldsymbol{x}_1) \\ \chi_1(\boldsymbol{x}_2) & \chi_2(\boldsymbol{x}_2) & \cdots & \chi_N(\boldsymbol{x}_2) \\ \vdots & \vdots & \ddots & \vdots \\ \chi_1(\boldsymbol{x}_N) & \chi_2(\boldsymbol{x}_N) & \cdots & \chi_N(\boldsymbol{x}_N) \end{vmatrix} \qquad (2.14)$$

where $\frac{1}{\sqrt{N!}}$ is the normalization constant. In the Slater determinant N spin orbitals are occupied by N electrons with no specific positions, *i.e.* the electrons are indistinguishable. Two identical columns represent two electrons in the same spin orbitals, which is impossible (Pauli Exclusion Principle) and makes the determinant zero. Thus, two electrons cannot have the same four quantum numbers. Permuting two columns of the Slater determinant corresponds to the interchange of the coordinates of two electrons, which changes the sign of the determinant, *i.e.* the wave function is antisymmetric.

Arising from the fact of introducing the antisymmetric Slater determinant a new quantity appears, the exchange energy term K. The exchange energy does not have a classical analogue, and it appears due to the fermion nature of electrons.

Fock redefined the monoelectronic operator in the Hartree's SCF method, giving birth to the Hartree-Fock (HF) theory. The monoelectronic Fock operator has the following form:

$$f_i = h_i^0 + v_i^{HF} \quad ; \quad h_i^0 = -\frac{1}{2}\nabla_i^2 - \sum_A \frac{Z_A}{d_{iA}} \quad ; \quad v_i^{HF} = \sum_j^{N/2}\left(2J_j(i) - K_j(i)\right) \tag{2.15}$$

where the v_i^{HF} is the average potential felt by the electron *i* created by the rest of the electrons in the system. The first term in the average potential represents the mean-field Coulombic repulsion term, and the second one is the exchange term, arising from the antisymmetric nature of the wave function.

The missing electronic correlation energy is a persistent problem in the Hartree-Fock theory. The Swedish physicist Per-Olov Löwdin defined the electronic correlation energy as the difference between the exact non-relativistic energy and the HF energy:

$$\varepsilon_{correlation} = E_{exact} - \varepsilon_{HF} \tag{2.16}$$

Although the HF method recovers 99% of the exact energy of polyelectronic systems, the missing 1% corresponding to the correlation energy has proven to be, over the years, very important to reproduce experimental observations. In 1964, the distinction between the dynamic and static electronic correlation was made by the Turkish physicist Oktay Sinanoglu. The missing static electronic correlation in the HF theory arises from the monodeterminantal nature of the wave function. The static correlation can be recovered to a good extend with multiconfigurational methods, which make use of many Slater determinants to construct the wave function, and other post-HF methods. Further, the missing dynamic electronic correlation in the HF theory arises from the substitution of the interelectronic term of the Hamiltonian $\sum_i \sum_{j>i} \frac{1}{d_{ij}}$ for the average potential v_i^{HF}. The dynamic correlation can be recovered not only with post-HF method (WFT), but with the Density Functional Theory as well. Note: DFT to some extend may also recover part of the static electronic correlation.[6]

2.1.3 Density Functional Theory

The two physicists Llewellyn Hilleth Thomas[7] and Enrico Fermi,[8] were the first physicists that developed a model based on the electronic density instead of the wave function. Their model, with some pitfalls, provided the basis for one of the most successful theories in modern quantum chemistry, the so-called Density Functional Theory. Modern DFT began with the theorems formulated by the theoretical physicists Pierre Hohenberg and Walter Kohn (HK)[9] and the subsequent mathematical orbital formulation by Kohn and the

physicist Lu Jeu Sham (KS).[10] The beauty of this theory resides in its intellectual and fundamental challenge. DFT is one of the most applied theories in electronic structure calculations, and in 1998 Walter Kohn was awarded with the Nobel Prize in Chemistry for his development of this theory.

One of the strongest points of DFT is the transformation of the *N*-electron problem into a one electron density problem. Being based on the electron density, which is a very simple quantity (3 variables compared to 3*N*), DFT is a simple theory. This is one of the main advantages of DFT over correlated methods based on the WFT, which scale poorly with system size and need large basis sets to describe electron-electron cusps. The WFT methods cannot be applied to very large molecules such as proteins or DNA chains. DFT has many points in common with the Hartree-Fock theory, with the advantage of being formally exact. Although HF and DFT share many conceptual and computational features, they are rarely presented together. As in the HF theory, the way the Schrödinger equation is solved remains a variational method in which a set of spin orbitals that minimize the energy of the system is found. The mathematical tool behind this variational minimization in DFT is the same SCF as in the HF theory.

Although DFT is formally exact, approximations need to be done in practice. Standard DFT approximations scale like Hartree-Fock. Furthermore, basis set must describe the density, not the wave function. Hence, less need for high angular momentum functions, which results in good quality correlated calculations at low cost that can be applied to very large systems.

a) The Hohenberg-Kohn Theorems

Theorem 1: *Two N-electron systems defined by two Hamiltonians with external potentials differing by more than one constant cannot have ground states with the same electronic density, i.e. the external potential is defined by the electron density of the ground state.*

This theorem can be easily proven assuming two different external potentials $\mathbf{V}_1(\mathbf{r})$ and $\mathbf{V}_2(\mathbf{r})$ which afford the same electron density $\rho(\mathbf{r})$. Each potential generate a different Hamiltonian, with the same ground state density, but different wave functions:

$$E_1 = \langle \Psi_1 | \hat{H}_1 | \Psi_1 \rangle \quad ; \quad E_2 = \langle \Psi_2 | \hat{H}_2 | \Psi_2 \rangle \tag{2.17}$$

Then, the energy of the system described by Ψ_1 can be computed with the Hamiltonian $\hat{H}_2$ and *vice versa*, obtaining the following equations:

$$E_2^0 < \langle \Psi_1 | \hat{H}_2 | \Psi_1 \rangle = \langle \Psi_1 | \hat{H}_1 | \Psi_1 \rangle + \langle \Psi_1 | \hat{H}_2 - \hat{H}_1 | \Psi_1 \rangle$$
$$= E_1^0 + \int \rho(r)[v_2(r) - v_1(r)] \tag{2.18}$$

and

$$E_1^0 < \langle \Psi_2 | \hat{H}_1 | \Psi_2 \rangle = \langle \Psi_2 | \hat{H}_2 | \Psi_2 \rangle + \langle \Psi_2 | \hat{H}_1 - \hat{H}_2 | \Psi_2 \rangle$$
$$= E_2^0 + \int \rho(r)[v_1(r) - v_2(r)] \tag{2.19}$$

These two inequalities are based on the variational principle. Adding both inequalities eq. (2.18) and eq. (2.19) yields:

$$E_2^0 + E_1^0 < E_1^0 + E_2^0 \tag{2.20}$$

which is a contradiction. Thus, the external potential must be uniquely determined by the electron density $\rho(\mathbf{r})$. The density also determines the number of electrons *N*:

$$\int \rho(\boldsymbol{r}) d\boldsymbol{r} = N \tag{2.21}$$

The first Hohenberg-Kohn theorem implies that the Hamiltonian of an *N*-electron system (and in particular its ground state wave function and energy) can be obtained from the electron density, $\rho(\mathbf{r})$. According to this theorem, there is a one-to-one correspondence between the energy of a system and the electron density. By extension, the electron density uniquely defines the expectation value of any ground state observable provided the operator is known.

Theorem 2: *Any approximate trial electronic density* $\tilde{\rho}(\boldsymbol{r})$ *that defines the* $\tilde{v}$ *and a trial wave function* $\tilde{\Psi}$*, can be used to determine variationally the electronic density that minimizes the energy of the ground state.*

The second Hohenberg-Kohn theorem introduces the variational principle for the Density Functional Theory. Using the trial wave function in the usual variational principle yields:

$$\left\langle \tilde{\Psi} \middle| \hat{H} \middle| \tilde{\Psi} \right\rangle = \int \tilde{\rho}(\boldsymbol{r}) v(\boldsymbol{r}) d\boldsymbol{r} + F[\tilde{\rho}] = E[\tilde{\rho}] \geq E[\rho_{exact}] \tag{2.22}$$

where $F[\tilde{\rho}]$ is the universal functional of $\tilde{\rho}$:

$$F[\tilde{\rho}] = T[\tilde{\rho}] + V_{ee}[\tilde{\rho}] = \left\langle \tilde{\Psi} \middle| \hat{T} + \hat{V}_{ee} \middle| \tilde{\Psi} \right\rangle \tag{2.23}$$

Unfortunately, the exact analytical form of $F[\tilde{\rho}]$ is unknown. In the formally exact DFT, the energy afforded by the variational principle is never below the exact ground state energy, $E[\rho_{exact}]$. This is not necessarily true when approximations to the universal functional $F[\tilde{\rho}]$ are introduced.

b) The Kohn-Sham Method

With the Kohn-Sham orbital formulation of DFT, the ground-state electron density can be obtained, in principle, solving the self-consistent one-electron Schrödinger equations for KS orbitals with occupations 0 or 1. The sum of the squares of the occupied orbitals gives the electron density. The energy of the system can be generally written, according to the KS formulation, as the sum of the kinetic energy $T_s[\rho]$ (not exact, due to the assumption of the non-interacting electrons), the interaction of the electron density with the external potential $E_{Ae}[\rho]$ (mainly generated by the nuclei), the Coulomb repulsion energy of the density interacting with itself $J[\rho]$ and the exchange-correlation energy $E_{xc}[\rho]$. Thus, the general energy expression for the real system is:

$$E_{DFT}[\rho] = T_s[\rho] + E_{Ae}[\rho] + J[\rho] + E_{xc}[\rho] \tag{2.24}$$

All the functionals corresponding to the energy terms of eq. (2.24) are known except for the exchange-correlation functional. Indeed, one of the principal aims in the development of modern DFT is to find the exact form of the functional that affords the exact exchange-correlation energy term, or at least a very good approximation.

c) The Exchange-Correlation Energy

Deriving the exact density functional for the exchange-correlation energy is an extremely hard task (not practical for *N*-electron systems). In spite of its physical importance,

the exchange-correlation energy is relatively small comparing with the rest of the energy terms of eq. (2.24). This is the reason why approximations can yield good and realistic results.

At this point, it is important to remember that the correlation energy arises from the fact that probabilities of finding one electron in a determined position and another electron in a different position are not independent, they are correlated probabilities. This is the main drawback in the HF theory, which does not take the correlation between probabilities into account. The physical explanation resides in the fact that electrons do not move randomly through the space but avoid one another.

The exchange-correlation energy term consists of three physical contributions. The first one is the exchange energy contribution, quite similar to the exchange integral in the HF theory. The second is the correlation energy related with the Coulomb repulsion, and the last but not least is the kinetic energy of correlation due to the 'extra' swerving motion of electrons as they avoid one another.

If the exact exchange-correlation energy could be determined, a self-interaction correction would be provided to the Hartree electrostatic energy, since the electrons never interact with themselves.

d) Spin Densities, Spin Symmetry and Spin Contamination

When the spin is introduced in DFT,[11] the exchange-correlation energy is obtained by a functional of the separate α and β -spin densities, thus the energies for the α and β electrons can be slightly different, since the α and β density matrixes are diagonalized independently. One of the main known issues of the DFT is the so-called spin contamination.[11] In open-shell systems the KS wave function is not an eigenfunction of the square of the total electron spin operator, phenomenon known as spin contamination (see §2.5.1, eq. (2.92)). Restricted open-shell KS[12] methods have been developed to avoid this problem.

The fact that the KS wave function is not an eigenfunction of S^2 does not have to be considered as a contamination, unless this wave function is regarded as an approximation of the real wave function. This might not be the best interpretation, since the KS theorem is conceived to yield the ground-state energy and spin-densities. Thus, a better interpretation is that the KS determinant is an auxiliary quantity that affords the true spin-densities.

A connection between the Kohn-Sham non-interacting system and the real interacting one exists through the average over the electron-electron coupling constant,[13,14] taking into account that the electron densities are always the same.

e) Different Approximations of the Density Functional

Many approximations to calculate the exchange-correlation energy exists, ranging from the lower level ones called Local Spin-Density Approximations (LDA) to the higher level more accurate ones called hyper- Generalized Gradient Approximations hyper-GGA, which include the exact exchange energy or the Random Phase Approximations which add the unoccupied orbitals.

According to J.P. Perdew a general classification of the different approximations can be regarded as the so-called '*Jacob's ladder of density functional approximations*'.[15] Climbing up the rungs of the ladder, new ingredients are added, making the approximations more accurate but at the same time more complicated and more expensive from a computational point of view.

It is extremely advisable to read and search in the literature what are the best approximations and functionals for a specific problem in order to choose the adequate functional for that specific problem.

f) Description of Strong Correlation

In general, semilocal density approximations do not describe properly the strong correlation phenomenon. Two different strong correlations can be defined: the one present in superconductors which may have a small effect on bonding energies, and the static correlation which can be large and important on the scale of these energies. Static correlation (also known as electron localization or the suppression of the electron fluctuation) can appear not only in solids but in molecules as well. In some systems containing *d* or *f* electrons these strong correlation phenomena are present. These systems can be treated by a general approximation method called 'DFT+U', where the empirical parameter U can be defined[16,17] as the energy correction for the fractional occupation error of the semilocal density approximation.

DFT calculations are done by solving self-consistent field equations like HF calculations but it includes correlation energies via the exchange-correlation functional. Semilocal density

functionals account for the static correlation in the exchange energy term and not in the correlation one.[18] Semilocal approximations generally yield not very accurate results for systems with stretched bonds. The accuracy can be increased using hybrid functionals but in some cases these functionals may yield even worse results than the semilocal ones. In these cases, accurate description of the strong correlation requires fully non-local high level functionals.

2.1.4 Time-Dependent Density Functional Theory

In principle, the solutions for the exact KS equations do not afford straightforward excited-state densities or energies, only under special conditions, since the HK theorems use the variational principle. In practice, excited-state energies can be obtained by excited-state DFT,[19,20] but a truly rigorous approach of the excited-state DFT problem is achieved by the time-dependent DFT (TD-DFT)[21] formulation within the framework of the linear-response theory.

In time-dependent DFT the vertical excitation energies ω are computed by solving the pseudo-eigenvalue equation formulated by the theoretical chemist Mark E. Casida:[22]

$$\begin{pmatrix} \boldsymbol{A} & \boldsymbol{B} \\ \boldsymbol{B}^* & \boldsymbol{A}^* \end{pmatrix} \begin{pmatrix} \boldsymbol{X} \\ \boldsymbol{Y} \end{pmatrix} = \omega \begin{pmatrix} \boldsymbol{1} & \boldsymbol{0} \\ \boldsymbol{0} & -\boldsymbol{1} \end{pmatrix} \begin{pmatrix} \boldsymbol{X} \\ \boldsymbol{Y} \end{pmatrix} \tag{2.25}$$

The precise form of the matrices $\boldsymbol{A}$ and $\boldsymbol{B}$ depends on the nature of the exchange-correlation functional used in the TD-DFT calculation. Casida's equation can be derived from the poles of the dynamic polarisability or by the density matrix linear-response approach. In practice, the problem can be reduced by one half taking advantage of the fact that the subtraction of matrices $\boldsymbol{A}$ and $\boldsymbol{B}$, ($\boldsymbol{A} - \boldsymbol{B}$) results in a positive definite matrix for real orbitals. Then, Casida's expression can be reformulated as:

$$(\boldsymbol{A}-\boldsymbol{B})^{1/2}(\boldsymbol{A}+\boldsymbol{B})(\boldsymbol{A}-\boldsymbol{B})^{1/2}\boldsymbol{Z} = \omega^2 \boldsymbol{Z} \tag{2.26}$$

where $\boldsymbol{Z} = (\boldsymbol{A}-\boldsymbol{B})^{1/2}(\boldsymbol{X}+\boldsymbol{Y})$. This new formulation provides information about the orbitals involved in the electronic transitions. TD-DFT calculations like regular DFT or HF calculations are also performed within the framework of the adiabatic approximation, meaning that the time-dependent exchange-correlation potential is replaced by the stationary time-independent potential which is evaluated using the time-dependent density.

42

The linear-response approach is a good approximation when the electronic structure of the excited states does not change drastically with respect to the electronic structure of the reference ground state. This is exactly what happens in regular UV-visible absorption spectra, where the bands experimentally observed are the result of electronic excitations from valence orbitals to the virtual unoccupied orbitals. Resulting from a TD-DFT calculation, the electronic transitions of the UV-visible absorption spectra are computed. Indeed, the core electronic structure is practically unmodified in these valence electronic transitions, *i.e.* the inner electronic structure of the ground and excited states is similar. Hence, an excited state can be considered as a slight perturbation of the electronic ground state. In this context, the linear-response is a very good approximation and has the great advantage of affording the vertical excitations just knowing the electronic structure of the reference ground state. This is quite interesting, since the reference ground state electronic structure is easily computed by the SCF iterative minimization procedure of a regular DFT calculation.

It is important to keep in mind that in a TD-DFT calculation, the electronic structure of all the computed excited states is built from the KS wave function of the ground state. Moreover, each electronic transition is built as a linear combination of monoelectronic excitations from the occupied to the virtual orbitals, which affords the nature of the electronic transition. In some cases there are few monoelectronic excitations which have quite similar coefficients and the excitation nature is quite difficult to determine. In these cases, the Natural Transition Orbitals[23] (NTOs) might help in the analysis of the electronic transition nature.

2.2 Exploring Potential Energy Surfaces

Due to the difference between the nuclear and electronic velocities, electrons adjust very fast to small changes in nuclear geometries. Thus, to a good extent, electronic and nuclear velocities can be decoupled. This means that from an electronic point of view, the nuclei are stationary. As mention in §2.1.1, this is known as the Born-Oppenheimer approximation. The electronic wave function depends only on the nuclear position (and not in their momentum), meaning that an electronic wave function exists for each possible nuclear configuration. Within the Born-Oppenheimer approximation the electronic wave function provides the necessary information to describe potential energy surfaces. The PES of a *N*-atom molecule depends on all nuclear coordinates defining the molecular geometry, hence, the dimensionality of that PES is 3*N*. Three of the 3*N* possible nuclear displacements correspond to

the overall rotations of the molecule and three correspond to the overall translations, leaving $3N - 6$ ($3N - 5$ for linear molecules) displacements which describe the internal motion of the nuclei in the molecule, the vibrational modes.

The Born-Oppenheimer approximation is essential in computational chemistry. Methods aimed at solving the electronic Schrödinger equation within this approximation are generally known as 'electronic structure methods'. Solving the electronic Schrödinger equation for a large number of nuclear configurations can give an idea of the general topology of the potential energy surface, but building a complete PES for molecules containing more than four or five atoms is practically impossible. However, it is possible to obtain useful 'chemical information' restricting the exploration of PESs to those nuclear configurations (geometries) which are relevant. Generally speaking, these molecular geometries correspond to the local and global minima on the PES. Once the minima on the PES are located, the minimum energy path (MEP) connecting them affords an energy profile of chemical reactions, with the maxima corresponding to the different transition states found in the reaction.

An important part of this PhD project focuses on exploring and characterizing the MEPs connecting the minima found on the PES of the ground state (singlet state) and the lowest triplet excited state of different ruthenium nitrosyl complexes within the hypothesis of adiabatic photochemical reactions. In order to explore possible non-adiabatic reaction mechanisms, crossing points between the PESs of the singlet and lowest triplet state have been searched as well. Characterization of the molecular geometries where the energy is minimized in the crossing region affords the minimum energy crossing points (MECP) which are explained in detail in §2.2.3.

2.2.1 Standard Approach to the MEP Problem

The aim of this section is to explain in detail the general procedure which is usually employed (and has been employed in the study of the photoisomerization of the *trans*-$[RuCl(NO)(py)_4]^{2+}$ complex) to explore the relevant reaction paths followed during a chemical reaction, *i.e.* the minimum energy paths on a PES connecting the products and the reactants (the minima on the PES). In general, this procedure can be divided in five steps a) the initial search and optimization of the minima on the PES, b) 'construction' of an educated guess for the search of a transition state (TS) connecting the minima c) optimization of the TS, d) frequency analysis of all the stationary points found and e) verification of the connection

between the different minima through the TS found by Intrinsic Reaction Coordinate (IRC) calculations or other computationally 'cheaper' alternatives like steepest descent optimizations.

a) Optimization of the Minima

Geometry optimizations are essential in the study of any chemical problem by means of electronic structure methods. They are one of the initial steps in the investigation of the reactivity in molecules. From a mathematical point of view, geometry optimizations are the search of stationary points in a PES, *i.e.* finding minima (or maxima) of the energy function which depends on the atomic coordinates (the geometric degrees of freedom). Over the years, a large number of efficient and adapted methods have been developed and refined to fulfill the special requirements of molecular geometry optimizations.

Within the framework of optimization theory in applied mathematics, a wide variety of sophisticated algorithms are available for optimizing molecular geometries. The optimal choice strongly depends on the problem and it is quite difficult to formulate a general recipe. It is worth noting that, in practice, the strategies adopted for the search of minima on a PES are different from those required to find transition states. From a widespread point of view, geometry optimizations can be divided in two major families; first-order methods using only first derivatives to find stationary points, and the so-called second-order methods which go a step further in the optimization procedure using first and second derivatives in the search of stationary points, assuming a quadratic model for the PES.

The gradient vector **g** containing the first derivatives of the energy function always points in the direction where the energy increases most. The gradient can be generally defined as a column vector with the following form:

$$\mathbf{g}(\boldsymbol{q}) = \begin{pmatrix} \dfrac{\partial E(\boldsymbol{q})}{\partial q_1} \\ \vdots \\ \dfrac{\partial E(\boldsymbol{q})}{\partial q_n} \end{pmatrix} \tag{2.27}$$

where $\boldsymbol{q}$ is an n-dimensional coordinate vector and E represents the potential energy function with n-geometric degrees of freedom. A straightforward approach in the search of a minimum on a PES would be to follow the opposite direction of the gradient, *i.e.* stepping in the

direction where the energy is lowered, until a minimum is found. This approach corresponds, indeed, to the first-order family of methods and it is known as the Steepest Descent (SD) optimization. This procedure can be generalized as:

$$\boldsymbol{q}^{k+1} = \boldsymbol{q}^{k} - \alpha \cdot \mathbf{g}^{k} \tag{2.28}$$

where $\boldsymbol{q}^{k+1}$ corresponds to the new geometry that will be computed, $\boldsymbol{q}^{k}$ and $\mathbf{g}^{k}$ are the previous (or reference) geometry and the gradient at that geometry, respectively; the superscript k refers to the step number and α is an arbitrary value which can be dynamically modified during the optimization to control the step size. The step vector, defined as $\boldsymbol{s}^{k} = \boldsymbol{q}^{k+1} - \boldsymbol{q}^{k}$, describes the displacement from the reference geometry $\boldsymbol{q}^{k}$. Since the iterative points are taken in a linear fashion, this movement along the PES is called a 'line search'. The advantage of the SD algorithm is that it is very simple and, by its intrinsic nature, it will always go towards a minimum of the energy function, lowering down its value at each step (if the line minimization is carried out sufficiently accurately). The main disadvantage is the slow convergence rate which decreases as the minimum is approached. The SD slow convergence can be improved by constructing a line search in such a way that it is the conjugate to the previous search direction. This method is generally known under the name of Conjugate Gradient (CG) and also belongs to the first-order family of methods where only the computation of the first derivatives is required. Though the CG method improves convergence, it does not hold rigorously for non-quadratic surfaces, and thus, it needs often to be restarted during geometry optimizations.[24] Further improvement on the convergence can be achieved with the family of second-order methods. Within this family of methods, the Newton-Raphson (NR) iterative algorithm may be considered as the simplest choice to compute the step vector during a geometry optimization. It represents a cornerstone in the general context of optimization theory. In this method, the true energy function is approximated as a multidimensional Taylor expansion truncated at the second order around a point[25] $\boldsymbol{q}^{k}$ as follows:

$$E\left(\boldsymbol{q}^{k+1}\right) = E\left(\boldsymbol{q}^{k}\right) + \mathbf{g}^{(k)\mathrm{t}}\left(\boldsymbol{q}^{k+1} - \boldsymbol{q}^{k}\right) + \frac{1}{2}\left(\boldsymbol{q}^{k+1} - \boldsymbol{q}^{k}\right)^{\mathrm{t}}\mathbf{H}^{(k)}\left(\boldsymbol{q}^{k+1} - \boldsymbol{q}^{k}\right) \tag{2.29}$$

where $\mathbf{g}^{(k)}$ and $\mathbf{H}^{(k)}$ are the gradient vector and the Hessian matrix (first and second derivatives of the energy function) at the reference geometry $\boldsymbol{q}^{k}$. Eq. (2.29) can be rewritten in terms of the step vector as:

$$E\left(\boldsymbol{q}^{k+1}\right) = E\left(\boldsymbol{q}^{k}\right) + \mathbf{g}^{(k)\mathrm{t}} \cdot (\boldsymbol{s}^{k}) + \frac{1}{2}(\boldsymbol{s}^{k})^{\mathrm{t}} \cdot \mathbf{H}^{(k)} \cdot (\boldsymbol{s}^{k}) \tag{2.30}$$

Differentiating eq. (2.30) with respect to the step vector and applying the stationary condition (the gradient of the potential energy function has to be equal to zero; $\partial E / \partial \boldsymbol{s}^{k} = 0$), the following equation is obtained:

$$0 = \mathbf{g}^{(k)} + \mathbf{H}^{(k)} \cdot (\boldsymbol{s}^{k}) \tag{2.31}$$

$$\boldsymbol{s}^{k} = -\left(\mathbf{H}^{(k)}\right)^{-1} \mathbf{g}^{(k)} \tag{2.32}$$

Equation 2.32 gives the so-called NR step in a geometry optimization performed with this method. By analogy with the SD algorithm, in the NR optimization the inverse of the second derivatives matrix (inverse Hessian) controls the step size (in the opposite direction of the gradient), as the α parameter does in eq. (2.28). The Hessian matrix can be diagonalized, $\boldsymbol{L}^{(k)t} \cdot \mathbf{H}^{(k)} \cdot \boldsymbol{L}^{(k)} = \tilde{\mathbf{H}}^{(k)}$ (*i.e.* performing an unitary transformation) so that the NR step can be conveniently represented in the Hessian eigenvector basis[26] as follows:

$$\tilde{\boldsymbol{s}}^{k} = -\left(\tilde{\mathbf{H}}^{(k)}\right)^{-1} \tilde{\mathbf{g}}^{(k)} \quad , \quad \tilde{s}_{i}^{k} = -\frac{\tilde{g}_{i}^{(k)}}{\tilde{\mathrm{H}}_{ii}^{(k)}} \tag{2.33}$$

where $\boldsymbol{L}^{(k)}$ is the matrix containing the column eigenvectors of the Hessian matrix, $\tilde{\mathbf{H}}^{(k)}$ is the diagonal Hessian matrix and $\tilde{\mathbf{g}}^{(k)} = \boldsymbol{L}^{(k)t} \cdot \mathbf{g}^{(k)}$ is the gradient expressed in the Hessian eigenvector basis.

If one of the Hessian eigenvalues is negative, from eq. (2.33) it can be seen that the step in the *i*th direction will be along the gradient component (not in the opposite direction) and thus the potential energy will increase. When this happens, the geometry optimization may lead to a stationary point with one negative Hessian eigenvalue, a TS. This feature might be pleasant, if a specific TS is searched, but quite bothersome if the optimization aim is to find a minimum. In general, without any constraint in the Hessian, the NR optimizations converge in the nearest stationary point from the initial geometry which can be a minimum or a saddle point of any order (various negative Hessian eigenvalues). Moreover, it is clear that if the true PES is based on the second-order Taylor expansion, only a restricted region about the point of expansion exists where this approximation is valid. This region is known as the trust region and can be described by a hypersphere with a trust radius T. As it can be observed from eq. (2.33), small eigenvalues $\tilde{\mathrm{H}}_{ii}^{(k)}$ can produce very large NR steps, taking the geometry far outside the

trust region, leading to divergence in the optimization. To avoid convergence problems, the step size of a NR optimization should be lower than or equal to the trust radius τ. NR methods controlling the step size with a defined trust radius are commonly known as Trust Radius Methods (TRM). A reasonable initial trust radius can be updated during the course of the optimization, depending on how well the second-order approximation describes the PES.[27] A simple approach to control the step size during the optimization is just reducing the step if it exceeds the defined τ, so that $\boldsymbol{s}^k < \tau^k$. A more sophisticated but much more rigorous scheme consists on constraining the optimization step using a Lagrangian multiplier, λ, to minimize the Lagrangian function defined as follows:

$$L\left(\boldsymbol{q}^{k+1}\right) = E\left(\boldsymbol{q}^{k+1}\right) - \frac{1}{2}\cdot\lambda\cdot\left((\boldsymbol{s}^k)^2 - \tau^2\right) \tag{2.34}$$

where $E(\boldsymbol{q}^{k+1})$ is the usual quadratic approximation of the PES in eq. (2.30).[28] Minimization of this Lagrangian function (stationary condition $\partial L / \partial \boldsymbol{s}^k = 0$) yields:

$$0 = \mathbf{g}^{(k)} + \mathbf{H}^{(k)}\cdot(\boldsymbol{s}^k) - \lambda\cdot(\boldsymbol{s}^k) \tag{2.35}$$

$$\boldsymbol{s}^k = -\left(\mathbf{H}^{(k)} - \lambda\cdot\mathbf{I}\right)^{-1}\mathbf{g}^{(k)} \tag{2.36}$$

where $\mathbf{I}$ is the identity matrix. If the shifted Hessian matrix ($\mathbf{H}^{(k)} - \lambda\,\mathbf{I}$) is diagonalized, the new control NR step can be represented in the shifted Hessian eigenvector basis as follows:

$$\tilde{s}_i^{\,k} = -\frac{\tilde{g}_i^{(k)}}{\tilde{H}_{ii}^{(k)} - \lambda} \tag{2.37}$$

where eq. (2.37) is the same diagonal representation of eq. (2.33) with the addition of the new parameter λ coming from the constraint Lagrangian optimization, known as the level-shift parameter. It is important to highlight that in order to reach a minimum, this level-shift parameter needs to be lower than the lowest Hessian eigenvalue, so that the denominator is always positive and the step direction will be always opposite to the gradient. On the contrary, if a TS is searched, the shifted Hessian must contain one negative eigenvalue, *i.e.* the level-shift parameter λ must be in between the lowest two eigenvalues of $\mathbf{H}^{(k)}$, $\tilde{H}_{n-1}^{(k)} > \lambda > \tilde{H}_n^{(k)}$. Other alternatives to optimize TSs will be mentioned in §2.1.1.c.

A second-order method alternative to the NR optimization can be used, the so-called Rational Function Optimization (RFO). In this popular method, used in many electronic structure packages, the optimization problem is reformulated, expanding this function in terms

of a rational function approximation,[29] instead of the Taylor expansion used in the NR method. In fact, the form of the function used in the RFO method is quite similar to a Taylor expansion truncated in the second order with just the addition of the denominator $(1+(\mathbf{q}^{k+1}-\mathbf{q}^{k})^{t}\mathbf{S}(\mathbf{q}^{k+1}-\mathbf{q}^{k}))$ as follows:

$$E\left(\boldsymbol{q}^{k+1}\right)-E\left(\boldsymbol{q}^{k}\right)=\frac{\mathbf{g}^{(k)\mathrm{t}}\left(\boldsymbol{q}^{k+1}-\boldsymbol{q}^{k}\right)+\frac{1}{2}\left(\boldsymbol{q}^{k+1}-\boldsymbol{q}^{k}\right)^{\mathrm{t}}\mathbf{H}^{(k)}\left(\boldsymbol{q}^{k+1}-\boldsymbol{q}^{k}\right)}{1+\left(\boldsymbol{q}^{k+1}-\boldsymbol{q}^{k}\right)^{t}\mathbf{S}\left(\boldsymbol{q}^{k+1}-\boldsymbol{q}^{k}\right)} \tag{2.38}$$

where the new matrix term **S** in eq. (2.38) is an identity matrix multiplied by an arbitrary constant α, meaning $\mathbf{S}=\alpha\cdot\mathbf{I}$, though usually α is set to one, so that the **S** matrix becomes the identity matrix. It is very common to rewrite eq. (2.38) as:

$$\Delta E\left(\boldsymbol{q}\right)=\frac{\frac{1}{2}\begin{bmatrix}\boldsymbol{s}^{k} & 1\end{bmatrix}\cdot\begin{bmatrix}\mathbf{H}^{(k)} & \mathbf{g}^{(k)}\\ \mathbf{g}^{(k)t} & 0\end{bmatrix}\cdot\begin{bmatrix}\boldsymbol{s}^{k}\\ 1\end{bmatrix}}{\begin{bmatrix}\boldsymbol{s}^{k} & 1\end{bmatrix}\cdot\begin{bmatrix}\mathbf{S} & 0\\ 0 & 1\end{bmatrix}\cdot\begin{bmatrix}\boldsymbol{s}^{k}\\ 1\end{bmatrix}} \tag{2.39}$$

so that when differentiating this eq. (2.39) with respect to the step vector and applying the stationary condition ($\partial\Delta E\left(\boldsymbol{q}\right)/\partial\boldsymbol{s}^{k}=0$), a eigenvalue equation involving the Hessian augmented by the gradient is obtained:

$$\begin{bmatrix}\mathbf{H}^{(k)} & \mathbf{g}^{(k)}\\ \mathbf{g}^{(k)t} & 0\end{bmatrix}\cdot\begin{bmatrix}\boldsymbol{s}^{k}\\ 1\end{bmatrix}=2\cdot\Delta E\left(\boldsymbol{q}\right)\cdot\begin{bmatrix}\mathbf{S} & 0\\ 0 & 1\end{bmatrix}\cdot\begin{bmatrix}\boldsymbol{s}^{k}\\ 1\end{bmatrix}\overset{\mathbf{S}=\mathbf{I}}{=}2\cdot\Delta E\left(\boldsymbol{q}\right)\cdot\begin{bmatrix}\boldsymbol{s}^{k}\\ 1\end{bmatrix} \tag{2.40}$$

where the augmented matrix on the left-hand side of eq (2.40), $\begin{bmatrix}\mathbf{H}^{(k)} & \mathbf{g}^{(k)}\\ \mathbf{g}^{(k)t} & 0\end{bmatrix}$, is called the augmented Hessian matrix of dimension *n* + *1*. Solving eq. (2.40) yields:

$$2\cdot\Delta E\left(\boldsymbol{q}\right)=\lambda=\mathbf{g}^{(k)t}\boldsymbol{s}^{k} \tag{2.41}$$

$$\boldsymbol{s}^{k}=-\left(\mathbf{H}^{(k)}-\lambda\cdot\mathbf{I}\right)^{-1}\mathbf{g}^{(k)} \tag{2.42}$$

As it can be observed, eq. (2.1) is the same as eq. (2.36) with a level-shift parameter λ, given by eq. (2.41). In this method, by natural choice, the level shift parameter is the double of the energy difference between consecutive geometries.

Taking a closer look to eq. (2.40) it becomes clear that $\begin{bmatrix}\boldsymbol{s}^{k}\\ 1\end{bmatrix}$ is an eigenvector of the augmented Hessian matrix with the eigenvalue $2\Delta E(\boldsymbol{q})=\lambda$. Thus, when $\mathbf{S}=\mathbf{I}$, a convenient way to determine the optimization step $\boldsymbol{s}^{k}$ is by diagonalizing the augmented Hessian matrix. Then,

the eigenvector belonging to the lowest eigenvalue is scaled so that its last component (of the eigenvector) becomes one. Removing the last element of the scaled eigenvector, (obviously it must be a one) the step $\boldsymbol{s}^k$ of the RFO method is obtained.[26] This RFO method can be combined with the idea of the trust radius. In fact, if the α parameter in $\mathbf{S} = \alpha \cdot \mathbf{I}$ is chosen so that $(\boldsymbol{s}^k)^2 = \tau^2$, this method is equivalent to the TRM.[30]

Second order geometry optimization methods have the great advantage of rapid convergence compared to those using only first derivatives; in contrast, they become very expensive for large molecules, since the full second derivatives matrix has to be computed, inverted and stored. Instead of computing the full true Hessian at each step of the iterative optimization algorithm, the Hessian can be updated based on the information provided by previous points. At the initial step, however, no previous information is available, hence, an initial Hessian must be provided. A true initial Hessian can be computed, at the same or at a lower level of theory than the geometry optimization. Another inexpensive option is to provide a model Hessian based on simple empirical procedures as initial guess. Among the models proposed in the literature, the most commonly used for geometry minimizations are the Schlegel,[31] Almlöf[32] and Lindh's[33] models. In the latter one, the original idea of the optimization algorithm was not only to compute the model Hessian at the initial step, but to recalculate it in every optimization step.

For the Hessian updating schemes, many formulas have been proposed for geometry optimizations. In the case of minimizations, the most widely used scheme is the one proposed by the mathematicians Broyden[34] Fletcher[35] Goldfarb[36] and Shanno[37] (known as the BFGS Hessian updating scheme) in 1970:

$$\mathbf{H}^{\mathrm{BFGS}} = \mathbf{H}^{(k)} + \frac{\Delta\mathbf{g} \cdot \Delta\mathbf{g}^t}{\Delta\mathbf{g}^t \cdot \boldsymbol{s}^k} - \frac{\mathbf{H}^{(k)} \cdot \boldsymbol{s}^k \cdot \left(\boldsymbol{s}^k\right)^t \cdot \mathbf{H}^{(k)}}{\left(\boldsymbol{s}^k\right)^t \cdot \mathbf{H}^{(k)} \cdot \boldsymbol{s}^k} \tag{2.43}$$

where $\mathbf{H}^{(k)}$ is the Hessian at the previous (or reference) geometry (old Hessian), $\Delta\mathbf{g}$ is the difference between the previous and current gradient and $\boldsymbol{s}^k$ is the step vector. The BFGS Hessian updating scheme is very popular for minimizations, since it tends to keep the Hessian positive definite (all its eigenvalues are positive), which is a requirement for minimizations. Negative Hessian eigenvalues can lead to uphill steps on the PES. When Newton-Raphson methods are combined with model Hessians and updating Hessian schemes, *i.e.* the true

Hessian is not computed, they are called Quasi-Newton (QN) or Quasi-Newton-Raphson methods.

Inversion and storage of the approximate Hessian matrix in standard QN methods is still somewhat problematic for large systems. The updating schemes may be reformulated so that the inverse of the Hessian is directly updated during the optimization.[27] The BFGS formula for updating the inverse Hessian becomes:

$$\mathbf{G}^{\mathrm{BFGS}} = \mathbf{G}^{(k)} + \frac{\boldsymbol{s}\cdot\boldsymbol{s}^{t}}{\boldsymbol{s}^{t}\cdot\Delta\mathbf{g}} - \frac{\mathbf{G}^{(k)}\cdot\Delta\mathbf{g}\cdot(\Delta\mathbf{g})^{t}\cdot\mathbf{G}^{(k)}}{(\Delta\mathbf{g})^{t}\cdot\mathbf{G}^{(k)}\cdot\Delta\mathbf{g}} \tag{2.44}$$

where $\mathbf{G}^{\mathrm{BFGS}}$ is the updated inverse Hessian matrix and $\mathbf{G}^{(k)}$ is the inverse Hessian at the previous (or reference) geometry (old inverse Hessian). To solve the storage inconvenient for large molecules, limited memory QN methods such as the so-called limited memory BFGS (L-BFGS) developed by Liu and Nocedal[38] can be used. The storage of the full old Hessian matrix (or its inverse) requires $(3N)^2$ 'memory positions' (assuming Cartesian coordinates), where N is the number of atoms in the molecule to be optimized. In the limited memory algorithms, instead of storing the full old inverse Hessian matrix $\mathbf{G}^{(k)}$ (in each iteration), a starting diagonal Hessian matrix, $\mathbf{G_0}^{(k)}$, which requires only $3N$ 'memory positions' is used, and it is updated using information from the $\Delta\mathbf{g}$ and the $\boldsymbol{s}$ of M previous steps (M is defined by the user; using $3 < M < 7$ is, in general, a good choice).

Although improvement on the convergence of geometry optimizations is achieved with the second-order family methods, it can be further improved. To accelerate convergence, reducing the number of iterations in optimizations (especially interesting for large molecules), methods such as the Direct Inversion in the Iterative Subspace (DIIS) can be used. This DIIS method developed by Pulay[39–41] initially conceived for wave function optimizations in the SCF iterative schemes, can be reformulated and used as well in geometry optimizations, under the name of GDIIS.[42] The idea behind this method is to build a new geometry as a linear combination of M previous geometries during the optimization, in order to find the best geometry in this M-dimensional iterative subspace. Each geometry obtained during the iterative optimization algorithm $\boldsymbol{q}_i$ can be expressed in terms of its deviation $\boldsymbol{e}_i$ with respect to the 'optimal' solution $\boldsymbol{q}^{k+1}$ as:

$$\boldsymbol{q}_i = \boldsymbol{q}^{new} + \boldsymbol{e}_i \tag{2.45}$$

Imposing the following two conditions:

$$\sum_i^M c_i \boldsymbol{e}_i = 0 \text{ and } \sum_i^M c_i = 1 \tag{2.46}$$

the relation:

$$\sum_i^M c_i \boldsymbol{q}_i = \boldsymbol{q}^{new} \tag{2.47}$$

is satisfied. Indeed, eq. (2.47) represents the new geometry expressed as a linear combination of M previous geometries, where c_i are the scalar coefficients of each geometry. The error vectors are not known, but if an energy quadratic function $E(\boldsymbol{q})$ is assumed, the error can be approximated as:

$$\boldsymbol{e}_i = -\left(\mathbf{H}_i\right)^{-1} \mathbf{g}_i \tag{2.48}$$

which is, in fact, the NR step vector. Defining a residual vector as $\boldsymbol{r} = \sum_i^M c_i \boldsymbol{e}_i$ and minimizing $|\boldsymbol{r}|^2$ reduces the problem to a minimization in a least-square sense. Minimizing with respect to c_i, *i.e.* setting the gradient to zero ($\frac{\partial}{\partial c_i}\left(|\boldsymbol{r}|^2\right) = 0$) with the constraint $\sum_i^M c_i = 1$ leads to the following set of equations:

$$\begin{pmatrix} B_{11} & \cdots & B_{1M} & 1 \\ \vdots & \ddots & \vdots & \vdots \\ B_{M1} & \cdots & B_{MM} & 1 \\ 1 & \cdots & 1 & 0 \end{pmatrix} \begin{pmatrix} c_1 \\ \vdots \\ c_M \\ \lambda \end{pmatrix} = \begin{pmatrix} 0 \\ \vdots \\ 0 \\ 1 \end{pmatrix} \tag{2.49}$$

where B_{ij} are the dot products of the error vectors $B_{ij} = (\boldsymbol{e}_i)^t \cdot (\boldsymbol{e}_j)$ and λ is the Lagrangian multiplier issue of the constraint imposed to the optimization. Of course, if a linear dependency exits between geometries $\boldsymbol{q}_i$, eq. (2.49) is ill-conditioned and alternative strategies should be taken such as omitting the error vectors with the largest norm. The coefficients obtained by solving eq. (2.49) are used to calculate the new geometry $\boldsymbol{q}^{new}$, eq. (2.47) and the new gradient $\mathbf{g}^{new}$, eq. (2.50) as well.

$$\mathbf{g}^{new} = \sum_i^M c_i \mathbf{g}\left(\boldsymbol{q}_i\right) \tag{2.50}$$

Note that the gradient computed with the coefficients c_i is not explicitly evaluated for the new geometry. A new step in the geometry optimization is taken $\boldsymbol{q}^{k+1}$ by subtracting to the geometry computed with the coefficients $\boldsymbol{q}^{\text{new}}$ a NR step computed as the 'new gradient' $\mathbf{g}^{new}$

by the inverse of the approximate Hessian which can be held constant or it can be updated, eq. (2.51).

$$\boldsymbol{q}^{k+1} = \boldsymbol{q}^{new} - (\mathbf{H})^{-1}\mathbf{g}^{new} \qquad (2.51)$$

Over the years, different modifications have been suggested to enhanced the control and stability of the GDIIS method such as the ones proposed in ref. [43]. A major modification known as the geometry optimization using the Energy-Represented Direct Inversion in the Iterative Subspace (GEDIIS)[44] uses the coefficients c_i to minimize an energy function instead of the NR step as in the standard GDIIS. In practice, the main difference between the GEDIIS and GDIIS methods resides in the definition of the B_{ij} matrix elements of eq. (2.49). The GEDIIS method uses $B_{ij} = (\mathbf{g}_i - \mathbf{g}_j) \cdot (\boldsymbol{q}_i - \boldsymbol{q}_j)$, instead of $B_{ij} = (\boldsymbol{e}_i)^t \cdot (\boldsymbol{e}_j)$ as in the GDIIS method.

In present days, geometry optimizations use sophisticated modifications and combinations of the methods mentioned before. Some optimization strategies go a step further switching optimization schemes during the calculation, depending on the predefined thresholds, e.g. when the root-mean-square (RMS) force of the latest point is smaller than the predefined threshold the algorithm switches to a different optimization scheme. This hybrid approach of switching methods during the geometry optimization can take advantage of the better performance of each method shown in different stages of the optimization. Here is presented the particular case of the optimization of the triplet isomer ^{3}**GS** of the *trans*-$[RuCl(NO)(py)_4]^{2+}$ complex (Figure 2.1) performed during this PhD. This is an example of a geometry optimization using a hybrid approach which combines the RFO, GDIIS and GEDIIS methods.

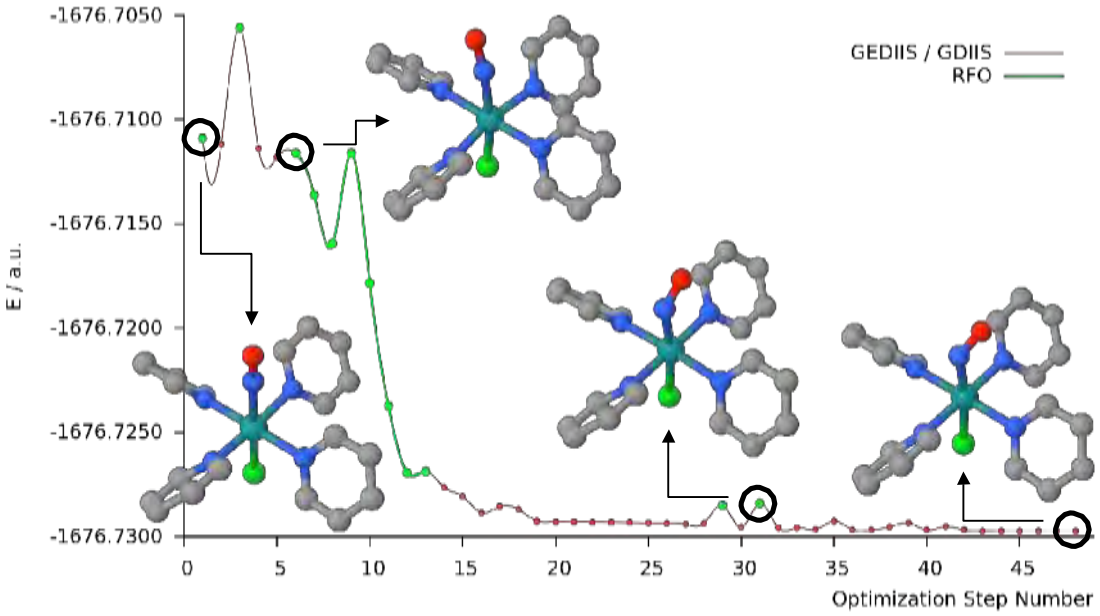

Figure 2.1: Geometry optimization of the ^{3}GS triplet isomer of the *trans*-[RuCl(NO)(py)$_4$]$^{2+}$ complex (last circled point on the right), starting from the GS isomer on the singlet ground state (first circled point on the left and first geometry shown in the picture). Optimization performed at the B3LYP/6-31G*(H, C, N, O)/6-31+G*(Cl)/ LANL2DZ(Ru) level of theory in vacuum. Steps taken with the RFO optimization algorithm are represented in green, whereas steps taken with a DIIS-based optimization method (GEDIIS / GDIIS) are represented in red.

The calculation shown in Figure 2.1 illustrates perfectly well the switching nature of the hybrid geometry optimization methodology. Obviously, the initial step in this hybrid approach needs to be a RFO step, since no 'iterative space' is yet available, *i.e.* no other previous geometry has been generated to build a new one by linear combination. Ideally, the optimization keeps doing RFO steps until the RMS force is smaller than 10^{-3} a.u. avoiding, at the beginning of the optimization, getting trapped in a possible undesired shallow potential well.[44] In the example shown, the optimization switches already at the second step to the GEDIIS algorithm. This 'sudden' switch can be explained looking at the RMS force during the optimization (Figure 2.2). Indeed, the RMS force at the second (and even at the first) geometry is lower than the established threshold equal to 10^{-3} a.u. thus, the algorithm switches to the GEDIIS method. Then, the algorithm keeps going back and forth switching between methods, until the optimization takes the molecular geometry into a region of the PES where the RMS force is larger than the threshold and several plain RFO steps are taken. As it can be seen in Figure 2.1, the RFO method takes down the energy very rapidly in only few steps. Once the RMS force is lower than the threshold the GEDIIS algorithm takes over, until a well-behaved quadratic region is reached (when the RMS step is lower than $2.5 \cdot 10^{-3}$ a.u.) and the GDIIS continues the optimization until convergence. In the example given, the GDIIS is switched on in the last three steps, taking advantage of its fast convergence near the minimum.

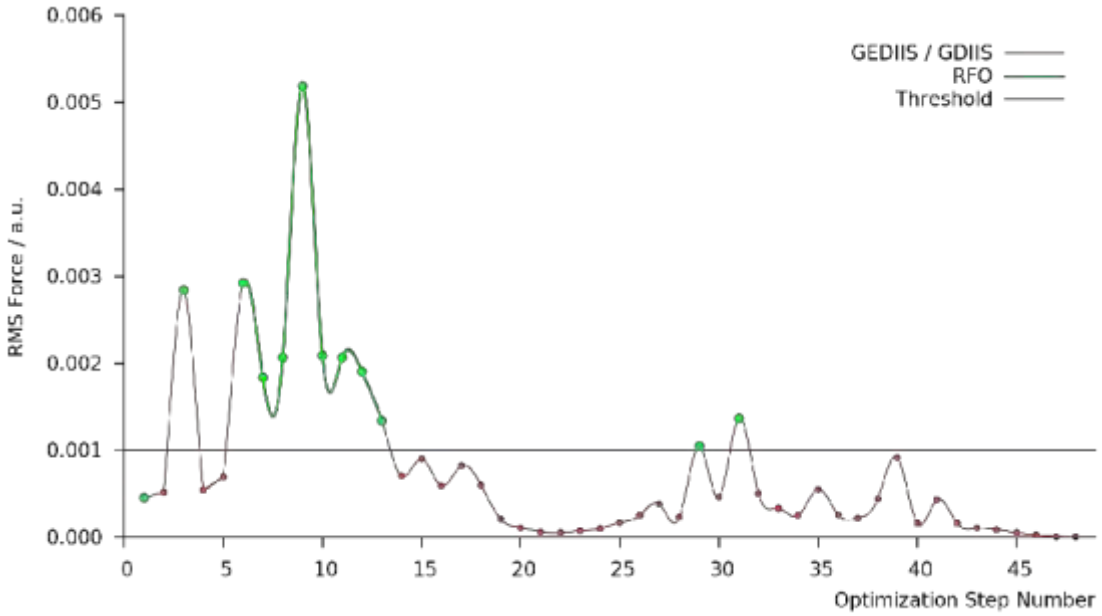

Figure 2.2: RMS force during the geometry optimization of the ^{3}GS triplet isomer of the *trans*-$[RuCl(NO)(py)_4]^{2+}$ complex. The same optimization represented in Figure 2.1 with RFO steps in green and GEDIIS / GDIIS steps in red. The blue line represents the RMS force threshold which is the criteria in the optimization algorithm to switch between methods.

In general, geometry optimizations using this hybrid approach begin with the RFO method, taking few steps depending on the case and the initial guess (in a standard optimization between three and eight initial steps). Then, the algorithm takes over with DIIS-based optimization methods, in the region of the PES where the RMS force is lower than the threshold. The example chosen is particularly interesting, since the algorithm only takes the initial step with the RFO method and switches to the GEDIIS optimization already at the second step. This may indicate that the optimization has started near a local minimum because of the low RMS force value. Further discussion of this particular case is outside the scope of this section and will be addressed in Chapter III. In some cases, geometry optimizations using GEDIIS may present small 'bumps' where the energy suddenly rises (steps 29 and 31 in Figure 2.1 and Figure 2.2). In these steps, the RMS force is generally over the threshold and thus, the optimization 'path' is corrected with one or several plain RFO steps, depending on the situation.

Summarizing, for geometry optimizations the best approaches are those using first and second order derivatives (second-order methods). The efficiency of these methods depends on the choice of the Hessian (exact or updated), the control of the step size and the maximum step allowed during the optimization (TRM, RFO) and even on the choice of coordinates used during the optimization (this matter has not been addressed in this section). In general, combinations of different methodologies[26,45] or even hybrid approaches where the algorithm

switches between different methods during the optimization yield the best optimization efficiencies. In the case of complicated geometry minimizations, the steepest descent can always be used as a last resort; despite of its slow convergence, by its intrinsic nature, it always takes down the molecular geometry towards the nearest local minimum.

b) Generating a Good Educated Guess for the TS Optimization

In the classical approach to the exploration of a PES in the quest of finding the pertinent MEP which connects two minima, the search of the TS characterizing this path is essential to have a full description of the reaction mechanism. In order to find the TS which connects two specific minima on a surface, a good starting geometry needs to be supplied for the optimization. While geometry minimizations can become routine calculations, being quite easily converged to the expected minima, optimizations of TSs are much more complicated, not only in algorithm terms, but also from a practical point of view; *i.e.* a precise transition state is much more difficult to find than a minima on a PES. This is one of the main reasons why a good initial guess for the TS optimization becomes imperative in the search for the right MEP connecting two minima.

Several approaches exist in order to generate the starting geometry to optimize a TS. This initial geometry should be already near the quadratic region of the transition structure. In some cases, this is easy to achieve by using the chemical intuition; a very good starting geometry can be created such as the ammoniac planar geometry of the transition state connecting the two identical conformers (Figure 2.3).

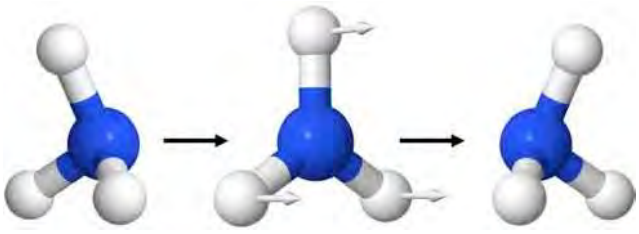

Figure 2.3: Ammoniac planar transition state (geometry in the middle) connecting two spatial conformations. Arrows in the TS structure represent the normal vibrational mode corresponding to the negative eigenvalue of the mass-weighted Hessian matrix (see §2.2.1d).

In the general case of bigger molecules, chemical knowledge may still prove to be quite useful. For example, bonds that are broken or made during a reaction such as bimolecular nucleophilic substitutions (S_N2) can be elongated ca. 50% for the initial guess of the TS structure (Figure 2.4). Another example is the Hammond's postulate[46] which in some cases

may be quite useful in order to estimate the position of the transition state along the reaction path. Hammond's postulate implies that for endothermic reactions the TS should be more similar to the products, and in the case of exothermic reactions should be more similar to the reactants.

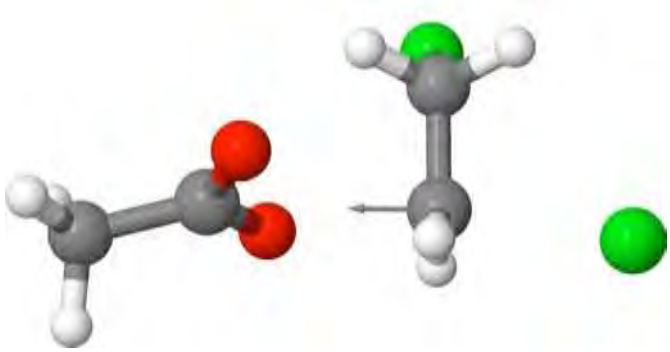

Figure 2.4: Optimized TS structure of the S_N2 attack of acetate to 1,2-dichloroethane. Bond distance between the electrophilic carbon and the chloride (breaking bond) are elongated (2.35 Å) with respect to the bond distance in the minimum geometry (*ca*. 1.80 Å). Distance between the oxygen and the electrophilic carbon that are forming a new bond is also elongated (2.09 Å) with respect to the final product (*ca*. 1.40 Å). The arrow represent the normal vibrational mode corresponding to the negative eigenvalue of the mass-weighted Hessian matrix (see §3.1.1c).

Unfortunately, in some cases simple chemical rules are not sufficient to build a suitable guess structure for the TS optimization and a deeper knowledge of the system and more information about the PES are required. In these cases, a rigid or relaxed surface scan may be performed. In these surface scans, one of the coordinates is progressively changed along the path from reactants to products, while the others are frozen (single points along the rigid scan) or optimized (in a relaxed scan). In complex cases, two or more coordinates are required to be scanned to gain some insight about the topology of the PES. When there is little or no knowledge at all about the pertinent coordinates which need to be modified, or simply the *N*-dimensional scan required in the search of a suitable TS is too expensive, a linear interpolation can always be done as a last resort.

At this point, it is important to highlight the crucial role of the complete set of coordinates chosen to describe a system. The most common set of coordinates routinely used by computational chemists are the well-known Cartesian coordinates, where the three spatial coordinates of the *N* atoms are completely defined, making the visualization of molecular structures straightforward with atoms completely defined as points in the tridimensional space. Internal coordinates are very common and used in daily tasks as well. Although computational chemists are quite familiar with this set of coordinates, they are anything but simple. This set of coordinates, less intuitive from a visualization point of view, consists on a

matrix containing ($N-1$) interatomic distances, ($N-2$) valence angles, and ($N-3$) dihedral angles, with a total of $3N-6$ variables for a complete set of internal coordinates describing a non-linear molecule. At first glimpse, from a mathematical point of view, internal coordinates seem to be a normal set of independent spherical polar coordinates defined with one distance (the radius) and two angles (the polar and the azimuthal angles), but they are not so. The main difference between spherical coordinates and internal coordinates is that the latter ones do not share the same origin (the center of a sphere) as it is the case of normal spherical coordinates. As a consequence of not sharing the same origin, strong linear dependencies are created between the internal coordinates, since each atom has as origin a previously defined atom which depends, at the same time, on the position of another atom. Transformation from Cartesian to internal coordinates is 'straight forward' (being careful with the valence angles of 0° and 180°). On the contrary, internal-to-Cartesian back transformation is not that simple. Since the beginning of computational chemistry, many methods to perform this transformation have been developed, and it is of such importance, that still new methods have been developed over the past few years.[47,48]

For linear interpolations, internal coordinates present many advantages over Cartesian coordinates. Internal coordinates are more 'natural' or 'chemical', since they are more descriptive of the molecular geometry with the bond lengths, valence angles and dihedrals as variables. It comes as no surprise that geometry optimizations with internal coordinates results in more efficient and reliable calculations than optimizations with plain rectilinear Cartesian coordinates (though of course it is well known that redundant internal coordinates[26] yield more efficient geometry optimizations). It is the same case for interpolations between two different conformations of a molecular system. A well-known problem of Cartesian coordinates is its poor performance for representing curvilinear motions such as valence angle bending or rotations about single bonds. The reason is quite simple, in a Cartesian linear interpolation the position of each atom is modified independently from the rest of the atoms following a straight line in space. If a rotation of an angle is involved in the geometrical change between molecular conformations, it might happen that atoms become unphysically close to one another. In order to illustrate this phenomenon, two different interpolation methods are shown in Figure 2.5 and compared with the Cartesian interpolation, using as an example the same particular case of the triplet isomer ^{3}**GS** of the *trans*-$[RuCl(NO)(py)_4]^{2+}$ complex used in the previous section.

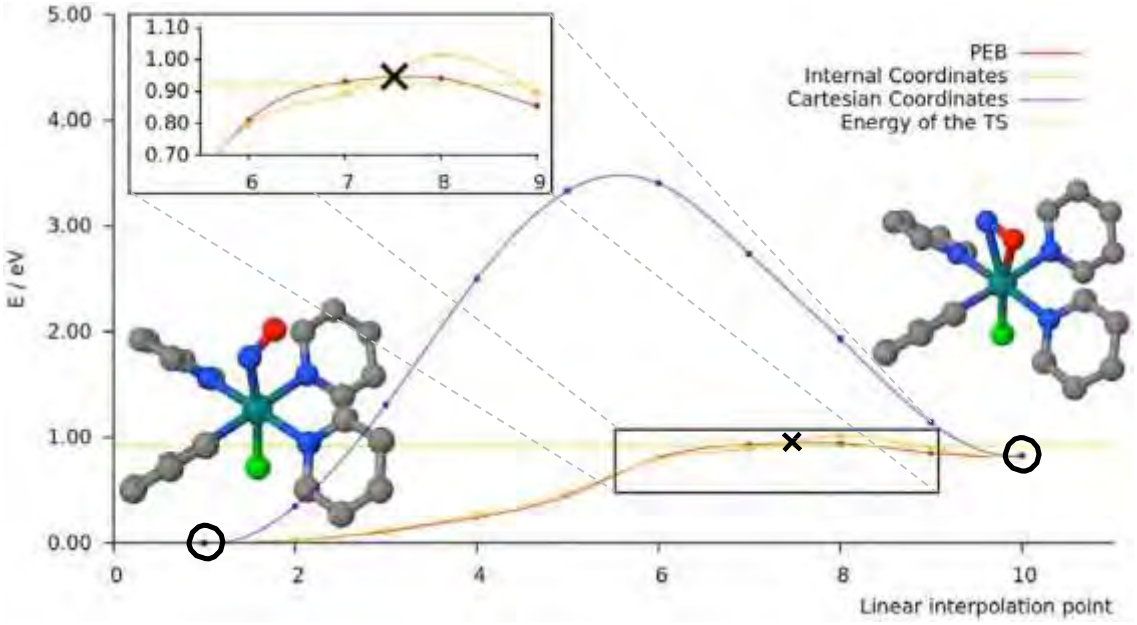

Figure 2.5: Educated-guess for the transition state search (black cross between the seventh and eighth interpolated points). Linear interpolation between ^{3}GS and ^{3}MS2 of the *trans*-$[RuCl(NO)(py)_4]^{2+}$ complex at the B3LYP/6-31G*(H, C, N, O)/6-31+G*(Cl)/ LANL2DZ(Ru) level of theory in vacuum. PEB: Plain Elastic Band interpolation methodology.

Continuing with the example of the previous section, the MEP connecting the optimized triplet **^{3}GS** isomer and another triplet isomer found in the lowest triplet PES, namely **^{3}MS2** will be optimized. In order to do so, the transition state connecting both minima needs to be found and optimized. Taking a closer look to the relative energies of both isomers, it can be said that the reaction is endothermic in the **^{3}GS** ▾▾ **^{3}MS2** direction. Thus, the TS connecting both isomers should be more similar to **^{3}MS2** than to **^{3}GS**, according to the Hammond's postulate. In order to find a good approximation of the molecular geometry of the TS, a linear interpolation is performed between **^{3}GS** (with a Ru−N−O valence angle of 133.6°) and **^{3}MS2** (with a Ru−N−O valence angle of 71.7°) Figure 2.5. This is a perfect example for illustrating the pathological behavior of Cartesian interpolations, since the rotation of the nitrosyl ligand generates unphysical bond lengths between the nitrogen and the oxygen, namely in the points five and six of the linear Cartesian interpolation (see Figure 2.5) the N−O distances are equal to 0.97 and 0.98 Å respectively.

Although internal coordinates outperform Cartesian coordinates in linear interpolations, they present a major drawback. There are many possible combinations to build a matrix of internal coordinates, and unfortunately depending on the interpolating problem, not all of them are suitable to perform the interpolation. For example, in the initial geometry a dihedral angle between four atoms is defined, the first three atoms of this definition form a

valence angle of 90° which is perfectly fine. However, in the final geometry the very same three atoms form a valence angle of 180° and then the dihedral angle defined in the initial geometry cannot be defined in the final geometry. This is just an example of many other problems that can be encountered when using internal coordinates for linear interpolations. Some of these problems are directly link to the fact that internal coordinates present linear dependencies and because of this fact, some combinations of internal coordinates may be better than others, depending on the atoms that take part in the molecular rearrangement.

A good knowledge of the molecular system and special attention with the changing signs of the dihedral angle definitions might be enough to generate a suitable internal coordinates matrix for the interpolation in few minutes. However, some difficult cases prove to be quite challenging and require many hours until a good internal coordinate matrix is found. Another problem is that automatizing this task is not simple, thus human interaction is required. If only a few interpolations are needed this might be acceptable, but if an important research project requires comparison of hundreds of species this might become a problem. That's the reason why another system of coordinates in which the interpolating procedure could be fully automatized is required. This can be achieved for example doing an interpolation with the matrix of distances, which contains much more variables than molecular degrees of freedom, $N(N-1)/2$ *vs*. $3N-6$. One of the main problems with this kind of procedures is that the information about the atomic coordinates is 'lost'. In order to recover the atomic coordinates, an objective function for each point of the interpolation can be defined. This objective function contains all the atom pair distances and it can be minimized in a least square sense with respect to the atomic coordinates.[49] This procedure may sometimes cause uniform translation of the different interpolated points, losing the continuity of the path. Recently, in 2014 a very original methodology to carry out these linear interpolations was proposed by Hannes Jónsson and co-workers.[50] In this procedure they use a simplified version of the objective function proposed in the original work, and in order to optimize the whole interpolated path, they use the Nudged Elastic Band (NEB) procedure to do it. Based on the work of Jónsson and co-workers, several definitions of the NEB algorithm have been tested. Finally, it has been shown by several test molecules of this PhD project and a small peptide, that a modified version of their proposed algorithm performs better using a Plain Elastic Band instead of the Nudged Elastic Band algorithm proposed in the original work. As it can be seen in Figure 2.5, the PEB methodology to generate an interpolated path yields very smooth results and it can be used to create the initial guess for the subsequent TS optimization (marked as a black cross in Figure

2.5). This PEB methodology presents the great advantage over the classical interpolation in internal coordinates of being a 100% automatized procedure that requires no human interaction (no previous preparation of the input to generate the interpolated path). This PEB interpolating procedure can be used as a starting point in full NEB optimizations as well.

c) TS optimization

For the transition state optimizations special attention needs to be taken. As explain in the previous section, a good educated guess needs to be given as a starting point, but this is not the only requirement, special algorithms designed specifically for this purpose are needed. For instance, one popular method called the eigenvector following (EF) consists on following the eigenvector corresponding to the lowest eigenvalue of the Hessian matrix until a stationary point is reached. The algorithm is a modified version of the trust radius Newton method where the level-shift parameter λ is chosen so that it is lower than the second lowest eigenvalue of the Hessian matrix $\mathbf{H}^{(k)}$, but greater than the lowest eigenvalue, *i.e.* $\tilde{H}^{(k)}_{n-1} > \lambda > \tilde{}^{(k)}_{n}$. Doing so, the optimization is minimizing the geometry in all coordinates but one (the one corresponding to the negative Hessian eigenvalue) where a maximum will be reached. Other much more sophisticated techniques exist, but are not presented in this manuscript. However, it is important to be aware that standard optimizations of TSs are not an easy task.

d) Characterization of the Stationary Points Optimized: Frequency Calculations

The vibrational Infra-Red (IR) spectrum is systematically computed after any minima or TS geometry optimization of a molecular system so that the nature of the stationary point found can be determined. These routine verifications are called frequency calculations because the frequencies of the vibrational normal modes of the molecule are computed (the vibrational IR spectrum is computed). The trick to perform such a calculation is to transform the potential and kinetic energy operators from Cartesian displacements to the so-called 'normal coordinates', doing so the Hamiltonian is re-written as a sum of independent harmonic oscillators.

Considering an equilibrium geometry of a molecular structure with *N* atoms, a Cartesian displacement coordinate system can be defined as $\Delta x_i \equiv \xi_{i1}$, $\Delta y_i \equiv \xi_{i2}$, $\Delta z_i \equiv \xi_{i3}$, where *i* represents the index for the atoms, and *x*, *y*, *z*, *i.e.* its Cartesian coordinates. The kinetic operator in this coordinate system is (in atomic units):

$$\hat{T} = -\frac{1}{2}\sum_{i}^{N}\frac{1}{m_i}\left(\sum_{j}^{3}\frac{\partial^2}{\partial\xi_{ij}^2}\right) \tag{2.52}$$

The explicit dependence on the atomic masses, m_i, can be removed by transforming the Cartesian displacement coordinate system into the mass-weighted Cartesian displacement coordinate system defined as:

$$q_1 \equiv \sqrt{m_1}\xi_{11},\ q_2 \equiv \sqrt{m_1}\xi_{12},\ q_3 \equiv \sqrt{m_1}\xi_{13},\ q_4 \equiv \sqrt{m_2}\xi_{21},\ \ldots\ q_{3N} \equiv \sqrt{m_N}\xi_{N3} \tag{2.53}$$

Hence, the kinetic operator becomes:

$$\hat{T} = -\frac{1}{2}\sum_{i}^{3N}\frac{\partial^2}{\partial q_i^2} \tag{2.54}$$

In order to represent analytically the potential energy operator, $\hat{V}$, for all the values of $\{q_i\}$ it would be necessary to construct the complete potential energy hypersurface, *i.e.* solving the electronic Schrödinger equation for all possible nuclear configurations. Limiting the analysis to small displacements around the equilibrium geometry, the potential energy operator can be approximated using a Taylor expansion as follows:

$$\hat{V} = V_{eq} + \sum_{i}^{3N}\left(\frac{\partial}{\partial q_i}\right)_{eq} q_i + \frac{1}{2}\sum_{i,j}^{3N}\left(\frac{\partial^2 V}{\partial q_i q_j}\right)_{eq} q_i q_j + \ldots \tag{2.55}$$

The first derivate is equal to zero, since the equilibrium geometry by definition is a stationary point in the potential energy hypersurface. Truncating the Taylor expansion in the quadratic term, assuming that terms beyond are negligible, and eliminating the first term by redefining the zero energy, the potential becomes:

$$\hat{V} = \frac{1}{2}\sum_{i,j}^{3N}\left(\frac{\partial^2 V}{\partial q_i q_j}\right)_{eq} q_i q_j = \frac{1}{2}\sum_{i,j}^{3N} F_{ij} q_i q_j \tag{2.56}$$

where the matrix of second-derivates, F_{ij}, is known as the mass-weighted Hessian matrix. Diagonalizing this Hessian matrix:

$$\boldsymbol{F}\,\boldsymbol{L} = \boldsymbol{L}\,\Lambda \tag{2.57}$$

the diagonal matrix Λ containing the eigenvalues (λ_i) of $\boldsymbol{F}$ is obtained. The columns of the transformation matrix $\boldsymbol{L}$ ($\boldsymbol{L}_j$) are the eigenvectors of $\boldsymbol{F}$. This diagonalization is an unitary transformation which introduces a new system of coordinates Q_k known as the 'normal'

coordinate system, which can be expressed as a function of the old coordinates using the matrix transformation ***L***, as follows:

$$Q_k \equiv \sum_i^{3N} L_{ik} q_i \tag{2.58}$$

In the new normal coordinate system, Q_k, the kinetic operator is still diagonal and the vibrational Schrödinger equation becomes:

$$\left[-\frac{1}{2} \sum_i^{3N} \frac{\partial^2}{\partial Q_i^2} + \frac{1}{2} \sum_i^{3N} \lambda_i Q_i^2 \right] \Psi_{nuc} = E_{nuc} \Psi_{nuc} \tag{2.59}$$

$$\left[\sum_i^{3N} \left(-\frac{1}{2} \frac{\partial^2}{\partial Q_i^2} + \frac{1}{2} \lambda_i Q_i^2 \right) \right] \Psi_{nuc} = E_{nuc} \Psi_{nuc} \tag{2.60}$$

$$\left[\sum_i^{3N} \hat{H}_i (Q_i) \right] \Psi_{nuc} = E_{nuc} \Psi_{nuc} \tag{2.61}$$

where the Hamiltonian have the form of a sum of independent harmonic oscillators. The 3*N*-dimensional Schrödinger equation problem is transformed into 3*N* mono-dimensional Schrödinger equations for the harmonic oscillator, with the solutions being the Hermite polynomials in the normal coordinate system Q_k. The second term in the Hamiltonian of equation 2.59 corresponds to the potential energy of a harmonic oscillator in normal coordinates, ½ $\omega^2 Q^2$, thus the eigenvalues of the mass-weighted Hessian matrix F_{ij} are by analogy, the square of the angular frequencies of each oscillator, *i.e.* $\lambda = \omega^2 = 4\pi^2 \nu^2$, where ν is the frequency characterizing each vibrational normal mode,

$$\nu_i = \frac{1}{2\pi} \sqrt{\lambda_i} \tag{2.62}$$

At the same time, the eigenvectors of F_{ij} , (L_j), are the vibrational normal modes in mass-weighted coordinates. It can be shown that six eigenvalues equal to zero should exist[51] (five for linear molecules). These eigenvalues correspond to the rotational and translational modes, remaining 3*N* – 6 vibrational modes (3*N* – 5 for linear molecules) with an oscillator frequency different from zero. In practice, due to the finite precision of the numerical operations, the eigenvalues for the translations and rotations are never exactly zero. The translational modes, in general show 'frequencies' very close to zero, however, the rotational modes can be problematic, with 'frequencies' that could go up to 50 cm^{-1}. If there are vibrational frequencies of the same magnitude, they can mix resulting in inaccurate values. To avoid this problem, the

rotational and translational modes are routinely removed by projection from the mass-weighted Hessian matrix, F_{ij}, before diagonalization. By eliminating the translations and rotations, equation 2.59 becomes:

$$\left[-\frac{1}{2}\sum_{i}^{3N-6}\frac{\partial^2}{\partial Q_i^2}+\frac{1}{2}\sum_{i}^{3N-6}\lambda_i Q_i^2\right]\Psi_{vib}=E_{vib}\Psi_{vib} \tag{2.63}$$

In any regular geometry optimization a stationary point is found in the potential energy surface of interest, having by mathematical definition a gradient equal to zero. At the same time, the eigenvalues of the Hessian matrix (second derivatives matrix) define the nature of the stationary point as follows:

$$\begin{aligned} &\text{if } \lambda_i > 0, \text{ then is a minimum in that vibrational normal mode } Q_i \\ &\text{if } \lambda_i < 0, \text{ then is a maximum in that vibrational normal mode } Q_i \end{aligned} \tag{2.64}$$

thus, if all the eigenvalues are positives, the stationary point corresponds to a minimum, but if all the eigenvalues are positive with the exception of one negative eigenvalue, the stationary point corresponds to a first order saddle point, *i.e.* a transition state in the potential energy surface (Figure 2.6). In a TS geometry, the energy is a maximum in one vibrational normal mode and a minimum in all other directions. The vibrational mode characterizing the TS (called the transition vector) corresponds to the local reaction coordinate, and it has an imaginary frequency, since it is equal to the square root of a negative number, eq. (2.62).

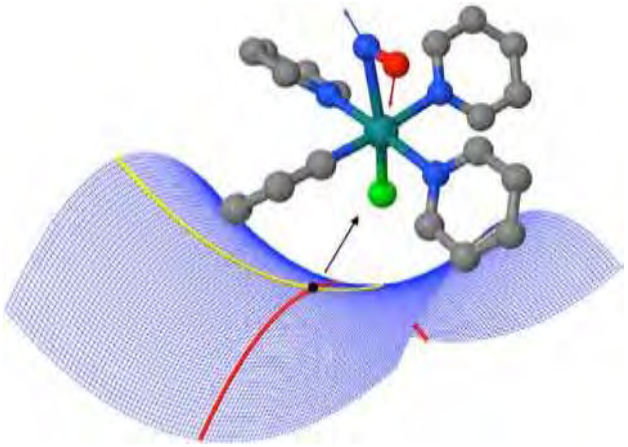

Figure 2.6: Transition state: $^{3}TS_{L}$ at the B3LYP/6-31G*(H, C, N, O)/6-31+G*(Cl)/ LANL2DZ(Ru) level of theory in vacuum. Arrows in the TS structure represent the normal vibrational mode corresponding to the negative eigenvalue of the mass-weighted Hessian matrix.

e) Minimum Energy Path Calculations: Intrinsic Reaction Coordinate vs. Steepest Descent

The PES describing chemical reactions are characterized by the stationary points, equilibrium geometries, corresponding to the minima, reactants, intermediates and products of the reaction, and first order saddle points corresponding to the TS structures. When a TS has been optimized, the connection between the corresponding minima needs to be verified. The imaginary frequency characterising a TS computed by a vibrational normal mode analysis corresponds to the reaction coordinate. Following the normal vibrational mode that corresponds to the negative eigenvalue of the mass-weighted Hessian matrix, the adiabatic reaction path through the PES can be optimized, freezing the normal mode followed and optimizing the rest of the coordinates. This type of calculations is known as Intrinsic Reaction Coordinate (IRC) optimization and is particularly expensive since each point of the path is optimized. Starting from the optimized TS structure, both directions of the MEP towards the products and the reactants are optimized, Figure 2.7.

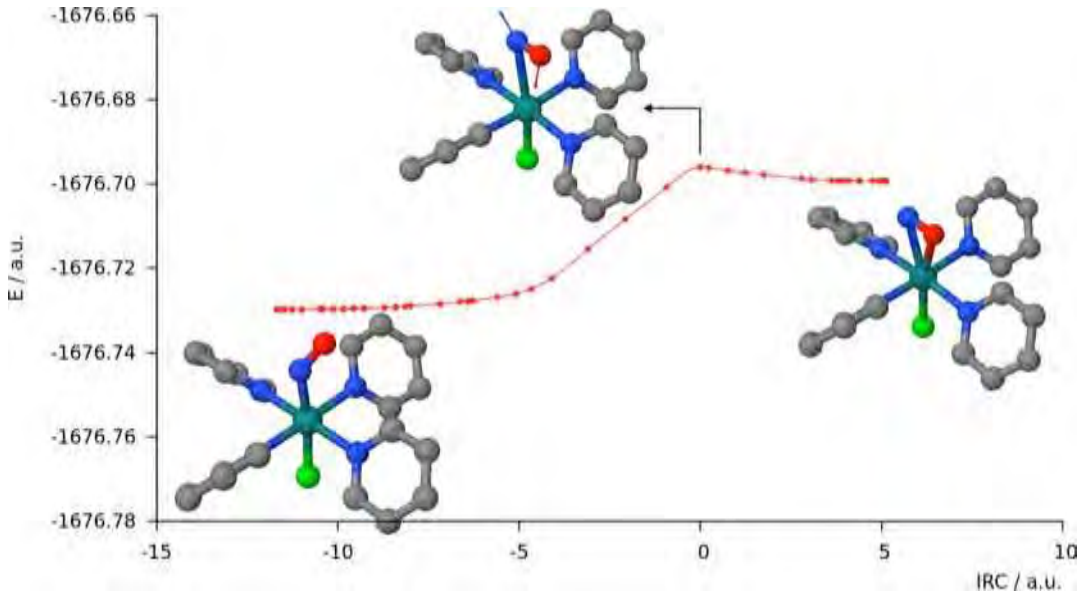

Figure 2.7: Intrinsic Reaction Coordinate (IRC) for the $^3TS_1$ at the B3LYP/6-31G*(H, C, N, O)/6-31+G*(Cl)/ LANL2DZ(Ru) level of theory in vacuum. The energy is represented as a function of the intrinsic reaction coordinate (zero set at the transition state, positive values corresponds to forward direction and negative values to reverse direction)

A computationally cheaper alternative to the expensive IRC calculations consists on performing steepest descent optimizations (eq. (2.28)) starting from a TS geometry deformed in the 'positive' and 'negative' directions along the transition vector. There are many examples in the literature which show that this procedure yields very similar profiles of the potential energy surfaces studied. If the computational electronic structure software employed in the calculation, uses a QN algorithm by default (see §2.2.1.a), a practical way of doing a steepest descent calculation, consists on giving an initial unit Hessian matrix, and ask the algorithm not to update it during the optimization. Doing so, the QN steps are equivalent to steepest descent steps.

2.2.2 Alternative Approach to the MEP Problem: The Nudged Elastic Band Method

In the characterization of PESs the location and optimization of minima is relatively easy. If commonly used methods like Newton-Raphson fail, a steepest descent algorithm always assures a lowering in the total energy of the system. By contrast, locating transition states is much more involved; it may require important human and computational efforts and there is no guarantee to find the right TS which connects the expected minima in the PES. An initial guess (starting geometry for the TS optimization) already close to the saddle point is required. In some cases, linear interpolations between minima may afford a good initial guess, however in problematic cases, this approach may not be good enough and, generating the

required initial guess may become quite difficult. Although TSs connecting a specific pair of minima in the hypersurface may not exist, it is essentially impossible to prove it.[24] On the other hand, not being able to find a TS does not mean that it does not exist. This is the reason why multi-structure interpolation methods need to be used when an energy barrier, or the minimum energy path, between two minima needs to be known whether a TS between them can be located or not.

In the early 90's, Daniel A. Liotard developed a multi-structure interpolation method for the semiempirical package AMPAC.[52] Few years later, Hannes Jónsson and his co-workers developed the so-called Nudged Elastic Band (NEB) method[53] which is another multi-structure interpolation method that became popular in the computation of MEPs using plane-wave based density functional theory. These methods use multiple (three or more) structures or images and are also known as *chain-of-states* methods. An initial distribution of images, typically a straight line between reactants and products, is optimized, relaxing the images and obtaining a good approximation of the 'true' reaction coordinate and also of the transition state molecular structure, if the number of images is large enough.

The target function defined in this method, f_{NEB}, consists on an 'elastic band' built up as the sum of energies of all images and a 'penalty' term which includes harmonic spring forces between adjacent images to distribute them along the pathway. The spring constants, k, can be the same to distribute the images evenly along the path, or they can be energy dependent in order to provide higher density of images in the higher energy regions, *i.e.* near the saddle point.

$$f_{NEB}\left(R_R, R_1, R_2, \ldots, R_M, R_P\right) = \sum_{i}^{M} E\left(R_i\right) + \frac{1}{2}\sum_{i}^{M-1} k_i \left(R_{i+1} - R_i\right)^2 \tag{2.65}$$

To understand the NEB method, it is necessary to explain the drawbacks of its predecessor method. The NEB method is based in the plain elastic band (PEB) method. The objective function to optimize is given by equation 2.66. The forces acting on each image of the string are defined as:

$$\vec{F}_i = -\vec{\nabla} V(\vec{R}_i) + \vec{F}_i^{\,s} \tag{2.66}$$

where

$$\vec{F}_i^{\,s} \equiv k_{i+1}(\vec{R}_{i+1} - \vec{R}_i) - k_i(\vec{R}_i - \vec{R}_{i-1}) \tag{2.67}$$

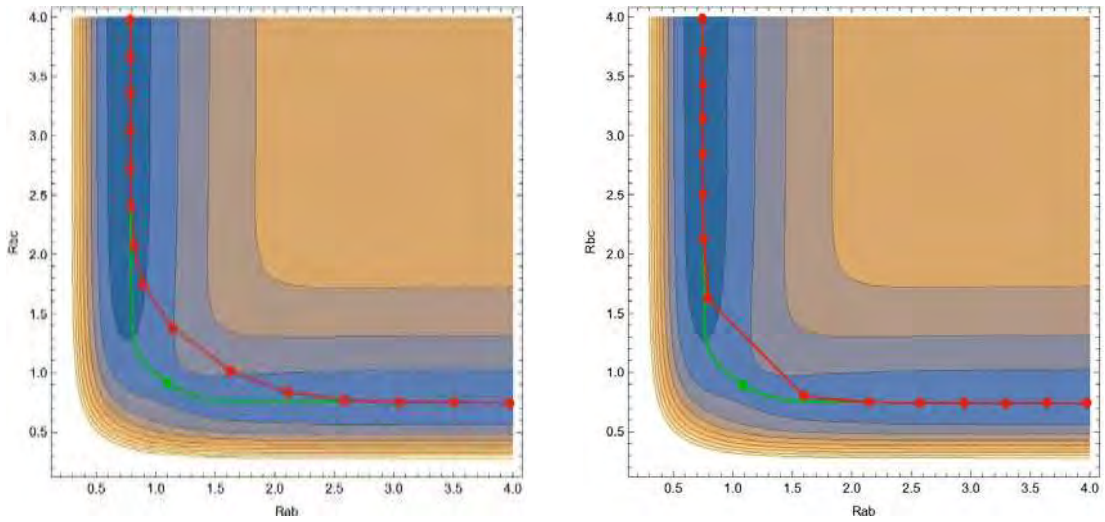

a) b)

Figure 2.8: Results of a calculation from a plain elastic band (PEB) a) with a spring constant equal for every image *k* = 1.0. It can be seen that the saddle point is missed, because the corner has been 'cut'. b) with a spring constant equal for every image *k* = 0.1. The cutting corner problem is partially solved, but the images slide down from the barrier region towards the minima. The red line represents the computed pathway, while the green line represents the optimized minimum energy path with the green dot being the position of the transition state (saddle point).

The 'corner-cutting' and 'down-sliding' problems that present the PEB method (Figure 2.8) can be easily solved by eliminating the true force component parallel to the path and the perpendicular component of the spring force, *i.e.* nudging the elastic band. With the component of the forces projected out, the force on image *i* then becomes:

$$\vec{F}_i^{\,0} = -\vec{\nabla} V(\vec{R}_i)\Big|_{\perp} + \vec{F}_i^{\,s} \cdot \hat{\tau}\Big\| \cdot \hat{\tau}\Big\| \tag{2.68}$$

where $\hat{\tau}\Big\|$ is the unit tangent to the path and $\vec{\nabla} V(\vec{R}_i)\Big|_{\perp} = \vec{\nabla} V(\vec{R}_i) - \vec{\nabla} V(\vec{R}_i) \cdot \hat{\tau}\Big\| \cdot \hat{\tau}\Big\|$.

It remains another problem in NEB calculations, the 'kinks' in the elastic band. To solve this problem a smooth switching function can be introduce. This function gradually turns on the perpendicular component of the spring force where the path becomes kinky. The force on image *i* then becomes:

$$\vec{F}_i^{\,NEB} = \vec{F}_i^{\,0} + f(\varphi_i)\left(\vec{F}_i^{\,s} - \vec{F}_i^{\,s} \cdot \hat{\tau}\Big\| \cdot \hat{\tau}\Big\|\right) \tag{2.69}$$

where $f(\varphi_i)$ is the switching function which goes from 0 to 1. For instance:

$$f(\varphi_i) = \frac{1}{2}\left(1 + \cos(\pi(\cos\varphi))\right) \tag{2.70}$$

where

$$\cos\varphi = \frac{(\vec{R}_{i+1} - \vec{R}_i)\cdot(\vec{R}_i - \vec{R}_{i-1})}{\left|\vec{R}_{i+1} - \vec{R}\right|_i \cdot \left|\vec{R}_i - \vec{R}_{i-1}\right|} \tag{2.71}$$

The Zero Temperature String (ZTS) method[54,55] is another important *chain-of-states* optimization method, quite similar to the NEB, which is also used to find the minimum energy paths. The ZTS method is not presented in the manuscript. Throughout the work of this PhD project both methods (NEB and ZTS) have been used. The production results presented in Chapter IV have been obtained with the ZTS method.

2.2.3 Minimum Energy Crossing Points

Within the hypothesis of non-adiabatic photoreactions, a detailed study of the crossing points between potential energy surfaces of different multiplicities becomes of crucial importance. When two hypersurfaces of different multiplicity cross each other, the ensemble of crossing points between them characterizes a hyperline (Figure 2.9). The point of this hyperline where the energy is minimal is known as the minimum energy crossing point (MECP).

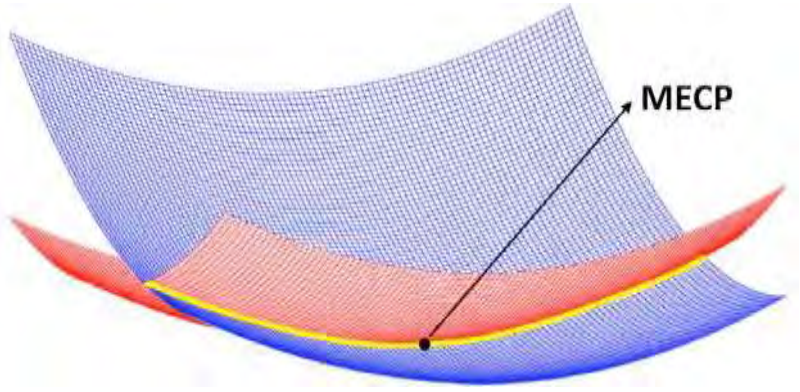

Figure 2.9: Hyperline (yellow line) defining an intersystem crossing between states of different spin multiplicity. In red a triplet state and in blue a singlet state. The minimum on the yellow line (black dot) represents the minimum energy crossing point (MECP).

Though MECPs may be very close in energy and in geometry to stationary points, it is important to highlight that a MECP is never a minimum or TS in any of the PESs involved. Thus, when the system is in a minimum of a PES, in order to cross to another PES through a MECP,

the system needs to overcome an energy activation barrier $\Delta E^{\ddagger}$. This activation barrier can be qualitatively characterized by the energy difference between the minimum equilibrium structure in the PES and the MECP (Figure 2.10).

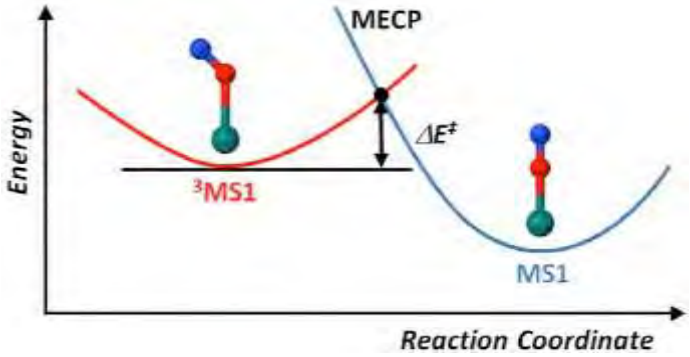

Figure 2.10: Schematic representation of a MECP in a non-adiabatic photoreaction coordinate. Non-adiabatic pathway from a triplet ^{3}MS1 (Ru−ON) linkage isomer (in red) to its correspondent singlet of lowest energy (in blue), with $\Delta E^{\ddagger}$ as activation barrier.

A MECP optimization is quite different from an optimization of a stationary point in a PES; due to the non-stationary nature of the MECPs another strategy needs to be adopted. In order to optimize MECPs two conditions must be fulfilled: minimization of the energy difference between the crossing surfaces $(E_1\text{-}E_2)^2$ and energy minimization of one of the PES. Thus, for MECP optimizations two different gradients are constructed.[56]

Defining the gradient difference vector, x_1, as:

$$x_1 = \left[\left(\frac{\partial E_1}{\partial q}\right) - \left(\frac{\partial E_2}{\partial q}\right)\right] \tag{2.72}$$

the two different gradients **f** and **g** used in the MECP optimization can be expressed as:

$$\mathbf{f} = \frac{\partial}{\partial q}(E_1 - E_2)^2 = 2(E_1 - E_2)\cdot x_1 \tag{2.73}$$

$$\mathbf{g} = \left(\frac{\partial E_1}{\partial q}\right) - \frac{x_1}{|x_1|}\left[\left(\frac{\partial E_1}{\partial q}\right)\cdot\frac{x_1}{|x_1|}\right] \tag{2.74}$$

where x_1 is orthogonal to the crossing hyperline near the MECP and **g** is orthogonal to x_1.

Finally, both gradients are summed up to afford the effective surface crossing gradient, $\mathbf{g}_{sc}$:

$$\mathbf{g}_{sc} = \mathbf{g} + \mathbf{f} \tag{2.75}$$

The final aim of a MECP optimization is to find the point of lowest energy within the crossing hyperline. This crossing hyperline is defined as a $3N - 7$ dimensional subspace of PES_1 which is orthogonal to x_1 (where N denotes the number of atoms).

2.3 Dispersion effects

A well-known problem in DFT is its difficulty to take into account weak interactions like the van der Waals (vdW) interactions also known as dispersion interactions. The main reason is that the electronic density ρ(r) is quite weak in those spatial regions where these dispersion interactions become important. Noble gases should present feeble attractive interactions between atomic dimers,[57,58] rather than purely repulsive potential energies that most density functionals predict. Few functionals show a correct behaviour for these interactions, but they tend to underestimate the differences between systems.[59] Moreover, taking as an example one of these functionals, namely TPSS, it only describes properly the short-range vdW interactions, not having the correct $1/R^6$ asymptotic behaviour in the long distance limit. It is possible to correct this by adding long-range empirical vdW interaction corrections. More generally, in order to take into account for the major part of these vdW contributions (short- and long-range) to the total energy it is possible to use a simple atom-pairwise correction, like in the family of the so-called DFT-D methods developed by Stefan Grimme. These dispersion correction methods have been used throughout this PhD thesis, in the DFT-D3[60] and DFT-D3(BJ)[61] formulations. Grimme's atom pair-wise dispersion correction scheme improves the results of standard density functionals at practically no extra cost. In this family of DFT-D methods the dispersion correction is added to the computed KS-DFT energy from a SCF calculation as follows:

$$E_{DFT-D} = E_{KS-DFT} + E_{disp} \tag{2.76}$$

where the dispersion correction E_{disp} can be computed as a sum of two- and three-body energies: $E_{disp} = E^{(2)} + E^{(3)}$. The most important (and only term used in the real calculations) is the two-body term which is given by the expression:

$$E^{(2)} = \sum_{A<B} \sum_{n=6,8,10,\ldots} s_n \cdot \frac{C_n^{AB}}{R_{AB}^n} \cdot f_{d,n}\left(R_{AB}\right) \tag{2.77}$$

where R_{AB}^{n} represents the internuclear distance between atoms A and B, C_{n}^{AB} is the *n*th-order dispersion coefficient (dependent on atoms A and B), s_n is an scaling factor (functional dependent) and $f_{d,n}(R_{AB})$ is the so-called damping function, which can have different expressions depending on the model. This damping function is needed to avoid near-singularities for small internuclear distances and also to avoid double-counting effects at intermediate distances.

2.4 Solvation Models

A lot of information can be extracted from an electronic structure calculation of a single molecule: its total potential energy, the molecular dipole moment, the electron density, and so on… Nevertheless, it has to be kept in mind that all these properties are computed in vacuum, *i.e.* the molecule is treated as an isolated system without any kind of external interaction. In some cases, the information extracted from these calculations may be enough to assist in the interpretation of experimental observations. In other cases, however, this information might not be sufficient to clarify the experiments and some interactions with the environment should be included in the theoretical model to understand the system's behaviour. For instance, if the reactivity of a molecule in solution is the problem of study, it is always better to include the solvent effects in the electronic structure calculations. Generally speaking, two main types of molecule-solvent interactions can be distinguished: a) short range interactions between the molecule (solute) and the solvent molecules within the first solvation sphere and b) the long range interactions between the molecule and the 'bulk' of the solvent. The former ones are essentially localised interactions (hydrogen bonds, supramolecular non-covalent interactions, dispersion interactions (vdW) …) which may considerably modify the electronic structure of the molecule. The long range interactions are related to the electrostatic interactions between a polar solvent and a charged or polar molecule. In comparison with the short range interactions, long range interactions may have a weak influence on the molecular electronic structure of the solute, still in many cases they prove to be of crucial importance in the modification of absorption properties of a molecule (Figure 2.11). Taking as an example one of the complexes studied throughout this PhD, the *cis*(Cl,Cl)-$[Ru(Cl)_2(NO)terpy]^+$ complex, it becomes evident the necessity to include the solvent effects in TD-DFT calculations in order to compute the absorption spectra.

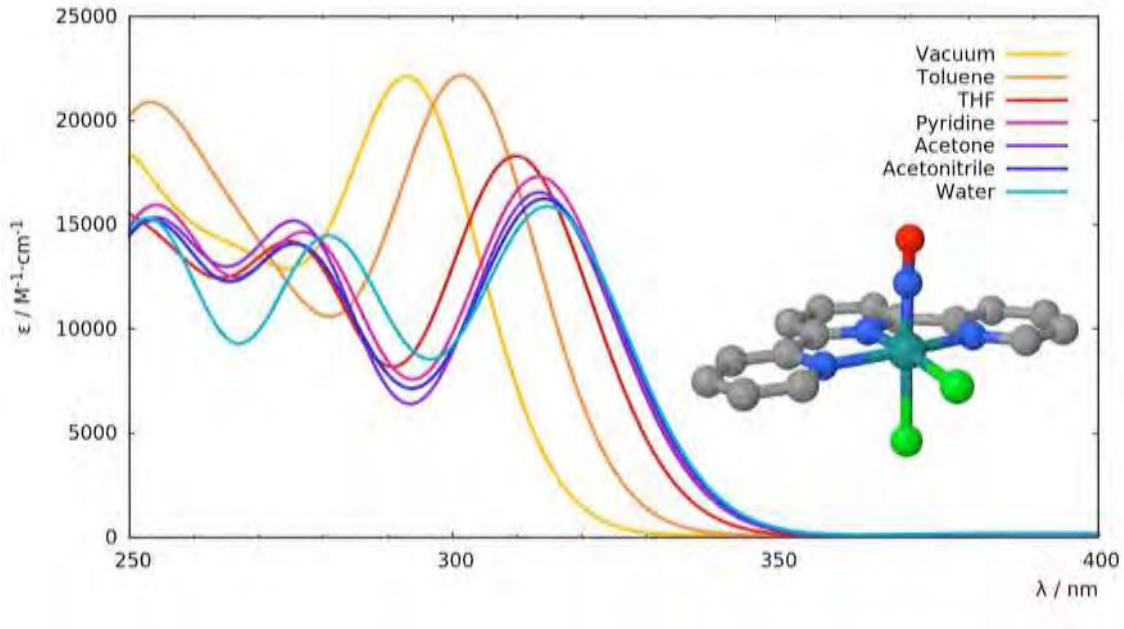

Figure 2.11: Theoretical example of TD-DFT absorption spectra of the *cis*-(Cl,Cl)[$RuCl_2$(NO)(terpy)]$^+$ complex using various solvents with different dielectric constants: toluene (orange; ε ≈ 2.4), THF (red; ε ≈ 7.25), pyridine (violet; ε ≈ 12.5), acetone (purple; ε ≈ 20.7), acetonitrile (blue; ε ≈ 36.6), water (cyan; ε ≈ 80.4). The TD-DFT absorption spectrum computed in vacuum is represented in yellow.

Another example of the importance of the solvent in the absorption properties is the so-called solvatochromism. Many examples can be found in the literature; Figure 2.12 illustrates the solvatochromism effect with an example of a Ru(II) complex which changes the color of the solution depending on the solvent used.[62]

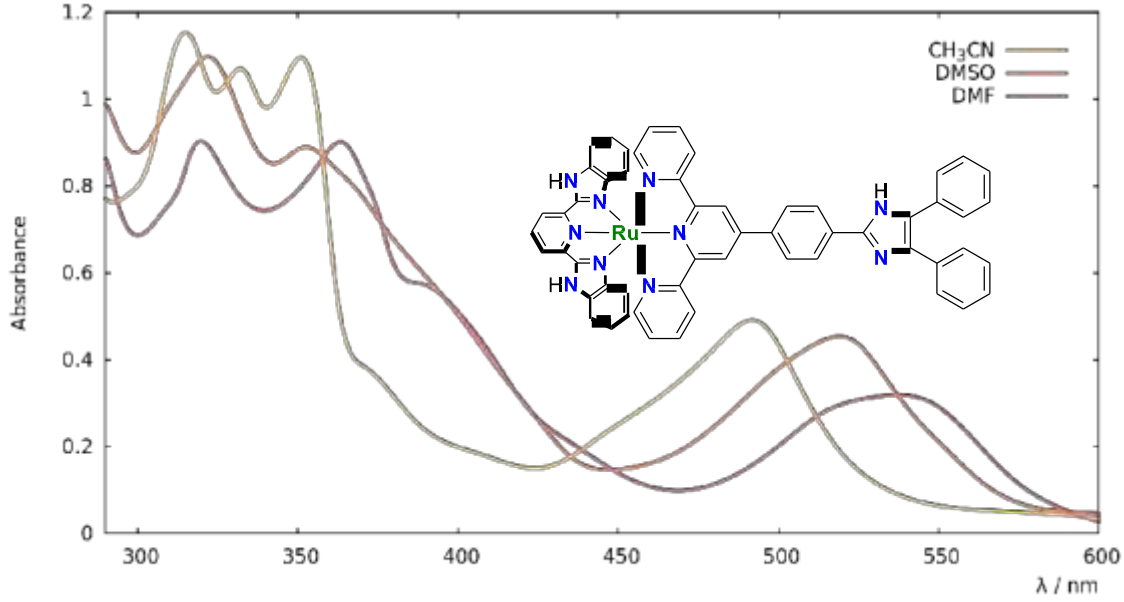

Figure 2.12: Experimental UV-Vis absorption spectra of a Ru(II) complex in three different solvents: acetonitrile (yellow), dimethyl sulfoxide (orange) and dimethylformamide (violet). The colors chosen try to mimic the resulting colors of the solutions in the different solvents. (Adapted from ref. 62)

In order to include solvent effects in the calculations two main strategies can be adopted: a) explicit inclusion of solvent molecules in the model, or b) continuum models where solute molecules are immerged in a dielectric polarizable 'bath' created by the solvent, being implicitly included in the model (or a mixed/hybrid strategy). For the first strategy many approaches can be followed, ranging from the simple inclusion of few solvent molecules treated at the same level of theory as the solute, to the popular hybrid methods like Quantum Mechanics / Molecular Mechanics (QM/MM) where the solute is treated with a Quantum Mechanic method and the solvent molecules with the classic approach of Molecular Mechanics. Depending on the problem and the accuracy required, an appropriate strategy may be employed. Explicit inclusion of solvent molecules allows the prediction of short range interactions between solvent and solute. On the other hand, it can be very expensive if no hybrid QM/MM approach is used. Besides, in some cases, parameterization of the force-field used in hybrid-based methods may become a quite long phase in the study, and it is the only possible approach if hundreds or even thousands of solvent molecules are to be included. Throughout the study of the different photoreactions described in this manuscript, no inclusion of solvent molecules has been done, unless stated otherwise. In the photoreactivity studies carried out during this PhD, treatment of long range molecule-solvent interactions has been done by mimicking the electric field created by the solvent using two different continuum models, the Polarizable Continuum Model (PCM)[63,64] and the COnductor-like Screening MOdel (COSMO).[65] In these models, solvent is treated like a dielectric polarizable isotropic environment, which is characterized (among other parameters) by a dielectric constant, ε, corresponding to the experimental value measured for each solvent.

One of the initial procedures that need to be done in the implementation of these solvation models consists on defining the limits of the molecule in the space. This might seem trivial but indeed, it is necessary to have well defined boundaries between the solute and solvent, *i.e.* the volume where the molecule is 'confined' needs to be well-described (Figure 2.7). A general procedure to obtain the surface which defines this volume is described in ref. 63.

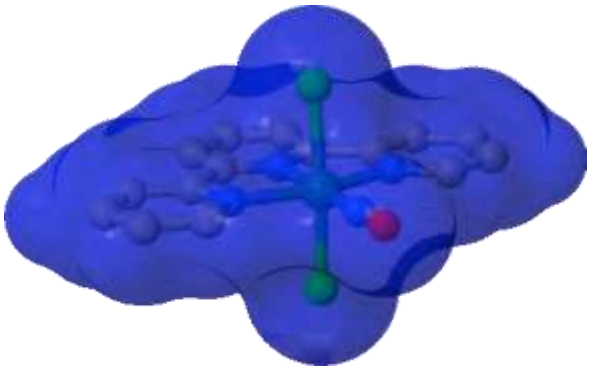

Figure 2.13: Example of the Solvent Excluding Surface (ESURF) on the *cis*-(Cl,Cl)[$RuCl_2$(NO)(terpy)]$^+$ complex.

This molecular surface labeled by Pascual-Ahuir and co-workers as the Solvent-Excluding Surface (ESURF) is built as the surface resulting from a set of interlocking spheres. Initially, atom-centered spheres are added to the model, preferably using the vdW radii for each atom. Then, spaces which are not accessible to the solvent are filled with a set of new spheres (Figure 2.8). Inside the cavity where the solute molecule is confined the dielectric constant is set to $\varepsilon = 1$ to simulate the vacuum, and outside, the dielectric constant is the one characteristic of the solvent used in the model, e.g. for the acetonitrile $\varepsilon = 36.64$ (at 20°C).

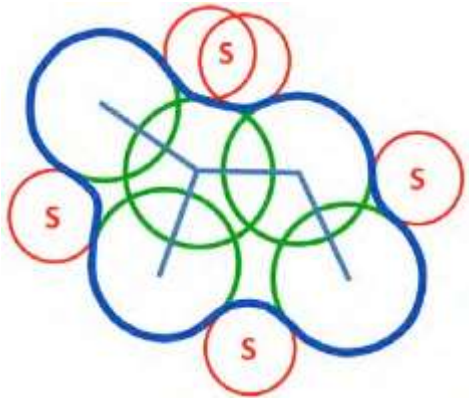

Figure 2.14: Solvent Excluding Surface (ESURF). The ends of the blue segments represent atomic centres, green spheres represent the vdW radii and the red ones are solvent molecules. The resulting surface from the set of interlocking spheres, the ESURF is traced in bold blue. (Adapted from ref. 63)

The electric fields created by the molecular dipole moment of the solute (inside the cavity) and the solvent environment (outside the cavity) interact and influence each other, generating an apparent charge distribution at the surface. In order to reproduce this charge distribution, the surface is divided in infinitesimal parts and to each part a partial charge q is assigned, the so-called Apparent Solvation Charge (ASC). The total electrostatic potential V_{tot} can be computed as the sum of the potential generated by the molecule (solute) V_m, and the

potential generated by the charges q_i at the surface V_q. These potentials can be computed at any spatial position $\boldsymbol{r}$ as follows:

$$V_{tot}(\boldsymbol{r}) = V_m(\boldsymbol{r}) + V_q(\boldsymbol{r}) \tag{2.78}$$

$$V_m(\boldsymbol{r}) = \int \frac{\rho(\boldsymbol{r}')}{|\boldsymbol{r} - \boldsymbol{r}'|} \cdot d\boldsymbol{r}' + \sum_A \frac{Z_A}{|\boldsymbol{r} - \boldsymbol{r}_A|} \tag{2.79}$$

$$V_q(\boldsymbol{r}) = \sum_i \frac{q_i}{|\boldsymbol{r} - \boldsymbol{r}_i|} \tag{2.80}$$

where $|\boldsymbol{r} - \boldsymbol{r}_x|$ represents Euclidean distances, $\rho(\boldsymbol{r}')$ the electron density at a $\boldsymbol{r}'$ point and Z_A the charge of nucleus A.

For a given molecular electrostatic potential $V_m(\mathbf{r})$, the charges q_i are determined so that a classical electrostatic problem (Poisson problem) is solved. The general Poisson equation needs to be satisfied inside (eq. 2.81) and outside (eq. 2.82) the cavity:

$$-\nabla^2 V_{tot}(\boldsymbol{r}) = 4\pi\rho(\boldsymbol{r}) \tag{2.81}$$

$$-\varepsilon\nabla^2 V_{tot}(\boldsymbol{r}) = 0 \tag{2.82}$$

It is worth noticing that two 'jump' conditions need to be satisfied at the surface. The first one:

$$[V_{tot}]_s = V_{in} - V_{out} = 0 \tag{2.83}$$

implies that the potential inside and outside the cavity need to be equal, ensuring the continuity of the potential across the surface. The second condition:

$$\left(-\frac{\partial V}{\partial \boldsymbol{n}}\right)_{in} - \varepsilon\left(-\frac{\partial V}{\partial \boldsymbol{n}}\right)_{out} = 0 \tag{2.84}$$

imposes the discontinuity of the component of the field that is perpendicular to the surface, where $\boldsymbol{n}$ is the outward-pointing vector perpendicular to the surface.

In these continuum solvation models (isotropic permittivity) with an empty cavity (or many), the polarization vector $\boldsymbol{P}(\boldsymbol{r})$ (required for the calculation of the charge distribution σ) is given by the gradient of the total potential $V_{tot}(\boldsymbol{r})$ as follows:

$$\boldsymbol{P}_{out}(\boldsymbol{r}) = -\frac{\varepsilon - 1}{4\pi}\nabla V_{tot}(\boldsymbol{r}) \tag{2.85}$$

At the surface the charge distribution (ASC) is given by:

$$\sigma = -(\boldsymbol{P}_{out} - \boldsymbol{P}_{in})\boldsymbol{n} \tag{2.86}$$

In the basic formulation of the PCM model, using the gradient on the internal part of the surface, the charge distribution is expressed as:

$$\sigma = \frac{\varepsilon - 1}{4\pi\varepsilon}\frac{\partial}{\partial \boldsymbol{n}}\left(V_m + V_\sigma\right)_{in} \tag{2.87}$$

where V_m is the potential created by the solute V_σ is the potential at the surface and $\boldsymbol{n}$ is the outwards-pointing unit normal vector at the surface. From eq. 2.87, in the PCM model the charges q_i can be numerically computed.

The strategy followed in the COSMO solvation model in order to compute the q_i charges is a little different. In this model, the external environment outside the cavity is considered to be a conductor material, which implies a dielectric constant with an infinite value. In practice, this approximation is acceptable for solvent with a dielectric constant higher than 5 ($\varepsilon > 5$). Within this approximation, the molecular charge distribution is completely screened by the charges at the surface q_i and the most important consequence is that the total potential V_{tot} is cancelled out at the surface of the cavity. Furthermore, this condition implies that the charge distribution is determined by the local value of the electrostatic potential and not by the normal component of its gradient. In order to recover a physical meaning, the ideal unscreened charge density, σ^*, is scaled by a proper function of ε as follows:

$$\sigma = f(\varepsilon)\cdot\sigma^* \tag{2.88}$$

where the scaling function $f(\varepsilon)$ has been empirically determined and has the following form:

$$f(\varepsilon) = \frac{\varepsilon - 1}{\varepsilon + k} \tag{2.89}$$

k being a small constant defined in the original paper as $k = 0.5$,[66] and modified depending on the version of COSMO which is implemented in the electronic structure code used. In a recent paper,[67] one of the original authors of COSMO, A. Klamt, shows that the method works perfectly well yielding similar results to other more sophisticated methods if for the constant k the value of 0.5 is given for neutral molecules and 0 in the case of ionic species.

The electron density in these solvation models is obtained iteratively within the Kohn-Sham SCF framework (in the case of DFT and TD-DFT) where the electric field outside the

cavity polarizes the electron density and the electron density polarizes the dielectric environment in return. Throughout the SCF iterative process dielectric environment and electron density are optimized until equilibrium is reached. The total energy of the system (solute) in these models is calculated as the sum of the energy given by the electron density issue of the SCF procedure and the interaction energy as follows:

$$E_{molecule} = E[\rho] + E_{int} \tag{2.90}$$

where the interaction energy E_{int} is:

$$E_{int} = \sum_i \int \frac{\rho(\boldsymbol{r}) q_i}{|\boldsymbol{r} - \boldsymbol{r}_i|} \cdot d\boldsymbol{r} + \sum_i \sum_A \frac{Z_A q_i}{|\boldsymbol{r} - \boldsymbol{r}_i|} \tag{2.91}$$

2.5 Analysis of the Triplet State Nature: Natural Orbitals

The wave function of a triplet state is spin polarized, with two α electrons in excess with respect to the β (Figure 2.15). In the unrestricted Kohn-Sham (UKS) calculations, like in the unrestricted Hartree-Fock (UHF) scheme, the α and β electrons are not restricted to be in the same spatial orbital, resulting in different orbitals for different spins, *i.e.* orbital φ_i^{α} does not necessarily correspond to orbital φ_i^{β}.

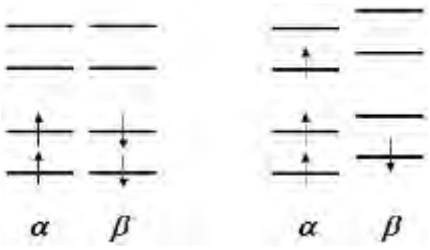

Figure 2.15: Schematic representation of a closed shell singlet from a restricted KS calculation (to the left) and an open shell triplet from an unrestricted KS calculation (to the right).

For open-shell systems an unrestricted Kohn-Sham wave function should be lower in energy than the restricted open-shell equivalent, since there are no 'spatial' constraints in the variational parameters. On the other hand, a UKS wave function is not an eigenfunction of the $\hat{S}^2$ operator, meaning that it may contain non-physical contributions from other states with different spin multiplicities. This phenomenon is known as spin contamination. Generally, the most important unphysical contributions to an UKS wave function come from the next higher

spin state than the desired one. Thus, for a UKS triplet wave function, the main source of undesired contributions comes from a quintet. The theoretical value for a pure triplet spin state is $S^2 = S_z\,(S_z + 1) = 2$, with $S_z = 1$. Although there is no much theoretical justification to compute the expectation value $< \hat{S}^2 >$ in UKS calculations as in wave-function-based methods, the computed $< \hat{S}^2 >$ value gives an indication of how reliable the DFT calculations are. In practice, the $< \hat{S}^2 >$ value for an UKS wave function is computed adding to the theoretical value of a pure spin state the difference between the total number of β electrons, N_β, and the spatial overlap between all pairs of α and β spin-orbitals, as follows:

$$\left\| \hat{S}^2 \right\| = S_z(S_z + 1) + N_\beta - \sum_{i,j}^{N_{MO}} \left\| \varphi_i^\alpha \left| \varphi_j^\beta \right\| \right\|^2 \qquad (2.92)$$

The last two terms in eq. (2.92) represent the deviation from the ideal expectation value $<\hat{S}^2>$, *i.e.* the spin contamination.

Since the α and β density matrixes are different in a UKS calculation, the optimized α and β canonical orbitals are not necessarily the same. Thus, the electronic nature of the triplet state is not always easy to define with the final set of canonical orbitals resulting from an UKS calculation. In this context, the triplet state nature is defined by the nature of the Single Occupied Molecular Orbitals (SOMOs) which characterize that triplet state (the two α occupied orbitals that should have their respective unoccupied β pairs). In photochemistry, the terminology '*hole*' and '*particle*' is widely used to describe the excited states of molecules. The molecular orbital from which the electron is initially excited is commonly known as the '*hole*', because of the 'vacant position' left in that MO after electronic excitation. At the same time, the empty orbital where the electron is promoted is called '*particle*' since the 'new coming' electron is considered as a new particle in that MO. By analogy, this terminology is extrapolated to the many different excited states that a molecule can visit during the photochemical reaction, even though they are not populated by electronic excitation. The first SOMO is considered as the hole and the second as the particle. In the same way, the lowest triplet states, which after initial absorption are populated as a consequence of a cascade of events, are characterized.

The characterization process can be illustrated taking as an example one of the lowest triplet states studied throughout this PhD thesis, the triplet isomer ^{3}**GS** of the *trans*-$[RuCl(NO)(py)_4]^{2+}$ complex (Figure 2.16). After the initial absorption of a photon ***1)***, the

ultrafast singlet-triplet ISC ***2)*** and the subsequent IC between triplet states[68,69] ***3)***, allow the population of ^{3}**GS**.[70]

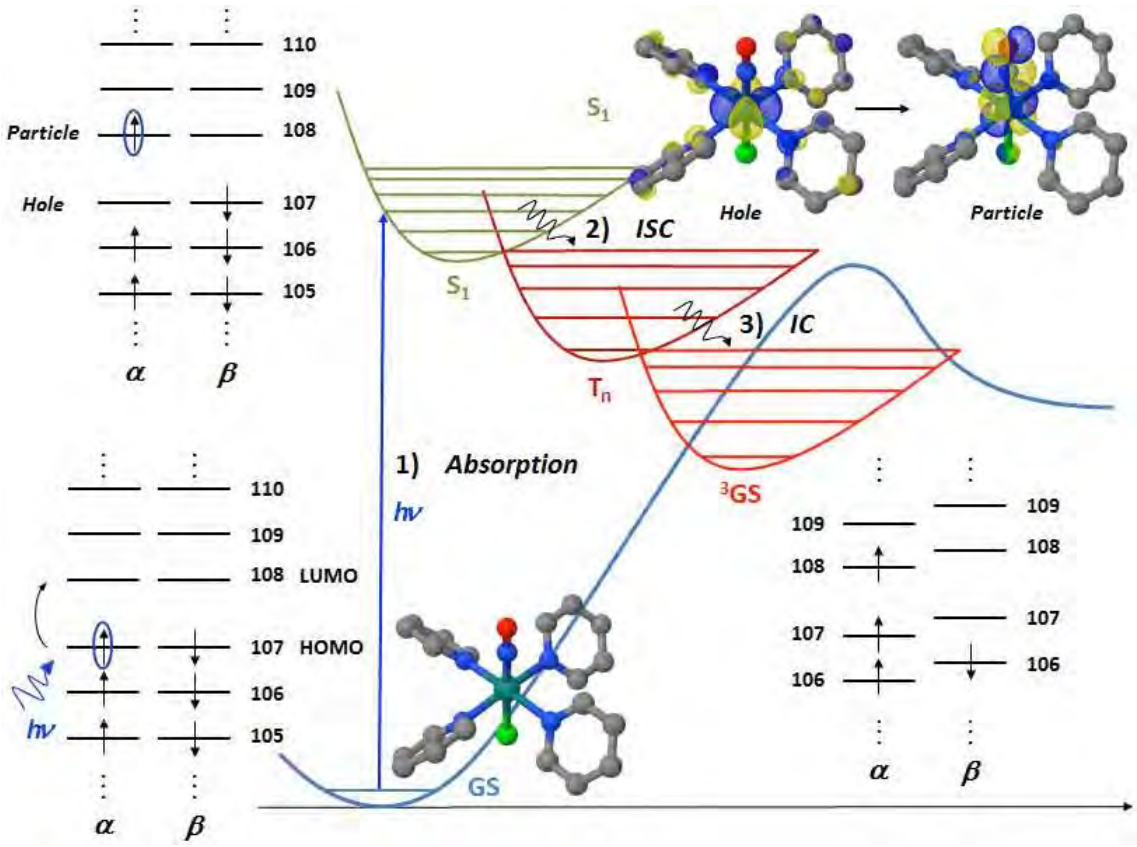

Figure 2.16: Schematic representation of the main processes taking place in the photoreaction to populate ^{3}GS from GS. After the initial photon absorption *1)* from the isomer GS on the singlet ground PES (blue line), the ultrafast singlet-triplet ISC *2)* followed by the IC between triplet states *3)* allows the population of ^{3}GS on the lowest triplet PES (red line). The Slater determinant for the GS isomer is represented at the bottom left corner, at this geometry at the top left corner is represented the Slater determinant for the first singlet excited state (green line) and at the bottom right corner the Slater determinant for the triplet ^{3}GS isomer (red line).

From Figure 2.16, the characterization of the electronic nature of the first singlet excited state becomes obvious, with no ambiguities in the identification of the hole being an atom centered Ru(d_{xy}) orbital and the particle being a Ru($d\pi$)NO(π^*) antibonding molecular orbital. On the contrary, defining the electronic nature of the triplet ^{3}**GS** becomes a much greater effort. In a first naive approach to this problem, the hole and particle might be assigned to the φ^{α}_{107} and φ^{α}_{108} MOs, then the complementary β orbitals need to be empty, otherwise these MOs are not the SOMOs which characterize the triplet state. Another difficulty arises from the fact that the φ^{α}_{i} does not necessarily correspond to orbital φ^{β}_{i}, meaning that the φ^{β}_{107} and φ^{β}_{108} MOs may not be the complementary β orbitals researched, increasing the orbital window to analyze. As a matter of fact, taking a closer look to the triplet

^{3}GS wave function, it can be shown that the φ^{α}_{107} MO is not a SOMO, since it exists a complementary β MO φ^{β}_{106} which is occupied (Figure 2.17).

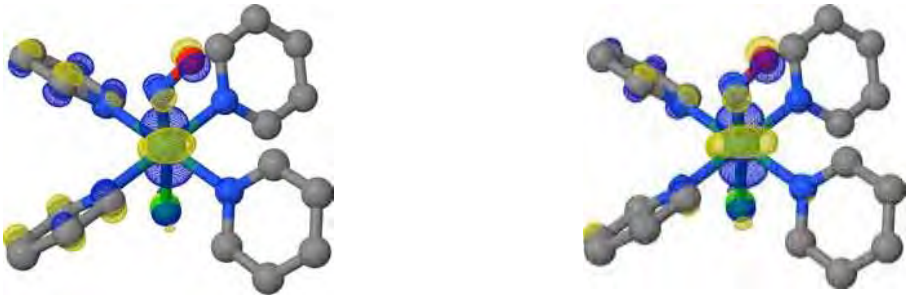

φ^{α}_{107} φ^{β}_{106}

Figure 2.17: φ^{α}_{107} and φ^{β}_{106} occupied molecular orbitals from the UKS canonical orbital set.

Further analysis on the **^{3}GS** triplet canonical orbitals affords the true nature of the SOMOs. The φ^{α}_{101} and φ^{α}_{108} MOs with their complementary β empty orbitals φ^{β}_{107} and φ^{β}_{108} respectively, correspond to the true SOMOs which characterize the triplet state (Figure 2.18).

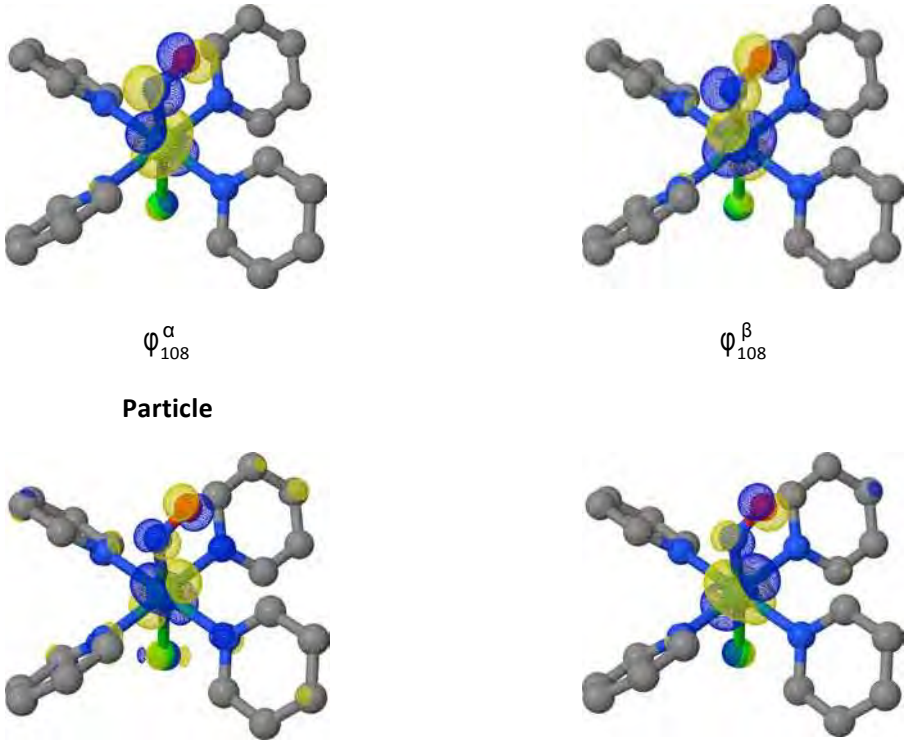

φ^{α}_{108} φ^{β}_{108}

Particle

φ^{α}_{101} φ^{β}_{107}

Hole

Figure 2.18: φ^{α}_{101} and φ^{β}_{108} SOMOs to the left and the complementary unoccupied β MOs φ^{α}_{101} and φ^{β}_{108} to the right.

Summarizing the triplet state characterization procedure:

4) Unrestricted DFT calculation on the lowest triplet state **^{3}GS** equilibrium geometry.
5) Careful inspection of sixteen canonical orbitals (eight α, β pairs), in this particular case.
6) Qualitative characterization of the SOMOs which define the electronic nature of the triplet (hole and particle), resulting from the canonical orbital analysis (Figure 2.19).

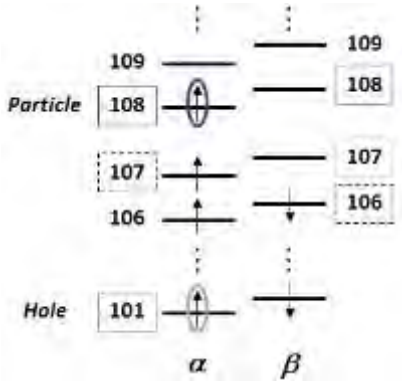

Figure 2.19: Schematic representation of the lowest triplet ^{3}GS electronic nature with the particle in blue and the hole in grey.

This procedure might seem quite tedious for just a qualitative description of the electronic structure of excited triplet states. An alternative procedure to the graphical analysis of the α, β partners is to compute the overlap between all α, β spin orbitals in order to decide between which pairs the overlap is maximized. Even using this numerical procedure, there is not 100% guaranty to find always the corresponding pairs for the SOMOs orbitals. Fortunately, a simple procedure can be applied to solve this inconvenient issue. If the first-order density matrix is diagonalized, an eigenvalue problem is solved, resulting in the truly intrinsic eigenvectors of the total density matrix, the so-called natural orbitals. The eigenvalues obtained are the occupation numbers of the natural orbitals, ranging from 0 to 2. Following this methodology, after the UKS calculations are converged the natural orbitals can be computed in order to identify the hole and the particle with occupancies of 1 (Figure 2.20).

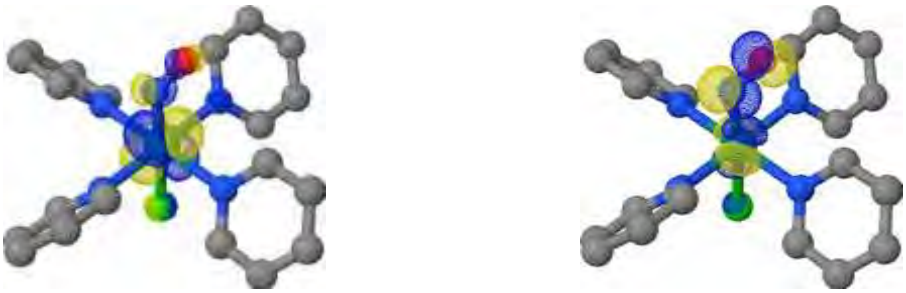

Hole **Particle**

Figure 2.20: Hole and Particle Natural Orbitals, qualitatively similar to those found in the canonical MO set.

2.6 Thermochemistry

Equations used to compute thermodynamic magnitudes throughout this PhD are derived from basic statistical thermodynamics. In order to calculate relevant thermodynamic information a frequency calculation becomes an essential tool in theoretical thermochemistry as it will be explained in this section.

When a chemical reaction is studied, it is always interesting to have information about the spontaneity of the process by computing the variation of the Gibbs free energy between products and reactants, ΔG, or to calculate the difference of the enthalpy between reactants and products, ΔH, in order to rationalize the process in terms of the exothermicity (endothermicity) of the reaction. These are just two examples of the various thermodynamic magnitudes that might help in the analysis and interpretation of experimental and theoretical results. Additionally, it exists another important magnitude: the so-called zero-point energy (ZPE) from the German term '*Nullpunktsenergie'*.[71] Introduced by O. Stern and A. Einstein in 1913, the physical meaning of the ZPE in quantum mechanics can be explained as the lowest energy that a system can have (the energy of the system at temperature equal to 0 Kelvin), *i.e.* the energy of its ground state. The origin of the ZPE lies in the Heisenberg uncertainty principle, and it can be understood as the energy that remains when all other energy is removed from the system, it is an irremovable 'intrinsic' energy of the system.

As a result of an electronic structure calculation within the B-O approximation, the total electronic energy of the system, E_{el}, (and the nuclear repulsion included in the term to simplify the notation) is computed, but… what about the other molecular energy contributions, namely the translational, rotational and vibrational energies? It comes as no

surprise that statistical molecular thermodynamics provides the necessary tools to compute these magnitudes. Statistical thermodynamics serves as a link between the macroscopic description of a system (entropy, heat capacity, …) and the microscopic magnitudes (molecular geometries, molecular energies, …) through the knowledge of the canonical partition function, *Q*. This partition function is based on the Boltzmann distribution and has the following general form:

$$Q = \sum_i g_i \cdot e^{-\frac{E_i}{k_B \cdot T}} \tag{2.93}$$

where g_i is the degeneracy factor of the *i*th state, E_i is its energy, k_B denotes the Boltzmann constant and *T* the temperature (being $k_B T$ the available thermal energy). It is important to be aware of the approximations done in order to derive the expressions for the different molecular energy contributions. In most electronic structure packages, unless state otherwise, during a computational thermochemistry analysis these few assumptions are made:

1) The macroscopic system is formed by *N* non-interacting indistinguishable particles, thus all equations apply only to ideal gases. The importance of the error introduced by this approximation depends on the extent of the non-ideal behaviour of the system. This approximation introduces the relation between the canonical partition function *Q* which depends on the *N* particles of the macroscopic system, and the microcanonical or molecular partition function *q* which depends on the molecular energy states of a single molecule.[72] For *N* non-interacting indistinguishable particles, *Q* can be written in terms of *q* as follows:

$$Q(N,V,T) = \frac{[q(V,T)]^N}{N!} \tag{2.94}$$

In a first approximation, the molecular energy $E_{molecule}$, can be split up into its different contributions as:

$$E_{molecule} = E_{el} + E_{trans} + E_{rot} + E_{vib} \tag{2.95}$$

Thus the molecular partition function *q* can be factorized as follows:

$$q_{molecule} = q = q_{el} \cdot q_{trans} \cdot q_{rot} \cdot q_{vib} \tag{2.96}$$

2) The electronic ground state is assumed to be, from a spatial-orbital point of view, non-degenerate and the first and higher excited states are not thermally accessible

since electronic excitation energies are much greater than k_BT. Thus, the electronic partition function can be simplified as follows:

$$q_{el} = \sum_i g_{el,i} \cdot e^{-\frac{\varepsilon_i}{k_B \cdot T}} = g_{el,0} \cdot e^{-\frac{\varepsilon_0}{k_B \cdot T}} + g_{el,1} \cdot e^{-\frac{\varepsilon_1}{k_B \cdot T}} + \ldots \approx g_{el,0} \cdot e^{-\frac{\varepsilon_0}{k_B \cdot T}} \tag{2.97}$$

Definitions and values of partition functions depend on the energy point of reference. Thus, a zero-energy point needs to be set to define the electronic molecular partition function, and it is chosen to be the energy computed issue of the SCF calculation from the electronic structure method; the energy of the ground state is set to zero. Indeed, the 'intrinsic' energy of the electronic ground state can be understood as the zero-point electronic energy, the electronic energy at 0 Kelvin. From eq. (2.42) the electronic partition function becomes:

$$q_{el} = g_{el,0} \tag{2.98}$$

where $g_{el,0}$ is the spin multiplicity of the molecule in the computed electronic ground state.

3) The quantum model of the particle in a box is used to derive the expression of the translational molecular partition function. Assuming a negligible translational ground state energy and practically a continuum in the translational energy, the sum in the expression of the translational partition function in one dimension becomes:

$$q_{trans,x} = \sum_{n_x=1}^{\infty} e^{-\frac{\theta_{trans,x}\,(n_x^2)}{T}\cdot n_x} \cong \int_0^{\infty} e^{-\frac{\theta_{trans,x}\,(n_x^2)}{T}} dn_x = \left(\frac{2\Pi \cdot m \cdot k_B \cdot T}{h^2}\right)^{\frac{1}{2}} \cdot L \tag{2.99}$$

where $\theta_{trans,x}$ is equal to the constant term $h^2/8 \cdot m \cdot L^2 \cdot k_B$, which depends on the molecular weight, m, and since it has temperature unities it is known under the name of translational temperature (characteristic of each molecule/atom). L is the length of the monodimensional box. Since the molecules are assumed to behave as an ideal gas, $PV = nRT = k_BT$, the translational partition function in three dimensions becomes:

$$q_{trans} = \left(\frac{2\Pi \cdot m \cdot k_B \cdot T}{h^2}\right)^{\frac{3}{2}} \cdot V = \left(\frac{2\Pi \cdot m \cdot k_B \cdot T}{h^2}\right)^{\frac{3}{2}} \frac{k_BT}{P} \tag{2.100}$$

$$\left(\quad^{2}\quad\right)\cdot P$$

4) To derive the expression of the rotational molecular partition function, the quantum rigid rotor model is used. For the general case of a non-linear polyatomic molecule, the rotational partition function becomes:

$$q_{rot} = \frac{\sqrt{\pi}}{\sigma_r}\left(\frac{T^{3/2}}{\sqrt{\theta_{r,a}\cdot\theta_{r,b}\cdot\theta_{r,c}}}\right) \qquad (2.101)$$

where σ_r is the rotational symmetry number, that can be derived from the molecular symmetry punctual group, counting the number of possible indistinguishable configurations obtained from rotations of the molecule. $\theta_{r,a}$, $\theta_{r,b}$ and $\theta_{r,c}$ represent the so-called characteristic rotational temperatures, which corresponds to the rotations around the three principal molecular inertia axis. Each rotational temperature is equal to $h^2/8\cdot\pi^2\cdot k_B\cdot I_i$, where I_i represents the inertia momentum that corresponds to each inertia axis.

It is worth to notice that in the quantum rigid rotor model the energy of the rotational ground state is equal to zero, since $E_j = \hbar^2/2I \cdot j\cdot(j+1) = B\cdot j\cdot(j+1)$, where j is the rotational quantum number, which is zero for the ground state, thus $E_0 = 0$. This implies that using this model the zero-point rotational energy is zero.

5) Finally, the model to derive the vibrational molecular partition function is the quantum harmonic oscillator, which means that all vibrations are considered strictly harmonic. This assumption is correct at temperatures where only the lower vibrational states are populated, in which case the harmonic oscillator approximation is still a good model.

2.7 References

(1) Hartree, D. R. *Math. Proc. Camb. Philos. Soc.* **1928**, *24* (1), 89.

(2) Pauli, W. *Z. Für Phys.* **1925**, *31* (1), 765–783.

(3) Pauli, W. *Exclusion principle and quantum mechanics*; Springer, 1994.

(4) Fock, V. *Z. Für Phys.* **1930**, *61* (1–2), 126–148.

(5) Slater, J. C. *Phys. Rev.* **1930**, *35* (2), 210–211.

(6) Fuchs, M.; Niquet, Y.-M.; Gonze, X.; Burke, K. *J. Chem. Phys.* **2005**, *122* (9), 94116.

(7) Thomas, L. H. *Math. Proc. Camb. Philos. Soc.* **1927**, *23* (5), 542–548.

(8) Fermi, E. *Z. Für Phys.* **1928**, *48* (1–2), 73–79.

(9) Hohenberg, P.; Kohn, W. *Phys. Rev.* **1964**, *136*, B864.

(10) Kohn, W.; Sham, L. J. *Phys. Rev.* **1965**, *140*, A1133.

(11) Barth, U.; Hedin, L. *J. Phys. C: Solid State Phys.* **1972**, *5*, 1629–1642.

(12) Filatov, M.; Shaik, S. *Chem. Phys. Lett.* **1998**, *288* (5–6), 689–697.

(13) Langreth, D. C.; Perdew, J. P. *Solid State Commun.* **1975**, *17* (11), 1425–1429.

(14) Gunnarsson, O.; Lundqvist, B. I. *Phys. Rev. B* **1976**, *13* (10), 4274–4298.

(15) Perdew, J. P. AIP, 2001; Vol. 577, pp 1–20.

(16) Cococcioni, M.; de Gironcoli, S. *Phys. Rev. B* **2005**, *71* (3), 35105.

(17) Perdew, J. P.; Ruzsinszky, A.; Csonka, G. I.; Vydrov, O. A.; Scuseria, G. E.; Staroverov, V. N.; Tao, J. *Phys. Rev. A* **2007**, *76* (4).

(18) HANDY, N. C.; COHEN, A. J. *Mol. Phys.* **2001**, *99* (5), 403–412.

(19) Parr, R. G.; Yang, W. *Density-functional theory of atoms and molecules*; Oxford Univ.: Oxford, 1989.

(20) Dreizler, R. M.; Gross, E. K. U. *Density Functional Theory*; Springer Berlin Heidelberg: Berlin, Heidelberg, 1990.

(21) Marques, M. A. L.; Gross, E. K. U. *Annu. Rev. Phys. Chem.* **2004**, *55* (1), 427–455.

(22) Casida, M. E. In *Recent Advances in Density Functional Methods, Part I*; World Sci.: Singapore, 1995; p 155.

(23) Martin, R. L. *J. Chem. Phys.* **2003**, *118* (11), 4775–4777.

(24) Jensen, F. In *Introduction to Computational Chemistry*; Wiley-VCH: Chichester, 2007; pp 380–420.

(25) Cramer, C. J. In *Essentials of Computational Chemistry*; Wiley-VCH: Chichester, 2004; pp 41–50.

(26) Bakken, V.; Helgaker, T. *J. Chem. Phys.* **2002**, *117* (20), 9160–9174.

(27) Schlegel, H. B. *Wiley Interdiscip. Rev. Comput. Mol. Sci.* **2011**, *1* (5), 790–809.

(28) Jensen, H. J. A.; Jo/rgensen, P.; Helgaker, T. *J. Chem. Phys.* **1986**, *85* (7), 3917–3929.

(29) Banerjee, A.; Adams, N.; Simons, J.; Shepard, R. *J. Phys. Chem.* **1985**, *89* (1), 52–57.

(30) Schlegel, H. B. In *Modern Electronic Structure Theory*; World Scientifc Publishing: Singapore, 1995; pp 459–500.

(31) Schlegel, H. B. *Theor. Chim. Acta* **1984**, *66* (5), 333–340.

(32) Fischer, T. H.; Almlof, J. *J. Phys. Chem.* **1992**, *96* (24), 9768–9774.

(33) Lindh, R.; Bernhardsson, A.; Karlström, G.; Malmqvist, P.-Å. *Chem. Phys. Lett.* **1995**, *241* (4), 423–428.

(34) Broyden, C. G. *IMA J. Appl. Math.* **1970**, *6* (1), 76–90.

(35) Fletcher, R. *Comput. J.* **1970**, *13* (3), 317–322.

(36) Goldfarb, D. *Math. Comput.* **1970**, *24* (109), 23–26. (37)

Shanno, D. F. *Math. Comput.* **1970**, *24* (111), 647–656.

(38) Liu, D. C.; Nocedal, J. *Math. Program.* **1989**, *45* (1–3), 503–528.

(39) Pulay, P. *Chem. Phys. Lett.* **1980**, *73* (2), 393–398.

(40) Pulay, P. *J. Comput. Chem.* **1982**, *3* (4), 556–560.

(41) Hamilton, T. P.; Pulay, P. *J. Chem. Phys.* **1986**, *84* (10), 5728–5734.

(42) Császár, P.; Pulay, P. *J. Mol. Struct.* **1984**, *114*, 31–34.

(43) Farkas, Ö.; Schlegel, H. B. *Phys. Chem. Chem. Phys.* **2002**, *4* (1), 11–15.

(44) Li, X.; Frisch, M. J. *J. Chem. Theory Comput.* **2006**, *2* (3), 835–839.

(45) Eckert, F.; Pulay, P.; Werner, H.-J. *J. Comput. Chem.* **1997**, *18* (12), 1473–1483.

(46) Hammond, G. S. *J. Am. Chem. Soc.* **1955**, *77* (2), 334–338.

(47) Parsons, J.; Holmes, J. B.; Rojas, J. M.; Tsai, J.; Strauss, C. E. M. *J. Comput. Chem.* **2005**, *26* (10), 1063–1068.

(48) Rybkin, V. V.; Ekström, U.; Helgaker, T. *J. Comput. Chem.* **2013**, *34* (21), 1842–1849.

(49) Halgren, T. A.; Lipscomb, W. N. *Chem. Phys. Lett.* **1977**, *49* (2), 225–232.

(50) Smidstrup, S.; Pedersen, A.; Stokbro, K.; Jónsson, H. *J. Chem. Phys.* **2014**, *140* (21), 214106.

(51) Bright Wilson, Jr., E.; Decius, J. C.; Cross, P. C. *Molecular Vibrations*; McGraw-Hill, 1955.

(52) Liotard, D. A. *Int. J. Quantum Chem.* **1992**, *44* (5), 723–741.

(53) Jónsson, H.; Mill, G.; Jacobsen, K. W. In *Classical and Quantum Dynamics in Condensed Phase Simulations*; World Sci.: Singapore, 1998; pp 385–404.

(54) E, W.; Ren, W.; Vanden-Eijnden, E. *J. Chem. Phys.* **2007**, *126* (16), 164103.

(55) Vanden-Eijnden, E.; Venturoli, M. *J. Chem. Phys.* **2009**, *130* (19), 194103.

(56) Harvey, J. N.; Aschi, M.; Schwarz, H.; Koch, W. *Theor. Chem. Acc.* **1998**, *99* (2), 95–99.

(57) Ogilvie, J. F.; Wang, F. Y. H. *J. Mol. Struct.* **1992**, *273*, 277–290.

(58) Ogilvie, J. F.; Wang, F. Y. *J. Mol. Struct.* **1993**, *291* (2), 313–322.

(59) Tao, J.; Perdew, J. P. *J. Chem. Phys.* **2005**, *122* (11), 114102.

(60) Grimme, S.; Antony, J.; Ehrlich, S.; Krieg, H. *J. Chem. Phys.* **2010**, *132* (15), 154104.

(61) Grimme, S.; Ehrlich, S.; Goerigk, L. *J. Comput. Chem.* **2011**, *32* (7), 1456–1465.

(62) Bhaumik, C.; Das, S.; Maity, D.; Baitalik, S. *Dalton Trans.* **2012**, *41* (8), 2427–2438.

(63) Pascual-ahuir, J. L.; Silla, E.; Tuñon, I. *J. Comput. Chem.* **1994**, *15* (10), 1127–1138.

(64) Tomasi, J.; Mennucci, B.; Cancès, E. *J. Mol. Struct. THEOCHEM* **1999**, *464* (1–3), 211–226.

(65) Klamt, A. *J. Phys. Chem.* **1995**, *99* (7), 2224–2235.

(66) Klamt, A.; Schüürmann, G. *J. Chem. Soc. Perkin Trans. 2* **1993**, No. 5, 799–805.

(67) Klamt, A.; Moya, C.; Palomar, J. *J. Chem. Theory Comput.* **2015**, *11* (9), 4220–4225.

(68) Balzani, V.; Ceroni, P.; Juris, A. *Photochemistry and Photophysics: Concepts, Research, Applications*, First.; Wiley-VCH: Weinheim, Germany, 2014.

(69) Freitag, L.; González, L. *Inorg. Chem.* **2014**, *53* (13), 6415–6426.

(70) Sanz García, J.; Alary, F.; Boggio-Pasqua, M.; Dixon, I. M.; Malfant, I.; Heully, J.-L. *Inorg. Chem.* **2015**, *54* (17), 8310–8318.

(71) Einstein, A.; Stern, O. *Ann. Phys.* **1913**, *40*, 551–560.

(72) Tuñon, I.; Silla, E. In *Química Molecular Estaística*; Editorial Síntesis, S. A.: Madrid, 2008; Vol. 27, pp 57–83.

Chapter III

Photoinduced Linkage Isomerization of the *trans*-$[RuClNO(py)_4]^{2+}$ Complex

In this chapter a detailed explanation of the photoinduced linkage isomerization mechanism of the *trans*-$[RuClNO(py)_4]^{2+}$ complex is presented. The chapter is organized as follows: First, the studied ruthenium-nitrosyl complex is briefly presented in order to situate this work in the appropriate context. Second, the ground-state (singlet closed-shell) and the lowest triplet potential energy surfaces (PESs) are described. Next, the TD-DFT absorption spectra of the three isomers found in the ground-state are discussed, and the different electronic transitions are characterized. This TD-DFT analysis proves to be especially important to rationalize the experimental conditions necessary for the forward and reverse photoisomerizations. Then, singlet-triplet minimum-energy crossing points (MECPs) are discussed in the context of nonradiative deactivation and intersystem crossing (ISC). All this information allows establishing the photoisomerization mechanism for the conversion from Ru−NO to Ru−ON and for the reverse conversion from Ru−ON to Ru−NO. Finally, the studied ruthenium-nitrosyl complex is compared with a previously studied polypyridyl ruthenium complexe (A detailed explanation of all technical details: method, basis set, and the programs used can be found in the Computational details in Appendix A).

3.1 Motivation

Since the discovery of the light-induced metastable isomers of the iron nitrosyl complex $Na_2[Fe(CN)_5(NO)]$ (sodium nitroprusside),[1,2] several iron compounds with similar photophysical properties have been found.[3–10] Due to their photochromic properties, these complexes offer not only a wide range of technological applications such as the design of new optical high-capacity storage devices but also an important knowledge in the fundamentals of chemical bonding and photochemical reactions.[11–14] A few years later, photoisomerizable ruthenium nitrosyl compounds have been developed.[15–26] By extension of the nitroprusside terminology, the lowest ground state species (denoted **GS**) is characterized by the commonly known N-bound form of the nitrosyl ligand to the metal; upon adequate irradiation **GS** turns into two different metastable (MS) isomers: the O-bonded isomer (isonitrosyl) called **MS1**, and the sideways bonded isomer called **MS2**. Besides photoisomerization, nitrosyl metal complexes can also undergo photorelease of NO and thus display a biological activity.[27–31] Despite numerous extensive experimental studies, as well as theoretical investigations, which have afforded a full structural and electronic description of the different isomers,[32–36] the photoisomerization mechanism is still unclear.

This chapter focuses on the photoinduced isomerization of the *trans*-$[RuCl(NO)(py)_4](PF_6)_2 \cdot ½H_2O$ complex.[37] Figure 3.1 displays a schematic representation of the structures involved in the photoisomerization process. Upon blue-light irradiation of a single crystal, the **GS** isomer (orange translucent crystal) turns into the **MS1** isomer (green translucent crystal). Subsequent irradiation with near-IR light generates a mixture of **GS** and **MS2** (black crystal); the latter eventually returns to the starting isomer **GS** (Figure 3.1). Alternatively, **MS1** returns to **GS** upon red light irradiation.[26] A remarkable conversion of *ca*. 100% from **GS** towards **MS1** was achieved on a single crystal upon irradiation for 1 hour.[24]

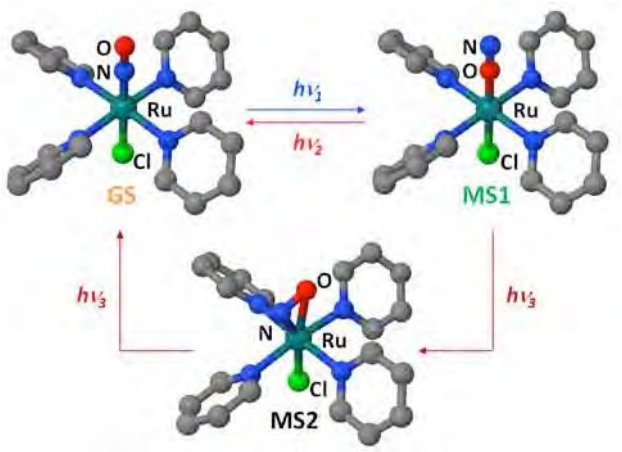

Figure 3.1: Schematic representation of the linkage isomers of the trans-$[RuCl(NO)(py)_4]^{2+}$ complex in its ground state (GS), metastable states (MS1 and MS2), and experimental irradiation conditions (blue, 473 nm; red, 782 nm; dark red, 980 nm).[23–26]

The leading motivation of the work presented in this chapter is to rationalize the full linkage photoisomerization mechanism of the *trans*-$[RuCl(NO)(py)_4]^{2+}$ complex, in both the forward and reverse directions by means of DFT and TD-DFT as it has been done before for a ruthenium monosulfoxide and other polypiridyl ruthenium complexes.[38–40] With the full characterization of the singlet and lowest triplet potential energy surfaces it will be shown that, despite of the unfavorable thermodynamic character of the forward process, the peculiar low energy character of the triplet 'excited' state (lower than the closed-shell singlet state in two critical regions) allows several crossing points between both surfaces along the reaction pathway which are crucial and favor the isomerization.

3.2 Exploring the Singlet and Triplet Potential Energy Surfaces of the *trans*-$[RuCl(NO)(py)_4]^{2+}$ Complex

3.2.1 Singlet Potential Energy Surface

The three *trans*-$[RuCl(NO)(py)_4]^{2+}$ isomers, **GS**, **MS1** and **MS2**, were optimized, and the computed geometries were compared to the experimental data (Table 3.1). As pointed out before,[25] the geometries of the three isomers are well reproduced with B3LYP. From a structural point of view, the four pyridine ligands appear as spectator ligands because their spatial arrangement in the three isomers is very similar. It is important to keep in mind that, as mentioned in ref. [24], the reduced data set available for **MS2** did not permit a perfect refinement of the X-ray crystallographic structure. Thus, the experimental bond lengths might not be fully reliable, in particular the N−O distance, which is reported to be only 1.08 Å (too short for a N−O bond length). A sideways-bonded NO ligand should indeed see its N−O distance increase, as was obtained by DFT. Further information on the optimized structures can be found in the Appendix A (Tables AA1−AA3). The energetic order of the isomers also perfectly fit the experimental data.

Table 3.1: Selected geometrical parameters (distances in Å, angles in °) for the three isomers in their singlet and lowest triplet states.

	Parameter	X-ray data[24]	Singlet	Triplet
GS	$Ru\text{-}N_{(NO)}$	1.755	1.745	1.975
	$Ru\text{-}O_{(NO)}$	--	2.886	2.901
	N-O	1.146	1.141	1.155
	Ru-Cl	2.321	2.317	2.290
	$Ru\text{-}N_{py}$	2.107[a]	2.139[b]	2.132[a]
	∠Ru-N-O	178.3	180.0[b]	134.2
MS2	$Ru\text{-}N_{(NO)}$	1.921	1.926	2.148
	$Ru\text{-}O_{(NO)}$	2.144	2.163	2.099
	N-O	1.08	1.177	1.216
	Ru-Cl	2.305	2.302	2.249
	$Ru\text{-}N_{py}$	2.101[a]	2.147[a]	2.144[a]
	∠Ru-N-O	87.3	84.7	71.1
MS1	$Ru\text{-}N_{(NO)}$	--	2.991	3.092
	$Ru\text{-}O_{(NO)}$	1.863	1.854	2.169
	N-O	1.140	1.137	1.159
	Ru-Cl	2.278	2.278	2.252
	$Ru\text{-}N_{py}$	2.097[a]	2.128[b]	2.121[a]
	∠Ru-N-O	--	0.0[b]	30.2

[a]Mean value for the four different $Ru\text{-}N_{py}$ distances. [b]Optimized in C_4 symmetry.

Location and subsequent optimization of the transition states connecting the three isomers, along with intrinsic reaction coordinate calculations, allowed full characterization of a possible thermal isomerization pathway. Following this procedure, the singlet PES was determined along the isomerization reaction coordinate, with $^1TS_1$ connecting the **GS** and **MS2** isomers and $^1TS_2$ connecting the **MS2** and **MS1** isomers (Appendix A, Tables AA4−AA5 and Figures AA5−AA6). The results are presented in Figure 3.2. Compared to previous work,[23] the trend is well reproduced.

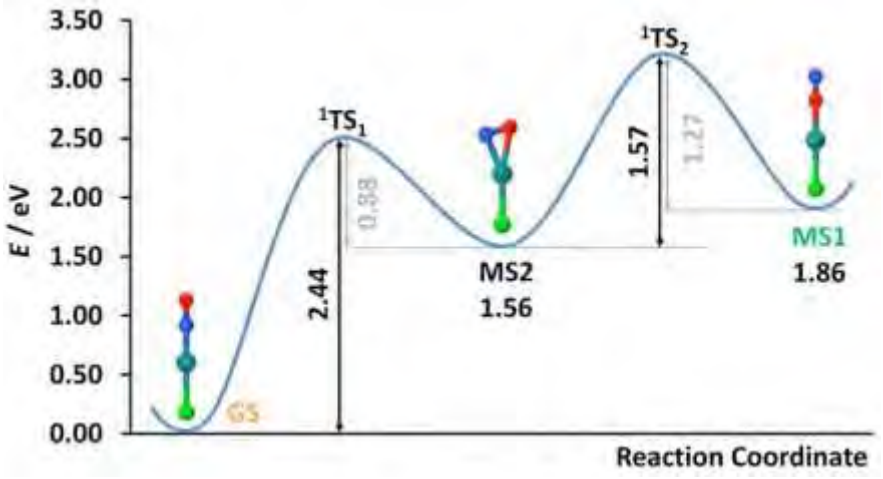

Figure 3.2: Singlet ground-state potential energy profile of *trans*-$[RuCl(NO)(py)_4]^{2+}$ along the isomerization reaction coordinate.

By analogy with the photoisomerizable iron(II) nitrosyl complexes, the first step of the thermal isomerization pathway would consist of the conversion of **GS** to **MS2**, 1.56 eV (150.5 kJ/mol) higher in energy, with a highly unfavorable 2.44 eV energy barrier (235.4 kJ/mol). With a sideways-bound NO ligand, the **MS2** geometry roughly corresponds to half of the geometric deformation between **GS** and **MS1**, and the nitrogen atom is much closer to the ruthenium atom than the oxygen atom (Table 3.1). The second step from **MS2** to **MS1** is also kinetically highly unfavorable [barrier of 1.57 eV (151.5 kJ/mol)], but only slightly thermodynamically unfavorable [**MS1** lies 0.30 eV (28.9 kJ/mol) higher than **MS2**]. Thus, from a kinetic and thermodynamic point of view, the **GS** ⇎ **MS1** isomerization cannot be achieved on the singlet state PES.

The reverse pathway from **MS1** to **GS** is thermodynamically favorable (exothermic), and from a kinetic point of view, it is more favorable than the forward process because the energy barriers are reduced: 1.27 eV (122.5 kJ/mol) from **MS1** to **MS2**, and 0.88 eV (84.9 kJ/mol) from **MS2** to **GS**. Thus, the thermal isomerization pathway from **MS1** to **GS** is

globally more favorable than the linkage isomerization from **GS** to **MS1**, but would remain challenging.

In an attempt to rationalize the energetic profile shown in Figure 3.2, a Natural Bond Orbital (NBO) analysis was undertaken. A second-order perturbation theory analysis of the Fock matrix in the NBO basis set allows a quantitative analysis, in terms of stabilizing energies gained upon electron delocalization between donors and acceptors, and a qualitative analysis based on interacting fragments in terms of two-center bonds and three-center four-electron (3c-4e) hyperbonds. Table 3.2 reports the main results from this NBO analysis.

Table 3.2: Delocalization energies (kJ/mol); donation and backdonation are defined with respect to the metal center. Nature of the fragments, and number of bonds and hyperbonds.

	Delocalization energy			Fragments	Bonds / Hyperbonds
	Donation	**Backdonation**	**Sum**		
GS	1367 ON:RuCl	744 RuCl:NO	2111	[Cl-Ru] / [NO]	0 / 3
MS2	995 ON:RuCl	217 RuCl:NO	1212	[Cl-Ru-NO]	1 / 1
MS1	693 NO:RuCl	267 RuCl:ON	960	[Cl-Ru] / [ON]	0 / 2

The energetic ordering of the three isomers is perfectly mirrored in the total delocalization energies. The energy gaps that appear on Figure 3.2 are also very well reproduced. From this analysis, **GS** is expected to be much more stabilized than **MS2** and **MS1**. **MS1** is expected to be slightly less stabilized than **MS2**. In terms of interacting fragments, **GS** and **MS1** are composed of two fragments, while **MS2** is described by one fragment only because one bonding orbital is found between the ruthenium and nitrogen atoms. Along the forward pathway, the largest activation barrier is associated with the disappearance of two highly stabilizing hyperbonds, in particular due to the tilting of the nitrogen lone pair and the loss of Cl−Ru−N linearity (from **GS** to **MS2**). When the Ru−N bond of **MS2** is broken (from **MS2** to **MS1**), a large activation barrier is also found. In the **MS1** isomer, it should be noticed that the (N)O : RuCl interaction is much weaker than the (O)N : RuCl interaction in **GS**. Along the reverse pathway, slightly smaller activation barriers are associated with the disappearance of one hyperbond (from **MS1** to **MS2**) or one bond (from **MS2** to **GS**). It can be seen that in this case the NBO analysis explains perfectly the relative positions of the three isomers as well as the energetic barriers between them.

3.2.2 Lowest Triplet Potential Energy Surface

The lowest triplet PES was explored in order to investigate a possible adiabatic N ⋯ O linkage photoisomerization on this surface, similarly to ruthenium sulfoxides,[38,40–44] and ruthenium phosphinidene oxides.[39] The singly occupied natural orbitals (SONOs), geometries, spin densities and other relevant information on the three minima can be found in the Appendix A Tables AA6–AA8. Starting from the singlet optimized structures, three different stationary points corresponding to three different minima were identified. These minima were labeled according to their affiliation with their corresponding closed-shell isomer: ^{3}**GS**, ^{3}**MS2** and ^{3}**MS1**. The nature of the triplet states cannot be defined as pure MLCT states since, from an orbital point of view, the hole corresponds to a Cl–Ru–NO (p–d–π*) orbital with a larger contribution from the Cl–Ru fragment and the particle corresponds to another Cl–Ru–NO (p–d–π*) orbital with a larger contribution from the NO ligand. Hence, the triplet states show electronic redistributions within the four atoms Cl, Ru, N and O. Nevertheless, on the basis of the Mulliken spin densities these triplet states may be considered as standard MLCT states (see Mulliken spin densities in Appendix A Tables AA6–AA8). It is worth noticing that, in contrast with polypyridyl ruthenium complexes, no triplet metal-centered states (^{3}MC) have been identified for this system on the lowest triplet PES.[38,40,43,44]

The lowest triplet state minima have been compared with their parent singlet geometries (Table 3.1) in order to highlight the main geometrical differences. It is remarkable that the Ru–N–O (or its homologous Ru–O–N for the **MS1**/^{3}**MS1** couple) bond angle bends from 180° (in **GS** and **MS1**) to 134° (in ^{3}**GS** and ^{3}**MS1**). Furthermore, the triplet states exhibit an elongated bond to the nitrosyl or isonitrosyl ligand, from 1.745 Å (**GS**) to 1.975 Å (^{3}**GS**) and from 1.854 Å (**MS1**) to 2.169 Å (^{3}**MS1**). Thus, for both the forward and reverse photoisomerizations, population of the triplet state initiates the rotation of the NO ligand.

In the Ru–NO ⋯ Ru–ON isomerization process (**GS** ⋯ **MS1**), the key geometrical change must involve a step where Ru–N < Ru–O becomes Ru–O < Ru–N. This key step is observed with the population of ^{3}**MS2**, whose geometry perfectly reflects this inversion (Table 3.1). From a structural point of view, it seems more favorable to go from one triplet to the other, rather than from one singlet to the other, because the changes in the Ru–N–O angles in the triplet state are smaller.

The location and optimization of the transition states, followed by intrinsic reaction coordinate calculations, is shown in Figure 3.3, with $^3TS_1$ connecting the **^{3}GS** and **^{3}MS2** minima and $^3TS_2$ connecting **^{3}MS2** and **^{3}MS1** minima (further information can be found in Appendix A Tables AA9−AA10 and Figures AA7−AA8).

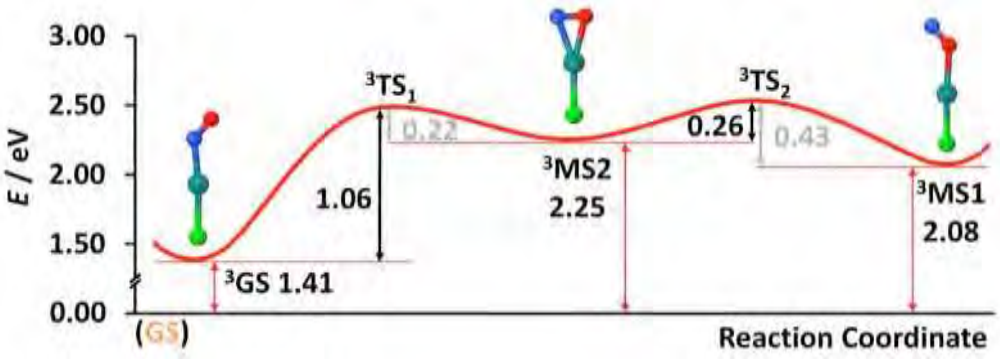

Figure 3.3: Triplet potential energy profile of *trans*-[RuCl(NO)(py)$_4$]$^{2+}$ along the photoisomerization reaction coordinate.

The energy gaps between the first two minima are smaller in the triplet case (**^{3}GS ▾▾ ^{3}MS2:** 0.84 eV, 81.1 kJ/mol) than in the singlet state case (**GS ▾▾ MS2**: 1.56 eV, 150.5 kJ/mol). With the **^{3}MS2** state being the highest of all triplet minima, the second step is now thermodynamically favorable (–0.17 eV, 16.4 kJ/mol) while it was unfavorable on the singlet state PES (+0.30 eV, 28.9 kJ/mol).

The energy barriers encountered on the lowest triplet PES are all reduced with respect to the singlet PES. However, the barrier found between **^{3}GS** and **^{3}MS2** (1.06 eV, 102.3 kJ/mol) is still large, but once **^{3}MS2** is reached, the progression of the reaction towards **^{3}MS1** is, from a thermodynamic and a kinetic (0.26 eV, 25.1 kJ/mol) point of view, favorable. Thus, the reaction would be easier on the lowest triplet PES than on the singlet PES.

The reverse pathway from **^{3}MS1** to **^{3}GS** is globally more favorable than the forward one, with an initial **^{3}MS1 ▾▾ ^{3}MS2** barrier of 0.43 eV (41.5 kJ/mol), and a second **^{3}MS2 ▾▾ ^{3}GS** barrier of 0.22 eV (21.2 kJ/mol). The backreaction **^{3}MS1 ▾▾ ^{3}GS** is exothermic; ΔE = –0.67 eV (–64.6 kJ/mol).

3.3 Absorption Spectra of GS, MS1 and MS2

Irradiation of **GS** with blue light at 473 nm happens to produce the largest amount of **MS1**. This point will be discussed in §3.5.1.a). On the way back, irradiation with red light at 782 nm can be used to generate **GS** from **MS1**.[26]

As it can be observed in Figure 3.4, isomers **GS** and **MS2** present absorption bands in the region from 400 to 500 nm and isomers **MS1** and **MS2** show a similar absorption band in the 600-750 nm spectral region. It should be noted that the extinction coefficients of the bands in those regions are quite small compared to those of polypyridyl ruthenium complexes. This is one of the reasons why the experimental irradiation times needed to achieve the photoisomerization are of the order of tens of minutes.

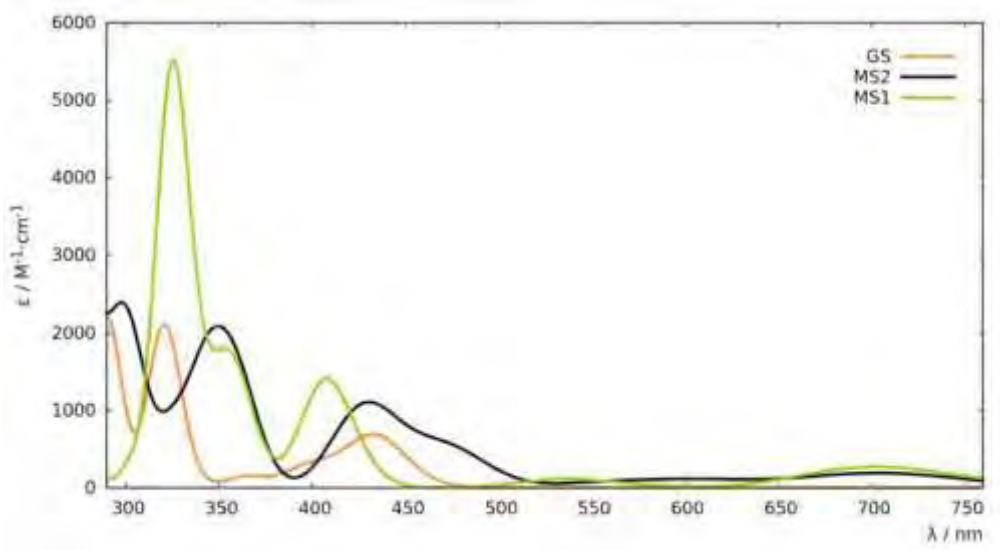

Figure 3.4: TD-DFT spectra of the three linkage isomers (GS in orange, MS2 in black and MS1 in green) of *trans*-$[RuCl(NO)(py)_4]^{2+}$ computed in acetonitrile.

In Table 3.3, the nature, absorption wavelengths, and oscillator strengths of the main transitions are summarized [natural transition orbitals (NTOs) for the selected states can be found in Appendix A Tables AA15−AA17].

Table 3.3: Selected TD-DFT states near the spectral irradiation wavelengths (*i.e.* in the 400-500 nm and 600-1100 nm ranges) computed in acetonitrile for the three isomers in their singlet states (oscillator strength threshold 10^{-3}).

	State	Wavelength / nm	f_{osc}	Nature
GS	S_1 & S_2	434	0.0031	Ru(d) ⋯ Ru(d)NO(π*)
	S_6 & S_7	402	0.0010	py(π) ⋯ Ru(d)NO(π*)
MS2	S_1	706	0.0017	Cl(p)Ru(d) ⋯ Ru(d)NO(π*)
	S_6	478	0.0016	Cl(p)Ru(d)NO(π*) ⋯ Ru(d)NO(π*) py(π)Ru(d) ⋯ Cl(p)Ru(d)NO(π *)
	S_7	476	0.0020	Cl(p)Ru(d) ⋯ Ru(d)NO(π*) Cl(p)Ru(d)NO(π*) ⋯ Cl(p)Ru(d)NO(π*)
	S_{10}	450	0.0012	py(π) ⋯ Cl(p)Ru(d)NO(π*)
	S_{11}	436	0.0028	Cl(p)Ru(d)py(π) ⋯ Ru(d)NO(π*)
	S_{12}	433	0.0021	Cl(p)Py(π) ⋯ Cl(p)Ru(d)NO(π*)
	S_{13}	427	0.0019	Cl(p)Ru(d)py(π) ⋯ Ru(d)NO(π*)
	S_{15}	417	0.0030	Cl(p)py(π) ⋯ Ru(d)NO(π*)
MS1	S_1 & S_2	703	0.0013	Ru(d) ⋯ Ru(d)ON(π*)
	S_{17}	408	0.0043	Cl(p)py(π) ⋯ Ru(d)ON(π*)
	S_{18} & S_{19}	408	0.0043	py(π) ⋯ Ru(d)ON(π*)

Experimentally, only the absorption of pure **GS** is available in solution (450 nm).[45] In order to reproduce this spectrum, it is necessary to take into account solvent effects (Appendix A Figures AA1−AA4). In these conditions, the lowest-energy absorption band is computed at 434 nm (416 nm without solvent). The 434 nm band in the spectrum of the **GS** isomer (Table 3.3) corresponds to two degenerate metal-to-ligand charge-transfer (MLCT) transitions from a Ru(d_{xy}) orbital to antibonding RuNO ($d_{xz} - \pi_x^*$ and $d_{yz} - \pi_y^*$) molecular orbitals (MOs). In general, the common ^{1}MLCT states in ruthenium(II) polypyridine complexes consist of electronic promotions from a Ru(*d*) orbital to a pure ligand orbital. In this particular case, the orbital that receives the electron is unusual because it also has a nonnegligible metallic contribution. At higher energies in the spectral region of interest, the two other states, S_6 and S_7, correspond to transitions from pyridyl MOs to the Ru−NO MOs described before.

The **MS2** spectrum displays its lowest-energy band at λ_{max} = 706 nm (Figure 3.4). The **MS2** isomer presents a band similar to that of **GS** in the region between 400 and 500 nm. This is crucial, as shown in the description of the photoisomerization mechanism (see §3.5.1.b). At the experimental irradiation wavelength (473 nm), **MS2** is the most efficient absorber of the three isomers. The excitation wavelength that produces the largest amount of **MS1** is 473 nm, which corresponds to a compromise between the absorption of **GS** and **MS2**.

The **MS1** isomer shows a band at the same position and intensity as **MS2** at 703 nm. It should be noted that, upon transposition of the 0.1 eV shift found for **GS** between theory and experiment, **MS1** does not absorb at the experimental irradiation wavelength (473 nm).

3.4 Singlet-Triplet Minimum Energy Crossing Points

In order to discuss possible nonadiabatic relaxation pathways, the MECPs between the lowest triplet PES and the singlet state PES have also been searched. This kind of relaxation through MECPs is decisive in the photoisomerization mechanism of ruthenium sulfoxide[38,40] and phosphinidene oxide complexes.[39] The size of the singlet-triplet spin-orbit coupling constant, about 1000 cm^{-1},[46,47] is sufficient to ensure that ISC will occur at these crossing points. Four MECPs between the singlet and the triplet PESs were found and are shown in Figure 3.5 (the geometries, gradients, triplet electronic structures, and relaxation pathways at these MECPs can be found in Appendix A Tables AA11–AA14 and Figures AA9–AA12). The energy is plotted against the Ru–N–O angle, which was selected as a relevant reaction coordinate for the photoisomerization process.

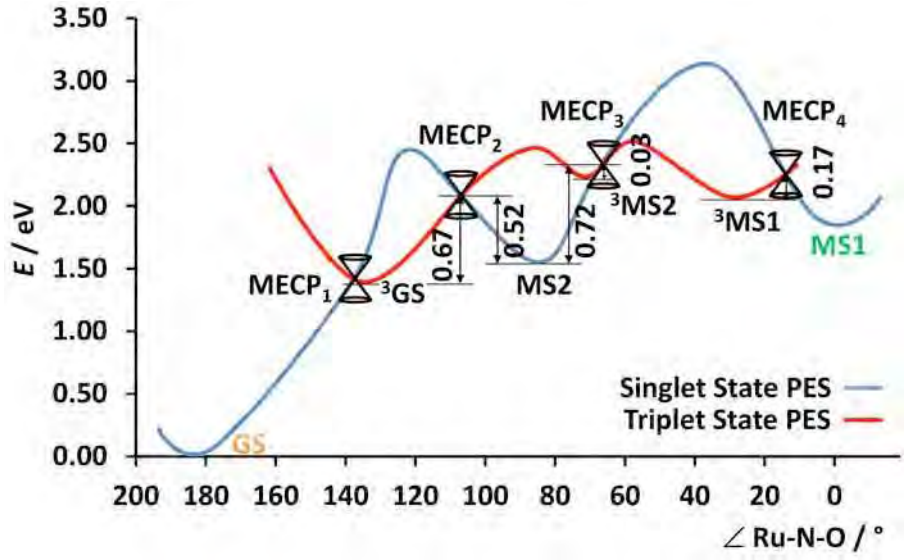

Figure 3.5: Energy profile showing the singlet-triplet minimum energy crossing points *vs.* Ru–N–O angle of *trans*-$[RuCl(NO)(py)_4]^{2+}$. The blue line represents the lowest-energy reaction path of the closed shell singlet state along the photoizomerization process. The red line represents the lowest triplet state energy path along the photoizomerization process. Triplet-singlet funnels are represented by double-cone pictograms.

The first MECP found, $MECP_1$, is almost similar in energy and geometry to ^{3}**GS**. $MECP_2$ is located between the geometries of the ^{3}**GS** and **MS2** species, 0.67 eV (64.6 kJ/mol) higher in energy than ^{3}**GS**. This MECP is very important, because it affords a way to go from ^{3}**GS** to **MS2**

at a reasonable cost. In comparison with the ^{3}**GS** ▾▾ $^3TS_1$ barrier (1.06 eV, 102.3 kJ/mol), the non-adiabatic barrier is substantially lower, making the passage from ^{3}**GS** to **MS2** possible. $MECP_3$ is almost similar in energy and geometry to ^{3}**MS2**. Finally, $MECP_4$ allows the ISC between ^{3}**MS1** and **MS1**, *i.e.* the population of the final photoisomerization product, **MS1**. It is easily accessible from ^{3}**MS1** (0.17 eV, 16.4 kJ/mol), and has an intermediate geometry between **MS1** and ^{3}**MS1** (especially in terms of Ru−O distance and Ru−O−N angle). As will be explained in the discussion (see §3.5), $MECP_4$ is important for both the forward and reverse isomerizations.

3.5 Forward and Reverse Photoisomerization Mechanisms

Before a discussion about the photoisomerization mechanisms of the *trans*-$[RuCl(NO)py_4]^{2+}$ system is presented in detail, three points have to be noted to describe this peculiar system:

1) From a structural point of view, the **MS2** geometry is an inevitable stopover and plays a central role in the mechanism, in the both forward and reverse directions. In addition, it has been shown that the absorption properties of **MS2** were partly overlapping those of **GS** (in the blue region) and partly overlapping those of **MS1** (in the red region). This property makes **MS2** the cornerstone of this photoisomerization.

2) The second remarkable specificity of this system is that, during the rotation of the NO fragment, two important regions of the PES exhibit the high-spin state (triplet states) as being more stable than the low-spin state (closed-shell singlet states). This is reminiscent of the physical properties of iron(II) magnetic compounds where spin crossover commonly occurs.

3) The initial working hypothesis is that the photoisomerization occurs on the lowest triplet PES. However, on the basis of the following calculations, the significant intervention of higher excited states (noted as T_n hereafter) has been envisaged in the mechanism, which avoids invoking thermodynamically uphill steps (see §3.5.1.a).

3.5.1. Mechanism for the Forward Isomerization (GS ▪▪ MS1)

The forward isomerization is performed by irradiation of the single crystal with λ = 473 nm at *ca*. 100 K during 1h.[24] The **GS ▪▪ MS1** photoisomerization can be viewed as a two-step sequence (**GS ▪▪ MS2** followed by **MS2 ▪▪ MS1**), in which **MS2** is an essential intermediate displaying an η^2 geometry**.** The corresponding mechanism is schematically presented in Figure 3.6.

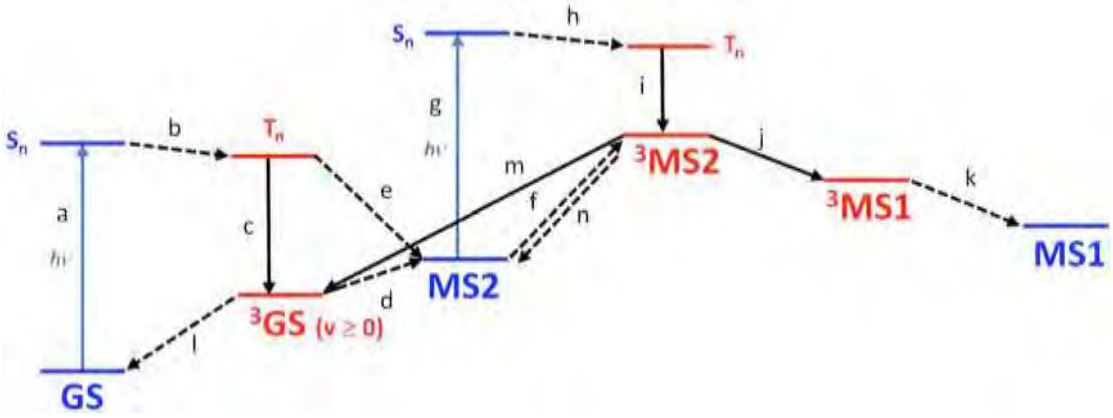

Figure 3.6: Schematic depiction of the major events involved in the photoisomerization mechanism from GS to MS1. The various steps that result in the population of the MS1 state are labeled sequentially (a-k). Solid arrows are used when states of the same multiplicity are involved, and dashed arrows are used otherwise. The singlet states are in blue and the triplet states in red.

a) Step 1: GS ▪▪ MS2

Following photoexcitation (elementary step a in Figure 3.6) **^{3}GS** is populated (steps b and c). The a, b, and c sequence is extremely well documented both experimentally and, more recently, theoretically, on the ruthenium complexes.[47–49] S_n refers to the lowest most absorbing singlet state. T_n, which is coupled by spin-orbit coupling with S_n, should be more or less degenerate with S_n and, furthermore, should be built on a determinant having one orbital orthogonal to the S_n determinant. Step c is the internal conversion from T_n to the lowest triplet state, *i.e.*, **^{3}GS**. From **^{3}GS**, ISC through $MECP_2$ (step d) populates **MS2** in its ground state. This step d involves an important change in the Ru−N−O angle (from 134.2° to 84.7°) and in the Ru−O distance (from 2.90 to 2.16 Å). Assuming a full thermal relaxation to **^{3}GS**(v=0), the activation energy barrier to reach $MECP_2$ amounts to 0.67 eV (64.6 kJ/mol). Alternatively, if **^{3}GS** is populated in high vibrational states, *i.e.*, **^{3}GS** (v>0), then the 0.67 eV value is just an upper limit of this activation energy. In addition, a direct connection between various T_n and **MS2** has also been considered (step e). In particular, two triplet states, which lie 0.47 and 0.70 eV (45.3 and 67.5 kJ/mol) above **^{3}GS** (at the **^{3}GS** geometry), are perfect candidates to populate **MS2** and

would avoid the system to fall in the **^{3}GS** potential well. It is even possible that these triplet states undergo ISC to **MS2**, but this point has not been addressed in this PhD thesis.

b) Step 2: MS2 ▾▾ MS1

To continue the isomerization process from **MS2** and literally to be dragged out of the **MS2** potential well, the system has to be excited to the **^{3}MS2** state. As seen in the geometries (Table 3.1), the **MS2 ▾▾ ^{3}MS2** step is crucial to switch in favour of the isonitrosyl coordination. Population of **^{3}MS2** can be achieved either by overcoming a 0.73 eV (70.4 kJ/mol) barrier to reach $MECP_3$ (step f), or much more probably by absorption of another blue photon (step g) and subsequent relaxation to **^{3}MS2** (steps h and i). Indeed, with such energy barriers to reach the $MECP_2$ or $MECP_3$ that surround **MS2**, the system should be trapped in the **MS2** isomer long enough to be detected by a colour change of the crystal. However, the irradiated crystal goes directly from orange to green. Hence, before the **MS2** isomer can be detected, it is depopulated by the absorption of a second photon. As seen in its absorption spectrum, **MS2** absorbs strongly at the experimental excitation wavelength. Thus, once the system reaches the **MS2** isomer, it absorbs a blue photon and relaxes preferentially to **^{3}MS2** (**GS ▾▾ MS1** photoisomerization completed in 1 hour), *vs* relaxing to **^{3}GS**.

The next step (**^{3}MS2 ▾▾ ^{3}MS1** *via* $^3TS_2$, step j) involves mainly a dramatic change in the Ru−N−O angle (from 71.1° to 30.2°) and a marked shortening of the N−O distance (from 1.216 to 1.159 Å). The last step of the photoisomerization (**^{3}MS1 ▾▾ MS1**, step k) consists of an ISC through $MECP_4$, with a small energy barrier of 0.17 eV (16.4 kJ/mol). The main coordinate involves a change in the Ru−N−O angle from 30.2° to 0.0°.

c) Pitfalls along the GS ▾▾ MS1 Path

Depending on their location and depending on which side they are accessed from, MECPs can act as either reactive or quenching funnels for the photoisomerization process. The first pitfall (step l) is encountered very close to **^{3}GS**, where $MECP_1$ takes the system back to the starting point. This relaxation back to **GS** is the most probable path because it only involves spin change (almost no energy barrier). This is an important trap that would make the photoisomerization quite inefficient. The second pitfall is that the **^{3}MS2** state can either go forward to **^{3}MS1** (as seen before) or return to **^{3}GS** (step m) with similar barriers (0.26 *vs.* 0.22 eV). In addition, in the vicinity of **^{3}MS2** lies $MECP_3$, which allows the system to return to **MS2** (step n).

It is noteworthy that, experimentally, the photoisomerization is achieved using a monochromatic excitation only because **GS** and **MS2** absorb at the same wavelength. This photoisomerization fulfills the general scheme proposed by Ishikawa and Tanaka,[50] where the absorption of a photon weakens the M−NO bond and crucial crossings are found between the singlet and triplet excited-state surfaces.

3.5.2. Mechanism for the Reverse Isomerization (MS1 ⋯ GS).

The oxygen-bound **MS1** isomer is formed upon blue-light irradiation at low temperature, *ca.* 100 K. It is stable in the dark, but conversion back to the **GS** isomer is observed upon heating and upon red light irradiation. Indeed, the **MS1** ⋯ **GS** transformation is achieved experimentally either by irradiation at 782 nm for 30 minutes[26] or by irradiation at 980 nm for 30 minutes to form a *ca.* 1:1 mixture of **MS2**/**GS**, which can eventually become the pure **GS** isomer upon heating.[24] The corresponding mechanisms have been studied separately and are schematically presented in Figures 3.7 and 3.8, respectively.

a) Red-Light Excitation (Figure 3.7)

In the red spectral range, **MS1** (and also **MS2**) shows a broad absorption band (650-800 nm) centered at 705 nm (Figure 3.4). Starting from **MS1**, the initial step of the mechanism consists of the absorption of a photon (step a in Figures 3.7). Similarly to the previous case, S_n undergoes ISC to T_n, which may directly convert into ^{3}**MS2** (step c). Which T_n converts into ^{3}**MS2** is an open question because two other triplets are available [0.50 and 0.55 eV (48.2 and 43.1 kJ/mol) higher in energy than ^{3}**MS1** at its proper geometry] that could populate ^{3}**MS2**. If the system relaxes to ^{3}**MS1** (step d), then there are two possibilities to depopulate this state: (i) by population of **MS2** through $MECP_3$ (step e); (ii) by population of ^{3}**MS2** via $^3TS_2$ (step f). If the system reaches ^{3}**MS2**, it can either relax to **MS2** through $MECP_3$ (step g) or relax to ^{3}**GS** through $^3TS_1$ (step h). In the latter case, only one photon is needed to complete the reaction.

If the system reaches **MS2**, it can absorb a second red photon (step i), because both **MS2** and **MS1** absorb at the excitation wavelength. This is consistent with the impossibility of observing **MS2** when irradiation is performed at 782 nm; *i.e.*, **MS2** is simultaneously produced and used; hence it does not accumulate.[26] As described before, depending on the excitation wavelength, excitation of **MS2** to an excited singlet S_n can lead to the population of either ^{3}**MS2** or ^{3}**GS**. The very fact that, at the end of the process a pure **GS** orange crystal is obtained, implies that at this wavelength (red light), the system evolves mainly to ^{3}**GS** (steps j and k). The

final step from ^{3}**GS** to **GS** involves the relaxation through $MECP_1$ (step l) *via* an efficient ISC with almost no energy barrier.

In summary, there are two pathways for the reverse **MS1** ⋮ **GS** photoisomerization: one that involves the absorption of only one photon, which avoids the **MS2** isomer, and a second one consisting in the sequential absorption of two photons by populating and depopulating the **MS2** isomer.

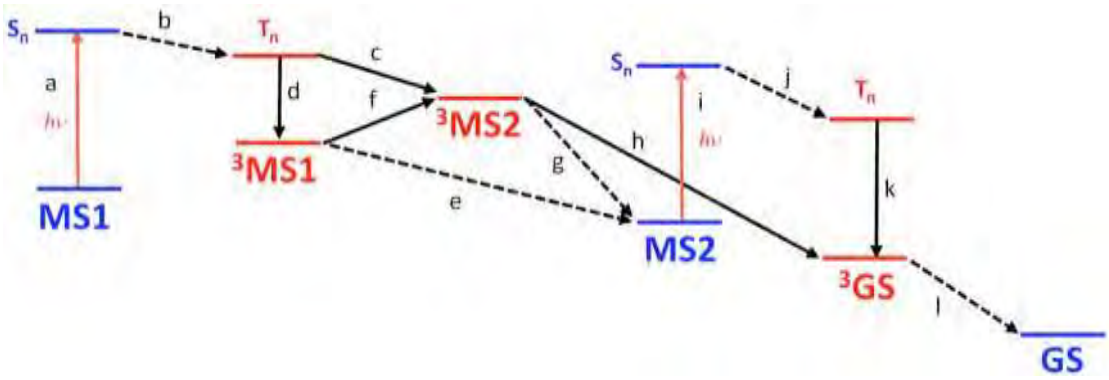

Figure 3.7: Schematic depiction of the major events involved in the photoisomerization mechanism from MS1 to GS with red light. The various steps that result in the population of the GS state are labeled sequentially (a-l). Solid arrows are used when states of the same multiplicity are involved, and dashed arrows are used otherwise. The singlet states are in blue and the triplet states in red.

b) Infrared Light Excitation (Figure 3.8)

Infrared (IR) light has been used to induce the stepwise photoisomerization from **MS1** to **GS** via **MS2**, the total disappearance of **MS1** being observed after 30 min irradiation.[24] A 1:1 mixture of **GS** and **MS2** is obtained, according to X-ray diffraction and IR spectroscopy,[23] which slowly evolves into a crystal of **GS** after a further 7 hours of irradiation or just by raising the temperature.

As seen in the TD-DFT spectrum of **MS1** (Appendix A Figure AA4), there is no absorption band in this region; this has been confirmed by using several functionals (B3LYP,[51,52] PBE0,[53] TPSSh,[54] X3LYP,[55] ωB97X,[56] LC-PBE[57,58]), and also by CASSCF/NEVPT2[59–61] calculations, which can be found in Appendix A (Tables AA18−AA19). Thus, IR-light is not capable of causing electronic excitations of **MS1**, and thus other explanations must be found to justify the disappearance of **MS1**. Two-photon absorption (TPA) cannot be excluded because many excited states fall in the suitable range. Alternatively, given that **MS1** can be thermally depopulated and by analogy with iron(II) spin crossover compounds,[62] one can propose that a

fraction of **MS1** exists as ^{3}**MS1**. Depopulation of ^{3}**MS1** by IR-light excitation ensures the gradual consumption of **MS1**. Variable temperature EPR measurements might confirm this hypothesis.

In the hypothesis of a TPA, **MS1** would be excited to higher singlet states, which by ISC could populate the ^{3}**MS1** state. Indeed, the *ca.* 1000 nm excitation wavelength (corresponding to a virtual excitation of 500 nm) matches several excited states of **MS1**. The TPA cross sections for these states have been computed, but these cross sections lie around 10^{-4} GM, which is too low to yield efficient excitations. Furthermore, calculations on **MS2** show similar cross sections. Hence, if **MS1** excitation (by TPA) was sufficient, **MS2** would be consumed as soon as produced and, thus, it could not be observed, in contrast to experimental evidence. Thus, TPA can be ruled out.

In the second hypothesis, which has been confirmed by very recent experimental data,[26] the system can partially exist as ^{3}**MS1** (step a in Figure 3.8) thanks to spin-orbit coupling and a low activation energy (0.38 eV). Interestingly, two transitions are found in the ^{3}**MS1** TD-DFT calculation, at 933 and 1396 nm, near the experimental irradiation wavelengths (980 nm and 1064 nm). Thus, absorption from ^{3}**MS1** takes the system to higher electronic triplet states (step b), and then the system can relax to ^{3}**MS2** *via* internal conversion (step c). Alternatively, ^{3}**MS1** can also populate ^{3}**MS2** via $^3TS_2$ (step d), but with this step being thermodynamically uphill, it is certainly less probable than step c. Once the system gets to ^{3}**MS2**, it can either relax to ^{3}**GS** through $^3TS_1$ (step e), or easily relax to **MS2** through $MECP_3$ (step f) (this explains why **MS2** is always observed as a blend of **GS** and **MS2**). The **MS2** isomer does not absorb in the IR region, and thus it is trapped long enough to be observed. This is fully consistent with the fact that experimentally, this is the only way to observe the **MS2** isomer.

From **MS2**, given that the system does not absorb IR-light (and TPA is not efficient enough), it can only relax to ^{3}**GS** through $MECP_2$ (step g) with a barrier of 0.52 eV (50.2 kJ/mol) for **MS2**(v=0). Finally, the last step of the mechanism consists in the ^{3}**GS** ▪▪ **GS** relaxation *via* $MECP_1$ (step h).

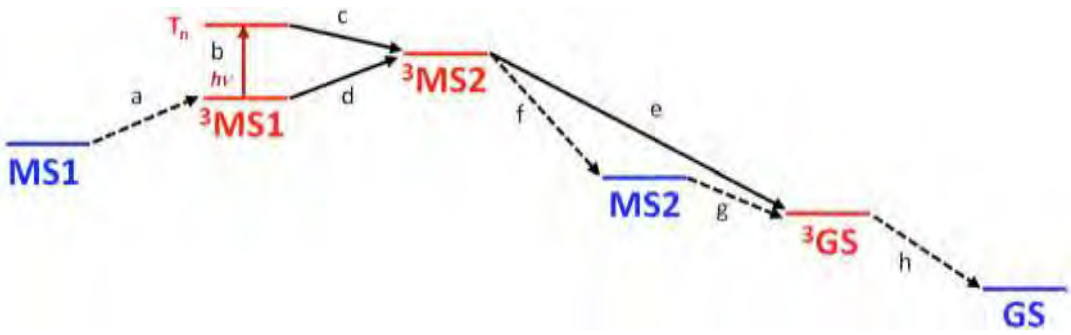

Figure 3.8: Schematic depiction of the major events involved in the photoisomerization mechanism from MS1 to GS with near-IR light. The various steps which result in the population of the GS state are labeled sequentially (a-h). Solid arrows are used when states of the same multiplicity are involved, and dashed arrows are used otherwise. The singlet states are in blue and the triplet states in red.

3.6 Conclusions

In this Chapter III, a mechanistic study of the reversible nitrosyl linkage photoisomerization in *trans*-$[RuCl(NO)(py)_4]^{2+}$ have been reported. Three isomers, Ru−NO (**GS**), Ru−η^2−NO (**MS2**) and Ru−ON (**MS1**), are successively populated during the process, which was already well established experimentally. The singlet and triplet PESs show that the forward isomerization, both thermodynamically and kinetically, is unfavorable and thus will necessitate the intervention of two photons. For the reverse photoisomerization with red-light excitation, two pathways coexist: one monophotonic process directly producing **GS** and one biphotonic process going to **GS** through **MS2**. For the reverse photoisomerization with IR-light excitation, only one species absorbs IR photons and thus only a monophotonic process is operative, yielding both **MS2** and **GS** in the same crystal.

For the forward and the reverse mechanisms, the Ru−η^2−NO isomer plays a pivotal role, both structurally and optically for the second photon absorption:

1) Its absorption spectrum overlaps that of **GS** in the blue region and that of **MS1** in the red region, which is a compulsory condition for the forward and backward photoisomerizations to proceed.

2) Its excitation allows the system to go past the tipping point toward **MS1** because Ru−O is shorter than Ru−N in ^{3}**MS2**.

It should also be noted that the singlet and triplet PESs are highly interwoven, which allows several spin changes along the reaction pathway. Furthermore, in certain regions of the PES, it is the triplet state that is the true ground state.

Note that the photoisomerization mechanism of two other ruthenium complexes, *trans*-$[RuBr(NO)(py)_4]^{2+}$ and *trans*-(Cl,Cl)$[RuCl_2(NO)(terpy)]^{+}$, has been studied and the trend of the photoconversion yields among these complexes has been rationalized (see Appendix B).

Besides linkage photoisomerization, metal nitrosyl complexes are promising candidates for NO photorelease. Understanding the factors controlling the competition between NO isomerization and NO release will be very challenging. In the following chapter, a comparison between these two processes in the studied system and four other nitrosyl ruthenium complexes is done, in order to understand and rationalize the relation between them. Approaches that combine static and dynamic studies[47] could bring further insight into the mechanisms involved in the versatile photosensitivity of ruthenium nitrosyl complexes.

3.7 Comparing Ru−NO with Ru−SO Complexes.

The documented studies and literature on photoisomerization of organic molecules, and more generally on the photochemistry of organic molecules, is quite extensive and many methods and techniques have been developed over the last decades in order to study these systems and to elucidate their photochemical mechanisms.[63–67] As explained in Chapter I, with the growth of computational power, theoretical photochemical studies have been developed quite rapidly during the past decades. Nowadays, computational investigations of photochemical reactions involving small organic chromophores have become a standard practice.[68–76] In comparison, theoretical studies on the photochemistry of organometallic compounds are much more recent; being on continuous development the methodologies and techniques used to study these compounds.

Photoinduced linkage isomerism of polypyridyl ruthenium complexes has been studied theoretically with the Density Functional Theory (DFT) since the last decade.[41,42] However, no complete mechanistic picture was ever reported until 2011, when the first full characterization of the lowest triplet excited state PES of a ruthenium sulfoxide complex (Figure 3.9) allowed

the full description of the linkage Ru–SO ⁚ Ru–OS photoisomerization mechanism.[38] After the seminal work of 2011, other studies on polypyridyl ruthenium complexes[39,40] have also proven that DFT and Time-Dependent DFT (TD-DFT) are powerful theories to describe the photoisomerization of this kind of organometallic complexes. In all these studies, triplet excited states appear to play an important role; this also holds for the *trans*-$[RuCl(NO)(py)_4]^{2+}$ complex. However a major difference exists; the lowest 'excited' triplet state is lower in energy than the singlet 'ground' state (closed shell) in two regions of the ruthenium-nitrosyl linkage photoisomerization pathway (Figure 3.10), whereas in the ruthenium monosulfoxide complex shown in Figure 3.9 and, generally speaking, in the majority of polypyridyl ruthenium(II) complexes the lowest triplet excited state is always higher in energy than the closed shell ground state throughout the whole photoisomerization pathway (as it is clearly illustrated with the example shown in the following Figure 3.9).

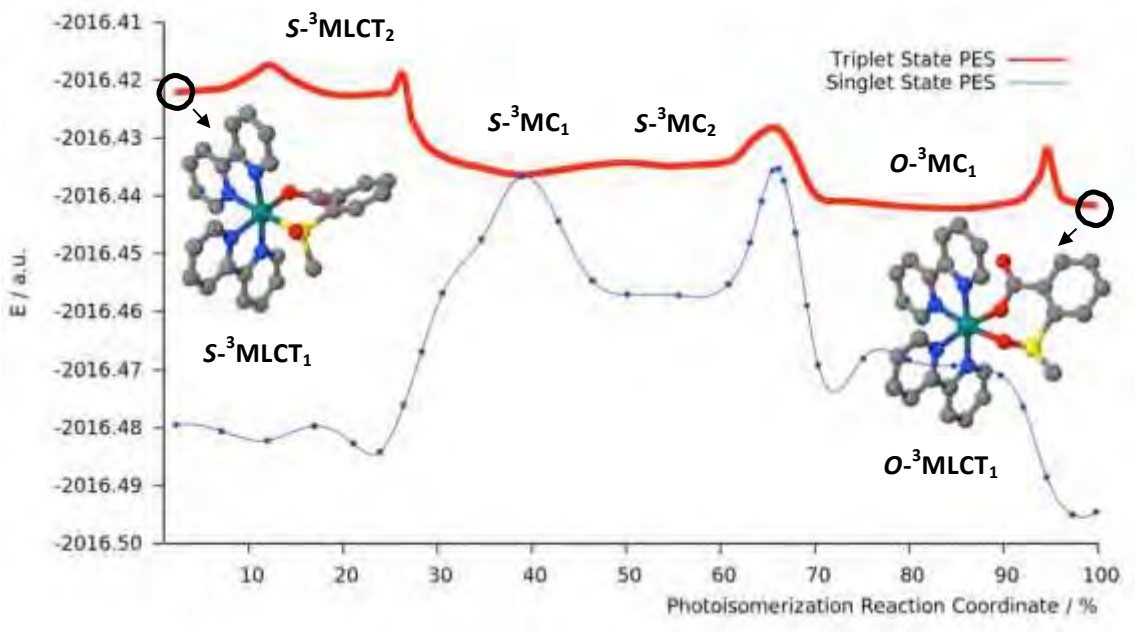

Figure 3.9: Complete photoisomerization pathway singlet ground-state (blue) and lowest triplet-state (red) along the reaction coordinate of the $[Ru(bpy)_2(OSO)]^+$ complex at the MPWB1K/6-31G*(H, C, N, O, S)/LANL2DZ(Ru) level of theory in vacuum. The triplet PES results from intrinsic reaction coordinate calculations, while the singlet ground-state PES results from single-point energy calculations at the triplet geometries along the triplet PES.[38] (Adapted from ref. 38)

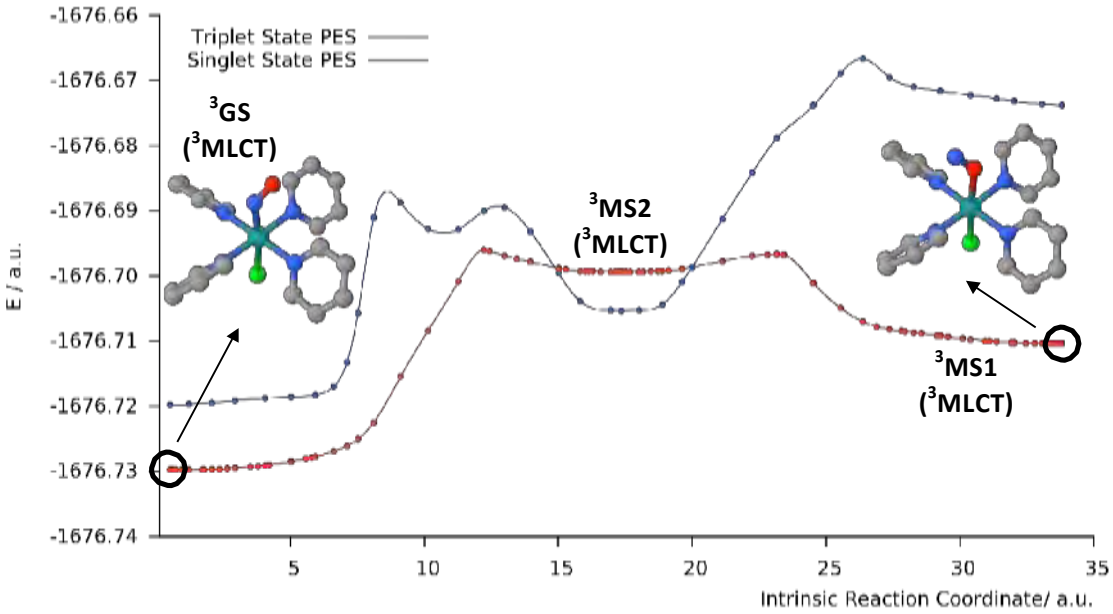

Figure 3.10: Complete photoisomerization pathway singlet ground-state (blue) and lowest triplet-state (red) along the reaction coordinate of the *trans*-[RuCl(NO)(py)$_4$]$^{2+}$ complex at the B3LYP/6-31G*(H, C, N, O)/6-31+G*(Cl)/LANL2DZ(Ru) level of theory in vacuum. The triplet PES results from intrinsic reaction coordinate calculations, while the singlet ground-state PES results from single-point energy calculations at the triplet geometries along the triplet PES.

In contrast with ruthenium sulfoxide complexes, for which metal-centered states play a crucial role because large geometric reorganizations are required,[38,40,43,44] the proposed photoisomerization mechanisms for the *trans*-[RuCl(NO)(py)$_4$]$^{2+}$ complex only involve moderately distorted triplet states of MLCT nature. Another remarkable feature of the triplet surface of this ruthenium nitrosyl is the global endothermic character of the Ru−NO (**^{3}GS**) ▪▪ Ru−ON (**^{3}MS1**) adiabatic isomerization on the lowest triplet PES (Figure 3.10), whereas for the ruthenium monosulfoxide, the adiabatic isomerization Ru−SO (**^{3}MLCT**) ▪▪ Ru−OS (**^{3}MLCT**) is globally exothermic (Figure 3.9), which corresponds to the general picture of lowest excited PES in reactions of photoactive systems.

3.8 References

(1) Hauser, U.; Oestreich, V.; Rohrweck, H. D. Z. *Phys. A* **1977**, *280*, 17.

(2) Hauser, U.; Oestreich, V.; Rohrweck, H. D. Z. *Phys. A* **1977**, *280*, 125.

(3) Pressprich, M. R.; White, M. A.; Vekhter, Y.; Coppens, P. *J. Am. Chem. Soc.* **1994**, *116* (12), 5233–5238.

(4) Delley, B.; Schefer, J.; Woike, T. *J. Chem. Phys.* **1997**, *107* (23), 10067–10074.

(5) Boulet, P.; Buchs, M.; Chermette, H.; Daul, C.; Gilardoni, F.; Rogemond, F.; Schläpfer, C. W.; Weber, J. *J. Phys. Chem. A* **2001**, *105* (39), 8991–8998.

(6) Boulet, P.; Buchs, M.; Chermette, H.; Daul, C.; Furet, E.; Gilardoni, F.; Rogemond, F.; Schläpfer, C. W.; Weber, J. *J. Phys. Chem. A* **2001**, *105* (39), 8999–9003.

(7) Chacón Villalba, M. E.; Güida, J. A.; Varetti, E. L.; Aymonino, P. J. *Inorg. Chem.* **2003**, *42* (8), 2622–2627.

(8) Lee, J.; Kovalevsky, A. Y.; Novozhilova, I. V.; Bagley, K. A.; Coppens, P.; Richter-Addo, G. B. *J. Am. Chem. Soc.* **2004**, *126* (23), 7180–7181.

(9) Novozhilova, I. V.; Coppens, P.; Lee, J.; Richter-Addo, G. B.; Bagley, K. A. *J. Am. Chem. Soc.* **2006**, *128* (6), 2093–2104.

(10) Lynch, M. S.; Cheng, M.; Van Kuiken, B. E.; Khalil, M. *J. Am. Chem. Soc.* **2011**, *133* (14), 5255–5262.

(11) Gütlich, P.; Garcia, Y.; Woike, T. *Coord. Chem. Rev.* **2001**, *250* (9–10), 839–879.

(12) Coppens, P.; Novozhilova, I.; Kovalevsky, A. *Chem. Rev.* **2002**, *102* (4), 861–884.

(13) Ford, P. C.; Wecksler, S. *Coord. Chem. Rev.* **2005**, *249* (13–14), 1382–1395.

(14) Bitterwolf, T. E. *Coord. Chem. Rev.* **2006**, *250* (9–10), 1196–1207.

(15) Fomitchev, D. V.; Coppens, P. *Inorg. Chem.* **1996**, *35* (24), 7021–7026.

(16) Fomitchev, D. V.; Coppens, P.; Li, T.; Bagley, K. A.; Chen, L.; Richter-Addo, G. B. *Chem. Commun.* **1999**, No. 19, 2013–2014.

(17) Da Silva, S. C.; Franco, D. W. *Spectrochim. Acta. A. Mol. Biomol. Spectrosc.* **1999**, *55* (7–8), 1515–1525.

(18) Gorelsky, S. I.; Lever, A. B. P. *Int. J. Quantum Chem.* **2000**, *80* (4–5), 636–645.

(19) Schaniel, D.; Woike, T.; Boskovic, C.; Güdel, H.-U. *Chem. Phys. Lett.* **2004**, *390* (4–6), 347–351.

(20) Bitterwolf, T. E. *Inorg. Chem. Commun.* **2008**, *11* (7), 772–773.

(21) Giglmeier, H.; Kerscher, T.; Klüfers, P.; Schaniel, D.; Woike, T. *Dalton Trans.* **2009**, No. 42, 9113.

(22) Zangl, A.; Klüfers, P.; Schaniel, D.; Woike, T. *Dalton Trans.* **2009**, No. 6, 1034–1045.

(23) Schaniel, D.; Cormary, B.; Malfant, I.; Valade, L.; Woike, T.; Delley, B.; Krämer, K. W.; Güdel, H.-U. *Phys. Chem. Chem. Phys.* **2007**, *9* (28), 3717–3724.

(24) Cormary, B.; Malfant, I.; Buron-Le Cointe, M.; Toupet, L.; Delley, B.; Schaniel, D.; Mockus, N.; Woike, T.; Fejfarová, K.; Petříček, V.; Dušek, M. *Acta Crystallogr. B* **2009**, *65* (6), 612–623.

(25) Cormary, B.; Ladeira, S.; Jacob, K.; Lacroix, P. G.; Woike, T.; Schaniel, D.; Malfant, I. *Inorg. Chem.* **2012**, *51* (14), 7492–7501.

(26) Khadeeva, L.; Kaszub, W.; Lorenc, M.; Malfant, I.; Buron-Le Cointe, M. *Inorg. Chem.* **2016**, *55* (9), 4117–4123.

(27) Tfouni, E.; Krieger, M.; McGarvey, B. R.; Franco, D. W. *Coord. Chem. Rev.* **2003**, *236* (1–2), 57–69.

(28) Pestana, C. R.; Phelippin, D. P. S.; Polizello, A. C. M.; Dorta, D. J.; Uyemura, S. A.; Santos, A. C.; Doro, F. G.; Rodrigues, F. P.; Tfouni, E.; Curti, C. *Nitric Oxide* **2009**, *20* (1), 24–30.

(29) Melo Pereira, J. C.; Carregaro, V.; Costa, D. L.; Santana da Silva, J.; Cunha, F. Q.; Franco, D. W. *Eur. J. Med. Chem.* **2010**, *45* (9), 4180–4187.

(30) Tfouni, E.; Truzzi, D. R.; Tavares, A.; Gomes, A. J.; Figueiredo, L. E.; Franco, D. W. *Nitric Oxide* **2012**, *26* (1), 38–53.

(31) Ford, P. C. *Nitric Oxide* **2013**, *34*, 56–64.

(32) Caramori, G. F.; Frenking, G. *Organometallics* **2007**, *26* (24), 5815–5825.

(33) Caramori, G. F.; Kunitz, A. G.; Andriani, K. F.; Doro, F. G.; Frenking, G.; Tfouni, E. *Dalton Trans.* **2012**, *41* (24), 7327.

(34) Andriani, K. F.; Caramori, G. F.; Doro, F. G.; Parreira, R. L. T. *Dalton Trans.* **2014**, *43* (23), 8792–8804.

(35) Delcey, M. G.; Freitag, L.; Pedersen, T. B.; Aquilante, F.; Lindh, R.; González, L. *J. Chem. Phys.* **2014**, *140* (17), 174103.

(36) Freitag, L.; Knecht, S.; Keller, S. F.; Delcey, M. G.; Aquilante, F.; Pedersen, T. B.; Lindh, R.; Reiher, M.; Gonzalez, L. *Phys. Chem. Chem. Phys.* **2015**.

(37) Also known as trans-[RuCl(py)4(NO)]2+ and trans-[Ru(py)4Cl(NO)]2+.

(38) Göttle, A. J.; Dixon, I. M.; Alary, F.; Heully, J.-L.; Boggio-Pasqua, M. *J. Am. Chem. Soc.* **2011**, *133* (24), 9172–9174.

(39) Vieuxmaire, O. P. J.; Piau, R. E.; Alary, F.; Heully, J.-L.; Sutra, P.; Igau, A.; Boggio-Pasqua, M. *J. Phys. Chem. A* **2013**, *117* (48), 12821–12830.

(40) Göttle, A. J.; Alary, F.; Dixon, I. M.; Heully, J.-L.; Boggio-Pasqua, M. *Inorg. Chem.* **2014**, *53* (13), 6752–6760.

(41) Ciofini, I.; Daul, C. A.; Adamo, C. *J. Phys. Chem. A* **2003**, *107* (50), 11182–11190.

(42) Ciofini, I.; Lainé, P. P.; Bedioui, F.; Daul, C. A.; Adamo, C. *Comptes Rendus Chim.* **2006**, *9* (2), 226–239.

(43) King, A. W.; Jin, Y.; Engle, J. T.; Ziegler, C. J.; Rack, J. J. *Inorg. Chem.* **2013**, *52* (4), 2086–2093.

(44) King, A. W.; McClure, B. A.; Jin, Y.; Rack, J. J. *J. Phys. Chem. A* **2014**, *118* (45), 10425–10432.

(45) Coe, B. J.; Meyer, T. J.; White, P. S. *Inorg. Chem.* **1995**, *34* (3), 593–602.

(46) Heully, J.-L.; Alary, F.; Boggio-Pasqua, M. *J. Chem. Phys.* **2009**, *131* (18), 184308.

(47) Freitag, L.; González, L. *Inorg. Chem.* **2014**, *53* (13), 6415–6426.

(48) Salassa, L.; Garino, C.; Salassa, G.; Gobetto, R.; Nervi, C. *J. Am. Chem. Soc.* **2008**, *130* (29), 9590–9597.

(49) Balzani, V.; Ceroni, P.; Juris, A. *Photochemistry and Photophysics: Concepts, Research, Applications*, First.; Wiley-VCH: Weinheim, Germany, 2014.

(50) Ishikawa, T.; Tanaka, K. *Z. Für Krist.* **2008**, *223* (4–5/2008), 334–342.

(51) Lee, C.; Yang, W.; Parr, R. G. *Phys. Rev. B* **1988**, *37* (2), 785.

(52) Becke, A. D. *J. Chem. Phys.* **1993**, *98* (7), 5648.

(53) Adamo, C.; Barone, V. *J. Chem. Phys.* **1999**, *110* (13), 6158–6170.

(54) Tao, J.; Perdew, J. P.; Staroverov, V. N.; Scuseria, G. E. *Phys. Rev. Lett.* **2003**, *91* (14), 146401.

(55) Xu, X.; Goddard, W. A. *Proc. Natl. Acad. Sci. U. S. A.* **2004**, *101* (9), 2673–2677.

(56) Chai, J.-D.; Head-Gordon, M. *J. Chem. Phys.* **2008**, *128* (8), 84106.

(57) Perdew, J. P.; Burke, K.; Ernzerhof, M. *Phys. Rev. Lett.* **1996**, *77* (18), 3865–3868.

(58) Perdew, J. P.; Burke, K.; Ernzerhof, M. *Phys. Rev. Lett.* **1997**, *78* (7), 1396–1396.

(59) Angeli, C.; Cimiraglia, R.; Evangelisti, S.; Leininger, T.; Malrieu, J.-P. *J. Chem. Phys.* **2001**, *114* (23), 10252–10264.

(60) Angeli, C.; Cimiraglia, R.; Malrieu, J.-P. *Chem. Phys. Lett.* **2001**, *350* (3–4), 297–305.

(61) Angeli, C.; Cimiraglia, R.; Malrieu, J.-P. *J. Chem. Phys.* **2002**, *117* (20), 9138–9153.

(62) Hauser, A.; Enachescu, C.; Daku, M. L.; Vargas, A.; Amstutz, N. *Coord. Chem. Rev.* **2006**, *250* (13–14), 1642–1652.

(63) Cowan, D. O.; Drisko, R. L. In *Elements of Organic Photochemistry*; Plenum Press: New York, 1976; pp 1–18.

(64) Turro, N. J. *Modern Molecular Photochemistry*; University Science Books: Mill Valley, 1991.

(65) Klessinger, M.; Josef, M. *Excited States and Photochemistry of Organic Molecules*; VCH: New York, 1995.

(66) Turro, N. J.; Scaiano, J. C. *Principles of Molecular Photochemistry*; University Science Books: Sausalito, 2009.

(67) Klan, P.; Wirz, J. *Photochemistry of Organic Compounds*; John Wiley & Sons: Chichester, 2009.

(68) Bernardi, F.; Olivucci, M.; Robb, M. A. *Chem. Soc. Rev.* **1996**, *25* (5), 321–328.

(69) Robb, M. A.; Garavelli, M.; Olivucci, M.; Bernardi, F. *Rev. Comput. Chem.* **2000**, *15*, 87–146.

(70) Bearpark, M. J.; Robb, M. A. In *Reviews of reactive intermediate chemistry*; Wiley: New Jersey, 2007; pp 379–414.

(71) Garavelli, M. *Theor. Chem. Acc.* **2006**, *116* (1–3), 87–105.

(72) Levine, B. G.; Martínez, T. J. *Annu. Rev. Phys. Chem.* **2007**, *58* (1), 613–634.

(73) Matsika, S.; Krause, P. *Annu. Rev. Phys. Chem.* **2011**, *62* (1), 621–643.

(74) Domcke, W.; Yarkony, D. R. *Annu. Rev. Phys. Chem.* **2012**, *63* (1), 325–352.

(75) Blancafort, L. *ChemPhysChem* **2014**, *15* (15), 3166–3181.

(76) Improta, R.; Santoro, F.; Blancafort, L. *Chem. Rev.* **2016**, *116* (6), 3540–3593.

Résumé

Chapitre III

Après la découverte des isomères métastables du nitroprussiate de sodium, complexe de fer à ligand nitrosyle ($Na_2[Fe(CN)_5(NO)]$), l'intérêt pour ce genre de complexes métalliques n'a pas cessé de croître dans le domaine de la photocristallographie. Cet intérêt est dû principalement à leur réponse photochromique sous irradiation électromagnétique, propriété qui rend ces composés susceptibles d'être utilisés pour la production de nouveaux dispositifs optiques de stockage massif. Le changement de couleur est dû à une photoisomérisation d'enchaînement du ligand nitrosyle, qui pour une longueur d'onde appropriée, bascule entre ses formes nitrosyle **GS** (lié par l'azote), isonitrosyle **MS1** (lié par l'oxygène) ainsi qu'une forme intermédiaire d'hapticité deux appelé **MS2**. Malgré les nombreuses études théoriques et expérimentales, la compréhension mécanistique de la photoisomérisation d'enchaînement depuis l'absorption initiale d'un photon jusqu'à la formation d'un nouvel isomère (photoproduit) restait à élucider.

La stratégie utilisée dans cette étude, similaire à celle mise à point pour décrire la photoréactivité de divers complexes polypyridines de ruthénium, a permis d'établir le mécanisme de photoisomérisation d'un complexe de ruthénium mononitrosyle, *trans*-$[RuCl(NO)(py)_4]^{2+}$, qui présente un taux de photoconversion sans précédent (*ca*. 100%). Cette étude basée sur la caractérisation du chemin photochimique sur la surface d'énergie potentielle de l'état excité triplet le plus bas, calculée à l'aide de la Théorie de la Fonctionnelle de la Densité (DFT), montre comment, grâce à plusieurs points de croisement inter-système le long de ce chemin, la photoisomérisation de Ru−NO vers Ru−ON peut se produire, malgré les hautes barrières énergétiques trouvées.

La caractérisation théorique par DFT de la surface d'énergie potentielle de l'état fondamental (singulet) reproduit parfaitement la tendance énergétique mesurée expérimentalement pour les trois isomères avec comme isomère le plus bas en énergie **GS** (ground-state), un isomère métastable **MS1** plus haut et un dernier isomère métastable **MS2** qui d'un point de vue énergétique et géométrique est à mi-chemin entre **GS** et **MS1**. L'ordre énergétique des trois isomères trouvés est parfaitement expliqué à l'aide d'une analyse par orbitales naturelles de liaison (NBO). **GS** étant l'isomère le plus stable, présente trois hyperliaisons, tandis que **MS2** en présente seulement une. En revanche, à la différence de **GS** et de **MS1**, **MS2** est décrit par un seul fragment car une orbitale de liaison est trouvée entre l'azote et le ruthénium. Finalement, avec une énergie légèrement plus élevée que **MS2**, **MS1** présente deux hyperliaisons. D'un point de vue cinétique, comme observées

expérimentalement, les barrières énergétiques trouvées dans l'état fondamental sont trop élevées pour que la réaction d'isomérisation se produise thermiquement.

La caractérisation de la surface triplet de plus basse énergie montre aussi l'existence de trois isomères le long de cette surface : ^{3}**GS** toujours lié par l'azote, ^{3}**MS1** lié par l'oxygène et une forme intermédiaire entre les deux, ^{3}**MS2**, également d'hapticité deux comme son homologue dans l'état fondamental. À la différence des autres complexes polypyridines de ruthénium aucun état triplet centré sur le métal (^{3}**MC**) n'a été identifié. En revanche, tous les états triplets trouvés peuvent être décrits comment étant des états à transfert de charge du métal vers le ligand (^{3}**MLCT**) nitrosyle. Quant aux barrières énergétiques trouvées, une photoisomérisation adiabatique de Ru−NO vers Ru−ON le long de cette surface triplet est encore défavorable dû à la hauteur de la première barrière ainsi qu'au caractère endothermique du processus.

La description des spectres d'absorption des trois isomères **GS**, **MS2** et **MS1** à l'état fondamental fournie par la DFT dépendante du temps (TD-DFT) donne des éléments fondamentaux pour la compréhension du mécanisme de photoisomérisation pour l'aller comme pour le retour du complexe *trans*-$[RuCl(NO)py_4]^{2+}$. **MS2** présente des bandes d'absorption communes à l'isomère **GS** ainsi qu'à l'isomère **MS1**, ce qui le singularise comme une structure clé pour les deux mécanismes de photoisomérisation d'enchaînement ; celui d'aller de Ru−NO (**GS**) vers Ru−ON (**MS1**) et celui de retour de Ru−ON (**MS1**) vers Ru−NO (**GS**). Une autre caractéristique très importante des spectres est l'absence de bandes d'absorption de l'isomère **MS1** dans la zone d'irradiation expérimentale. Une fois formé, **MS1** ne subit pas de réaction photochimique. C'est ainsi que des taux de photoconversion aussi élevés peuvent être expliqués.

Grâce à la caractérisation des différents croisements entre la surface de l'état fondamental et la surface de plus basse énergie de l'état triplet, les différents mécanismes de photoisomérisation d'aller-retour ont pu être éclaircis. Le mécanisme de photoisomérisation d'enchaînement de **GS** vers **MS1** peut être conçu comme un processus séquentiel à deux étapes : l'absorption d'un premier photon permet la photoisomérisation du **GS** vers **MS2**, tandis que l'absorption d'un deuxième photon permet la transformation du **MS2** en **MS1**. Après l'absorption initiale d'un premier photon bleu à 473 nm à partir de l'isomère **GS** dans son état fondamental, le système est excité vers des états singulets. Grâce au phénomène

relativiste du couplage spin-orbite la désactivation non-radiative du système vers des états triplets depuis les états singlets excités par croisement inter-système est tout à fait possible. En effet, la transition non-radiative très efficace vers les états triplets est très bien documentée pour les complexes polypyridines de ruthénium. En supposant que le système se désactive vers les états triplets, il peut, par conversion interne, se relaxer vers le triplet de plus basse énergie **^{3}GS,** et ensuite se dépeupler par croisement inter-système vers l'isomère **MS2**. Alternativement, l'isomère **MS2** pourrait être peuplé depuis des états triplets de plus haute énergie. Pour essayer de clarifier ce dernier point, une étude dynamique qui complèterait cette étude statique d'exploration des surfaces d'énergie potentielles pourrait être envisagée (voir Chapitre V). Une fois que le système est relaxé à la géométrie de l'isomère **MS2** à l'état fondamental, il est ré-excité par absorption d'un deuxième photon bleu, et en suivant un processus de relaxation similaire à celui décrit pour l'isomère **GS**, le système peut se relaxer vers l'isomère **^{3}MS2**. Une fois dans l'état **^{3}MS2**, la réaction de photoisomérisation devient favorable du point de vue cinétique (petite barrière énergétique pour passer de **^{3}MS2** à **^{3}MS1**) ainsi que du point de vue thermodynamique (étape exothermique). Un croisement entre les surfaces triplet de plus basse énergie et la surface de l'état fondamental permet le passage du **^{3}MS1** à **MS1** par un dernier croisement inter-système, qui amène le système au photoproduit final.

La photoisomérisation de retour de l'isomère **MS1** vers l'état fondamental **GS** peut être déclenchée par deux types différents de longueurs d'onde (rouge et infrarouge), lesquels conduisent à des chemins de réaction différents. Expérimentalement, sous irradiation dans le rouge, l'isomère **MS1** est directement converti en isomère **GS**, alors que sous irradiation infrarouge, un mélange 1:1 de **GS** et **MS2** est observé.

Le premier mécanisme de photoisomérisation du **MS1** vers **GS** a beaucoup de points en commun avec celui du sens inverse (**GS** vers **MS1**). Il peut impliquer soit un mécanisme séquentiel à deux photons, soit un mécanisme à un photon. Après l'absorption initiale d'un premier photon rouge à 782 nm à partir de l'isomère **MS1** à l'état fondamental, le système est excité vers des états singulets plus hauts en énergie. En suivant un mécanisme de relaxation similaire à celui décrit pour l'isomère **GS**, le système peut se relaxer vers **^{3}MS1**, et ensuite surmonter une petite barrière pour former **^{3}MS2**. Alternativement, l'état **^{3}MS2** pourrait être peuplé depuis des états triplets de plus haute énergie. À partir de **^{3}MS2**, le système peut se relaxer par croisement inter-système vers **MS2** à l'état fondamental singulet, lequel absorbe

aussi à 782 nm. L'absorption d'un deuxième photon rouge à partir du **MS2** amène le système vers des états excités qui peuvent se relaxer vers le triplet ^{3}**MS2** ou directement vers le triplet ^{3}**GS** qui ensuite conduit à l'isomère **GS**. De plus, il existe une voie de réaction alternative une fois que le système atteint ^{3}**MS2**, impliquant un seul photon. En franchissant une petite barrière, ^{3}**MS2** peut former ^{3}**GS**, qui par un croisement inter-système reconduit à la formation de l'isomère **GS**.

Le deuxième mécanisme de photoisomérisation du **MS1** vers **GS** est initié par l'absorption d'un photon infrarouge à 980 nm. Afin de pouvoir expliquer cette photoréactivité il faut admettre que dans une première étape du mécanisme un croisement inter-système amène le complexe de l'isomère **MS1** vers le triplet ^{3}**MS1**, et c'est justement cet état triplet qui absorbe un photon dans l'infrarouge. L'absorption d'un photon à partir de ^{3}**MS1** excite le système vers des états triplets plus hauts en énergie, lesquels peuvent se relaxer par conversion interne vers l'état triplet ^{3}**MS2**. Exactement comme dans le mécanisme avec des photons rouges, une fois que le système atteint ^{3}**MS2**, il peut soit se relaxer vers l'isomère **MS2** à l'état fondamental singulet, soit se transformer en ^{3}**GS** qui ensuite devient l'isomère **GS**. À la différence des deux autres mécanismes avec de la lumière bleue et rouge, **MS2** n'absorbe pas dans l'infrarouge, et c'est pour cette raison qu'expérimentalement un mélange de **GS** et **MS2** est observé à l'issue d'une irradiation avec de la lumière infrarouge.

Pour conclure, cette étude mécanistique de la photoisomérisation d'enchaînement réversible du complexe *trans*-$[RuCl(NO)py_4]^{2+}$ a pu montrer que trois isomères, Ru−NO (**GS**), Ru−η^2−NO (**MS2**) et Ru−ON (**MS1**) sont successivement peuplés pendant la photoisomérisation comme il avait déjà été bien établi expérimentalement. Les surfaces de l'état fondamental singulet ainsi que de l'état triplet de plus basse énergie montrent que l'isomérisation de **GS** vers **MS1** est un processus non favorable ni d'un point de vue cinétique ni d'un point de vue thermodynamique, et c'est pour cette raison que l'intervention de deux photons est nécessaire. Pour la photoisomérisation du **MS1** vers **GS** avec la lumière rouge, deux mécanismes différents qui impliquent l'absorption d'un ou de deux photons coexistent. En revanche, un seul mécanisme mettant en jeu uniquement un photon est impliqué dans la photoconversion avec l'infrarouge donnant un mélange du **GS** et **MS2** dans le même cristal. Il est important de rappeler le rôle crucial de l'isomère **MS2**, autant au niveau géométrique, car il a une structure intermédiaire entre **GS** et **MS1**, qu'au niveau optique, car il présente des bandes d'absorption communes à **GS** et **MS1**, condition fondamentale pour les mécanismes

séquentiels à deux photons. Pour compléter ce travail, il faudrait mener une étude dynamique qui pourrait répondre aux questions qui restent encore en suspens comme par exemple celle concernant le chemin de relaxation conduisant à l'isomère **MS2** dans son état fondamental lors du mécanisme de photoisomérisation du **GS** vers **MS1**.

Chapter IV

Photorelease *vs.* Photoisomerization in Ruthenium Nitrosyl Complexes

In this chapter the competition between intramolecular NO photoinduced linkage isomerization and NO photorelease in five nitrosyl ruthenium complexes is presented. The chapter is organized as follows: First the five nitrosyl ruthenium complexes in their ground state (**GS**) and in their two metastable states (**MS1** and **MS2**) are presented, followed by a characterisation of the associated lowest triplet states (^{3}**GS**, ^{3}**MS1** and ^{3}**MS2**). This is followed by a discussion of the TD-DFT absorption spectra of the four complexes in their **GS** and MS states to assign the main electronic transitions and to establish a general picture of the subtle wavelength dependency of the photoreactivity on these complexes. Finally, the lowest triplet PESs are reported to discuss the fate of the intermediates involved in the photoisomerization process and to introduce the photorelease pathway in a general scheme. All this information contributes to shed some light on the difference of photoreactivity of these complexes. (A detailed explanation of all technical details: method, basis set, and the programs used can be found in the Computational details in Appendix C).

4.1 Motivation

As explained in Chapter I, ruthenium nitrosyl complexes receive a lot of attention from the research community as they could be of interest as optical switches, in data storage, or in the medical field. Indeed, these molecules are an important family of NO delivering agents. NO is a signalling molecule in vascular biology (Nobel prize in medicine, 1998) and is involved in various physiological processes such as neurotransmission and death of cancer cells.[1] Moreover, NO causes also apoptosis (cell death) of healthy cells. Thus, numerous studies now aim at photocontrolling the release of NO locally, which could be useful in the treatment of cancer by photodynamic therapy.

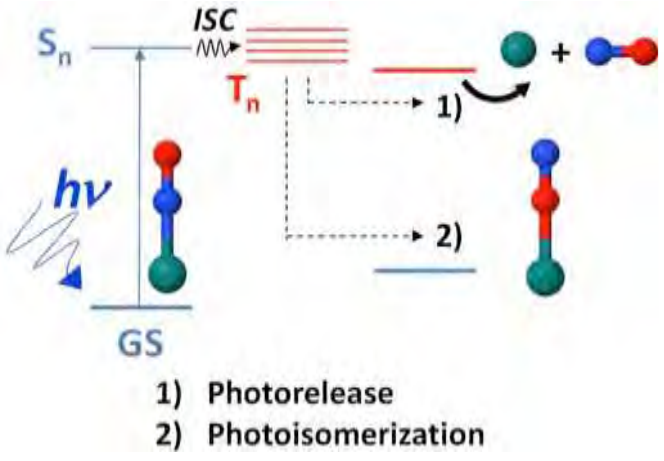

Figure 4.1: Scheme of the possible photoreactions pathways that ruthenium nitrosyl complexes may undergo after irradiation.

For this purpose, theory may help in providing mechanistic insights regarding the photoactivity of these complexes. The aim of this study consists in gaining a detailed understanding of the NO photorelease mechanism. This will require the identification of the electronic state(s) involved in this process and the characterization of the photochemical pathways. Once the mechanism is understood, it will be possible to propose new candidates bearing appropriate ligands which will lead to a higher NO release efficiency and which can provoke this photorelease under visible-near IR irradiation, as UV light is harmful for the living cells.

Beside their ability to photorelease NO and as schematized on Figure 4.1, ruthenium nitrosyl complexes are able to undergo photoinduced isomerization.[2–12] In solution, it is more or less admitted that these two processes are exclusive, *i.e* complexes known to photoisomerize are less efficient to photorelease NO. At lower temperature and/or in solid state, coexistence of these two photoprocesses has been uncovered in the founding works of Woike *et al.*[10] and of Bitterwolf.[9] They highlight the role of the linkage isomers in the photorelease of NO and suggest that they could be intermediates in the photochemical NO loss. They also discuss about a possible connection between photo linkage isomerism and photorelease, which may be either consecutive or competing or non-related phenomena. Recent theoretical studies have proposed a mechanistic picture of the intramolecular photoisomerization of NO in *trans*-$[RuCl(NO)(py)_4]^{2+}$ (see Chapter III),[13] and have also investigated the initial stages of the NO photorelease in another ruthenium nitrosyl complex.[14] Based on these preliminary results, DFT calculations have been performed on two sets of ruthenium nitrosyl complexes in order to identify the factors controlling the photoactivity: photoisomerization *vs*. photorelease.

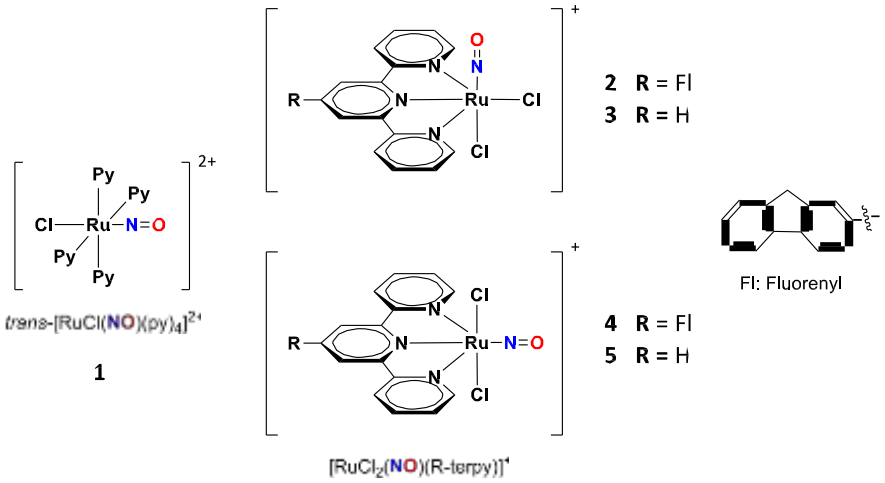

Figure 4.2: Families of ruthenium nitrosyl complexes studied in this work.

These complexes are: the well-studied *trans*-$[RuCl(NO)(py)_4]^{2+}$, compound **1**, and a series of $[RuCl_2(NO)(R\text{-terpy})]^+$ compounds **2**, **3**, **4** and **5** (Figure 4.2). **1** is well-known to undergo a photoisomerization process in a crystalline environment,[6–8] while under suitable conditions **2**, **3** and **4** photorelease NO in solution with different yields.[15,16] De Candia *et al.*[17] have shown that **1** may also photorelease NO but with quite low quantum yields,[17] namely $\varphi_{NO} = 1.6 \cdot 10^{-3}$ mol·einstein^{-1} while compounds **2** and **4** show a quantum yield two orders of magnitude higher, being $\varphi_{NO} = 3.1$ and $1.1 \cdot 10^{-1}$ mol·einstein^{-1} respectively. Complex **3** has been extensively studied by Karidi *et al.*, but no quantum yield of photorelease has been reported. Regarding complex **5**, to our knowledge, experimental data deal only with ground state reactivity.[18]

The aim of the present investigation is first to propose photophysical pathways consistent with the ability of nitrosyl ruthenium complexes to undergo photoisomerization and/or photorelease of NO. The second objective is an attempt to rationalise the different photorelease quantum yields, in particular between the *cis*- and *trans*-$[RuCl_2(NO)(R\text{-terpy})]^+$ complexes. To reach these goals, two hypotheses based on previous theoretical works[13,14] were made. To discuss the factors which govern the balance between photoisomerization and photorelease, it has been assumed that:

1) population of initial singlet states by photon absorption was followed by rapid intersystem crossing (ISC) and thus

2) photoactivity (photoisomerization and photorelease) takes place on the lowest triplet potential energy surface (PES), as it is generally assumed for ruthenium complexes.

4.2 Characteristics of the Ru−NO Complexes Studied

The existence of different linkage isomers in ruthenium nitrosyl complexes, for instance in complex **1**, is well documented experimentally[19–21] and theoretically.[22–26] The lowest ground-state species (**GS**) is characterized by an N-bound form of the nitrosyl ligand to the ruthenium atom, while the isonitrosyl metastable isomer called **MS1** (metastable 1) is oxygen-bound and the sideways-bound isomer is called **MS2**. Hereafter, we assumed that the active structures, which take part in the photoisomerization process for complexes **2**, **3**, **4** and **5**, are similar to those commonly and previously encountered. As shown before,[13] the structures of the three isomers **GS**, **MS1** and **MS2** of compound **1** are well reproduced with B3LYP. With the same methodology, **GS**, **MS2** and **MS1** structures have been found in the singlet and in their corresponding lowest triplet state (^{3}**GS**, ^{3}**MS2** and ^{3}**MS1**) for the other four complexes. The existence as minima of all the isomers suggests that all four complexes may potentially photoisomerize in solution like for complex **1**. From a structural point of view, during the photoisomerization the main geometrical changes occur within the ruthenium nitrosyl moiety as for compound **1**. The most relevant geometrical parameters of the optimized structures, selected bond lengths, bond and dihedral angles are listed in Appendix C Tables AC1−AC30. The structure of the RuCl(R-terpy) core is almost unaltered and changes very little with the nature of the ligand. The exploration of the lowest triplet PESs shows that the electronic nature, spin densities, and geometries of the three minima found for the $[RuCl_2(NO)(R\text{-terpy})]^+$ complexes are comparable to those found for *trans*-$[RuCl(NO)py_4]^{2+}$, being of MLCT nature (Ru(*d*) ▪▪ NO(π*)) with a spin density on the ruthenium atom which varies between 0.70 and 0.97. As in the case of compound **1**, no metal-centered (^{3}MC) state has been identified for any of the complexes studied. More information about the electronic nature and the geometries at each minima found on the triplet PES can be found in Appendix C Tables AC4−AC6, AC10−AC12, AC17−AC18, AC22−AC24, AC28−AC30.

4.3 Absorption Spectra of the GS, MS1 and MS2 Isomers of all Complexes

In this section the computed TD-DFT spectra are compared for the five complexes in order to pinpoint key factors that rationalize the photoactivity of this family of nitrosyl complexes. At 473 nm, under continuous irradiation, complex **1** (solid state) undergoes linkage photoisomerization (Ru−NO ⁘ Ru−ON) with a yield approaching 100%,[7] while continuous irradiation of this same complex in solution at 455 nm leads to the photorelease of NO.[17] In previous theoretical and experimental studies,[13] we have already highlighted the importance of the existence of overlapping absorption bands (400 to 500 nm) for the **GS** and **MS2** isomers for the photoisomerization process. Indeed this peculiarity provides the framework to a sequential two-photon absorption mechanism. Now, we suspect that the similarity in the **GS** and **MS2** absorption wavelengths is able to trigger two very different outcomes.

Experimental data for compounds **2, 3** and **4** are scarce. Continuous irradiation of **2** and **4** in solution at 405 nm[16] and continuous irradiation with a mercury lamp of compound **3**[15] bring about the departure of their nitrosyl ligand. Figures 4.4−4.8 show the TD-DFT simulated spectra of the five compounds, and the NTOs of interest. The excitations are shown in detail in Appendix C Table AC31. TD-DFT calculations compare very well with experiment, with maximum discrepancies of about 0.2 eV, which falls in the accepted range of error for such a method.

It should be noted that the lowest singlet states with a significant oscillator strength for complexes **2**, **3**, **4** and **5** were identified to be essentially ligand to metal ligand charge transfer (^{1}LMLCT) fluorenyl (π) ⁘ Ru(*d*)NO(π*) in nature, in contrast to the lowest excited singlet state of compound **1** which is a true ^{1}MLCT Ru(*d*) ⁘ (Ru(*d*)NO(π*). Another striking feature is the hyperchromic effect observed for compounds **2**, **3**, **4** and **5** with respect to compound **1**. This dramatic effect is due to the substitution of pyridine by more extended π-conjugated systems. The terpyridine ligand acts as an antenna increasing the intensity of the LMLCT absorption bands near the visible region. Complexes **2** and **4** show the most intense absorption bands due to the extended conjugated system brought by the fluorenyl moiety (Figures 4.5 and 4.7). The same reasons can be invoked to explain the bathochromic effect of the fluorenyl ligand. Introduction of this more extended ligand causes a redshift of the main

absorption band in the visible region by lowering the energy of the fluorenyl(π) ⁚ Ru(*d*)NO(π*) transitions.

Table 4.1: Energy gaps (eV) between the HOMO and the antibonding RuNO and RuON MOs for the GS and MS1 isomers, and corresponding Mayer bond orders.

	1	**2**	**3**	**4**	**5**
GS ΔE(HOMO-(RuNO)*)	3.6	4.6	5.8	4.4	5.6
Mayer Bond Order Ru−N	1.65	1.47	1.47	1.47	1.47
MS1 ΔE(HOMO-(RuON)*)	2.6	3.6	4.8	3.5	4.6
Mayer Bond Order Ru−O	0.90	0.71	0.72	0.65	0.57

Another general trend observed for all these compounds concerns the redshift of the **MS1** spectra with respect to the **GS** ones. In the case of **MS1**, the interaction between the Ru(d_{xz}, d_{yz}) and the NO(π_x^*, π_y^*) orbitals can be expected to be weaker, leading to smaller energy gaps between the bonding and the corresponding antibonding molecular orbitals resulting in lower electronic transition energies for **MS1** than for **GS**. Mayer bond order analysis, as an estimate of the L_5-Ru and NO/ON orbital overlap, is displayed in Table 4.1 and supports this observation showing that the Ru−ON bond order is smaller by a factor of two than the Ru−NO one. These results are consistent with NBO analysis previously published on **1**.[13] As a consequence, the Ru−ON bonding (antibonding) MOs are higher (lower) in energy than the corresponding Ru−NO MOs (Figure 4.3). Moreover the increase of **ΔE HOMO-(RuNO)*** in **2**, **3**, **4** and **5** with respect to **1** can be explained by the increased π-acceptor capability of terpy *vs.* py, thus resulting in the stabilisation of the L_5-Ru orbital set.

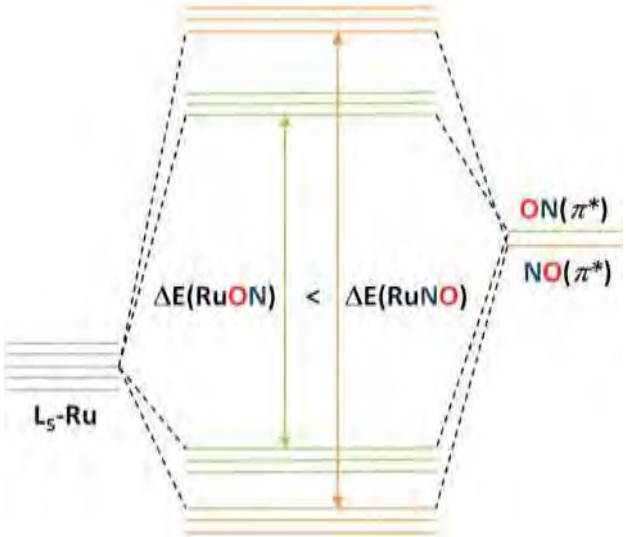

Figure 4.3: Schematic representation of the RuNO MO diagram for the isomer GS (in orange) and the RuON MO diagram for the isomer MS1 (in green).

The most remarkable difference between the two isomers for both couples of complexes (2,4) and (3,5) appears in the spectrum of the sideways bound isomer, **MS2**. While **MS2** of the *cis*- complex absorbs at 338 nm, near the main absorption band of **GS** (314 nm), **MS2** of the *trans*- complex absorbs at 389 nm (*ca*. 0.5 eV lower in energy). This band poorly overlaps with the main absorption band of **GS** at 325 nm, disfavouring the sequential absorption of a second photon by *trans*-**MS2** and subsequently the population of *trans*-^{3}**MS2**, which has been identified as a key step for the photoisomerization process in nitrosyl ruthenium complexes. This observation should be kept in mind as it may provide an explanation for the lower quantum yield of photorelease of *trans*- isomers. Finally, an important difference emerges for the *cis*- and the *trans*- complexes bearing a fluorenyl ligand. Indeed, in compound **2,** the *cis*-**MS2** isomer shows two absorption bands at 396 nm and 352 nm surrounding the main absorption band of **GS** (384 nm). In complex **4** one of these bands is absent in the *trans*-**MS2** species, making the absorption of a second photon by *trans*-**MS2** less efficient. Moreover, the excitation corresponding to the remaining band at 360 nm (transition number 2 on Figure 4.7) does not involve the nitrosyl ligand (fluorenyl(π)Ru(*d*) ▪▪ terpy(π*)Ru(*d*)), which may affect the quantum yield of the photochemical reaction in **4**. This suggests that differences in the photoreactivity between *cis*- and *trans*- isomers might be connected with the different absorption properties shown by the sideways bound isomer **MS2** and emphasizing the particular role of the **MS2** isomer in the photochemistry of this family of complexes.

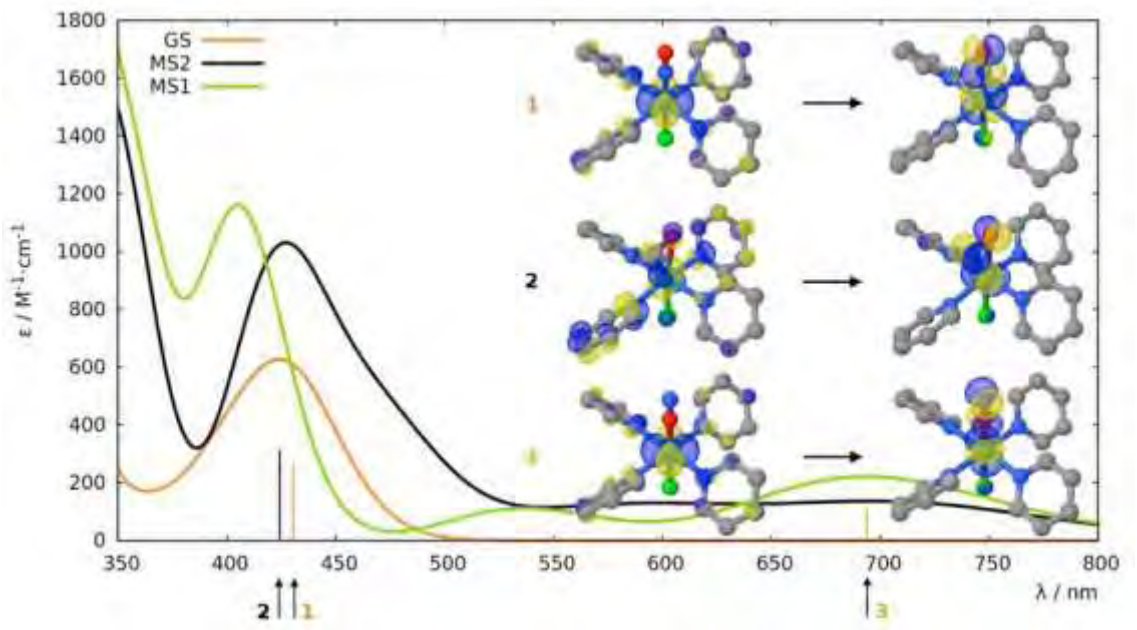

Figure 4.4: TD-DFT spectra of the three linkage isomers (GS in orange, MS2 in black and MS1 in green) of *trans*-[RuCl(NO)(py)$_4$]$^{2+}$ (complex 1) computed in acetonitrile. Occupied (left) and virtual (right) NTOs for selected transitions.

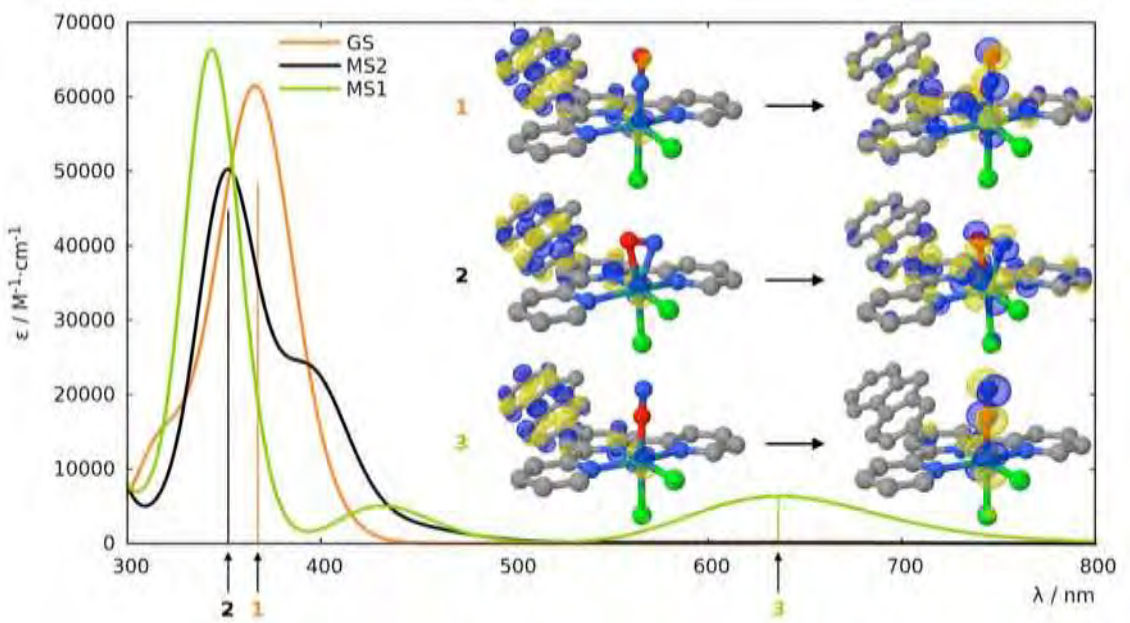

Figure 4.5: TD-DFT spectra of the three linkage isomers (GS in orange, MS2 in black and MS1 in green) of *cis*-(Cl,Cl)[$RuCl_2$(NO)(Fl-terpy)]$^+$ (complex 2) computed in acetonitrile. Occupied (left) and virtual (right) NTOs for selected transitions.

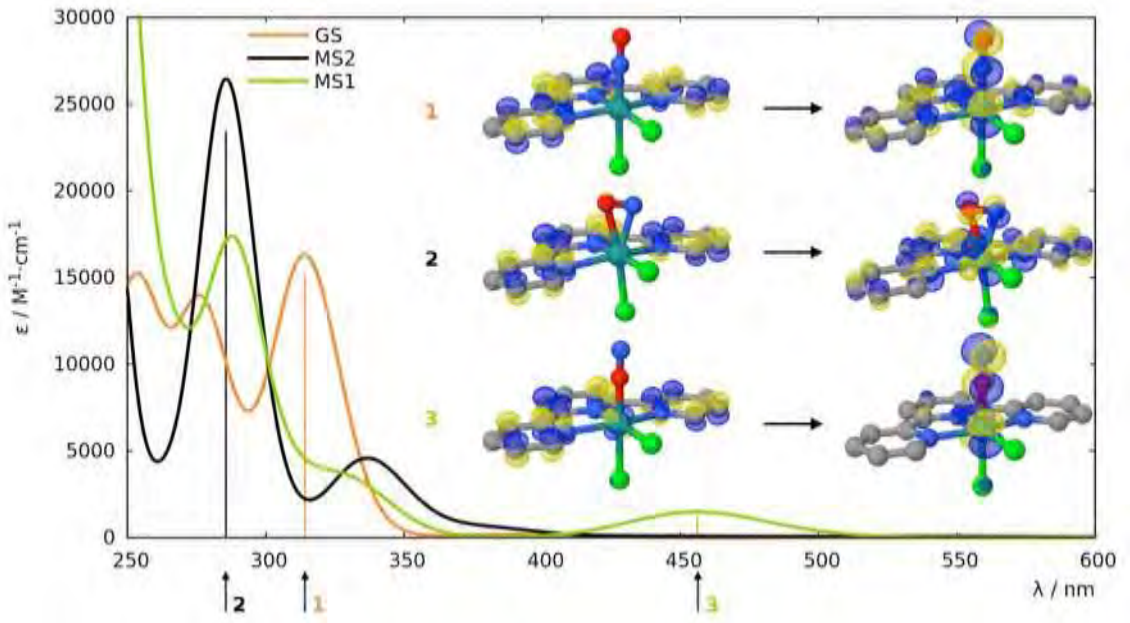

Figure 4.6: TD-DFT spectra of the three linkage isomers (GS in orange, MS2 in black and MS1 in green) of *cis*-(Cl,Cl)[$RuCl_2$(NO)(terpy)]$^+$ (complex 3) computed in acetonitrile. Occupied (left) and virtual (right) NTOs for selected transitions.

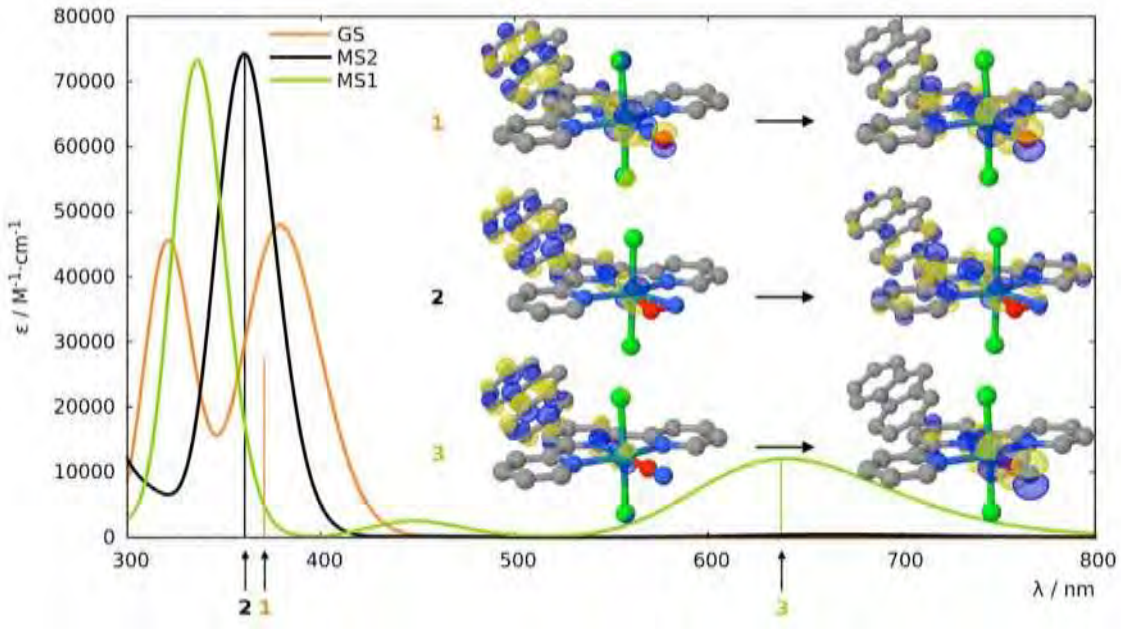

Figure 4.7: TD-DFT spectra of the three linkage isomers (GS in orange, MS2 in black and MS1 in green) of *trans*-(Cl,Cl)[RuCl$_2$(NO)(Fl-terpy)]$^+$ (complex 4) computed in acetonitrile. Occupied (left) and virtual (right) NTOs for selected transitions.

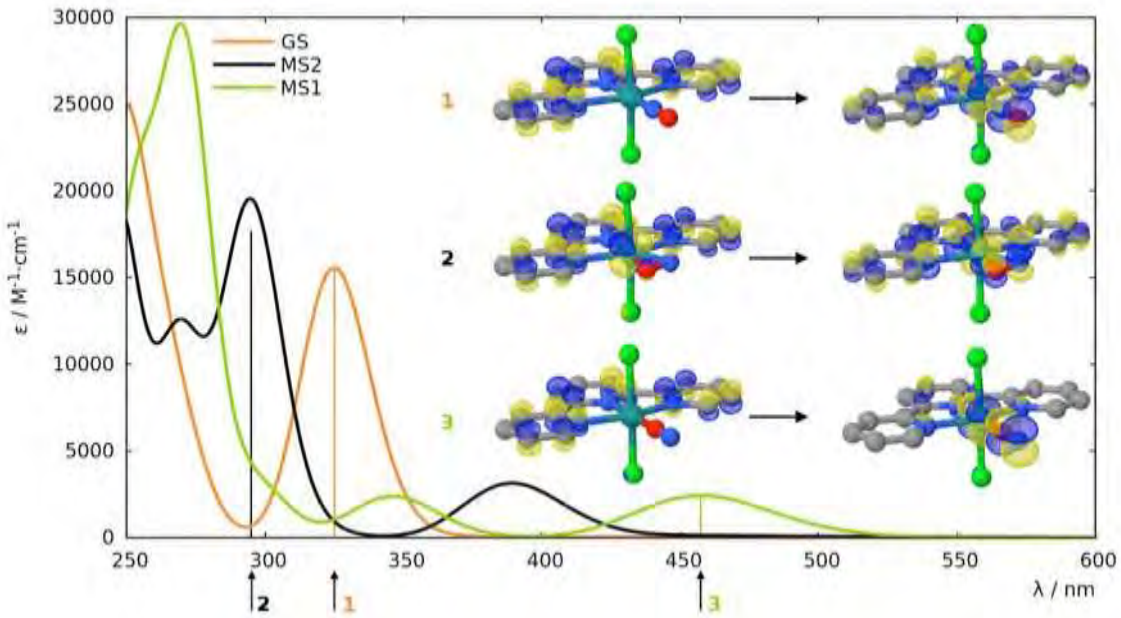

Figure 4.8: TD-DFT spectra of the three linkage isomers (GS in orange, MS2 in black and MS1 in green) of *trans*- (Cl,Cl)[RuCl(NO)(terpy)]$^+$ (complex 5) computed in acetonitrile. Occupied (left) and virtual (right) NTOs for selected transitions.

4.4 Thermal Isomerization and Photoisomerization Pathways

Assuming similar mechanisms as for the photoisomerization of the *trans*-$[RuCl(NO)py_4]^{2+}$ complex, for complexes **2**, **3**, **4** and **5** the full excited adiabatic pathway supporting the photoisomerization mechanism for the conversion from **GS** to **MS1** has been stablished. The main results are summarized in Table 4.2 and in Figure 4.9.

To investigate the validity of the Zero Temperature String (ZTS) methodology used in the calculations of the energy barriers, the previous results obtained on compound **1** through TS optimization followed by IRC calculations were compared to those obtained with the ZTS methodology. As shown in Table 4.2, ZTS results obtained for barriers B1-B4 are comparable with those obtained through TS optimizations, all being contained within 0.2 eV. All the ZTS calculations are shown in Appendix C Figures AC1−AC20.

4.4.1 Thermal Isomerization Pathway

The first step in the thermal isomerization pathway (B1, adiabatic conversion of **GS** to **MS2**) shows similar barriers for all the $[RuCl_2(NO)(R\text{-terpy})]^+$ complexes. Even if all these barriers are smaller by 0.3 eV than the one found for the *trans*-$[RuCl(NO)py_4]^{2+}$ complex **1,** it would be very difficult to overcome B1. B2 (adiabatic conversion from **MS2** to **MS1**) is smaller than B1 but remains highly unfavourable for all the compounds. These results confirm, as pointed out before for *trans*-$[RuCl(NO)py_4]^{2+}$,[13] the thermal stability of these compounds in their ground and metastable states.

4.4.2 Triplet State Adiabatic Pathway

The adiabatic isomerization on the lowest triplet PES involves barriers B3 and B4, which do not vary significantly from one complex to another. The energy barriers to overcome on the triplet PES are reduced with respect to the singlet PES. However, B3 (*ca.* 0.97 eV) is still large and compromises an adiabatic isomerization pathway for the five complexes.

4.4.3 Non Adiabatic Pathway

The four singlet-triplet MECPs found for **1** have also been characterized for each $[RuCl_2(NO)(R\text{-terpy})]^+$ complex. In Table 4.2, barrier B5 is the energy difference found between the ^{3}**GS** isomer and $MECP_2$, as surmounting this barrier represents a crucial step in the photoisomerization pathway. Indeed the existence of $MECP_2$ enables the population of **MS2** from ^{3}**GS**, through intersystem crossing. It is important to remember that B5 is an upper limit for this activation energy, and that **MS2** may be directly populated from higher triplet states, during the relaxation processes of the triplet state(s) initially populated just after photon absorption. Finally, the fact that B4 is always small renders the population of the O-bound isomer (**MS1**) favourable. To conclude, from a mechanistic point of view and as shown for **1**, all the studied complexes may undergo a photoisomerization reaction involving several intersystem crossings.

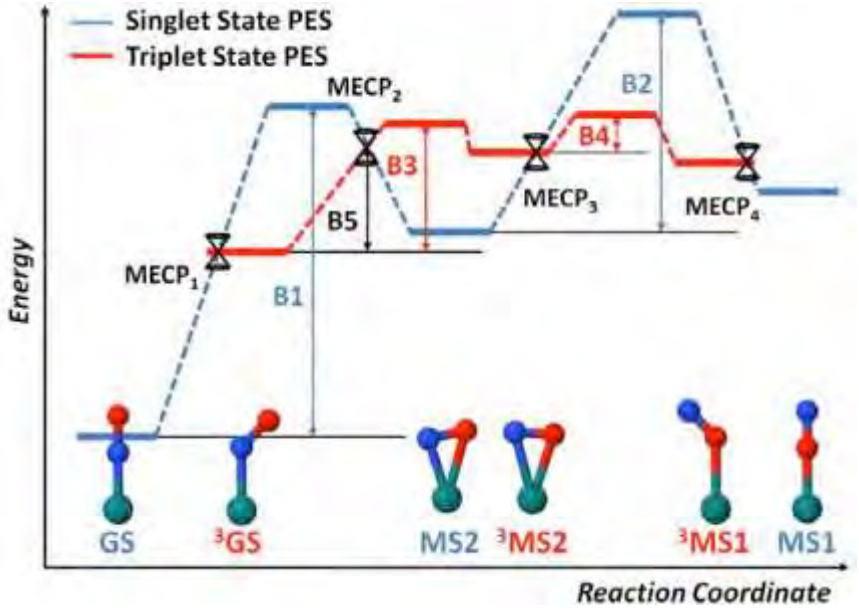

Figure 4.9: Scheme of the entanglement between the singlet and the lowest triplet state potential energy surfaces. The reaction coordinate considered is the Ru-N-O angle. Blue lines represent the singlet state and red lines the triplet state. Singlet-triplet funnels (MECPs) are represented by double-cone pictograms. Barriers B1 (GS-MS2), B2 (MS2-MS1), B3 (^{3}GS-^{3}MS2), B4 (^{3}MS2-^{3}MS1) and B5 (^{3}GS-^{1}MS2) are scaled.

Table 4.2: Comparison of the different energy barriers for the complexes studied for the photoisomerization reaction.

Complex / Barrier	1	2	3	4	5
B1	2.61 (2.44)[a]	2.31	2.29	2.33	2.30
B2	1.48 (1.57)[a]	1.31	1.39	1.62	1.44
B3	1.04 (1.06)[a]	0.96	1.02	0.96	0.98
B4	0.22 (0.26)[a]	0.15	0.18	0.25	0.16
B5	0.63 (0.67)[a]	0.69	0.67	0.83	0.86

[a]In brackets, values obtained from TS optimizations.[13]

4.5 Capability of NO Photorelease from the Three Different Triplet States, ^{3}GS, ^{3}MS2 and ^{3}MS1

Simultaneously, the possible photorelease of NO was investigated. The lowest triplet PES was explored following the bond distances Ru-N_{NO} or Ru-O_{ON} as relevant reaction coordinates. The dissociation curves were computed for all the complexes in their three isomers (**^{3}GS, ^{3}MS2, ^{3}MS1)**, which all are credible candidates for NO photorelease. It is noteworthy that the role of such triplet states in the photorelease process has been already pointed by Karidi *et al.*[15] and De Candia *et al.*[17] The curves representative of the Minimum

Energy Pathway (MEP), optimized using ZTS calculations, are sketched for **2** in Figure 4.10. MEPs for all the other complexes are available in Appendix C Figures AC21−AC25 and the results are summarized in Table 4.3.

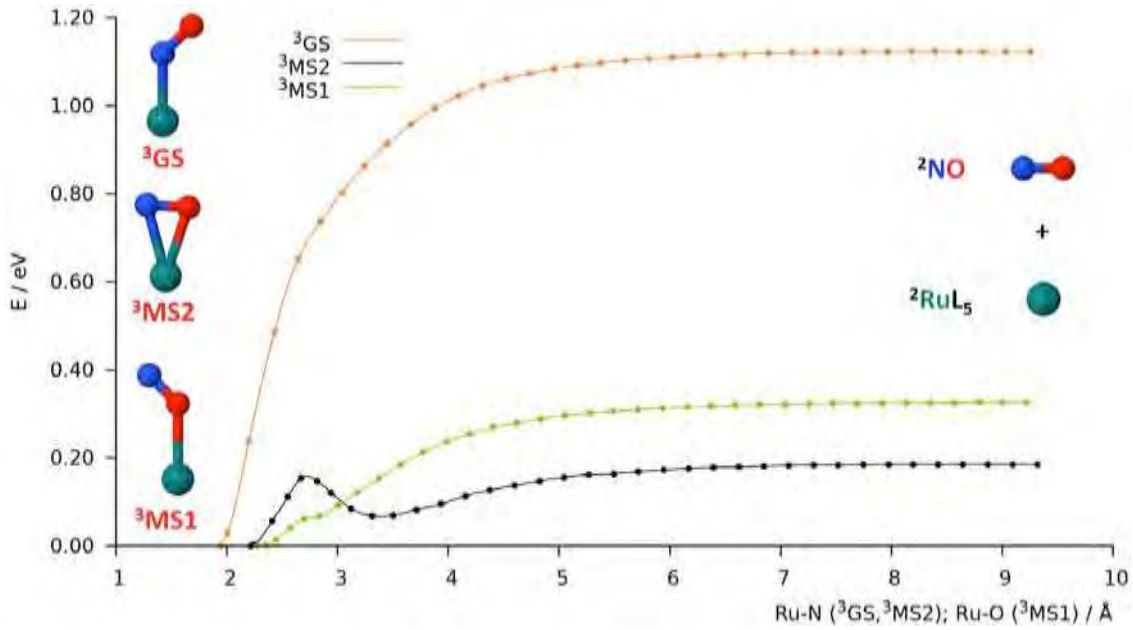

Figure 4.10: Triplet energy profiles for the photorelease pathways from ^{3}GS (orange), ^{3}MS2 (black) and ^{3}MS1 (green) along Ru-N or Ru-O distances for complex 2. For each curve, the zero is set at the respective triplet minimum.

De Candia *et al.*[17] proposed to use the photorelease barrier (bond dissociation energy, D_e), defined from the **^{3}GS**, and to correlate it qualitatively with the experimental quantum yield. In the case of this study, as shown in Table 4.3, the similarly high D_e values found for all the complexes suggest that such a correlation does not apply (here), and that the origin of the different φ_{NO} values cannot be solely justified by D_e calculations. The conclusion of this work is that the mechanism of NO photorelease does not involve a direct release from **^{3}GS**. Thus, the light-induced release of nitric oxide involves other intermediate states, which might determine the quantum yields of the reaction. This is the reason why bond dissociation energies from **^{3}MS$_1$** (D_{e1}) and **^{3}MS$_2$** (D_{e2}) states (Table 4.3) have also been computed. Two important points emerge from these calculations:

1) the D_{e1} and D_{e2} values are much lower than the D_e ones, and

2) the D_{e1} and D_{e2} follow the trend **2**<**4**<**1**, which matches the relative experimental quantum yields. In all cases, the smaller values for D_{e2} confirm the greater ease of

photodissociation from **^{3}MS2** and thus confirm the crucial role of this intermediate for any photoactivity of ruthenium nitrosyl compounds.

Table 4.3: Dissociation energies (eV) D_e, D_{e2}, D_{e1} from the different triplet isomers ^{3}GS, ^{3}MS1, ^{3}MS2, respectively for the five complexes and comparison with the B4 barrier.

	1	2	3	4	5
^{3}GS(D_e)	1.17	1.12	1.08	1.17	1.17
^{3}MS2 (D_{e2})	0.39	0.19	0.21	0.31	0.30
^{3}MS1(D_{e1})	0.52	0.33	0.38	0.46	0.43
D_{e2}–B4[a]	0.17	0.04	0.02	0.06	0.14
D_{e1}–B4[a]	0.30	0.18	0.20	0.21	0.27

[a]**B4 is the energy barrier value associated with ^{3}MS2-^{3}MS1 step defined in Figure 4.9.**

4.6 Discussion: Photorelease *vs.* Photoisomerization

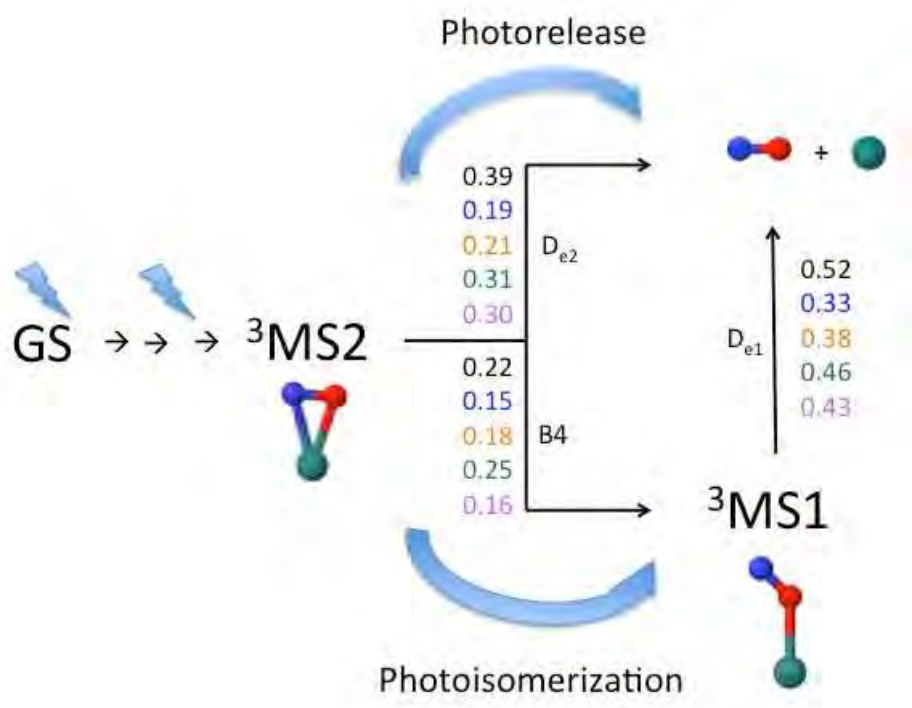

Figure 4.11: Energetic data (eV) of the photorelease (D_{e2} and D_{e1}) of nitric oxide and photoisomerization (B4) of nitrosyl ligand. Data for 1 in black, for 2 in blue, for 3 in orange, for 4 in green and for 5 in purple.

The current understanding of the PESs of the complexes under consideration allows proposing the mechanistic picture shown in Figure 4.11. According to TD-DFT calculations and due to the absorption overlap between **GS** and **MS2**, the sequential two-photon absorption established for complex **1** can be generalized to complexes **2**-**5**. Therefore photoisomerization

and photorelease processes involve the same initial elementary steps. Upon irradiation, the population of a singlet excited state occurs, followed by ultrafast internal conversion and intersystem crossings that lead to the population of ^{3}**GS**. From ^{3}**GS**, the **MS2** isomer can be populated by intersystem crossing at $MECP_2$. **MS2** is a closed-shell species with a rather deep potential well, thus the subsequent step requires the excitation of **MS2** by the means of a second photon, thus populating a new singlet excited states species, which is assumed to decay to ^{3}**MS2**. At this stage two outcomes are possible from the sideways-bound isomer ^{3}**MS2**: NO photorelease or the end of the photoisomerization. The competition between these two processes is most probably controlled by kinetics, *i.e.*, by the difference between the D_{e2} dissociation energy and the B4 isomerization barrier.

The manifold of low-lying excited states looks qualitatively very similar for all the complexes, but is in fact quantitatively different. Indeed, upon comparing the values of D_{e2} (Table 4.3) and B4 (Table 4.2), two situations can be distinguished, associated with two diverging pathways: D_{e2} < B4 would favour the departure of nitric oxide, while D_{e2} > B4 would promote the linkage isomerization of NO. As shown in Figure 4.11, the predicted D_{e2} values are on the order of those of B4 for the two *cis*-isomers, indicating that the two photoprocesses should compete. In contrast, for complexes **1** and **5**, D_{e2} is larger than B4. This promotes the formation of ^{3}**MS1** and subsequent relaxation to **MS1**, directing these complexes toward isomerization. The energy difference (D_{e2} − B4) is 0.06 eV for **4**, which is lower than those for **1** and **5.** This result is in agreement with the experimentally observed photorelease quantum yields, *i.e.*, φ_{NO}(**1**) < φ_{NO}(**4**). In addition, the energy difference (D_{e2} − B4) is similar for **2** and **4**. However, the dissociation energy D_{e2} is 0.12 eV higher for 4, and the absorption properties of **4**, as discussed before, make it less photoactive than its *cis* counterpart; together, these observations explain why the experimental quantum yield for photorelease is larger for the *cis* isomers. Comparison of the energy values D_{e1} and B4 clearly indicates that the participation of the ^{3}**MS1** state in the photorelease process would be more energetically demanding (but < 0.5 eV), and thus less favourable, than the photorelease from ^{3}**MS2**. The photorelease of NO from ^{3}**MS2** is quite facile due to the particular geometry of the sideways-bound intermediate, with a Ru−N bond in ^{3}**MS2** being longer than that in ^{3}**GS**, while dissociation from ^{3}**GS** or ^{3}**MS1** is more difficult because of the stronger Ru−N or Ru−O bond.

4.7 Conclusions

This work represents a theoretical attempt to explore the connection between photoinduced linkage isomers of nitrosyl ligand and photorelease of nitric oxide. Investigations by TD-DFT and by DFT of the relevant excited states involved in the photolytic cleavage of the Ru−NO bond show that, the ^{3}**MS2** state appears as a key metastable state. Indeed, its population is able to induce both processes with the following scenario: First a two-step process involving sequential two-photon absorption is required to produce the critical ^{3}**MS2** excited-state intermediate. Then, NO release or NO rotation occurs depending on the energy costs involved in these two processes (*i.e.*, NO dissociation energy D_{e2} *vs.* NO isomerization barrier B4). The ^{3}**MS2** state plays a similar role to that of ^{3}**MC** dissociative states, which are completely absent of the lowest triplet manifold of this family of complex. Moreover, the calculated activation energies (B1-B5) and dissociation energies (D_e-D_{e2}) indicate that for the *cis*-species **2** and **3** two pathways coexist and that it is quite facile to photorelease NO, while NO loss from **1**, **4** and **5** might be more difficult which is in agreement with the experimental observations.

4.8 References

(1) Tfouni, E.; Truzzi, D. R.; Tavares, A.; Gomes, A. J.; Figueiredo, L. E.; Franco, D. W. *Nitric Oxide* **2012**, *26* (1), 38–53.

(2) Fomitchev, D. V.; Coppens, P.; Li, T.; Bagley, K. A.; Chen, L.; Richter-Addo, G. B. *Chem. Commun.* **1999**, No. 19, 2013–2014.

(3) Da Silva, S. C.; Franco, D. W. *Spectrochim. Acta. A. Mol. Biomol. Spectrosc.* **1999**, *55* (7–8), 1515–1525.

(4) Gorelsky, S. I.; Lever, A. B. P. *Int. J. Quantum Chem.* **2000**, *80* (4–5), 636–645.

(5) Schaniel, D.; Woike, T.; Boskovic, C.; Güdel, H.-U. *Chem. Phys. Lett.* **2004**, *390* (4–6), 347–351.

(6) Schaniel, D.; Cormary, B.; Malfant, I.; Valade, L.; Woike, T.; Delley, B.; Krämer, K. W.; Güdel, H.-U. *Phys. Chem. Chem. Phys.* **2007**, *9* (28), 3717–3724.

(7) Cormary, B.; Malfant, I.; Buron-Le Cointe, M.; Toupet, L.; Delley, B.; Schaniel, D.; Mockus, N.; Woike, T.; Fejfarová, K.; Petříček, V.; Dušek, M. *Acta Crystallogr. B* **2009**, *65* (6), 612–623.

(8) Cormary, B.; Ladeira, S.; Jacob, K.; Lacroix, P. G.; Woike, T.; Schaniel, D.; Malfant, I. *Inorg. Chem.* **2012**, *51* (14), 7492–7501.

(9) Bitterwolf, T. E. *Inorg. Chem. Commun.* **2008**, *11* (7), 772–773.

(10) Giglmeier, H.; Kerscher, T.; Klüfers, P.; Schaniel, D.; Woike, T. *Dalton Trans.* **2009**, No. 42, 9113.

(11) Zangl, A.; Klüfers, P.; Schaniel, D.; Woike, T. *Dalton Trans.* **2009**, No. 6, 1034–1045.

(12) Khadeeva, L.; Kaszub, W.; Lorenc, M.; Malfant, I.; Buron-Le Cointe, M. *Inorg. Chem.* **2016**, *55* (9), 4117–4123.

(13) Sanz García, J.; Alary, F.; Boggio-Pasqua, M.; Dixon, I. M.; Malfant, I.; Heully, J.-L. *Inorg. Chem.* **2015**, *54* (17), 8310–8318.

(14) Freitag, L.; González, L. *Inorg. Chem.* **2014**, *53* (13), 6415–6426.

(15) Karidi, K.; Garoufis, A.; Tsipis, A.; Hadjiliadis, N.; Dulk, H. den; Reedijk, J. *Dalton Trans.* **2005**, No. 7, 1176–1187.

(16) Akl, J.; Sasaki, I.; Lacroix, P. G.; Malfant, I.; Mallet-Ladeira, S.; Vicendo, P.; Farfán, N.; Santillan, R. *Dalton Trans.* **2014**, *43* (33), 12721–12733.

(17) De Candia, A. G.; Marcolongo, J. P.; Etchenique, R.; Slep, L. D. *Inorg. Chem.* **2010**, *49* (15), 6925–6930.

(18) Hirano, T.; Ueda, K.; Mukaida, M.; Nagao, H.; Oi, T. *J. Chem. Soc. Dalton Trans.* **2001**, No. 16, 2341–2345.

(19) Coppens, P.; Novozhilova, I.; Kovalevsky, A. *Chem. Rev.* **2002**, *102* (4), 861–884.

(20) Tfouni, E.; Krieger, M.; McGarvey, B. R.; Franco, D. W. *Coord. Chem. Rev.* **2003**, *236* (1–2), 57–69.

(21) Bitterwolf, T. E. *Coord. Chem. Rev.* **2006**, *250* (9–10), 1196–1207.

(22) Caramori, G. F.; Frenking, G. *Organometallics* **2007**, *26* (24), 5815–5825.

(23) Caramori, G. F.; Kunitz, A. G.; Andriani, K. F.; Doro, F. G.; Frenking, G.; Tfouni, E. *Dalton Trans.* **2012**, *41* (24), 7327.

(24) Andriani, K. F.; Caramori, G. F.; Doro, F. G.; Parreira, R. L. T. *Dalton Trans.* **2014**, *43* (23), 8792–8804.

(25) Delcey, M. G.; Freitag, L.; Pedersen, T. B.; Aquilante, F.; Lindh, R.; González, L. *J. Chem. Phys.* **2014**, *140* (17), 174103.

(26) Freitag, L.; Knecht, S.; Keller, S. F.; Delcey, M. G.; Aquilante, F.; Pedersen, T. B.; Lindh, R.; Reiher, M.; González, L. *Phys. Chem. Chem. Phys.* **2015**, *17* (22), 14383–14392.

Résumé

Chapitre IV

De plus en plus, les complexes organométalliques à ligand nitrosyle attirent l'attention de la communauté scientifique. Cet intérêt croissant s'explique par leurs propriétés d'isomérisation d'enchaînement induit par irradiation, ce qui rend ces composés idéals pour la conception des nouveaux commutateurs moléculaires, ainsi que pour la fabrication d'unitées de stockage optique. Non seulement la propriété de photoisomériser rend ce genre de complexes particulièrement intéressants, mais aussi leur propriété de photolibérer NO fait de ces composés les candidats parfaits pour le développement de nouveaux médicaments pour le traitement de maladies cardiovasculaires, neuronales ou même pour le traitement du cancer.

Une étude théorique peut aider à éclaircir les aspects mécanistiques qui renforcent un des processus au détriment de l'autre, et elle peut également aider à comprendre quels sont les paramètres moléculaires plus adaptés pour favoriser la photoisomérisation ou bien la photolibération. L'enjeu de cette étude est justement de comprendre le mécanisme de photolibération de NO ainsi que sa relation avec le mécanisme de photoisomérisation. Pour cela, l'étude comparative de cinq complexes de ruthénium à ligand nitrosyle a été menée. Les complexes utilisés dans cette étude sont : le *trans*-$[RuCl(NO)(py)_4]^{2+}$ appelé complexe **1**, déjà présenté dans le chapitre précédent, et les isomères *cis*- et *trans*- d'une famille de complexes avec une formule de base $[RuCl_2(NO)(R\text{-terpy})]^+$, où R est soit un hydrogène (complexes **3** et **5**), soit un ligand fluorényle (complexes **2** et **4)**. Le complexe **1** est bien connu par sa photoconversion pratiquement totale de **GS** à **MS1** dans des monocristaux, toutefois, il n'est pas si connu par sa capacité à libérer NO en solution. D'un autre côte, il a été montré expérimentalement que les complexes **2** et **4** libèrent NO en solution avec des rendements quantiques plus importants que le complexe **1**.

En suivant une méthode similaire à celle utilisée pour caractériser les différentes structures impliquées dans l'isomérisation du complexe **1** à l'état fondamental singulet (**GS**, **MS2** et **MS1**) et à l'état excité triplet (^{3}**GS**, ^{3}**MS2**, ^{3}**MS1**), tous les isomères des complexes **2**, **3**, **4** et **5** ont été trouvés en solution. Une caractérisation exhaustive des surfaces d'énergie potentielle de l'état fondamental singulet ainsi que de l'état triplet de plus basse énergie pour tous les complexes étudiés a pu montrer que tous les composés sont également capables de subir une photoisomérisation d'enchaînement en solution comme celle décrite pour le complexe **1** dans le chapitre précédent. Comme il a déjà été observé pour le complexe **1**, la structure de base RuCl(R-terpy) reste pratiquement inchangée pour tous les différents isomères des complexes **2**, **3**, **4** et **5**. La nature des triplets trouvés pour les complexes

$[RuCl_2(NO)(R\text{-terpy})]^+$ (**2**, **3**, **4** et **5**) est tout à fait comparable à celle trouvée pour les triplets du complexe **1**, *trans*-$[RuCl(NO)(py)_4]^{2+}$, soit des états à transfert de charge du métal vers le ligand nitrosyle (Ru(*d*) ⋾ NO(π*)). Aucun état triplet centré sur le métal (^{3}**MC**) n'a été identifié dans ces complexes.

La caractérisation des spectres d'absorption par TD-DFT des isomères **GS**, **MS2** et **MS1** dans leurs états fondamentaux dévoile beaucoup d'information cruciale pour la compréhension des divers mécanismes des réactions photochimiques. Ces spectres fournissent aussi des informations importantes pour la rationalisation des différents rendements quantiques observés expérimentalement. Il est important de rappeler qu'une des propriétés clés pour expliquer la photoisomérisation séquentielle à deux photons du complexe **1** est la superposition des bandes d'absorption des isomères **GS** et **MS2** dans une région commune du spectre UV-visible. C'est également cette superposition des bandes qui permet aussi d'expliquer un mécanisme séquentiel à deux photons pour la photolibération de NO. Une des différences remarquables entre les complexes $[RuCl_2(NO)(R\text{-terpy})]^+$ (**2**, **3**, **4** et **5**) et le complexe **1** est la nature des états singulets excités vers lesquels les composés sont excités après l'absorption d'un premier photon. La transition initiale est un transfert de charge de la partie fluorényle (dans le cas des complexes **2** et **4**) ou bien du ligand terpyridine (dans le cas des complexes **3** et **5**) vers la partie Ru−NO, tandis que pour le complexe **1**, il s'agit plutôt d'un transition d'un électron *d* du ruthénium vers l'ensemble ruthénium-nitrosyle (Ru(*d*) ⋾ Ru(*d*)NO(π*)). Une autre différence marquante est l'effet hyperchromique exacerbé observé dans les complexes **2**, **3**, **4** et **5** en comparaison avec l'absorbance observée dans le complexe **1**. Cet effet est dû à la substitution des quatre pyridines par des systèmes π-conjugués plus étendus. La terpyridine est un chromophore qui joue le rôle d'antenne dans l'absorption initiale d'un photon, augmentant l'intensité des bandes dans les spectres UV-Vis par rapport à celles du complexe **1**. Dans cette logique, il n'est pas surprenant que les complexes **2** et **4** avec des ligands fluorényle-terpyridine soient les complexes qui présentent les bandes d'absorption les plus intenses. Par ailleurs, exactement pour la même raison, un effet bathochromique est observé quand la partie fluorényle est introduite dans la terpyridine. Dû au système π-conjugué plus étendu présent dans les complexes **2** et **4**, les premières bandes d'absorption importantes dans ces complexes sont plus basses en énergie que celles des complexes **3** et **5**.
Une autre propriété caractéristique des complexes de ruthénium à ligand nitrosyle, observé dans tous les spectres des complexes étudiés, est le décalage vers le rouge de tous les spectres des isomères **MS1** par rapport à celles des isomères **GS**. Dans le cas de l'isomère **MS1**,

l'interaction entre les orbitales *d* du ruthénium et les orbitales antiliantes du ligand nitrosyle et plus faible, ce qui a comme conséquence une différence énergétique entre orbitales moléculaires liantes et antiliantes moins importantes. Une des différences trouvées entres les isomères *cis*- et *trans*- des complexes **2**, **4** et **3**, **5** peut aider à rationaliser les rendements quantiques trouvés expérimentalement. Par analogie avec la photoisomérisation, la superposition des bandes d'absorption de **GS** et **MS2** permet la rationalisation du mécanisme par une absorption séquentielle à deux photons, le premier absorbé par **GS** et le deuxième absorbé par **MS2** qui amène le système au triplet ^{3}**MS2**. La libération de NO à partir du triplet ^{3}**MS2** est relativement facile. Par ailleurs, les isomères *cis*- (complexes **2** et **3**) présentent des superpositions de bandes plus importantes que celles des isomères *trans*- (complexes **4** et **5**). Cette propriété est cohérente avec un rendement quantique plus faible du complexe **4** (*trans*-) par rapport à celui du complexe **2** (*cis*-) observé expérimentalement.

Les énergies de dissociation à partir des états triplets ^{3}**GS**, ^{3}**MS2** et ^{3}**MS1** de tous les complexes montrent que la libération de NO est seulement possible à partir de ^{3}**MS2** et ^{3}**MS1**, en privilégiant le premier. De plus, les grandeurs relatives de dissociation calculées reflètent parfaitement les rendements quantiques relatifs trouvés expérimentalement, c'est-à-dire le rendement de photolibération du complexe **2** supérieur à celui du complexe **4**, lui-même supérieur à celui du complexe **1**. La petite barrière de dissociation à partir du ^{3}**MS2** trouvé pour tous les complexes montre que ce triplet joue un rôle crucial dans la photolibération de NO, ainsi que dans la photoisomérisation.

Tous les résultats obtenus dans cette étude (pour tous les complexes) montrent que les mécanismes de photoréactivité peuvent être expliqués par l'absorption séquentielle de deux photons à partir de **GS** et **MS2**. Donc les deux processus, photolibération et photoisomérisation, commencent par les mêmes étapes élémentaires. Sous irradiation continue avec la longueur d'onde appropriée pour chaque complexe, la population initiale des états singulets excités à partir de l'état fondamental **GS** est suivie par une relaxation non-radiative *via* croisement inter-système vers des états triplets grâce au couplage spin-orbite. Ensuite, le système peut se relaxer par voie non-radiative vers l'état triplet de plus basse énergie ^{3}**GS**, produisant ensuite l'isomère **MS2** dans son état fondamental. Une fois que le système est dans son isomère **MS2**, il réabsorbe un deuxième photon qui amène le système vers des états excités lesquels se relaxent vers le triplet ^{3}**MS2**. C'est dans cet état ^{3}**MS2** que la compétition entre photolibération et photoisomérisation a lieu. L'analyse des barrières

énergétiques à partir du triplet ^{3}**MS2** montre que pour les complexes *cis*- (**2** et **3**) les deux processus ont la même probabilité d'avoir lieu. En revanche, pour le complexe **1**, ainsi que pour le complexe **5**, la photoisomérisation est favorisée car l'énergie d'activation de ce processus est substantiellement plus faible que l'énergie de libération de NO.

Pour conclure, cette étude théorique est une tentative pour essayer de comprendre le lien entre la photolibération et la photoisomérisation d'enchaînement du ligand nitrosyle. Il est montré que l'état triplet ^{3}**MS2** est un intermédiaire fondamental dans les deux processus. Par analogie, les états ^{3}**MC** sont les intermédiaires critiques pour la photoisomérisation de complexes de ruthénium à ligands sulfoxyde et pour la photolibération de complexes de ruthénium à ligands thioéther. C'est dans cet état ^{3}**MS2** que la vraie compétition entre les deux processus se déclenche. Cette étude a montré, qu'en solution, les deux phénomènes coexistent pour les complexes *cis*-, tandis que pour les complexes *trans*- la photoisomérisation est favorisée au détriment de la photolibération. Ces résultats reflètent parfaitement la tendance des rendements quantiques observés expérimentalement.

Chapitre V

Conclusion Générale et Perspectives

5.1 Conclusions

L'idée principale de cette thèse a consisté à étudier divers mécanismes photochimiques se produisant dans des complexes de ruthénium à ligand nitrosyle à l'aide d'outils fournis par la chimie théorique. En particulier, les mécanismes de photoisomérisation d'enchaînement ainsi que de photolibération du ligand NO ont été explorés dans différents complexes présentant des rendements quantiques différents pour ces deux processus. La stratégie de calcul utilisée repose sur une approche statique basée sur le calcul de chemins photochimiques le long des surfaces d'énergie potentielle (SEP) impliquées dans ces mécanismes. Ces surfaces ont été calculées à l'aide de la Théorie de la Fonctionnelle de la Densité (DFT). Une telle approche avait déjà été appliquée précédemment dans l'étude de photoisomérisation d'enchaînement, de photosubstitution et de photolibération dans des complexes de ruthénium à ligand sulfoxyde, thioéther et oxyde de phosphinidène.[1–4] Cette stratégie a montré toute son utilité pour obtenir des informations mécanistiques sur ces processus, permettant ainsi de rationaliser qualitativement les observations expérimentales. Lors des travaux effectués au cours de cette thèse, cette stratégie computationnelle a montré sa capacité à apporter les informations nécessaires pour la compréhension et la description des mécanismes de photoisomérisation[5] ainsi que de photolibération[6] de NO dans les complexes de ruthénium à ligand nitrosyle. Les résultats présentés dans ce manuscrit constituent une avancée importante dans la compréhension des propriétés photophysiques et de photoréactivité de ces complexes, qui attirent de plus en plus l'attention de la communauté scientifique par ses applications potentielles technologiques[7,8] et médicales.[9] Ces résultats comportent, entre autres, la détermination des différents chemins réactionnels pour la photoisomérisation ainsi que pour la photolibération. Ces chemins ont pu être trouvés grâce à la caractérisation exhaustive des SEP de l'état fondamental singulet, de l'état excité triplet de plus basse énergie, ainsi que l'identification de leurs croisements. Deux stratégies bien différentes pour la caractérisation de ces SEP ont été utilisées lors de ce travail de thèse : a) une première approche standard similaire à celle suivie lors de l'étude des complexes de ruthénium sulfoxyde, et b) une deuxième approche plus originale dans le domaine de la photoréactivité des états excités des complexes organométalliques basée sur les méthodes de la chaîne d'états comme le '*Nudged Elastic Band*' (NEB) et le '*Zero Temperature String*' (ZTS). L'approche plus standard consiste essentiellement à optimiser les minima sur les différentes SEP, suivi d'une recherche des états de transitions (ET) qui connectent ces minima, en utilisant l'information apportée par leurs structures. Ensuite, des calculs de chemins d'énergie

minimum sont réalisés à partir des ET trouvés afin de relier tous les points stationnaires trouvés. L'approche basée sur les méthodes de la chaîne d'états, dans un premier temps, nécessite aussi une optimisation initiale des minima sur les SEP. En revanche, il n'y a pas une recherche directe des ET. C'est à partir des minima qu'un chemin initial est construit. Ce chemin est, en général, obtenu à partir d'une interpolation linéaire entre les minima. Par la suite, ce chemin est optimisé pour trouver le chemin d'énergie minimum sur la SEP impliquée. Malgré leur apparente simplicité, aucun de ces approches n'est routinière et la détermination de chemins réactionnels reste un travail complexe et délicat, tout particulièrement lorsque des états électroniques excités sont impliqués.

La caractérisation des surfaces d'énergie potentielle du complexe *trans*-$[RuCl(NO)(py)_4]^{2+}$ ainsi que l'optimisation de leurs croisements ont permis de mettre en évidence la complexité des chemins réactionnels mis en jeu lors de la photoisomérisation d'enchaînement Ru−NO ⁚⁚ Ru−ON. En effet, il apparaît que ce processus est défavorable à la fois d'un point de vue thermodynamique et d'un point de vue cinétique. Le profil d'énergie potentielle à l'état excité triplet monte en énergie le long du chemin d'isomérisation et montre des barrières énergétiques importantes. Ce comportement est très différent de ce qui avait été obtenu pour la photoisomérisation de complexes de ruthénium à ligand sulfoxyde et d'oxyde de phosphinidène, pour lesquels un profil énergétique favorable (thermodynamiquement et cinétiquement) avait été trouvé à l'état excité triplet. Néanmoins, ce travail a permis de montrer que, grâce aux croisements entre les SEP singulet et triplet, la photoisomérisation peut se produire de manière non-adiabatique. Ce mécanisme de photoréactivité consiste en l'absorption séquentielle de deux photons à partir de **GS** et **MS2**. En résumé, le mécanisme peut être décrit comme l'absorption initiale d'un premier photon qui permet la photoisomérisation du **GS** vers **MS2**. Ceci se produit par une succession de croisements inter-système et de conversions internes conduisant au minimum ^{3}**GS**, à partir duquel **MS2** peut être peuplé dû à un croisement singulet/triplet accessible énergétiquement. Une fois que le complexe est à la géométrie de l'isomère **MS2**, un deuxième photon est absorbé, amenant le système vers des états excités qui par voies non-radiatives vont être désactivés vers l'état triplet ^{3}**MS2**. Enfin, cet état peut se relaxer vers ^{3}**MS1**, qui lui-même se désactive grâce à un autre croisement singulet/triplet vers le photoproduit **MS1**.

Le mécanisme de la photoisomérisation d'enchaînement retour Ru−ON ⁚⁚ Ru−NO a également été étudié. Cette isomérisation de l'isomère **MS1** vers l'état fondamental **GS** peut

être déclenchée par irradiations soit rouge, soit infrarouge, lesquelles conduisent à des chemins de réaction différents. Expérimentalement, sous irradiation dans le rouge, l'isomère **MS1** est directement converti en isomère **GS**, alors que sous irradiation infrarouge, un mélange 1:1 de **GS** et **MS2** est observé après 30 minutes d'irradiation. Ce comportement a pu être rationalisé théoriquement. Sous irradiation dans le rouge, un mécanisme séquentiel à deux photons et un mécanisme à un photon ont pu être identifiés. Après l'absorption initiale d'un premier photon rouge à 782 nm à partir de l'isomère **MS1** à l'état fondamental, le système est excité vers des états singulets qui conduisent à la formation de l'intermédiaire ^{3}**MS1** par désactivation non-radiative. Ensuite, le système peut se relaxer vers l'état ^{3}**MS2** en franchissant une petite barrière de potentiel. À partir de ^{3}**MS2**, l'isomère **MS2** peut être peuplé par croisement inter-système. Cet isomère absorbe aussi à 782 nm et l'absorption d'un deuxième photon rouge amène le système vers le triplet ^{3}**MS2**, puis vers le triplet ^{3}**GS**, qui ensuite conduit à l'isomère **GS**. Le mécanisme à un photon diffère puisqu'il ne met pas en jeu l'absorption de l'isomère **MS2**. A partir de l'intermédiaire ^{3}**MS2**, ^{3}**GS** peut être formé en franchissant une petite barrière de potentiel. L'irradiation dans l'infrarouge à 980 nm, elle, n'induit pas de transition électronique de l'isomère **MS1**, comme le montre les calculs de spectres d'absorption de cette espèce. Par contre, c'est le cas pour l'intermédiaire ^{3}**MS1**. Cet intermédiaire peut être peuplé thermiquement par croisement inter-système dû à la présence d'un croisement des SEP singulet et triplet facilement accessible le long du chemin entre **MS1** et ^{3}**MS1**. L'absorption dans l'infrarouge de ^{3}**MS1** peuple des états triplets plus hauts en énergie, lesquels peuvent se relaxer par conversion interne vers l'état triplet ^{3}**MS2**. Puis, comme dans le mécanisme précédent sous irradiation dans le rouge, le système peut se relaxer vers l'isomère **MS2**. **MS2** n'absorbant pas dans l'infrarouge, il n'est pas consommé immédiatement et **GS** est formé alors que **MS2** est encore présent dans le milieu. Il n'est donc pas surprenant qu'expérimentalement un mélange de **GS** et **MS2** soit observé.

Par ailleurs, pour compléter l'étude mécanistique du complexe *trans*-$[RuCl(NO)(py)_4]^{2+}$, une analyse des orbitales naturelles de liaison (NBO) en termes d'énergies de délocalisation électronique entre donneurs et accepteurs a permis quantitativement d'expliquer l'ordre énergétique trouvé pour les trois isomères sur la SEP de l'état fondamental, **GS**, **MS2** et **MS1**. De plus, une analyse qualitative en termes de liaisons simples et d'hyperliaisons reflète aussi la tendance énergétique des isomères.

Par la suite, l'étude du mécanisme de photolibération de NO ainsi que sa relation avec le mécanisme de photoisomérisation a été entrepris pour cinq complexes différents. Il s'agit du complexe *trans*-$[RuCl(NO)(py)_4]^{2+}$ étudié précédemment (dénoté complexe **1**), et des isomères *cis*- et *trans*- d'une famille de complexes avec une formule de base $[RuCl_2(NO)(R\text{-terpy})]^+$, où R est soit un hydrogène (complexes **3** et **5**), soit un ligand fluorényle (complexes **2** et **4)**. Le complexe **1** est bien connu par sa photoconversion pratiquement totale de **GS** à **MS1** dans des monocristaux, mais présente un rendement faible de photolibération de NO en solution. D'un autre côte, il a été montré expérimentalement que les complexes **2** et **4** libèrent NO en solution avec des rendements quantiques bien plus importants. Ce comportement a également été rationalisé au cours de ce travail. Une caractérisation exhaustive des SEP de l'état fondamental singulet ainsi que de l'état triplet de plus basse énergie pour tous ces complexes a pu montrer que les composés **2**-**5** sont également capables de subir une photoisomérisation d'enchaînement en solution comme celle décrite pour le complexe **1**. Les énergies de dissociation calculées à partir des états triplets ^{3}**GS**, ^{3}**MS2** et ^{3}**MS1** de tous les complexes montrent que la libération de NO est seulement possible à partir de ^{3}**MS2** et ^{3}**MS1**, en privilégiant le premier. Il apparaît donc que photoisomérisation et photolibération ont un mécanisme de départ en commun avec les mêmes étapes initiales conduisant à la formation de l'intermédiaire ^{3}**MS2**. Les deux nécessitent donc un mécanisme à deux photons. C'est une fois que cet intermédiaire ^{3}**MS2** est formé que la compétition entre ces deux processus a lieu. Les grandeurs relatives de dissociation calculées ainsi que la comparaison avec la barrière d'isomérisation entre ^{3}**MS2** et ^{3}**MS1** ont permis de rationaliser les rendements quantiques relatifs trouvés expérimentalement, c'est-à-dire des rendements de photolibération des complexes **2** et **4** supérieurs à celui du complexe **1**. Par ailleurs, les isomères *cis*- (complexes **2** et **3**) présentent des superpositions de bandes d'absorption entre **GS** et **MS2** plus importantes que celles des isomères *trans*- (complexes **4** et **5**). Cet argument permet d'expliquer le rendement quantique plus faible du complexe **4** par rapport à celui du complexe **2** observé expérimentalement.

Il est important de souligner que, contrairement à ce qui est généralement accepté pour les complexes de ruthénium à ligand NO, la même longueur d'onde peut déclencher les deux processus (*i.e.*, photoisomérisation et photolibération). Ce n'est pas l'absorption initiale qui joue un rôle clé dans la prédestination de la photoréaction, mais c'est surtout dans les états excités que la compétition entre photolibération et photoisomérisation a lieu, notamment quand le système atteint l'état excité triplet ^{3}**MS2**. Ce travail a permis de montrer

l'influence cruciale de la nature des ligands et de leurs positions autour de la sphère de coordination sur la photoréactivité de ce type de complexe.

En comparaison avec les complexes de ruthénium sulfoxyde et thioéther, où des états triplet centré sur le métal (^{3}**MC**) jouent un rôle fondamental dans les réactions de photoisomérisation, de photodissociation, ainsi que de photosubstitution, aucun ^{3}**MC** n'est impliqué dans les mécanismes de photoréactivité identifiés dans les complexes de ruthénium nitrosyle étudiés. En revanche, une analogie peut être faite entre le rôle du triplet ^{3}**MS2** dans les complexes de ruthénium à ligand nitrosyle avec celui des états ^{3}**MC** dans les complexes de ruthénium sulfoxyde et thioéther. C'est cet état triplet ^{3}**MS2** qui est incontournable dans les processus de photoisomérisation et de photolibération.

Lors de ce travail, l'analyse des spectres d'absorption UV-Vis a fourni des informations précieuses pour les descriptions mécanistiques des deux processus en compétition. Par exemple, il a été montré que la superposition des bandes d'absorption de **GS** et **MS2** est une condition *sine qua non* pour expliquer les mécanismes à deux photons absorbés séquentiellement. Cette superposition est également importante pour expliquer les différents rendements quantiques observés. Une autre caractéristique remarquable des spectres, très importante pour la description du mécanisme de photoisomérisation dans le complexe *trans*-$[RuCl(NO)(py)_4]^{2+}$, est la position des bandes d'absorption de l'isomère **MS1**. L'absence des bandes d'absorption de **MS1** dans la zone où il existe un recouvrement important des bandes de **GS** et **MS2** explique les rendements si élevés de photoconversion **GS** ❜❜ **MS1** observés expérimentalement. L'analyse des spectres d'absorption a également permis de rationaliser la décroissance observée pour les rendements de photoisomérisation dans une famille de complexes de ruthénium à ligand nitrosyle, plus concrètement les complexes *trans*-$[RuCl(NO)(py)_4]^{2+}$, *trans*-$[RuBr(NO)(py)_4]^{2+}$ et *trans*-(Cl,Cl)$[RuCl_2(NO)(terpy)]^{+}$. Pour le complexe *trans*-$[RuBr(NO)(py)_4]^{2+}$, l'apparition d'une petite bande d'absorption de l'isomère **MS1** dans la même région où **GS** et **MS2** absorbent explique la chute d'environ 40% du rendement de photoconversion par rapport au complexe analogue avec du chlore. Dans le cas du complexe *trans*-(Cl,Cl)$[RuCl_2(NO)(terpy)]^{+}$, cette bande d'absorption de l'isomère **MS1** est beaucoup plus intense que dans le cas précédent (et même plus intense que les bandes trouvées pour **GS** et **MS2**), ce qui explique aussi parfaitement les faibles rendements observés expérimentalement pour ce complexe.

L'analyse de la nature électronique des transitions dans les spectres a permis de mettre en évidence la différence entre les états excités des complexes étudiés. La transition initiale qui déclenche les deux photoréactions dans le complexe *trans*-$[RuCl(NO)(py)_4]^{2+}$ correspond à une excitation d'un électron *d* du ruthénium vers l'ensemble Ru−NO, tandis que pour les complexes de la famille $[RuCl_2(NO)(R-terpy)]^+$, elle est décrite par un transfert de charge de la partie R−terpy vers Ru−NO. L'effet hyperchromique observé dans la famille de complexes $[RuCl_2(NO)(R-terpy)]^+$ est remarquable. Il est dû à la substitution des pyridines par des systèmes π-conjugués plus étendus. Ceux-ci jouent le rôle d'antenne dans l'absorption initiale d'un photon, augmentant l'intensité des bandes, ce qui améliore le rendement quantique. Ce phénomène explique en partie les rendements plus importants observés pour les complexes $[RuCl_2(NO)(R-terpy)]^+$ dans la photolibération de NO en solution. L'effet bathochromique, observé dans les spectres quand la partie fluorényle est ajoutée à la terpyridine, peut être aussi expliqué par l'effet du système π-conjugué plus étendu. Une dernière caractéristique des spectres intéressante à souligner est le décalage vers le rouge des transitions de l'isomère **MS1** par rapport à celles de l'isomère **GS**. Ce phénomène, observé dans tous les complexes étudiés, reflète parfaitement la différence entre la force de la liaison $Ru\text{-}N_{(NO)}$ dans l'isomère **GS,** et $Ru\text{-}O_{(ON)}$ dans l'isomère **MS1**, cette dernière étant la liaison la plus faible.

Pour conclure, il est important de rappeler l'enjeu des études réalisées au cours de cette thèse, lequel n'est pas de reproduire quantitativement les expériences avec une précision absolue, mais d'être en mesure d'expliquer et de rationaliser, avec les modèles et les outils employés, les comportements photochimiques observés expérimentalement. Ceci a permis de comprendre la relation entre photoisomérisation et photolibération dans les complexes de ruthénium à ligand nitrosyle, ce qui n'avait jamais été établi auparavant. Il serait aussi intéressant d'utiliser les méthodologies et stratégies suivies dans ce travail comme outils prédictifs pour être capable de connaître, *a priori*, la réactivité d'un complexe avant même qu'il ne soit synthétisé. C'est pour ces raisons que le dialogue entre la théorie et l'expérience est toujours important et enrichissant. En effet, les études présentées dans ce manuscrit ont eu comme point de départ l'analyse détaillée des résultats expérimentaux fournis directement par les expérimentateurs, avec lesquels il y a eu une communication directe au cours de cette thèse.

5.2 Perspectives

Les études mécanistiques réalisées lors de ce travail reposent sur une hypothèse principale : il est supposé que toutes les propriétés de photoréactivité des complexes de ruthénium à ligand nitrosyle étudiés peuvent être rationalisées à partir de l'état excité triplet le plus bas. Il est donc admis dans ce travail que cet état est peuplé très rapidement et efficacement après la photoexcitation initiale des complexes. Ceci implique que les états singulets excités initialement peuplés se désactivent non-radiativement très rapidement par croisement inter-système vers les états triplets excités, qui eux-mêmes se relaxent vers le triplet de plus basse énergie. Il serait intéressant de vérifier cette hypothèse par des calculs de chemins photophysiques caractérisant ces voies de désactivation non-radiative. Pour cela, il faudrait calculer les énergies des états triplets le long du chemin de relaxation de l'état singulet excité initialement peuplé, de localiser les éventuels croisements entre ces états et de calculer les couplages spin-orbite le long de ce chemin afin de savoir si le transfert de population des états singulets vers les états triplets est efficace. Il est tout de même important de rappeler qu'expérimentalement, il est reconnu que pour ce type de complexe (complexe de ruthénium polypyridine), ce transfert de population est efficace (durée de vie de l'état singulet excité très courte). Par ailleurs, une étude basée sur des simulations dynamiques d'un complexe de ruthénium à ligand nitrosyle a confirmé ce comportement.[10]

Par ailleurs, les études réalisées dans ce travail de thèse se sont basées uniquement sur des approches statiques utilisant la topologie des surfaces d'énergie potentielle de l'état fondamental et de l'état triplet excité le plus bas. Le rôle joué par les états excités plus hauts en énergie n'a pas été caractérisé. Notamment, des états triplets MLCT sont invoqués pour former potentiellement directement l'isomère **MS2** sans passer par la formation de ^{3}**GS**, comme illustré sur la Figure 5.1. Ces chemins sont simplement hypothétiques et il serait intéressant de les explorer afin de confirmer ou d'infirmer ce scénario. De plus, les voies de désactivation non-radiative décrites dans nos études mécanistiques sont basées sur la localisation des croisements singulet/triplet, points critiques qui permettent un croisement inter-système très efficace. La possibilité de désactivation non-radiative hors de ces points de croisement a été négligée. Une approche dynamique serait tout particulièrement adaptée à ce type de problème. Il faudrait pour cela utiliser des méthodes de type semi-classique (trajectoires avec saut de surfaces) incluant les couplages spin-orbite.[11] Ainsi, les transferts de population entre tous les états singulets et triplets pertinents pourraient être décrits sans *a*

priori. Ce type d'approche reste néanmoins compliqué à mettre en œuvre et nécessite de calculer en tout point de chaque trajectoire le potentiel quantique (e.g., par TD-DFT), sa dérivée (forces agissant sur les noyaux) et les couplages inter-états. Diverses approximations sont néanmoins possibles afin de rendre ces simulations réalisables d'un point de vue pratique[10,12] et ce type d'étude sera envisagé à l'avenir pour étudier ces complexes fascinants.

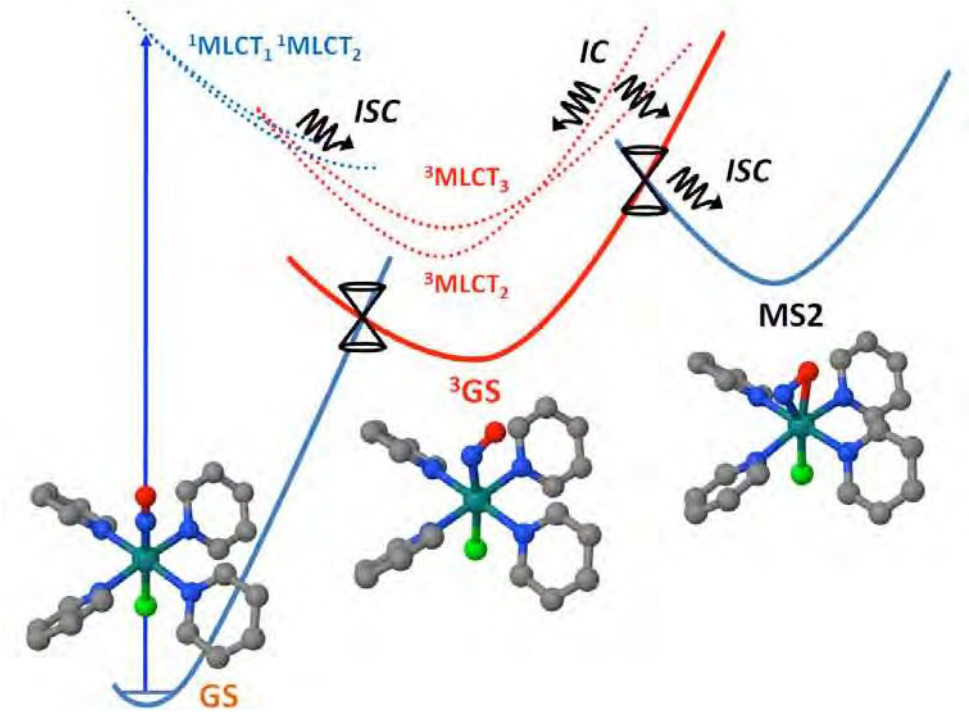

Figure 5.1: Illustration du rôle potentiel des états excités triplets plus hauts en énergie. La courbe bleue continue représente la surface d'énergie potentielle de l'état fondamental, tandis que la courbe rouge continue représente la surface d'énergie potentielle de l'état triplet de plus basse énergie. Les courbes pointillées représentent les surfaces d'énergie potentielle des états excités plus hauts en énergie (singulets en bleu, et triplets en rouge). Les doubles cônes représentent les croisements singulet-triplet caractérisés dans ce travail de thèse.

Toutes les études théoriques sur les complexes de ruthénium nitrosyle présentées dans ce manuscrit ont été réalisées à l'aide de la DFT et de sa version dépendante du temps, la TD-DFT, comme dans les études précédentes sur les complexes de ruthénium sulfoxyde. Il pourrait être aussi très intéressant et enrichissant de compléter les études de ces complexes à ligand nitrosyle à l'aide de méthodes basées sur la fonction d'onde corrélée. En effet, il est important de s'assurer de la fiabilité et de la précision des calculs de surfaces d'énergie potentielle obtenues par DFT. Cette exploration apportera des informations complémentaires à celles obtenues par les méthodes basées sur la densité électronique, notamment quant au caractère multiconfigurationnel de la fonction d'onde. Il serait donc intéressant de réaliser les calculs des SEP pertinentes, par exemple au niveau '*Complete Active Space Self-Consistent Field*' (CASSCF), complétés par des calculs de théorie des perturbations à l'ordre 2 (CASPT2,

NEVPT2, etc.). Ces méthodes permettent de caractériser naturellement les états excités d'énergie supérieure et permettraient donc d'obtenir des informations sur le rôle joué par ces états dans les mécanismes photochimiques.

Les études expérimentales sur ces complexes montrent également le rôle important joué par l'environnement sur leur photoréactivité. Par exemple, le complexe *trans*-$[RuCl(NO)(py)_4]^{2+}$ est capable de photoisomériser avec un rendement de photoconversion proche de l'unité dans le cristal, alors qu'il est très inefficace en solution. Par ailleurs, comme montré dans le Tableau 5.1, la nature des contre-ions dans le cristal a un effet important sur l'efficacité de la photoconversion pour un même complexe. Il serait donc souhaitable de prendre en compte les effets de l'environnement dans la modélisation de ces complexes de ruthénium à ligand nitrosyle. Des approches hybrides décrivant le complexe (et, par exemple, quelques contre-ions) quantiquement et le reste du système classiquement, voire par des charges ponctuelles, pourraient être envisagées afin de décrire ces effets d'environnement. Il serait notamment intéressant de savoir si la photolibération est bloquée dans le cristal due aux contraintes stériques imposées par la taille des contre-ions dans la maille cristalline.

Tableau 5.1: Différents rendements de photoconversion trouvés pour le complexe *trans*-[RuCl(NO)(py)$_4$]$^{2+}$ avec des contre-ions différents.[13,14]

Complexe	Rendement de photoconversion[a]	Longueur d'onde expérimentale / nm
trans-[RuCl(NO)(py)$_4$]$(PF_6)_2\cdot½H_2O$	76%	476
trans-[RuCl(NO)(py)$_4$]$(BF_4)_2\cdot H_2O$	50%	458-488
trans-[RuCl(NO)(py)$_4$]$Br_2\cdot 2H_2O$	17%	488
trans-[RuCl(NO)(py)$_4$]$Cl_2\cdot 4H_2O$	11%	476

[a] **Rendements obtenus à partir de poudres.**

En conclusion, il reste encore beaucoup de travail à réaliser sur le plan théorique afin de comprendre la photoréactivité de ces complexes de ruthénium à ligand nitrosyle. Ce travail de thèse a permis de faire des avancées très importantes et prometteuses dans cette compréhension, qui encourage à poursuivre l'étude de ce type de complexes. Un point particulier qui est en cours d'investigation concerne notamment la nature du photoproduit final formé après photolibération du ligand NO.

5.3 Références

(1) Göttle, A. J.; Dixon, I. M.; Alary, F.; Heully, J.-L.; Boggio-Pasqua, M. *J. Am. Chem. Soc.* **2011**, *133* (24), 9172–9174.

(2) Vieuxmaire, O. P. J.; Piau, R. E.; Alary, F.; Heully, J.-L.; Sutra, P.; Igau, A.; Boggio-Pasqua, M. *J. Phys. Chem. A* **2013**, *117* (48), 12821–12830.

(3) Göttle, A. J.; Alary, F.; Dixon, I. M.; Heully, J.-L.; Boggio-Pasqua, M. *Inorg. Chem.* **2014**, *53* (13), 6752–6760.

(4) Göttle, A. J.; Alary, F.; Boggio-Pasqua, M.; Dixon, I. M.; Heully, J.-L.; Bahreman, A.; Askes, S. H. C.; Bonnet, S. *Inorg. Chem.* **2016**, *55* (9), 4448–4456.

(5) Sanz García, J.; Alary, F.; Boggio-Pasqua, M.; Dixon, I. M.; Malfant, I.; Heully, J.-L. *Inorg. Chem.* **2015**, *54* (17), 8310–8318.

(6) Sanz García, J.; Alary, F.; Boggio-Pasqua, M.; Dixon, I. M.; Heully, J.-L. *J. Mol. Model.* **2016**, *22*, 284.

(7) Coppens, P.; Novozhilova, I.; Kovalevsky, A. *Chem. Rev.* **2002**, *102* (4), 861–884.

(8) Bitterwolf, T. E. *Coord. Chem. Rev.* **2006**, *250* (9–10), 1196–1207.

(9) Tfouni, E.; Truzzi, D. R.; Tavares, A.; Gomes, A. J.; Figueiredo, L. E.; Franco, D. W. *Nitric Oxide* **2012**, *26* (1), 38–53.

(10) Freitag, L.; González, L. *Inorg. Chem.* **2014**, *53* (13), 6415–6426.

(11) Mai, S.; Marquetand, P.; González, L. *Int. J. Quantum Chem.* **2015**, *115* (18), 1215–1231.

(12) Warshel, A.; Karplus, M. *Chem. Phys. Lett.* **1975**, *32* (1), 11–17.

(13) Cormary, B. Photocommutation à l'état solide dans les complexes de ruthénium à ligand nitrosyle. Vers la réalisation de matériaux composites photochromes, Université Toulouse III - Paul Sabatier, 2009.

(14) Cormary, B.; Ladeira, S.; Jacob, K.; Lacroix, P. G.; Woike, T.; Schaniel, D.; Malfant, I. *Inorg. Chem.* **2012**, *51* (14), 7492–7501.

Appendix A

Supporting Information for Chapter III

Table of Contents

Computational Details AA2
Table AA1. Structure, energies and orbitals of **GS** AA3
Table AA2. Structure, energies and orbitals of **MS2** AA4
Table AA3. Structure, energies and orbitals of **MS1** AA5
Table AA4. Structure, energies and orbitals of $^{1}TS_{1}$ AA6
Table AA5. Structure, energies and orbitals of $^{1}TS_{2}$ AA7
Table AA6. Structure, energies and orbitals of ^{3}**GS** AA8
Table AA7. Structure, energies and orbitals of ^{3}**MS2** AA9
Table AA8. Structure, energies and orbitals of ^{3}**MS1** AA10
Table AA9. Structure, energies and orbitals of $^{3}TS_{1}$ AA11
Table AA10. Structure, energies and orbitals of $^{3}TS_{2}$ AA12
Table AA11. Structure, energies and orbitals of $MECP_{1}$ AA13
Table AA12. Structure, energies and orbitals of $MECP_{2}$ AA14
Table AA13. Structure, energies and orbitals of $MECP_{3}$ AA15
Table AA14. Structure, energies and orbitals of $MECP_{4}$ AA16
Figure AA1. Absorption TD-DFT spectrum of **GS** AA17
Figure AA2. Absorption TD-DFT spectrum of **MS2** AA18
Figure AA3. Absorption TD-DFT spectrum of **MS1** AA19
Figure AA4. Absorption TD-DFT spectrum of the 3 isomers in vacuum and in acetonitrile AA20
Table AA15. Natural Transition Orbitals for the singlet states of the **GS** isomer AA21
Table AA16. Natural Transition Orbitals for the singlet states of the **MS2** isomer AA22
Table AA17. Natural Transition Orbitals for the singlet states of the **MS1** isomer AA24
Table AA18. Active space orbitals of the **MS1** CASSCF(6,6) calculation AA26
Table AA19. First transitions computed for the **MS1** isomer AA26
Figure AA5. Intrinsic reaction coordinate for the $^{1}TS_{1}$ AA27
Figure AA6. Intrinsic reaction coordinate for the $^{1}TS_{2}$ AA28
Figure AA7. Intrinsic reaction coordinate for the $^{3}TS_{1}$ AA29
Figure AA8. Intrinsic reaction coordinate for the $^{3}TS_{2}$ AA30
Figure AA9. Steepest decent optimization from the $MECP_{1}$ AA31
Figure AA10. Steepest decent optimization from the $MECP_{2}$ AA32
Figure AA11. Steepest decent optimization from the $MECP_{3}$ AA33
Figure AA12. Steepest decent optimization from the $MECP_{4}$ AA34
References AA35

Computational Details

Gas-phase geometry optimizations of all the stationary points found on the closed shell singlet (hereafter called singlet for simplicity) and the lowest triplet PES were carried out with the Gaussian 09 quantum package.[1] Starting from the crystallographic X-ray structures[2] the isomers **GS** and **MS1** were optimized in C_4 symmetry. DFT was used in order to perform these calculations using the standard hybrid functional B3LYP,[3,4] including Grimme's dispersion correction,[5] with a double-ζ Ahlrichs-type basis set[6] with a *p* polarization function for the hydrogen atoms, a triple-ζ Ahlrichs-type basis set[6] with one *d* polarization function for the second- and third-row elements, and for the ruthenium a Stuttgart relativistic effective core potential[7] (including 28 core electrons) with its associated basis set[7] and two *f* and one *g* polarization functions.[8] After geometry optimizations, vibration frequency analyses were performed at the same level of theory to verify the nature of the stationary points. At the transition state (TS) geometries, steepest descent (SD) optimizations and subsequent intrinsic reaction coordinate (IRC) calculations were carried out to confirm the connections between the isomers on the singlet and triplet PESs.

In the vicinity of singlet and triplet minima, a search for minimum energy crossing points (MECPs) has been performed. Optimization of the MECPs was performed with the ORCA 3.0.2 quantum package[9] at the same level of theory. The UV-Vis absorption spectra of **GS**, **MS1** and **MS2** in acetonitrile,[10] were computed using the COSMO[11] solvation model with ORCA, applying TDDFT using the TPSSh[12] functional within the Tamm-Dancoff approximation,[13,14] and the same basis sets as described above. In these TDDFT calculations the resolution-of-identity (RI) approximation for hybrid functionals[15] (as implemented in ORCA) was employed to calculate the Coulomb energy term using the Ahlrichs/Weigand Def2-TZV auxiliary basis set and the exchange term by the so-called 'chain-of-spheres exchange' (COSX) algorithm.[16] The natural transition orbitals[17] (NTOs) corresponding to the different singlet excited states at the **GS**, **MS1** and **MS2** geometries were also computed in order to analyse the nature of the electronic transitions. Complete active-space self-consistent field (CASSCF) plus second order *n*-electron valence states for multireference perturbation theory (NEVPT2)[18–20] calculations have been done also on the **MS1** state in order to confirm the results of TDDFT calculations in the lowest energy part of the absorption spectrum (six electrons, six orbitals, see Table AA18). For the reverse photoisomerization **MS1** ⋯ **GS**, two-photon absorption (TPA) was envisaged for **MS1** and **MS2**. The TPA probability was computed using GAMESS-US[21] within the formalism presented in the work of Zahariev *et al.*[22] For the final results, equation 93 from the work of Friese *et al.*[23] has been used. Natural bond orbital (NBO) analyses are a powerful tool for the study of the chemical bonding. These NBO analyses were performed at the optimized geometries of **GS**, **MS1** and **MS2**. It was performed with NBO 6[24,25] which is directly accessible from ORCA.

Table AA1. Optimized Cartesian coordinates, energies, molecular parameters and electronic structure of the **GS** isomer at the B3LYP-D3/Ahlrichs-basis level of theory in its ground state (singlet) in vacuum.

Ru	0.000000000000	0.000000000000	0.075373000098
Cl	0.000000000000	0.000000000000	-2.241876998087
N	0.000715000003	2.137759000999	0.008602000003
N	2.137759000999	-0.000715000003	0.008602000003
N	-0.000715000003	-2.137759000999	0.008602000003
N	-2.137759000999	0.000715000003	0.008602000003
N	0.000000000000	0.000000000000	1.820093001914
O	0.000000000000	0.000000000000	2.960970001222
C	-0.805272998832	2.842570998263	0.832481999705
H	-1.447122999683	2.277536001171	1.498677999269
C	-0.833355999367	4.224145002329	0.833475000737
H	-1.498087998432	4.743048002577	1.516766001232
C	-0.008361999988	4.918275002001	-0.044745999978
H	-0.012454000022	6.004203996837	-0.067041000172
C	0.818857999089	4.194434998841	-0.893259002257
H	1.477028999825	4.689415998321	-1.600218998603
C	0.801454001002	2.811346997614	-0.842417000166
H	1.422719998000	2.219019998203	-1.501717000477
C	2.842570998263	0.805272998832	0.832481999705
H	2.277536001171	1.447122999683	1.498677999269
C	4.224145002329	0.833355999367	0.833475000737
H	4.743048002577	1.498087998432	1.516766001232
C	4.918275002001	0.008361999988	-0.044745999978
H	6.004203996837	0.012454000022	-0.067041000172
C	4.194434998841	-0.818857999089	-0.893259002257
H	4.689415998321	-1.477028999825	-1.600218998603
C	2.811346997614	-0.801454001002	-0.842417000166
H	2.219019998203	-1.422719998000	-1.501717000477
C	-0.801454001002	-2.811346997614	-0.842417000166
H	-1.422719998000	-2.219019998203	-1.501717000477
C	-0.818857999089	-4.194434998841	-0.893259002257
H	-1.477028999825	-4.689415998321	-1.600218998603
C	0.008361999988	-4.918275002001	-0.044745999978
H	0.012454000022	-6.004203996837	-0.067041000172
C	0.833355999367	-4.224145002329	0.833475000737
H	1.498087998432	-4.743048002577	1.516766001232
C	0.805272998832	-2.842570998263	0.832481999705
H	1.447122999683	-2.277536001171	1.498677999269
C	-2.811346997614	0.801454001002	-0.842417000166
H	-2.219019998203	1.422719998000	-1.501717000477
C	-4.194434998841	0.818857999089	-0.893259002257
H	-4.689415998321	1.477028999825	-1.600218998603
C	-4.918275002001	-0.008361999988	-0.044745999978
H	-6.004203996837	-0.012454000022	-0.067041000172
C	-4.224145002329	-0.833355999367	0.833475000737
H	-4.743048002577	-1.498087998432	1.516766001232
C	-2.842570998263	-0.805272998832	0.832481999705
H	-2.277536001171	-1.447122999683	1.498677999269

Energies (a.u.)	
E	-1678.292739
Zero-point correction	0.375038
Sum of electronic and thermal enthalpies	-1677.891367
Sum of electronic and thermal free energies	-1677.972816
Selected molecular parameters	
Ru-$N_{(NO)}$	1.745 Å
Ru-$O_{(NO)}$	2.886 Å
N-O	1.141 Å
Ru-Cl	2.317 Å
Ru-N_{py1}	2.139 Å
Ru-N_{py2}	2.139 Å
Ru-N_{py3}	2.139 Å
Ru-N_{py4}	2.139 Å
∠Ru-N-O	180.000 °
∠Ru-O-N	0.000 °
NO stretching vibration	
ν_{NO} (cm^{-1})	1947.18 cm^{-1}

Electronic structure

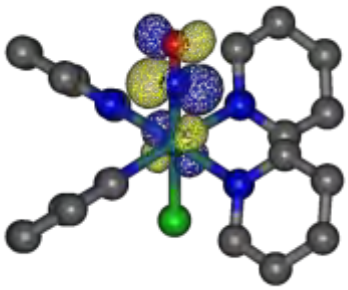
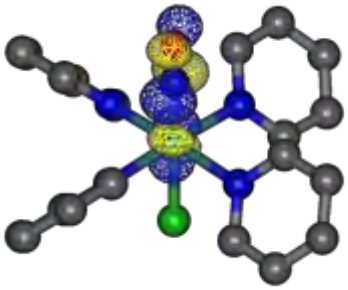

LUMOs (degenerate)

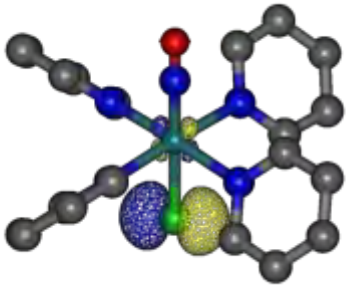
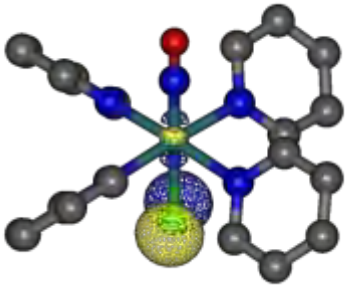

HOMOs (degenerate)

Table AA2. Optimized Cartesian coordinates, energies, molecular parameters and electronic structure of the **MS2** isomer at the B3LYP-D3/Ahlrichs-basis level of theory in its ground state (singlet) in vacuum.

Ru	-0.161797675233	-0.000484407770	0.022594707618
Cl	2.132925867041	-0.103880706629	0.165861360927
N	0.083633431350	1.344873189658	-1.614848799801
N	-0.162393057376	1.692196007102	1.316110093760
N	-0.011115130559	-1.392250851126	1.699055774043
N	-0.132674199670	-1.642858624511	-1.348445084001
N	-1.984203797413	-0.412946041402	0.489462774945
O	-2.260753090415	0.341932163466	-0.369527152746
C	-0.664316061446	1.195378380425	-2.730440934715
H	-1.364140101740	0.368780923531	-2.748848376419
C	-0.554225189227	2.051264722659	-3.809385206617
H	-1.180649821981	1.890519957103	-4.681020799813
C	0.359752989653	3.097686555244	-3.754191609167
H	0.469129068477	3.781791028862	-4.590799848132
C	1.131302553858	3.248545351301	-2.609194408008
H	1.861074496820	4.046795436002	-2.518967497816
C	0.971029434446	2.360521723544	-1.560855419004
H	1.566777526570	2.444057537796	-0.661304274577
C	-1.006171474327	2.718401300438	1.073025093180
H	-1.646045811992	2.637642940404	0.201612343578
C	-1.062005384432	3.837949009890	1.882216693869
H	-1.761751342559	4.632900514786	1.644936762203
C	-0.211455447403	3.922323716492	2.978620121276
H	-0.229549657263	4.793189158319	3.627548033528
C	0.666004833554	2.873460930116	3.223172193433
H	1.354780227173	2.895822259731	4.061701370389
C	0.666199853205	1.777609452481	2.378430682023
H	1.345078142165	0.949562989459	2.535996491123
C	0.727675982304	-2.515114817405	1.594835821961
H	1.247218673855	-2.678067564604	0.660332355842
C	0.845032606771	-3.416117097934	2.637932693388
H	1.453738705447	-4.304515329344	2.503445097704
C	0.189212382599	-3.161553525606	3.835482256167
H	0.269929373851	-3.851798797145	4.670184877359
C	-0.572008988708	-2.004350743764	3.943063649372
H	-1.105249217858	-1.758513579943	4.855781426645
C	-0.652351501202	-1.148748765340	2.859804091673
H	-1.245906764946	-0.244142228387	2.918795828141
C	0.784532149054	-1.691974633538	-2.338848399727
H	1.496758271756	-0.878450568479	-2.386344460658
C	0.836556831110	-2.735036880111	-3.246720169992
H	1.597790355583	-2.725304341512	-4.020323905759
C	-0.080551561815	-3.772902093129	-3.146382490335
H	-0.060091956959	-4.602576852577	-3.847066601149
C	-1.022705489124	-3.729495787241	-2.125180705883
H	-1.758343491951	-4.517432055830	-1.998208211299
C	-1.017220996704	-2.660734944204	-1.249071238130
H	-1.731109554554	-2.618909001647	-0.433494002146

Energies (a.u.)	
E	-1678.235488
Zero-point correction	0.373709
Sum of electronic and thermal enthalpies	-1677.835431
Sum of electronic and thermal free energies	-1677.917151
Selected molecular parameters	
Ru-$N_{(NO)}$	1.926 Å
Ru-$O_{(NO)}$	2.163 Å
N-O	1.177 Å
Ru-Cl	2.302 Å
Ru-N_{py1}	2.133 Å
Ru-N_{py2}	2.130 Å
Ru-N_{py3}	2.184 Å
Ru-N_{py4}	2.140 Å
∠Ru-N-O	84.723 °
∠Ru-O-N	62.476 °
NO stretching vibration	
ν_{NO} (cm^{-1})	1662.24 cm^{-1}

Electronic structure

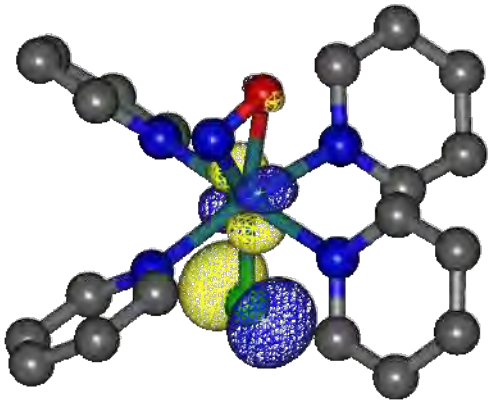

HOMO

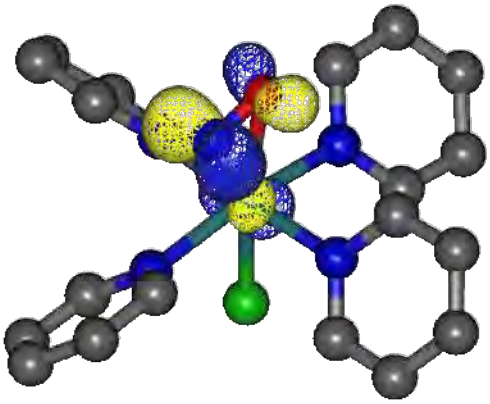

LUMO

Table AA3. Optimized Cartesian coordinates, energies, molecular parameters and electronic structure of the **MS1** isomer at the B3LYP-D3/Ahlrichs-basis level of theory in its ground state (singlet) in vacuum.

Ru	0.000000000000	0.000000000000	0.000209000000
Cl	0.000000000000	0.000000000000	-2.277904000000
N	-0.000060000000	2.128222000000	-0.017851000000
N	2.128222000000	0.000060000000	-0.017851000000
N	0.000060000000	-2.128222000000	-0.017851000000
N	-2.128222000000	-0.000060000000	-0.017851000000
O	0.000000000000	0.000000000000	1.853867000000
N	0.000000000000	0.000000000000	2.990883000000
C	-0.799437000000	2.811765000000	0.829567000000
H	-1.445463000000	2.229088000000	1.477124000000
C	-0.821844000000	4.193094000000	0.875420000000
H	-1.481827000000	4.693644000000	1.576750000000
C	-0.000061000000	4.910623000000	0.013217000000
H	-0.000874000000	5.996718000000	0.023445000000
C	0.818178000000	4.209959000000	-0.863487000000
H	1.472536000000	4.724674000000	-1.559834000000
C	0.796798000000	2.826084000000	-0.853375000000
H	1.414134000000	2.250874000000	-1.531766000000
C	2.811765000000	0.799437000000	0.829567000000
H	2.229088000000	1.445463000000	1.477124000000
C	4.193094000000	0.821844000000	0.875420000000
H	4.693644000000	1.481827000000	1.576750000000
C	4.910623000000	0.000061000000	0.013217000000
H	5.996718000000	0.000874000000	0.023445000000
C	4.209959000000	-0.818178000000	-0.863487000000
H	4.724674000000	-1.472536000000	-1.559834000000
C	2.826084000000	-0.796798000000	-0.853375000000
H	2.250874000000	-1.414134000000	-1.531766000000
C	-0.796798000000	-2.826084000000	-0.853375000000
H	-1.414134000000	-2.250874000000	-1.531766000000
C	-0.818178000000	-4.209959000000	-0.863487000000
H	-1.472536000000	-4.724674000000	-1.559834000000
C	0.000061000000	-4.910623000000	0.013217000000
H	0.000874000000	-5.996718000000	0.023445000000
C	0.821844000000	-4.193094000000	0.875420000000
H	1.481827000000	-4.693644000000	1.576750000000
C	0.799437000000	-2.811765000000	0.829567000000
H	1.445463000000	-2.229088000000	1.477124000000
C	-2.826084000000	0.796798000000	-0.853375000000
H	-2.250874000000	1.414134000000	-1.531766000000
C	-4.209959000000	0.818178000000	-0.863487000000
H	-4.724674000000	1.472536000000	-1.559834000000
C	-4.910623000000	-0.000061000000	0.013217000000
H	-5.996718000000	-0.000874000000	0.023445000000
C	-4.193094000000	-0.821844000000	0.875420000000
H	-4.693644000000	-1.481827000000	1.576750000000
C	-2.811765000000	-0.799437000000	0.829567000000
H	-2.229088000000	-1.445463000000	1.477124000000

Energies (a.u.)	
E	-1678.224215
Zero-point correction	0.373971
Sum of electronic and thermal enthalpies	-1677.823696
Sum of electronic and thermal free energies	-1677.905463
Selected molecular parameters	
Ru-$O_{(NO)}$	1.854 Å
Ru-$N_{(NO)}$	2.991 Å
N-O	1.137 Å
Ru-Cl	2.278 Å
Ru-N_{py1}	2.128 Å
Ru-N_{py2}	2.128 Å
Ru-N_{py3}	2.128 Å
Ru-N_{py4}	2.128 Å
∠Ru-N-O	0.000 °
∠Ru-O-N	180.000 °
NO stretching vibration	
ν_{NO} (cm^{-1})	1889.58 cm^{-1}

Electronic structure

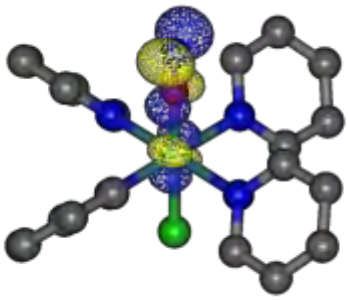
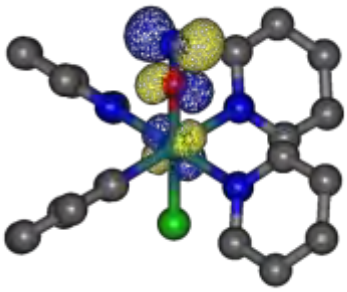

LUMOs (degenerate)

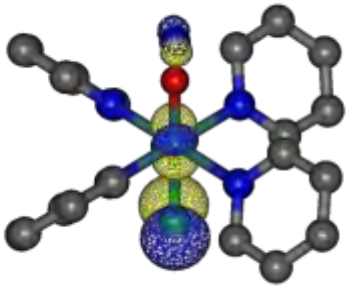
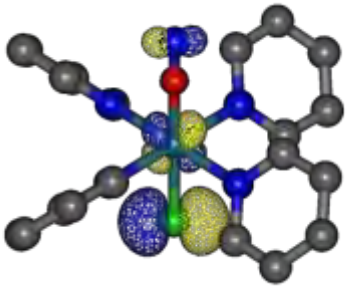

HOMOs (degenerate)

Table AA4. Optimized Cartesian coordinates, energies, molecular parameters and electronic structure of the transition state $^{1}TS_{1}$ at the B3LYP-D3/Ahlrichs-basis level of theory in vacuum.

Ru	-0.017965743688	-0.005179087101	0.048197671652
Cl	2.244021652398	0.066848472777	0.406570132814
N	0.041529554061	1.307497067668	-1.603816436690
N	-0.078819763460	1.750238523297	1.312532798088
N	-0.010563206199	-1.446016199150	1.656383870760
N	0.039406757580	-1.619228142484	-1.288618292934
N	-1.987383046417	-0.116879642486	0.591871625883
O	-2.697668324729	0.741104515547	0.348099803758
C	-0.873434639112	1.165722729318	-2.588247821459
H	-1.604328663107	0.371263313661	-2.472208869675
C	-0.893435848425	1.979406546064	-3.705265659435
H	-1.654307793939	1.827414016102	-4.464140739015
C	0.070291377033	2.974398745446	-3.831787383854
H	0.082069620400	3.625548638917	-4.701055777324
C	1.017673799756	3.116485707925	-2.825879531905
H	1.791404500164	3.875671801096	-2.881443418220
C	0.975615300314	2.273634051716	-1.728678984852
H	1.699260667836	2.354898974498	-0.926992943340
C	-0.759955723146	2.857319314691	0.948490196645
H	-1.268728745628	2.832855610198	-0.006507085406
C	-0.817369264379	3.990792131733	1.739752984659
H	-1.381062366991	4.851885314142	1.395279357236
C	-0.147182426441	4.002384502991	2.956367694807
H	-0.171960359390	4.879990379247	3.595753758563
C	0.558030313754	2.867081197180	3.334464231302
H	1.103468548981	2.825362402788	4.271883735774
C	0.573198245269	1.767223409788	2.495396757356
H	1.128223938179	0.877228799396	2.761367945903
C	0.757789645044	-2.550670631701	1.572854089175
H	1.369635227601	-2.655189079693	0.686692550887
C	0.795549802085	-3.506219241120	2.573931636857
H	1.438679491711	-4.372498421317	2.455547132316
C	0.018656546373	-3.332918966915	3.713187326614
H	0.030977631387	-4.068818736491	4.511847152146
C	-0.763851253186	-2.190290269026	3.811837720251
H	-1.380351431418	-1.998233289133	4.684268039203
C	-0.745588632134	-1.271605830953	2.776402107332
H	-1.314368390766	-0.352428813101	2.859070294739
C	0.993055029598	-1.677257077772	-2.245326399457
H	1.734151694367	-0.886942245424	-2.240417959741
C	1.038859980854	-2.700264866799	-3.174257983120
H	1.830082321843	-2.708464882893	-3.917177737499
C	0.070859281386	-3.697926008253	-3.136753224079
H	0.084411320781	-4.509778811748	-3.858278157564
C	-0.912686024247	-3.639089037834	-2.155202475098
H	-1.687354684219	-4.395967921570	-2.083902733824
C	-0.894933279566	-2.597538543910	-1.247418190593
H	-1.634200638170	-2.532272419315	-0.456627809635

Energies (a.u.)	
E	-1678.202889
Zero-point correction	0.371615
Sum of electronic and thermal enthalpies	-1677.804602
Sum of electronic and thermal free energies	-1677.887915
Selected molecular parameters	
Ru-$N_{(NO)}$	2.046 Å
Ru-$O_{(NO)}$	2.798 Å
N-O	1.140 Å
Ru-Cl	2.291 Å
Ru-N_{py1}	2.111 Å
Ru-N_{py2}	2.164 Å
Ru-N_{py3}	2.159 Å
Ru-N_{py4}	2.097 Å
∠Ru-N-O	120.113 °
∠Ru-O-N	39.245 °
Imaginary frequency	
ν (cm^{-1})	701.03*i* cm^{-1}

Electronic structure

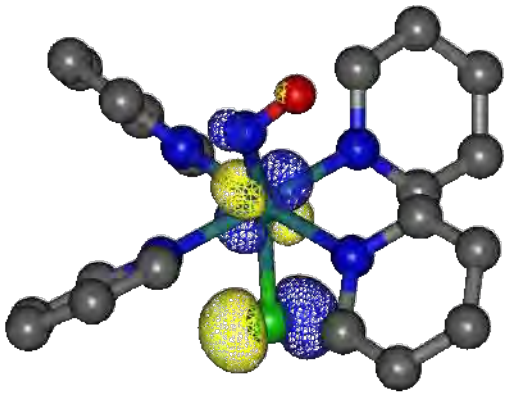

HOMO

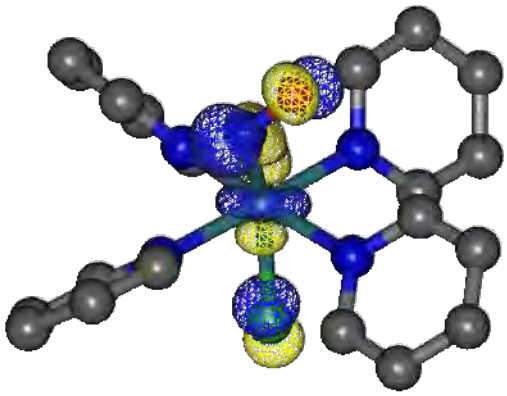

LUMO

Table AA5. Optimized Cartesian coordinates, energies, molecular parameters and electronic structure of the transition state $^{1}TS_{2}$ at the B3LYP-D3/Ahlrichs-basis level of theory in vacuum.

Ru	0.057065000000	-0.005331000000	-0.016454000000
Cl	2.318498000000	-0.072626000000	-0.151695000000
N	0.106734000000	1.395082000000	-1.642123000000
N	0.043663000000	1.637826000000	1.309964000000
N	0.020017000000	-1.313684000000	1.638148000000
N	0.001748000000	-1.687748000000	-1.316473000000
N	-2.803949000000	-0.695547000000	-0.323225000000
O	-2.043279000000	0.127250000000	-0.510733000000
C	-0.639970000000	1.235849000000	-2.756452000000
H	-1.251124000000	0.343218000000	-2.818936000000
C	-0.624607000000	2.138431000000	-3.804529000000
H	-1.248794000000	1.957681000000	-4.673882000000
C	0.200257000000	3.253688000000	-3.723294000000
H	0.237486000000	3.977040000000	-4.532557000000
C	0.982806000000	3.415744000000	-2.587550000000
H	1.654498000000	4.261495000000	-2.480082000000
C	0.912462000000	2.475779000000	-1.573688000000
H	1.524008000000	2.572190000000	-0.686235000000
C	-0.863362000000	2.630449000000	1.172923000000
H	-1.542446000000	2.558909000000	0.330178000000
C	-0.931181000000	3.699174000000	2.046781000000
H	-1.682204000000	4.467669000000	1.893821000000
C	-0.026034000000	3.769201000000	3.100281000000
H	-0.051983000000	4.601083000000	3.798127000000
C	0.913975000000	2.755479000000	3.239321000000
H	1.645520000000	2.769178000000	4.041009000000
C	0.919750000000	1.707536000000	2.335742000000
H	1.643225000000	0.904736000000	2.411126000000
C	0.876434000000	-2.350911000000	1.753392000000
H	1.597911000000	-2.473902000000	0.955061000000
C	0.849671000000	-3.210670000000	2.837902000000
H	1.564297000000	-4.026223000000	2.885960000000
C	-0.089114000000	-3.012122000000	3.842526000000
H	-0.130237000000	-3.674417000000	4.702412000000
C	-0.972543000000	-1.943691000000	3.728170000000
H	-1.720887000000	-1.743668000000	4.488390000000
C	-0.882747000000	-1.115887000000	2.624920000000
H	-1.540890000000	-0.258188000000	2.524225000000
C	0.720595000000	-1.704490000000	-2.460969000000
H	1.344543000000	-0.841833000000	-2.655906000000
C	0.685937000000	-2.769875000000	-3.342039000000
H	1.290683000000	-2.732882000000	-4.242606000000
C	-0.116142000000	-3.868435000000	-3.053982000000
H	-0.159477000000	-4.716938000000	-3.730608000000
C	-0.849653000000	-3.862632000000	-1.875188000000
H	-1.479201000000	-4.701266000000	-1.595260000000
C	-0.758507000000	-2.769337000000	-1.030608000000
H	-1.286103000000	-2.767342000000	-0.084772000000

Energies (a.u.)	
E	-1678.177658
Zero-point correction	0.371248
Sum of electronic and thermal enthalpies	-1677.779553
Sum of electronic and thermal free energies	-1677.862022
Selected molecular parameters	
Ru-$N_{(NO)}$	2.959 Å
Ru-$O_{(NO)}$	2.162 Å
N-O	1.136 Å
Ru-Cl	2.266 Å
Ru-N_{py1}	2.146 Å
Ru-N_{py2}	2.112 Å
Ru-N_{py3}	2.110 Å
Ru-N_{py4}	2.127 Å
∠Ru-N-O	36.949 °
∠Ru-O-N	124.635 °
Imaginary frequency	
ν (cm^{-1})	572.95*i* cm^{-1}

Electronic structure

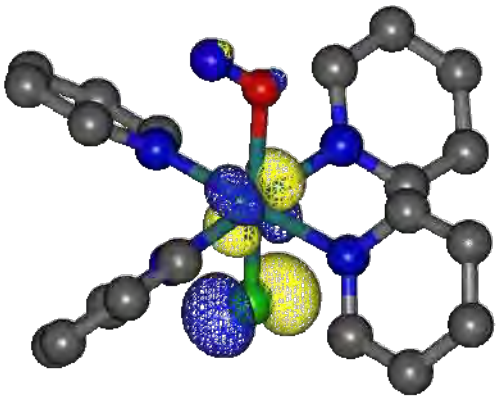

HOMO

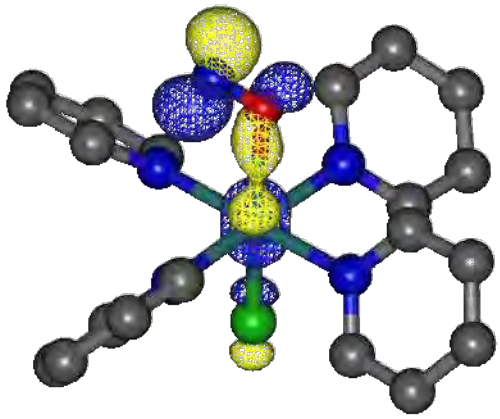

LUMO

Table AA6. Optimized Cartesian coordinates, energies, molecular parameters and electronic structure of the **^{3}GS** triplet state at the B3LYP-D3/Ahlrichs-basis level of theory in vacuum.

Ru	0.034508782019	0.013758245326	0.010817075424
Cl	2.324007899780	0.043928223221	0.041810832486
N	0.044288674940	1.342145107489	-1.673753293168
N	0.049061909178	1.661509036451	1.374394494242
N	-0.076562014786	-1.313065759325	1.647080057519
N	0.060752480594	-1.633229568118	-1.344398549992
N	-1.931893475047	0.168263764539	-0.082076783849
O	-2.807960492765	-0.550398434811	0.142858501287
C	-0.780895607555	1.134726451414	-2.722084963128
H	-1.423748524902	0.263400439463	-2.679026507926
C	-0.816083347002	1.979861777209	-3.815407481646
H	-1.500735726486	1.768224411571	-4.630533538031
C	0.029500843093	3.082791694398	-3.845966707394
H	0.024596997314	3.761634696203	-4.693819229885
C	0.881376114813	3.297127446062	-2.770087072232
H	1.565116979106	4.139783926777	-2.748317169454
C	0.863429916050	2.414672696284	-1.704325304915
H	1.522921958051	2.551051029447	-0.856665451773
C	-0.764673239070	2.720851757232	1.173702000243
H	-1.405195654732	2.689061654154	0.299841403941
C	-0.790704624698	3.805641042575	2.030389523108
H	-1.465321834302	4.630702068044	1.824996889589
C	0.050954073058	3.814769740659	3.136804397003
H	0.053202621404	4.655645241952	3.824317844531
C	0.890178939619	2.727069699861	3.343529858248
H	1.569029218668	2.689085639914	4.189524724177
C	0.865304551010	1.672051405160	2.448596620452
H	1.517632109528	0.817239163511	2.575065943326
C	0.728266548147	-2.398580444784	1.704491783549
H	1.420450952090	-2.534909842684	0.883070693561
C	0.691938032983	-3.284241894136	2.764751142187
H	1.364931695938	-4.135762947273	2.768614417200
C	-0.201999784262	-3.062675605240	3.806318257130
H	-0.250129006997	-3.745753678042	4.649553568322
C	-1.029962578101	-1.946813290708	3.750467986465
H	-1.741842255372	-1.729744803313	4.540418582108
C	-0.937839903710	-1.095179007548	2.666572686993
H	-1.559426459692	-0.209995101037	2.605153595892
C	0.920226122678	-1.657647388055	-2.384862420358
H	1.597914764640	-0.818809017831	-2.478157617220
C	0.954047302431	-2.707025992538	-3.286115219183
H	1.669707550746	-2.681617619176	-4.101728414936
C	0.075657040006	-3.771240997373	-3.126602125506
H	0.082781481014	-4.605783594746	-3.821721693840
C	-0.811009210473	-3.747305640355	-2.056382080111
H	-1.515937531480	-4.554819112205	-1.886175087177
C	-0.788426738115	-2.671894429676	-1.187622164624
H	-1.462041549351	-2.637926189938	-0.339265002634

Energies (a.u.)	
E	-1678.240799
Zero-point correction	0.372586
Sum of electronic and thermal enthalpies	-1677.841085
Sum of electronic and thermal free energies	-1677.926311
Selected molecular parameters	
Ru-$N_{(NO)}$	1.975 Å
Ru-$O_{(NO)}$	2.901 Å
N-O	1.155 Å
Ru-Cl	2.290 Å
Ru-N_{py1}	2.145 Å
Ru-N_{py2}	2.139 Å
Ru-N_{py3}	2.110 Å
Ru-N_{py4}	2.133 Å
∠Ru-N-O	134.214 °
∠Ru-O-N	29.201 °
NO stretching vibration	
ν_{NO} (cm^{-1})	1823.11 cm^{-1}

Electronic structure

$<S^2>$: 2.0089

Mulliken Spin Populations: Ru: 0.8915 Cl: 0.2575 $N_{(NO)}$: 0.4488 $O_{(NO)}$: 0.3810

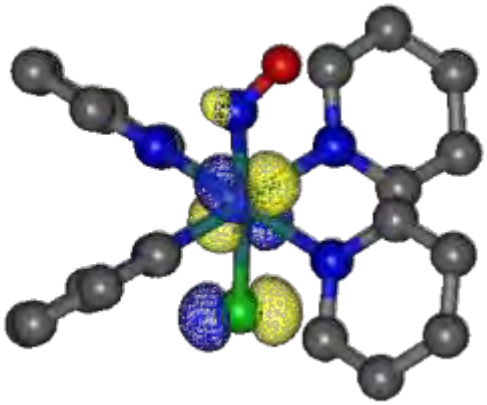

SONO (Hole)

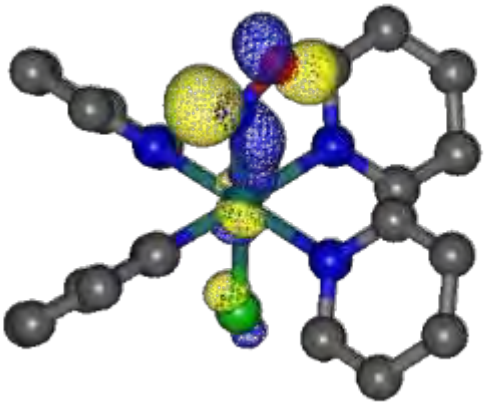

SONO (Particle)

Table AA7. Optimized Cartesian coordinates, energies, molecular parameters and electronic structure of the ^{3}**MS2** triplet state at the B3LYP-D3/Ahlrichs-basis level of theory in vacuum.

Ru	-0.064400000000	-0.000219000000	0.003822000000
Cl	2.181513000000	-0.058799000000	0.105360000000
N	0.140810000000	1.365585000000	-1.641889000000
N	-0.147020000000	1.675337000000	1.312414000000
N	0.030336000000	-1.385157000000	1.676441000000
N	-0.113908000000	-1.649891000000	-1.332551000000
N	-2.124439000000	-0.359360000000	0.495931000000
O	-2.073628000000	0.354157000000	-0.487714000000
C	-0.587592000000	1.205917000000	-2.767542000000
H	-1.274281000000	0.369509000000	-2.796518000000
C	-0.481854000000	2.068912000000	-3.842496000000
H	-1.091402000000	1.895610000000	-4.723621000000
C	0.399437000000	3.140808000000	-3.768788000000
H	0.501433000000	3.833149000000	-4.599461000000
C	1.145194000000	3.308795000000	-2.609204000000
H	1.847017000000	4.129530000000	-2.500749000000
C	0.993851000000	2.408757000000	-1.569810000000
H	1.569725000000	2.513188000000	-0.659684000000
C	-1.006444000000	2.688171000000	1.065526000000
H	-1.633149000000	2.599550000000	0.186864000000
C	-1.098914000000	3.792036000000	1.892801000000
H	-1.811079000000	4.575472000000	1.654101000000
C	-0.275845000000	3.874928000000	3.009226000000
H	-0.326020000000	4.733829000000	3.672282000000
C	0.615110000000	2.837405000000	3.258629000000
H	1.284250000000	2.858382000000	4.112966000000
C	0.652882000000	1.755867000000	2.398988000000
H	1.340220000000	0.935942000000	2.563977000000
C	0.803528000000	-2.488069000000	1.600008000000
H	1.354358000000	-2.643641000000	0.681955000000
C	0.911267000000	-3.387723000000	2.645186000000
H	1.547927000000	-4.259075000000	2.529914000000
C	0.208775000000	-3.152870000000	3.819828000000
H	0.278882000000	-3.842191000000	4.656241000000
C	-0.588178000000	-2.017849000000	3.899619000000
H	-1.163044000000	-1.790255000000	4.791608000000
C	-0.658345000000	-1.162876000000	2.815110000000
H	-1.289224000000	-0.284145000000	2.846116000000
C	0.741311000000	-1.716643000000	-2.377969000000
H	1.451399000000	-0.906123000000	-2.482563000000
C	0.731327000000	-2.774225000000	-3.266912000000
H	1.444590000000	-2.786066000000	-4.084940000000
C	-0.189316000000	-3.801706000000	-3.092270000000
H	-0.218332000000	-4.642153000000	-3.779861000000
C	-1.068300000000	-3.733984000000	-2.018183000000
H	-1.803938000000	-4.511298000000	-1.837647000000
C	-1.000931000000	-2.654582000000	-1.156924000000
H	-1.668207000000	-2.576891000000	-0.307082000000

Energies (a.u.)	
E	-1678.209955
Zero-point correction	0.372929
Sum of electronic and thermal enthalpies	-1677.810400
Sum of electronic and thermal free energies	-1677.893793
Selected molecular parameters	
Ru-$N_{(NO)}$	2.148 Å
Ru-$O_{(NO)}$	2.099 Å
N-O	1.216 Å
Ru-Cl	2.249 Å
Ru-N_{py1}	2.148 Å
Ru-N_{py2}	2.128 Å
Ru-N_{py3}	2.174 Å
Ru-N_{py4}	2.124 Å
∠Ru-N-O	71.131 °
∠Ru-O-N	75.612 °
NO stretching vibration	
ν_{NO} (cm^{-1})	1536.07 cm^{-1}

Electronic structure

$\langle S^2 \rangle$: 2.0073

Mulliken Spin Populations: Ru: 0.8027 Cl: 0.1774 $N_{(NO)}$: 0.7385 $O_{(NO)}$: 0.2794

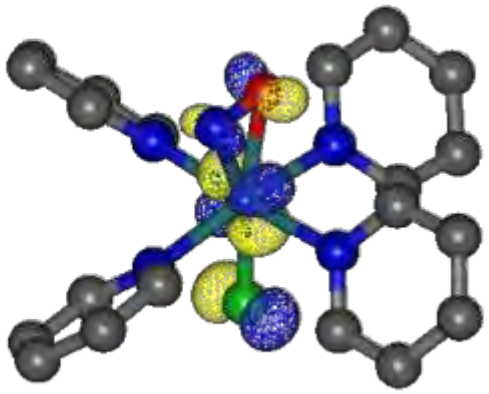

SONO (Hole)

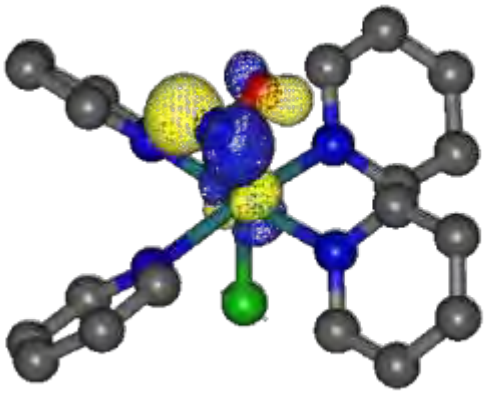

SONO (Particle)

Table AA8. Optimized Cartesian coordinates, energies, molecular parameters and electronic structure of the ^{3}**MS1** triplet state at the B3LYP-D3/Ahlrichs-basis level of theory in vacuum.

Ru	0.141926343332	-0.000160722241	-0.002085975605
Cl	2.393558283046	-0.033667807681	0.037811968688
N	0.094714886903	1.330858958770	-1.650095996005
N	0.116208287032	1.642488945428	1.348885174206
N	-0.017896399137	-1.304511095070	1.651834010139
N	0.125966644346	-1.634230154704	-1.359430063734
N	-2.886633084043	-0.597375368239	0.170101845939
O	-2.021250786359	0.124675825423	-0.102263875611
C	-0.758863047422	1.131824628559	-2.677792594956
H	-1.388840361980	0.251496636931	-2.629991531850
C	-0.835281507902	1.995129386270	-3.754489899923
H	-1.542161051043	1.791879157212	-4.552563377115
C	0.003500304261	3.103243799424	-3.793376621826
H	-0.030947016645	3.794514985418	-4.630491969838
C	0.888765036152	3.306658996074	-2.741614908581
H	1.568228528890	4.152938343834	-2.729771246207
C	0.906716371307	2.410365627056	-1.688695612772
H	1.588554084157	2.536683386172	-0.856948730154
C	-0.758092537242	2.656196424246	1.168600786446
H	-1.411533405253	2.593806376190	0.305378260269
C	-0.829309459606	3.736186978722	2.029040636096
H	-1.552273045496	4.523173732889	1.839378779424
C	0.033697236373	3.790985104367	3.117843143238
H	0.003094533245	4.629711240074	3.807249138347
C	0.936673636591	2.752073213283	3.303613283515
H	1.633656579642	2.750783261734	4.135633667606
C	0.951437061946	1.697485182192	2.407146395519
H	1.648661756074	0.876732598767	2.520332829918
C	0.740031097358	-2.421299878270	1.727694225266
H	1.433055478212	-2.594880686244	0.913754690808
C	0.656442886834	-3.295502412211	2.795753739851
H	1.294793188441	-4.173119151892	2.814484595508
C	-0.240443742990	-3.030427828898	3.823947384814
H	-0.326192631569	-3.703810608650	4.671895094902
C	-1.021617672980	-1.882789645500	3.748664379877
H	-1.732628259872	-1.629704136857	4.528619613035
C	-0.879115711227	-1.043175017613	2.660057796682
H	-1.456024987812	-0.128514661436	2.589602652896
C	0.956840576827	-1.658487552088	-2.423240185120
H	1.641184295330	-0.825773781892	-2.525181527987
C	0.954887402044	-2.697574127247	-3.337036035422
H	1.648532742319	-2.671390408165	-4.171439380158
C	0.068978071805	-3.753938281857	-3.165829327164
H	0.048088968504	-4.580616178932	-3.869988456963
C	-0.786424999429	-3.733743824580	-2.070353575733
H	-1.492703038574	-4.537462779441	-1.888139081913
C	-0.725703835486	-2.668801023777	-1.190079806358
H	-1.366906698903	-2.643892655553	-0.315889311995

Energies (a.u.)	
E	-1678.216481
Zero-point correction	0.371695
Sum of electronic and thermal enthalpies	-1677.817311
Sum of electronic and thermal free energies	-1677.903349

Selected molecular parameters	
Ru-$O_{(NO)}$	2.169 Å
Ru-$N_{(NO)}$	3.092 Å
N-O	1.159 Å
Ru-Cl	2.252 Å
Ru-N_{py1}	2.119 Å
Ru-N_{py2}	2.127 Å
Ru-N_{py3}	2.112 Å
Ru-N_{py4}	2.124 Å
∠Ru-N-O	30.177 °
∠Ru-O-N	134.236 °

NO stretching vibration	
ν_{NO} (cm^{-1})	1785.45 cm^{-1}

Electronic structure

$\langle S^2 \rangle$: 2.0090

Mulliken Spin Populations: Ru: 0.8714 Cl: 0.1911 $N_{(NO)}$: 0.7787 $O_{(NO)}$: 0.1517

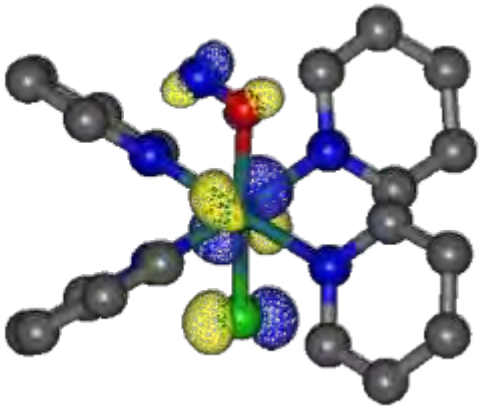

SONO (Hole)

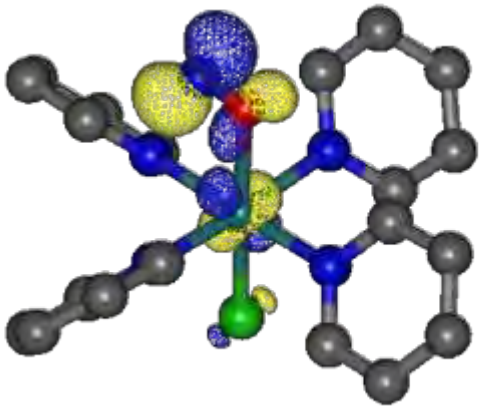

SONO (Particle)

Table AA9. Optimized Cartesian coordinates, energies, molecular parameters and electronic structure of the transition state $^{3}TS_{1}$ at the B3LYP-D3/Ahlrichs-basis level of theory in vacuum.

Ru	-0.023769000000	0.005364000000	-0.015506000000
Cl	-0.028581000000	-0.011678000000	2.229089000000
N	2.120904000000	0.053066000000	0.034906000000
N	0.019780000000	2.111205000000	-0.150969000000
N	-2.175792000000	0.001044000000	0.109377000000
N	-0.030330000000	-2.117493000000	-0.104694000000
N	-0.643177000000	-0.084333000000	-2.174887000000
O	0.505307000000	-0.145674000000	-2.411139000000
C	2.869562000000	-0.758225000000	-0.744445000000
H	2.340514000000	-1.432735000000	-1.405761000000
C	4.251591000000	-0.745412000000	-0.717208000000
H	4.801669000000	-1.417806000000	-1.367862000000
C	4.905711000000	0.130776000000	0.140833000000
H	5.990634000000	0.160915000000	0.182069000000
C	4.140540000000	0.966244000000	0.943605000000
H	4.600995000000	1.666746000000	1.632954000000
C	2.760437000000	0.902020000000	0.867372000000
H	2.143441000000	1.536153000000	1.490614000000
C	0.801277000000	2.712755000000	-1.074376000000
H	1.401035000000	2.068380000000	-1.706435000000
C	0.844521000000	4.086890000000	-1.218385000000
H	1.481590000000	4.522253000000	-1.981611000000
C	0.076516000000	4.880871000000	-0.374480000000
H	0.098868000000	5.963418000000	-0.461062000000
C	-0.717010000000	4.262972000000	0.585402000000
H	-1.326899000000	4.840591000000	1.272789000000
C	-0.729263000000	2.883167000000	0.667754000000
H	-1.334283000000	2.369805000000	1.404774000000
C	-2.814487000000	-0.862938000000	0.926174000000
H	-2.199436000000	-1.544715000000	1.498744000000
C	-4.192311000000	-0.884217000000	1.048908000000
H	-4.653403000000	-1.599873000000	1.722065000000
C	-4.954599000000	0.013566000000	0.312910000000
H	-6.037743000000	0.018982000000	0.393029000000
C	-4.300289000000	0.904019000000	-0.529321000000
H	-4.848525000000	1.623501000000	-1.129058000000
C	-2.920046000000	0.869280000000	-0.607034000000
H	-2.389738000000	1.547456000000	-1.263607000000
C	0.828355000000	-2.829069000000	0.661565000000
H	1.494059000000	-2.264813000000	1.302135000000
C	0.850617000000	-4.210358000000	0.652319000000
H	1.552502000000	-4.734007000000	1.293554000000
C	-0.029384000000	-4.899930000000	-0.174683000000
H	-0.028329000000	-5.985853000000	-0.201987000000
C	-0.914748000000	-4.172041000000	-0.960513000000
H	-1.624118000000	-4.663364000000	-1.618780000000
C	-0.896235000000	-2.791411000000	-0.894889000000
H	-1.584449000000	-2.200185000000	-1.487161000000

Energies (a.u.)	
E	-1678.201864
Zero-point correction	0.371397
Sum of electronic and thermal enthalpies	-1677.803729
Sum of electronic and thermal free energies	-1677.887632
Selected molecular parameters	
Ru-$N_{(NO)}$	2.248 Å
Ru-$O_{(NO)}$	2.458 Å
N-O	1.174 Å
Ru-Cl	2.245 Å
Ru-N_{py1}	2.146 Å
Ru-N_{py2}	2.111 Å
Ru-N_{py3}	2.156 Å
Ru-N_{py4}	2.125 Å
∠Ru-N-O	85.748 °
∠Ru-O-N	65.804 °
Imaginary frequency	
ν (cm^{-1})	1075.06*i* cm^{-1}

Electronic structure

$<S^2>$: 2.0186

Mulliken Spin Populations: Ru: 0.9200 Cl: 0.1832 $N_{(NO)}$: 0.5840 $O_{(NO)}$: 0.2996

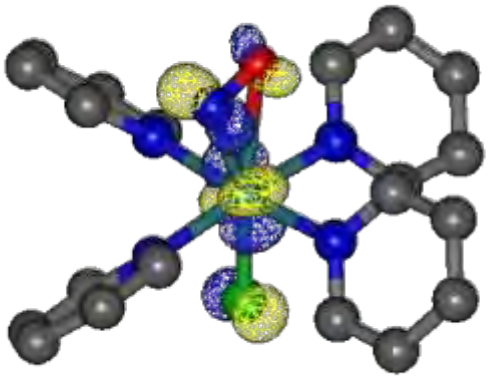

SONO (Hole)

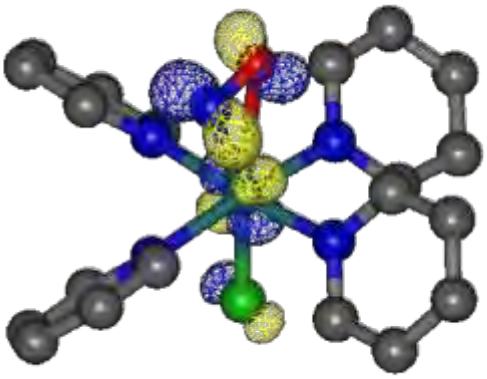

SONO (Particle)

Table AA10. Optimized Cartesian coordinates, energies, molecular parameters and electronic structure of the transition state $^3TS_2$ at the B3LYP-D3/Ahlrichs-basis level of theory in vacuum.

Ru	-0.002475000000	0.002343000000	0.017137000000
Cl	-0.061868000000	-0.011028000000	2.248373000000
N	2.130378000000	-0.003796000000	0.090936000000
N	0.051579000000	2.112391000000	-0.101005000000
N	-2.146280000000	-0.000639000000	0.004193000000
N	-0.035930000000	-2.098485000000	-0.138943000000
O	0.515688000000	0.056977000000	-2.336195000000
N	-0.594918000000	0.087267000000	-2.685871000000
C	2.853749000000	-0.807754000000	-0.717812000000
H	2.302370000000	-1.446410000000	-1.397035000000
C	4.236196000000	-0.831645000000	-0.698268000000
H	4.766888000000	-1.496599000000	-1.372179000000
C	4.915591000000	-0.002829000000	0.186695000000
H	6.001031000000	-0.003315000000	0.225051000000
C	4.175726000000	0.825062000000	1.021006000000
H	4.657713000000	1.488992000000	1.731532000000
C	2.794134000000	0.800646000000	0.948210000000
H	2.193898000000	1.430160000000	1.592581000000
C	0.918899000000	2.745202000000	-0.923005000000
H	1.579971000000	2.122998000000	-1.513605000000
C	0.972178000000	4.123080000000	-1.019583000000
H	1.680216000000	4.581570000000	-1.702494000000
C	0.123552000000	4.891229000000	-0.231101000000
H	0.151650000000	5.975931000000	-0.281459000000
C	-0.757922000000	4.243801000000	0.627339000000
H	-1.432724000000	4.799910000000	1.270326000000
C	-0.773967000000	2.862554000000	0.664794000000
H	-1.444590000000	2.328279000000	1.326086000000
C	-2.828081000000	-0.856468000000	0.794806000000
H	-2.241939000000	-1.518517000000	1.419064000000
C	-4.211260000000	-0.894274000000	0.829243000000
H	-4.706080000000	-1.601948000000	1.486740000000
C	-4.935727000000	-0.023382000000	0.026445000000
H	-6.021760000000	-0.032511000000	0.034830000000
C	-4.239138000000	0.861723000000	-0.788138000000
H	-4.756342000000	1.562093000000	-1.436188000000
C	-2.856982000000	0.847055000000	-0.771617000000
H	-2.295786000000	1.533516000000	-1.394490000000
C	0.751190000000	-2.862960000000	0.652148000000
H	1.371146000000	-2.342402000000	1.371436000000
C	0.757334000000	-4.242214000000	0.566958000000
H	1.397834000000	-4.812293000000	1.232412000000
C	-0.057971000000	-4.870120000000	-0.368169000000
H	-0.066795000000	-5.952705000000	-0.456889000000
C	-0.866079000000	-4.086055000000	-1.183346000000
H	-1.522706000000	-4.529667000000	-1.924954000000
C	-0.839740000000	-2.711806000000	-1.036100000000
H	-1.473197000000	-2.076002000000	-1.643257000000

Energies (a.u.)	
E	-1678.200617
Zero-point correction	0.371281
Sum of electronic and thermal enthalpies	-1677.802316
Sum of electronic and thermal free energies	-1677.887366
Selected molecular parameters	
Ru-$N_{(NO)}$	2.768 Å
Ru-$O_{(NO)}$	2.410 Å
N-O	1.165 Å
Ru-Cl	2.232 Å
Ru-N_{py1}	2.134 Å
Ru-N_{py2}	2.114 Å
Ru-N_{py3}	2.144 Å
Ru-N_{py4}	2.107 Å
∠Ru-N-O	60.135 °
∠Ru-O-N	95.090 °
Imaginary frequency	
ν (cm^{-1})	497.30*i* cm^{-1}

Electronic structure

$<S^2>$: 2.0074

Mulliken Spin Populations: Ru: 0.8419 Cl: 0.1523 $N_{(NO)}$: 0.7303 $O_{(NO)}$: 0.2562

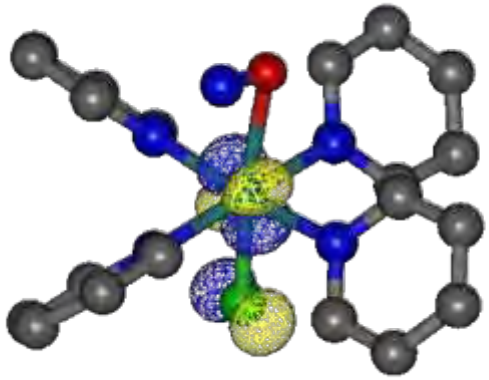

SONO (Hole)

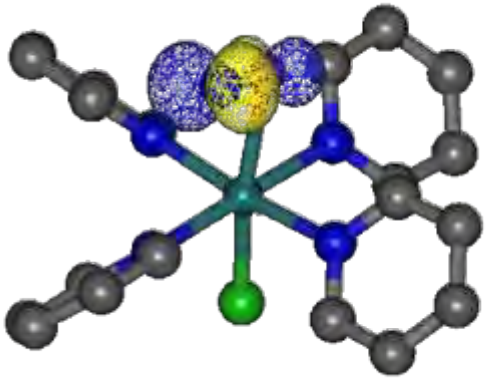

SONO (Particle)

Table AA11. Optimized Cartesian coordinates, energy, molecular parameters and electronic structure of the $MECP_1$ (triplet and singlet) at the B3LYP-D3/Ahlrichs-basis level of theory in vacuum.

Ru	0.024419750822	0.015449407521	0.012486264395
Cl	2.317243292142	0.035239182135	0.049137646372
N	0.040842102686	1.344464958339	-1.670401113721
N	0.042240032245	1.661721443943	1.375385114992
N	-0.081085959789	-1.316209185990	1.646529319646
N	0.053871735310	-1.629644226991	-1.345862619391
N	-1.930331188115	0.150965914833	-0.066524351351
O	-2.824210165132	-0.548992312878	0.146048319627
C	-0.785555245649	1.140385168269	-2.718298092200
H	-1.434080822191	0.273409223660	-2.672561118866
C	-0.813789653049	1.982431717482	-3.814150873104
H	-1.499087424756	1.773479000726	-4.629598440399
C	0.040453573556	3.078652553181	-3.847711482706
H	0.041762148939	3.754169613380	-4.698485846502
C	0.892580366870	3.290384510032	-2.771484728569
H	1.582030984313	4.128671007621	-2.751727133587
C	0.867312008450	2.411272402550	-1.702983106372
H	1.525784105398	2.546257265755	-0.854076826208
C	-0.767852028774	2.722952550144	1.170679578012
H	-1.406308913797	2.690028090273	0.295385852045
C	-0.791271947339	3.810356625075	2.023988865959
H	-1.462240299132	4.637718104077	1.815341914293
C	0.049496796589	3.820050246167	3.131087033684
H	0.054532162867	4.663817547972	3.815391676819
C	0.884192753985	2.729591728561	3.342659382847
H	1.561355953445	2.691918218882	4.190242059083
C	0.856593399216	1.671904082562	2.451099065155
H	1.504400602666	0.814084794455	2.581666834097
C	0.723897203050	-2.401961681784	1.699140226329
H	1.410222340933	-2.539124864369	0.872922424924
C	0.694259221866	-3.287356634257	2.759886156160
H	1.366847607064	-4.139419565407	2.759810547948
C	-0.192415565907	-3.065001418140	3.807575884236
H	-0.234548149305	-3.746907537728	4.652328990887
C	-1.021178734114	-1.949505716003	3.756244933408
H	-1.727585972078	-1.731949524118	4.551123734640
C	-0.936549378678	-1.098721889111	2.670982980130
H	-1.558557991173	-0.213591899740	2.613358844238
C	0.913127041582	-1.649911680165	-2.386480367409
H	1.585907559017	-0.807003448836	-2.480660894853
C	0.952430567452	-2.699541874599	-3.287198101997
H	1.668090739343	-2.671004932082	-4.103020660691
C	0.079617764677	-3.768260601495	-3.127122546876
H	0.091403957969	-4.603828001991	-3.821321517031
C	-0.807528288690	-3.747911488683	-2.057235722205
H	-1.508169683971	-4.559317620407	-1.886743058761
C	-0.790190710266	-2.672074164397	-1.189058361590
H	-1.462978650549	-2.641559088429	-0.339752685539

Energies (a.u.)	
E	-1678.240658
Selected molecular parameters	
Ru-$N_{(NO)}$	1.961 Å
Ru-$O_{(NO)}$	2.907 Å
N-O	1.155 Å
Ru-Cl	2.293 Å
Ru-N_{py1}	2.144 Å
Ru-N_{py2}	2.137 Å
Ru-N_{py3}	2.111 Å
Ru-N_{py4}	2.134 Å
∠Ru-N-O	136.229 °
∠Ru-O-N	27.817 °

Gradient of the triplet	**Gradient of the singlet**
	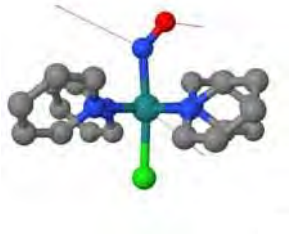
x300	x30

Electronic structure in the lowest triplet state

$\langle S^2 \rangle$: 2.0092

Mulliken Spin Populations: Ru: 0.8898 Cl: 0.2550 $N_{(NO)}$: 0.4527 $O_{(NO)}$: 0.3793

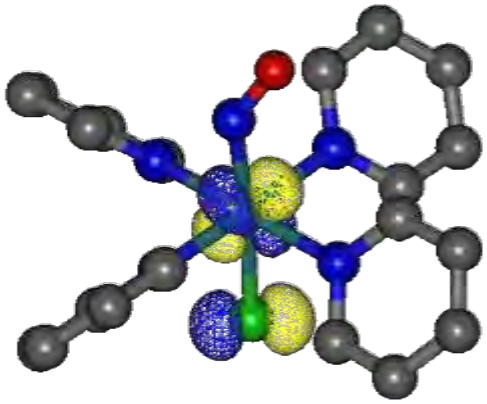

SONO (Hole)

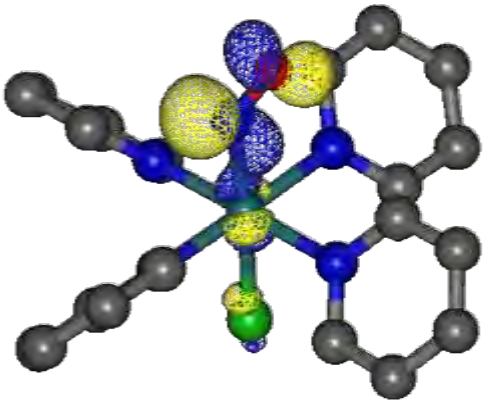

SONO (Particle)

Table AA12. Optimized Cartesian coordinates, energy, molecular parameters and electronic structure of the $MECP_2$ (triplet and singlet) at the B3LYP-D3/Ahlrichs-basis level of theory in vacuum.

Ru	-0.043119763404	0.005216872011	0.003083935309
Cl	2.238035359920	0.081109288161	0.160801890946
N	-0.004601921537	-1.643521926743	-1.315029186359
N	0.020476274728	1.324777574070	-1.665901656900
N	-0.011101733102	1.685952673562	1.371672476293
N	-0.055672045174	-1.376679403461	1.640739685727
N	-1.990877886236	0.376010489062	0.329121151629
O	-2.584375975146	-0.195233473206	-0.481594806478
C	-0.857667752778	-2.678846052312	-1.148244632708
C	-0.868852566923	-3.769698457843	-1.995868331032
C	0.040396881632	-3.818696728680	-3.047157315243
C	0.927864026286	-2.761760534293	-3.212762420642
C	0.878122947103	-1.692835340344	-2.337097271284
C	-0.788077218429	1.112561904106	-2.727029729520
C	-0.797345880971	1.945417774918	-3.830734048632
C	0.065325006770	3.034843091644	-3.862292533513
C	0.904787715184	3.250475623281	-2.776376460873
C	0.856958211746	2.383997849797	-1.698748672008
C	0.711281330098	1.635419676314	2.510198771146
C	0.749842347434	2.687731045780	3.407435737775
C	0.023307741904	3.840630348598	3.136863562068
C	-0.721525975885	3.895905397793	1.965517608086
C	-0.715016539627	2.807772852953	1.111919345635
C	0.802332375211	-2.418671431329	1.664805130187
C	0.831401865080	-3.329609758687	2.706134221680
C	-0.048325634870	-3.176157706723	3.769635424842
C	-0.931877649898	-2.103069546859	3.750365657414
C	-0.906082170795	-1.228355339873	2.680437862804
H	-1.543293535148	-2.620342465511	-0.310748163434
H	-1.580219936864	-4.571531046235	-1.824452769930
H	0.059247466162	-4.669369112582	-3.722719799264
H	1.660930406840	-2.758878196013	-4.013460943829
H	1.560004079556	-0.856590931051	-2.432033359857
H	-1.437690824281	0.245631820071	-2.687078883915
H	-1.470183796765	1.731313359925	-4.655134426374
H	0.084782618172	3.701179788113	-4.720086373074
H	1.600059982823	4.083936530543	-2.755961381677
H	1.502817820515	2.522777266162	-0.841225686467
H	1.280844546693	0.733196501925	2.690353547258
H	1.352390364585	2.596618263530	4.305616414100
H	0.039065086382	4.681562000407	3.824394289071
H	-1.305145804147	4.773409564498	1.706139832098
H	-1.283222880731	2.832023089777	0.189714348505
H	1.485806958583	-2.508454672148	0.829948210224
H	1.545259833292	-4.146928346562	2.675965451327
H	-0.045077731390	-3.877132453402	4.599613221226
H	-1.638625049032	-1.936761079210	4.557437704077
H	-1.574560973567	-0.375339643936	2.650344373588

Energies (a.u.)	
E	-1678.216122
Selected molecular parameters	
Ru-$N_{(NO)}$	2.009 Å
Ru-$O_{(NO)}$	2.595 Å
N-O	1.156 Å
Ru-Cl	2.288 Å
Ru-N_{py1}	2.111 Å
Ru-N_{py2}	2.129 Å
Ru-N_{py3}	2.168 Å
Ru-N_{py4}	2.143 Å
∠Ru-N-O	107.022 °
∠Ru-O-N	47.770 °

Gradient of the triplet	**Gradient of the singlet**
	
x30	x30

Electronic structure in the lowest triplet state

$\langle S^2 \rangle$: 2.0072

Mulliken Spin Populations: Ru: 0.9173 Cl: 0.2795 $N_{(NO)}$: 0.3835 $O_{(NO)}$: 0.4142

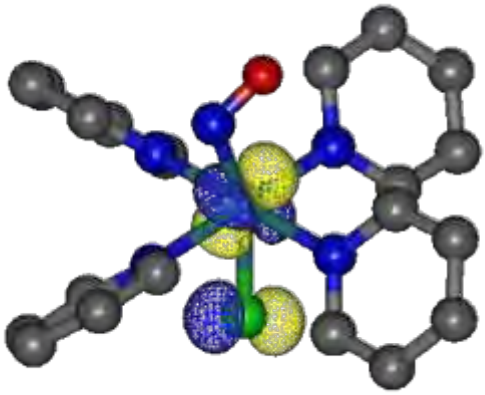

SONO (Hole)

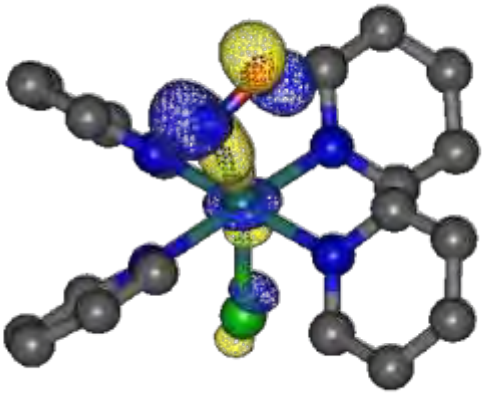

SONO (Particle)

Table AA13. Optimized Cartesian coordinates, energy, molecular parameters and electronic structure of the $MECP_3$ (triplet and singlet) at the B3LYP-D3/Ahlrichs-basis level of theory in vacuum.

Ru	-0.015614682016	0.001576057044	0.006114560692
Cl	2.213837022108	-0.050816401568	0.104062078113
N	0.166716605099	1.368392087969	-1.642002106290
N	-0.140965051931	1.671434053483	1.310166328354
N	0.053081815689	-1.387197903742	1.674578140220
N	-0.103418714876	-1.643069374719	-1.327163270600
N	-2.151650461958	-0.317915575172	0.533823814630
O	-2.045081259929	0.327980253411	-0.503504082774
C	-0.568399076971	1.207279592687	-2.762520770218
H	-1.252773082442	0.369016363680	-2.785913173175
C	-0.473319291132	2.071864772731	-3.837418461347
H	-1.087776511223	1.896870610593	-4.714893673706
C	0.402574102670	3.148079609496	-3.768664150738
H	0.495686090600	3.841962226317	-4.599376332863
C	1.153972631417	3.319336155164	-2.613084585573
H	1.850971903381	4.144780015369	-2.507634984881
C	1.013461448946	2.416857872933	-1.574240685005
H	1.592416134331	2.526311759159	-0.666513098500
C	-1.002662793709	2.677956633521	1.045709701855
H	-1.616072718958	2.579721138502	0.159323647532
C	-1.113703359544	3.782686743557	1.869821919760
H	-1.827070801145	4.561283609690	1.618832745394
C	-0.308418987945	3.872841065373	2.998432911234
H	-0.373804156013	4.733551871110	3.658071932767
C	0.583717887698	2.840104260208	3.266001446304
H	1.237927025654	2.866998087422	4.131792156838
C	0.639972422411	1.756108526337	2.411159694225
H	1.325749744467	0.937910020080	2.591329460629
C	0.823911481607	-2.492212788998	1.597304433062
H	1.378615476665	-2.646514381718	0.681384215560
C	0.924167401183	-3.398638751078	2.637313996914
H	1.559008128119	-4.271211324978	2.520337647851
C	0.215681194021	-3.169149628194	3.809428787480
H	0.279037714421	-3.863745025253	4.642279934843
C	-0.578933024403	-2.032889250365	3.890612273025
H	-1.159187290547	-1.810064336785	4.780348463832
C	-0.641618544805	-1.171086814266	2.811050143707
H	-1.272681205842	-0.293043208261	2.841786880742
C	0.739525794401	-1.720571498267	-2.382377733424
H	1.454660987239	-0.915982050011	-2.499856523519
C	0.709509101225	-2.782212453140	-3.265379194994
H	1.414010905926	-2.806058616547	-4.090991839280
C	-0.221558970539	-3.798321768924	-3.076430300809
H	-0.267278870168	-4.641576065970	-3.760008743964
C	-1.090096442403	-3.715498049705	-1.995096337442
H	-1.834530607354	-4.482477153829	-1.805800788672
C	-1.002027064655	-2.634431821747	-1.137427647750
H	-1.662220048765	-2.541175142599	-0.284237830041

Energies (a.u.)	
E	-1678.208742
Selected molecular parameters	
Ru-$N_{(NO)}$	2.223 Å
Ru-$O_{(NO)}$	2.118 Å
N-O	1.227 Å
Ru-Cl	2.232 Å
Ru-N_{py1}	2.149 Å
Ru-N_{py2}	2.122 Å
Ru-N_{py3}	2.172 Å
Ru-N_{py4}	2.119 Å
∠Ru-N-O	68.908 °
∠Ru-O-N	78.381 °

Gradient of the triplet	**Gradient of the singlet**
	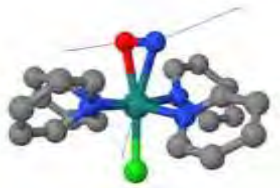
x60	x30

Electronic structure in the lowest triplet state

$\langle S^2 \rangle$: 2.0073

Mulliken Spin Populations: Ru: 0.7940 Cl: 0.1824 $N_{(NO)}$: 0.7458 $O_{(NO)}$: 0.2715

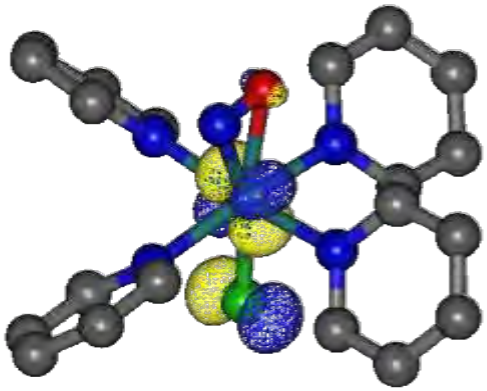

SONO (Hole)

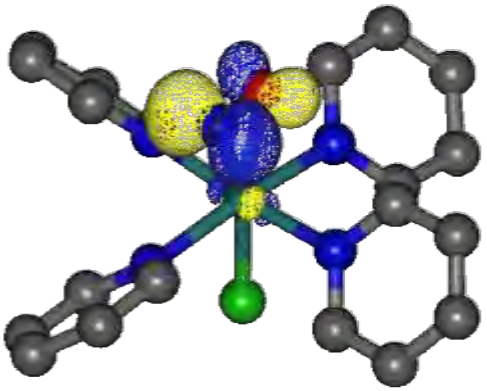

SONO (Particle)

Table AA14. Optimized Cartesian coordinates, energy, molecular parameters and electronic structure of the $MECP_4$ (triplet and singlet) at the B3LYP-D3/Ahlrichs-basis level of theory in vacuum.

Ru	0.093693876712	0.002774585909	-0.004086461390
Cl	2.349645791169	-0.064274087609	0.052364338186
N	0.093081227263	1.342958293968	-1.645267170885
N	0.082764897787	1.648511933793	1.341574329915
N	-0.020534323798	-1.318453594657	1.653257292260
N	0.095636217583	-1.634635936340	-1.362249951403
N	-2.959346025723	-0.494118217642	0.143448282083
O	-1.926076914435	-0.011708561646	-0.042769822312
C	-0.764923127790	1.166958677940	-2.673268517400
H	-1.417645827195	0.302862941584	-2.625436089753
C	-0.817182436929	2.031837724892	-3.750100229375
H	-1.527952823891	1.847632072345	-4.549584864345
C	0.051001226186	3.117415654093	-3.787562045680
H	0.036201085715	3.809078827106	-4.625221486842
C	0.939583853570	3.297309301788	-2.734474005446
H	1.640571670832	4.126127149329	-2.721494367142
C	0.933121585495	2.399831928884	-1.681913626923
H	1.616858910130	2.507192633004	-0.848745173134
C	-0.786859130068	2.664369304633	1.152712079342
H	-1.439071543556	2.597346582822	0.288741936146
C	-0.852816460452	3.751762181360	2.003906522650
H	-1.571594690070	4.541175311195	1.807711958025
C	0.011061658901	3.811255369639	3.091945400915
H	-0.014859477950	4.656644955836	3.773697987809
C	0.908166673887	2.768981517250	3.287101471509
H	1.604449995087	2.771002052808	4.119976600640
C	0.917472110534	1.706362437939	2.399971782172
H	1.608986778353	0.881704147938	2.521160560854
C	0.748800121058	-2.427117523109	1.718682532972
H	1.431540886069	-2.595567066996	0.895208442670
C	0.688115095953	-3.302748673494	2.787878812782
H	1.334024391966	-4.175120948658	2.796797329961
C	-0.194847220594	-3.045798163038	3.829790460842
H	-0.260891750728	-3.718607172829	4.680115491802
C	-0.988725230856	-1.906569442415	3.764635942371
H	-1.690699122655	-1.659545780831	4.554803028988
C	-0.871855719156	-1.067394690122	2.671992846300
H	-1.461989422592	-0.160598711610	2.608595753892
C	0.925432429392	-1.653415644964	-2.426502990437
H	1.598506495938	-0.812087137704	-2.534239984625
C	0.935932779128	-2.697814069348	-3.334218496584
H	1.628016982171	-2.667671174248	-4.170039216200
C	0.064460381555	-3.764739123098	-3.155077722197
H	0.054186139101	-4.596735047981	-3.853568277172
C	-0.790845581958	-3.748671292552	-2.059383491283
H	-1.486553555209	-4.560602585275	-1.872121712287
C	-0.743890411734	-2.677443828612	-1.186250214657
H	-1.384801464200	-2.654614111278	-0.311960267617

Energies (a.u.)	
E	-1678.210359
Selected molecular parameters	
Ru-$N_{(NO)}$	3.097 Å
Ru-$O_{(NO)}$	2.020 Å
N-O	1.155 Å
Ru-Cl	2.258 Å
Ru-N_{py1}	2.119 Å
Ru-N_{py2}	2.126 Å
Ru-N_{py3}	2.123 Å
Ru-N_{py4}	2.127 Å
∠Ru-N-O	16.997 °
∠Ru-O-N	153.378 °

Gradient of the triplet	**Gradient of the singlet**
	
x30	x30

Electronic structure in the lowest triplet state

$<S^2>$: 2.0078

Mulliken Spin Populations: Ru: 0.8427 Cl: 0.1891 $N_{(NO)}$: 0.7990 $O_{(NO)}$: 0.1688

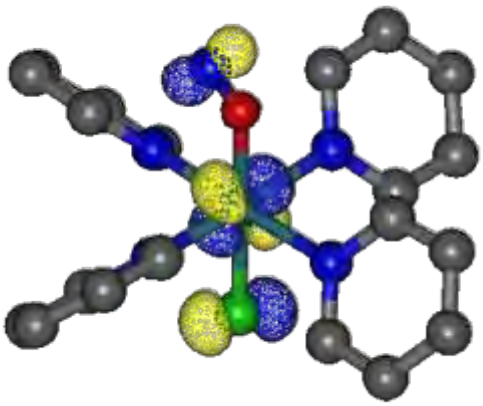

SONO (Hole)

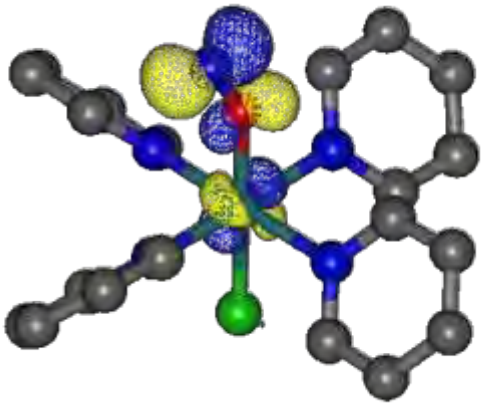

SONO (Particle)

Figure AAl. Absorption TD-DFT spectrum of GS at the TPSSh-03/Ahlrichs-basis levelof theory.

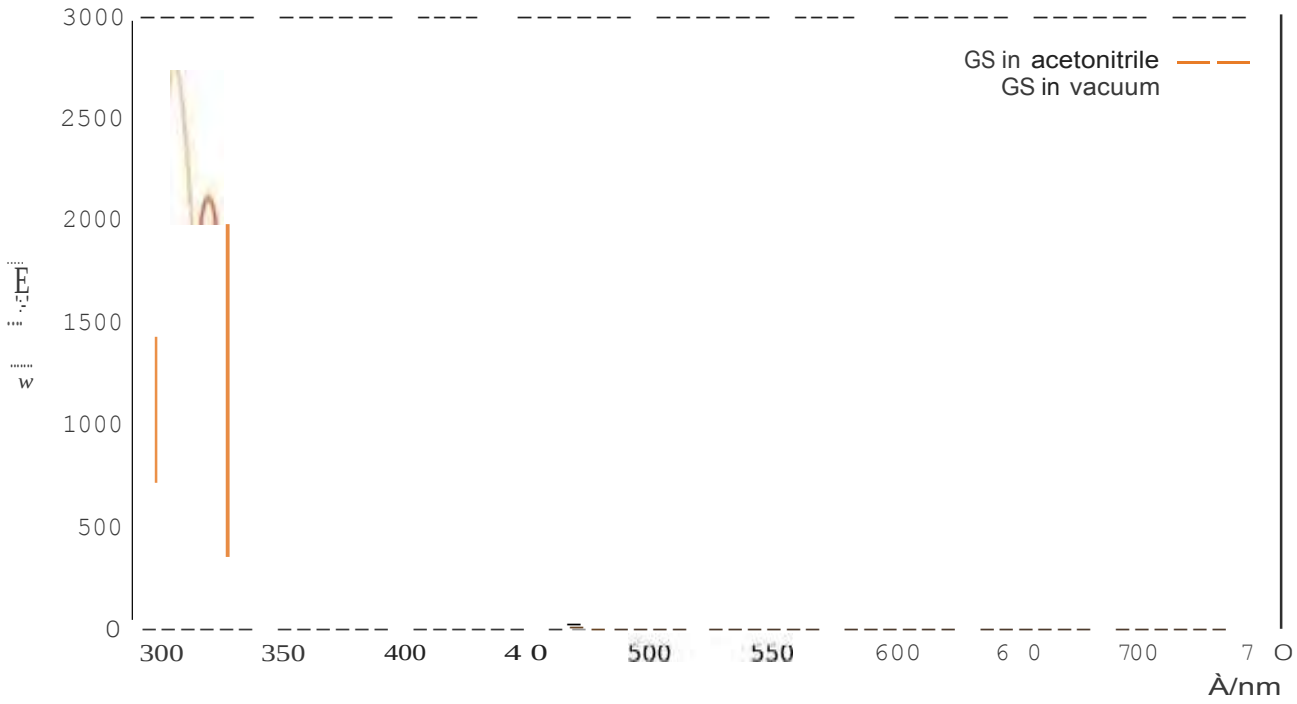

Figure AA2. Absorption TD-DFT spectrum of MS2 at the TPSSh-03/Ahlrichs-basis level of theory.

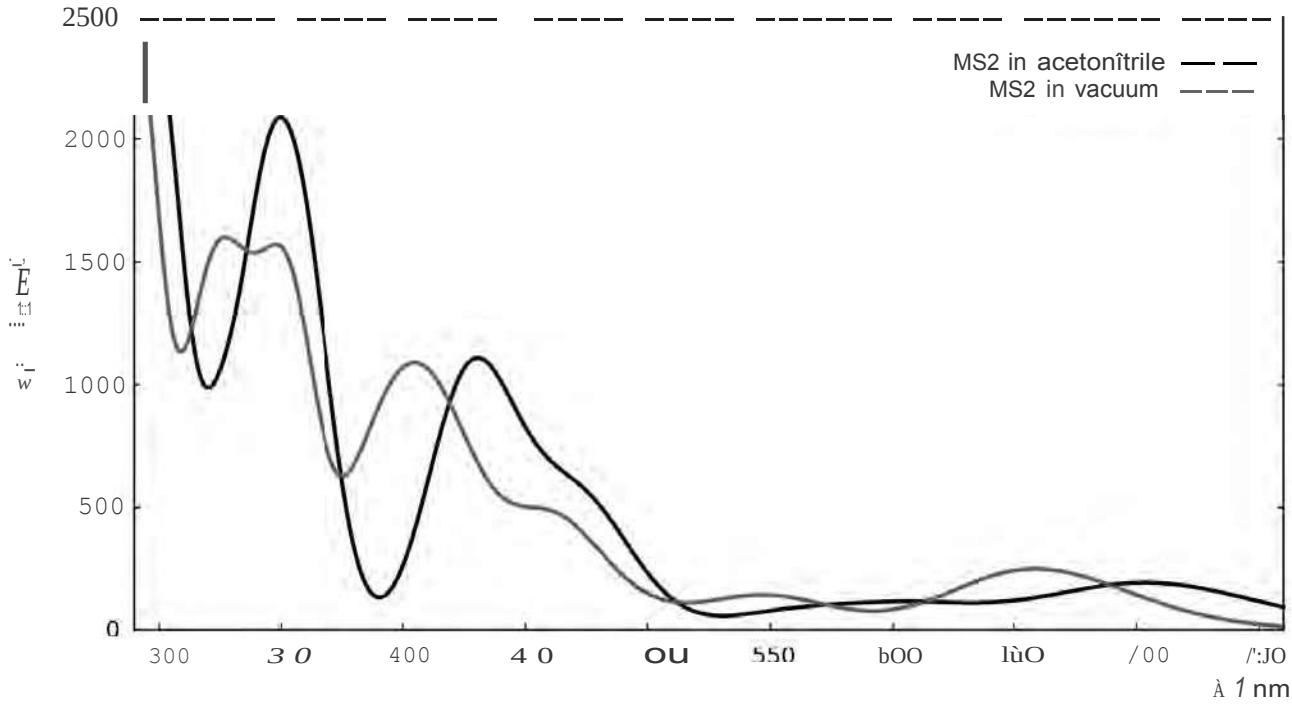

Figure AA3. Absorption TD-DFT spectrum of MSl at the TPSSh-03/Ahlrichs-basis level of theory.

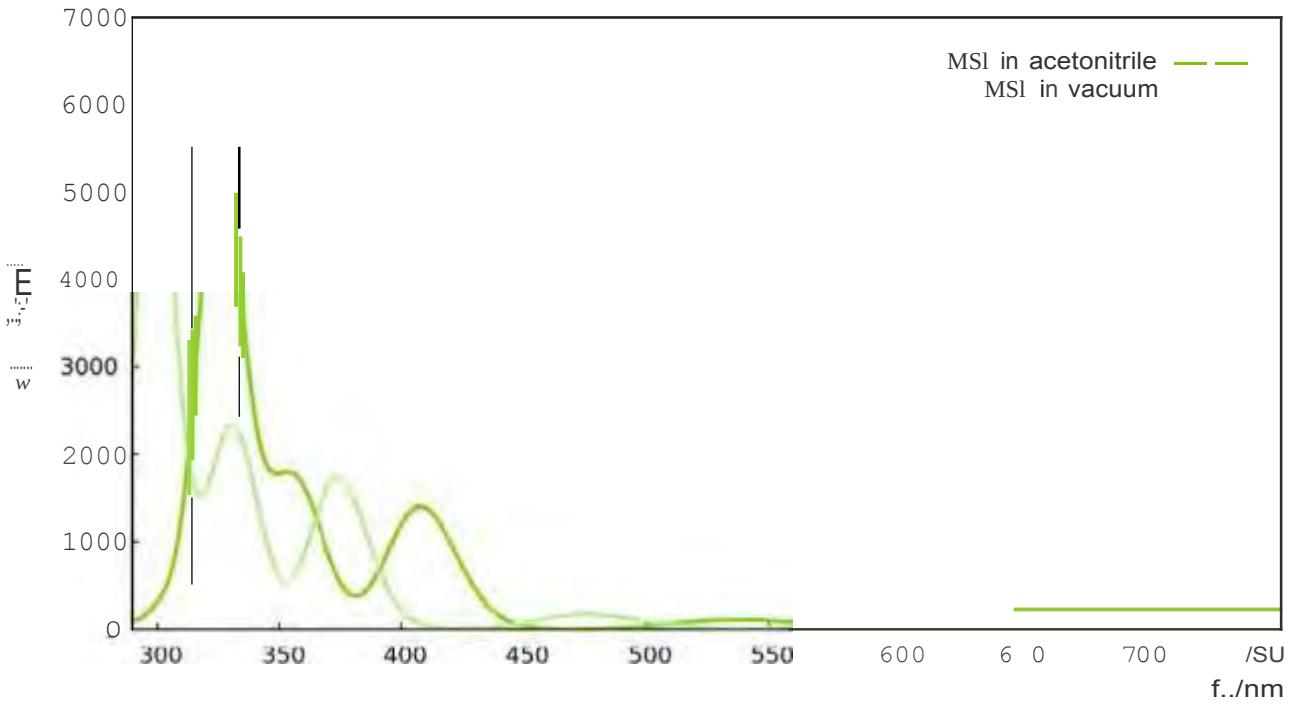

Figure AA4. Absorption TD-DFT spectrum of GS (orange), MSl (green), and MS2 (black) at the TPSSh-03/Ahlrichs-basis level of theory in vacuum and in acetonitrile.

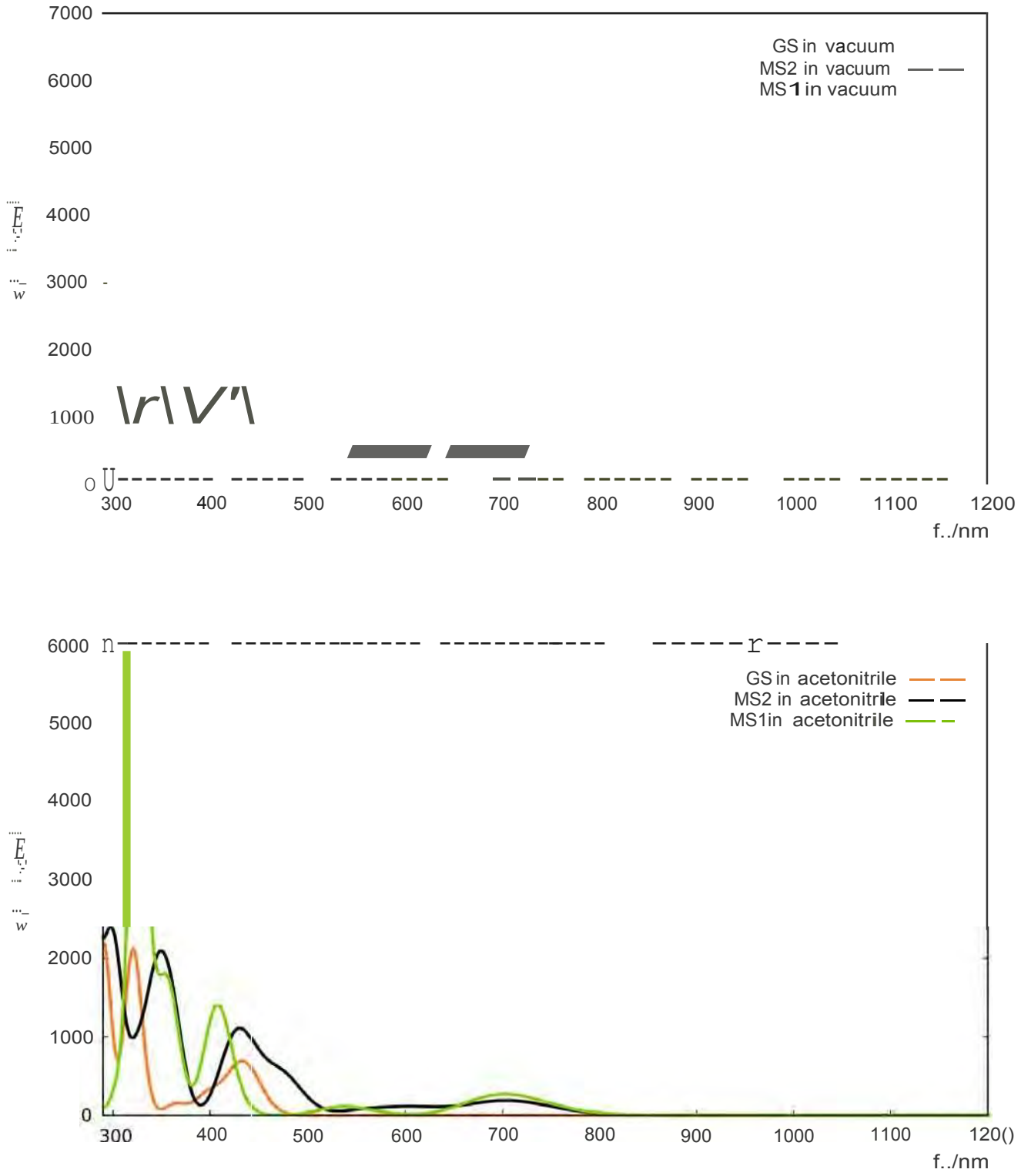

Table AA15. TD-DFT states of the **GS** isomer at TPSSh-03/Ahlrichs-basis level of theory in acetonitrile. Natural transition orbitals involved are shawn in the following table for each state.

State	À/ nm	f.,..	Nature	Natural Transition Orbitals (NTO}
	434	0.0031	Ru(d) ..... Ru(d}NO(n*)	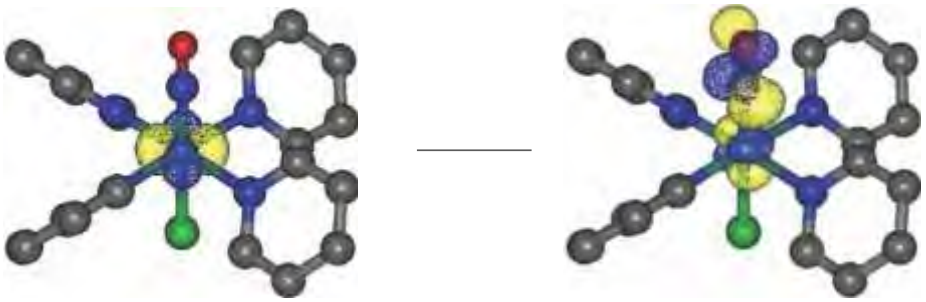
	434	0.0031	Ru(d) ..... Ru(d)NO(n*)	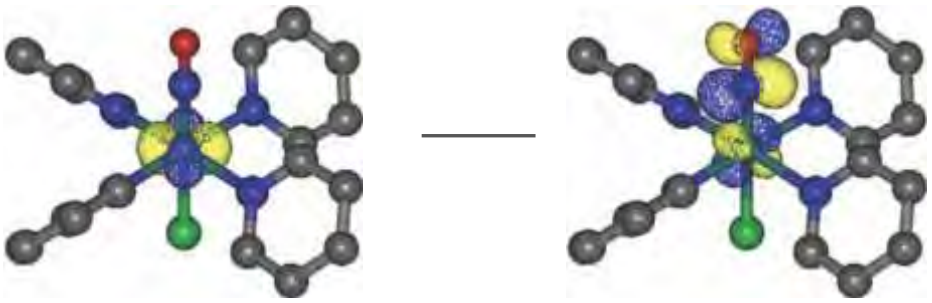
	402	0.0010	py(n) ..... Ru(d)NO(n*)	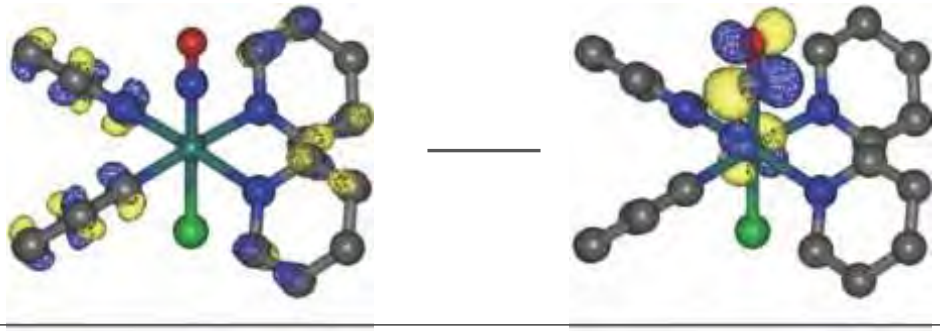
S,	402	0.0010	py(n) .... Ru(d)NO(n*)	

Table AA16. TD-DFT states of the MS2 isomer at TPSSh-03/Ahlrichs-basis level of theory in acetonitrile. Natural transition orbitais involved are shawn in the following table for each state.

State	À/ nm	f_{osc}	Nature	Natural Transition Orbitais (NTO)	
51	706	0.0017	Cl(p)Ru(d) ..... Ru(d)NO(n*)		
S.	478	0.0016	Cl(p)Ru(d)NO(n*) ..... Ru(d)NO(n*)	ca. 0.70 e 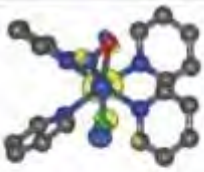	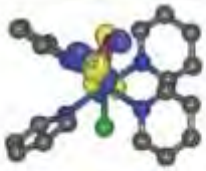
			py(n)Ru(d) ..... Cl(p)Ru(d)NO(n*)	ca. 0.30 e 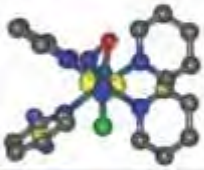	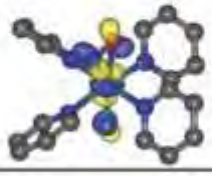
57	476	0.0020	Cl(p)Ru(d) ..... Ru(d)NO(n*)	ca. 0.80 e 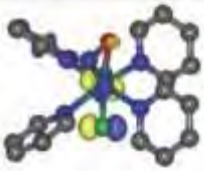	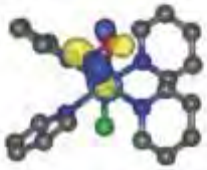
			Cl(p)Ru(d) NO(n*) Cl(p)Ru(d)NO(n*)	ca. 0.20 e 	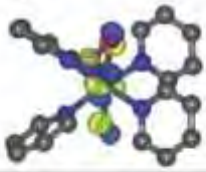
5_{10}	450	0.0012	py(n) -+ Cl(p)Ru(d)NO(n*)		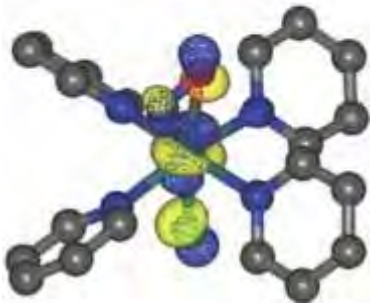

S_{11}	436	0.0028	Cl(p)Ru(d)py(π) → Ru(d)NO(π*)	
S_{12}	433	0.0021	Cl(p)py(π) → Cl(p)Ru(d)NO(π*)	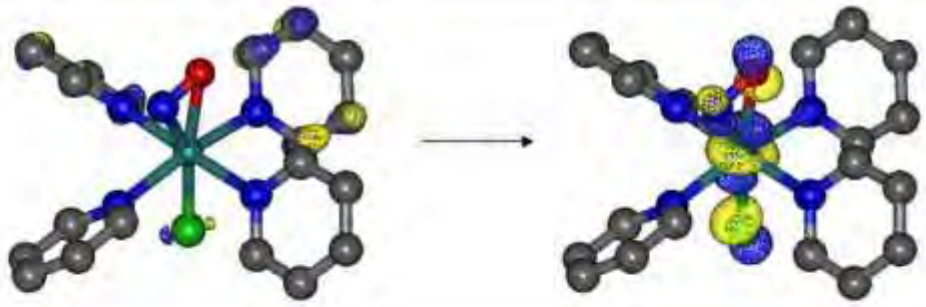
S_{13}	427	0.0019	Cl(p)Ru(d)py(π) → Ru(d)NO(π*)	
S_{15}	417	0.0030	Cl(p)py(π) → Ru(d)NO(π*)	

Table AA17. TD-DFT states of the **MS1** isomer at TPSSh-D3/Ahlrichs-basis level of theory in acetonitrile. Natural transition orbitals involved are shown in the following table for each state.

State	λ / nm	f_{osc}	Nature	Natural Transition Orbitals (NTO)
S_1	703	0.0013	Ru(d) → Ru(d)ON(π*)	
S_2	703	0.0013	Ru(d) → Ru(d)ON(π*)	
S_{17}	408	0.0043	Cl(p)py(π) → Ru(d)ON(π*)	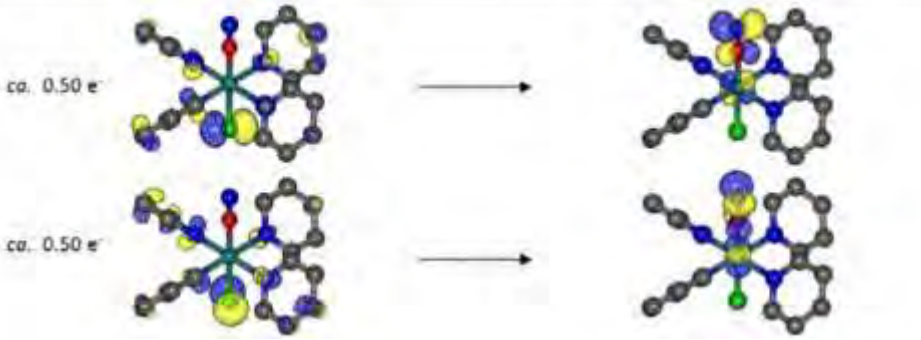

S_{18}	408	0.0043	py(π) → Ru(d)ON(π*)	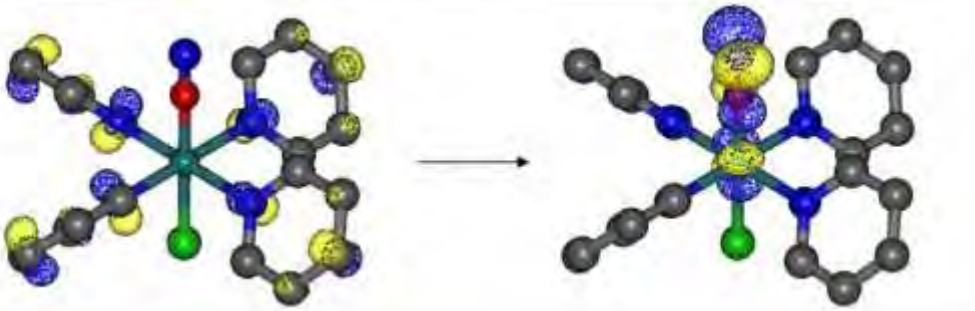
S_{19}	408	0.0043	py(π) → Ru(d)ON(π*)	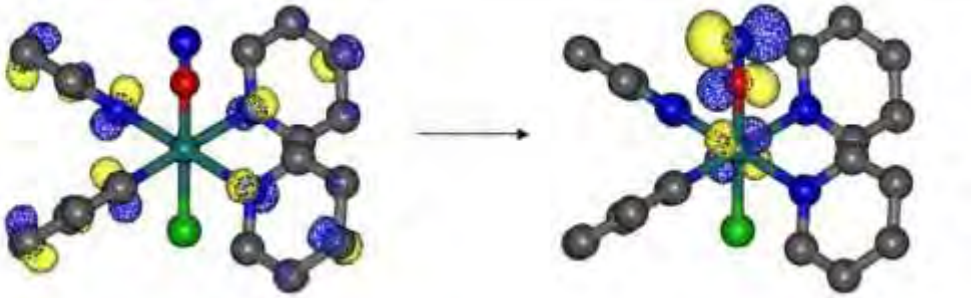

Table AA18. Active space orbitals and their occupation numbers of the CASSCF(6,6) calculation for the **MS1** isomer.

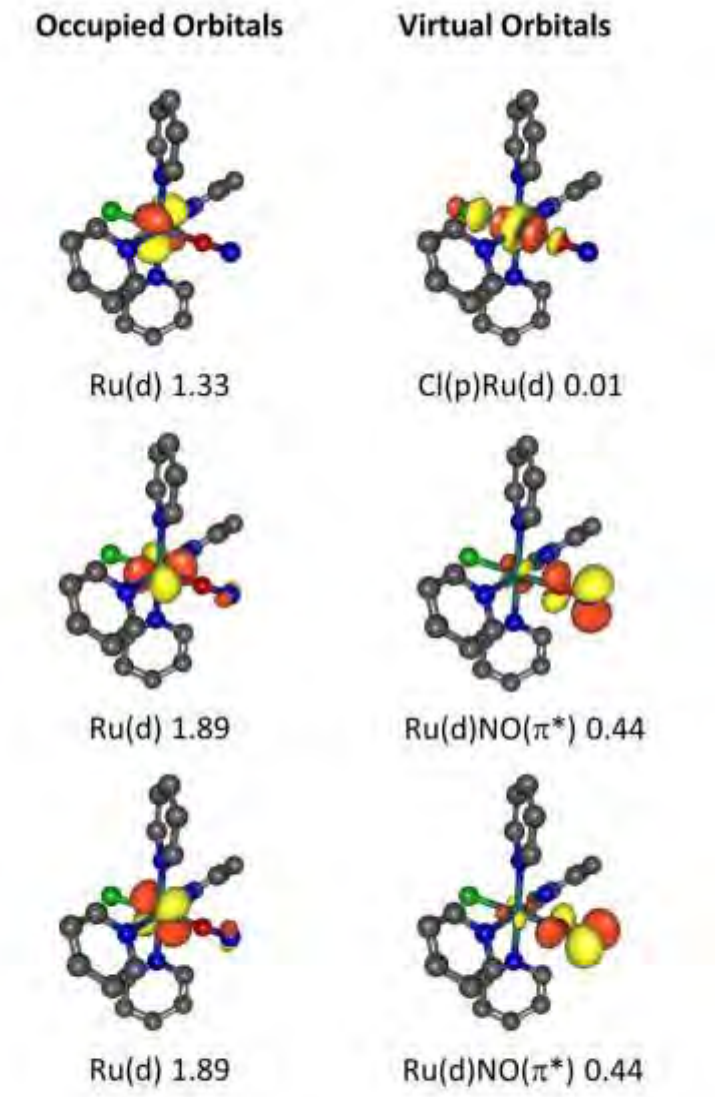

Table AA19. First electronic transitions computed at different levels of theory for the MS1 isomer.

Level of Theory	Wavelength / nm	f_{osc}
B3LYP	696	0.0010
PBE0	662	0.0009
TPSSh	703	0.0013
X3LYP	689	0.0005
ωB97X	581	0.0004
LC-PBE	577	0.0006
CASSCF(6,6)/NEVPT2	638	0.0001

Figure AA5. Intrinsic Reaction Coordinate (IRC) for the $^{1}TS_{1}$ at the B3LYP/6-31G*(H, C, N, O)/6-31+G*(Cl)/LANL2DZ(Ru) level of theory in vacuum. The energy is represented as a function of the intrinsic reaction coordinate (zero set at the transition state, positive values corresponds to forward direction and negative values to reverse direction). Structures and transition vector (scaled up by 2) are shown.

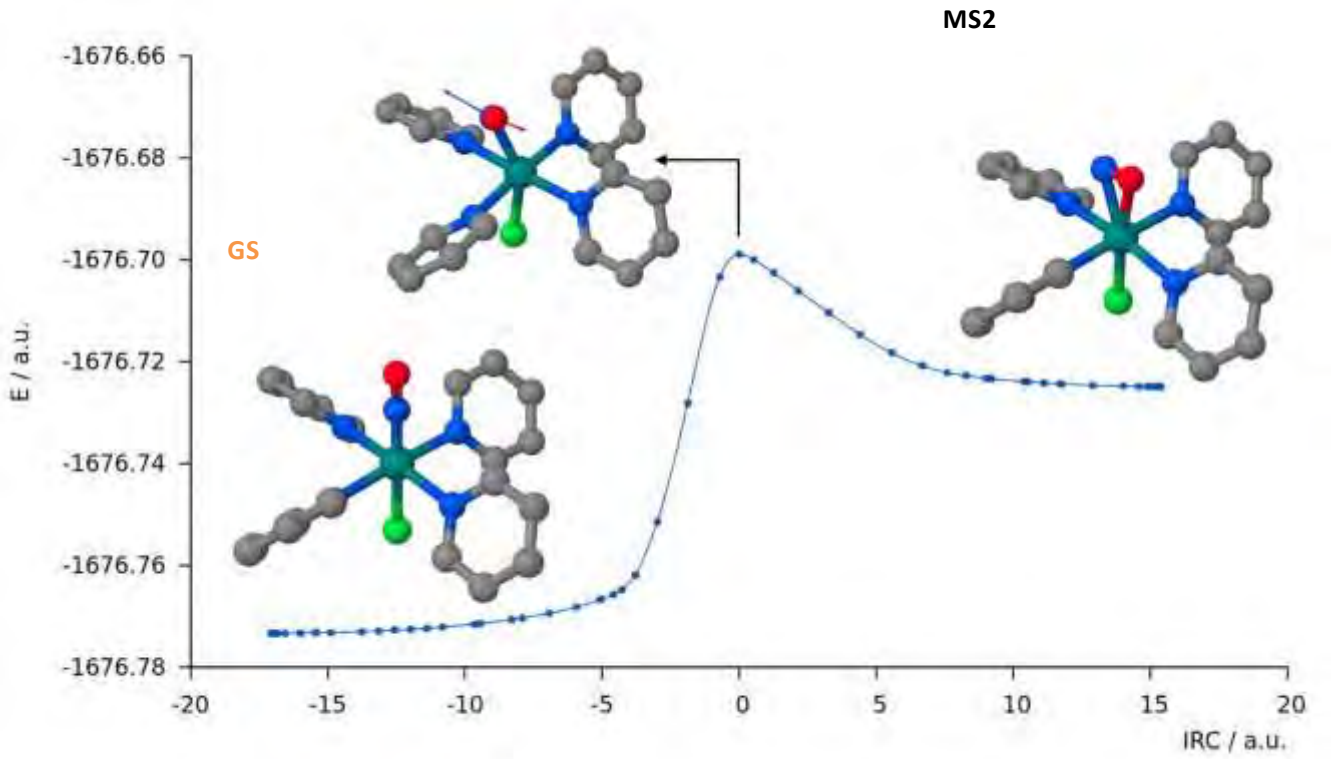

Figure AA6. Intrinsic Reaction Coordinate (IRC) for the $^1TS_2$ at the B3LYP/6-31G*(H, C, N, O)/6-31+G*(Cl)/ LANL2DZ(Ru) level of theory in vacuum. The energy is represented as a function of the intrinsic reaction coordinate (zero set at the transition state, positive values corresponds to forward direction and negative values to reverse direction). Structures and transition vector (scaled up by 2) are shown.

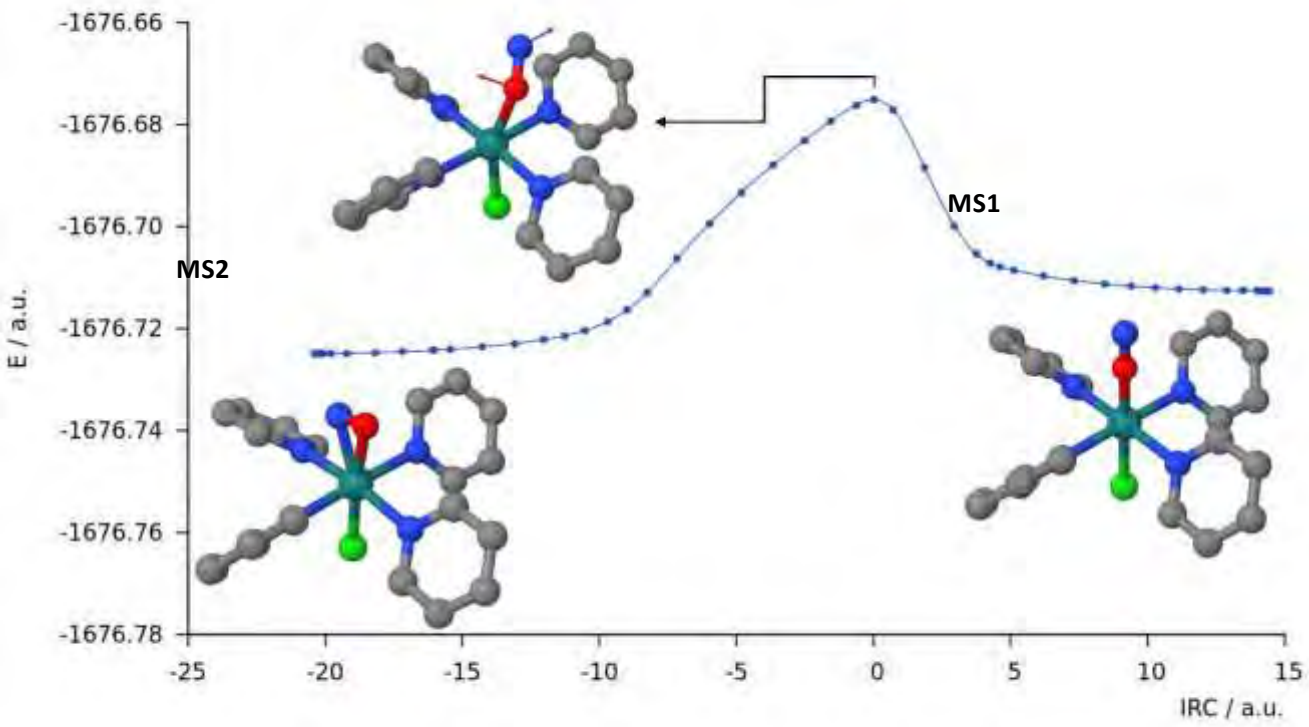

Figure AA7. Intrinsic Reaction Coordinate (IRC) for the $^{3}TS_{1}$ at the B3LYP/6-31G*(H, C, N, O)/6-31+G*(Cl)/LANL2DZ(Ru) level of theory in vacuum. The energy is represented as a function of the intrinsic reaction coordinate (zero set at the transition state, positive values corresponds to forward direction and negative values to reverse direction). Structures and transition vector (scaled up by 2) are shown.

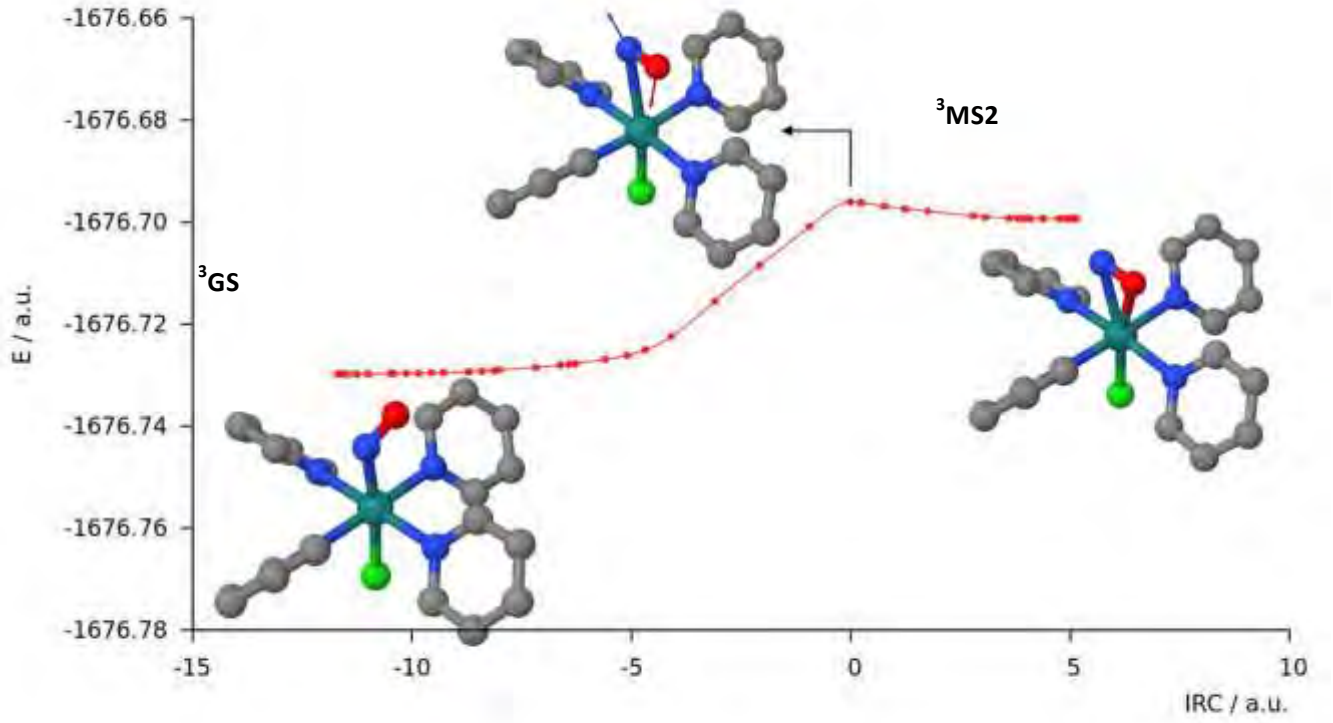

Figure AA8. Intrinsic Reaction Coordinate (IRC) for the $^3TS_2$ at the B3LYP/6-31G*(H, C, N, O)/6-31+G*(Cl)/LANL2DZ(Ru) level of theory in vacuum. The energy is represented as a function of the intrinsic reaction coordinate (zero set at the transition state, positive values corresponds to forward direction and negative values to reverse direction). Structures and transition vector (scaled up by 2) are shown.

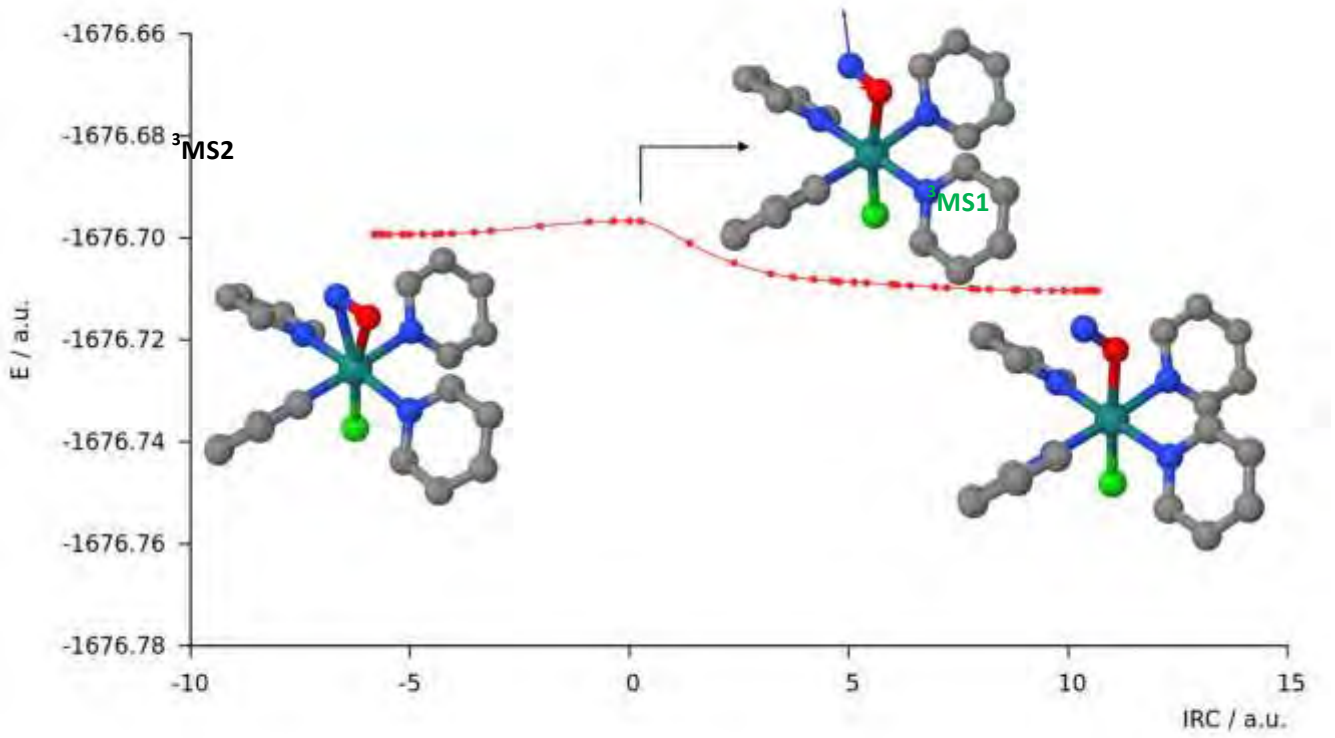

Figure AA9. Steepest decent optimization from the $MECP_1$ in vacuum at the level of theory specified in the computational details. The energy is represented as a function of the optimization step number (zero set arbitrarily at the $MECP_1$, positive values correspond to the optimization towards the triplet state ^{3}**GS** and negative values correspond to the optimization towards the singlet state **GS).**

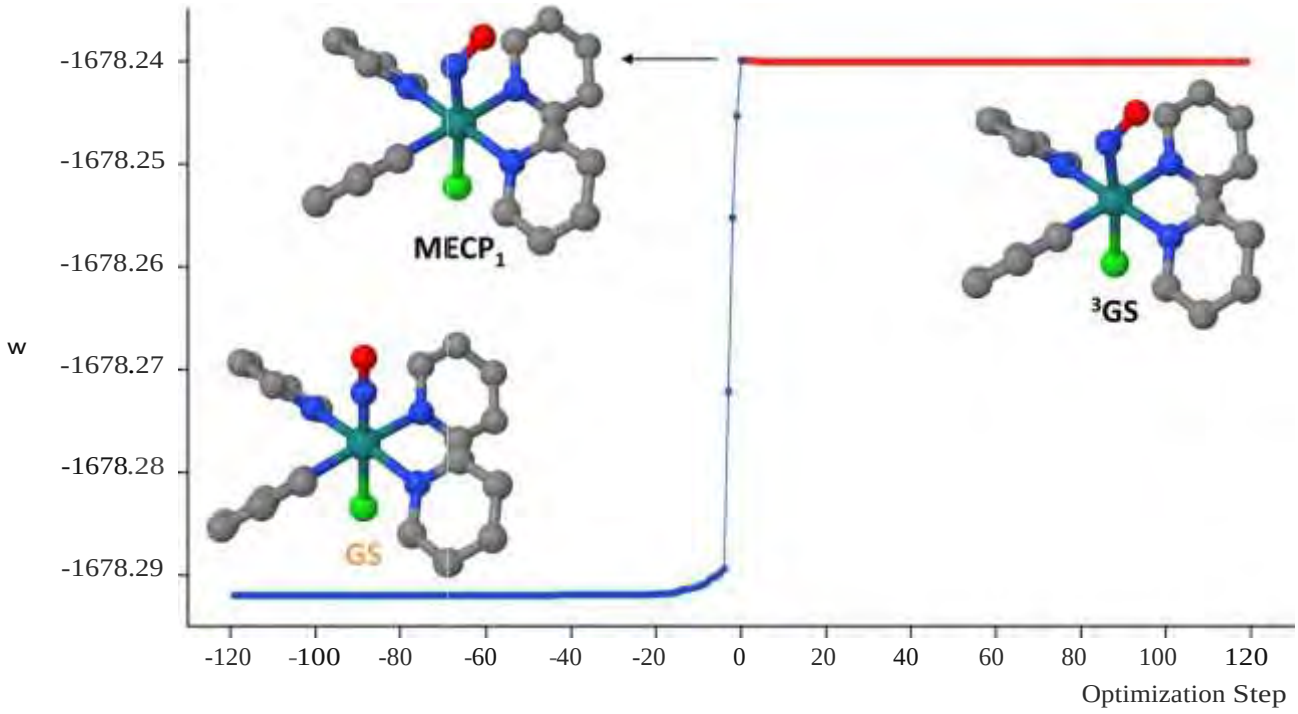

Note: Negative values have been given to emphasize the reverse direction of the global photoreaction (Ru-ON-+ Ru-NO) characterized by the increment ofthe Ru-N-O angle, when going from the $MECP_1$to **GS.**

Figure AAlO. Steepest decent optimization from the $MECP_2$ in vacuum at the level of theory specified in the computational details. The energy is represented as a function of the optimization step number (zero set arbitrarily at the $MECP_2$, positive values correspond to the optimization towards the singlet state **MS2** and negative values correspond to the optimization towards the triplet state ^{3}GS).

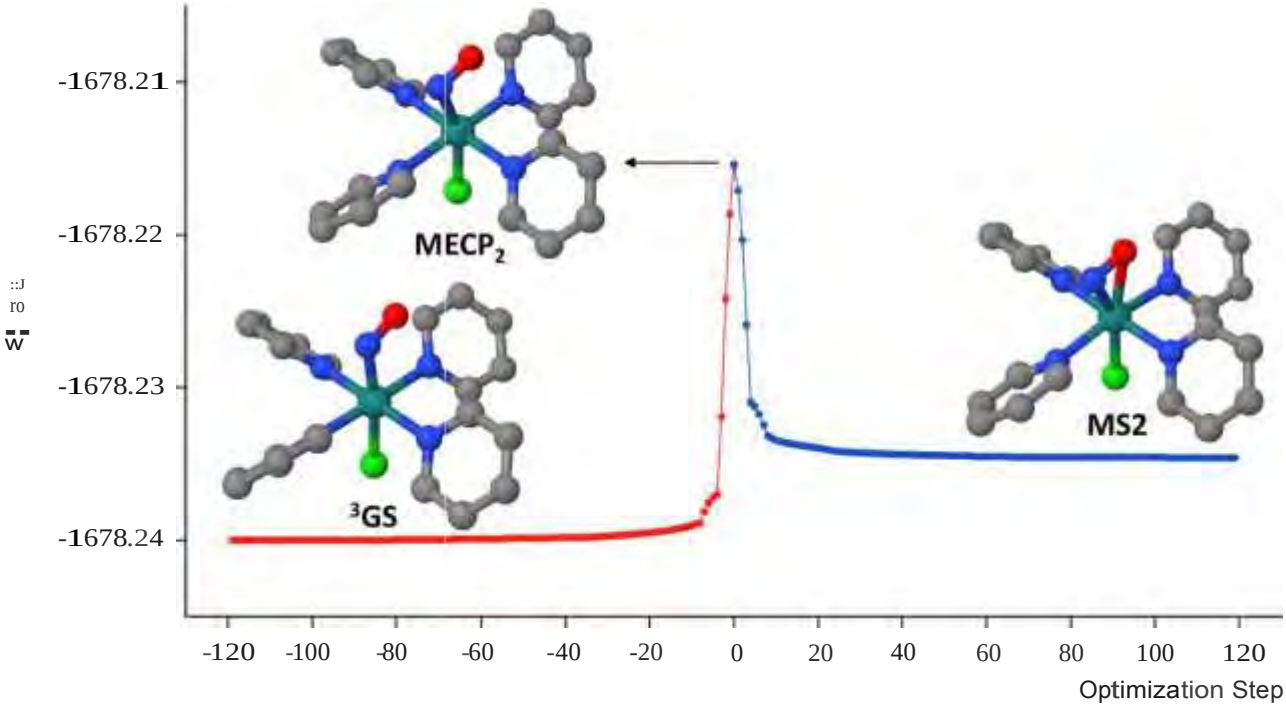

Note: Negative values have been given to empha size the reverse direction of the global photoreaction (Ru-ON-+ Ru-NO) characterized by the increment ofthe Ru-N-O angle, when going from the $MECP_2$ to ^{3}GS.

Figure AAII. Steepest decent optimization from the $MECP_3$ in vacuum at the level of theory specified in the computational details. The energy is represented as a function of the optimization step number (zero set arbitrarily at the $MECP_3$, red points correspond to the optimization towards the triplet state ^{3}**MS2** while the blue ones correspond to the optimization towards the singlet state **MS2).**

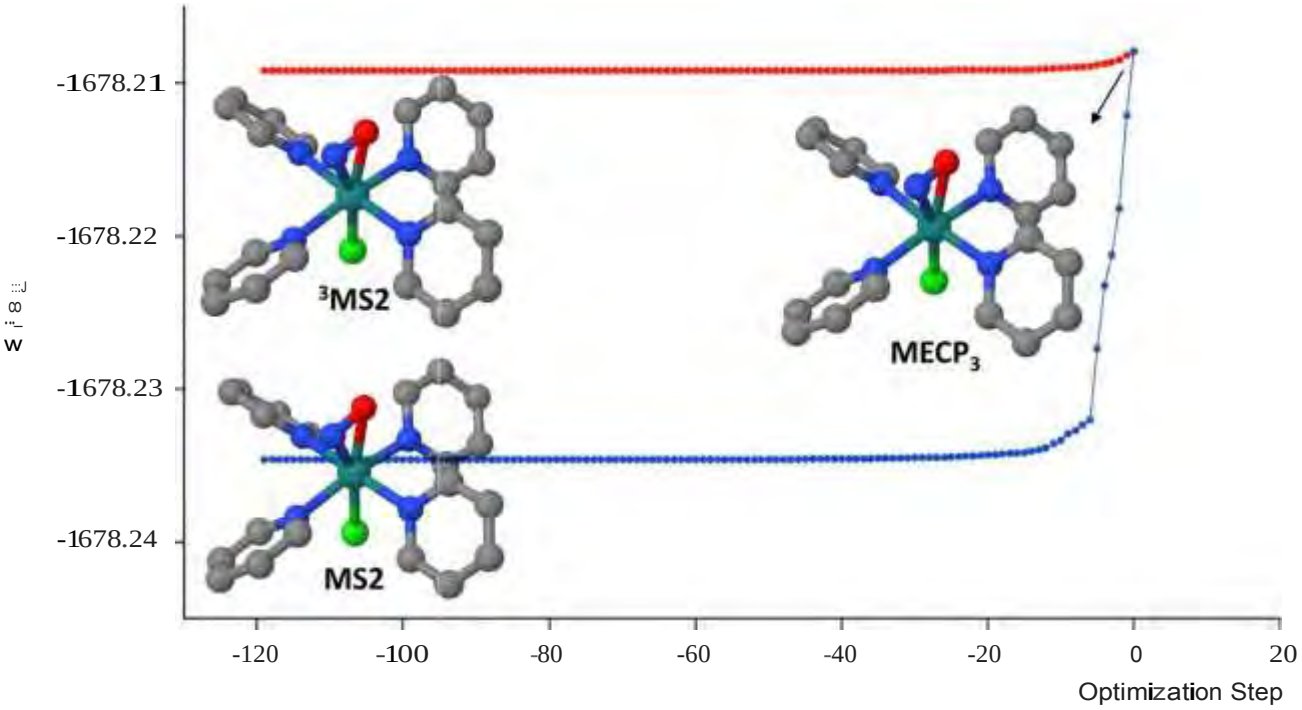

Note: Negative values have been given to emphasize the reverse direction of the global photoreaction (Ru-ON-+ Ru-NO) characterized by the increment of the Ru-N-O angle, when going from the $MECP_3$ to **MS2** and ^{3}**MS2.**

Figure AA12. Steepest decent optimization from the $MECP_4$ in vacuum at the level of theory specified in the computational details. The energy is represented as a function of the optimization step number (zero set arbitrarily at the $MECP_4$, positive values correspond to the optimization towards the singlet state **MSl** and negative values correspond to the optimization towards the triplet state ^{3}**MS1).**

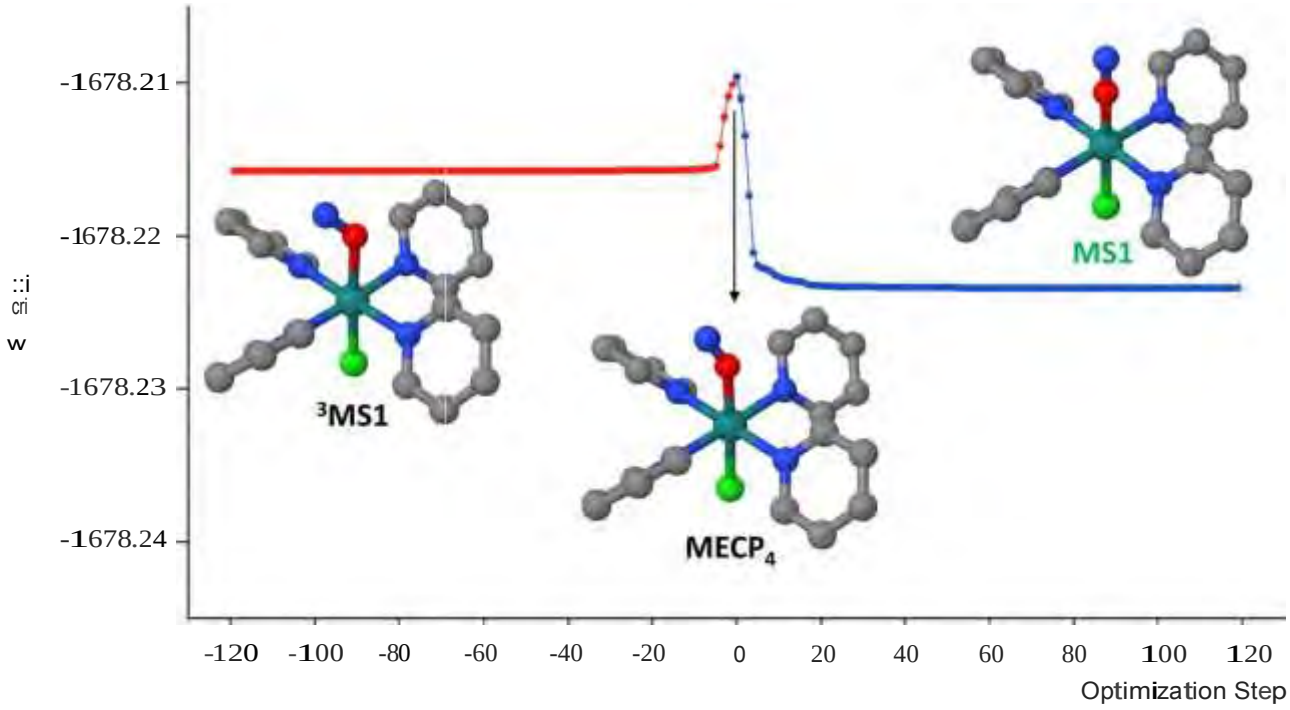

Note: Negative values have been given to emphasize the reverse direction of the global photoreaction (Ru-ON-+ Ru-NO) characterized by the increment ofthe Ru-N-O angle, when going from the $MECP_4$ to ^{3}**MS1.**

References

(1) Frisch M. J., et al. *Gaussian 09, revision D.01*; Gaussian, Inc.: Wallingford, CT, 2010.

(2) Cormary, B.; Malfant, I.; Buron-Le Cointe, M.; Toupet, L.; Delley, B.; Schaniel, D.; Mockus, N.; Woike, T.; Fejfarová, K.; Petříček, V.; Dušek, M. *Acta Crystallogr. B* **2009**, *65* (6), 612–623.

(3) Lee, C.; Yang, W.; Parr, R. G. *Phys. Rev. B* **1988**, *37* (2), 785.

(4) Becke, A. D. *J. Chem. Phys.* **1993**, *98* (7), 5648.

(5) Grimme, S.; Antony, J.; Ehrlich, S.; Krieg, H. *J. Chem. Phys.* **2010**, *132* (15), 154104.

(6) Schäfer, A.; Horn, H.; Ahlrichs, R. *J. Chem. Phys.* **1992**, *97* (4), 2571.

(7) Andrae, D.; Haeussermann, U.; Dolg, M.; Stoll, H.; Preuss, H. *Theor. Chim. Acta* **1990**, *77* (2), 123–141.

(8) Martin, J. M. L.; Sundermann, A. *J. Chem. Phys.* **2001**, *114* (8), 3408.

(9) Neese, F. *WIREs: Comput. Mol. Sci.* **2012**, *2* (1), 73–78.

(10) Coe, B. J.; Meyer, T. J.; White, P. S. *Inorg. Chem.* **1995**, *34* (3), 593–602.

(11) Sinnecker, S.; Rajendran, A.; Klamt, A.; Diedenhofen, M.; Neese, F. *J. Phys. Chem. A* **2006**, *110* (6), 2235–2245.

(12) Tao, J.; Perdew, J. P.; Staroverov, V. N.; Scuseria, G. E. *Phys. Rev. Lett.* **2003**, *91* (14), 146401.

(13) Hirata, S.; Head-Gordon, M. *Chem. Phys. Lett.* **1999**, *314* (3–4), 291–299.

(14) Hirata, S.; Head-Gordon, M. *Chem. Phys. Lett.* **1999**, *302* (5–6), 375–382.

(15) Neese, F. *J. Comput. Chem.* **2003**, *24* (14), 1740–1747.

(16) Neese, F.; Wennmohs, F.; Hansen, A.; Becker, U. *Chem. Phys.* **2009**, *356* (1–3), 98–109.

(17) Martin, R. L. *J. Chem. Phys.* **2003**, *118* (11), 4775–4777.

(18) Angeli, C.; Cimiraglia, R.; Evangelisti, S.; Leininger, T.; Malrieu, J.-P. *J. Chem. Phys.* **2001**, *114* (23), 10252–10264.

(19) Angeli, C.; Cimiraglia, R.; Malrieu, J.-P. *Chem. Phys. Lett.* **2001**, *350* (3–4), 297–305.

(20) Angeli, C.; Cimiraglia, R.; Malrieu, J.-P. *J. Chem. Phys.* **2002**, *117* (20), 9138–9153.

(21) Schmidt, M. W.; Baldridge, K. K.; Boatz, J. A.; Elbert, S. T.; Gordon, M. S.; Jensen, J. H.; Koseki, S.; Matsunaga, N.; Nguyen, K. A.; Su, S.; Windus, T. L.; Dupuis, M.; Montgomery, J. A. *J. Comput. Chem.* **1993**, *14* (11), 1347–1363.

(22) Zahariev, F.; Gordon, M. S. *J. Chem. Phys.* **2014**, *140* (18), 18A523.

(23) Friese, D. H.; Beerepoot, M. T. P.; Ringholm, M.; Ruud, K. *J. Chem. Theory Comput.* **2015**.

(24) Glendening E. D., et al. *NBO 6.0*; Theoretical Chemistry Institute, University of Wisconsin, Madison, 2013.

(25) Glendening, E. D.; Landis, C. R.; Weinhold, F. *J. Comput. Chem.* **2013**, *34* (16), 1429–1437.

Appendix B

Photochromic Response of Various Ru–NO Complexes

Table of Contents

AB.1 Motivation AB2
AB.2 Computational Details AB2
AB.3 Exploring the Singlet and Triplet Potential Energy Surfaces of the *trans*-[RuBr(NO)(py)$_4$]$^{2+}$ Complex .. AB3
AB.3.1 Singlet Potential Energy surface AB3
AB.3.2 Lowest Triplet Potential Energy surface AB5
AB.4 Thermal Isomerization and Photoisomerization Pathways of the Three Complexes AB7
AB.5 Absorption Spectra of GS, MS1 and MS2 of the Three Complexes AB9
AB.6 Discussion AB11
Table AB1. Structure, energies and orbitals of the isomer **GS** of *trans*-[RuBr(NO)(py)$_4$]$^{2+}$ AB13
Table AB2. Structure, energies and orbitals of the isomer **MS2** of *trans*-[RuBr(NO)(py)$_4$]$^{2+}$ AB14
Table AB3. Structure, energies and orbitals of the isomer **MS1** of *trans*-[RuBr(NO)(py)$_4$]$^{2+}$ AB15
Table AB4. Structure, energies and orbitals of ^{1}TS$_1$ of *trans*-[RuBr(NO)(py)$_4$]$^{2+}$ AB16
Table AB5. Structure, energies and orbitals of ^{1}TS$_2$ of *trans*-[RuBr(NO)(py)$_4$]$^{2+}$ AB17
Table AB6. Structure, energies and orbitals of ^{3}**GS** of *trans*-[RuBr(NO)(py)$_4$]$^{2+}$ AB18
Table AB7. Structure, energies and orbitals of ^{3}**MS2** of *trans*-[RuBr(NO)(py)$_4$]$^{2+}$ AB19
Table AB8. Structure, energies and orbitals of ^{3}**MS1** of *trans*-[RuBr(NO)(py)$_4$]$^{2+}$ AB20
Table AB9. Structure, energies and orbitals of ^{3}TS$_1$ of *trans*-[RuBr(NO)(py)$_4$]$^{2+}$ AB21
Table AB10. Structure, energies and orbitals of ^{3}TS$_2$ of *trans*-[RuBr(NO)(py)$_4$]$^{2+}$ AB22
Table AB11. Structure, energies and orbitals of the isomer **GS** of *trans*-(Cl,Cl)[RuCl$_2$(NO)(terpy)]$^+$ AB23
Table AB12. Structure, energies and orbitals of the isomer **MS2** of *trans*-(Cl,Cl)[RuCl$_2$(NO)(terpy)]$^+$ AB24
Table AB13. Structure, energies and orbitals of the isomer **MS1** of *trans*-(Cl,Cl)[RuCl$_2$(NO)(terpy)]$^+$ AB25
Table AB14. Absorption TD-DFT spectra and selected states of the *trans*-[RuCl(NO)(py)$_4$]$^{2+}$ isomers AB26
Table AB15. Absorption TD-DFT spectra and selected states of the *trans*-[RuBr(NO)(py)$_4$]$^{2+}$ isomers..... AB27
Table AB16. Absorption TD-DFT spectra and selected states of the *trans*-(Cl,Cl)[RuCl$_2$(NO)(terpy)]$^+$ isomers AB28
AB.7 References AB29

AB.1 Motivation

The main motivation of this Appendix is to show how the experimental photoconversion yields reported in references 1,2 can be rationalized once the photoisomerization mechanism Ru−NO (**GS**) ▾▾ Ru−ON (**MS1**) has been established (Chapter III). The three complexes that are compared in this Appendix (Table AB.1.1) have the same counter anion PF_6^-, but present very different photoconversion yields.

Table AB.1.1: Photoconversion yields reported for three different complexes in references 1 and 2.

Complex	Photoconversion Yield	Experimental λ used / nm
trans-[RuCl(NO)(py)$_4$]$^{2+}$	76%	476[a]
trans-[RuBr(NO)(py)$_4$]$^{2+}$	46%	488-496
trans-(Cl,Cl) [RuCl$_2$(NO)(terpy)]$^+$	8%	-[b]

[a] This is the wavelength reported in references 1 and 2, while in Chapter III, 473 nm is used instead, since that wavelength is also used, depending on the available experimental lasers. [b] Irradiation wavelength not specified in reference 1.

The Appendix is organized as follows: First the potential energy surfaces (PESs) of the ground and lowest triplet state of the *trans*-[RuBr(NO)(py)$_4$]$^{2+}$ are presented and compared to the ones of the other two complexes. Next, the TD-DFT absorption spectra of the three isomers **GS**, **MS1** and **MS2** are shown for the three different complexes. Finally, with all this information, the trend in the photoconversion yield is rationalized mainly in terms of the spectroscopic properties of the isomers of each complex.

AB.2 Computational Details

Gas-phase geometry optimizations of all the stationary points found on the closed shell singlet (hereafter called singlet for simplicity) and the lowest triplet PES were carried out with the Gaussian 09 quantum package.[3] The isomers **GS** and **MS1** of the *trans*-[RuBr(NO)(py)$_4$]$^{2+}$ were optimized in C_4 symmetry. DFT was used in order to perform these calculations using the standard hybrid functional B3LYP,[4,5] including Grimme's dispersion correction,[6] with a double-ζ Ahlrichs-type basis set[7] with a *p* polarization function for the hydrogen atoms, a triple-ζ Ahlrichs-type basis set[7] with one *d* polarization function for the second- and fourth-row elements, and for the ruthenium a Stuttgart relativistic effective core potential[8] (including 28 core electrons) with its associated basis set[8] and two *f* and one *g* polarization functions.[9] After geometry optimizations, vibration frequency analyses were performed at the same level of theory to verify the nature of the stationary points.

The UV-Vis absorption spectra of **GS**, **MS1** and **MS2** were computed with the ORCA 3.0.2 quantum package,[10] applying TD-DFT using the TPSSh[11] functional for the *trans*-$[RuX(NO)(py)_4]^{2+}$ complexes (X = Cl, Br) and the BHandHLYP[4,12] functional for the *trans*-(Cl,Cl)$[RuCl_2(NO)(terpy)]^+$ complex (as used in Chapter IV), within the Tamm-Dancoff approximation,[13,14] and the same basis sets as described above. In these TD-DFT calculations the resolution-of-identity (RI) approximation for hybrid functionals[15] (as implemented in ORCA) was employed to calculate the Coulomb energy term using the Ahlrichs/Weigand Def2-TZV auxiliary basis set and the exchange term by the so-called 'chain-of-spheres exchange' (COSX) algorithm.[16]

AB.3 Exploring the Singlet and Triplet Potential Energy Surfaces of the *trans*-$[RuBr(NO)(py)_4]^{2+}$ Complex

AB.3.1 Singlet Potential Energy Surface

Starting from the previously optimized geometries obtained at the same level of theory for the *trans*-$[RuCl(NO)(py)_4]^{2+}$ complex, the three *trans*-$[RuBr(NO)(py)_4]^{2+}$ isomers, **GS**, **MS1** and **MS2**, were optimized. From a structural point of view, all the isomers found are very similar to those of the *trans*-$[RuCl(NO)(py)_4]^{2+}$ complex with no major differences. The HOMO and LUMO orbitals found are very similar as well. Starting from the transition states found for the complex studied in Chapter III, the transition states connecting **GS** and **MS2** ($^1TS_1$) and the **MS2** and **MS1** ($^1TS_2$) were optimized. Due to an optimization problem found during the characterization of the triplet PES, all the structures found in the ground state singlet PES (isomers and TSs) were optimized again with no dispersion corrections, in order to be able to compare all the results found. As shown in Table AB.3.1 and Table AB.3.2, the energy profile of the PES with and without dispersion corrections is practically the same for both complexes. Further information of the most relevant geometrical parameters (selected bond lengths and angles) as well as the HOMO and LUMO orbitals of the optimized structures (without dispersion corrections) are shown in Tables AB1−AB5. The full profile of the thermal isomerization pathway for the *trans*-$[RuBr(NO)(py)_4]^{2+}$ is shown in Figure AB.3.1.

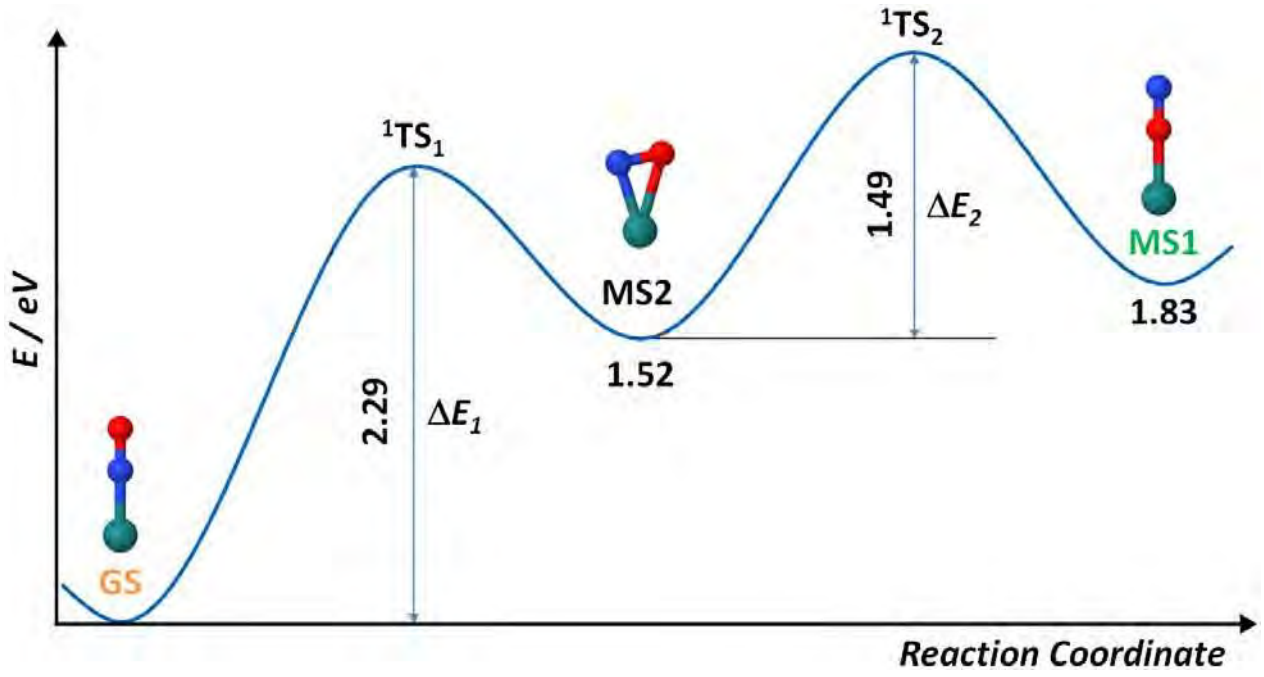

Figure AB.3.1: Singlet ground-state potential energy profile of *trans*-$[RuBr(NO)(py)_4]^{2+}$ along the isomerization reaction coordinate at the B3LYP/Ahlrichs-basis level of theory (without Grimme's dispersion correction).

Table AB.3.1: Comparison of the ground-state energy profile of the complex *trans*-$[RuBr(NO)(py)_4]^{2+}$ computed at the B3LYP/Ahlrichs-basis level of theory with and without dispersion correction.

Energy Gap	B3LYP/Ahlrichs-basis (Without Dispersion Correction) *trans*-$[RuBr(NO)(py)_4]^{2+}$	B3LYP-D3/Ahlrichs-basis (With Dispersion Correction) *trans*-$[RuBr(NO)(py)_4]^{2+}$
ΔE (MS2 - GS)	1.52	1.51
ΔE (MS1 - GS)	1.83	1.82
ΔE_1	2.29	2.30
ΔE_2	1.49	1.49

Table AB.3.2: Comparison of the ground-state energy profile of the complex *trans*-$[RuCl(NO)(py)_4]^{2+}$ computed at the B3LYP/Ahlrichs-basis level of theory with and without dispersion correction.

Energy Gap	B3LYP/Ahlrichs-basis (Without Dispersion Correction) *trans*-$[RuCl(NO)(py)_4]^{2+}$	B3LYP-D3/Ahlrichs-basis (With Dispersion Correction) *trans*-$[RuCl(NO)(py)_4]^{2+}$
ΔE (MS2 - GS)	1.57	1.56
ΔE (MS1 - GS)	1.87	1.86
ΔE_1	2.44	2.44
ΔE_2	1.57	1.57

AB.3.2 Lowest Triplet Potential Energy Surface

The lowest triplet PES of the *trans*-$[RuBr(NO)(py)_4]^{2+}$ complex was explored to characterize the adiabatic isomerization Ru−NO ⁚⁚ Ru−ON on this surface, as it was done for the *trans*-$[RuCl(NO)(py)_4]^{2+}$ complex[17] (see Chapter III). Following the same procedure explained for the singlet ground state PES, starting from the optimized geometries obtained at the same level of theory for the *trans*-$[RuCl(NO)(py)_4]^{2+}$ complex, the three *trans*-$[RuBr(NO)(py)_4]^{2+}$ triplet states, ^{3}**GS**, ^{3}**MS1** and ^{3}**MS2**, were optimized. Once more, from a structural point of view, all the triplets found are very similar to those of the *trans*-$[RuCl(NO)(py)_4]^{2+}$ complex with no major differences. The electronic nature of the triplet states of both complexes is quite similar as well, with the minor difference in the bromine atom, which presents slightly higher spin densities than the chlorine atom, as expected. In contrast with the ground-state TSs optimizations which were successfully carried out using the structures found for the previously studied complex, the optimizations of the TSs in the lowest triplet surface for the *trans*-$[RuBr(NO)(py)_4]^{2+}$ complex were much more difficult. In fact, after trying different strategies and approaches, only the $^3TS_1$, which connects ^{3}**GS** and ^{3}**MS2**, could be found. In Table AB.3.3 the last value reported (in the right corner) corresponds to the hypothetical activation energy barrier between ^{3}**MS2** and a wrong TS (Figure AB.3.2) which does not connect ^{3}**MS2** and ^{3}**MS1** (after the first '$^3TS_2$' optimization, subsequent steepest descent calculations showed that the TS found do not connect the corresponding triplet states, ^{3}**MS2** and ^{3}**MS1**). Nevertheless, without the Grimme's dispersion corrections both TSs connecting the minima in the lowest triplet surface were found (see Tables AB9 and AB10 for further information). All the triplets found were optimized again with no dispersion corrections (see Tables AB6−AB8). As for the energy profile in the ground-state, the lowest triplet energy profile with and without dispersion corrections is practically the same for both complexes (see Table AB.3.3 and Table AB.3.4). The full profile of the adiabatic isomerization pathway on the lowest triplet PES for the *trans*-$[RuBr(NO)(py)_4]^{2+}$ is shown in Figure AB.3.3.

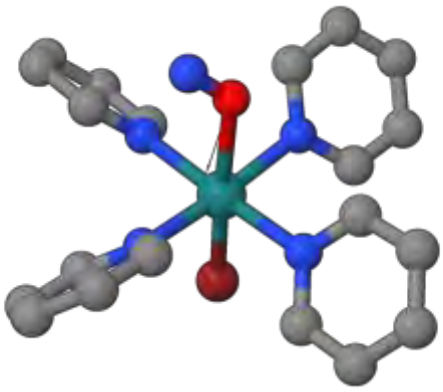

Figure AB.3.2: Initial TS found in the lowest triplet potential energy surface of the *trans*-[RuCl(NO)(py)$_4$]^2 at the B3LYP-D3/Ahlrichs-basis level of theory (with the Grimme's dispersion correction).This TS corresponds to the energy value given in Table AB.3.3, but it does not connect the minima ^{3}MS2 and ^{3}MS1. As it can be seen it is different from the 'real' ^{3}TS$_2$ found without the dispersion correction (Table AB10).This TS presents a Ru−O−N angle of 131.3 degrees while the 'real' ^{3}TS$_2$ shows a Ru−O−N angle of 91.4 degrees (Table AB10).

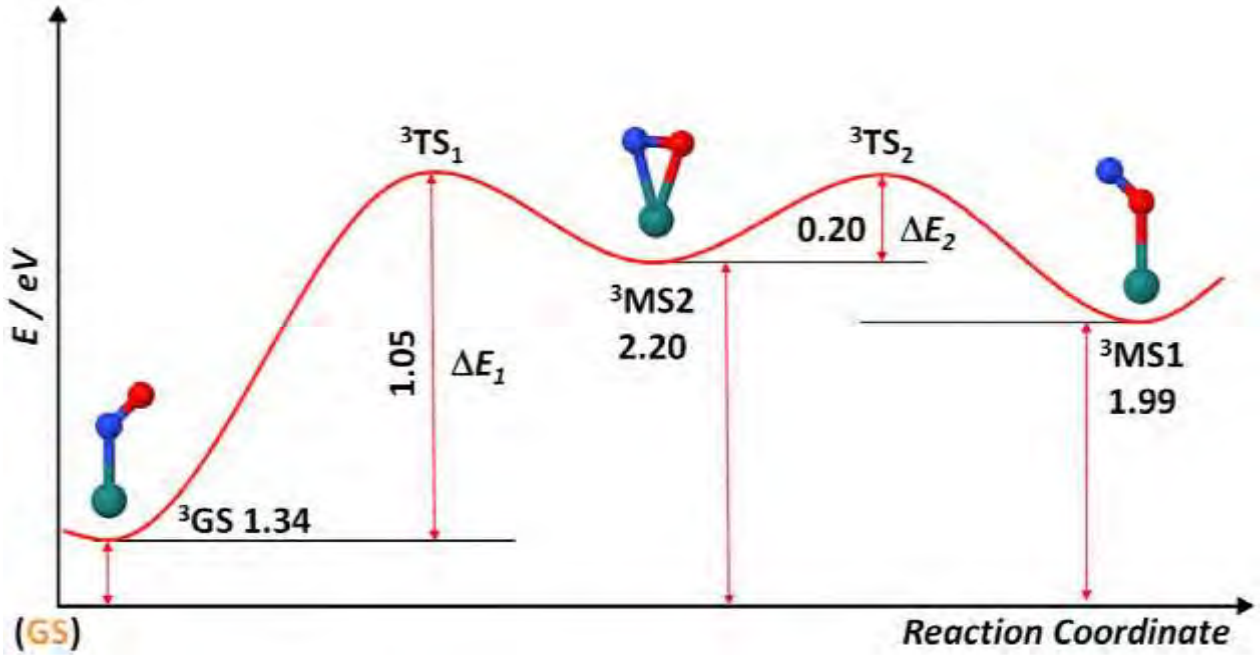

Figure AB.3.3: Triplet potential energy profile of *trans*-[RuCl(NO)(py)$_4$]$^{2+}$ along the adiabatic isomerization reaction coordinate at the B3LYP/Ahlrichs-basis level of theory (without the Grimme's dispersion correction).

Table AB.3.3: Comparison of the lowest triplet state energy profile of the complex *trans*-$[RuBr(NO)(py)_4]^{2+}$ computed at the B3LYP/Ahlrichs-basis level of theory with and without dispersion correction.

Energy Gap	B3LYP/Ahlrichs-basis (Without Dispersion Corrections) *trans*-$[RuBr(NO)(py)_4]^{2+}$	B3LYP-D3/Ahlrichs-basis (With Dispersion Corrections) *trans*-$[RuBr(NO)(py)_4]^{2+}$
ΔE (^{3}GS - GS)	1.34	1.32
ΔE (^{3}MS2 - GS)	2.20	2.19
ΔE (^{3}MS1 - GS)	1.99	1.98
ΔE_1	1.05	1.05
ΔE_2	0.20	-0.16

Table AB.3.4: Comparison of the lowest triplet state energy profile of the complex *trans*-$[RuCl(NO)(py)_4]^{2+}$ computed at the B3LYP/Ahlrichs-basis level of theory with and without dispersion correction.

Energy Gap	B3LYP/Ahlrichs-basis (Without Dispersion Correction) *trans*-$[RuCl(NO)(py)_4]^{2+}$	B3LYP-D3/Ahlrichs-basis (With Dispersion Correction) *trans*-$[RuCl(NO)(py)_4]^{2+}$
ΔE (^{3}GS - GS)	1.41	1.43
ΔE (^{3}MS2 - GS)	2.25	2.27
ΔE (^{3}MS1 - GS)	2.08	2.09
ΔE_1	1.06	1.06
ΔE_2	0.26	0.26

AB.4 Thermal Isomerization and Photoisomerization Pathways of the Three Complexes

Thermal Isomerization Pathway. The first step in the thermal isomerization pathway B1 (Figure AB.4.1 and Table AB.4.1) shows similar barriers for the *trans*-$[RuBr(NO)py_4]^{2+}$ and *trans*-$(Cl,Cl)[RuCl_2(NO)(terpy)]^{+}$ complexes. These barriers are smaller than the one found for the *trans*-$[RuCl(NO)py_4]^{2+}$, but still it would be very difficult to overcome them. B2 is smaller than B1 (Table AB.4.1) but remains highly unfavourable for all the complexes. As pointed out in Chapters III and IV, the thermal stability of these compounds in their three isomers is confirmed by these results.

Adiabatic *vs*. Non-Adiabatic Isomerization Pathway. Generally speaking, the energy barriers found on the triplet PES are lower than those found in the singlet PES. However, the first energy barriers found in the forward direction (Ru–NO → Ru–ON) of the adiabatic isomerization along the lowest triplet PES are too large to be easily overcome (B3 adiabatic conversion from **^{3}GS** to **^{3}MS2**). On the other hand, the second barrier (B4

adiabatic conversion from ^{3}**MS2** to ^{3}**MS1**) can be easily attained once the system reaches the triplet ^{3}**MS2** (Figure AB.4.1 and Table AB.4.1). The main difference found between the complexes of the family *trans*-[RuX(NO)(py)$_4$]$^{2+}$ (X = Cl, Br) and the *trans*-(Cl,Cl)[RuCl$_2$(NO)(terpy)]$^+$ complex is the non-adiabatic barrier found between ^{3}**GS** and **MS2**, B5. The *trans*-[RuX(NO)(py)$_4$]$^{2+}$ (X = Cl, Br) complexes present a barrier of *ca*. 0.7 eV, while the *trans*-(Cl,Cl)[RuCl$_2$(NO)(terpy)]$^+$ complex shows a barrier of *ca*. 0.9 eV. The non-adiabatic conversion from ^{3}**GS** to **MS2** is a key step in the photoisomerization mechanism described in Chapter III and might play an important role in the rationalization of the photoconversion yields found experimentally.

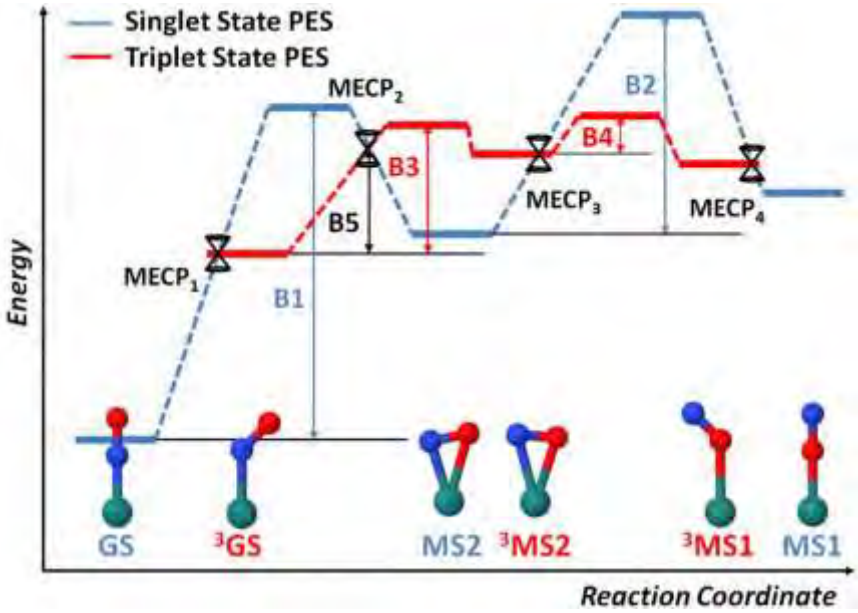

Figure AB.4.1: Scheme of the interweaving between the singlet and the lowest triplet state potential energy surfaces. The reaction coordinate considered is the Ru−N−O angle. Blue lines represent the singlet state and red lines the triplet state. Singlet-triplet funnels (MECPs) are represented by double-cone pictograms. Barriers B1 (GS-MS2), B2 (MS2-MS1), B3 (^{3}GS-^{3}MS2), B4 (^{3}MS2-^{3}MS1) and B5 (^{3}GS-^{1}MS2) are scaled.

Table AB.4.1: Comparison of the different energy barriers for the three studied complexes: *trans*-[RuCl(NO)(py)$_4$]$^{2+}$, *trans*-[RuCl(NO)(py)$_4$]$^{2+}$, *trans*-(Cl,Cl)[RuCl$_2$(NO)(terpy)]$^+$.

Complex Barrier	*trans*-[RuCl(NO)(py)$_4$]$^{2+}$	*trans*-[RuBr(NO)(py)$_4$]$^{2+}$	*trans*-(Cl,Cl)[RuCl$_2$(NO)(terpy)]$^+$
B1	2.44	2.29	2.30
B2	1.57	1.49	1.44
B3	1.06	1.05	0.98
B4	0.26	0.20	0.16
B5	0.67	0.65	0.86

AB.5 Absorption Spectra of GS, MS1 and MS2 of the Three Complexes

The TD-DFT absorption spectra of the three isomers (**GS**, **MS2** and **MS1** optimized including the Grimme's dispersion correction) of all the complexes presented in this Appendix have been computed. All the results obtained are shown in the following Figures AB.5.1, AB.5.2 and AB.5.3. For further details of the transition wavelengths and oscillators strength see Tables AB14–AB16.

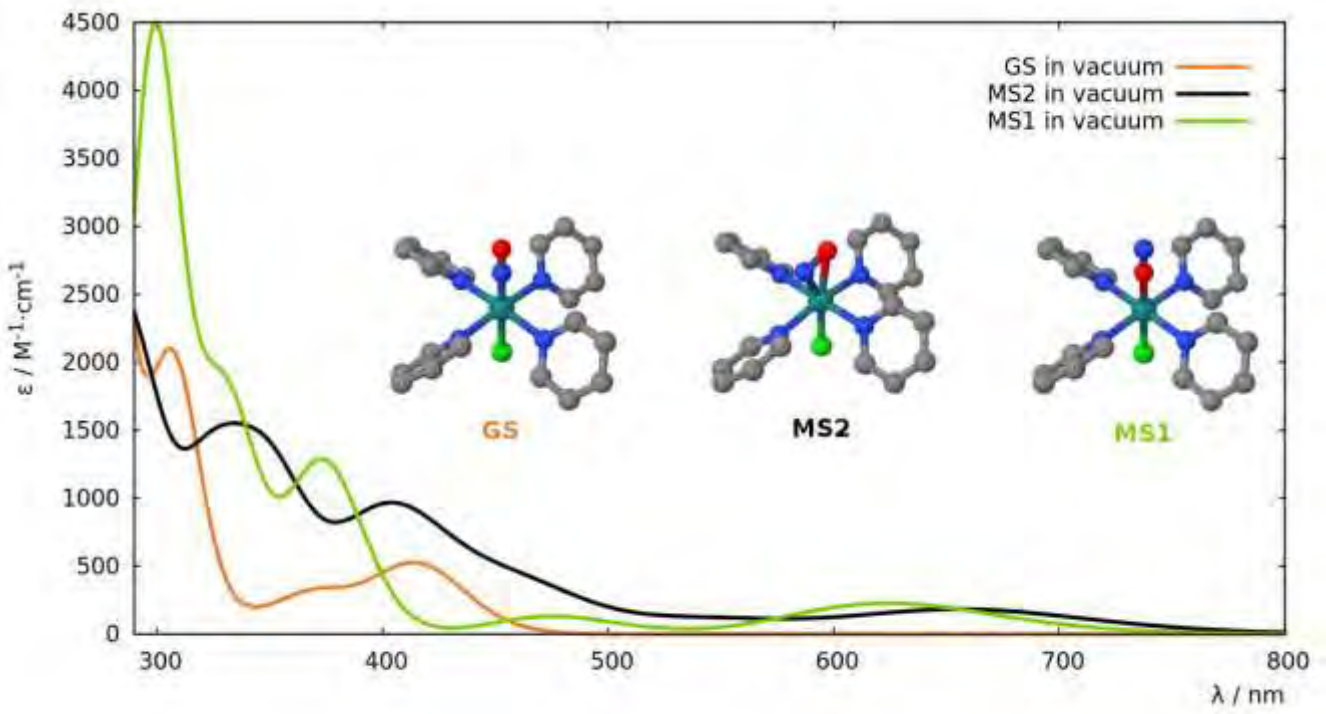

Figure AB.5.1: TD-DFT spectra of the three linkage isomers (GS in orange, MS2 in black and MS1 in green) of *trans*-$[RuCl(NO)(py)_4]^{2+}$ computed in vacuum.

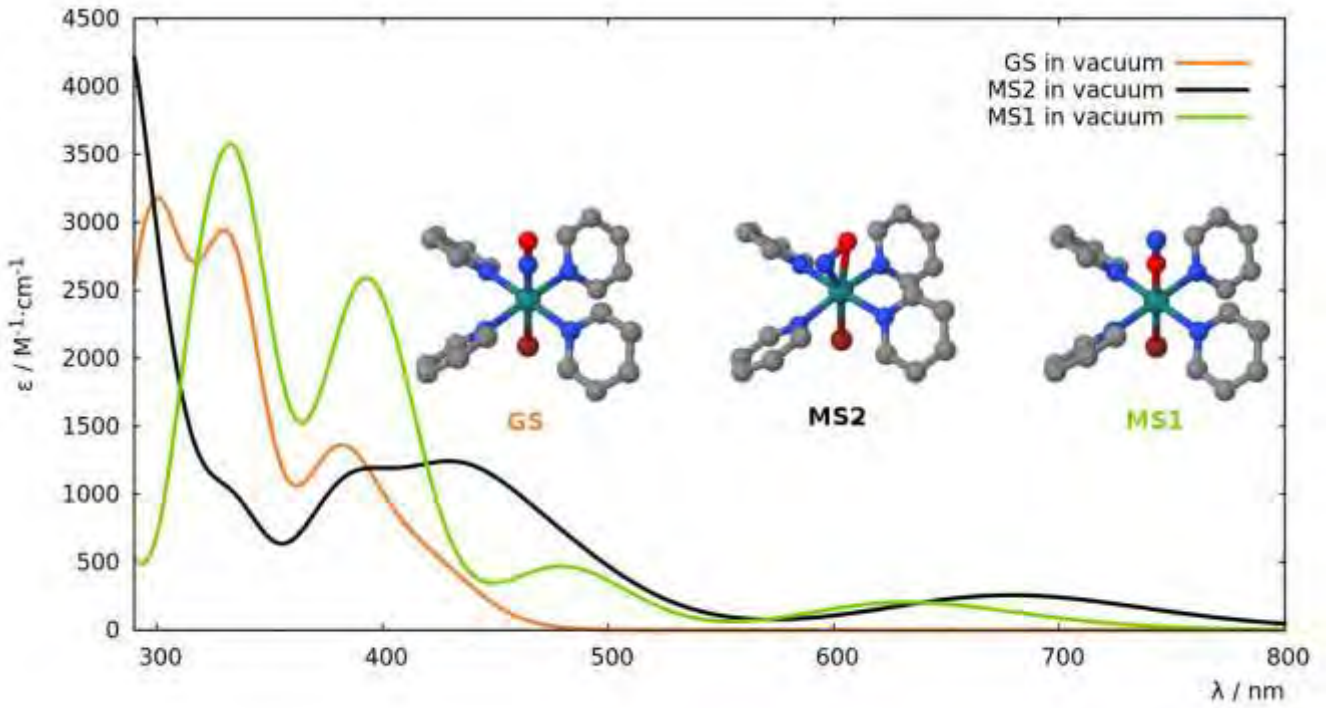

Figure AB.5.2: TD-DFT spectra of the three linkage isomers (GS in orange, MS2 in black and MS1 in green) of *trans*-$[RuBr(NO)(py)_4]^{2+}$ computed in vacuum.

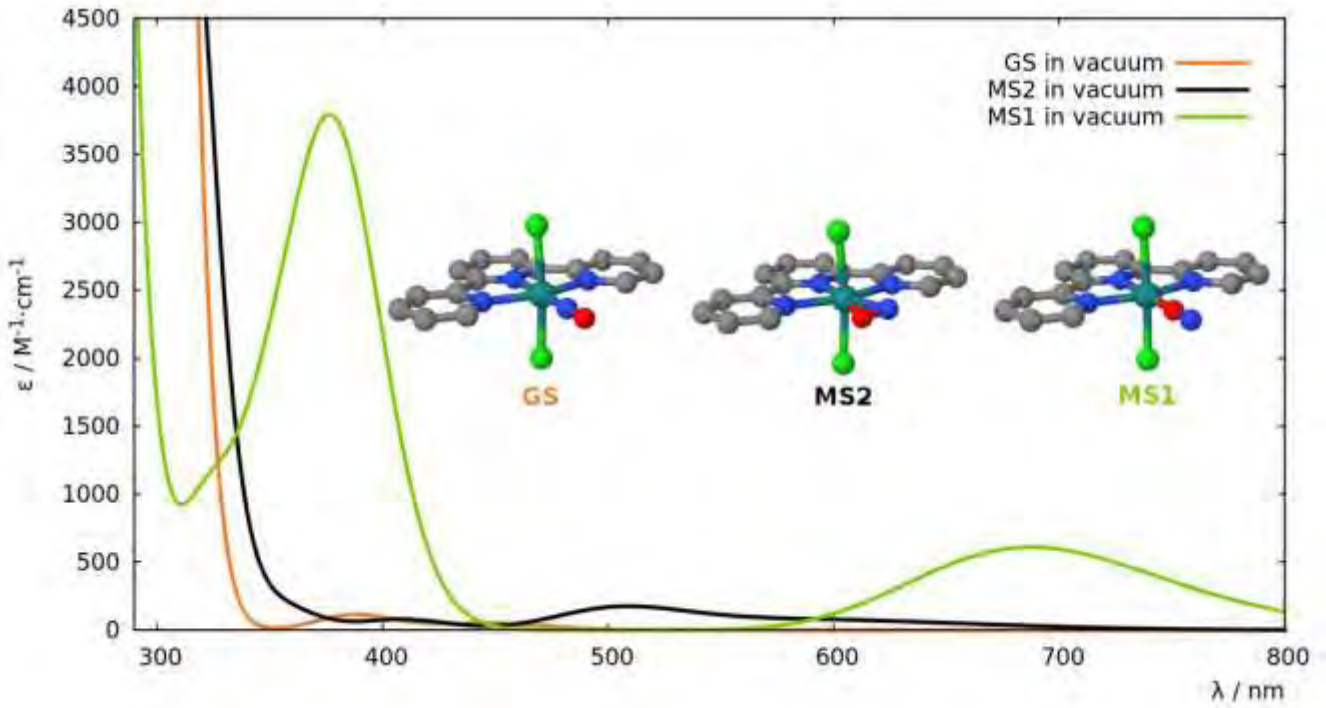

Figure AB.5.3: TD-DFT spectra of the three linkage isomers (GS in orange, MS2 in black and MS1 in green) of *trans*-(Cl,Cl)$[RuCl_2(NO)(terpy)]^+$ computed in vacuum.

N.B. The geometries used to performed the TD-DFT calculations of the three *trans*-(Cl,Cl)$[RuCl_2(NO)(terpy)]^+$ isomers optimized in vacuum including the Grimme's dispersion correction can be found in Tables AB11–AB13.

AB.6 Discussion

The photoconversion trend experimentally observed in the family of ruthenium nitrosyl compounds presented in this Appendix (Table AB.1.1) can be rationalized making use of the absorption properties of the different isomers (**GS**, **MS2** and **MS1**) of each complex. As explained in Chapter III and IV, one of the key factors necessary for the photoreactivity of this kind of compounds is the overlap between the absorption bands of the **GS** and **MS2** isomers. This is a requirement for the description of a sequential two-photon mechanism, where initially **GS** absorbs one photon and subsequently **MS2** absorbs a second one. In the particular case of the *trans*-$[RuCl(NO)py_4]^{2+}$ complex, which shows the higher photoconversion yield, two remarkable characteristics of the spectra permit the rationalization of the mechanism and experimental yield: a) there is a spectral region near the experimental irradiation wavelengths (400 – 500 nm) where an important superposition of the absorption bands of **GS** and **MS2** exits, and b) **MS1** does not absorb in that specific region. While the first property is obviously a *sine qua non* condition for a sequential two-photon absorption mechanism, the second property allows the rationalization of large photoconversion yields after long experimental irradiations times. If the system is progressively transformed from **GS** to **MS1**, and **MS1** is not consumed (since it does not absorb), at some point all the isomer **GS** will be transformed into **MS1**, reaching very large photoconversion yields.

It is important to have in mind the notion of spectral range rather than monochromatic irradiation wavelengths, since many different wavelengths in the spectral region of 400 to 500 nm can be used in order to trigger the photoreactivity of the *trans*-$[RuCl(NO)py_4]^{2+}$ complex. Not all the experimental wavelengths in this region afford the same conversion yields, which may also be explained with the characteristic features of the computed spectra, taking into account the possible transposition of the error of *ca*. 1 eV ascribed to the method. In the particular case of the *trans*-$[RuBr(NO)py_4]^{2+}$ complex, there is also a spectral region where an important overlap between the absorption bands of **GS** and **MS2** exists. In contrast with the *trans*-$[RuCl(NO)py_4]^{2+}$ complex, **MS1** also presents a small band that overlaps those of **GS** and **MS2**. This observation may explain the lowering by *ca.* 40 % in the photoconversion yield, since a fraction of **MS1** is lost by absorption of a photon. During the experimental irradiation times, **MS1** is formed and consumed continuously, and depending on the chemical rates, different conversion yields will be attained once the photostationary state is obtained. The fact that the optimal irradiation wavelength found for the complex with the bromine atom (488 – 496 nm) is higher with respect to the one found for the complex with the chlorine can be explained comparing the different spectra. The optimal irradiation wavelength for that complex should be one where **GS** and **MS2** absorb significantly compared to **MS1**. The important region of the spectra where the **GS** and **MS2** isomers absorb but not **MS1** for the *trans*-$[RuCl(NO)py_4]^{2+}$ complex is blue-shifted with respect to the region

where **GS** and **MS2** absorb and the **MS1** band is less important in the *trans*-$[RuBr(NO)py_4]^{2+}$ complex.

Last but not least, the low photoconversion yield observed for the *trans*-(Cl,Cl)$[RuCl_2(NO)(terpy)]^{+}$ complex can also be rationalized following the same line of thinking. As it can be observed in the computed spectra (Figure AB.5.3), near the spectral range of 400 to 500 nm **MS1** presents an important absorption band (*ca*. 6 times larger than the one observed for the *trans*-$[RuBr(NO)py_4]^{2+}$ complex), while the isomers **GS** and **MS2** barely absorb in that region. This particular characteristic reflects perfectly the very low photoconversion yield found for this complex. Moreover, it appears that, for this particular complex, there is no wavelength that would trigger an efficient photoisomerization in the 400 – 500 nm range.

Table AB3. Optimized Cartesian coordinates, energies, molecular parameters and electronic structure of the **GS** isomer of the *trans*-$[RuBr(NO)(py)_4]^{2+}$ complex, at the B3LYP/Ahlrichs-basis level of theory in its ground state (singlet) in vacuum.

Ru	-0.000000006275	0.000000135702	0.037965074280
Br	0.000000354589	0.000000415401	-2.431947007374
N	-0.000306208796	2.155721313493	-0.013506806048
N	2.155721196984	0.000306215662	-0.013506522980
N	0.000306188590	-2.155721078650	-0.013506821096
N	-2.155721195162	-0.000306181717	-0.013507104109
N	-0.000000200344	0.000000184217	1.787072406211
O	-0.000000361096	0.000000124027	2.928327241888
C	-0.789272918744	2.851822724028	0.834906826104
H	-1.421128551981	2.281004529610	1.505414858745
C	-0.814107673555	4.233610619140	0.860747372475
H	-1.466438292094	4.740865610543	1.564548903057
C	-0.002585521303	4.941972534315	-0.017714670953
H	-0.004241431950	6.028183779185	-0.021053739560
C	0.808475247883	4.230207867955	-0.890747596835
H	1.457275888431	4.734838703980	-1.599701835230
C	0.787877439761	2.846126858712	-0.863550931741
H	1.396706174539	2.266949620322	-1.545453698779
C	2.851822506016	0.789273733581	0.834906444677
H	2.281004233263	1.421130102148	1.505413717808
C	4.233610396919	0.814108436145	0.860747220481
H	4.740865295615	1.466439756066	1.564548167950
C	4.941972427049	0.002585320912	-0.017713839624
H	6.028183672786	0.004241148716	-0.021052695287
C	4.230207871768	-0.808476337497	-0.890746028185
H	4.734838799756	-1.457277792968	-1.599699455310
C	2.846126857094	-0.787878408191	-0.863549653307
H	2.266949713291	-1.396707885299	-1.545451835038
C	-0.787879500393	-2.846126728249	-0.863548975985
H	-1.396709991780	-2.266949575914	-1.545450242538
C	-0.808477316044	-4.230207743410	-0.890745481664
H	-1.457279688334	-4.734838657795	-1.599698079548
C	0.002585610103	-4.941972315671	-0.017714485645
H	0.004241558970	-6.028183560905	-0.021053477624
C	0.814109840307	-4.233610300344	0.860745554798
H	1.466442191366	-4.740865209390	1.564545539190
C	0.789274935378	-2.851822409841	0.834904987964
H	1.421132188230	-2.281004155022	1.505411443674
C	-2.846126729926	0.787878532171	-0.863550254140
H	-2.266949483072	1.396708281435	-1.545452105870
C	-4.230207739657	0.808476226645	-0.890747049937
H	-4.734838562122	1.457277784198	-1.599700458890
C	-4.941972422941	-0.002585810485	-0.017715316743
H	-6.028183667306	-0.004241842182	-0.021054521587
C	-4.233610522514	-0.814109077910	0.860745706795
H	-4.740865524218	-1.466440727751	1.564546274181
C	-2.851822627805	-0.789274120720	0.834905369317
H	-2.281004451275	-1.421130638400	1.505412584349

Energies (a.u.)	
E	-3792.117204
Zero-point correction	0.373888
Sum of electronic and thermal enthalpies	-3791.716386
Sum of electronic and thermal free energies	-3791.801261
Selected molecular parameters	
$Ru\text{-}N_{(NO)}$	1.749 Å
$Ru\text{-}O_{(NO)}$	2.890 Å
N-O	1.141 Å
Ru-Br	2.470 Å
$Ru\text{-}N_{py1}$	2.156 Å
$Ru\text{-}N_{py2}$	2.156 Å
$Ru\text{-}N_{py3}$	2.156 Å
$Ru\text{-}N_{py4}$	2.156 Å
∠Ru-N-O	180.000 °
∠Ru-O-N	0.000 °
NO stretching vibration	
ν_{NO} (cm^{-1})	1940.79 cm^{-1}

Electronic structure

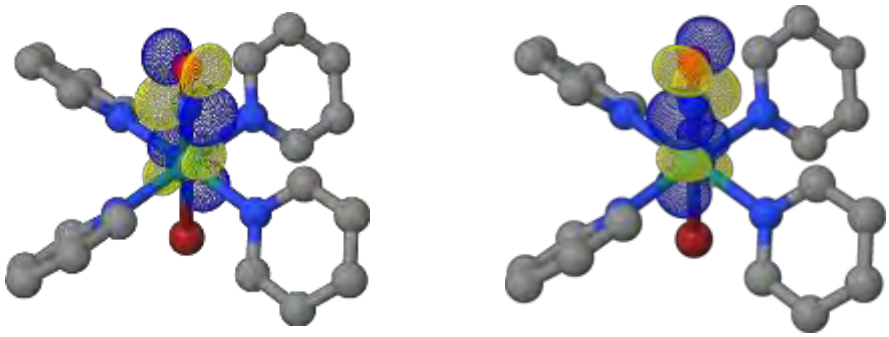

LUMOs (degenerate)

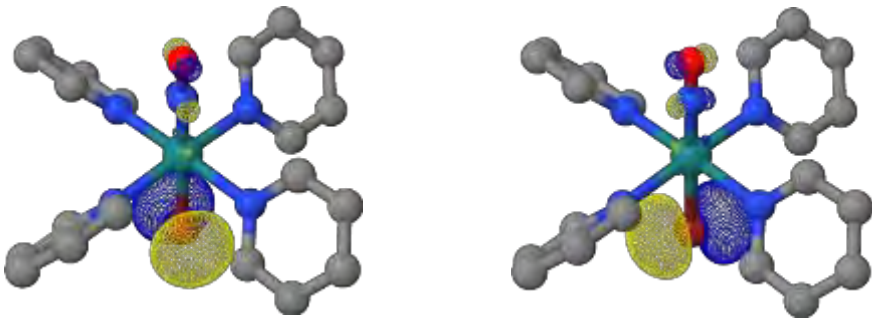

HOMOs (degenerate)

Table AB2. Optimized Cartesian coordinates, energies, molecular parameters and electronic structure of the **MS2** isomer of the *trans*-$[RuBr(NO)(py)_4]^{2+}$ complex, at the B3LYP/Ahlrichs-basis level of theory in its ground state (singlet) in vacuum.

Ru	-0.120722006796	-0.000240055851	0.022544572187
Br	2.323954805746	-0.113916090874	0.183330600943
N	0.109888128720	1.354842510251	-1.630540050020
N	-0.140758803666	1.708255445161	1.326009473367
N	0.021618382422	-1.403680782166	1.715437539858
N	-0.107415000787	-1.656188964426	-1.358284895136
N	-1.942752382247	-0.423987485150	0.496819455672
O	-2.249728637398	0.328804604007	-0.351895731575
C	-0.659519391429	1.209399769108	-2.732714140182
H	-1.361533206441	0.384679638649	-2.740977440731
C	-0.573855178156	2.067623779287	-3.812619768415
H	-1.218875514938	1.906695402930	-4.670645095621
C	0.338251637888	3.115702911089	-3.775619462632
H	0.428970722239	3.801594185467	-4.613065214982
C	1.131531972147	3.265426735663	-2.646069724606
H	1.861283329672	4.065125851656	-2.568120206416
C	0.994121793783	2.374797244119	-1.596191579679
H	1.610246366450	2.459927356611	-0.710809834610
C	-1.008369849886	2.716463735067	1.088047605768
H	-1.649504276574	2.624178369926	0.218834091439
C	-1.093196684039	3.832408949231	1.900418471018
H	-1.812741000034	4.609759003444	1.663696604810
C	-0.247577488955	3.935474628564	2.998275613169
H	-0.288085329940	4.803694963727	3.649819929618
C	0.653433890732	2.906988398429	3.240571282154
H	1.340130157418	2.942368257119	4.080494509136
C	0.681194452461	1.813690036443	2.392310692405
H	1.381789568242	1.004217320087	2.550864601578
C	0.751792517113	-2.533930208457	1.627776800527
H	1.289791773874	-2.702610854020	0.704933900712
C	0.839886929647	-3.438277809371	2.671374147374
H	1.443835755696	-4.331510639490	2.547010594426
C	0.161874749817	-3.181255296092	3.855455745253
H	0.219344287589	-3.873599448560	4.690410024863
C	-0.592356645994	-2.018893120081	3.947471444620
H	-1.144360396902	-1.770030017005	4.848223560595
C	-0.642712377223	-1.161041972781	2.863462242139
H	-1.234960131983	-0.255234226838	2.912767277300
C	0.805600823520	-1.726572589768	-2.351765730578
H	1.540349528402	-0.933246465327	-2.396890279268
C	0.829945714877	-2.765954822677	-3.265714889704
H	1.590831096019	-2.771009235929	-4.039849606523
C	-0.113234215279	-3.780018091202	-3.171133073921
H	-0.115253122642	-4.606047613735	-3.876492177459
C	-1.052697660571	-3.716253467480	-2.149174317382
H	-1.809773341501	-4.484268142920	-2.025552165878
C	-1.018088686672	-2.652383673664	-1.267249881138
H	-1.734250064638	-2.596923012540	-0.454452516224

Energies (a.u.)	
E	-3792.061443
Zero-point correction	0.372617
Sum of electronic and thermal enthalpies	-3791.661874
Sum of electronic and thermal free energies	-3791.745590

Selected molecular parameters	
Ru-$N_{(NO)}$	1.930 Å
Ru-$O_{(NO)}$	2.187 Å
N-O	1.175 Å
Ru-Br	2.453 Å
Ru-N_{py1}	2.150 Å
Ru-N_{py2}	2.149 Å
Ru-N_{py3}	2.204 Å
Ru-N_{py4}	2.156 Å
∠Ru-N-O	85.899 °
∠Ru-O-N	61.681 °

NO stretching vibration	
ν_{NO} (cm^{-1})	1664.73 cm^{-1}

Electronic structure

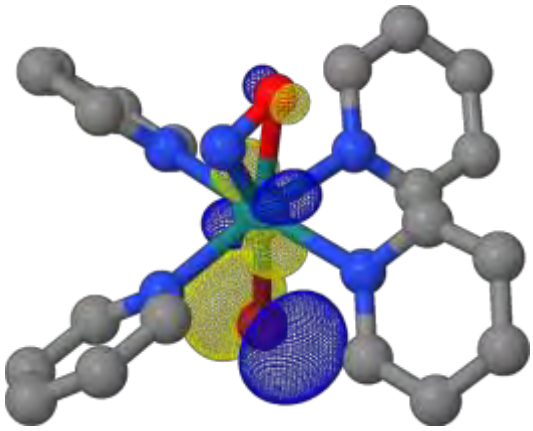

HOMO

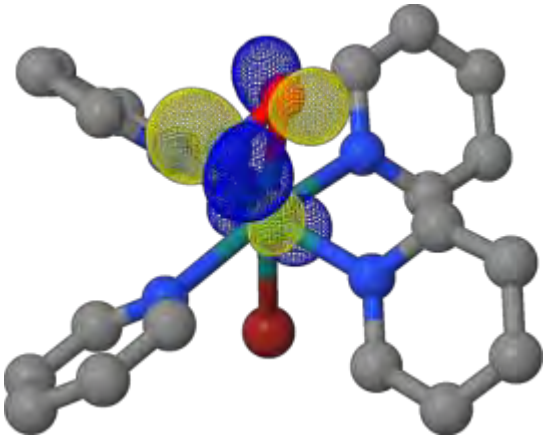

LUMO

Table AB3. Optimized Cartesian coordinates, energies, molecular parameters and electronic structure of the **MS1** isomer of the *trans*-$[RuBr(NO)(py)_4]^{2+}$ complex, at the B3LYP/Ahlrichs-basis level of theory in its ground state (singlet) in vacuum.

Ru	-0.000000090620	-0.000000045218	-0.020994678194
Br	-0.000000349072	0.000000122167	-2.446052928451
N	-0.000315745816	2.147742469646	-0.030094956155
N	2.147742429028	0.000315728676	-0.030095242422
N	0.000315734914	-2.147742551632	-0.030095346898
N	-2.147742592257	-0.000315752035	-0.030095060571
O	-0.000000074350	-0.000000206755	1.845003701039
N	-0.000000009218	-0.000000337797	2.982245860595
C	-0.791612355431	2.827839589089	0.828650652303
H	-1.434625118620	2.244112107606	1.477915187979
C	-0.812308982887	4.209081068155	0.889230301135
H	-1.467273707621	4.701852822617	1.600813395823
C	0.003595069849	4.935515451606	0.029999533654
H	0.004163832368	6.021498829157	0.051364806140
C	0.814365247835	4.241868830074	-0.858209756075
H	1.465325955111	4.761740189815	-1.554063606108
C	0.790835847905	2.857671578438	-0.861810361537
H	1.403035231184	2.292589888721	-1.552867562207
C	2.827839602516	0.791612916937	0.828649789584
H	2.244112159199	1.434626039939	1.477914004047
C	4.209081088198	0.812309707733	0.889229226846
H	4.701852885407	1.467274909950	1.600811852447
C	4.935515421835	-0.003594789130	0.029998839544
H	6.021498802593	-0.004163436606	0.051363952773
C	4.241868745379	-0.814365545515	-0.858209879265
H	4.761740063947	-1.465326609194	-1.554063426737
C	2.857671490748	-0.790836268749	-0.861810305316
H	2.292589759573	-1.403036102079	-1.552867072673
C	-0.790835277353	-2.857671563320	-0.861811388020
H	-1.403034296694	-2.292589787788	-1.552868842379
C	-0.814364513416	-4.241868817731	-0.858211114872
H	-1.465324744921	-4.761740096529	-1.554065470554
C	-0.003594758158	-4.935515544817	0.029998479417
H	-0.004163393867	-6.021498927480	0.051363494350
C	0.812308739586	-4.209081261346	0.889229858755
H	1.467273141300	-4.701853101603	1.600813191217
C	0.791611986219	-2.827839770334	0.828650511257
H	1.434624339190	-2.244112356702	1.477915514316
C	-2.857671651047	0.790834856514	-0.861811444170
H	-2.292589917000	1.403033425754	-1.552869331907
C	-4.241868902462	0.814364215793	-0.858210991517
H	-4.761740222457	1.465324090879	-1.554065649757
C	-4.935515574589	0.003595039011	0.029999173785
H	-6.021498954041	0.004163789807	0.051364348049
C	-4.209081241276	-0.812308014587	0.889230933295
H	-4.701853038763	-1.467271938761	1.600814734912
C	-2.827839756885	-0.791611424617	0.828651374129
H	-2.244112305064	-1.434623417756	1.477916698397

Energies (a.u.)	
E	-3792.049878
Zero-point correction	0.372836
Sum of electronic and thermal enthalpies	-3791.649895
Sum of electronic and thermal free energies	-3791.734990

Selected molecular parameters	
$Ru\text{-}O_{(NO)}$	1.866 Å
$Ru\text{-}N_{(NO)}$	3.003 Å
N-O	1.137 Å
Ru-Br	2.425 Å
$Ru\text{-}N_{py1}$	2.148 Å
$Ru\text{-}N_{py2}$	2.148 Å
$Ru\text{-}N_{py3}$	2.148 Å
$Ru\text{-}N_{py4}$	2.148 Å
∠Ru-O-N	180.000 °
∠Ru-N-O	0.000 °

NO stretching vibration	
ν_{NO} (cm^{-1})	1884.43 cm^{-1}

Electronic structure

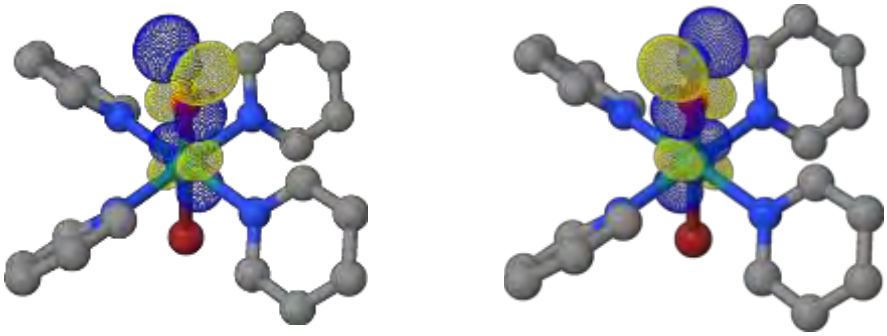

LUMOs (degenerate)

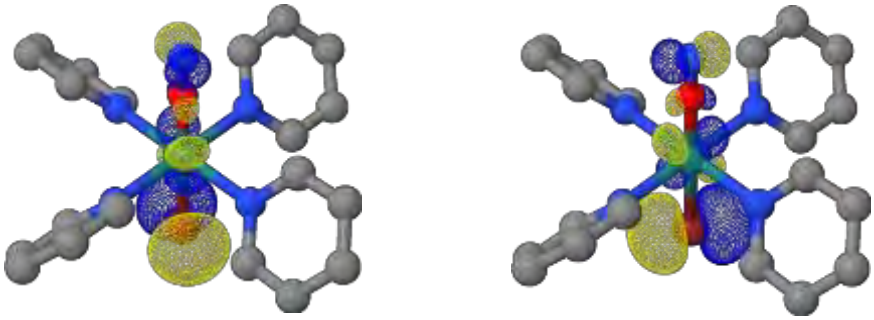

HOMOs (degenerate)

Table AB4. Optimized Cartesian coordinates, energies, molecular parameters and electronic structure of the transition state $^{1}TS_{1}$ of the *trans*-$[RuBr(NO)(py)_4]^{2+}$ complex, at the B3LYP/Ahlrichs-basis level of theory in vacuum.

Ru	0.014805660760	0.001911222318	0.063089820881
Br	2.419664077478	0.099970027604	0.489811316018
N	0.051173387553	1.320992833724	-1.611483411663
N	-0.066673884396	1.778945577453	1.329622665347
N	0.018559419209	-1.467270619578	1.671469930291
N	0.061022031939	-1.623596929809	-1.285567906480
N	-1.950508314791	-0.114309116805	0.614252506990
O	-2.671146064086	0.733510980235	0.360676522668
C	-0.899765659266	1.197755340154	-2.564533664226
H	-1.651018770113	0.428113348149	-2.417524833683
C	-0.936889138271	1.999857559688	-3.690009845789
H	-1.728125776762	1.859842473083	-4.419690684189
C	0.046442430656	2.967690208008	-3.861597680164
H	0.045077308983	3.609704329069	-4.737781092025
C	1.029950280612	3.093969567566	-2.889656217555
H	1.821011868822	3.832003748380	-2.978385027792
C	1.003493331144	2.262517628036	-1.782709629842
H	1.759229510326	2.333929315617	-1.010118841848
C	-0.739640045215	2.884197834188	0.944948560820
H	-1.224046268929	2.856963438772	-0.022218018675
C	-0.823095597001	4.021326248609	1.729752365239
H	-1.379822933347	4.878621668444	1.364853332449
C	-0.189466393915	4.041055544318	2.964934596473
H	-0.235192486335	4.921213112440	3.599717249680
C	0.505462527554	2.908472343512	3.367538604632
H	1.022739695325	2.870386131164	4.321049759288
C	0.547553319165	1.805481963493	2.533085165924
H	1.096182011551	0.919209254430	2.822993698325
C	0.785048837032	-2.573617439353	1.587074927968
H	1.408100256700	-2.672008304026	0.708344960294
C	0.808915000279	-3.542397737246	2.576406685461
H	1.452587835611	-4.407861481146	2.454322446558
C	0.018355334862	-3.383264661784	3.707400321974
H	0.019531991105	-4.128811722781	4.497214116947
C	-0.765566569465	-2.242293274876	3.807308669717
H	-1.396639316221	-2.061043668350	4.671693229039
C	-0.732910703796	-1.310925751838	2.783021847872
H	-1.311278673043	-0.398343362521	2.868318988232
C	1.021759003443	-1.709142308341	-2.233694187771
H	1.788608443042	-0.944057403920	-2.218372745096
C	1.047307020184	-2.728201399620	-3.168307241867
H	1.847054344107	-2.755963052586	-3.901696799901
C	0.048942522956	-3.695214933654	-3.149355933442
H	0.045667607906	-4.503018527093	-3.875609204827
C	-0.943350562783	-3.609572909246	-2.179570445967
H	-1.743202825291	-4.341081823432	-2.121542975850
C	-0.903298949468	-2.573752926811	-1.265256236017
H	-1.653204125812	-2.491314343639	-0.486174664412

Energies (a.u.)	
E	-3792.032919
Zero-point correction	0.370686
Sum of electronic and thermal enthalpies	-3791.635015
Sum of electronic and thermal free energies	-3791.720287

Selected molecular parameters	
Ru-$N_{(NO)}$	2.044 Å
Ru-$O_{(NO)}$	2.800 Å
N-O	1.141 Å
Ru-Br	2.444 Å
Ru-N_{py1}	2.132 Å
Ru-N_{py2}	2.184 Å
Ru-N_{py3}	2.178 Å
Ru-N_{py4}	2.113 Å
∠Ru-N-O	120.323 °
∠Ru-O-N	39.075 °

Imaginary frequency	
ν (cm^{-1})	640.64*i* cm^{-1}

Electronic structure

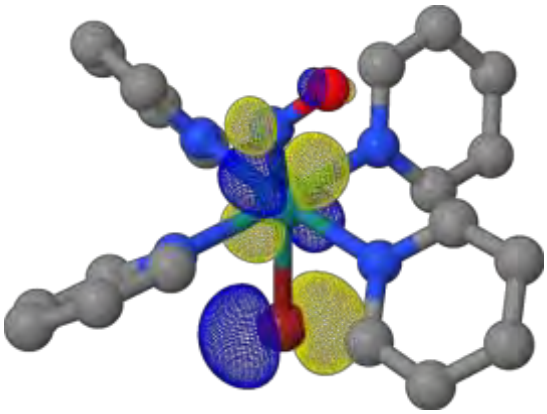

HOMO

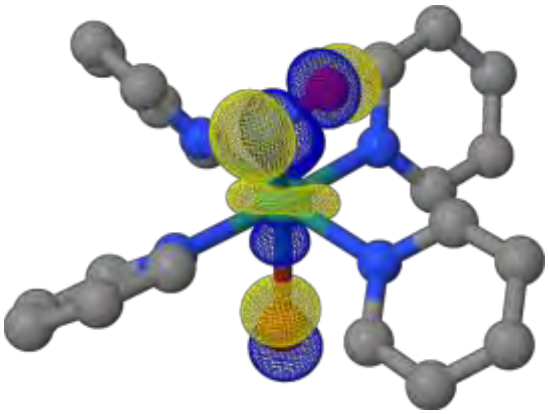

LUMO

Table AB5. Optimized Cartesian coordinates, energies, molecular parameters and electronic structure of the transition state $^{1}TS_{2}$ of the *trans*-$[RuBr(NO)(py)_4]^{2+}$ complex, at the B3LYP/Ahlrichs-basis level of theory in vacuum.

Ru	0.088417576593	-0.006460307091	-0.024497920101
Br	2.491917178008	-0.091620445551	-0.203062902796
N	0.130294200241	1.414219515495	-1.656564363251
N	0.063678511778	1.647690598481	1.315306804581
N	0.035631791796	-1.325352832964	1.645574972166
N	0.012167716340	-1.706401851820	-1.330718309534
N	-2.798109349789	-0.697612390229	-0.378433882341
O	-2.034338288323	0.124442157235	-0.551225607705
C	-0.619042465225	1.260331586306	-2.770145900946
H	-1.226341663751	0.365897964191	-2.839594937473
C	-0.617054076807	2.171060866781	-3.811988517972
H	-1.244689647516	1.990482899250	-4.678981483078
C	0.197297405405	3.292989774291	-3.727494699521
H	0.224361689275	4.022640866764	-4.531548791709
C	0.981942276057	3.452918922851	-2.593580024558
H	1.646094280119	4.304084824672	-2.481204872913
C	0.924265943316	2.504080597853	-1.586727679153
H	1.539556489735	2.602863836223	-0.702473593453
C	-0.872672613885	2.616196325407	1.197748904691
H	-1.561858878457	2.533055466018	0.364370569089
C	-0.963135220962	3.677862087850	2.078899351625
H	-1.738806775173	4.423923437726	1.937778370941
C	-0.049913226331	3.769860090786	3.122834721209
H	-0.092713543033	4.596682875725	3.825930983732
C	0.920176094877	2.783292080549	3.244465218406
H	1.660101344487	2.812889358965	4.038123703385
C	0.946192689023	1.740790398641	2.334450415781
H	1.695022234887	0.960946327822	2.400496497410
C	0.894844313175	-2.357531882990	1.786955760607
H	1.635575290138	-2.481438333775	1.006698090886
C	0.853616447965	-3.211920227022	2.875757381130
H	1.573609480608	-4.021648018895	2.941298649350
C	-0.105133136616	-3.015911700702	3.861028700260
H	-0.158274918957	-3.673677196009	4.723792400050
C	-0.993289252409	-1.955209106075	3.721694878379
H	-1.758892168207	-1.755955106522	4.464841604295
C	-0.887314753300	-1.133035501066	2.615143402302
H	-1.553750800711	-0.283874846826	2.499181786915
C	0.711822055069	-1.741884284348	-2.487021158078
H	1.341602177667	-0.888424300834	-2.701844350902
C	0.654681020771	-2.813585803395	-3.360020188620
H	1.247148681725	-2.788112302825	-4.269230152935
C	-0.153188691724	-3.902136820687	-3.053552046971
H	-0.214158336431	-4.755412053716	-3.722841994516
C	-0.870747713052	-3.877829856625	-1.865990890372
H	-1.506891587061	-4.706373542751	-1.571012392218
C	-0.756427810635	-2.778424329259	-1.030985576570
H	-1.275922970699	-2.764327817904	-0.081097929503

Energies (a.u.)	
E	-3792.006838
Zero-point correction	0.370317
Sum of electronic and thermal enthalpies	-3791.609101
Sum of electronic and thermal free energies	-3791.694812

Selected molecular parameters	
Ru-$N_{(NO)}$	2.989 Å
Ru-$O_{(NO)}$	2.191 Å
N-O	1.135 Å
Ru-Br	2.412 Å
Ru-N_{py1}	2.164 Å
Ru-N_{py2}	2.129 Å
Ru-N_{py3}	2.129 Å
Ru-N_{py4}	2.145 Å
∠Ru-N-O	36.962 °
∠Ru-O-N	124.884 °

Imaginary frequency	
ν (cm^{-1})	503.47*i* cm^{-1}

Electronic structure

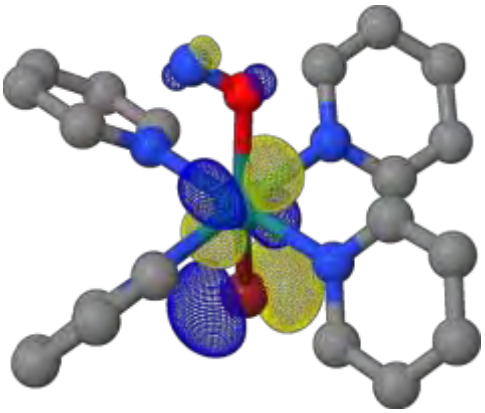

HOMO

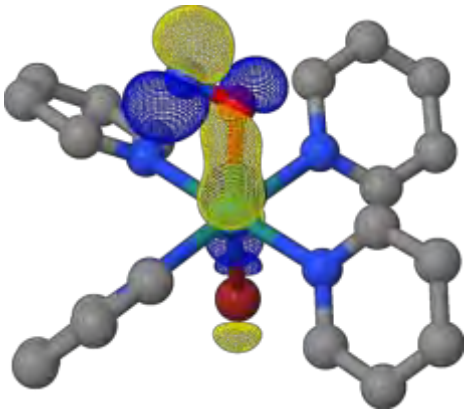

LUMO

Table AB6. Optimized Cartesian coordinates, energies, molecular parameters and electronic structure of the **^{3}GS** triplet state of the *trans*-$[RuBr(NO)(py)_4]^{2+}$ complex, at the B3LYP/Ahlrichs-basis level of theory in vacuum.

Ru	0.065142760406	0.011778619819	0.012611505798
Br	2.506080940657	0.052302907241	0.045151176811
N	0.069385140600	1.354043636013	-1.688719256575
N	0.064675747559	1.673021292780	1.389925584009
N	-0.059422366657	-1.326738104324	1.661993165862
N	0.076334838508	-1.649245958653	-1.355412180458
N	-1.899335126781	0.186486538829	-0.087423742861
O	-2.794934474613	-0.514411213616	0.114762423667
C	-0.783367454696	1.156962078333	-2.717273839913
H	-1.433814032068	0.292274228528	-2.661207659981
C	-0.842796077455	2.003273969166	-3.809381769406
H	-1.550532151787	1.795305503934	-4.605627923776
C	0.006693206979	3.101431278011	-3.862394582785
H	-0.016515299854	3.781216768060	-4.709243190264
C	0.885912871067	3.308996049374	-2.808162308862
H	1.574301805069	4.148249233092	-2.801591402212
C	0.890547697759	2.424595550671	-1.743315081607
H	1.573020277237	2.561107723305	-0.914300175171
C	-0.771313212025	2.716353482491	1.194029849457
H	-1.416025336602	2.672171290123	0.324005477418
C	-0.820044735412	3.801126512268	2.050535152083
H	-1.513527884639	4.610495171348	1.845119991330
C	0.021752865265	3.829937950686	3.155664608979
H	0.006824793945	4.670852072327	3.843046044412
C	0.882980507158	2.759959425323	3.360713192601
H	1.563394560507	2.735165835347	4.206069367280
C	0.879389571877	1.704449602710	2.465379255642
H	1.551784466125	0.865910501904	2.594141415094
C	0.736908136415	-2.418195277001	1.732826809200
H	1.441124595208	-2.560465926651	0.923009313051
C	0.682222328416	-3.305985135053	2.790925521966
H	1.351305409487	-4.160647571037	2.801278436196
C	-0.223564649132	-3.082806798631	3.821206939974
H	-0.286117219125	-3.766678783265	4.662895839110
C	-1.044383849901	-1.963439437994	3.754032553668
H	-1.766988677425	-1.743143091698	4.533384444019
C	-0.933102069677	-1.110775223545	2.671795827879
H	-1.553685253435	-0.225357508620	2.606354316684
C	0.933638777583	-1.689474305079	-2.397868325394
H	1.626335044985	-0.863390522848	-2.492520846822
C	0.952444614193	-2.738525916984	-3.300460538773
H	1.668983662364	-2.722051309267	-4.115661078019
C	0.059071720188	-3.789816624429	-3.143121849068
H	0.053889826307	-4.623932543879	-3.838849946572
C	-0.826889856146	-3.751689200984	-2.073615556749
H	-1.545183812243	-4.547506740308	-1.903733837818
C	-0.787975560623	-2.676794093314	-1.203968726704
H	-1.465231065569	-2.635819934499	-0.358955392396

Energies (a.u.)	
E	-3792.068009
Zero-point correction	0.371590
Sum of electronic and thermal enthalpies	-3791.668690
Sum of electronic and thermal free energies	-3791.756142

Selected molecular parameters	
Ru-$N_{(NO)}$	1.975 Å
Ru-$O_{(NO)}$	2.910 Å
N-O	1.155 Å
Ru-Br	2.441 Å
Ru-N_{py1}	2.167 Å
Ru-N_{py2}	2.158 Å
Ru-N_{py3}	2.128 Å
Ru-N_{py4}	2.152 Å
∠Ru-N-O	135.134 °
∠Ru-O-N	28.604 °

NO stretching vibration	
ν_{NO} (cm^{-1})	1820.88 cm^{-1}

Electronic structure

$\langle S^2 \rangle$: 2.0098

Mulliken Spin Populations: Ru: 0.8403 Br: 0.3198 $N_{(NO)}$: 0.4485 $O_{(NO)}$: 0.3725

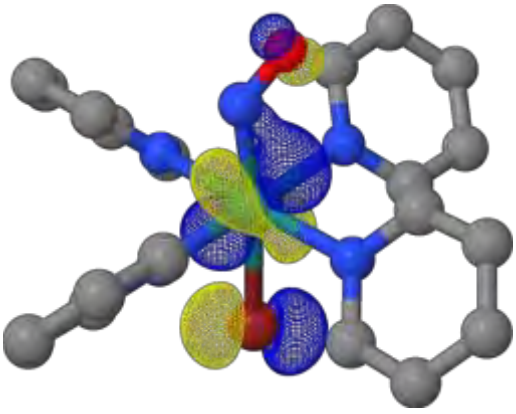

SONO (Hole)

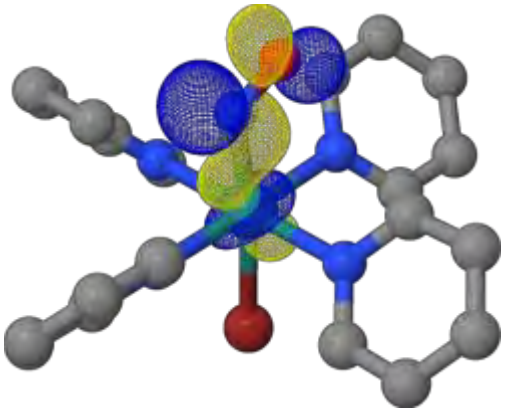

SONO (Particle)

Table AB7. Optimized Cartesian coordinates, energies, molecular parameters and electronic structure of the ^{3}**MS2** triplet state of the *trans*-[RuBr(NO)(py)$_4$]$^{2+}$ complex, at the B3LYP/Ahlrichs-basis level of theory in vacuum.

Ru	-0.019755006705	-0.000141217583	0.006205118007
Br	2.370012917661	-0.060545684384	0.117049512924
N	0.169810831344	1.375729732725	-1.655149113839
N	-0.123971957859	1.689796369129	1.325978752400
N	0.060071823759	-1.396493064302	1.690941563771
N	-0.088185002703	-1.662194060993	-1.343054260156
N	-2.093973997174	-0.363331518626	0.499160629106
O	-2.051191228769	0.351171263412	-0.480612817014
C	-0.582136168243	1.218353564490	-2.766118679746
H	-1.271209240655	0.383827310453	-2.782060154481
C	-0.502614143015	2.081707390164	-3.843720735092
H	-1.132393045511	1.906610225606	-4.710237437454
C	0.377142941290	3.155278990384	-3.790984423942
H	0.459201327975	3.847877377308	-4.623711555421
C	1.146593119964	3.324216546644	-2.647736224222
H	1.848478864298	4.146760076467	-2.553341765617
C	1.019772042541	2.423275058309	-1.605362259169
H	1.616884532017	2.532007680624	-0.709815614887
C	-1.006808971927	2.683712670392	1.082679465661
H	-1.633275878709	2.582651074242	0.205304125361
C	-1.129158824937	3.784305036651	1.911540275707
H	-1.860437301215	4.549520060881	1.671177120592
C	-0.312802775433	3.886554761736	3.030299610598
H	-0.385743451573	4.742853367035	3.694673278661
C	0.601003872768	2.869771255444	3.279757730829
H	1.266839881388	2.904039356121	4.136380040330
C	0.667455339560	1.791138124677	2.417583256820
H	1.374898583706	0.989531615572	2.587051015830
C	0.825957472214	-2.505946995416	1.631226954249
H	1.394122682387	-2.666739114369	0.724932807503
C	0.907500839597	-3.408541925163	2.676689130086
H	1.540744693924	-4.283777040466	2.571561868359
C	0.183737488277	-3.172222712587	3.837517125504
H	0.232713855247	-3.863417263365	4.673953314049
C	-0.608023122714	-2.033306165391	3.901545305967
H	-1.201237138813	-1.803750631874	4.781024302342
C	-0.650546442224	-1.176010898801	2.816757563009
H	-1.281296516466	-0.297141461692	2.837190851919
C	0.760186301452	-1.749533264610	-2.393001335478
H	1.490923643912	-0.957976195979	-2.499901770244
C	0.721916911948	-2.803131147579	-3.286557608844
H	1.433020123981	-2.828521669660	-4.106296619415
C	-0.222886417118	-3.808269799261	-3.114759687420
H	-0.274419407797	-4.645170147235	-3.805410796384
C	-1.097118473088	-3.720759813214	-2.039237899861
H	-1.853338503169	-4.478448202931	-1.859810093281
C	-1.000242736975	-2.645849885443	-1.174082123234
H	-1.668872338416	-2.554424027538	-0.326682744384

Energies (a.u.)	
E	-3792.036201
Zero-point correction	0.371863
Sum of electronic and thermal enthalpies	-3791.637102
Sum of electronic and thermal free energies	-3791.722489
Selected molecular parameters	
Ru-N$_{(NO)}$	2.163 Å
Ru-O$_{(NO)}$	2.118 Å
N-O	1.213 Å
Ru-Br	2.393 Å
Ru-N$_{py1}$	2.165 Å
Ru-N$_{py2}$	2.147 Å
Ru-N$_{py3}$	2.190 Å
Ru-N$_{py4}$	2.142 Å
∠Ru-N-O	71.533 °
∠Ru-O-N	75.557 °
NO stretching vibration	
ν_{NO} (cm^{-1})	1545.51 cm^{-1}

Electronic structure

<S^2>: 2.0076

Mulliken Spin Populations: Ru: 0.7666 Br: 0.2161 N$_{(NO)}$: 0.7379 O$_{(NO)}$: 0.2787

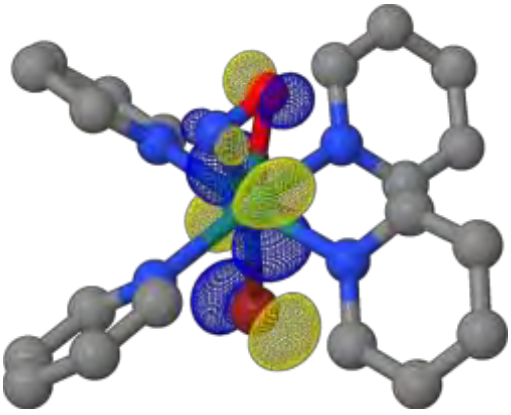

SONO (Hole)

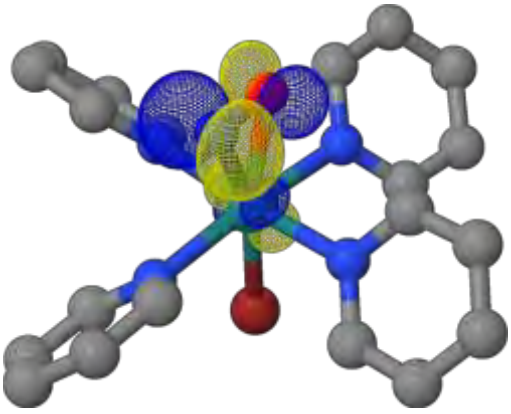

SONO (Particle)

Table AB8. Optimized Cartesian coordinates, energies, molecular parameters and electronic structure of the ^{3}**MS1** triplet state of the *trans*-[RuBr(NO)(py)$_4$]$^{2+}$ complex, at the B3LYP/Ahlrichs-basis level of theory in vacuum.

Ru	0.164689771303	-0.000794394385	-0.000906083041
Br	2.559550828775	-0.036779988479	0.042674446561
N	0.110588970040	1.342927831308	-1.663395952047
N	0.126756656142	1.654062326568	1.364499517101
N	-0.002576920137	-1.319817854416	1.665800231847
N	0.138400089400	-1.645517984741	-1.373512460629
N	-2.919796344638	-0.577434436647	0.141966983757
O	-2.045780499443	0.138863169581	-0.107260794125
C	-0.752711851805	1.144997924173	-2.683793301933
H	-1.381095875605	0.263948252498	-2.633542193754
C	-0.846102204871	2.008667827185	-3.759623297217
H	-1.561834504036	1.801469648458	-4.548846583152
C	-0.014332138068	3.120650981657	-3.808726993292
H	-0.061450656465	3.812244961416	-4.645011750897
C	0.880610195827	3.326326281468	-2.766388435865
H	1.556329126052	4.175776156174	-2.760128244074
C	0.914562341167	2.428582407231	-1.714664718550
H	1.606903484958	2.561474298413	-0.893022895147
C	-0.758944248679	2.659224486747	1.187256133375
H	-1.415159696525	2.591331913663	0.326797842292
C	-0.843544076760	3.739809102070	2.046487191389
H	-1.577003019164	4.516764543377	1.855344634691
C	0.018561782995	3.808086656439	3.134396467775
H	-0.021711658990	4.647462114655	3.822597455630
C	0.933346274399	2.780211452191	3.319735576473
H	1.631420199091	2.787452096697	4.150937000148
C	0.959945796471	1.724610945022	2.424236045483
H	1.670005336630	0.915634693367	2.540232549001
C	0.745636872334	-2.443149322944	1.750701059739
H	1.445642975770	-2.624115802568	0.944761822430
C	0.649086099452	-3.318407298973	2.817197188853
H	1.282485499916	-4.199652290368	2.838693118160
C	-0.252720863387	-3.050041862877	3.839458875878
H	-0.348362858718	-3.723252620374	4.686538435726
C	-1.025791491233	-1.898355303187	3.757385726695
H	-1.742107347138	-1.640736692573	4.531088192360
C	-0.869772452684	-1.059016552831	2.669611075240
H	-1.444696404260	-0.143392416973	2.598402022552
C	0.970224757011	-1.687205299338	-2.436615491969
H	1.668391465840	-0.866663668341	-2.540935652179
C	0.957447733991	-2.728610696352	-3.348299458404
H	1.654504181302	-2.712903146049	-4.180244069864
C	0.057587640037	-3.772557058945	-3.178527654268
H	0.027964059816	-4.600904494836	-3.880487299296
C	-0.801282772099	-3.735814777430	-2.086933576874
H	-1.520901187448	-4.527806455992	-1.905124077709
C	-0.728364849709	-2.668989232474	-1.209206358880
H	-1.377247216861	-2.633617418269	-0.341067249992

Energies (a.u.)	
E	-3792.044194
Zero-point correction	0.370717
Sum of electronic and thermal enthalpies	-3791.645355
Sum of electronic and thermal free energies	-3791.733648

Selected molecular parameters	
Ru-O$_{(NO)}$	2.217 Å
Ru-N$_{(NO)}$	3.141 Å
N-O	1.157 Å
Ru-Br	2.396 Å
Ru-N$_{py1}$	2.138 Å
Ru-N$_{py2}$	2.146 Å
Ru-N$_{py3}$	2.132 Å
Ru-N$_{py4}$	2.142 Å
∠Ru-O-N	134.717 °
∠Ru-N-O	30.108 °

NO stretching vibration	
ν_{NO} (cm^{-1})	1802.86 cm^{-1}

Electronic structure

<S^2>: 2.0097

Mulliken Spin Populations: Ru: 0.8545 Br: 0.2158 N$_{(NO)}$: 0.7682 O$_{(NO)}$: 0.1597

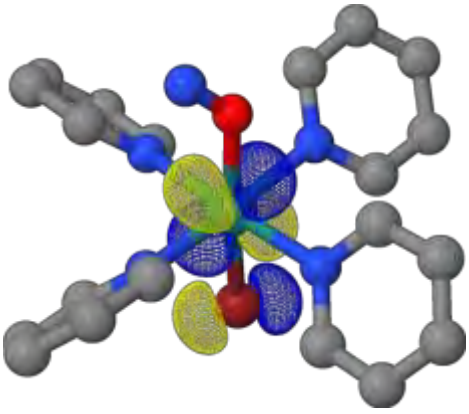

SONO (Hole)

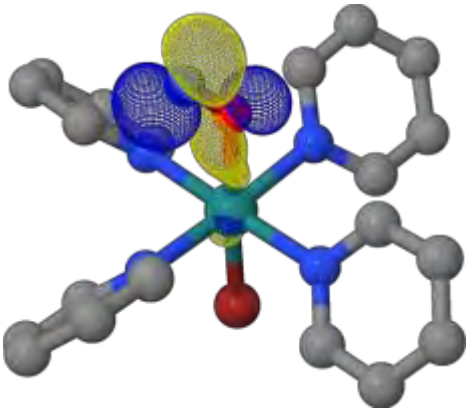

SONO (Particle)

Table AB9. Optimized Cartesian coordinates, energies, molecular parameters and electronic structure of the transition state $^3TS_1$ of the *trans*-$[RuBr(NO)(py)_4]^{2+}$ complex, at the B3LYP/Ahlrichs-basis level of theory in vacuum.

Ru	-0.023539934307	0.005339562803	0.019163801821
Br	-0.035437022867	-0.010318931485	2.406706822419
N	2.137927867611	0.053321815746	0.058046836788
N	0.019264097880	2.130003024402	-0.131340729523
N	-2.194096419898	-0.000333190058	0.130969879759
N	-0.026627816300	-2.135146024737	-0.080914186660
N	-0.663548709939	-0.090744136975	-2.158404316504
O	0.483464502759	-0.146741122352	-2.399849995746
C	2.877969669329	-0.746318918617	-0.742224225079
H	2.342187738743	-1.410834904029	-1.408095580495
C	4.260766027829	-0.734157546868	-0.736283728789
H	4.799737091869	-1.398054745891	-1.404834510969
C	4.928922510410	0.129972160002	0.122196592942
H	6.014406922109	0.159347867817	0.147536057550
C	4.175431428272	0.955454310862	0.945276458601
H	4.645551693105	1.648548856262	1.635737816392
C	2.793997730002	0.892208765972	0.888556400158
H	2.189605555503	1.520261013744	1.529613391580
C	0.790266321437	2.721273482896	-1.070805286821
H	1.383989245839	2.070509597356	-1.701758181205
C	0.831382224350	4.093370496912	-1.238856117863
H	1.461626209696	4.514915589997	-2.015502205412
C	0.070588262728	4.901672472987	-0.403405628944
H	0.091152023435	5.982677894519	-0.508268694197
C	-0.714161745440	4.297979209043	0.571819247558
H	-1.320129038059	4.885446405948	1.254471071629
C	-0.723482435538	2.919378023875	0.677364785764
H	-1.323489173631	2.422392614889	1.429308680954
C	-2.849464479605	-0.858114148977	0.941745075627
H	-2.246837762376	-1.538263530954	1.528845115467
C	-4.229337114093	-0.878156841008	1.044279746284
H	-4.700119141142	-1.590167806682	1.714743195665
C	-4.980540875733	0.014876511926	0.292260802081
H	-6.064815683392	0.021489609892	0.355992291049
C	-4.312055514905	0.897866149125	-0.545720733986
H	-4.849729999605	1.613206548897	-1.159940844406
C	-2.930347576925	0.861380347898	-0.602018323565
H	-2.392712370207	1.532563953112	-1.259368575895
C	0.828856193581	-2.861363012125	0.675783927016
H	1.490691117600	-2.309904871276	1.331100592245
C	0.856203846034	-4.242518338456	0.642197092862
H	1.556367050190	-4.774467894921	1.278630150587
C	-0.015512728816	-4.920957837854	-0.201866171213
H	-0.010965683206	-6.006262907657	-0.248260214441
C	-0.895865301763	-4.181008794934	-0.980616117155
H	-1.598251782232	-4.661394177180	-1.654390962088
C	-0.881669497909	-2.801056068517	-0.889912336343
H	-1.564136522425	-2.203861535330	-1.482620165498

Energies (a.u.)	
E	-3792.029360
Zero-point correction	0.370163
Sum of electronic and thermal enthalpies	-3791.631792
Sum of electronic and thermal free energies	-3791.718046

Selected molecular parameters	
Ru-$N_{(NO)}$	2.272 Å
Ru-$O_{(NO)}$	2.476 Å
N-O	1.173 Å
Ru-Br	2.388 Å
Ru-N_{py1}	2.162 Å
Ru-N_{py2}	2.130 Å
Ru-N_{py3}	2.173 Å
Ru-N_{py4}	2.143 Å
∠Ru-N-O	85.634 °
∠Ru-O-N	66.168 °

Imaginary frequency	
ν (cm^{-1})	995.45*i* cm^{-1}

Electronic structure

$\langle S^2 \rangle$: 2.0165

Mulliken Spin Populations: Ru: 0.8838 Br: 0.2053 $N_{(NO)}$: 0.6044 $O_{(NO)}$: 0.2981

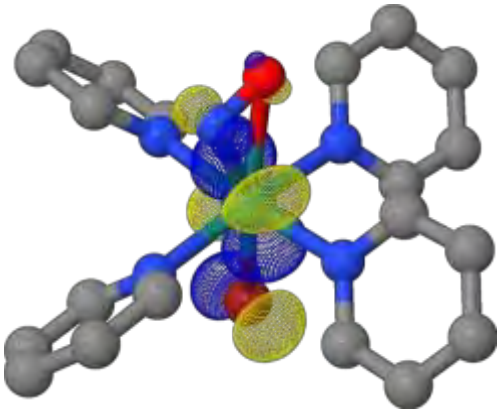

SONO (Hole)

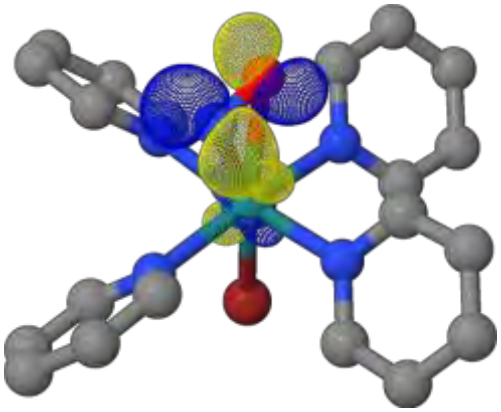

SONO (Particle)

Table AB10. Optimized Cartesian coordinates, energies, molecular parameters and electronic structure of the transition state $^3TS_2$ of the *trans*-$[RuBr(NO)(py)_4]^{2+}$ complex, at the B3LYP/Ahlrichs-basis level of theory in vacuum.

Ru	-0.003355752769	0.001953429176	0.062671147958
Br	-0.062402467536	-0.021023474798	2.433770626941
N	2.147461388842	-0.001445536159	0.119582769402
N	0.046936693155	2.126176490952	-0.069975251792
N	-2.161735251667	-0.001121745034	0.034115237194
N	-0.031664523459	-2.114707444491	-0.117614348389
O	0.532648184296	0.028448638532	-2.431017081236
N	-0.594615595524	0.095340871063	-2.701413269016
C	2.864344166623	-0.796746583407	-0.704520423948
H	2.307632880634	-1.427843696755	-1.386114274319
C	4.247357723302	-0.820841857072	-0.703567110282
H	4.768114796986	-1.479543144450	-1.391350848036
C	4.939263588696	-0.000693412017	0.178862792431
H	6.025163068404	-0.001457209444	0.203108984579
C	4.209454542572	0.819822968334	1.028253852175
H	4.699606503694	1.478836163904	1.737914472651
C	2.826737582672	0.795467586038	0.972713031018
H	2.238676836507	1.420541360020	1.632036451297
C	0.899209491594	2.745753985445	-0.918011301379
H	1.553418211642	2.114140288375	-1.506120163901
C	0.946739238128	4.121648053697	-1.048568844773
H	1.643837682599	4.564854651994	-1.752614252445
C	0.107433391333	4.906268799942	-0.267724941037
H	0.131478085311	5.989627644553	-0.343559971097
C	-0.760275189104	4.275522180001	0.616088418428
H	-1.429260692044	4.843798295471	1.254667990116
C	-0.771204174072	2.895168167987	0.685780719275
H	-1.433644862396	2.378123345068	1.368407538587
C	-2.861435098817	-0.847700200185	0.820175404475
H	-2.289698184368	-1.506790355427	1.460352572152
C	-4.245227639369	-0.881561240616	0.834387059828
H	-4.751258678904	-1.582345864904	1.490881906966
C	-4.955608128627	-0.016878581176	0.013125637717
H	-6.041726564637	-0.022694097113	0.005406946407
C	-4.243409711082	0.856231977513	-0.799748091524
H	-4.747793621224	1.550593793090	-1.464271702046
C	-2.861117555496	0.838195025398	-0.761523635599
H	-2.290659697318	1.512364841870	-1.388889682686
C	0.750331303901	-2.898613887393	0.660538170210
H	1.367005928771	-2.396328755029	1.395172111190
C	0.757995033550	-4.276155843317	0.548341587838
H	1.395016053333	-4.858214616574	1.206886407050
C	-0.050387856197	-4.886834496306	-0.403424089018
H	-0.058412490615	-5.967530186799	-0.513289428399
C	-0.851430589998	-4.086187145374	-1.208009887981
H	-1.501803963741	-4.513752568570	-1.964509396646
C	-0.826387313897	-2.714671480914	-1.032677418776
H	-1.452692773685	-2.070240135099	-1.638088421565

Energies (a.u.)	
E	-3792.028699
Zero-point correction	0.370059
Sum of electronic and thermal enthalpies	-3791.630830
Sum of electronic and thermal free energies	-3791.718805

Selected molecular parameters	
Ru-$O_{(NO)}$	2.828 Å
Ru-$N_{(NO)}$	2.551 Å
N-O	1.161 Å
Ru-Br	2.372 Å
Ru-N_{py1}	2.152 Å
Ru-N_{py2}	2.129 Å
Ru-N_{py3}	2.159 Å
Ru-N_{py4}	2.125 Å
∠Ru-O-N	91.390 °
∠Ru-N-O	64.377 °

Imaginary frequency	
ν (cm^{-1})	196.32*i* cm^{-1}

Electronic structure

$<S^2>$: 2.0078

Mulliken Spin Populations: Ru: 0.8209 Br: 0.1630 $N_{(NO)}$: 0.7253 $O_{(NO)}$: 0.2738

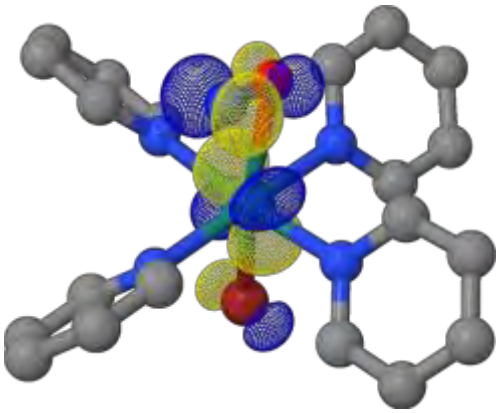

SONO (Hole)

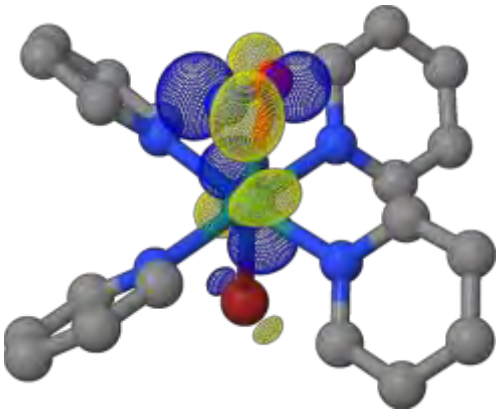

SONO (Particle)

N.B. From an electronic and structural point of view and regarding the transition vector, this TS seems to be the correct one compared with the one found for the *trans*-$[RuCl(NO)(py)_4]^{2+}$ complex. However, depending on the distortion applied to perform steepest decent calculations, the TS leads to the isomerization product or to the dissociation product. This is probably due to the vicinity of the reaction pathways of both processes. Further analysis on this matter needs to be done.

Table AB11. Optimized Cartesian coordinates, energies, molecular parameters and electronic structure of the **GS** isomer of the *trans*-(Cl,Cl)[$RuCl_2$(NO)(terpy)]$^+$ complex, at the B3LYP-D3/Ahlrichs-basis level of theory in its ground state (singlet) in vacuum.

Ru	3.359060564218	0.053046264782	-0.061801673164
Cl	3.126959144576	-0.093564109673	-2.429503212980
Cl	3.163259296268	0.173226719527	2.310787511369
N	5.096082712590	0.159784820963	-0.079884868709
N	1.330149798790	-0.072049755274	-0.039040009727
N	2.805868860327	2.067770292163	-0.171438743501
N	3.060101111288	-2.014181321133	0.056617448801
O	6.233601996745	0.229442623279	-0.090645845467
C	0.626372706245	1.067844058972	-0.097970234280
C	1.460265903665	2.280026505233	-0.173068663941
H	-2.457071383857	-0.305640861633	0.002887539160
C	3.180980835353	4.416926607611	-0.308248926867
H	3.896433533899	5.230664489072	-0.360231518407
C	0.773225096040	-1.289686377267	0.033933535162
C	-0.612525974529	-1.400218221001	0.050824531070
H	-1.094698252236	-2.368555787968	0.109201994411
C	3.723956700937	-4.299436421429	0.179011777088
H	4.534956531326	-5.019079917799	0.212742979169
C	1.751161270029	-2.390160672040	0.088115940582
C	-1.373595638311	-0.238810913977	-0.009030234247
C	0.947056638050	3.567153137585	-0.242395855863
H	-0.124976019776	3.726491414187	-0.243223962921
C	-0.762495165191	1.007227893734	-0.084062774887
H	-1.361179505220	1.908886281033	-0.130546948588
C	3.639569741860	3.110233025142	-0.237424399744
H	4.700413512283	2.890973887647	-0.233426459849
C	4.016828948404	-2.946328278742	0.100962690781
H	5.042375577872	-2.598525224817	0.073069764446
C	1.401669452451	-3.730570205795	0.165812601320
H	0.357624220776	-4.020423830268	0.190262407980
C	2.396821311679	-4.697634147389	0.211940356959
H	2.134824884239	-5.749310874253	0.272842854407
C	1.814570719298	4.649019761083	-0.310762327832
H	1.424037869914	5.660395138450	-0.365362271731

Energies (a.u.)	
E	-1888.067876
Zero-point correction	0.241889
Sum of electronic and thermal enthalpies	-1887.805551
Sum of electronic and thermal free energies	-1887.874900
Selected molecular parameters	
Ru-$N_{(NO)}$	1.740 Å
Ru-$O_{(NO)}$	2.880 Å
N-O	1.140 Å
Ru-Cl_1	2.384 Å
Ru-Cl_2	2.384 Å
Ru-N_{tpy1}	2.033 Å
Ru-N_{tpy2}	2.092 Å
Ru-N_{tpy3}	2.092 Å
∠Ru-N-O	179.944 °
∠Ru-O-N	0.034 °
NO stretching vibration	
ν_{NO} (cm^{-1})	1964.19 cm^{-1}

Electronic structure

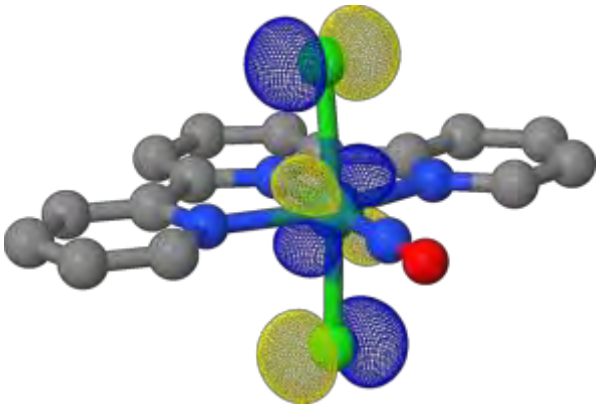

HOMO

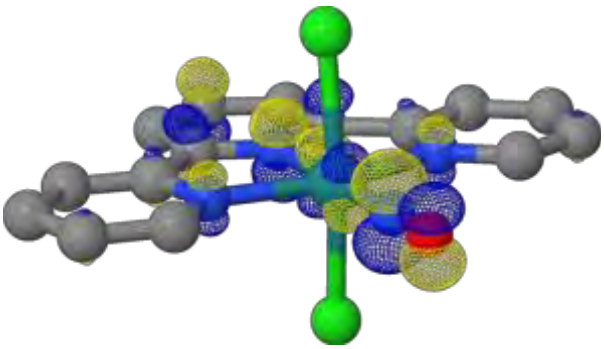

LUMO

Table AB12. Optimized Cartesian coordinates, energies, molecular parameters and electronic structure of the **MS2** isomer of the *trans*-(Cl,Cl)[$RuCl_2$(NO)(terpy)]$^+$ complex, at the B3LYP-D3/Ahlrichs-basis level of theory in its ground state (singlet) in vacuum.

Ru	3.360115543841	-0.041933915395	-0.042159884162
Cl	3.275506529709	-0.293434194591	-2.408572691650
Cl	3.274304232110	-0.026544626635	2.338612942289
N	5.110072428252	0.726657323169	-0.080438316918
N	1.352825529905	-0.085588403504	-0.035227107698
N	2.798717259281	2.034500176315	-0.164292075612
N	3.010958469179	-2.092699444995	0.073300827605
O	5.451025589757	-0.398051600667	-0.020746873108
C	0.639563505578	1.050036845477	-0.096527319580
C	1.459619156567	2.256051760502	-0.171767544863
H	-2.462872328494	-0.290995332082	-0.000783781783
C	3.164039905440	4.389457847636	-0.312117017479
H	3.881789852767	5.201073883223	-0.366445080685
C	0.764800410364	-1.300278570213	0.038328858782
C	-0.620128883995	-1.393102571255	0.051645494035
H	-1.103688109468	-2.360516966131	0.110420594138
C	3.617011933654	-4.388595865048	0.198452554015
H	4.409204529039	-5.128612982473	0.235808089800
C	1.696864160528	-2.430685864780	0.098230678549
C	-1.379114537067	-0.232182929758	-0.010751694201
C	0.937532085843	3.541153667504	-0.248078403130
H	-0.135182732320	3.693746061181	-0.252551113730
C	-0.751065138852	0.999934103582	-0.085528711429
H	-1.333631589609	1.911627697584	-0.134456962820
C	3.624982007648	3.084376971581	-0.233983660072
H	4.686905097839	2.881200581800	-0.227401773722
C	3.947637873276	-3.044701937583	0.121712981583
H	4.980250690996	-2.723251200330	0.098264597621
C	1.309783678360	-3.761115637325	0.174494903280
H	0.258985513663	-4.024480039056	0.194023051426
C	2.279630899644	-4.752434571335	0.225416902682
H	1.990513454948	-5.797072468809	0.285294826302
C	1.798382039043	4.624926425579	-0.319073113176
H	1.406760942577	5.635546776833	-0.379349176292

Energies (a.u.)	
E	-1888.013345
Zero-point correction	0.240626
Sum of electronic and thermal enthalpies	-1887.752086
Sum of electronic and thermal free energies	-1887.821565
Selected molecular parameters	
Ru-$N_{(NO)}$	1.912 Å
Ru-$O_{(NO)}$	2.121 Å
N-O	1.177 Å
Ru-Cl_1	2.381 Å
Ru-Cl_2	2.382 Å
Ru-N_{tpy1}	2.008 Å
Ru-N_{tpy2}	2.083 Å
Ru-N_{tpy3}	2.154 Å
∠Ru-N-O	83.105 °
∠Ru-O-N	63.475 °
NO stretching vibration	
ν_{NO} (cm^{-1})	1658.30 cm^{-1}

Electronic structure

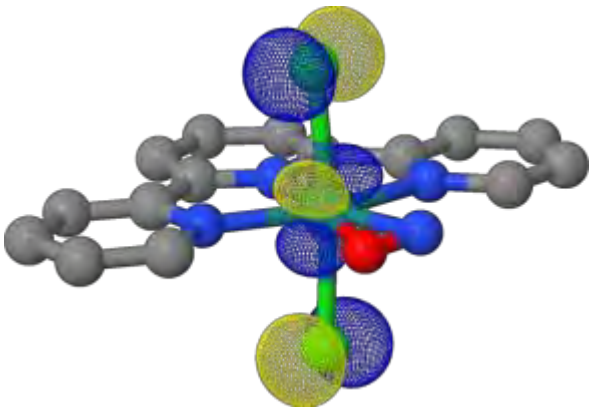

HOMO

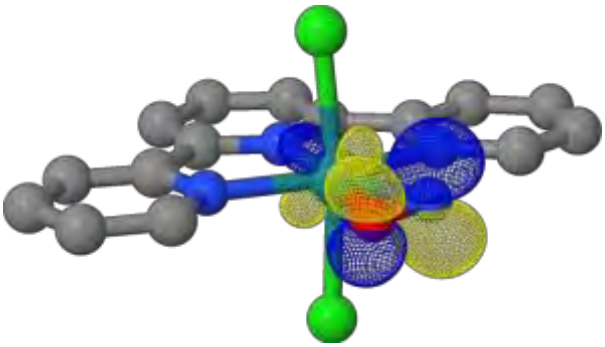

LUMO

Table AB13. Optimized Cartesian coordinates, energies, molecular parameters and electronic structure of the **MS1** isomer of the *trans*-(Cl,Cl)[$RuCl_2$(NO)(terpy)]$^+$ complex, at the B3LYP-D3/Ahlrichs-basis level of theory in its ground state (singlet) in vacuum.

Ru	3.307865993315	0.049511943364	-0.064859082418
Cl	3.172140632048	-0.093611734044	-2.428847964265
Cl	3.221243495436	0.178676056435	2.302406378757
N	1.329275772945	-0.071973443446	-0.037193032940
N	2.794824538949	2.067011833862	-0.176314346314
N	3.048679238521	-2.015424593831	0.056408512158
O	5.153682825118	0.163040960248	-0.088127142489
N	6.284362107555	0.232796915112	-0.099667266675
C	0.621496398618	1.070255841742	-0.095841506095
C	1.451119646182	2.283892690344	-0.174755363232
H	-2.462246105271	-0.304834719814	0.014661548242
C	3.177591146670	4.414097373981	-0.317425561473
H	3.894799205211	5.226086515927	-0.372541467382
C	0.768414896459	-1.292093384507	0.039035156939
C	-0.616987497814	-1.398811223315	0.059355488822
H	-1.097861555538	-2.367669110598	0.120194675157
C	3.719459562231	-4.297986754222	0.179858790196
H	4.531854546123	-5.016126543234	0.212136346625
C	1.742106898854	-2.395027829528	0.092322543332
C	-1.378848216072	-0.238291522668	-0.000029735936
C	0.939772758454	3.571909976719	-0.244382422994
H	-0.131704907133	3.735320400135	-0.242621379459
C	-0.766592788859	1.006621194576	-0.078149637994
H	-1.363885057995	1.909245151899	-0.124364932098
C	3.630898573648	3.105126753847	-0.245992458548
H	4.691723091779	2.881412101654	-0.244703414193
C	4.007077087507	-2.943463324205	0.098976932469
H	5.032123743816	-2.591783091726	0.067220459282
C	1.394296588460	-3.735860685683	0.172975381342
H	0.351227223507	-4.029100749724	0.201013466421
C	2.393070847833	-4.699639970660	0.217443656037
H	2.134613067843	-5.752032583364	0.280660370230
C	1.811509993698	4.650471116743	-0.316497214313
H	1.424583247903	5.663190437979	-0.371410777186

Energies (a.u.)	
E	-1887.997655
Zero-point correction	0.240768
Sum of electronic and thermal enthalpies	-1887.736176
Sum of electronic and thermal free energies	-1887.806266
Selected molecular parameters	
Ru-$O_{(NO)}$	1.849 Å
Ru-$N_{(NO)}$	2.982 Å
N-O	1.133 Å
Ru-Cl_1	2.372 Å
Ru-Cl_2	2.372 Å
Ru-N_{tpy1}	1.983 Å
Ru-N_{tpy2}	2.085 Å
Ru-N_{tpy3}	2.085 Å
∠Ru-O-N	179.862 °
∠Ru-N-O	0.085 °
NO stretching vibration	
ν_{NO} (cm^{-1})	1923.47 cm^{-1}

Electronic structure

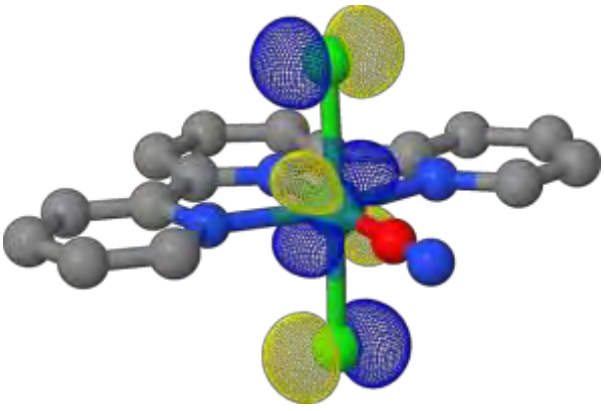

HOMO

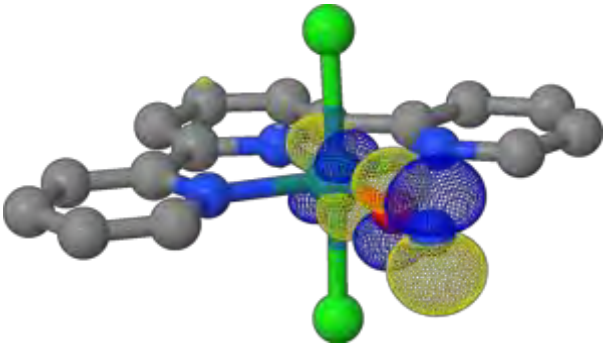

LUMO

Table AB14. Absorption TD-DFT spectra and selected states of the **GS** (orange), **MS1** (green), and **MS2** (black) isomers of the *trans*-[RuCl(NO)(py)$_4$]$^{2+}$ complex at the TPSSh/Ahlrichs-basis level of theory in vacuum.

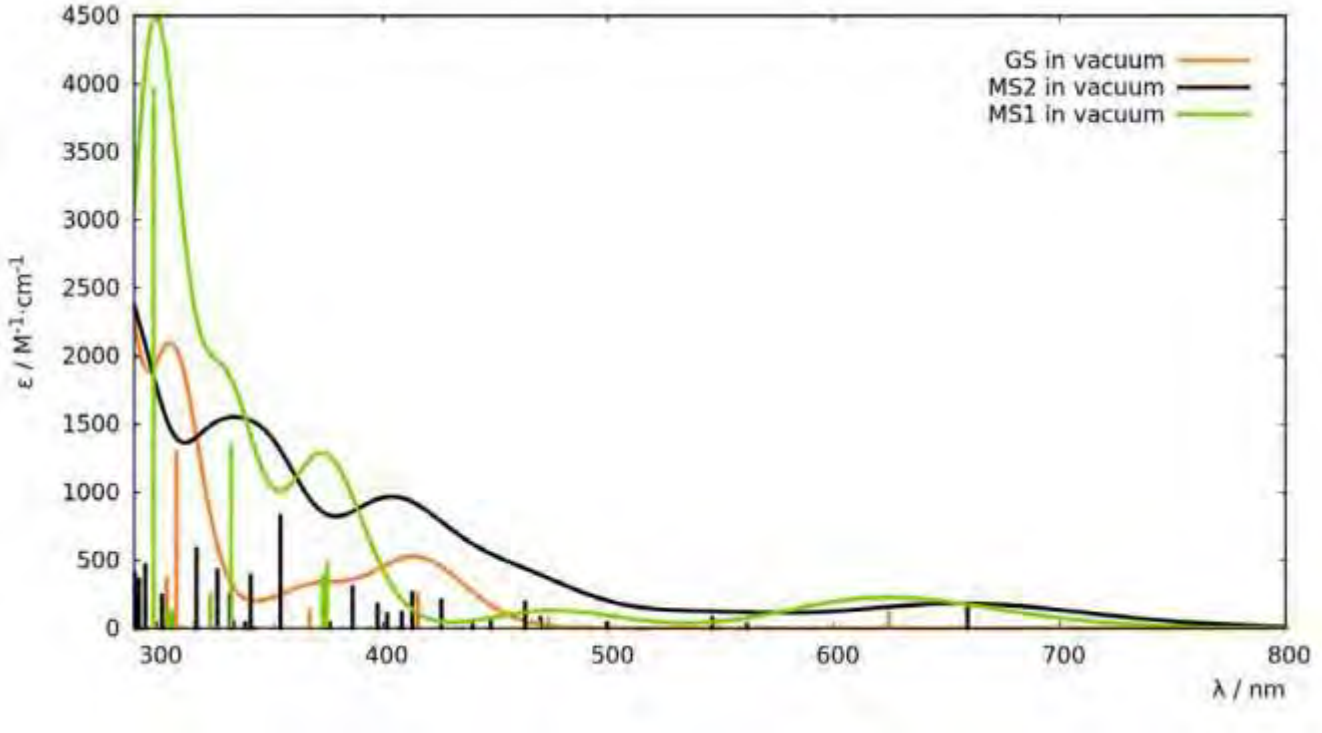

	State	Wavelength / nm	f_{osc}
GS	S_1 & S_2	416	0.0032
	S_6 & S_7	375	0.0010
MS2	S_6	470	0.0010
	S_7	463	0.0024
	S_{10}	426	0.0026
	S_{11}	413	0.0033
	S_{12}	408	0.0015
	S_{13}	402	0.0013
	S_{14}	398	0.0022
	S_{15}	387	0.0039
MS1	S_{17}	375	0.0062
	S_{18} & S_{19}	373	0.0049

Table AB15. Absorption TD-DFT spectra and selected states of the **GS** (orange), **MS1** (green), and **MS2** (black) isomers of the *trans*-[RuBr(NO)(py)$_4$]$^{2+}$ complex at the TPSSh/Ahlrichs-basis level of theory in vacuum.

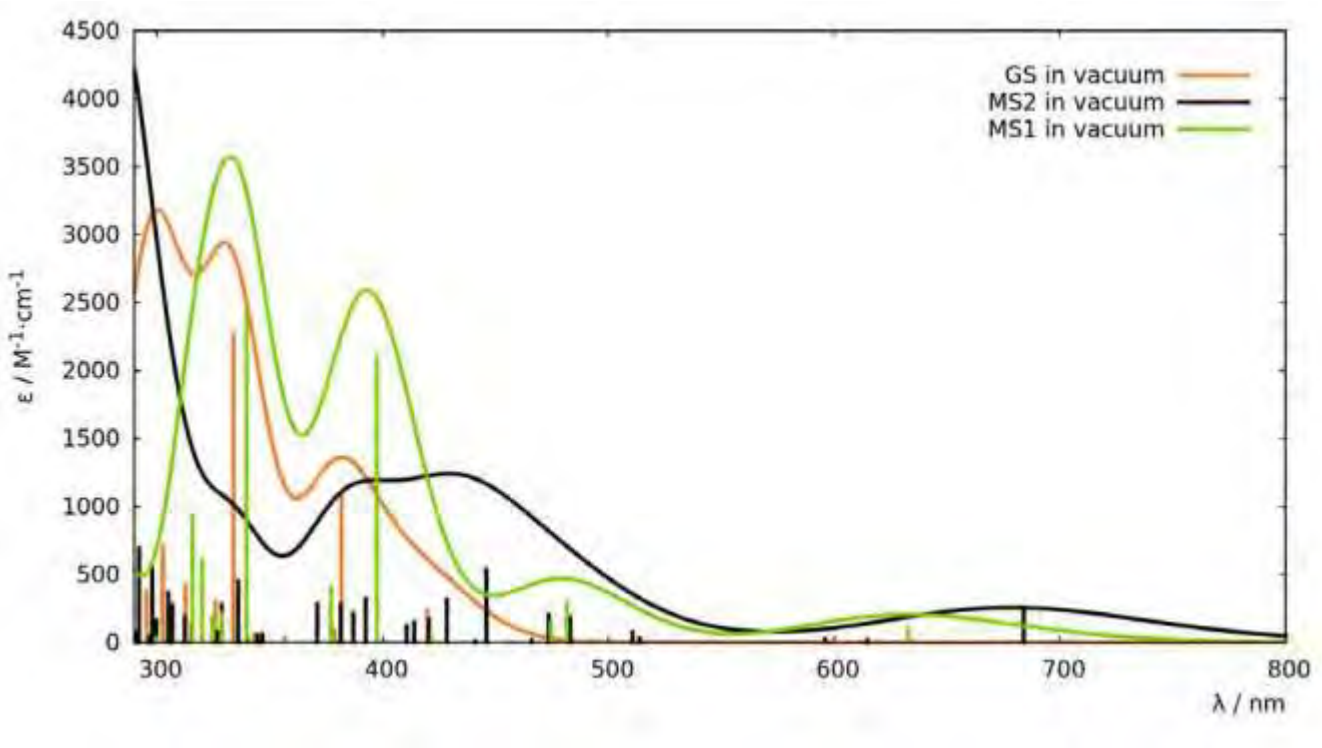

	State	Wavelength / nm	f_{osc}
GS	S_4 & S_5	420	0.0029
	S_6	382	0.0141
	S_7 & S_8	379	0.0011
MS2	S_5	511	0.0010
	S_6	483	0.0024
	S_7	473	0.0026
	S_9	446	0.0069
	S_{11}	428	0.0040
	S_{12}	421	0.0021
	S_{13}	414	0.0019
	S_{14}	411	0.0016
MS1	S_8	482	0.0037
	S_9	474	0.0019
	S_{17}	397	0.0269

Table AB16. Absorption TD-DFT spectra and selected states of the **GS** (orange), **MS1** (green), and **MS2** (black) isomers of the *trans*-(Cl,Cl)[$RuCl_2$(NO)(terpy)]$^+$ complex at the BHandHLYP/Ahlrichs-basis level of theory in vacuum.

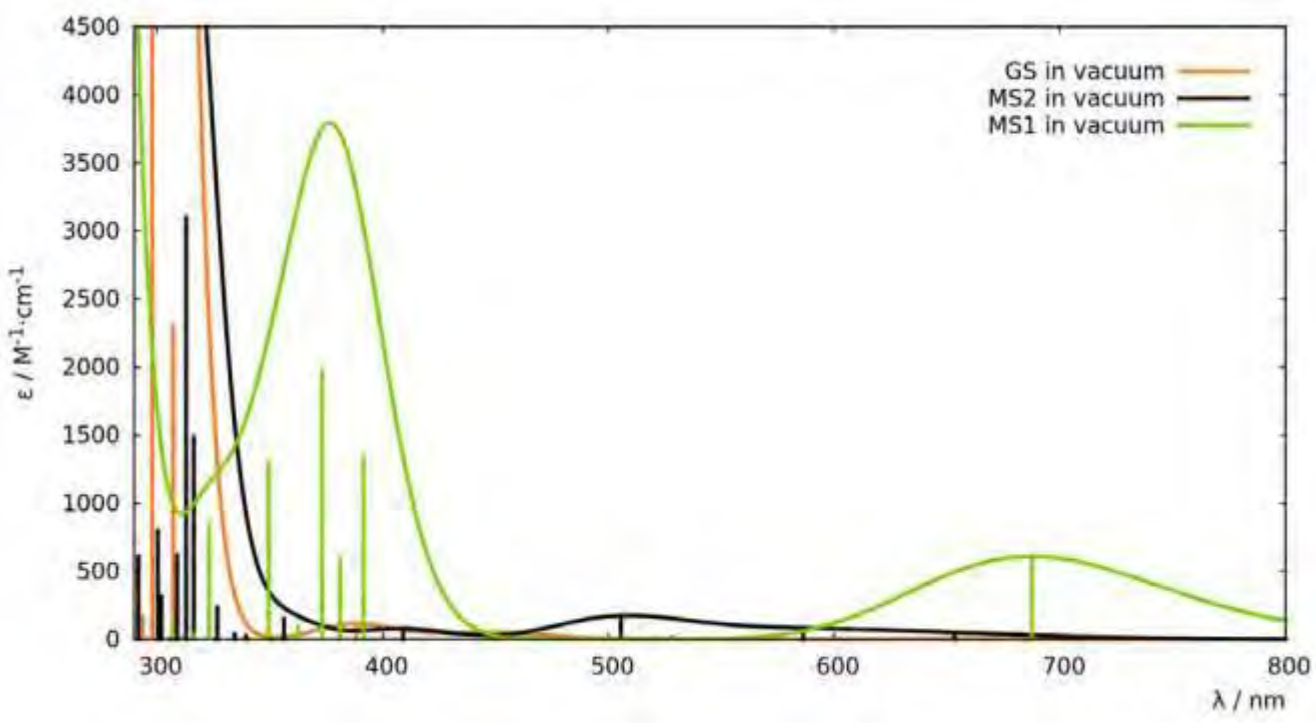

	State	Wavelength / nm	f_{osc}
GS	S_5	388	0.0014
MS2	S_4	505	0.0020
	S_6	409	0.0010
	S_7	356	0.0019
MS1	S_8	392	0.0172
	S_9	381	0.0076
	S_{10}	373	0.0253
	S_{11}	362	0.0013

AB.7 References

(1) Cormary, B. Photocommutation à l'état solide dans les complexes de ruthénium à ligand nitrosyle. Vers la réalisation de matériaux composites photochromes, Université Toulouse III - Paul Sabatier, 2009.

(2) Cormary, B.; Ladeira, S.; Jacob, K.; Lacroix, P. G.; Woike, T.; Schaniel, D.; Malfant, I. *Inorg. Chem.* **2012**, *51* (14), 7492–7501.

(3) Frisch M. J., et al. *Gaussian 09, revision D.01*; Gaussian, Inc.: Wallingford, CT, 2010.

(4) Lee, C.; Yang, W.; Parr, R. G. *Phys. Rev. B* **1988**, *37* (2), 785.

(5) Becke, A. D. *J. Chem. Phys.* **1993**, *98* (7), 5648.

(6) Grimme, S.; Antony, J.; Ehrlich, S.; Krieg, H. *J. Chem. Phys.* **2010**, *132* (15), 154104.

(7) Schäfer, A.; Horn, H.; Ahlrichs, R. *J. Chem. Phys.* **1992**, *97* (4), 2571.

(8) Andrae, D.; Haeussermann, U.; Dolg, M.; Stoll, H.; Preuss, H. *Theor. Chim. Acta* **1990**, *77* (2), 123–141.

(9) Martin, J. M. L.; Sundermann, A. *J. Chem. Phys.* **2001**, *114* (8), 3408.

(10) Neese, F. *WIREs: Comput. Mol. Sci.* **2012**, *2* (1), 73–78.

(11) Tao, J.; Perdew, J. P.; Staroverov, V. N.; Scuseria, G. E. *Phys. Rev. Lett.* **2003**, *91* (14), 146401.

(12) Becke, A. D. *Phys. Rev. A* **1988**, *38* (6), 3098–3100.

(13) Hirata, S.; Head-Gordon, M. *Chem. Phys. Lett.* **1999**, *314* (3–4), 291–299.

(14) Hirata, S.; Head-Gordon, M. *Chem. Phys. Lett.* **1999**, *302* (5–6), 375–382.

(15) Neese, F. *J. Comput. Chem.* **2003**, *24* (14), 1740–1747.

(16) Neese, F.; Wennmohs, F.; Hansen, A.; Becker, U. *Chem. Phys.* **2009**, *356* (1–3), 98–109.

(17) Sanz García, J.; Alary, F.; Boggio-Pasqua, M.; Dixon, I. M.; Malfant, I.; Heully, J.-L. *Inorg. Chem.* **2015**, *54* (17), 8310–8318.

Appendix C

Supporting Information for Chapter IV

Table of Contents

Computational Details AC3
Table AC1. Structure, energies and orbitals of the **GS** isomer of complex **1** AC4
Table AC2. Structure, energies and orbitals of the **MS2** isomer of complex **1** AC5
Table AC3. Structure, energies and orbitals of the **MS1** isomer of complex **1** AC6
Table AC4. Structure, energies and orbitals of the ^{3}**GS** triplet state of complex **1** AC7
Table AC5. Structure, energies and orbitals of the ^{3}**MS2** triplet state of complex **1** AC8
Table AC6. Structure, energies and orbitals of the ^{3}**MS1** triplet state of complex **1** AC9
Table AC7. Structure, energies and orbitals of the **GS** isomer of complex **2** AC10
Table AC8. Structure, energies and orbitals of the **MS2** isomer of complex **2** AC11
Table AC9. Structure, energies and orbitals of the **MS1** isomer of complex **2** AC12
Table AC10. Structure, energies and orbitals of the ^{3}**GS** triplet state of complex **2** AC13
Table AC11. Structure, energies and orbitals of the ^{3}**MS2** triplet state of complex **2** AC14
Table AC12. Structure, energies and orbitals of the ^{3}**MS1** triplet state of complex **2** AC15
Table AC13. Structure, energies and orbitals of the **GS** isomer of complex **3** AC16
Table AC14. Structure, energies and orbitals of the **MS2** isomer of complex **3** AC17
Table AC15. Structure, energies and orbitals of the **MS1** isomer of complex **3** AC18
Table AC16. Structure, energies and orbitals of the ^{3}**GS** triplet state of complex **3** AC19
Table AC17. Structure, energies and orbitals of the ^{3}**MS2** triplet state of complex **3** AC20
Table AC18. Structure, energies and orbitals of the ^{3}**MS1** triplet state of complex **3** AC21
Table AC19. Structure, energies and orbitals of the **GS** isomer of complex **4** AC22
Table AC20. Structure, energies and orbitals of the **MS2** isomer of complex **4** AC23
Table AC21. Structure, energies and orbitals of the **MS1** isomer of complex **4** AC24
Table AC22. Structure, energies and orbitals of the ^{3}**GS** triplet state of complex **4** AC25
Table AC23. Structure, energies and orbitals of the ^{3}**MS2** triplet state of complex **4** AC26
Table AC24. Structure, energies and orbitals of the ^{3}**MS1** triplet state of complex **4** AC27
Table AC25. Structure, energies and orbitals of the **GS** isomer of complex **5** AC28
Table AC26. Structure, energies and orbitals of the **MS2** isomer of complex **5** AC29
Table AC27. Structure, energies and orbitals of the **MS1** isomer of complex **5** AC30
Table AC28. Structure, energies and orbitals of the ^{3}**GS** triplet state of complex **5** AC31
Table AC29. Structure, energies and orbitals of the ^{3}**MS2** triplet state of complex **5** AC32
Table AC30. Structure, energies and orbitals of the ^{3}**MS1** triplet state of complex **5** AC33
Table AC31. TDDFT states of all the isomers of each complex in the singlet state AC34

Figure AC1. MEP between the **GS** and **MS2** isomers of complex **1**..... AC35
Figure AC2. MEP between the **MS2** and **MS1** isomers of complex **1**..... AC36
Figure AC3. MEP between the triplets ^{3}**GS** and ^{3}**MS2** of complex **1** AC37
Figure AC4. MEP between the triplets ^{3}**MS2** and ^{3}**MS1** of complex **1** AC38
Figure AC5. MEP between the **GS** and **MS2** isomers of complex **2**..... AC39
Figure AC6. MEP between the **MS2** and **MS1** isomers of complex **2**..... AC40
Figure AC7. MEP between the triplets ^{3}**GS** and ^{3}**MS2** of complex **2** AC41
Figure AC8. MEP between the triplets ^{3}**MS2** and ^{3}**MS1** of complex **2** AC42
Figure AC9. MEP between the **GS** and **MS2** isomers of complex **3**..... AC43
Figure AC10. MEP between the **MS2** and **MS1** isomers of complex **3**..... AC44
Figure AC11. MEP between the triplets ^{3}**GS** and ^{3}**MS2** of complex **3** AC45
Figure AC12. MEP between the triplets ^{3}**MS2** and ^{3}**MS1** of complex **3** AC46
Figure AC13. MEP between the **GS** and **MS2** isomers of complex **4**..... AC47
Figure AC14. MEP between the **MS2** and **MS1** isomers of complex **4**..... AC48
Figure AC15. MEP between the triplets ^{3}**GS** and ^{3}**MS2** of complex **4** AC49
Figure AC16. MEP between the triplets ^{3}**MS2** and ^{3}**MS1** of complex **4** AC50
Figure AC17. MEP between the **GS** and **MS2** isomers of complex **5**..... AC51
Figure AC18. MEP between the **MS2** and **MS1** isomers of complex **5**..... AC52
Figure AC19. MEP between the triplets ^{3}**GS** and ^{3}**MS2** of complex **5** AC53
Figure AC20. MEP between the triplets ^{3}**MS2** and ^{3}**MS1** of complex **5** AC54
Figure AC21. MEP for the dissociation of complex **1** AC55
Figure AC22. MEP for the dissociation of complex **2** AC56
Figure AC23. MEP for the dissociation of complex **3** AC57
Figure AC24. MEP for the dissociation of complex **4** AC58
Figure AC25. MEP for the dissociation of complex **5** AC59
References AC60

Computational Details

Geometry optimizations of all the stationary points found on the closed shell singlet (hereafter called singlet for simplicity) and the lowest triplet PESs were carried out using the Polarizable Continuum Model[1] (PCM) with acetonitrile, with the Gaussian 09 quantum chemistry package.[2] DFT was used in order to perform these calculations using the standard hybrid functional B3LYP,[3,4] including Grimme's dispersion correction (D3BJ),[5] with a triple-ζ Ahlrichs basis set, namely def2-TZVP(-*f*),[6] with a *p* polarization function for the H atoms, two *d* polarization functions for the second and third row elements, and for the ruthenium the triple-ζ basis set def2-TZVPP[6] with two *f* and one *g* polarization functions and its associated relativistic effective core potential[7] (including 28 core electrons) (this basis set hereafter called **BS1**). After the geometry optimizations, vibration frequency analyses were performed at the same level of theory to verify the nature of the stationary points.

Zero Temperature String (ZTS)[8,9] calculations, based on the chain-of-states method, connect the minima on a PES, minimizing the energy paths and thus, characterizing the adiabatic activation barriers. These methods are a powerful alternative to the classical transition state (TS) optimizations and intrinsic reaction coordinate (IRC) calculations. ZTS calculations were performed in vacuum with the same previously used hybrid functional and a quite similar triple-ζ basis set,[10] but using a more modest contraction scheme, including only one *d* polarization function for the second and third row elements and only one *f* function for the ruthenium atom def2-TZVP[6] (this basis set hereafter called **BS2**). The ZTS calculations were carried out with the NWCHEM 6 quantum package.[11] For these calculations, B3LYP functional has been used including Grimme's dispersion correction D3.[12]

The optimization of the minimum energy crossing points (MECPs) between singlet and triplet minima was performed with the ORCA 3.0.3 quantum package[13] with B3LYP, including D3-BJ, in vacuum with the basis set **BS1**. The UV-Vis absorption spectra of the singlet species **GS**, **MS1** and **MS2** in acetonitrile were computed for all the complexes using the COSMO[14] solvation model with ORCA, applying TD-DFT using the TPSSh[15] and BHandHLYP[3,16] functional within the Tamm-Dancoff approximation,[17,18] and the same basis sets **BS1**. In these TD-DFT calculations the resolution-of-identity (RI) approximation for hybrid functionals[19] (as implemented in ORCA) was employed to calculate the Coulomb energy term using the Ahlrichs/Weigand Def2-TZV basis as the auxiliary basis set and the exchange term by the so-called 'chain-of-spheres exchange' (COSX) algorithm.[20] In order to analyse the nature of the electronic transitions in the TD-DFT spectra, the Natural Transition Orbitals[21] (NTOs) were computed.

In addition, to calculate the dissociation energies, reported as D_e in Chapter IV §4.5, the Ru-X (X=N, O, NO) bond was elongated up to *ca.* 9 Å with 36 initially equally separated points. The starting point is the optimized triplet state of interest, which at the dissociation limit gives two doublets as dissociation products, *i.e* $[Ru^{(III)}Cl_2(terpy)]^+$ and neutral $NO^{\bullet}$.

Table AC1. Optimized Cartesian coordinates, energies, molecular parameters and electronic structure of the **GS** isomer of complex **1**, *trans*-$[RuCl(NO)(py)_4]^{2+}$, at the B3LYP-D3BJ/**BS1** level of theory in its ground state (singlet) in acetonitrile.

Ru	0.000000001793	-0.000000001156	0.107396088010
Cl	0.000000005918	-0.000000006120	-2.228110647217
N	-0.008476447398	2.122229249996	0.025838349412
N	2.122229252792	0.008476447838	0.025838354624
N	0.008476447182	-2.122229252342	0.025838359331
N	-2.122229249539	-0.008476446724	0.025838354086
N	0.000000004738	0.000000003152	1.855366060667
O	-0.000000003115	0.000000003688	2.987638446175
C	-0.833375247611	2.832183871421	0.818340938887
H	-1.489958533112	2.280092121736	1.472213509305
C	-0.859565718707	4.212133491239	0.799462434889
H	-1.539922345470	4.735541904816	1.454591965105
C	-0.010689704708	4.892093285869	-0.062354284536
H	-0.011680763149	5.972493290089	-0.097033035767
C	0.837638218788	4.158822911481	-0.878479659254
H	1.515317224386	4.640206637520	-1.567827049519
C	0.814054527566	2.779182801866	-0.810963617361
H	1.449221274442	2.178420273205	-1.440118389813
C	2.832183873045	0.833375232738	0.818340960983
H	2.280092122320	1.489958506109	1.472213542700
C	4.212133492943	0.859565702627	0.799462460930
H	4.735541905633	1.539922316699	1.454592005036
C	4.892093288793	0.010689703543	-0.062354272254
H	5.972493293101	0.011680761431	-0.097033020770
C	4.158822915539	-0.837638204582	-0.878479663994
H	4.640206642558	-1.515317198295	-1.567827065259
C	2.779182805794	-0.814054513195	-0.810963624926
H	2.178420277931	-1.449221248136	-1.440118410239
C	-0.814054531374	-2.779182806823	-0.810963601822
H	-1.449221278733	-2.178420280086	-1.440118375645
C	-0.837638225489	-4.158822916751	-0.878479636518
H	-1.515317233708	-4.640206645034	-1.567827022638
C	0.010689698492	-4.892093288586	-0.062354259990
H	0.011680754732	-5.972493292989	-0.097033005641
C	0.859565715536	-4.212133491199	0.799462454276
H	1.539922342447	-4.735541902747	1.454591985963
C	0.833375247213	-2.832183871231	0.818340951192
H	1.489958534688	-2.280092119309	1.472213517799
C	-2.779182802852	0.814054545774	-0.810963594309
H	-2.178420275289	1.449221305045	-1.440118355266
C	-4.158822912647	0.837638239761	-0.878479631852
H	-4.640206639922	1.515317259870	-1.567827006988
C	-4.892093285653	-0.010689699558	-0.062354272346
H	-5.972493289968	-0.011680756317	-0.097033020725
C	-4.212133489523	-0.859565731530	0.799462428178
H	-4.735541901986	-1.539922371113	1.454591945971
C	-2.832183869634	-0.833375262038	0.818340929060
H	-2.280092118782	-1.489958561652	1.472213484385

Energies (a.u.)	
E	-1678.637915
Zero-point correction	0.378499
Sum of electronic and thermal enthalpies	-1678.233149
Sum of electronic and thermal free energies	-1678.315703
Selected molecular parameters	
$Ru\text{-}N_{(NO)}$	1.748 Å
$Ru\text{-}O_{(NO)}$	2.880 Å
N-O	1.132 Å
Ru-Cl	2.336 Å
$Ru\text{-}N_{py1}$	2.124 Å
$Ru\text{-}N_{py2}$	2.124 Å
$Ru\text{-}N_{py3}$	2.124 Å
$Ru\text{-}N_{py4}$	2.124 Å
∠Ru-N-O	180.000 °
∠Ru-O-N	0.000 °
NO stretching vibration	
ν_{NO} (cm^{-1})	1943.99 cm^{-1}

Electronic structure

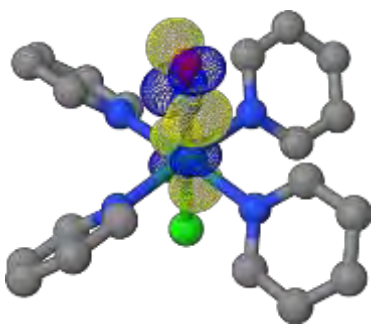
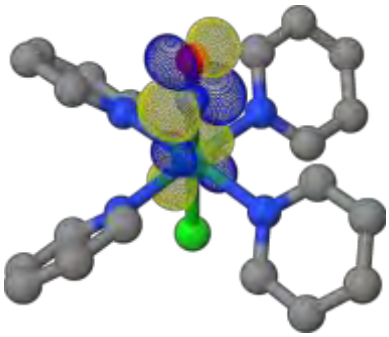

LUMOs (degenerate)

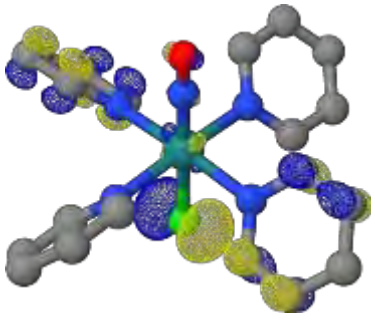
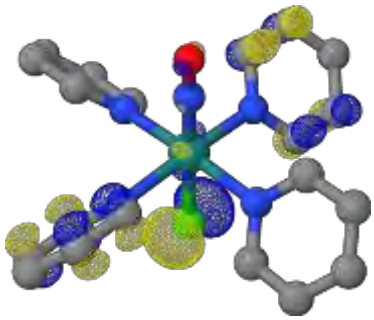

HOMOs (degenerate)

Table AC2. Optimized Cartesian coordinates, energies, molecular parameters and electronic structure of the **MS2** isomer of complex **1**, *trans*-$[RuCl(NO)(py)_4]^{2+}$, at the B3LYP-D3BJ/**BS1** level of theory in its ground state (singlet) in acetonitrile.

Ru	-0.168418617606	-0.000592780544	0.017613803798
Cl	2.130477835775	-0.101823884161	0.151746768124
N	0.076060654959	1.331445285273	-1.606262032460
N	-0.161008888184	1.676827149053	1.304296459945
N	-0.014156333679	-1.372408724314	1.681354441018
N	-0.134053150793	-1.633406072040	-1.339423570925
N	-2.001919062379	-0.423530815819	0.483627729107
O	-2.267221633648	0.342499017159	-0.358047205534
C	-0.658260954049	1.170798305714	-2.723726103931
H	-1.341575267437	0.337013147218	-2.749276545775
C	-0.548106823984	2.028668211079	-3.798645839569
H	-1.159601844622	1.859016739284	-4.672337319799
C	0.348394173904	3.085848401200	-3.730022834421
H	0.455910860152	3.770527604623	-4.559620845394
C	1.105311027897	3.246425476273	-2.578721684964
H	1.816956091849	4.052219313623	-2.476843077775
C	0.947147114150	2.354490610096	-1.536834702712
H	1.526490391404	2.441652371402	-0.633048939749
C	-0.980171813310	2.714513115428	1.051872111916
H	-1.607691061260	2.646584652825	0.176697050763
C	-1.020764460032	3.832148467194	1.861508262260
H	-1.696359459915	4.638103366654	1.616639463925
C	-0.183801348742	3.894314718514	2.966425798493
H	-0.191491989963	4.759653404400	3.614238121037
C	0.667045784151	2.828330041408	3.220474692655
H	1.339800925346	2.831467104500	4.065276361567
C	0.655076205905	1.738401802714	2.372582363567
H	1.310631349261	0.898524606139	2.532714419994
C	0.729126941072	-2.487300567734	1.579084062484
H	1.246538296194	-2.647971219819	0.648726123774
C	0.842938772311	-3.386682587965	2.621043043254
H	1.449660852025	-4.270225472154	2.488437043402
C	0.179013709679	-3.132741695961	3.812344224066
H	0.256268599034	-3.819255145413	4.643826735041
C	-0.587000701893	-1.981082613728	3.915145427769
H	-1.124243548608	-1.735158872636	4.819039724582
C	-0.665215142609	-1.128659319789	2.831452939163
H	-1.259819718554	-0.230086997142	2.883005253071
C	0.768008844123	-1.665428907493	-2.338820553984
H	1.458486249402	-0.840501061999	-2.398767707767
C	0.824831689815	-2.707692054374	-3.243520319653
H	1.567482294085	-2.683447239456	-4.027316945679
C	-0.069704774863	-3.760716062217	-3.123497446415
H	-0.045146000325	-4.588228388093	-3.818616028228
C	-0.994580048384	-3.732690882446	-2.089617665016
H	-1.709873716956	-4.528960087274	-1.946485766392
C	-0.996778090826	-2.661142827222	-1.219956837101
H	-1.697347220087	-2.624693622348	-0.399229453282

Energies (a.u.)	
E	-1678.579288
Zero-point correction	0.376524
Sum of electronic and thermal enthalpies	-1678.176286
Sum of electronic and thermal free energies	-1678.258768

Selected molecular parameters	
$Ru\text{-}N_{(NO)}$	1.938 Å
$Ru\text{-}O_{(NO)}$	2.160 Å
N-O	1.169 Å
Ru-Cl	2.305 Å
$Ru\text{-}N_{py1}$	2.114 Å
$Ru\text{-}N_{py2}$	2.114 Å
$Ru\text{-}N_{py3}$	2.162 Å
$Ru\text{-}N_{py4}$	2.123 Å
∠Ru-N-O	84.178 °
∠Ru-O-N	63.252 °

NO stretching vibration	
ν_{NO} (cm^{-1})	1664.66 cm^{-1}

Electronic structure

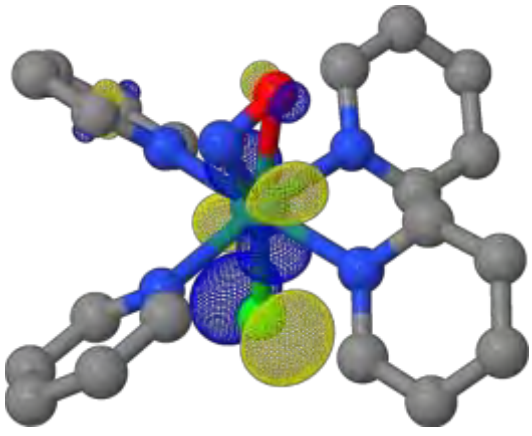

HOMO

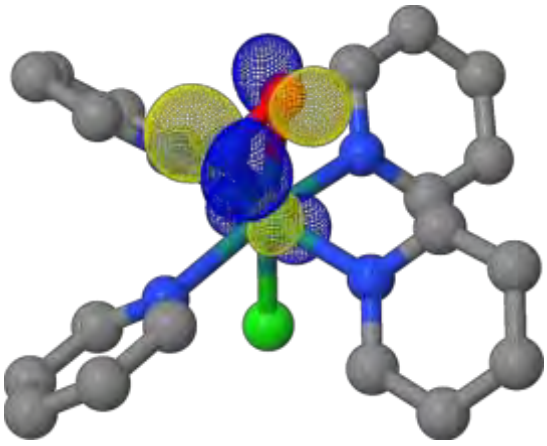

LUMO

Table AC3. Optimized Cartesian coordinates, energies, molecular parameters and electronic structure of the **MS1** isomer of complex **1**, *trans*-$[RuCl(NO)(py)_4]^{2+}$, at the B3LYP-D3BJ/**BS1** level of theory in its ground state (singlet) in acetonitrile.

Ru	0.000000004634	-0.000000001199	0.054767971433
Cl	-0.000000002707	-0.000000011589	-2.239065105717
N	-0.006796710234	2.116408402415	0.012832345083
N	2.116408408051	0.006796715299	0.012832326729
N	0.006796707944	-2.116408404273	0.012832355493
N	-2.116408397098	-0.006796716079	0.012832335550
O	0.000000001626	-0.000000000108	1.916403296284
N	0.000000018215	0.000000011923	3.042404297797
C	-0.827523930987	2.812841776380	0.820940643595
H	-1.483810852135	2.248560922726	1.464776826405
C	-0.852346262465	4.193356054889	0.832958039286
H	-1.529745318274	4.703615512641	1.501470979342
C	-0.007905279684	4.890018325261	-0.019500545957
H	-0.008642899983	5.970921665066	-0.033028998431
C	0.835404795675	4.172285106714	-0.855051152862
H	1.509491539750	4.667696439373	-1.538055492633
C	0.811712700032	2.791678826450	-0.814164133796
H	1.445858343959	2.202623835249	-1.455832199457
C	2.812841793080	0.827523885818	0.820940665663
H	2.248560950670	1.483810764429	1.464776901058
C	4.193356072713	0.852346216884	0.832958041891
H	4.703615540018	1.529745226423	1.501471021585
C	4.890018331051	0.007905294636	-0.019500613871
H	5.970921670574	0.008642920081	-0.033029086849
C	4.172285099866	-0.835404720941	-0.855051271151
H	4.667696422536	-1.509491411463	-1.538055671158
C	2.791678820105	-0.811712631329	-0.814164226153
H	2.202623818690	-1.445858225647	-1.455832332510
C	-0.811712670963	-2.791678825823	-0.814164156473
H	-1.445858282116	-2.202623832532	-1.455832252768
C	-0.835404774055	-4.172285106047	-0.855051171938
H	-1.509491491003	-4.667696436662	-1.538055539960
C	0.007905259406	-4.890018327155	-0.019500524937
H	0.008642872838	-5.970921667017	-0.033028973226
C	0.852346208615	-4.193356059339	0.832958095675
H	1.529745230218	-4.703615519229	1.501471068764
C	0.827523887213	-2.812841780690	0.820940693860
H	1.483810781164	-2.248560929244	1.464776906094
C	-2.791678813445	0.811712660847	-0.814164183698
H	-2.202623815477	1.445858278618	-1.455832270014
C	-4.172285093483	0.835404752147	-0.855051219447
H	-4.667696420116	1.509491467078	-1.538055592498
C	-4.890018319921	-0.007905292670	-0.019500587490
H	-5.970921659529	-0.008642917220	-0.033029053939
C	-4.193356056865	-0.852346243983	0.832958035644
H	-4.703615520444	-1.529745275914	1.501470995490
C	-2.812841777304	-0.827523912706	0.820940651998
H	-2.248560930356	-1.483810812494	1.464776862213

Energies (a.u.)	
E	-1678.569316
Zero-point correction	0.376942
Sum of electronic and thermal enthalpies	-1678.165592
Sum of electronic and thermal free energies	-1678.250381

Selected molecular parameters	
$Ru\text{-}O_{(NO)}$	1.862 Å
$Ru\text{-}N_{(NO)}$	2.988 Å
N-O	1.126 Å
Ru-Cl	2.294 Å
$Ru\text{-}N_{py1}$	2.117 Å
$Ru\text{-}N_{py2}$	2.117 Å
$Ru\text{-}N_{py3}$	2.117 Å
$Ru\text{-}N_{py4}$	2.117 Å
∠Ru-N-O	0.000 °
∠Ru-O-N	180.000 °

NO stretching vibration	
ν_{NO} (cm^{-1})	1911.56 cm^{-1}

Electronic structure

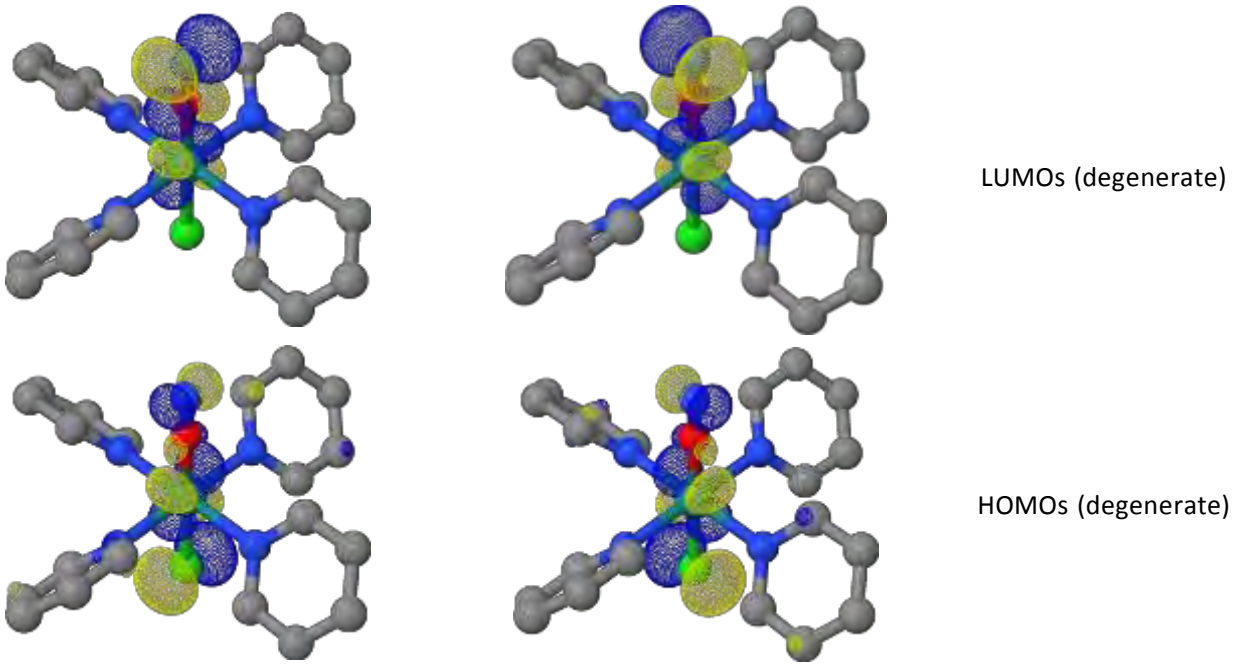

LUMOs (degenerate)

HOMOs (degenerate)

Table AC4. Optimized Cartesian coordinates, energies, molecular parameters and electronic structure of the ^{3}**GS** triplet state of complex **1**, *trans*-[RuCl(NO)(py)$_4$]$^{2+}$, at the B3LYP-D3BJ/**BS1** level of theory in acetonitrile.

Ru	0.024738062939	0.015020935029	0.015233498760
Cl	2.329109222272	0.048080135181	0.042571088768
N	0.042962083909	1.325525960473	-1.665580925027
N	0.044289894366	1.652749840048	1.361506544721
N	-0.078909752982	-1.299201539869	1.642201591947
N	0.054582655550	-1.623969423552	-1.327979058767
N	-1.938951253961	0.189887136980	-0.077070244641
O	-2.819390243358	-0.526707310301	0.102436177268
C	-0.773805674817	1.113205607505	-2.713650257419
H	-1.409897879380	0.243226440716	-2.675787711876
C	-0.805672403171	1.960099821686	-3.803500058595
H	-1.479969270239	1.745142205469	-4.619100810883
C	0.030586132833	3.067177127404	-3.823234833425
H	0.025584380110	3.746087237955	-4.664397279048
C	0.872260477320	3.285289625070	-2.742642087360
H	1.543116626164	4.131013388700	-2.710141094000
C	0.853920196458	2.399198802528	-1.682879996141
H	1.500352415544	2.535386799611	-0.831495319775
C	-0.758375352076	2.713439179065	1.153265515998
H	-1.394661896089	2.683068180511	0.282582939707
C	-0.775997561968	3.798328641696	2.006892058681
H	-1.438472765995	4.624845335488	1.796968367589
C	0.060191826149	3.798953807699	3.114231487818
H	0.067043622767	4.636125690306	3.798092292672
C	0.887792376461	2.705403359942	3.326801623856
H	1.556942912899	2.659626127911	4.173239085860
C	0.857017253350	1.652888436502	2.433487813297
H	1.494350442501	0.793179456861	2.559899514630
C	0.716988166237	-2.387423785848	1.683180609784
H	1.396877823036	-2.522491034962	0.857936171908
C	0.679957372789	-3.279244277429	2.734610003307
H	1.339091915332	-4.134498825018	2.725073259656
C	-0.202843776256	-3.054889483254	3.782444632507
H	-0.251303121928	-3.740232837896	4.616970139234
C	-1.019831548017	-1.933386574009	3.742088806969
H	-1.719710806778	-1.714606947488	4.534584792966
C	-0.930957005588	-1.077546031365	2.664048764904
H	-1.545252383574	-0.192813012968	2.610515964877
C	0.902616394206	-1.630900610980	-2.372768519364
H	1.560141719885	-0.783065443733	-2.471120194931
C	0.943250170633	-2.676622762679	-3.274089066302
H	1.643523097613	-2.636657624913	-4.095318227657
C	0.085394515436	-3.753560860374	-3.103827813901
H	0.097647842824	-4.583379726836	-3.796469732057
C	-0.787720865984	-3.745813093677	-2.025792456367
H	-1.474217451356	-4.559722287883	-1.846055282878
C	-0.775096295235	-2.670814115423	-1.159447540064
H	-1.439896290831	-2.644825669876	-0.310465237208

Energies (a.u.)	
E	-1678.583200
Zero-point correction	0.375528
Sum of electronic and thermal enthalpies	-1678.180360
Sum of electronic and thermal free energies	-1678.266500
Selected molecular parameters	
Ru-N$_{(NO)}$	1.974 Å
Ru-O$_{(NO)}$	2.897 Å
N-O	1.149 Å
Ru-Cl	2.305 Å
Ru-N$_{py1}$	2.131 Å
Ru-N$_{py2}$	2.120 Å
Ru-N$_{py3}$	2.094 Å
Ru-N$_{py4}$	2.119 Å
∠Ru-N-O	134.400 °
∠Ru-O-N	29.132 °
NO stretching vibration	
ν_{NO} (cm^{-1})	1821.95 cm^{-1}

Electronic structure

<S^2>: 2.0103

Mulliken Spin Populations: Ru: 0.9601 Cl: 0.2068 N$_{(NO)}$: 0.4506 O$_{(NO)}$: 0.3749

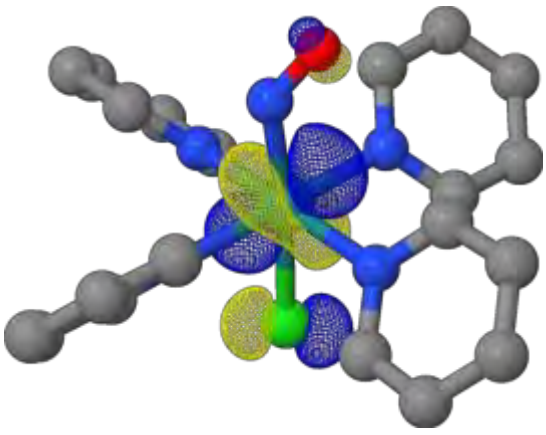

SONO (Hole)

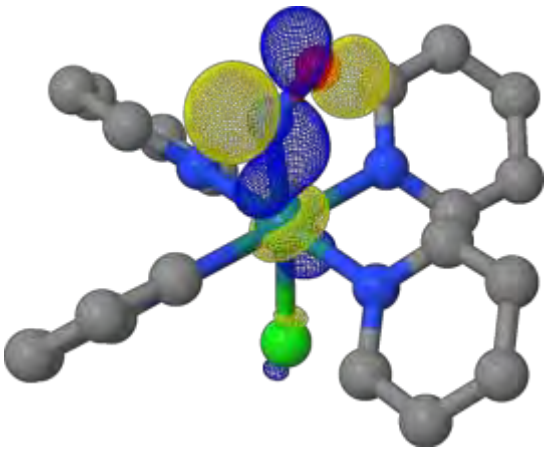

SONO (Particle)

Table AC5. Optimized Cartesian coordinates, energies, molecular parameters and electronic structure of the ^{3}**MS2** triplet state of complex **1**, *trans*-$[RuCl(NO)(py)_4]^{2+}$, at the B3LYP-D3BJ/**BS1** level of theory in acetonitrile.

Ru	-0.075783053696	-0.000733896069	0.002634509723
Cl	2.166017429070	-0.058336638882	0.107154607473
N	0.130532123522	1.350794708068	-1.629619084167
N	-0.148833356911	1.661350761555	1.304711781826
N	0.021098307425	-1.371504174545	1.662295268788
N	-0.115498227072	-1.638004627302	-1.325827481771
N	-2.131468232304	-0.366198867104	0.492676549685
O	-2.083473955026	0.356968024763	-0.482613784680
C	-0.591362282901	1.183530285727	-2.752828290550
H	-1.270230801293	0.347067018118	-2.781429112151
C	-0.481807265167	2.042764214783	-3.827653253096
H	-1.081441127598	1.863406669739	-4.707649328221
C	0.393631191872	3.116156123114	-3.748937360136
H	0.496990103834	3.804589096210	-4.575934020024
C	1.131587113491	3.290069942837	-2.587583600028
H	1.824170042426	4.110785708476	-2.474006507420
C	0.978762566603	2.391500679042	-1.550077013290
H	1.544236505606	2.495659401608	-0.639388485439
C	-0.978994563183	2.688541520163	1.041221326074
H	-1.587591105288	2.613441627364	0.154753226360
C	-1.059892761784	3.791656460325	1.867077508534
H	-1.743441619749	4.588786295059	1.615709200855
C	-0.257958867963	3.850779842309	2.997449101977
H	-0.299921333646	4.705320033026	3.658032372894
C	0.602013736383	2.794157914267	3.262741289705
H	1.250260034449	2.795312780024	4.126331818301
C	0.631800645196	1.716976303357	2.401361462399
H	1.294795260234	0.885045870348	2.572706386071
C	0.801800326318	-2.463522945990	1.585242219954
H	1.347144232012	-2.615972793079	0.669363813088
C	0.915759622458	-3.358409485669	2.631248572727
H	1.553305179475	-4.222414783361	2.515906589459
C	0.212936319712	-3.123519438759	3.803342635171
H	0.288561320347	-3.805926565146	4.638313815672
C	-0.592029109685	-1.996514571262	3.880744602289
H	-1.163696125979	-1.767861089426	4.767942990893
C	-0.669844570582	-1.148222090090	2.794071674258
H	-1.301775652667	-0.276079742414	2.819900020043
C	0.726971044160	-1.686075095514	-2.377292186323
H	1.419331078363	-0.867557108657	-2.487493371763
C	0.721094494216	-2.739862856261	-3.266968590085
H	1.418565649990	-2.737331235453	-4.091341531163
C	-0.180421916206	-3.779266723213	-3.080887504641
H	-0.205282797464	-4.615110622767	-3.765883884525
C	-1.045662990850	-3.728248706198	-1.997771891017
H	-1.762630336764	-4.513051553654	-1.808356481149
C	-0.984983901957	-2.650016630904	-1.138314358131
H	-1.639986380073	-2.579874049027	-0.284541217186

Energies (a.u.)	
E	-1678.551171
Zero-point correction	0.375821
Sum of electronic and thermal enthalpies	-1678.148590
Sum of electronic and thermal free energies	-1678.232904
Selected molecular parameters	
Ru-$N_{(NO)}$	2.145 Å
Ru-$O_{(NO)}$	2.096 Å
N-O	1.215 Å
Ru-Cl	2.245 Å
Ru-N_{py1}	2.129 Å
Ru-N_{py2}	2.113 Å
Ru-N_{py3}	2.155 Å
Ru-N_{py4}	2.109 Å
∠Ru-N-O	71.175 °
∠Ru-O-N	75.551 °
NO stretching vibration	
ν_{NO} (cm^{-1})	1519.89 cm^{-1}

Electronic structure

$\langle S^2 \rangle$: 2.0076

Mulliken Spin Populations: Ru: 0.8132 Cl: 0.1649 $N_{(NO)}$: 0.7359 $O_{(NO)}$: 0.2790

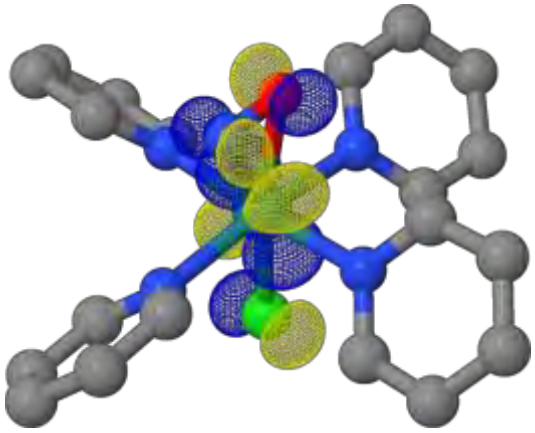

SONO (Hole)

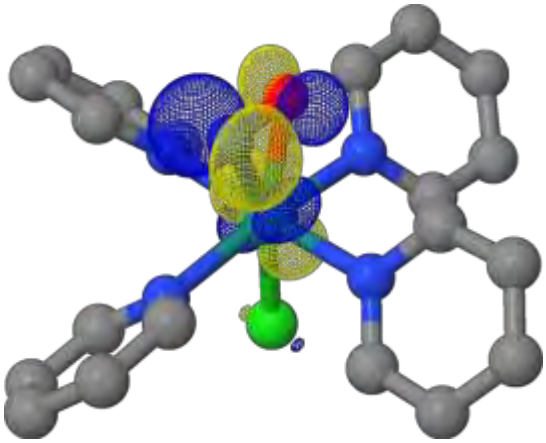

SONO (Particle)

Table AC6. Optimized Cartesian coordinates, energies, molecular parameters and electronic structure of the ^{3}**MS1** triplet state of complex **1**, *trans*-$[RuCl(NO)(py)_4]^{2+}$, at the B3LYP-D3BJ/**BS1** level of theory in acetonitrile.

Ru	0.129099252992	0.006751338696	-0.003780133347
Cl	2.388249709822	-0.021475917458	0.034098209227
N	0.083679449957	1.319772215152	-1.649246744182
N	0.111420566123	1.639479820634	1.338738210915
N	-0.021272924910	-1.286322721119	1.643543170492
N	0.122225854113	-1.622680303411	-1.346014823715
N	-2.872502671009	-0.585779645735	0.191994094470
O	-2.031104458328	0.141557669945	-0.112142512391
C	-0.735068439518	1.092261086754	-2.693859336668
H	-1.342391761992	0.201946911985	-2.659241859449
C	-0.802860829675	1.949511088925	-3.773743684459
H	-1.478708505740	1.724635978367	-4.585300795476
C	0.005341779790	3.077257694594	-3.791648023350
H	-0.024876613629	3.762420468569	-4.627223508820
C	0.854210448037	3.308342901661	-2.718128388390
H	1.504566669459	4.169932370079	-2.687762811987
C	0.866789160554	2.416215444630	-1.665102875852
H	1.515898682627	2.561341956021	-0.816915272114
C	-0.747676238567	2.660145346844	1.158300367413
H	-1.395254739142	2.611303723027	0.296288253625
C	-0.809817501583	3.732865005464	2.025749635617
H	-1.518814801324	4.525185646199	1.836787487503
C	0.044422742702	3.766145805018	3.118735099116
H	0.018279982071	4.594512047845	3.812806181339
C	0.932344799543	2.716174258633	3.302792114446
H	1.617440459655	2.696376918687	4.137499882681
C	0.940028258729	1.672055391512	2.398099152597
H	1.619031508315	0.842143504236	2.507292501810
C	0.717832887518	-2.412462863306	1.695271120536
H	1.388036907896	-2.591640522782	0.870293877785
C	0.637326446470	-3.291500738350	2.755977254697
H	1.254801247866	-4.177398393907	2.754622588292
C	-0.235645851874	-3.016495585025	3.799618494287
H	-0.319250143859	-3.691813761154	4.639495785659
C	-0.995590336615	-1.856697109463	3.747414994046
H	-1.684960176478	-1.595667239813	4.536416197534
C	-0.858378324102	-1.013264772463	2.663438442962
H	-1.419883591811	-0.094388262274	2.606808161009
C	0.951753285908	-1.640349839262	-2.405753273636
H	1.623406311223	-0.803835524988	-2.508825118995
C	0.954418664699	-2.678307226284	-3.317036914128
H	1.640322530603	-2.646733168615	-4.150716941696
C	0.075819845175	-3.737948979870	-3.141365362334
H	0.057635618654	-4.561307727074	-3.841595741728
C	-0.777275020502	-3.721809621603	-2.047496816406
H	-1.477187265133	-4.523002968880	-1.862335866866
C	-0.722940518839	-2.655446461578	-1.171521383865
H	-1.365571355868	-2.626962239070	-0.304788088204

Energies (a.u.)	
E	-1678.558360
Zero-point correction	0.375107
Sum of electronic and thermal enthalpies	-1678.155766
Sum of electronic and thermal free energies	-1678.242159
Selected molecular parameters	
Ru-$N_{(NO)}$	3.066 Å
Ru-$O_{(NO)}$	2.167 Å
N-O	1.153 Å
Ru-Cl	2.260 Å
Ru-N_{py1}	2.106 Å
Ru-N_{py2}	2.114 Å
Ru-N_{py3}	2.100 Å
Ru-N_{py4}	2.111 Å
∠Ru-N-O	31.437 °
∠Ru-O-N	132.452 °

NO stretching vibration	
ν_{NO} (cm^{-1})	1801.73 cm^{-1}

Electronic structure

$\langle S^2 \rangle$: 2.0090

Mulliken Spin Populations: Ru: 0.9213 Cl: 0.1634 $N_{(NO)}$: 0.7712 $O_{(NO)}$: 0.1500

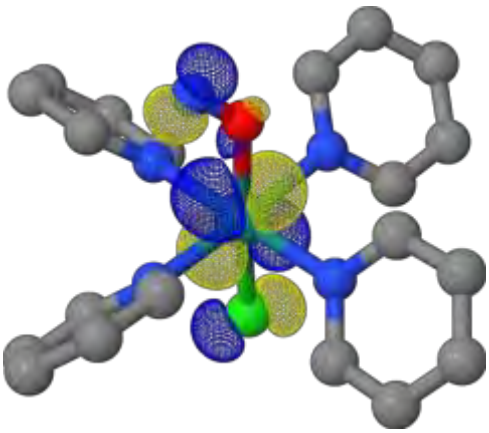

SONO (Hole)

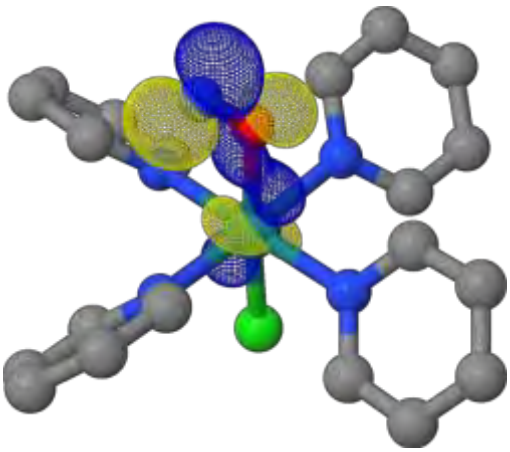

SONO (Particle)

Table AC7. Optimized Cartesian coordinates, energies, molecular parameters and electronic structure of the **GS** isomer of complex **2**, *cis*(Cl,Cl)-[$RuCl_2(NO)(FT)]^+$, at the B3LYP-D3BJ/**BS1** level of theory in its ground state (singlet) in acetonitrile.

Ru	3.289942384039	0.085630201459	0.111543100703
Cl	3.141472351823	-0.072378346927	-2.243272842596
Cl	5.700517943160	0.235586543666	-0.110694140777
N	1.305284688999	-0.050423487446	0.076654403250
N	2.773835903786	2.105780833591	-0.117301798172
N	3.050329396030	-1.997415807589	0.139435315110
N	3.481647715883	0.204818663500	1.837604881973
O	3.676898560155	0.285806090410	2.952106031814
C	0.596814236801	1.082504526703	-0.043165530919
C	1.424839767035	2.299627064974	-0.145042364225
C	-2.882301616227	-0.339976588054	-0.110562277031
C	-7.110171976333	-0.392425289926	-0.167252868894
C	3.140625074778	4.435158904213	-0.376888719651
H	3.845117737977	5.248454830659	-0.466965624481
C	0.755324360745	-1.274013195590	0.094778513445
C	-0.621137835768	-1.392557378264	0.040900627654
H	-1.082354392454	-2.365986012246	0.085158078328
C	3.729064501585	-4.270183240506	0.176412254702
H	4.537024582884	-4.986411680060	0.186193668664
C	1.739750684290	-2.372439225982	0.145420948950
C	-1.418024569771	-0.241047193280	-0.051327470541
C	0.905884564842	3.575290976021	-0.286916187171
H	-0.162249986866	3.727568092364	-0.310498966560
C	-0.782128850384	1.009043610368	-0.103556837105
H	-1.365738353885	1.907104000964	-0.225817578914
C	3.607936492243	3.138110044015	-0.231493574208
H	4.661265583590	2.899775712756	-0.206849369995
C	4.016631230259	-2.914272789698	0.151858685530
H	5.028140398467	-2.535249494631	0.138974766647
C	1.398399281187	-3.713956059514	0.170129954177
H	0.360870167993	-4.010481620209	0.172821083052
C	2.403414001265	-4.672315098914	0.187589641708
H	2.147351214203	-5.722130591194	0.206911647773
C	1.772874345326	4.654060880190	-0.402909631235
H	1.377639674509	5.653694584023	-0.514682874050
C	-7.397039292694	0.814887281962	0.494490485381
C	-9.736630292091	0.380895393325	0.241494984295
H	-10.767132223627	0.673306416381	0.395792789521
C	-8.136373236448	-1.214206895425	-0.624872947769
H	-7.919049007798	-2.143983461437	-1.134796911034
C	-9.451793016534	-0.817229652663	-0.414946875508
H	-10.263733734627	-1.442012376985	-0.763455520519
C	-8.709815527647	1.204452123429	0.700169142546
H	-8.939789813471	2.132454052982	1.208567281260
C	-3.683845530306	0.678728788134	0.429561918611
H	-3.229558182740	1.529301189240	0.920482599040
C	-4.873791141083	-1.557260368045	-0.787872612138
H	-5.324128319068	-2.414775459134	-1.269868382327
C	-5.056567214966	0.569581348646	0.367154306174
C	-3.494343254393	-1.450630845268	-0.711910694284
H	-2.883220504948	-2.224212232019	-1.155825994899
C	-5.659355252021	-0.545729062986	-0.243371668158
C	-6.115921363567	1.511238440789	0.885201189892
H	-6.034483116276	2.503391813850	0.433323392872
H	-6.040103237859	1.651264045377	1.966865570092

Energies (a.u.)	
E	-2388.701758
Zero-point correction	0.411128
Sum of electronic and thermal enthalpies	-2388.260514
Sum of electronic and thermal free energies	-2388.353665

Selected molecular parameters	
Ru-$N_{(NO)}$	1.741 Å
Ru-$O_{(NO)}$	2.874 Å
N-O	1.134 Å
Ru-$Cl_{1(trans\text{-}NO)}$	2.365 Å
Ru-$Cl_{2(cis\text{-}NO)}$	2.425 Å
Ru-N_{tpy1}	1.990 Å
Ru-N_{tpy2}	2.098 Å
Ru-N_{tpy3}	2.097 Å
∠Ru-N-O	176.406 °
∠Ru-O-N	2.176 °

NO stretching vibration	
ν_{NO} (cm^{-1})	1929.60 cm^{-1}

Electronic structure

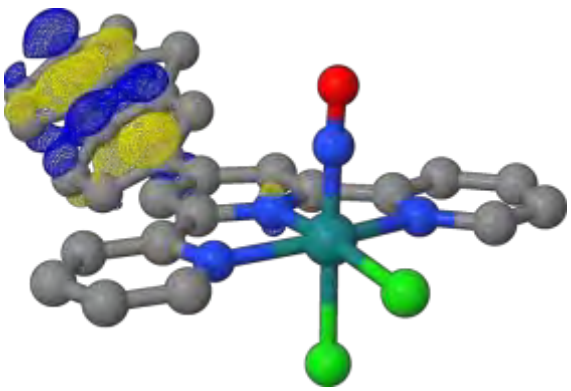

HOMO

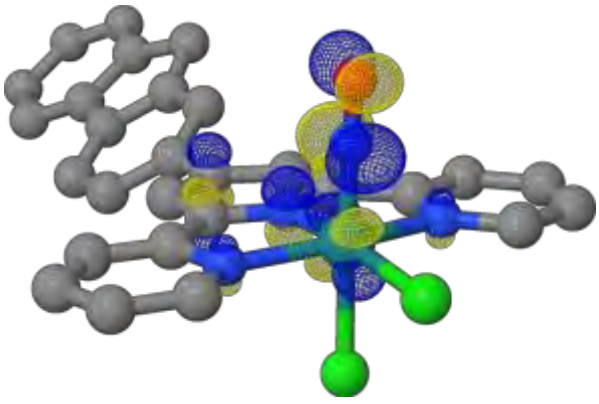

LUMO

Table AC8. Optimized Cartesian coordinates, energies, molecular parameters and electronic structure of the **MS2** isomer of complex **2**, *cis*(Cl,Cl)-[$RuCl_2(NO)(FT)]^+$, at the B3LYP-D3BJ/**BS1** level of theory in its ground state (singlet) in acetonitrile.

Ru	3.139702361557	0.071157657961	0.162109928460
Cl	3.085289744260	0.060271774719	-2.155530496238
Cl	5.562657938166	0.100454030087	0.087196479085
N	1.154989284694	-0.057294917117	0.127930663824
N	2.610484530734	2.093247708264	-0.159415100318
N	2.886430911214	-2.003975806358	0.083700762561
O	3.302146308884	-0.250597805002	2.292249955830
N	3.234449785075	0.860193517509	1.929801496879
C	0.440909567873	1.072283992111	-0.016360319663
C	1.263901395522	2.286479975028	-0.159198803615
C	-3.042383645166	-0.345311236202	-0.072155539829
C	-7.270660926587	-0.390802703541	-0.120182324302
C	2.979682848332	4.405667729662	-0.519040490764
H	3.683590699938	5.212363687641	-0.658982185186
C	0.596806250086	-1.278619649305	0.128313123885
C	-0.779657605217	-1.397788692459	0.073101808540
H	-1.238602580554	-2.372771761549	0.106888864564
C	3.567022912624	-4.274702743664	0.023192225454
H	4.374188374987	-4.990304952976	-0.023476376198
C	1.576909017971	-2.379403348621	0.131004179298
C	-1.577551809099	-0.247942910874	-0.015350194852
C	0.744896920307	3.559986089329	-0.332315145272
H	-0.322961386866	3.715795392643	-0.331932245595
C	-0.938504507589	0.998964529370	-0.078247515790
H	-1.519767855140	1.896572891419	-0.215144959658
C	3.446601586392	3.113721831705	-0.335928766721
H	4.499657025996	2.872625173381	-0.327093315768
C	3.854388474440	-2.919733496438	0.024723360162
H	4.863610452098	-2.536892830526	-0.017349725307
C	1.237442821230	-3.721525544958	0.137001845739
H	0.201074037847	-4.019125712899	0.177585887212
C	2.242464104676	-4.678121965177	0.084111519248
H	1.987556798614	-5.728416494387	0.086838143583
C	1.611553476913	4.629050408258	-0.512307628197
H	1.216900479360	5.625888516238	-0.648315929152
C	-7.554212159860	0.819505406711	0.537448255441
C	-9.895106740153	0.388386269994	0.290937093277
H	-10.924808854743	0.683097867347	0.446211591331
C	-8.299139780010	-1.212647019115	-0.572425251711
H	-8.084384506954	-2.144817381381	-1.079089239329
C	-9.613538495044	-0.812732079360	-0.361340672430
H	-10.427179040199	-1.437630750998	-0.705685767599
C	-8.865932752072	1.212019448188	0.744264792226
H	-9.093350918280	2.142384029424	1.249511201498
C	-3.841036850127	0.676369860938	0.466208365099
H	-3.383879630022	1.527734734343	0.953202621785
C	-5.037377319859	-1.561434901183	-0.741154150461
H	-5.490119328462	-2.419976718941	-1.219086842289
C	-5.214262078055	0.569630518028	0.406517535206
C	-3.657508350622	-1.456621107781	-0.668818073809
H	-3.048858563689	-2.232705412039	-1.111779061321
C	-5.820149659242	-0.546779267858	-0.198642750987
C	-6.271050236416	1.515150951620	0.922916147914
H	-6.188779839397	2.505372613938	0.466945309713
H	-6.192945690367	1.659384604855	2.003865714545

Energies (a.u.)	
E	-2388.645537
Zero-point correction	0.409614
Sum of electronic and thermal enthalpies	-2388.205662
Sum of electronic and thermal free energies	-2388.297662

Selected molecular parameters	
$Ru\text{-}N_{(NO)}$	1.938 Å
$Ru\text{-}O_{(NO)}$	2.160 Å
N-O	1.170 Å
$Ru\text{-}Cl_{1(trans\text{-}NO)}$	2.318 Å
$Ru\text{-}Cl_{2(cis\text{-}NO)}$	2.424 Å
$Ru\text{-}N_{tpy1}$	1.989 Å
$Ru\text{-}N_{tpy2}$	2.115 Å
$Ru\text{-}N_{tpy3}$	2.092 Å
∠Ru-N-O	84.197 °
∠Ru-O-N	63.190 °

NO stretching vibration	
ν_{NO} (cm^{-1})	1651.61 cm^{-1}

Electronic structure

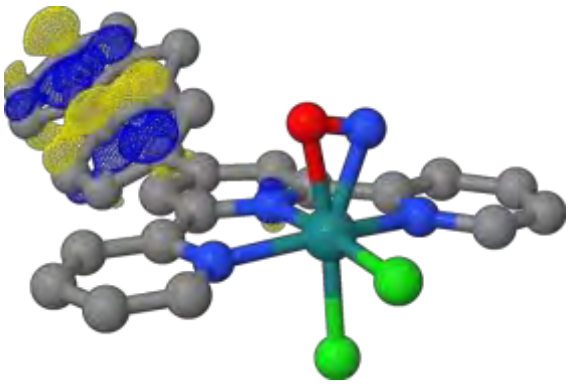

HOMO

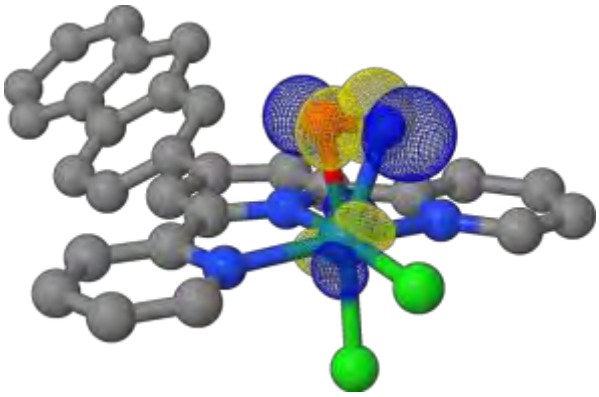

LUMO

Table AC9. Optimized Cartesian coordinates, energies, molecular parameters and electronic structure of the **MS1** isomer of complex **2**, *cis*(Cl,Cl)-[$RuCl_2(NO)(FT)]^+$, at the B3LYP-D3BJ/**BS1** level of theory in its ground state (singlet) in acetonitrile.

Ru	3.287924899252	0.084625794200	0.113558505931
Cl	3.246229901218	-0.065923956955	-2.196135673038
Cl	5.705917369835	0.241503560099	0.082899577634
N	1.313763945099	-0.051250486757	0.056818762070
N	2.780613695496	2.105955250323	-0.082026165529
N	3.054598862060	-1.994405013112	0.183040274550
O	3.388111197660	0.215342634659	1.959635450898
N	3.523276703127	0.303515187269	3.072943093562
C	0.602956416940	1.081498226244	-0.064850904942
C	1.431963638849	2.300609874704	-0.142811528102
C	-2.876791939931	-0.339456273337	-0.143277556447
C	-7.105217843049	-0.393255314201	-0.193643770454
C	3.147068380457	4.441711002470	-0.308619248988
H	3.851681528305	5.257476809756	-0.372611885479
C	0.760095293739	-1.274563152322	0.078293458271
C	-0.616284677059	-1.392752092209	0.017111535881
H	-1.078971031679	-2.365391961574	0.065715709411
C	3.730010276241	-4.270186440219	0.263077082013
H	4.537028368229	-4.986586685969	0.302358218266
C	1.744156468025	-2.372685010703	0.156732560711
C	-1.412132920787	-0.241261268616	-0.082198461913
C	0.913178938546	3.576524522886	-0.284537621915
H	-0.154451338354	3.726853130935	-0.333117141441
C	-0.775803024538	1.008471875347	-0.131591030860
H	-1.359396177498	1.906905745583	-0.251933801233
C	3.612856392340	3.143713725741	-0.165971418514
H	4.666009236814	2.907390708548	-0.118216824495
C	4.018134066485	-2.914449828190	0.231129351346
H	5.030066074194	-2.536016912005	0.241035420218
C	1.401109846270	-3.713832956755	0.186041256762
H	0.363692195641	-4.010135052431	0.163473561289
C	2.404438884747	-4.672570453038	0.240994750861
H	2.147455404264	-5.722142077811	0.263232631231
C	1.779895747746	4.658581688896	-0.367544526266
H	1.385351872210	5.658520195682	-0.479407158681
C	-7.391366902119	0.810635219620	0.474683773063
C	-9.731360777680	0.376214237952	0.225752094012
H	-10.761653695791	0.667087746000	0.384296289526
C	-8.132101979398	-1.213362546110	-0.652674170590
H	-7.915485398675	-2.140456934259	-1.167774276468
C	-9.447311902388	-0.818348908679	-0.437400711666
H	-10.259694515632	-1.442012027644	-0.786904649991
C	-8.703848464656	1.198203882687	0.685757594329
H	-8.933098525580	2.123481591882	1.199451687630
C	-3.678141079075	0.676541493323	0.401997497696
H	-3.223383337335	1.524947196024	0.896258647803
C	-4.869026389040	-1.554162792003	-0.823557593899
H	-5.319732341494	-2.409866538149	-1.308471089860
C	-5.050994039652	0.567317901167	0.340909919480
C	-3.489367299104	-1.447462453498	-0.748738534411
H	-2.878104023817	-2.219201470932	-1.195804938052
C	-5.654353885322	-0.545408324722	-0.273564805140
C	-6.109763080480	1.505971326407	0.865649067256
H	-6.030033202627	2.500290204798	0.418229784558
H	-6.031600811026	1.641069199002	1.947784932118

Energies (a.u.)	
E	-2388.632269
Zero-point correction	0.410193
Sum of electronic and thermal enthalpies	-2388.191786
Sum of electronic and thermal free energies	-2388.284791

Selected molecular parameters	
Ru-$O_{(NO)}$	1.853 Å
Ru-$N_{(NO)}$	2.977 Å
N-O	1.125 Å
Ru-$Cl_{1(trans\text{-}NO)}$	2.315 Å
Ru-$Cl_{2(cis\text{-}NO)}$	2.423 Å
Ru-N_{tpy1}	1.980 Å
Ru-N_{tpy2}	2.093 Å
Ru-N_{tpy3}	2.093 Å
∠Ru-N-O	2.385 °
∠Ru-O-N	176.168 °

NO stretching vibration	
ν_{NO} (cm^{-1})	1911.56 cm^{-1}

Electronic structure

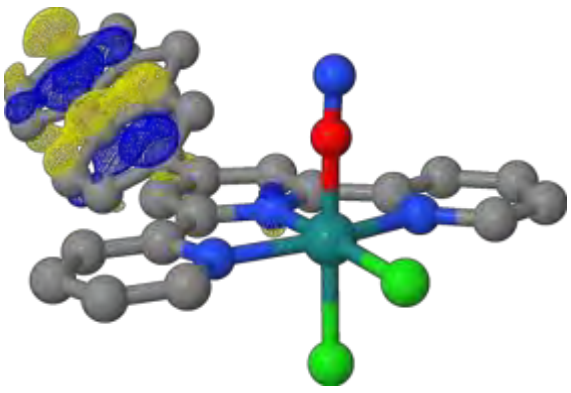

HOMO

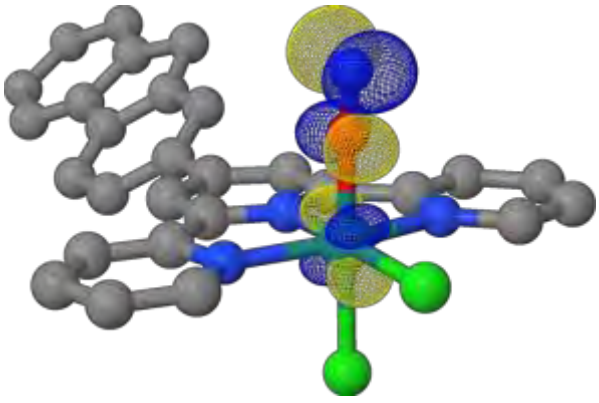

LUMO

Table AC10. Optimized Cartesian coordinates, energies, molecular parameters and electronic structure of the ^{3}**GS** triplet state of complex **2**, *cis*(Cl,Cl)-[$RuCl_2$(NO)(FT)]$^{+}$, at the B3LYP-D3BJ/**BS1** level of theory in acetonitrile.

Ru	3.345094327406	0.049400400879	-0.095761276637
Cl	3.045238221746	-0.084046366313	-2.473006822155
Cl	5.644520152076	0.240782937328	-0.422859887384
N	1.323726450503	-0.079046816925	0.003214175913
N	2.757767167704	2.055252695694	-0.117740853875
N	3.020249668176	-2.008460710979	0.100725277397
N	3.655123261481	0.189226876711	1.803013762764
O	3.936261819469	1.001771910798	2.571082116460
C	0.599089457896	1.048603069464	-0.079134566899
C	1.414991185828	2.265895954497	-0.133688359057
C	-2.889834040918	-0.355289818734	-0.129516002026
C	-7.118243230053	-0.392895886115	-0.177234090726
C	3.141523769049	4.397440723947	-0.203422031777
H	3.854086366288	5.208198206309	-0.230952898607
C	0.75076729881	-1.293681221703	0.036365937541
C	-0.626413186631	-1.409072763720	0.004015721745
H	-1.083613671099	-2.383700818994	0.062714282212
C	3.711471132838	-4.273295825626	0.268623880586
H	4.524343290036	-4.981327225020	0.329757052988
C	1.717684386881	-2.393853444150	0.110239003818
C	-1.425130929905	-0.260722329791	-0.079069109238
C	0.903147880929	3.551325059884	-0.186359115422
H	-0.164295901874	3.708936181133	-0.195080310992
C	-0.780572502376	0.982763870769	-0.120153576152
H	-1.356478920000	1.889097857309	-0.214155421909
C	3.600956142287	3.092690248351	-0.146869967009
H	4.653760381312	2.857449179121	-0.133898397100
C	3.993844269823	-2.920488534902	0.181981318005
H	5.006236563441	-2.546986281432	0.169312038487
C	1.380265149910	-3.734365977180	0.194947502851
H	0.343347878477	-4.032722887089	0.201426271434
C	2.387803129947	-4.684746303067	0.273689141673
H	2.137984962812	-5.734015505239	0.340259950268
C	1.775330985935	4.629439413532	-0.224072395318
H	1.388186738555	5.637413327780	-0.266617302027
C	-7.399296848552	0.818580985990	0.479359265416
C	-9.741027672457	0.393642347622	0.230526993787
H	-10.770094829333	0.691313387199	0.384336742397
C	-8.148452114529	-1.212282731177	-0.630023350608
H	-7.935667216966	-2.145266870412	-1.135997208549
C	-9.461978879964	-0.808685055095	-0.420615046281
H	-10.276935770931	-1.431553036304	-0.765504522651
C	-8.710168411211	1.214784160896	0.684469817723
H	-8.935610200475	2.146176537025	1.188702262948
C	-3.686730730915	0.667551641814	0.409424951069
H	-3.229094161283	1.518673961919	0.896187963790
C	-4.887164935060	-1.568823114746	-0.796683265257
H	-5.341455734327	-2.426895027754	-1.273962926718
C	-5.059978656534	0.563099413455	0.350065199736
C	-3.507094445170	-1.466052345278	-0.725068730096
H	-2.899572867728	-2.243192701296	-1.167820171700
C	-5.668070652080	-0.552388798764	-0.254758707831
C	-6.114801405115	1.511289204122	0.865474789516
H	-6.029831194175	2.501121095909	0.409162203591
H	-6.037074661020	1.655743748351	1.946421689883

Energies (a.u.)	
E	-2388.658278
Zero-point correction	0.408906
Sum of electronic and thermal enthalpies	-2388.218468
Sum of electronic and thermal free energies	-2388.313884

Selected molecular parameters	
Ru-$N_{(NO)}$	1.929 Å
Ru-$O_{(NO)}$	2.893 Å
N-O	1.153 Å
Ru-$Cl_{1(trans\text{-}NO)}$	2.400 Å
Ru-$Cl_{2(cis\text{-}NO)}$	2.330 Å
Ru-N_{tpy1}	2.028 Å
Ru-N_{tpy2}	2.090 Å
Ru-N_{tpy3}	2.093 Å
∠Ru-N-O	138.249 °
∠Ru-O-N	26.361 °

NO stretching vibration	
ν_{NO} (cm^{-1})	1800.74 cm^{-1}

Electronic structure

$\langle S^2 \rangle$: 2.0157

Mulliken Spin Populations: Ru: 0.9718 Cl_1: 0.0670 Cl_2: 0.1372 $N_{(NO)}$: 0.4593 $O_{(NO)}$: 0.2928

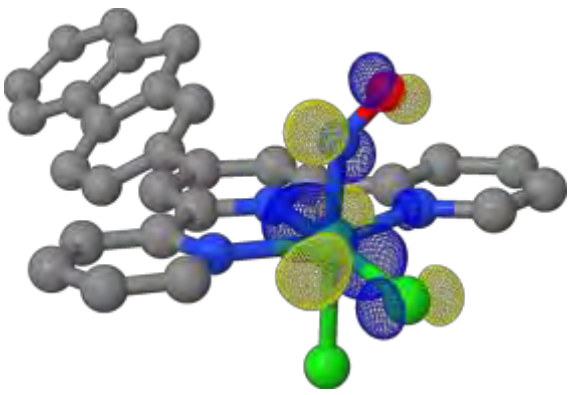

SONO (Hole)

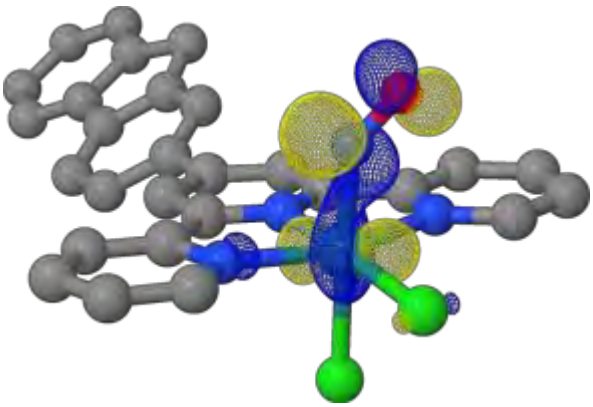

SONO (Particle)

Table AC11. Optimized Cartesian coordinates, energies, molecular parameters and electronic structure of the ^{3}**MS2** triplet state of complex **2**, *cis*(Cl,Cl)-[$RuCl_2(NO)(FT)]^+$, at the B3LYP-D3BJ/**BS1** level of theory in acetonitrile.

Ru	3.126963151727	0.069914737670	0.125361465274
Cl	3.238666276310	0.021809973420	-2.155020538277
Cl	5.476561121151	0.218296980465	0.363508515342
N	1.168336213235	-0.061078623053	0.029863099416
N	2.625574091416	2.102090439793	-0.136166167773
N	2.903123518997	-2.014156139378	0.071169856221
O	3.009789836002	-0.375004705754	2.200637912574
N	2.961663139663	0.835249218773	2.140523001442
C	0.453731462509	1.077359159616	-0.075351668748
C	1.279576066660	2.295448983801	-0.179089886621
C	-3.020082386012	-0.346289413479	-0.119972635710
C	-7.246271779196	-0.401514401588	-0.116528408997
C	2.996595564757	4.426085660376	-0.418552538929
H	3.702959682414	5.237529022402	-0.511078418902
C	0.611792093083	-1.288926456597	0.034539851803
C	-0.761213180261	-1.404258336755	-0.010270194808
H	-1.221152107771	-2.378141824286	0.028054625679
C	3.582423670773	-4.286066899950	0.032461403407
H	4.390901639842	-5.001674998035	0.019738750350
C	1.593866242208	-2.389945301534	0.059840436728
C	-1.561219069222	-0.248904136234	-0.078998189014
C	0.760882335879	3.569453700997	-0.339514175493
H	-0.306893959409	3.722019145298	-0.374815005465
C	-0.922010814079	1.003609630493	-0.123919805693
H	-1.504836815861	1.903435577154	-0.233542074056
C	3.461488695181	3.129484433181	-0.251840535950
H	4.514514167785	2.893287502217	-0.205314652862
C	3.869429164242	-2.929231386956	0.055101890541
H	4.881172797836	-2.550989540521	0.064528066417
C	1.251567693218	-3.731321357808	0.041813715371
H	0.214265432720	-4.028503119172	0.033443558083
C	2.257412139643	-4.689326484745	0.029123198640
H	2.002016259234	-5.739340122742	0.014053893792
C	1.629815801363	4.646410468883	-0.459807740104
H	1.236709514580	5.645088498965	-0.586267867012
C	-7.525962318853	0.832720855614	0.498924191449
C	-9.866692364261	0.382381024412	0.299224262077
H	-10.895619001528	0.678373997435	0.456830286613
C	-8.277088799890	-1.245109314112	-0.524198733711
H	-8.064300460495	-2.194831270548	-0.997710032425
C	-9.589143969879	-0.842448851152	-0.310988045520
H	-10.405056982807	-1.482442534043	-0.620006744788
C	-8.836377511205	1.227525907784	0.707650223219
H	-9.061989105605	2.175201424760	1.180140413258
C	-3.816982835282	0.697354636153	0.385333034884
H	-3.358476734957	1.567471901952	0.835408504943
C	-5.021010213316	-1.590810050178	-0.720803394858
H	-5.478348303342	-2.466765578051	-1.160740890276
C	-5.188262659518	0.585801852352	0.347216829525
C	-3.642965866073	-1.482926637768	-0.666150626203
H	-3.040464426632	-2.275515702725	-1.086610152134
C	-5.799664192089	-0.555816853297	-0.207641100783
C	-6.241272134845	1.546708289330	0.841259220390
H	-6.168453639550	2.519194400639	0.347350713554
H	-6.149450140490	1.731160616522	1.914879304119

Energies (a.u.)	
E	-2388.624663
Zero-point correction	0.408730
Sum of electronic and thermal enthalpies	-2388.185435
Sum of electronic and thermal free energies	-2388.279072
Selected molecular parameters	
Ru-$N_{(NO)}$	2.162 Å
Ru-$O_{(NO)}$	2.126 Å
N-O	1.213 Å
Ru-$Cl_{1(trans\text{-}NO)}$	2.284 Å
Ru-$Cl_{2(cis\text{-}NO)}$	2.366 Å
Ru-N_{tpy1}	1.965 Å
Ru-N_{tpy2}	2.109 Å
Ru-N_{tpy3}	2.097 Å
∠Ru-N-O	71.934 °
∠Ru-O-N	75.221 °
NO stretching vibration	
ν_{NO} (cm^{-1})	1526.61 cm^{-1}

Electronic structure

$<S^2>$: 2.0095

Mulliken Spin Populations: Ru: 0.7225 Cl_1: 0.0788 Cl_2: 0.0952 $N_{(NO)}$: 0.7484 $O_{(NO)}$: 0.2749

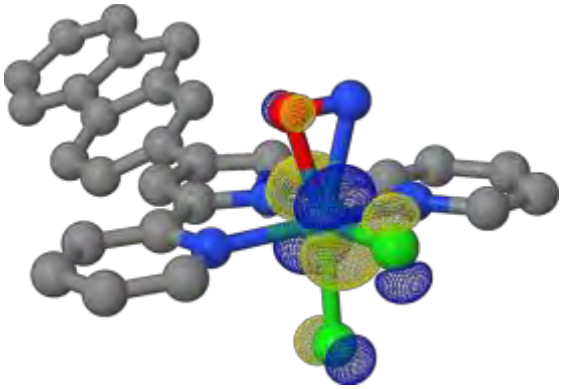

SONO (Hole)

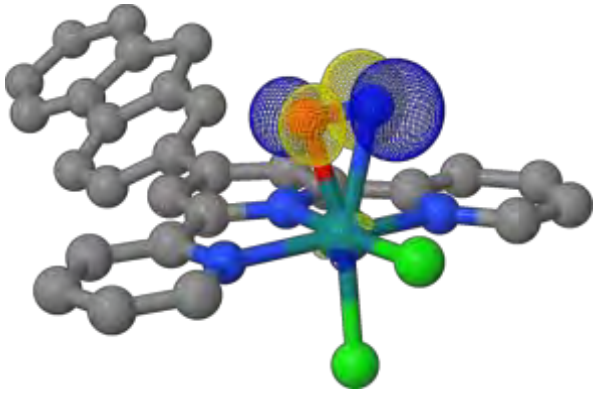

SONO (Particle)

Table AC12. Optimized Cartesian coordinates, energies, molecular parameters and electronic structure of the ^{3}**MS1** triplet state of complex **2**, *cis*(Cl,Cl)-[$RuCl_2(NO)(FT)]^+$, at the B3LYP-D3BJ/**BS1** level of theory in acetonitrile.

Ru	3.120217111850	0.076630874634	-0.030173734954
Cl	3.250025699353	-0.042513056633	-2.305005239538
Cl	5.433693943831	0.267166543733	0.409595024625
N	1.160830708911	-0.056149049570	-0.062834101862
N	2.621299236442	2.106544669829	-0.160255658548
N	2.895708400625	-2.000134956647	0.076708579029
O	2.803857603312	0.177596387726	2.161608410122
N	3.534635613227	0.192117663359	3.047933669112
C	0.445012744951	1.082858044980	-0.140209224137
C	1.272642509432	2.304468488535	-0.210608759376
C	-3.032186855629	-0.339508773433	-0.137494176146
C	-7.259776934222	-0.401321738229	-0.091846200923
C	2.978773318808	4.450071072110	-0.348025663280
H	3.682228347292	5.267729911151	-0.401546326070
C	0.602853844889	-1.281959812609	-0.016588375590
C	-0.772220586206	-1.396152328485	-0.037986711757
H	-1.234984239769	-2.367481537837	0.027495126524
C	3.565115839070	-4.279519331029	0.183831259087
H	4.371912834108	-4.995821128360	0.231307915554
C	1.586054140390	-2.381645076172	0.057197262721
C	-1.569964720532	-0.241187791495	-0.112273506177
C	0.748516064849	3.580534781034	-0.326469484377
H	-0.319793393784	3.729043692347	-0.365953732315
C	-0.932619801182	1.010731322281	-0.164473335716
H	-1.518345537144	1.911133117642	-0.253703813364
C	3.447543385511	3.149371612680	-0.230048638714
H	4.502096724771	2.918892157016	-0.186876110789
C	3.854705059425	-2.923408108004	0.135355781790
H	4.868519039887	-2.550407506608	0.145419165281
C	1.238809502188	-3.721051089491	0.103020537964
H	0.200595125596	-4.015252496883	0.087029600318
C	2.240134953122	-4.681888285669	0.167681756705
H	1.981671847160	-5.730694030609	0.202920316834
C	1.611902284042	4.666861134734	-0.396139247161
H	1.214751140948	5.667691250519	-0.488841462949
C	-7.534217683738	0.820677985191	0.548486733040
C	-9.877319979956	0.372969694457	0.364378837660
H	-10.904749037787	0.665494040468	0.537662572672
C	-8.293988152938	-1.237407009099	-0.504271195934
H	-8.085627744776	-2.178243814871	-0.997310269539
C	-9.604800097032	-0.839740601646	-0.270715920153
H	-10.423071897535	-1.474989553161	-0.583532450757
C	-8.842849291078	1.210773290414	0.777650842549
H	-9.063799392422	2.149682260683	1.269643601972
C	-3.824510150604	0.691777442150	0.395860357848
H	-3.362154293708	1.554450395260	0.856657201304
C	-5.037376511749	-1.575673896350	-0.739824877058
H	-5.497565798074	-2.444655379648	-1.190789937955
C	-5.197144399136	0.578693407512	0.369145180972
C	-3.657745404007	-1.465722189303	-0.698113547627
H	-3.056830440042	-2.249017974221	-1.138453891537
C	-5.812102104521	-0.552518137080	-0.200194841971
C	-6.246351052293	1.529586841384	0.890786935773
H	-6.179299427706	2.510859310812	0.413580083422
H	-6.144241096422	1.695342260500	1.966584683399

Energies (a.u.)	
E	-2388.628338
Zero-point correction	0.407626
Sum of electronic and thermal enthalpies	-2388.189230
Sum of electronic and thermal free energies	-2388.286738

Selected molecular parameters	
Ru-$N_{(NO)}$	3.108 Å
Ru-$O_{(NO)}$	2.217 Å
N-O	1.149 Å
Ru-$Cl_{1(trans\text{-}NO)}$	2.282 Å
Ru-$Cl_{2(cis\text{-}NO)}$	2.363 Å
Ru-N_{tpy1}	1.964 Å
Ru-N_{tpy2}	2.094 Å
Ru-N_{tpy3}	2.092 Å
∠Ru-N-O	31.858 °
∠Ru-O-N	132.267 °

NO stretching vibration	
ν_{NO} (cm^{-1})	1830.69 cm^{-1}

Electronic structure

$\langle S^2 \rangle$: 2.0091

Mulliken Spin Populations: Ru: 0.8305 Cl_1: 0.1107 Cl_2: 0.0862 $N_{(NO)}$: 0.7674 $O_{(NO)}$: 0.1566

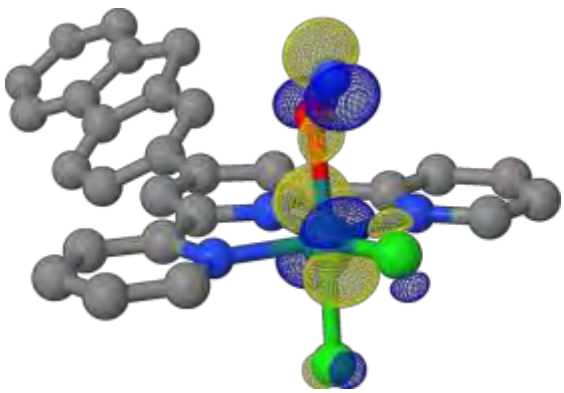

SONO (Hole)

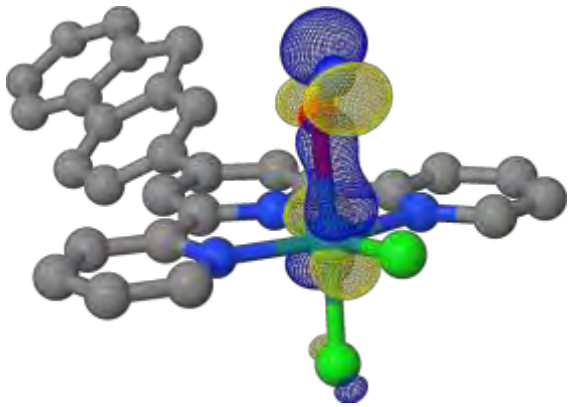

SONO (Particle)

Table AC13. Optimized Cartesian coordinates, energies, molecular parameters and electronic structure of the **GS** isomer of complex **3**, *cis*(Cl,Cl)-$[RuCl_2(NO)(terpy)]^+$, at the B3LYP-D3BJ/**BS1** level of theory in its ground state (singlet) in acetonitrile.

Ru	3.286912659298	0.085488479816	0.110288295610
Cl	3.143796762219	-0.072425510257	-2.242512665373
Cl	5.694898815873	0.236146737034	-0.099871101332
N	1.296474364319	-0.051453419540	0.068786248532
N	2.776141057064	2.105546959324	-0.119415664706
N	3.052484230143	-1.996957603125	0.138074006867
N	3.464019448047	0.203748589013	1.838873623479
O	3.642994647758	0.283170297162	2.955518268311
C	0.596722777291	1.086284507921	-0.049396100592
C	1.427423539047	2.300563255251	-0.149405131495
C	3.144415299731	4.434388928444	-0.380095841027
H	3.849737932299	5.247011277407	-0.469669625809
C	0.755441652205	-1.278188387666	0.096706698512
C	-0.627267378704	-1.396640439077	0.048141093149
H	-1.103450073082	-2.364389790001	0.071248364504
C	3.732509802038	-4.269181953676	0.174105214897
H	4.541143533403	-4.984636246626	0.183804528012
C	1.742354888874	-2.373300627168	0.144019247198
C	0.909003472056	3.576151672739	-0.293361273842
H	-0.158993618526	3.728815585170	-0.319666901128
C	-0.788727085492	1.013074771038	-0.099474209082
H	-1.388384544294	1.905099223278	-0.190529007532
C	3.610954238489	3.136875308437	-0.233119233277
H	4.664104313318	2.898010357388	-0.206747791564
C	4.019292606553	-2.912714032983	0.150443190409
H	5.030555425327	-2.533043113531	0.138458480737
C	1.401494396773	-3.714856835998	0.168171885145
H	0.364184117572	-4.012007516435	0.171080197581
C	2.407499844790	-4.672536657813	0.184820431395
H	2.152297948358	-5.722540356894	0.203442776659
C	1.777128826880	4.654389297131	-0.408554927537
H	1.382826777493	5.654186112553	-0.521825891849
C	-1.390450103725	-0.238374362921	-0.041043695986
H	-2.467701573395	-0.312786505396	-0.079094488862

Energies (a.u.)	
E	-1888.248255
Zero-point correction	0.243416
Sum of electronic and thermal enthalpies	-1887.984469
Sum of electronic and thermal free energies	-1888.053397

Selected molecular parameters	
$Ru\text{-}N_{(NO)}$	1.742 Å
$Ru\text{-}O_{(NO)}$	2.874 Å
N-O	1.134 Å
$Ru\text{-}Cl_{1(trans\text{-}NO)}$	2.362 Å
$Ru\text{-}Cl_{2(cis\text{-}NO)}$	2.422 Å
$Ru\text{-}N_{tpy1}$	1.996 Å
$Ru\text{-}N_{tpy2}$	2.096 Å
$Ru\text{-}N_{tpy3}$	2.096 Å
∠Ru-N-O	176.749 °
∠Ru-O-N	1.969 °

NO stretching vibration	
ν_{NO} (cm^{-1})	1933.68 cm^{-1}

Electronic structure

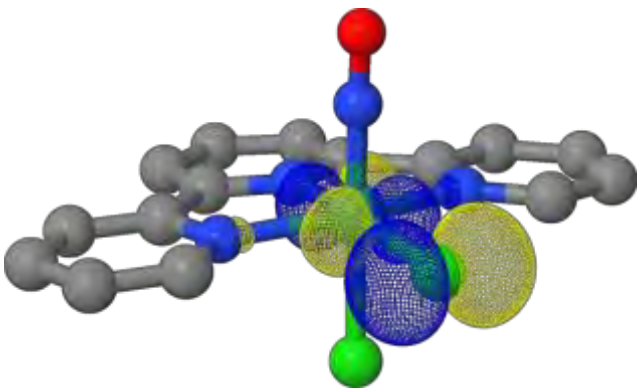

HOMO

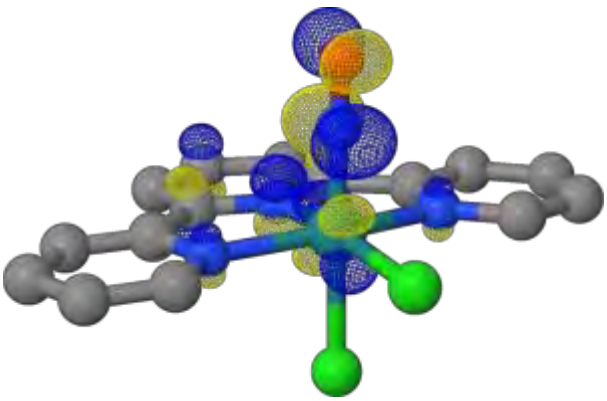

LUMO

Table AC14. Optimized Cartesian coordinates, energies, molecular parameters and electronic structure of the **MS2** isomer of complex **3**, *cis*(Cl,Cl)-[$RuCl_2$(NO)(terpy)]$^+$, at the B3LYP-D3BJ/**BS1** level of theory in its ground state (singlet) in acetonitrile.

Ru	3.114469077556	0.068249649087	0.214948384064
Cl	3.152493880912	0.087530015604	-2.102321496544
Cl	5.532652553325	0.112825171784	0.245381029120
N	1.128420940197	-0.064522495238	0.092277834665
N	2.599495438492	2.093893378712	-0.099911633202
N	2.874577470869	-2.004672715561	0.097690311865
O	3.195935441294	-0.282850464668	2.346018554701
N	3.111484433937	0.830807537641	1.999492889012
C	0.426290165259	1.070988591679	-0.058246279313
C	1.253834725643	2.285759801192	-0.150504653543
H	-2.636551550702	-0.327228164473	-0.212945921345
C	2.978453828040	4.411295086261	-0.412220294116
H	3.686027595169	5.220741120042	-0.512058829538
C	0.581039135487	-1.289948157268	0.062665883939
C	-0.798420575472	-1.410093623940	-0.040374400710
H	-1.270742031288	-2.379881875552	-0.059037381607
C	3.565221362245	-4.272139757319	0.031496257884
H	4.376407157346	-4.984301872902	0.007737901249
C	1.565756299508	-2.385157384982	0.085597174937
C	-1.561524643766	-0.252920882710	-0.134881290997
C	0.739422291484	3.560301912395	-0.328644155742
H	-0.327837347359	3.714407517053	-0.371218667165
C	-0.956416390621	0.997265389757	-0.160925215892
H	-1.550902528642	1.890502095969	-0.272194940007
C	3.440301981928	3.117208343131	-0.228498766517
H	4.492539891724	2.877154693698	-0.180861489743
C	3.847388307185	-2.916226123226	0.065283717817
H	4.856140333570	-2.529947181392	0.070788907672
C	1.230914013924	-3.728044352268	0.057133110545
H	0.194808376237	-4.029111649737	0.050190537910
C	2.241022574176	-4.680662347544	0.031239751285
H	1.990185876620	-5.731637613868	0.007349812402
C	1.611017597063	4.632899371894	-0.458653412167
H	1.220488318663	5.630931986749	-0.597552230923

Energies (a.u.)	
E	-1888.192156
Zero-point correction	0.241790
Sum of electronic and thermal enthalpies	-1887.929789
Sum of electronic and thermal free energies	-1887.998314
Selected molecular parameters	
Ru-$N_{(NO)}$	1.941 Å
Ru-$O_{(NO)}$	2.161 Å
N-O	1.169 Å
Ru-$Cl_{1(trans\text{-}NO)}$	2.318 Å
Ru-$Cl_{2(cis\text{-}NO)}$	2.419 Å
Ru-N_{tpy1}	1.994 Å
Ru-N_{tpy2}	2.114 Å
Ru-N_{tpy3}	2.090 Å
∠Ru-N-O	84.155 °
∠Ru-O-N	63.281 °
NO stretching vibration	
ν_{NO} (cm^{-1})	1655.73 cm^{-1}

Electronic structure

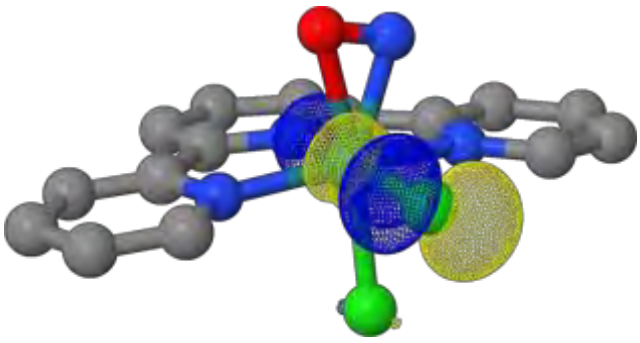

HOMO

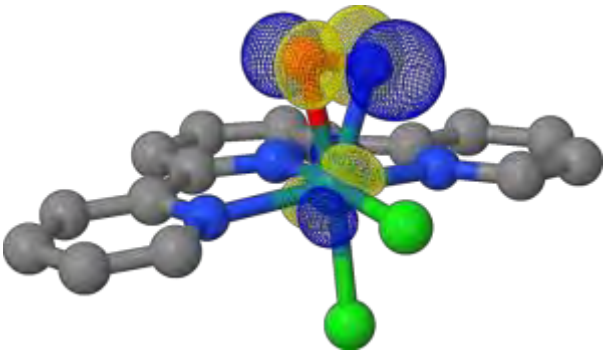

LUMO

Table AC15. Optimized Cartesian coordinates, energies, molecular parameters and electronic structure of the **MS1** isomer of complex **3**, *cis*(Cl,Cl)-[$RuCl_2$(NO)(terpy)]$^+$, at the B3LYP-D3BJ/**BS1** level of theory in its ground state (singlet) in acetonitrile.

Ru	3.285721926209	0.080928754064	0.037202990250
Cl	3.171382479722	-0.070403414542	-2.268121820204
Cl	5.698423931190	0.237616637747	-0.067914361471
N	1.304446048971	-0.052562112507	0.036982680212
N	2.779609247834	2.103354107378	-0.142034085425
N	3.056325065114	-1.996876568794	0.113872088692
O	3.438838376767	0.202422782983	1.881425822549
N	3.599530524749	0.279618221381	2.991266350992
C	0.599932604472	1.085305717085	-0.067878556153
C	1.430282751978	2.300971100984	-0.164170823888
C	3.143659694279	4.438727035768	-0.375374796435
H	3.847890649151	5.253082178825	-0.458560224311
C	0.758998108548	-1.278553721604	0.077889107786
C	-0.624336699686	-1.396071094010	0.049569706591
H	-1.100963317669	-2.363342066024	0.083949222218
C	3.732503835502	-4.272677143682	0.180669748570
H	4.540086882984	-4.989279071652	0.198572674306
C	1.745723808204	-2.374703244437	0.127730507059
C	0.909718983146	3.577898777323	-0.289206164286
H	-0.158566344944	3.730138386808	-0.307822375757
C	-0.786109513810	1.013180197387	-0.098002560737
H	-1.386525636252	1.905867789764	-0.177685363623
C	3.611042031303	3.139444856496	-0.247916765048
H	4.664686760863	2.901211033030	-0.230711127787
C	4.020368615993	-2.916963782224	0.136094659871
H	5.032360085616	-2.539162452124	0.115369608006
C	1.402630395407	-3.715407415843	0.171422213678
H	0.364857543898	-4.011052695713	0.181609236797
C	2.406930950059	-4.674542850001	0.199291871050
H	2.150315695585	-5.723882330846	0.232678470647
C	1.776014295624	4.658508135227	-0.395058751885
H	1.380447797134	5.659322311771	-0.494521790402
C	-1.388314350621	-0.237749552245	-0.032442439876
H	-2.466074227318	-0.311450427774	-0.055975951984

Energies (a.u.)	
E	-1888.178886
Zero-point correction	0.242426
Sum of electronic and thermal enthalpies	-1887.915872
Sum of electronic and thermal free energies	-1887.985176

Selected molecular parameters	
$Ru\text{-}O_{(NO)}$	1.855 Å
$Ru\text{-}N_{(NO)}$	2.977 Å
N-O	1.124 Å
$Ru\text{-}Cl_{1(trans\text{-}NO)}$	2.313 Å
$Ru\text{-}Cl_{2(cis\text{-}NO)}$	2.420 Å
$Ru\text{-}N_{tpy1}$	1.986 Å
$Ru\text{-}N_{tpy2}$	2.092 Å
$Ru\text{-}N_{tpy3}$	2.092 Å
∠Ru-N-O	2.173 °
∠Ru-O-N	176.511 °

NO stretching vibration	
ν_{NO} (cm^{-1})	1904.05 cm^{-1}

Electronic structure

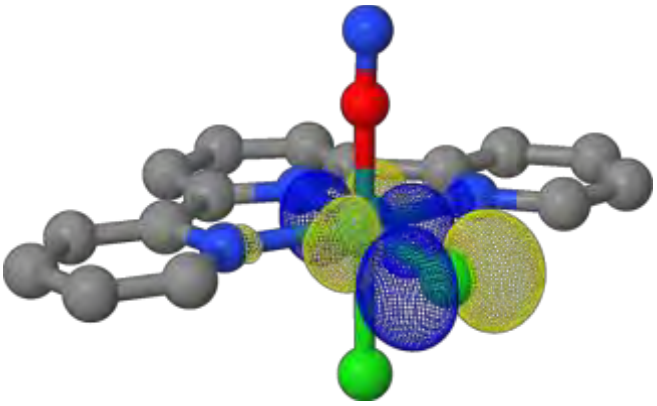

HOMO

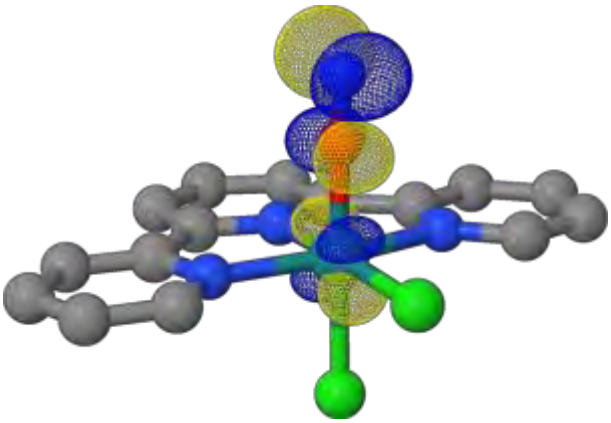

LUMO

Table AC16. Optimized Cartesian coordinates, energies, molecular parameters and electronic structure of the **^{3}GS** triplet state of complex **3**, *cis*(Cl,Cl)-[$RuCl_2$(NO)(terpy)]$^+$, at the B3LYP-D3BJ/**BS1** level of theory in acetonitrile.

Ru	3.332154765751	0.043533379855	-0.089331326766
Cl	3.061642527966	-0.089682117764	-2.467541454042
Cl	5.633919791084	0.225002291882	-0.384460443603
N	1.304261565245	-0.077441443583	-0.015128123434
N	2.757832778809	2.051643885593	-0.118597320770
N	3.003007719238	-2.012159119173	0.105417006315
N	3.618833380392	0.182957146332	1.815955934378
O	3.902412459560	0.993073873939	2.584728395523
C	0.592712723109	1.057669008271	-0.104837438514
C	1.416516748836	2.268690911647	-0.154359051136
H	-2.486481513129	-0.312563292606	-0.133335898521
C	3.153317893644	4.391597457542	-0.208244194704
H	3.870116514752	5.198843902883	-0.228128271019
C	0.735110933207	-1.293225536322	0.022619050130
C	-0.648108857553	-1.403778877745	-0.016531011155
H	-1.123927011507	-2.371431979706	0.016542505418
C	3.684584521443	-4.279230569125	0.281941186066
H	4.494582331507	-4.989697627666	0.352210832902
C	1.699372452065	-2.393805367592	0.102378412564
C	-1.408680500100	-0.245919974679	-0.100384806859
C	0.911095883080	3.555839485266	-0.222852254851
H	-0.155303315104	3.718041141301	-0.251647196245
C	-0.792981083898	0.997193347496	-0.145120885190
H	-1.381148791083	1.898867801311	-0.212218041915
C	3.606070588584	3.084772677216	-0.139575334351
H	4.657525279432	2.844974499098	-0.110694397670
C	3.972518855233	-2.927148362175	0.197447176006
H	4.986271185786	-2.557266369009	0.195088746855
C	1.356215733469	-3.732967824684	0.184214405574
H	0.318298191584	-4.027755332289	0.180417278076
C	2.359928290634	-4.686698240454	0.273328878469
H	2.106080475182	-5.735120810045	0.337538200633
C	1.788982554191	4.629873870958	-0.252240448584
H	1.407378928589	5.639359164028	-0.306765109579

Energies (a.u.)	
E	-1888.204739
Zero-point correction	0.241092
Sum of electronic and thermal enthalpies	-1887.942432
Sum of electronic and thermal free energies	-1888.014736

Selected molecular parameters	
Ru-$N_{(NO)}$	1.932 Å
Ru-$O_{(NO)}$	2.894 Å
N-O	1.152 Å
Ru-$Cl_{1(trans\text{-}NO)}$	2.397 Å
Ru-$Cl_{2(cis\text{-}NO)}$	2.328 Å
Ru-N_{tpy1}	2.033 Å
Ru-N_{tpy2}	2.089 Å
Ru-N_{tpy3}	2.091 Å
∠Ru-N-O	138.185 °
∠Ru-O-N	26.423 °

NO stretching vibration	
ν_{NO} (cm^{-1})	1805.42 cm^{-1}

Electronic structure

$\langle S^2 \rangle$: 2.0156

Mulliken Spin Populations: Ru: 0.9683 Cl_1: 0.0673 Cl_2: 0.1385 $N_{(NO)}$: 0.4605 $O_{(NO)}$: 0.2943

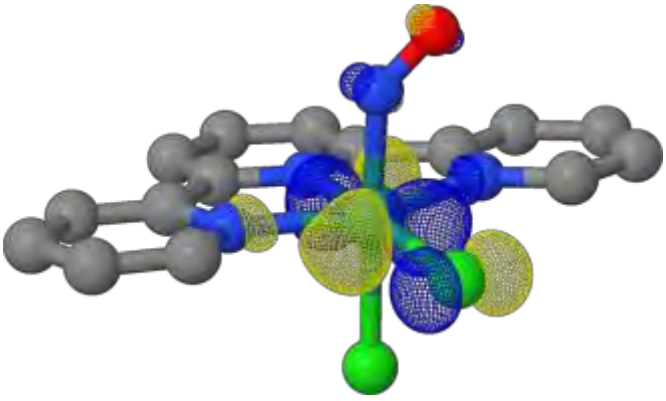

SONO (Hole)

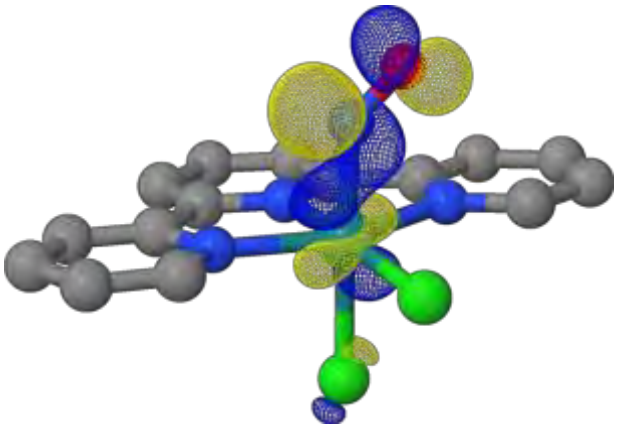

SONO (Particle)

Table AC17. Optimized Cartesian coordinates, energies, molecular parameters and electronic structure of the ^{3}**MS2** triplet state of complex **3**, *cis*(Cl,Cl)-[$RuCl_2$(NO)(terpy)]$^+$, at the B3LYP-D3BJ/**BS1** level of theory in acetonitrile.

Ru	3.120393068590	0.069312316013	0.120856985712
Cl	3.217619098884	0.020755520443	-2.151395925565
Cl	5.455102928859	0.214011939427	0.377457636202
N	1.145128038490	-0.063193650128	0.020536909287
N	2.619738404890	2.102233180103	-0.138392205275
N	2.897059494514	-2.015119260015	0.068724872534
O	2.969782670482	-0.376331479818	2.195176358315
N	2.928909232705	0.833351807574	2.139037387188
C	0.443839090485	1.079656587773	-0.085275490880
C	1.273257796860	2.294696660718	-0.185285535287
H	-2.618962581176	-0.320053307966	-0.102373229021
C	2.988780847232	4.426965430952	-0.416801165262
H	3.694952029864	5.238904393779	-0.506107116425
C	0.601641338681	-1.293397961735	0.039088791996
C	-0.779947990012	-1.408645068484	0.000497804307
H	-1.258995133138	-2.374931603842	0.019680360549
C	3.574449537428	-4.287497327047	0.027301416188
H	4.382798936112	-5.003167706692	0.011936172925
C	1.587190258328	-2.390618120983	0.061363291176
C	-1.541265119563	-0.246928167919	-0.072890268821
C	0.753846380012	3.567942941568	-0.347251833617
H	-0.313938744174	3.719056184121	-0.387509148985
C	-0.940510133136	1.005929546503	-0.127086339700
H	-1.542095617790	1.897633571793	-0.206772781784
C	3.454744081196	3.130185647231	-0.249907503211
H	4.508007159300	2.895873966701	-0.200357557267
C	3.862464326562	-2.930291962216	0.049410564804
H	4.874709750450	-2.553451526616	0.056194602791
C	1.244095862818	-3.731545242731	0.044969801717
H	0.206637721291	-4.028119932411	0.040418564475
C	2.249811607859	-4.690264399692	0.028599486904
H	1.993863211002	-5.740112530315	0.014448517249
C	1.622461582055	4.646139577309	-0.463317161606
H	1.228824864040	5.644434976603	-0.590735261614

Energies (a.u.)	
E	-1888.169331
Zero-point correction	0.240926
Sum of electronic and thermal enthalpies	-1887.907610
Sum of electronic and thermal free energies	-1887.977600
Selected molecular parameters	
Ru-$N_{(NO)}$	2.166 Å
Ru-$O_{(NO)}$	2.127 Å
N-O	1.212 Å
Ru-$Cl_{1(trans\text{-}NO)}$	2.275 Å
Ru-$Cl_{2(cis\text{-}NO)}$	2.353 Å
Ru-N_{tpy1}	1.982 Å
Ru-N_{tpy2}	2.110 Å
Ru-N_{tpy3}	2.097 Å
∠Ru-N-O	71.826 °
∠Ru-O-N	75.406 °
NO stretching vibration	
ν_{NO} (cm^{-1})	1530.70 cm^{-1}

Electronic structure

$\langle S^2 \rangle$: 2.0077

Mulliken Spin Populations: Ru: 0.7535 Cl_1: 0.0959 Cl_2: 0.1084 $N_{(NO)}$: 0.7474 $O_{(NO)}$: 0.2754

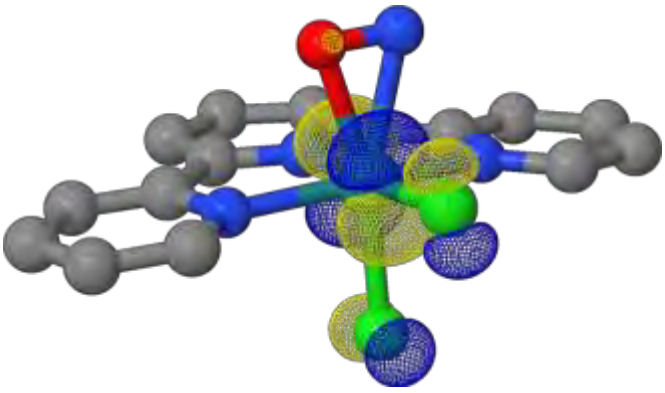

SONO (Hole)

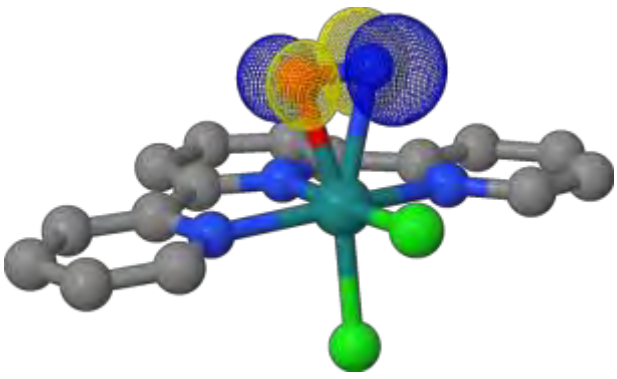

SONO (Particle)

Table AC18. Optimized Cartesian coordinates, energies, molecular parameters and electronic structure of the ^{3}**MS1** triplet state of complex **3**, *cis*(Cl,Cl)-[$RuCl_2$(NO)(terpy)]$^{+}$, at the B3LYP-D3BJ/**BS1** level of theory in acetonitrile.

Ru	3.302913595195	0.042565506487	-0.192320813475
Cl	3.077410564289	-0.111646478830	-2.494347270769
Cl	5.636827438275	0.205782042511	-0.338449731395
N	1.294115553904	-0.077329720946	-0.087802144740
N	2.747335135444	2.044547533552	-0.152636897570
N	2.996200199170	-1.995350387340	0.088269821166
O	3.569984593074	0.141583444871	1.986400729316
N	4.117051498669	0.944250741985	2.599656306260
C	0.578844215753	1.057962562149	-0.153903159852
C	1.405273575464	2.268158689346	-0.192563112482
H	-2.501362024093	-0.311293991775	-0.100825945647
C	3.151121681233	4.386260860964	-0.190649826243
H	3.869647363095	5.192257106847	-0.189349208084
C	0.723459866030	-1.291775096112	-0.018168123830
C	-0.660372579224	-1.402584412778	-0.020980048548
H	-1.135672648762	-2.369361106763	0.039287536099
C	3.689599288982	-4.257898247031	0.301501877482
H	4.502545042338	-4.963202143581	0.388140951239
C	1.693376829196	-2.387265454043	0.077112861804
C	-1.423047867235	-0.244938617816	-0.096751406387
C	0.904915598742	3.558316189215	-0.237371146475
H	-0.160763771052	3.725518259191	-0.268803357884
C	-0.807958799822	0.997931306431	-0.158512790648
H	-1.397585803781	1.900151107687	-0.204872128082
C	3.598671834405	3.076757873614	-0.147588616608
H	4.648881889777	2.829226626291	-0.120889879181
C	3.969630909494	-2.905521501907	0.202035240424
H	4.980209428536	-2.526258100552	0.201740073902
C	1.358078106788	-3.727071576801	0.174709656171
H	0.322079465790	-4.028653134292	0.164798557525
C	2.367120242774	-4.673341363316	0.285261677213
H	2.118989020198	-5.722526462805	0.359692343096
C	1.787212585525	4.629491992754	-0.238874912684
H	1.409381971827	5.641296952794	-0.275112111109

Energies (a.u.)	
E	-1888.175975
Zero-point correction	0.239952
Sum of electronic and thermal enthalpies	-1887.914289
Sum of electronic and thermal free energies	-1887.987479

Selected molecular parameters	
Ru-$N_{(NO)}$	3.045 Å
Ru-$O_{(NO)}$	2.197 Å
N-O	1.149 Å
Ru-$Cl_{1(trans\text{-}NO)}$	2.318 Å
Ru-$Cl_{2(cis\text{-}NO)}$	2.344 Å
Ru-N_{tpy1}	2.015 Å
Ru-N_{tpy2}	2.078 Å
Ru-N_{tpy3}	2.080 Å
∠Ru-N-O	34.537 °
∠Ru-O-N	128.222 °

NO stretching vibration	
ν_{NO} (cm^{-1})	1831.58 cm^{-1}

Electronic structure

$\langle S^2 \rangle$: 2.0081

Mulliken Spin Populations: Ru: 0.8929 Cl_1: 0.0505 Cl_2: 0.0790 $N_{(NO)}$: 0.7589 $O_{(NO)}$: 0.1627

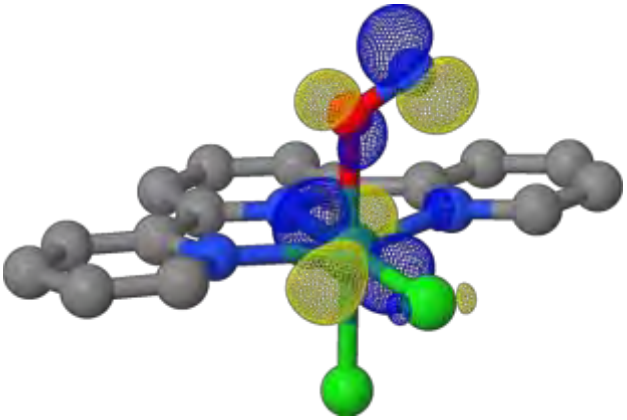

SONO (Hole)

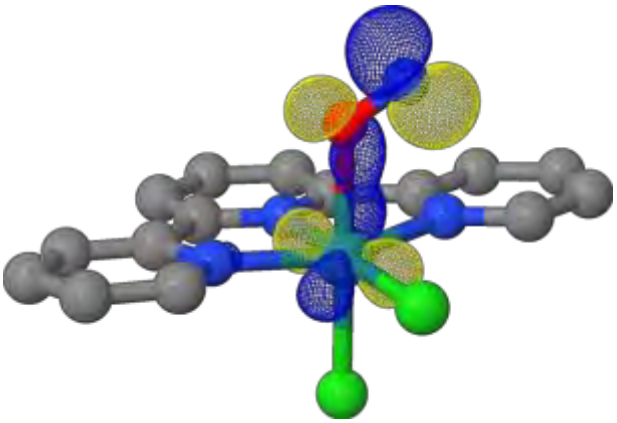

SONO (Particle)

Table AC19. Optimized Cartesian coordinates, energies, molecular parameters and electronic structure of the **GS** isomer of complex **4**, *trans*(Cl,Cl)-[$RuCl_2(NO)(FT)]^+$, at the B3LYP-D3BJ/**BS1** level of theory in its ground state (singlet) in acetonitrile.

Ru	3.341069085218	0.081066459860	-0.015824305493
Cl	3.257352624939	-0.076129264009	-2.405361527517
Cl	3.088778923626	0.216844027254	2.363511453637
N	1.328598293030	-0.054847871048	-0.075222888288
N	2.774738965265	2.092149102319	-0.158556058402
N	3.042246591414	-1.986739528464	0.099950717844
N	5.086174799543	0.190610074727	0.043201316994
O	6.217288723373	0.254294696795	0.087546055118
C	-6.091945666331	1.514449641892	0.877539729207
C	-7.378972718433	0.812949276277	0.516753006441
C	-7.102624649004	-0.396566573464	-0.145514713025
C	-5.653539466293	-0.546674195506	-0.250695375306
C	-5.041008837341	0.573052329970	0.342133788848
C	-8.688284326685	1.199574140922	0.748396272904
C	-9.722006276685	0.370921131134	0.315112918579
C	-9.447560654449	-0.829279392206	-0.342069280988
C	-8.135740258735	-1.223395719444	-0.577910875611
C	-4.877077310649	-1.559741246213	-0.805472976378
C	-3.496783092941	-1.450706561168	-0.756286193122
C	-2.875020799128	-0.335711448392	-0.172673163273
C	-3.667700133758	0.685154186306	0.376878023371
C	-1.410808357768	-0.238158116514	-0.139312213145
C	-0.612952414271	-1.388354892891	-0.051954750439
C	0.763199804721	-1.270641040394	-0.022197272645
C	0.609458506685	1.074743546885	-0.157888560627
C	-0.769882764930	1.008123589150	-0.192505616422
C	1.429872426432	2.292225878607	-0.211355573563
C	3.601701982305	3.139947892516	-0.200229963176
C	3.133529625493	4.439839705298	-0.296847752900
C	1.767023401503	4.658706312468	-0.352112819838
C	0.907278863515	3.571087036775	-0.308709056257
C	1.736009610727	-2.367079319275	0.077504626161
C	4.000349869014	-2.912729926504	0.189539315159
C	3.708173725853	-4.264553302712	0.262151758835
C	2.383103482029	-4.666974913256	0.239327990835
C	1.387539017827	-3.705796189957	0.145212099107
H	3.840064132336	5.255753276111	-0.327511214838
H	-1.073242010959	-2.360414360048	0.019225489234
H	4.515896391719	-4.977454461482	0.333962159602
H	-0.161108560618	3.716291960012	-0.350795734713
H	-1.350587236415	1.911349750966	-0.285366914731
H	4.658955492231	2.931972284499	-0.156105345355
H	5.020408969149	-2.562890197667	0.202110494728
H	0.348371405832	-3.995386533478	0.124302040245
H	2.122951687318	-5.714413468546	0.293097305668
H	1.370494285914	5.661019785325	-0.428030812506
H	-10.749898337330	0.660900946916	0.490032482570
H	-7.926243392058	-2.154817856203	-1.088142069319
H	-10.264850781476	-1.457944028666	-0.670509215023
H	-8.910291637188	2.129044701414	1.257637951142
H	-3.205781064822	1.538800735660	0.855031375568
H	-5.335497566821	-2.420574241297	-1.273700097650
H	-2.892636622572	-2.226029440318	-1.206736369662
H	-6.022561186401	2.504720601516	0.419573744111
H	-5.994029562949	1.659628017549	1.956732594307

Energies (a.u.)	
E	-2388.704426
Zero-point correction	0.411359
Sum of electronic and thermal enthalpies	-2388.262909
Sum of electronic and thermal free energies	-2388.356082

Selected molecular parameters	
Ru-$N_{(NO)}$	1.750 Å
Ru-$O_{(NO)}$	2.883 Å
N-O	1.134 Å
Ru-Cl_1	2.396 Å
Ru-Cl_2	2.397 Å
Ru-N_{tpy1}	2.018 Å
Ru-N_{tpy2}	2.094 Å
Ru-N_{tpy3}	2.092 Å
∠Ru-N-O	179.519 °
∠Ru-O-N	0.292 °

NO stretching vibration	
ν_{NO} (cm^{-1})	1936.94 cm^{-1}

Electronic structure

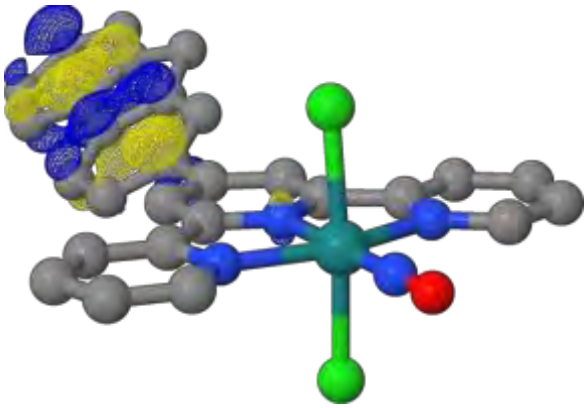

HOMO

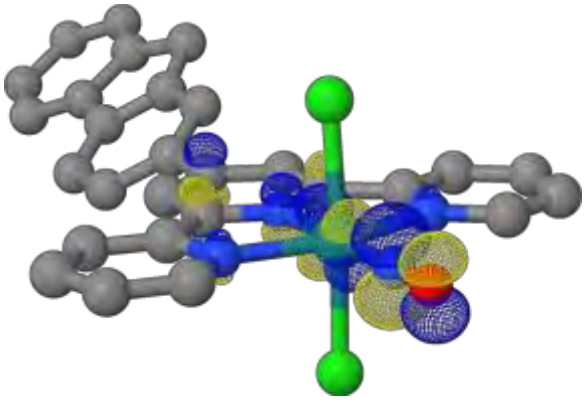

LUMO

Table AC20. Optimized Cartesian coordinates, energies, molecular parameters and electronic structure of the **MS2** isomer of complex **4**, *trans*(Cl,Cl)-[$RuCl_2(NO)(FT)]^+$, at the B3LYP-D3BJ/**BS1** level of theory in its ground state (singlet) in acetonitrile.

Ru	-0.598712108180	-4.672421127202	0.079913771304
Cl	-1.111114877145	-4.779730629433	-2.257264570485
Cl	-0.272646888292	-4.494187445487	2.444484653650
N	-0.959144108628	-2.706060278145	0.016364620352
N	1.329698480917	-3.804177163575	-0.308256798122
N	-2.646925486575	-4.624553131737	0.442253390228
N	0.435688616419	-6.290756037644	-0.012851814143
O	-0.596668474943	-6.797683945769	0.206509653195
C	-0.368572274225	4.915471921900	0.587572041153
C	-1.284970604944	6.076278801721	0.285696612333
C	-2.514662664556	5.607144616357	-0.210045152224
C	-2.467970396420	4.147941895846	-0.259288430866
C	-1.208558865953	3.722419815178	0.202924285971
C	-1.063122362368	7.435158890983	0.432706912021
C	-2.077144336929	8.324992556415	0.082362221744
C	-3.297731045783	7.859373651175	-0.408548360620
C	-3.527105644095	6.496812344674	-0.558719040483
C	-3.418856010099	3.215337040570	-0.663296709637
C	-3.108627183543	1.866858708475	-0.593336456855
C	-1.854201959614	1.431560937315	-0.138157899810
C	-0.898109363806	2.380755321319	0.258336378877
C	-1.543519140252	-0.001214743436	-0.082102695890
C	-2.542867439866	-0.953406679276	0.157455597993
C	-2.233438475865	-2.297381504653	0.201593067679
C	0.027760920403	-1.825949616238	-0.212150251925
C	-0.239629415883	-0.470251904739	-0.266005008649
C	1.331472992740	-2.450802812707	-0.396033197613
C	2.483001378880	-4.462232521043	-0.458617879234
C	3.679847965968	-3.810495232118	-0.703377045556
C	3.690736946431	-2.428908405459	-0.796279314893
C	2.498499222452	-1.742695098322	-0.639068289476
C	-3.185296139611	-3.379743226203	0.448292452763
C	-3.422808843795	-5.690359835418	0.658694772275
C	-4.780833711508	-5.563965546750	0.891980867805
C	-5.347462773911	-4.299321765177	0.900679249533
C	-4.539413156161	-3.195710966812	0.675910057697
H	4.581441175681	-4.393654279352	-0.816876637952
H	-3.558554693307	-0.638351840085	0.332484673724
H	-5.371660854658	-6.451294657555	1.062559878663
H	2.473763376937	-0.666316626231	-0.704030211980
H	0.559697625968	0.220544314634	-0.478070880051
H	2.458678047848	-5.535705482469	-0.383183970059
H	-2.947894098265	-6.657258178610	0.644345113332
H	-4.957995976838	-2.201724690654	0.679158267380
H	-6.405078191739	-4.169882324944	1.080200340858
H	4.608835477367	-1.891817377826	-0.986626922184
H	-1.917055824281	9.389651183667	0.192386877790
H	-4.475319094850	6.139586972643	-0.939437095932
H	-4.072002600174	8.567077365676	-0.674411968132
H	-0.119332889568	7.804969168492	0.813464726740
H	0.064394980954	2.062098336850	0.636399879009
H	-4.386230084685	3.528753738795	-1.032530994637
H	-3.838432388808	1.143126972914	-0.929049025764
H	0.558152217002	4.963603547579	0.009640813425
H	-0.080407975842	4.885457971892	1.641796445681

Energies (a.u.)	
E	-2388.651589
Zero-point correction	0.409892
Sum of electronic and thermal enthalpies	-2388.211253
Sum of electronic and thermal free energies	-2388.305293

Selected molecular parameters	
Ru-$N_{(NO)}$	1.923 Å
Ru-$O_{(NO)}$	2.129 Å
N-O	1.171 Å
Ru-Cl_1	2.395 Å
Ru-Cl_2	2.394 Å
Ru-N_{tpy1}	2.000 Å
Ru-N_{tpy2}	2.150 Å
Ru-N_{tpy3}	2.081 Å
∠Ru-N-O	83.168 °
∠Ru-O-N	63.737 °

NO stretching vibration	
ν_{NO} (cm^{-1})	1655.52 cm^{-1}

Electronic structure

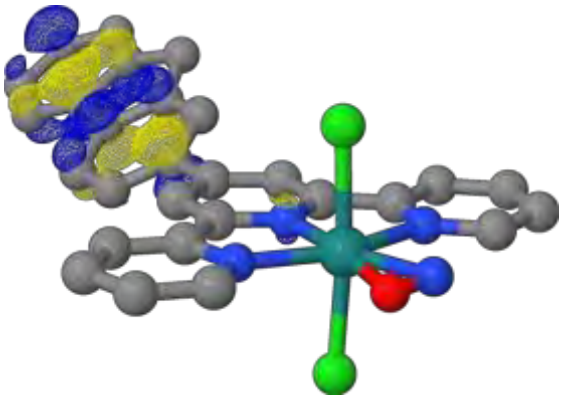

HOMO

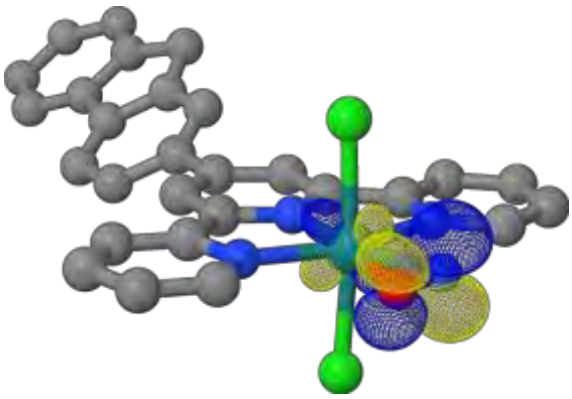

LUMO

Table AC21. Optimized Cartesian coordinates, energies, molecular parameters and electronic structure of the **MS1** isomer of complex **4**, *trans*(Cl,Cl)-[$RuCl_2(NO)(FT)]^+$, at the B3LYP-D3BJ/**BS1** level of theory in its ground state (singlet) in acetonitrile.

Ru	3.320350717393	0.080266275169	-0.018287876907
Cl	3.324106561158	-0.058557910326	-2.402843148242
Cl	3.160332635136	0.215967331385	2.362907501416
N	1.353647659278	-0.051265645770	-0.073020952778
N	2.790933266373	2.096938547679	-0.156384891215
N	3.057563880973	-1.987721955812	0.090470712328
N	6.296254459377	0.243037688677	0.109596700896
O	5.175074324945	0.189307775371	0.051131862215
C	-6.074170934760	1.522978736249	0.864711401265
C	-7.360093239471	0.816435160046	0.509805765356
C	-7.081736465592	-0.398695421970	-0.141348130917
C	-5.632611667324	-0.547611598705	-0.244699944846
C	-5.021661059204	0.578082713534	0.338558140683
C	-8.670065328521	1.203125036710	0.737466886313
C	-9.702350369562	0.368827955221	0.311607582282
C	-9.425896694506	-0.837029139672	-0.334338674769
C	-8.113455034260	-1.231198880197	-0.566293212103
C	-4.854574037608	-1.564399403148	-0.790508050002
C	-3.474619961281	-1.453127203145	-0.741641485767
C	-2.853998812561	-0.332707674366	-0.166654503301
C	-3.648558532373	0.691902537372	0.373553378142
C	-1.390168058453	-0.234329422879	-0.133044504340
C	-0.591355094291	-1.383594010985	-0.046769497860
C	0.784551716275	-1.269496263065	-0.019184937706
C	0.630902337450	1.080592907702	-0.153693145076
C	-0.747951113927	1.011041378141	-0.185936314478
C	1.447545250588	2.300033285934	-0.208872411080
C	3.618996016847	3.141784705496	-0.201823104349
C	3.154052741625	4.443348666507	-0.301441401667
C	1.787635991349	4.664690656706	-0.355908317769
C	0.925147599712	3.579037429632	-0.308936239048
C	1.752924633776	-2.369514742263	0.075519753191
C	4.016258336349	-2.911967591498	0.168682168920
C	3.727040351198	-4.265056604895	0.240579514604
C	2.401762342621	-4.668495140012	0.228111152976
C	1.403962046458	-3.708419055935	0.142981502524
H	3.861548166547	5.258370001523	-0.335264027659
H	-1.050178583187	-2.356352698606	0.024706805889
H	4.535434802017	-4.978088343173	0.303686217114
H	-0.142962192806	3.726757832326	-0.350984005288
H	-1.327385561646	1.915241119750	-0.277669299208
H	4.676772842521	2.932049342325	-0.158149197292
H	5.036741433884	-2.560553360397	0.172027561729
H	0.365021035446	-3.999440029880	0.128756280489
H	2.143342475118	-5.716369219393	0.282184023041
H	1.393318302590	5.667714644317	-0.434358927300
H	-10.730742529925	0.658775861206	0.483594617111
H	-7.902350372532	-2.167013490692	-1.067733621837
H	-10.242132351964	-1.470038133567	-0.656996066712
H	-8.893738525183	2.136890750052	1.238031915412
H	-3.188220513015	1.550164796615	0.844851088422
H	-5.311648940481	-2.429725738427	-1.251704406304
H	-2.869705575709	-2.231424285686	-1.185759821417
H	-6.005889007113	2.508989692973	0.397480142503
H	-5.977048369751	1.678398085846	1.942537442416

Energies (a.u.)	
E	-2388.635740
Zero-point correction	0.410443
Sum of electronic and thermal enthalpies	-2388.194914
Sum of electronic and thermal free energies	-2388.288570

Selected molecular parameters	
Ru-$O_{(NO)}$	1.859 Å
Ru-$N_{(NO)}$	2.983 Å
N-O	1.124 Å
Ru-Cl_1	2.389 Å
Ru-Cl_2	2.390 Å
Ru-N_{tpy1}	1.972 Å
Ru-N_{tpy2}	2.090 Å
Ru-N_{tpy3}	2.087 Å
∠Ru-N-O	0.652 °
∠Ru-O-N	178.954 °

NO stretching vibration	
ν_{NO} (cm^{-1})	1922.38 cm^{-1}

Electronic structure

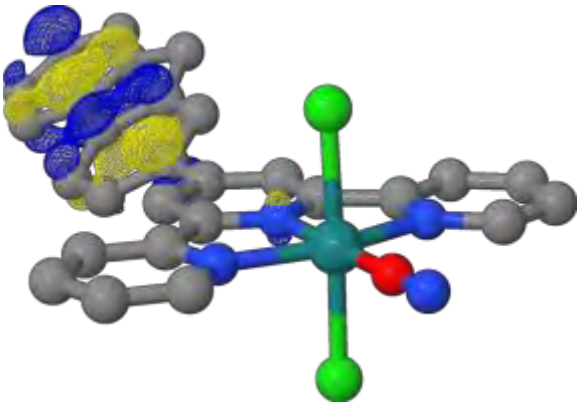

HOMO

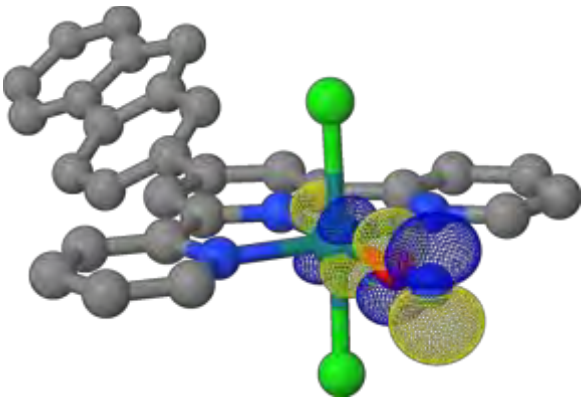

LUMO

Table AC22. Optimized Cartesian coordinates, energies, molecular parameters and electronic structure of the ^{3}**GS** triplet state of complex **4**, *trans*(Cl,Cl)-[$RuCl_2$(NO)(FT)]$^{+}$, at the B3LYP-D3BJ/**BS1** level of theory in acetonitrile.

Ru	3.318919000000	0.078384000000	-0.042987000000
Cl	3.404287000000	-0.069154000000	-2.380637000000
Cl	3.193370000000	0.220919000000	2.283587000000
N	1.318683000000	-0.058948000000	-0.121093000000
N	2.776991000000	2.095443000000	-0.192602000000
N	3.046296000000	-1.995011000000	0.074790000000
N	5.251896000000	0.217571000000	0.068320000000
O	6.103884000000	0.321834000000	0.841414000000
C	-6.093705000000	1.500985000000	0.912104000000
C	-7.384059000000	0.806831000000	0.548387000000
C	-7.113237000000	-0.394053000000	-0.131400000000
C	-5.664316000000	-0.545149000000	-0.246193000000
C	-5.047090000000	0.565097000000	0.358513000000
C	-8.691409000000	1.193003000000	0.791596000000
C	-9.729257000000	0.372588000000	0.352254000000
C	-9.460316000000	-0.819052000000	-0.322209000000
C	-8.150214000000	-1.212610000000	-0.569666000000
C	-4.892174000000	-1.550886000000	-0.819174000000
C	-3.510889000000	-1.443013000000	-0.777841000000
C	-2.885028000000	-0.337731000000	-0.182098000000
C	-3.672836000000	0.674789000000	0.387542000000
C	-1.418192000000	-0.240713000000	-0.158650000000
C	-0.621784000000	-1.390712000000	-0.068572000000
C	0.757181000000	-1.272893000000	-0.051807000000
C	0.603376000000	1.070521000000	-0.198735000000
C	-0.778648000000	1.004839000000	-0.222905000000
C	1.427966000000	2.288082000000	-0.256171000000
C	3.603444000000	3.144842000000	-0.238865000000
C	3.134080000000	4.441504000000	-0.349483000000
C	1.765604000000	4.653873000000	-0.414852000000
C	0.906050000000	3.566086000000	-0.367753000000
C	1.734304000000	-2.368838000000	0.050158000000
C	4.002814000000	-2.924580000000	0.161174000000
C	3.707388000000	-4.274278000000	0.232224000000
C	2.379017000000	-4.670125000000	0.210314000000
C	1.384787000000	-3.707325000000	0.116921000000
H	3.836659000000	5.260589000000	-0.383574000000
H	-1.084266000000	-2.361205000000	0.013122000000
H	4.511101000000	-4.991818000000	0.301800000000
H	-0.161906000000	3.711291000000	-0.419485000000
H	-1.361659000000	1.907124000000	-0.313617000000
H	4.659715000000	2.931588000000	-0.186953000000
H	5.022253000000	-2.571671000000	0.171102000000
H	0.345577000000	-3.996618000000	0.094877000000
H	2.115420000000	-5.716869000000	0.263185000000
H	1.367128000000	5.654582000000	-0.502413000000
H	-10.755662000000	0.662432000000	0.535959000000
H	-7.945247000000	-2.137513000000	-1.093495000000
H	-10.280381000000	-1.441707000000	-0.655249000000
H	-8.908842000000	2.116089000000	1.314320000000
H	-3.206489000000	1.521155000000	0.874619000000
H	-5.354131000000	-2.405018000000	-1.296268000000
H	-2.909404000000	-2.212099000000	-1.242720000000
H	-6.024851000000	2.497328000000	0.467363000000
H	-5.990205000000	1.631435000000	1.992685000000

Energies (a.u.)	
E	-2388.662558
Zero-point correction	0.408980
Sum of electronic and thermal enthalpies	-2388.222741
Sum of electronic and thermal free energies	-2388.317717

Selected molecular parameters	
Ru-$N_{(NO)}$	1.941 Å
Ru-$O_{(NO)}$	2.932 Å
N-O	1.155 Å
Ru-Cl_1	2.344 Å
Ru-Cl_2	2.334 Å
Ru-N_{tpy1}	2.006 Å
Ru-N_{tpy2}	2.094 Å
Ru-N_{tpy3}	2.095 Å
∠Ru-N-O	141.194 °
∠Ru-O-N	24.512 °

NO stretching vibration	
ν_{NO} (cm^{-1})	1809.54 cm^{-1}

Electronic structure

<S^2>: 2.0141

Mulliken Spin Populations: Ru: 0.9097 Cl_1: 0.1218 Cl_2: 0.1044 $N_{(NO)}$: 0.4988 $O_{(NO)}$: 0.3075

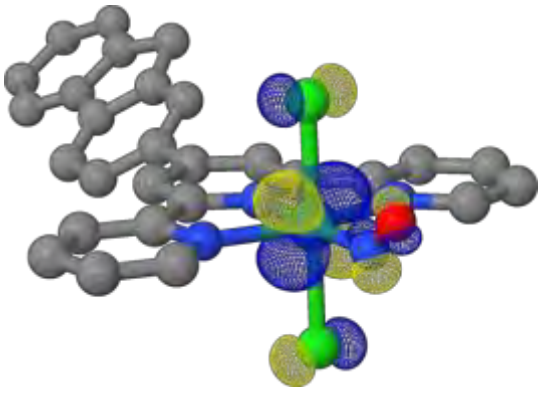

SONO (Hole)

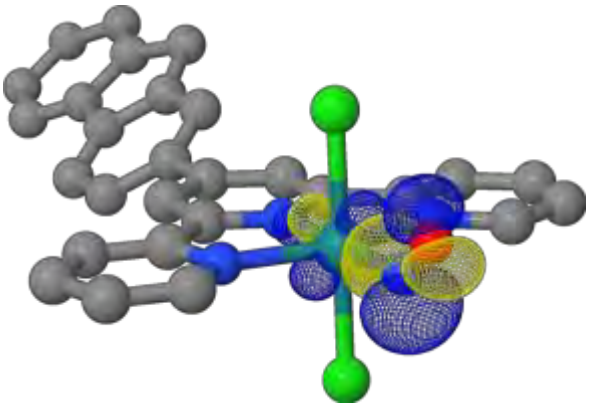

SONO (Particle)

Table AC23. Optimized Cartesian coordinates, energies, molecular parameters and electronic structure of the ^{3}**MS2** triplet state of complex **4**, *trans*(Cl,Cl)-[$RuCl_2(NO)(FT)]^+$, at the B3LYP-D3BJ/**BS1** level of theory in acetonitrile.

Ru	-0.593234887081	-4.621430764340	0.087213384591
Cl	-0.996030437516	-4.806318057752	-2.197246432157
Cl	-0.202303476264	-4.478146271296	2.376839054394
N	-0.979399291895	-2.689816139520	0.014560681535
N	1.336030462211	-3.806072635771	-0.305839971766
N	-2.643695357968	-4.625964135832	0.444728135354
N	0.482159652344	-6.515248196273	0.038152845511
O	-0.669050012296	-6.778378387172	0.252786278956
C	-0.370913225016	4.918172393264	0.591405684980
C	-1.283706604491	6.082014087905	0.290399593960
C	-2.513595403269	5.617156775526	-0.209066420255
C	-2.470534271705	4.158079330555	-0.261565546422
C	-1.213288341391	3.728216180719	0.202475125943
C	-1.058790394634	7.439930705372	0.441310496753
C	-2.069934441778	8.333147043993	0.091229301233
C	-3.290734694953	7.871811952474	-0.403274965599
C	-3.523174402943	6.510258857998	-0.557458770234
C	-3.422825720605	3.228697107419	-0.670108672239
C	-3.116282618099	1.879365733069	-0.602345683751
C	-1.864318922287	1.439593349277	-0.144359069734
C	-0.906590270891	2.385622077329	0.255934423861
C	-1.558981063937	0.005431904937	-0.086786024671
C	-2.561581748928	-0.941135172318	0.153690198122
C	-2.252235741375	-2.287558220022	0.199285405691
C	0.017532986880	-1.817647681302	-0.216204476116
C	-0.251227787717	-0.463956037422	-0.271442839286
C	1.326967238373	-2.448690197288	-0.399221098255
C	2.486532222519	-4.467735098047	-0.458344024962
C	3.680865095484	-3.813726145365	-0.710943906622
C	3.684626556857	-2.432492794723	-0.808033821759
C	2.491550481269	-1.743068805527	-0.649240495418
C	-3.192492376785	-3.380626909291	0.446218413809
C	-3.415717480776	-5.694814883881	0.661690376214
C	-4.775045673803	-5.575660950421	0.891232342343
C	-5.349499937927	-4.313888113020	0.895406913363
C	-4.548582748889	-3.205267444157	0.669867141143
H	4.585099221777	-4.392184700730	-0.827308033664
H	-3.576190583026	-0.622354894332	0.328398246166
H	-5.362447840123	-6.465168888208	1.062695386671
H	2.469573042897	-0.666936285999	-0.720095469302
H	0.545877341516	0.229604718691	-0.483680839884
H	2.445668320856	-5.540123992489	-0.375989282155
H	-2.931121557940	-6.657069645929	0.650359046717
H	-4.973943928214	-2.213980276387	0.669311658714
H	-6.408437771757	-4.190871141688	1.072024605347
H	4.600595458007	-1.893640859464	-1.004332032556
H	-1.907456284546	9.397117614205	0.204338530108
H	-4.471541587128	6.156354195844	-0.940856542261
H	-4.062741519573	8.582129722881	-0.668735555185
H	-0.114876359000	7.806439844198	0.824926181255
H	0.054108319167	2.063995321547	0.636034309512
H	-4.388357078411	3.545448908448	-1.041332006955
H	-3.846929214681	1.158087298478	-0.941510073873
H	0.556992142123	4.965160572765	0.015277126295
H	-0.084775482661	4.885098029071	1.646085166539

Energies (a.u.)	
E	-2388.632530
Zero-point correction	0.408481
Sum of electronic and thermal enthalpies	-2388.193174
Sum of electronic and thermal free energies	-2388.288460

Selected molecular parameters	
Ru-$N_{(NO)}$	2.178 Å
Ru-$O_{(NO)}$	2.165 Å
N-O	1.200 Å
Ru-Cl_1	2.327 Å
Ru-Cl_2	2.327 Å
Ru-N_{tpy1}	1.971 Å
Ru-N_{tpy2}	2.131 Å
Ru-N_{tpy3}	2.081 Å
∠Ru-N-O	73.326 °
∠Ru-O-N	74.590 °

NO stretching vibration	
ν_{NO} (cm^{-1})	1567.05 cm^{-1}

Electronic structure

$<S^2>$: 2.0078

Mulliken Spin Populations: Ru: 0.7290 Cl_1: 0.1250 Cl_2: 0.1247 $N_{(NO)}$: 0.7508 $O_{(NO)}$: 0.2589

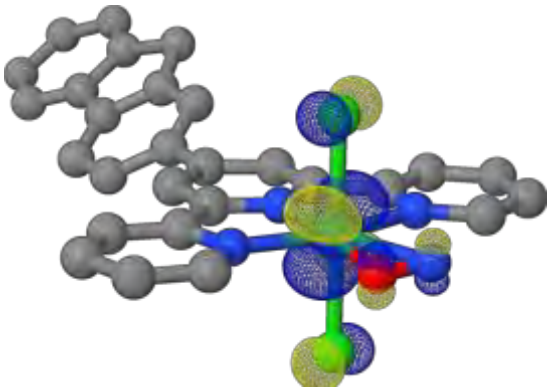

SONO (Hole)

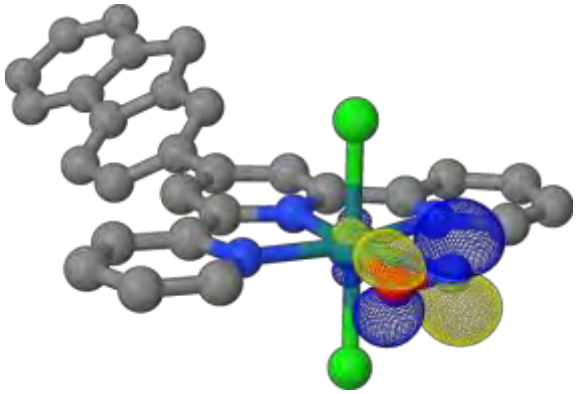

SONO (Particle)

Table AC24. Optimized Cartesian coordinates, energies, molecular parameters and electronic structure of the ^{3}**MS1** triplet state of complex **4**, *trans*(Cl,Cl)-[$RuCl_2(NO)(FT)]^+$, at the B3LYP-D3BJ/**BS1** level of theory in acetonitrile.

Ru	3.279520050456	0.090987141640	-0.054746632886
Cl	3.388005133703	-0.047598583189	-2.383349527220
Cl	3.291977413514	0.237169612116	2.274184287387
N	1.340224093593	-0.049780570768	-0.091123224446
N	2.784866304310	2.113303376284	-0.195060238441
N	3.063735615608	-1.984871931519	0.071939954450
N	6.296907917705	-0.073519232945	0.655456456442
O	5.469323367552	0.358265230649	-0.017117001374
C	-6.081438313153	1.497798004378	0.912470528932
C	-7.369794973896	0.804291480654	0.540439239509
C	-7.095194869773	-0.395219558371	-0.140279642450
C	-5.645580078943	-0.545903338538	-0.247662192775
C	-5.031768313291	0.563212207653	0.362416436444
C	-8.678438890529	1.190014385952	0.777266381644
C	-9.713949832729	0.370584059955	0.330574125204
C	-9.441300028752	-0.819668489548	-0.344792771112
C	-8.129829258533	-1.212776504317	-0.585858649739
C	-4.870020187235	-1.550030156905	-0.818807796977
C	-3.488943725656	-1.441246149809	-0.771029007181
C	-2.866363633216	-0.337036186758	-0.169926843261
C	-3.657661957745	0.673394269473	0.398533580701
C	-1.399660336150	-0.238078906514	-0.140575808509
C	-0.600428477746	-1.385335605404	-0.054477528846
C	0.778320280986	-1.269069906752	-0.032327984597
C	0.619174976868	1.082124025064	-0.172848879568
C	-0.761509701779	1.008257224709	-0.199531632609
C	1.435884553300	2.304593374442	-0.237093346152
C	3.609710432841	3.161309015194	-0.253009510916
C	3.138291413914	4.458773227886	-0.353214889452
C	1.768259877889	4.669666551974	-0.395637989670
C	0.908897124490	3.581761263350	-0.337412625028
C	1.754421440840	-2.364747044657	0.062091508987
C	4.022986599677	-2.909039510403	0.159584633749
C	3.734952715586	-4.260277898549	0.241037529987
C	2.407575183508	-4.661717262603	0.228772138533
C	1.408014482085	-3.704126981697	0.138357327002
H	3.838345038693	5.279616971285	-0.396742094150
H	-1.059333741488	-2.358275622744	0.018969250202
H	4.541280260625	-4.974869638067	0.311207533098
H	-0.159726868735	3.727721116491	-0.371246088436
H	-1.345330478159	1.910008701353	-0.290911491258
H	4.667010434925	2.944847891136	-0.218762689087
H	5.041394592667	-2.550839003098	0.166389046147
H	0.369843524562	-3.998019002976	0.127707953487
H	2.149184979057	-5.709403112478	0.289034920293
H	1.368020378489	5.670492663585	-0.473994590928
H	-10.741335853517	0.660141925572	0.509188879516
H	-7.922079922332	-2.136615988842	-1.110473792188
H	-10.259520886963	-1.441618628983	-0.683654297737
H	-8.898681564353	2.112089115280	1.300620060125
H	-3.194177980104	1.518995395908	0.889682921918
H	-5.329121261323	-2.403448424775	-1.299961682259
H	-2.884896329169	-2.208836722796	-1.235061567570
H	-6.010367340086	2.495087755639	0.470193634012
H	-5.983720382084	1.626021976381	1.993863689053

Energies (a.u.)	
E	-2388.635437
Zero-point correction	0.407878
Sum of electronic and thermal enthalpies	-2388.196113
Sum of electronic and thermal free energies	-2388.292483
Selected molecular parameters	
Ru-$N_{(NO)}$	3.104 Å
Ru-$O_{(NO)}$	2.206 Å
N-O	1.151 Å
Ru-Cl_1	2.335 Å
Ru-Cl_2	2.334 Å
Ru-N_{tpy1}	1.945 Å
Ru-N_{tpy2}	2.087 Å
Ru-N_{tpy3}	2.091 Å
∠Ru-N-O	31.479 °
∠Ru-O-N	132.720 °
NO stretching vibration	
ν_{NO} (cm^{-1})	1851.05 cm^{-1}

Electronic structure

$<S^2>$: 2.0087

Mulliken Spin Populations: Ru: 0.8463 Cl_1: 0.0927 Cl_2: 0.0899 $N_{(NO)}$: 0.7625 $O_{(NO)}$: 0.1861

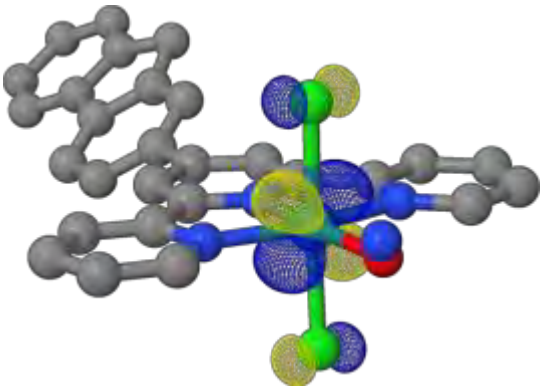

SONO (Hole)

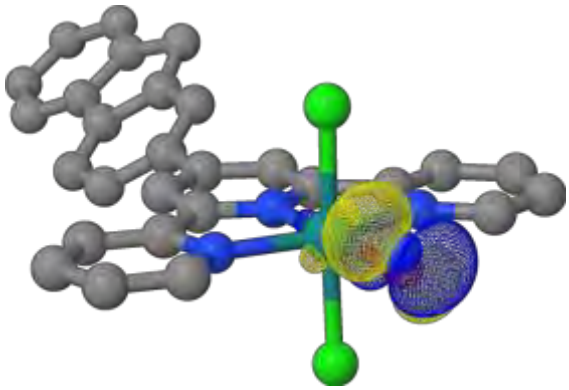

SONO (Particle)

Table AC25. Optimized Cartesian coordinates, energies, molecular parameters and electronic structure of the **GS** isomer of complex **5**, *trans*(Cl,Cl)-[$RuCl_2(NO)(terpy)]^+$, at the B3LYP-D3BJ/**BS1** level of theory in its ground state (singlet) in acetonitrile.

Ru	3.357890271540	0.053255546088	-0.064310339557
Cl	3.164927322618	-0.093485861994	-2.446305574416
Cl	3.197835777316	0.178841227651	2.321449916429
N	5.103754308541	0.153768920166	-0.079328459795
N	1.336339062603	-0.071681461965	-0.042387359164
N	2.802406498544	2.067849188780	-0.173899509015
N	3.056402489181	-2.013079303646	0.055681003096
O	6.235363069170	0.211707463926	-0.084683825733
C	0.630229540401	1.066783231533	-0.098076541729
C	1.457937434037	2.277028683294	-0.173408540488
H	-2.445361058021	-0.303138912244	0.008951720053
C	3.170607980024	4.414019157694	-0.309053294897
H	3.880957304551	5.225511462198	-0.361174938185
C	0.776294604899	-1.287889770402	0.030109362316
C	-0.606963176484	-1.398400660679	0.049654766708
H	-1.085580430275	-2.363243262923	0.107900501418
C	3.715766563418	-4.294930143702	0.183266730222
H	4.522105170118	-5.012004130914	0.220832273821
C	1.748420223351	-2.386995634564	0.083749520296
C	-1.366959770532	-0.237312946276	-0.006019763841
C	0.939942527522	3.559583531295	-0.241227098192
H	-0.128303267658	3.711631469302	-0.241126961767
C	-0.755911357246	1.007543245292	-0.080171899385
H	-1.349268517959	1.907170926848	-0.122265305533
C	3.633926562138	3.110245996424	-0.240180698599
H	4.690795651219	2.895948347648	-0.238682611650
C	4.012149344982	-2.944000075561	0.104549106842
H	5.033865444321	-2.599880006784	0.078930903266
C	1.395427634558	-3.723976691892	0.159745913404
H	0.354707184749	-4.007844024010	0.179757005323
C	2.389085856227	-4.690734602921	0.210539760322
H	2.125866972157	-5.737052988834	0.270244691446
C	1.804757647131	4.642179447247	-0.309583744927
H	1.412272132859	5.647518633928	-0.362531708088

Energies (a.u.)	
E	-1888.250551
Zero-point correction	0.243636
Sum of electronic and thermal enthalpies	-1887.986484
Sum of electronic and thermal free energies	-1888.055829

Selected molecular parameters	
$Ru\text{-}N_{(NO)}$	1.749 Å
$Ru\text{-}O_{(NO)}$	2.882 Å
N-O	1.133 Å
$Ru\text{-}Cl_1$	2.394 Å
$Ru\text{-}Cl_2$	2.394 Å
$Ru\text{-}N_{tpy1}$	2.026 Å
$Ru\text{-}N_{tpy2}$	2.092 Å
$Ru\text{-}N_{tpy3}$	2.093 Å
∠Ru-N-O	179.574 °
∠Ru-O-N	0.258 °

NO stretching vibration	
ν_{NO} (cm^{-1})	1941.06 cm^{-1}

Electronic structure

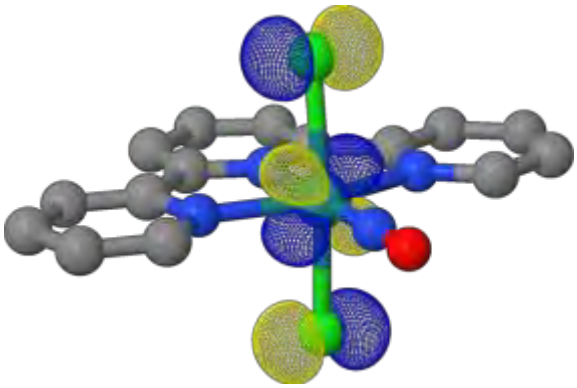

HOMO

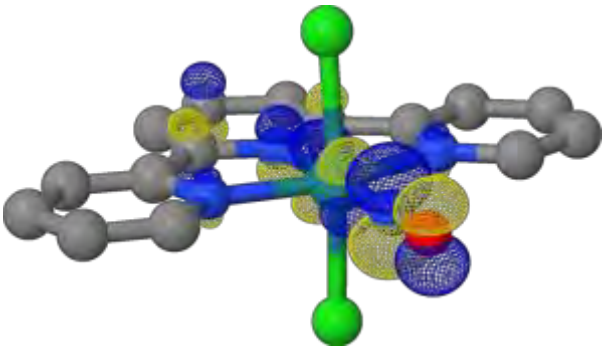

LUMO

Table AC26. Optimized Cartesian coordinates, energies, molecular parameters and electronic structure of the **MS2** isomer of complex **5**, *trans*(Cl,Cl)-[$RuCl_2(NO)(terpy)]^+$, at the B3LYP-D3BJ/**BS1** level of theory in its ground state (singlet) in acetonitrile.

Ru	3.356327560346	-0.043577318018	-0.036672495010
Cl	3.320862655653	-0.268339453048	-2.418546866269
Cl	3.289272691265	0.003109118313	2.356064235434
N	5.115543429941	0.736914050167	-0.060223620994
N	1.352260564298	-0.089616866822	-0.036084133770
N	2.796484496703	2.026642894690	-0.165716455852
N	3.003983887927	-2.090129887010	0.075459282522
O	5.456066222501	-0.380547399605	0.000165061422
C	0.640363897334	1.045813343881	-0.092233179338
C	1.458581049294	2.247740053447	-0.168733144333
H	-2.454992872116	-0.288940160342	0.012446019938
C	3.161152718392	4.376422347384	-0.323851959305
H	3.875709299365	5.183571404922	-0.385435366147
C	0.762506247688	-1.302257247342	0.036696455335
C	-0.620129499124	-1.394045298883	0.055122374947
H	-1.100703930448	-2.357712074029	0.114415775049
C	3.609919873745	-4.382742267270	0.196688401046
H	4.398611498706	-5.118937697635	0.236067824042
C	1.691003737714	-2.429203424358	0.093342235120
C	-1.376339370997	-0.232256130285	-0.001876509367
C	0.935814115970	3.529638168919	-0.245414855383
H	-0.132556876798	3.678104820772	-0.245794969976
C	-0.747677648699	0.998592248353	-0.076394394534
H	-1.325032908106	1.908125340543	-0.120940670161
C	3.623181948570	3.073316820709	-0.243854085467
H	4.681188003140	2.875188043347	-0.243577999884
C	3.940906780976	-3.040699108945	0.125272958501
H	4.969748398657	-2.721446662209	0.107206444875
C	1.303351641377	-3.757354118813	0.161257239343
H	0.256374524268	-4.016469006852	0.173096104654
C	2.273148604933	-4.746661163591	0.214506477251
H	1.984891121893	-5.786623938870	0.268634226463
C	1.796669401159	4.611498370912	-0.323346662754
H	1.405608734473	5.616893197569	-0.383988747399

Energies (a.u.)	
E	-1888.197554
Zero-point correction	0.242342
Sum of electronic and thermal enthalpies	-1887.934549
Sum of electronic and thermal free energies	-1888.004058
Selected molecular parameters	
$Ru\text{-}N_{(NO)}$	1.925 Å
$Ru\text{-}O_{(NO)}$	2.127 Å
N-O	1.170 Å
$Ru\text{-}Cl_1$	2.393 Å
$Ru\text{-}Cl_2$	2.394 Å
$Ru\text{-}N_{tpy1}$	2.005 Å
$Ru\text{-}N_{tpy2}$	2.080 Å
$Ru\text{-}N_{tpy3}$	2.148 Å
∠Ru-N-O	82.996 °
∠Ru-O-N	63.920 °
NO stretching vibration	
ν_{NO} (cm^{-1})	1661.20 cm^{-1}

Electronic structure

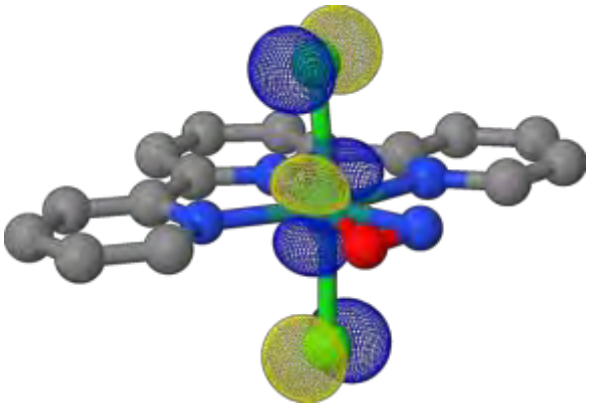

HOMO

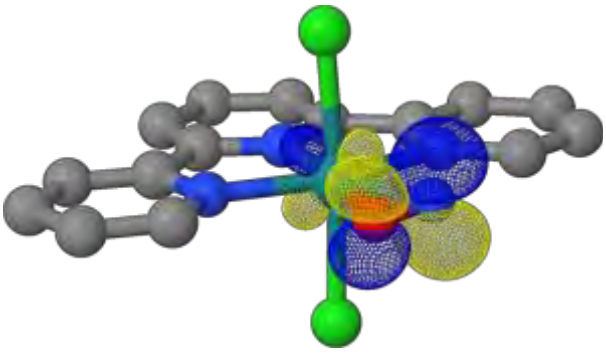

LUMO

Table AC27. Optimized Cartesian coordinates, energies, molecular parameters and electronic structure of the **MS1** isomer of complex **5**, *trans*(Cl,Cl)-[$RuCl_2(NO)(terpy)]^+$, at the B3LYP-D3BJ/**BS1** level of theory in its ground state (singlet) in acetonitrile.

Ru	3.313201719652	0.051041178755	-0.060203184946
Cl	3.216872788801	-0.089630223046	-2.441587645719
Cl	3.236763329562	0.186000926031	2.323058252505
N	1.338065890451	-0.070704220492	-0.039124932958
N	2.793424948775	2.071012431106	-0.175658884059
N	3.047665436936	-2.015912657013	0.056515105337
O	5.169486696749	0.150966829396	-0.067541918623
N	6.291519465588	0.198266542186	-0.063934126052
C	0.627693104364	1.069569647048	-0.094098413372
C	1.450323015683	2.282052702419	-0.175243995643
H	-2.448200176813	-0.301810098238	0.031131237686
C	3.162729658775	4.416241005232	-0.326446692771
H	3.873089199834	5.227347943041	-0.384954965981
C	0.774209808395	-1.289027764308	0.039484816114
C	-0.608735260232	-1.396045082821	0.065892232671
H	-1.085762315798	-2.361401392825	0.129314782541
C	3.709490130642	-4.297589590168	0.172235136439
H	4.516117943604	-5.014784950388	0.201719185222
C	1.741534957196	-2.391441348456	0.090326736238
C	-1.369928645952	-0.236210279893	0.010654459812
C	0.930873007837	3.564002491320	-0.249766852373
H	-0.137254579582	3.717216827327	-0.249421693631
C	-0.757814386961	1.007296965887	-0.069803335461
H	-1.350124497915	1.907668645181	-0.111621110051
C	3.624345878183	3.111649070244	-0.249950482233
H	4.681898816549	2.896993693364	-0.247794747183
C	4.003296692923	-2.945389922880	0.095102764232
H	5.025524641132	-2.600849200471	0.061450262600
C	1.387720914072	-3.728574099380	0.165651935560
H	0.347418492195	-4.013732220931	0.190746685569
C	2.382979053740	-4.694395816849	0.208231609450
H	2.121294662674	-5.741152394550	0.267417819922
C	1.796774680471	4.645427992145	-0.326083063710
H	1.405191928472	5.650832372024	-0.384751977128

Energies (a.u.)	
E	-1888.181780
Zero-point correction	0.242803
Sum of electronic and thermal enthalpies	-1887.918350
Sum of electronic and thermal free energies	-1887.988094

Selected molecular parameters	
$Ru\text{-}O_{(NO)}$	1.859 Å
$Ru\text{-}N_{(NO)}$	2.982 Å
N-O	1.123 Å
$Ru\text{-}Cl_1$	2.387 Å
$Ru\text{-}Cl_2$	2.388 Å
$Ru\text{-}N_{tpy1}$	1.979 Å
$Ru\text{-}N_{tpy2}$	2.089 Å
$Ru\text{-}N_{tpy3}$	2.087 Å
∠Ru-N-O	179.217 °
∠Ru-O-N	0.488 °

NO stretching vibration	
ν_{NO} (cm^{-1})	1929.06 cm^{-1}

Electronic structure

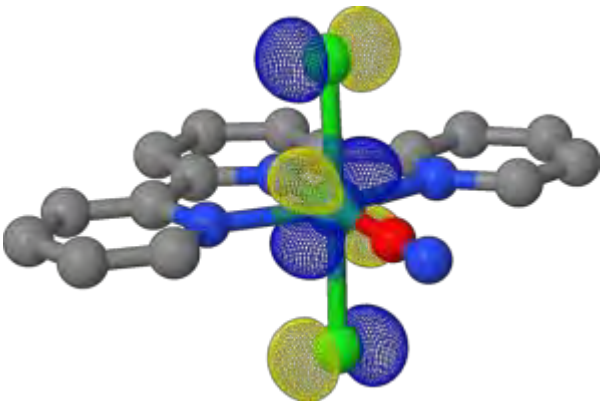

HOMO

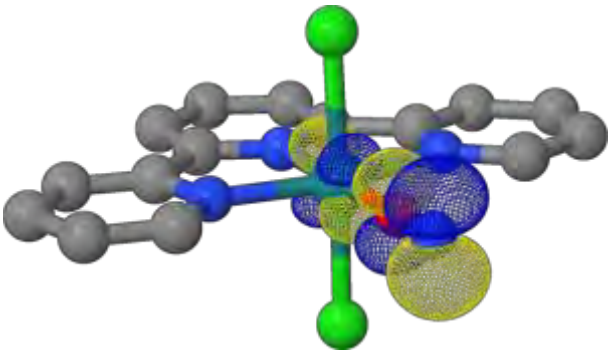

LUMO

Table AC28. Optimized Cartesian coordinates, energies, molecular parameters and electronic structure of the **^{3}GS** triplet state of complex **5**, *trans*(Cl,Cl)-[$RuCl_2(NO)(terpy)]^+$, at the B3LYP-D3BJ/**BS1** level of theory in acetonitrile.

Ru	3.318027000000	0.012221000000	-0.007908000000
Cl	3.322917000000	-0.130661000000	-2.338018000000
Cl	3.271754000000	0.148621000000	2.330672000000
N	5.256462000000	0.119324000000	-0.021260000000
N	1.310927000000	-0.096672000000	-0.018882000000
N	2.806033000000	2.037460000000	-0.135149000000
N	3.025427000000	-2.057230000000	0.107648000000
O	6.152764000000	0.123504000000	-0.749265000000
C	0.617155000000	1.046111000000	-0.097607000000
C	1.458897000000	2.250383000000	-0.157789000000
H	-2.471867000000	-0.300915000000	-0.070341000000
C	3.191643000000	4.380641000000	-0.264500000000
H	3.904964000000	5.190138000000	-0.304289000000
C	0.742798000000	-1.308215000000	0.035323000000
C	-0.642874000000	-1.409436000000	0.017861000000
H	-1.130697000000	-2.370636000000	0.062563000000
C	3.660120000000	-4.344914000000	0.248650000000
H	4.456002000000	-5.072479000000	0.302300000000
C	1.708909000000	-2.414620000000	0.110068000000
C	-1.393085000000	-0.242860000000	-0.056859000000
C	0.951864000000	3.536828000000	-0.235091000000
H	-0.114987000000	3.697391000000	-0.253042000000
C	-0.770932000000	0.997527000000	-0.116145000000
H	-1.357227000000	1.901086000000	-0.174889000000
C	3.645558000000	3.075832000000	-0.187110000000
H	4.699914000000	2.848668000000	-0.165531000000
C	3.971388000000	-2.998590000000	0.176159000000
H	4.995280000000	-2.659090000000	0.172128000000
C	1.343267000000	-3.748592000000	0.179460000000
H	0.300108000000	-4.024012000000	0.179500000000
C	2.326944000000	-4.724325000000	0.249401000000
H	2.051299000000	-5.767862000000	0.303830000000
C	1.825311000000	4.613353000000	-0.288689000000
H	1.439067000000	5.620868000000	-0.348258000000

Energies (a.u.)	
E	-1888.209445
Zero-point correction	0.241021
Sum of electronic and thermal enthalpies	-1887.947203
Sum of electronic and thermal free energies	-1888.019401
Selected molecular parameters	
$Ru\text{-}N_{(NO)}$	1.941 Å
$Ru\text{-}O_{(NO)}$	2.932 Å
N-O	1.155 Å
$Ru\text{-}Cl_1$	2.334 Å
$Ru\text{-}Cl_2$	2.343 Å
$Ru\text{-}N_{tpy1}$	2.093 Å
$Ru\text{-}N_{tpy2}$	2.010 Å
$Ru\text{-}N_{tpy3}$	2.093 Å
∠Ru-N-O	141.219 °
∠Ru-O-N	24.501 °
NO stretching vibration	
ν_{NO} (cm^{-1})	1812.58 cm^{-1}

Electronic structure

$\langle S^2 \rangle$: 2.0141

Mulliken Spin Populations: Ru: 0.9067 Cl_1: 0.1047 Cl_2: 0.1238 $N_{(NO)}$: 0.4986 $O_{(NO)}$: 0.3092

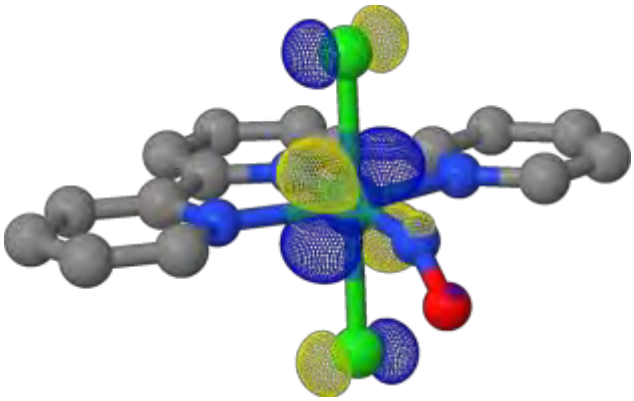

SONO (Hole)

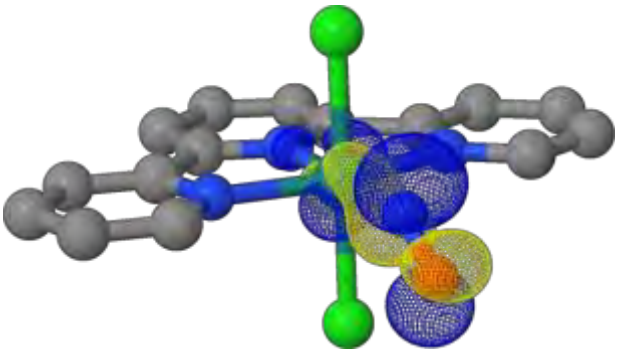

SONO (Particle)

Table AC29. Optimized Cartesian coordinates, energies, molecular parameters and electronic structure of the ^{3}**MS2** triplet state of complex **5**, *trans*(Cl,Cl)-[$RuCl_2$(NO)(terpy)]$^+$, at the B3LYP-D3BJ/**BS1** level of theory in acetonitrile.

Ru	3.297768587609	-0.028402532379	-0.044942990568
Cl	3.318117310472	-0.161370271214	-2.364818424709
Cl	3.325761086509	0.103687021395	2.274890216586
N	5.362236270719	0.727696023362	-0.085987173150
N	1.325574396163	-0.103935822850	-0.035466843920
N	2.793882832658	2.028468470185	-0.164598268962
N	2.998546606122	-2.089167961490	0.073927190523
O	5.431756545029	-0.464941527302	-0.024514159934
C	0.622957203309	1.039348836569	-0.095887324615
C	1.449857952084	2.243313253013	-0.170807449162
H	-2.472951998244	-0.295102592898	0.001663507075
C	3.164074890541	4.374539618735	-0.310136279152
H	3.875858056937	5.184650661183	-0.364035893644
C	0.741742483927	-1.315376486155	0.036502120332
C	-0.643255502931	-1.405888051513	0.051072058500
H	-1.128028169042	-2.367633755296	0.109547101009
C	3.613336287159	-4.379847901056	0.204146542477
H	4.403552040278	-5.114307374261	0.245929044496
C	1.682206601570	-2.434644746358	0.095180270720
C	-1.394115380405	-0.241286100703	-0.009349271851
C	0.932099662324	3.525526930015	-0.245986430557
H	-0.135623247968	3.679349964712	-0.250621837354
C	-0.764443275407	0.991900063354	-0.083484532196
H	-1.343520404107	1.900463462470	-0.130305844760
C	3.626315846033	3.071741657426	-0.233324608865
H	4.680326332785	2.854192568768	-0.227261734323
C	3.938744295987	-3.037006886940	0.127100807042
H	4.964582592919	-2.708359124285	0.106940540832
C	1.301774168928	-3.764236975108	0.168849202871
H	0.256190197155	-4.029141757689	0.183430566858
C	2.277241186298	-4.748392325742	0.224638541253
H	1.993428624979	-5.789443607239	0.283125917578
C	1.798438426772	4.605936932849	-0.316286979198
H	1.407667492838	5.611681336442	-0.375372581233

Energies (a.u.)	
E	-1888.178928
Zero-point correction	0.241212
Sum of electronic and thermal enthalpies	-1887.916716
Sum of electronic and thermal free energies	-1887.987575
Selected molecular parameters	
Ru-$N_{(NO)}$	2.199 Å
Ru-$O_{(NO)}$	2.178 Å
N-O	1.196 Å
Ru-Cl_1	2.324 Å
Ru-Cl_2	2.324 Å
Ru-N_{tpy1}	1.974 Å
Ru-N_{tpy2}	2.086 Å
Ru-N_{tpy3}	2.121 Å
∠Ru-N-O	73.190 °
∠Ru-O-N	75.095 °
NO stretching vibration	
ν_{NO} (cm^{-1})	1618.14 cm^{-1}

Electronic structure

$\langle S^2 \rangle$: 2.0078

Mulliken Spin Populations: Ru: 0.7273 Cl_1: 0.1304 Cl_2: 0.1310 $N_{(NO)}$: 0.7461 $O_{(NO)}$: 0.2623

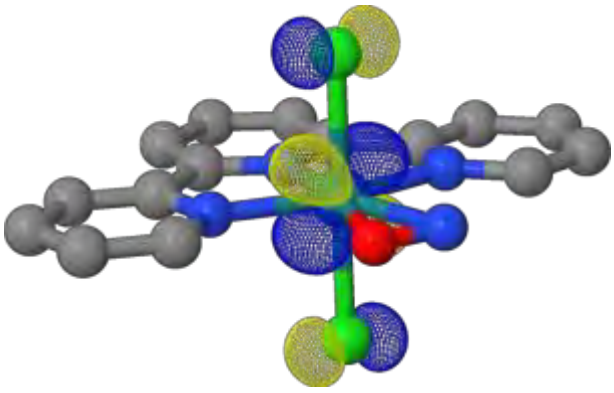

SONO (Hole)

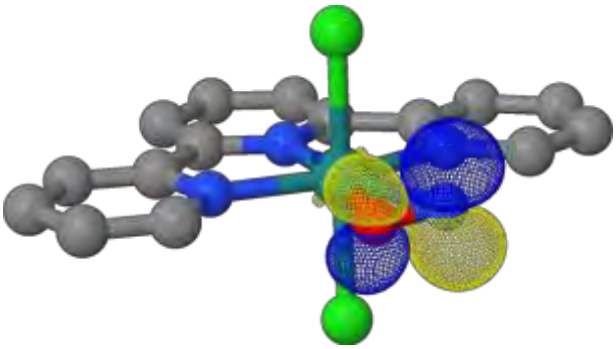

SONO (Particle)

Table AC30. Optimized Cartesian coordinates, energies, molecular parameters and electronic structure of the ^{3}**MS1** triplet state of complex **5**, *trans*(Cl,Cl)-[$RuCl_2$(NO)(terpy)]$^{+}$, at the B3LYP-D3BJ/**BS1** level of theory in acetonitrile.

Ru	3.256231000000	0.044280000000	-0.101583000000
Cl	3.313591000000	-0.085200000000	-2.429603000000
Cl	3.446685000000	0.193377000000	2.213985000000
N	1.313766000000	-0.071652000000	-0.048370000000
N	2.781583000000	2.078882000000	-0.211066000000
N	3.036049000000	-2.029068000000	0.025862000000
O	5.477639000000	0.148187000000	-0.258168000000
N	6.321391000000	0.229569000000	0.519617000000
C	0.609749000000	1.076539000000	-0.093496000000
C	1.436424000000	2.288941000000	-0.189167000000
H	-2.461301000000	-0.297224000000	0.088440000000
C	3.139336000000	4.427698000000	-0.365684000000
H	3.846027000000	5.241229000000	-0.435269000000
C	0.756559000000	-1.295489000000	0.044759000000
C	-0.625355000000	-1.396741000000	0.095868000000
H	-1.106164000000	-2.359346000000	0.171219000000
C	3.683940000000	-4.316847000000	0.139043000000
H	4.486413000000	-5.039179000000	0.157575000000
C	1.727097000000	-2.399795000000	0.082819000000
C	-1.383378000000	-0.233007000000	0.049337000000
C	0.911266000000	3.568908000000	-0.254306000000
H	-0.157033000000	3.720529000000	-0.236949000000
C	-0.774319000000	1.012322000000	-0.045102000000
H	-1.369641000000	1.911047000000	-0.078586000000
C	3.605068000000	3.122517000000	-0.297243000000
H	4.662349000000	2.905866000000	-0.313600000000
C	3.983649000000	-2.964982000000	0.051952000000
H	5.005848000000	-2.622351000000	-0.000475000000
C	1.365670000000	-3.733989000000	0.169282000000
H	0.324563000000	-4.014210000000	0.213019000000
C	2.356653000000	-4.706031000000	0.199011000000
H	2.089660000000	-5.750953000000	0.266836000000
C	1.773592000000	4.653419000000	-0.343558000000
H	1.378082000000	5.657690000000	-0.395453000000

Energies (a.u.)	
E	-1888.177625
Zero-point correction	0.240522
Sum of electronic and thermal enthalpies	-1887.915532
Sum of electronic and thermal free energies	-1887.988098
Selected molecular parameters	
Ru-$O_{(NO)}$	2.229 Å
Ru-$N_{(NO)}$	3.133 Å
N-O	1.150 Å
Ru-Cl_1	2.332 Å
Ru-Cl_2	2.328 Å
Ru-N_{tpy1}	1.947 Å
Ru-N_{tpy2}	2.092 Å
Ru-N_{tpy3}	2.089 Å
∠Ru-O-N	133.363 °
∠Ru-N-O	31.153 °
NO stretching vibration	
ν_{NO} (cm^{-1})	1849.93 cm^{-1}

Electronic structure

$\langle S^2 \rangle$: 2.0084

Mulliken Spin Populations: Ru: 0.8141 Cl_1: 0.1011 Cl_2: 0.1021 $N_{(NO)}$: 0.7697 $O_{(NO)}$: 0.1754

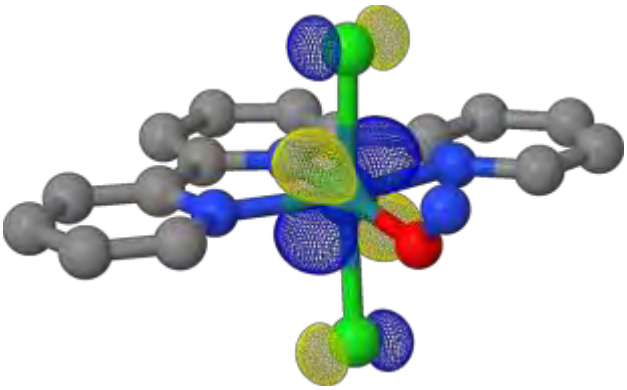

SONO (Hole)

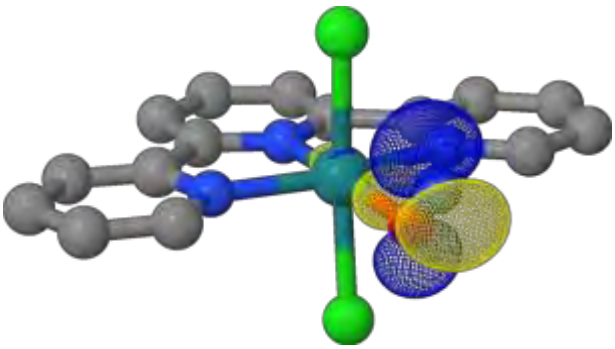

SONO (Particle)

Table AC31. TDDFT states computed in acetonitrile for the three isomers **GS**, **MS2** and **MS1** of the five complexes in their singlet states (oscillator strength threshold 10^{-3}).

1	2	3	4	5
GS	**GS**	**GS**	**GS**	**GS**
430 Ru(d) •• (Ru(d)NO(π*))-	**384** (Fluorenyl(π)(Ru(d)NO(π*))+)- •• (Ru(d)NO(π*))- (Ru(d)NO(π*))+ •• (Ru(d)NO(π*))-	**314** Terpy(π) •• (Terpy(π*)(Ru(d)NO(π*))-)+	**388** (Fluorenyl(π)(Ru(d)NO(π*))+)- •• (Ru(d)NO(π*))-	**325** Terpy(π) •• (Terpy(π*)(Ru(d)NO(π*))-)+
401 pyridine(π) •• (Ru(d)NO(π*))-	**367** Fluorenyl(π) •• (Ru(d)NO(π*))-	**277** Terpy(π) + Ru(d) •• (Terpy(π*)(Ru(d)NO(π*))-)-	**371** (Fluorenyl(π)(Ru(d)NO(π*))+)+ •• (Ru(d)NO(π*))-	**252** (Terpy(π)Ru(d))- •• (Terpy(π*)(Ru(d)NO(π*))-)+ (ClRu(d)Cl)- •• (Terpy(π*)(Ru(d)NO(π*))-)+
	345 Fluorenyl(π) •• (Ru(d)NO(π*))-	**256** (Terpy(π)(Ru(d)NO(π*))+)- •• (Terpy(π*)(Ru(d)NO(π*))-)+ Terpy(π) •• (Terpy(π*)(Ru(d)NO(π*))-)-	**324** Terpy(π) •• (Terpy(π*)(Ru(d)NO(π*))-)+ **320** Fluorenyl(π) •• (Ru(d)NO(π*))-	
	319 Fluorenyl(π) •• (Ru(d)NO(π*))- Fluorenyl(π) •• (Ru(d)NO(π*))-			
MS2	**MS2**	**MS2**	**MS2**	**MS2**
715 Cl(p)Ru(d) •• Ru(d)NO(π*)	**396** Fluorenyl(π) •• (Ru(d)NO(π*))-	**338** Terpy(π) •• (Ru(d)NO(π*))-	**360** Fluorenyl(π)Ru(d) •• Terpy(π*)Ru(d)	**389** Terpy(π) •• (Ru(d)NO(π*))-
477 Cl(p)Ru(d)NO(π*) •• Ru(d)NO(π*)	**352** Fluorenyl(π) •• (Ru(d)NO(π*))-	**286** Terpy(π) •• (Terpy(π)(Ru(d)NO(π*))-)-		**295** (Terpy(π)Ru(d))- •• (Terpy(π*)(Ru(d)NO(π*))-)-
475 Cl(p)Ru(d) •• Ru(d)NO(π*) Cl(p)Ru(d)NO(π*) •• Cl(p)Ru(d)NO(π*)				**271** Cl(p)Ru(d)Cl(p) •• (Ru(d)NO(π*))- (Cl_2Ru(d)NO(π*))+ •• (Terpy(π∗)Ru(d))-
MS1	**MS1**	**MS1**	**MS1**	**MS1**
694 Ru(d) •• (Ru(d)ON(π*))-	**636** Fluorenyl(π) •• (Ru(d)NO(π*))-	**456** Terpy(π) •• (Ru(d)NO(π*))-	**638** Fluorenyl(π) •• (Ru(d)NO(π*))-	**458** Terpy(π) •• (Ru(d)NO(π*))-
404 pyridine(π) •• (Ru(d)ON(π*))-	**449** Terpy(π) •• (Ru(d)NO(π*))-	**335** (Cl(p)Ru(d)Cl(p))+ •• (Ru(d)NO(π*))-	**449** Terpy(π) •• (Ru(d)NO(π*))-	**349** (Terpy(π)Ru(d)Cl_2)+ •• (Ru(d)NO(π*))- Cl_2Ru(d)•• (Ru(d)NO(π*))-
	426 Terpy(π) •• (Ru(d)NO(π*))-	**325** (Cl(p)Ru(d)Cl(p))+ •• (Ru(d)NO(π*))-	**336** Cl_2 •• (Ru(d)NO(π*))- (Fluorenyl(π)(Ru(d)NO(π*))+) •• (Terpy(π)(Ru(d)NO(π*))-)-	**337** (Terpy(π)(Cl(p)Ru(d)Cl(p))+)- •• (Ru(d)NO(π*))-
	344 Fluorenyl(π) •• Terpy(π*)	**289** Terpy(π) + Ru(d) •• (Terpy(π*)(Ru(d)NO(π*))-)-	**336** Fluorenyl(π) Terpy(π) Cl •• (Ru(d)NO(π*))- Fluorenyl(π) •• Terpy(π*)	**273** Terpy(π) + Ru(d) •• (Terpy(π*)(Ru(d)NO(π*))-)- (Ru(d)NO(π*))+ •• (Ru(d)NO(σ))-
		264 (Cl(π)Ru(d)NO(π*))+ •• (Terpy(π∗)Ru(d))-		**270** (Ru(d)NO(π*))+ •• (Ru(d)NO(σ))-
		250 (Cl(π)Ru(d)NO(π*))+ •• (Terpy(π∗)Ru(d))-		**251** Terpy(π) •• (Ru(d)NO(π*))-

Figure AC1. Minimum Energy Path (MEP) between the **GS** and **MS2** isomers of complex **1**, *trans*-$[RuCl(NO)(py)_4]^{2+}$, at the B3LYP-D3/**BS2** level of theory in vacuum.

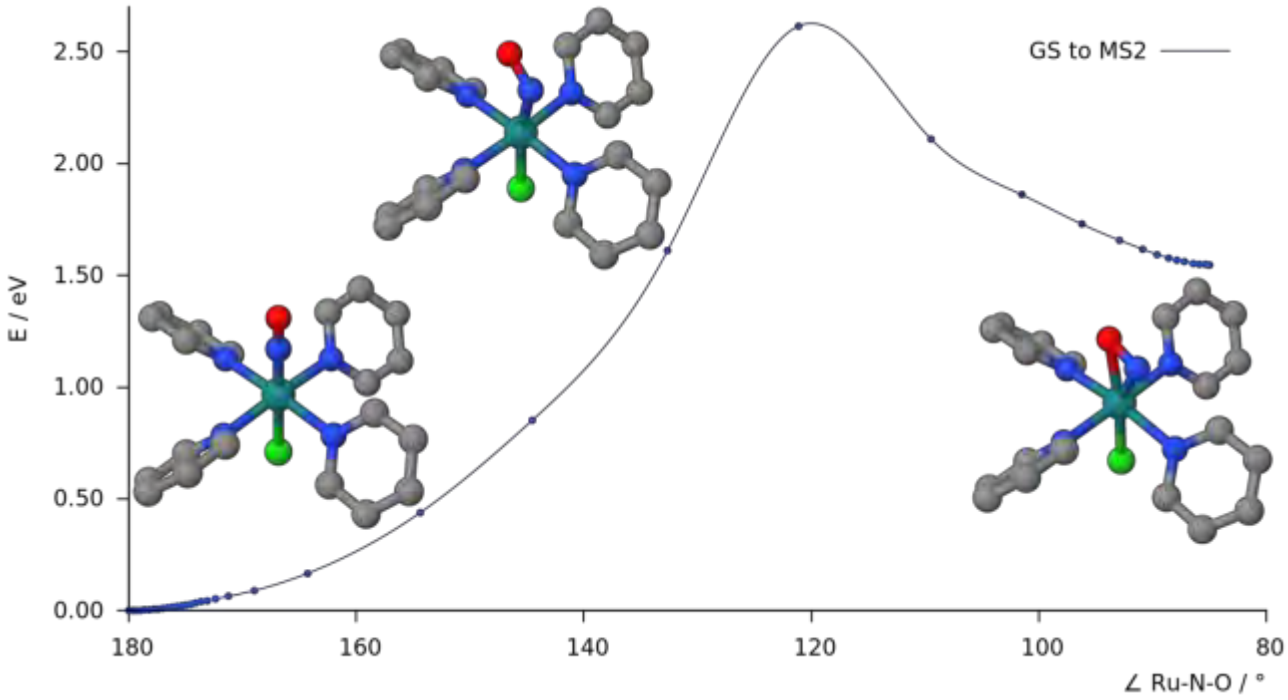

Figure AC2. Minimum Energy Path (MEP) between the **MS2** and **MS1** isomers of complex **1**, *trans*-$[RuCl(NO)(py)_4]^{2+}$, at the B3LYP-D3/**BS2** level of theory in vacuum.

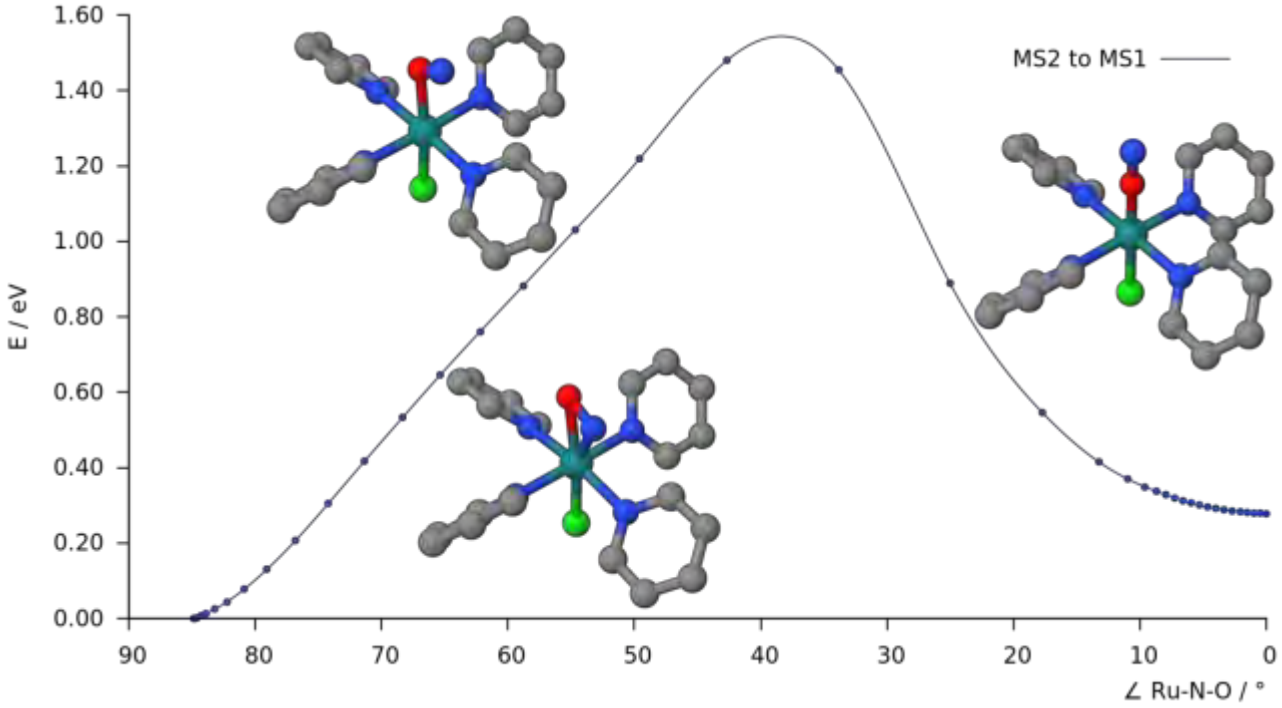

Figure AC3. Minimum Energy Path (MEP) between the triplets ^{3}**GS** and ^{3}**MS2** of complex **1**, *trans*-$[RuCl(NO)(py)_4]^{2+}$, at the B3LYP-D3/**BS2** level of theory in vacuum.

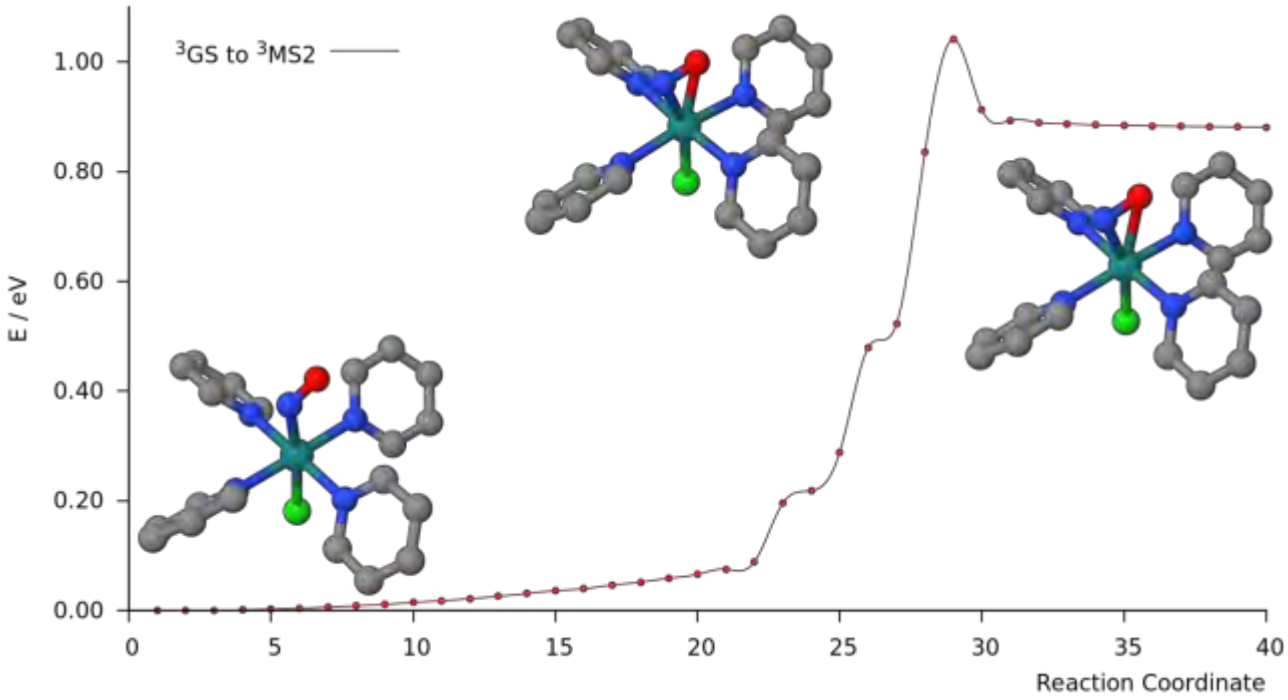

Figure AC4. Minimum Energy Path (MEP) between the triplets ^{3}**MS2** and ^{3}**MS1** of complex **1**, *trans*-$[RuCl(NO)(py)_4]^{2+}$, at the B3LYP-D3/**BS2** level of theory in vacuum.

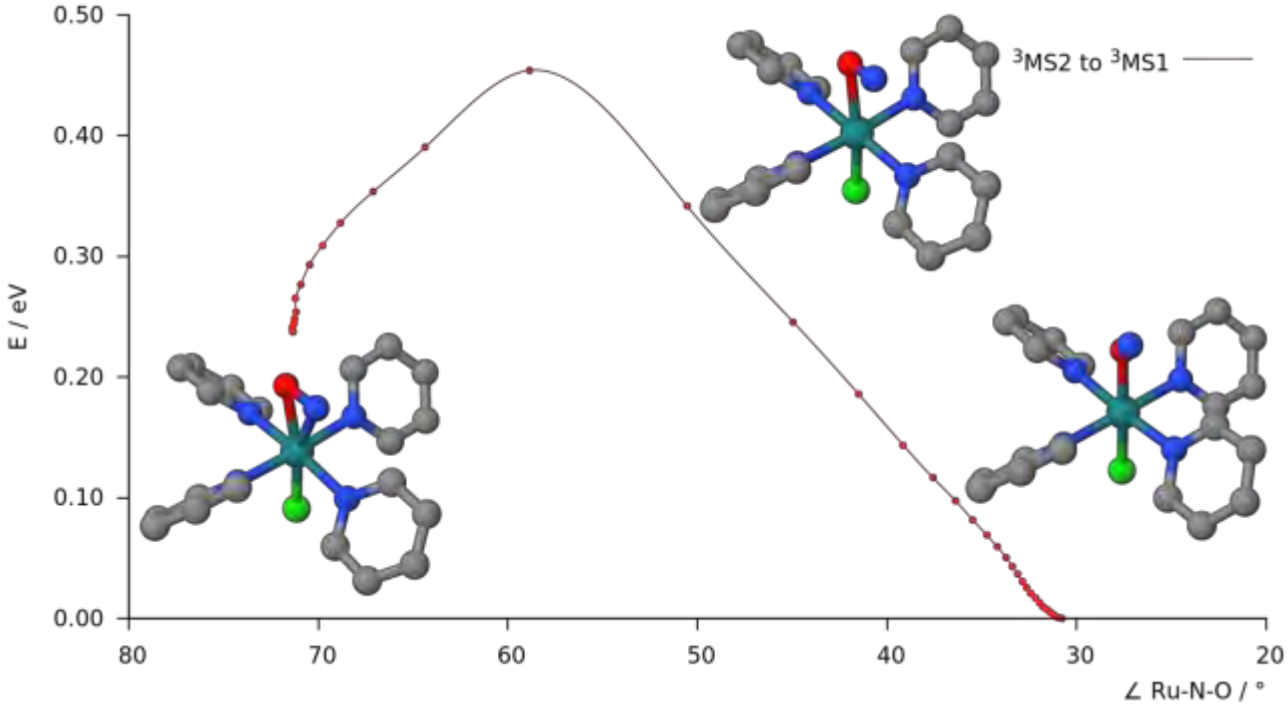

Figure AC5. Minimum Energy Path (MEP) between the **GS** and **MS2** isomers of complex **2**, *cis*(Cl,Cl)-$[RuCl_2(NO)(FT)]^+$, at the B3LYP-D3/**BS2** level of theory in vacuum.

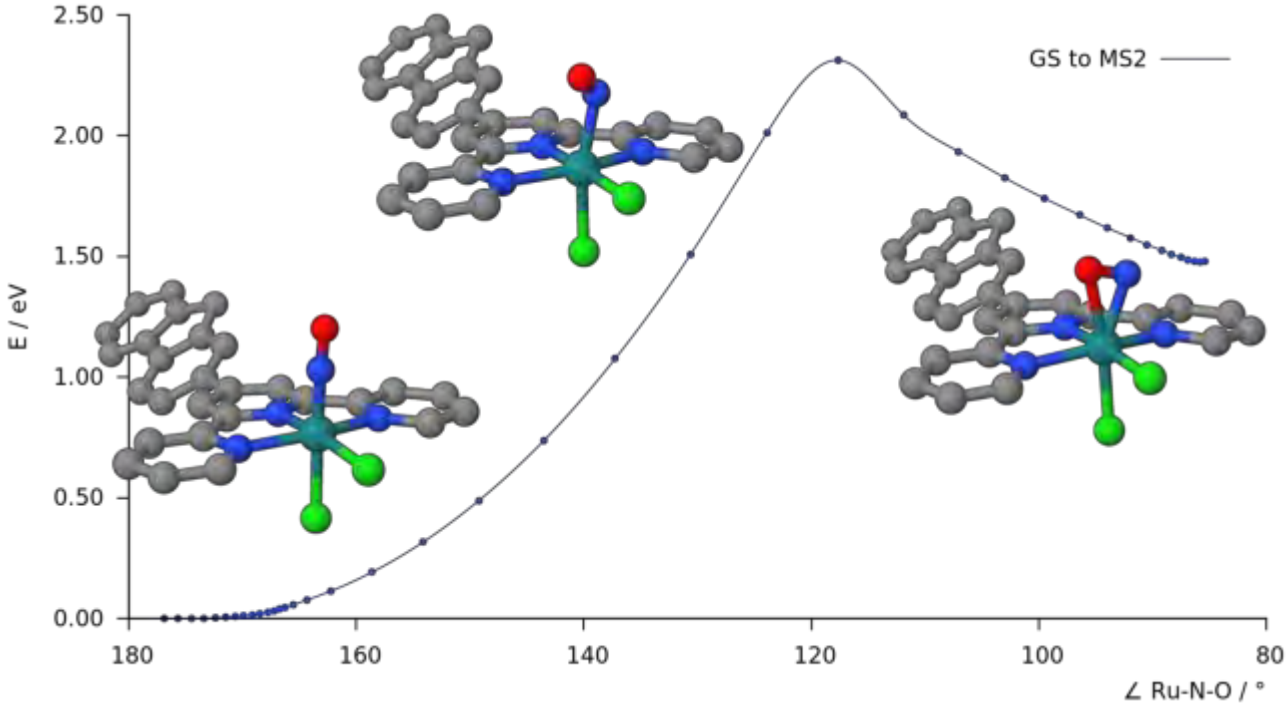

Figure AC6. Minimum Energy Path (MEP) between the **MS2** and **MSl** isomers of complex 2, cis(Cl,Cl)-[RuCl2(NO)(FT)f, at the B3LYP-D3/BS21evel oftheory in vacuum.

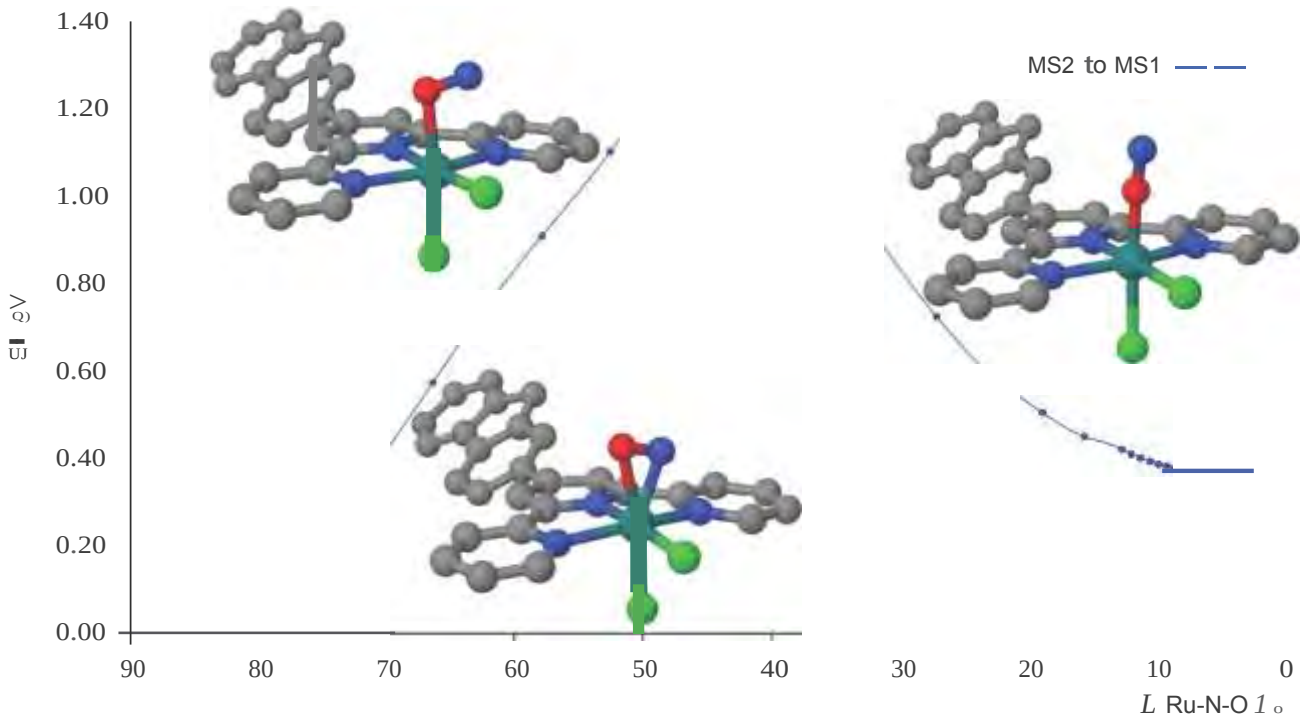

Figure AC7. Minimum Energy Path (MEP) between the triplets ^{3}**GS** and ^{3}**MS2** of complex **2**, *cis*(Cl,Cl)-$[RuCl_2(NO)(FT)]^+$, at the B3LYP-D3/**BS2** level of theory in vacuum.

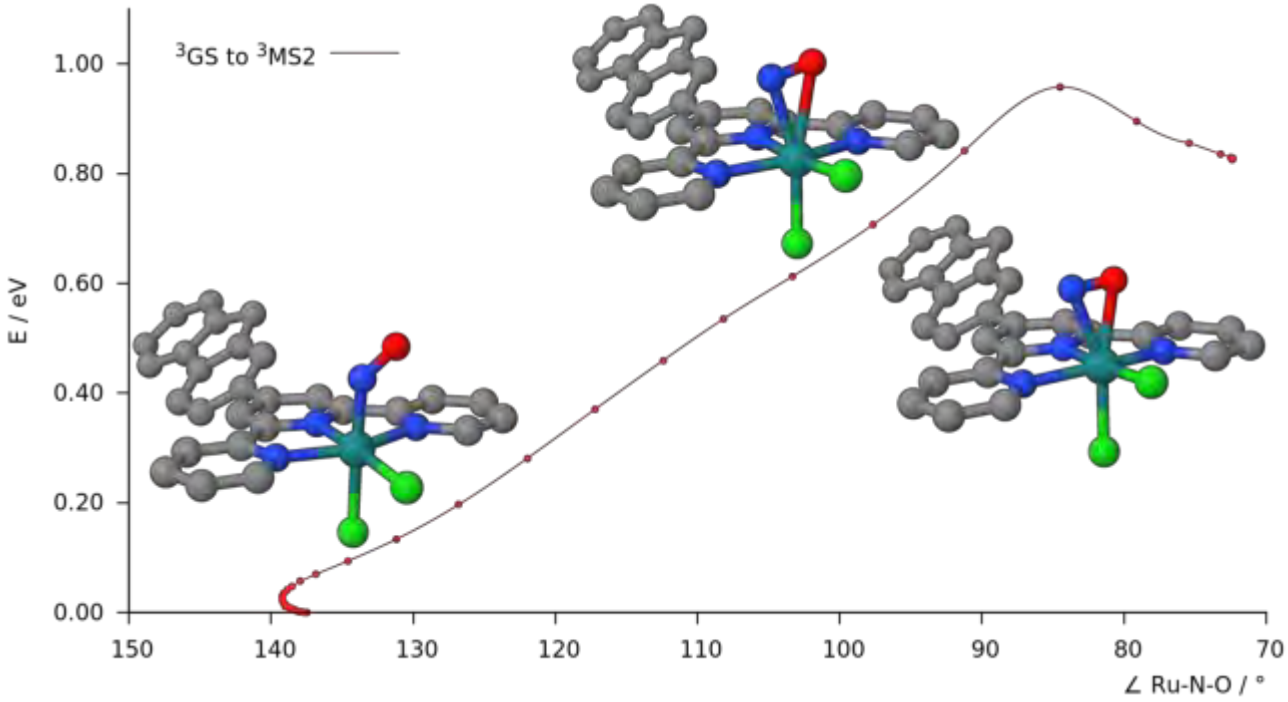

Figure AC8. Minimum Energy Path (MEP) between the triplets ^{3}**MS2** and ^{3}**MS1** of complex **2**, *cis*(Cl,Cl)-$[RuCl_2(NO)(FT)]^+$, at the B3LYP-D3/**BS2** level of theory in vacuum.

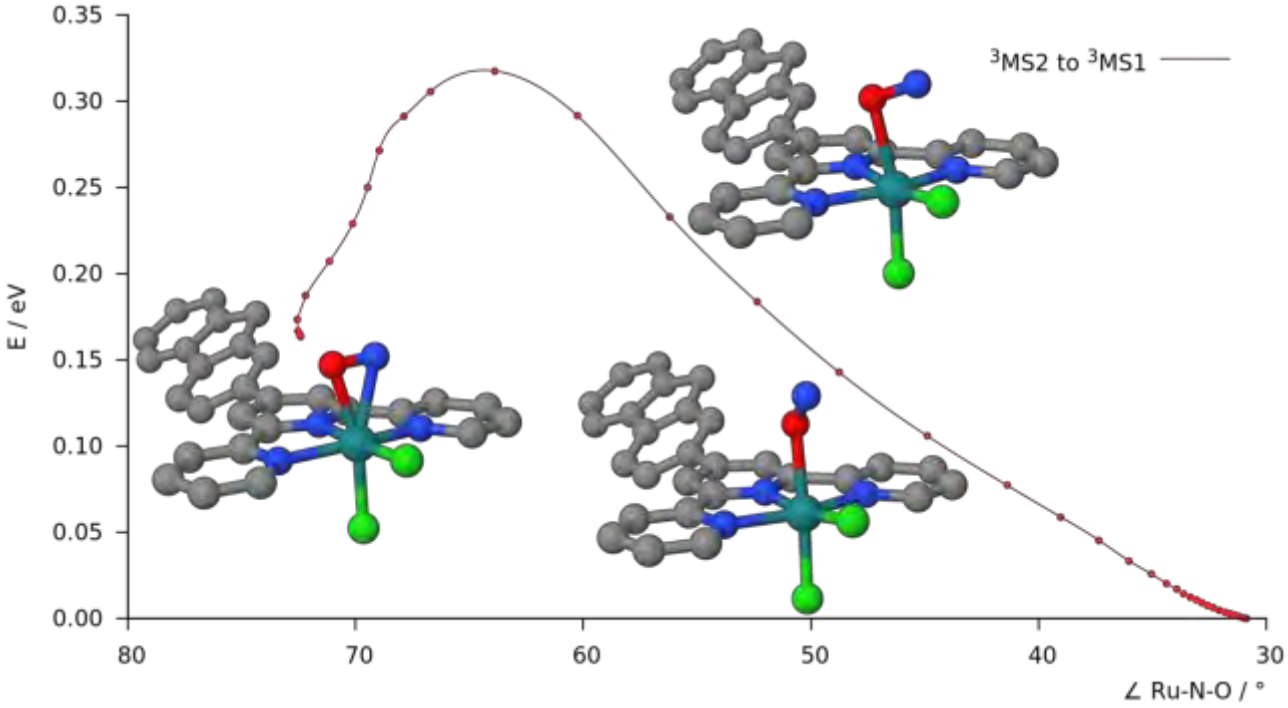

Figure AC9. Minimum Energy Path (MEP) between the **GS** and **MS2** isomers of complex **3**, *cis*(Cl,Cl)-$[RuCl_2(NO)(terpy)]^+$, at the B3LYP-D3/**BS2** level of theory in vacuum.

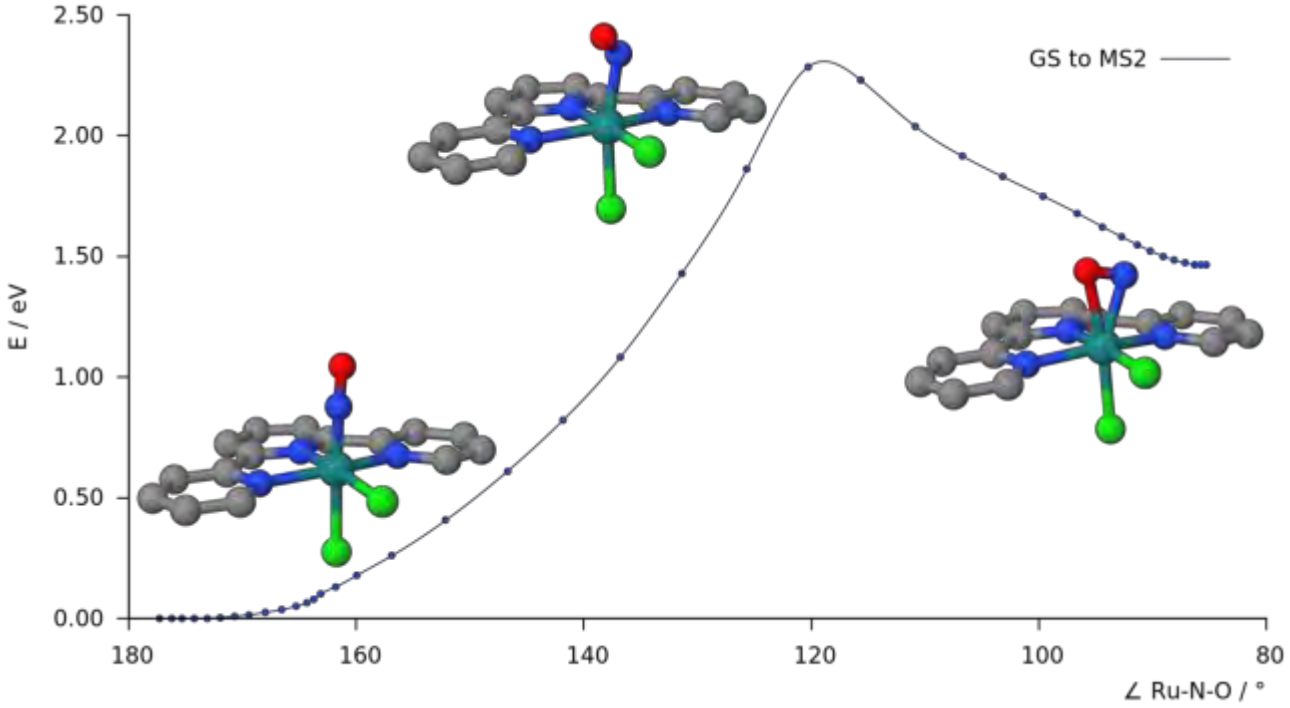

Figure AClO. Minimum Energy Path (MEP) between the **MS2** and **MSl** isomers of complex 3, cis(Cl,Cl)-[RuCl2(NO)(terpy)f, at the B3LYP-D3/BS2 level of theory in vacuum.

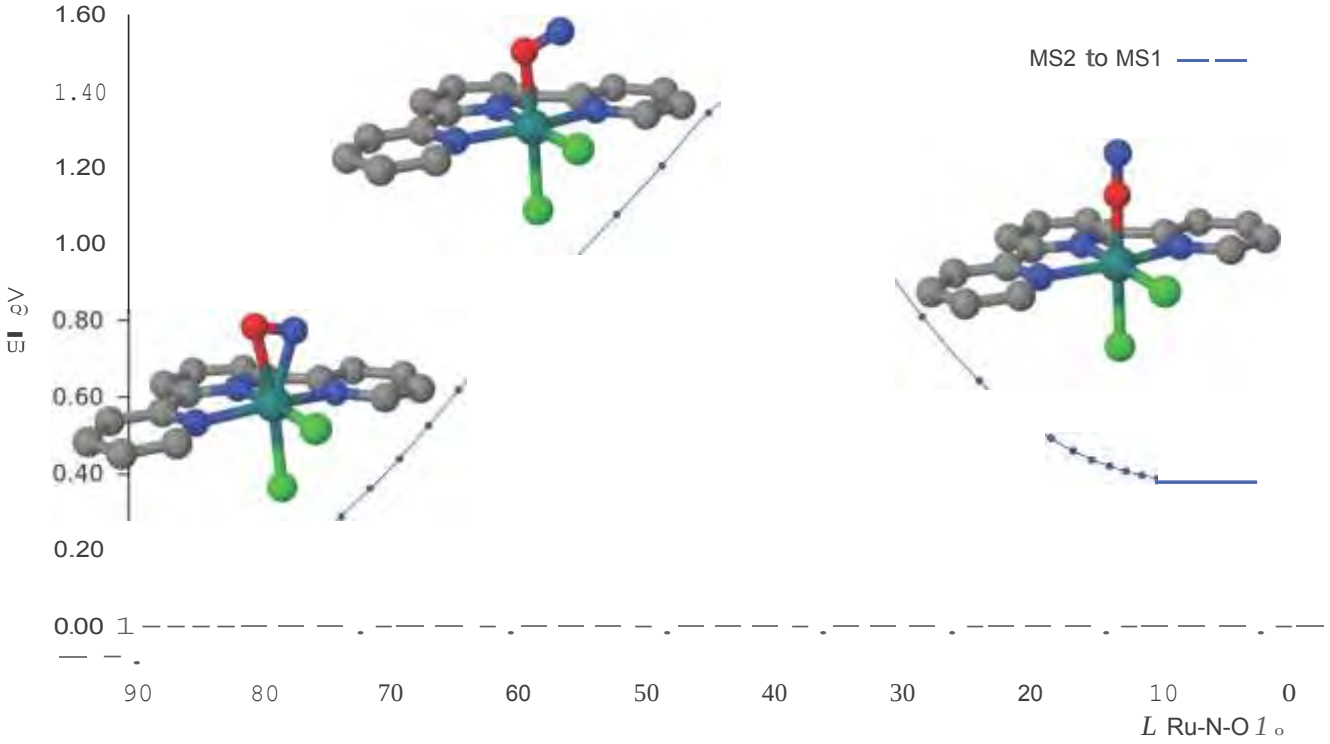

Figure AC11. Minimum Energy Path (MEP) between the triplets **^{3}GS** and **^{3}MS2** of complex **3**, *cis*(Cl,Cl)-$[RuCl_2(NO)(terpy)]^+$, at the B3LYP-D3/**BS2** level of theory in vacuum.

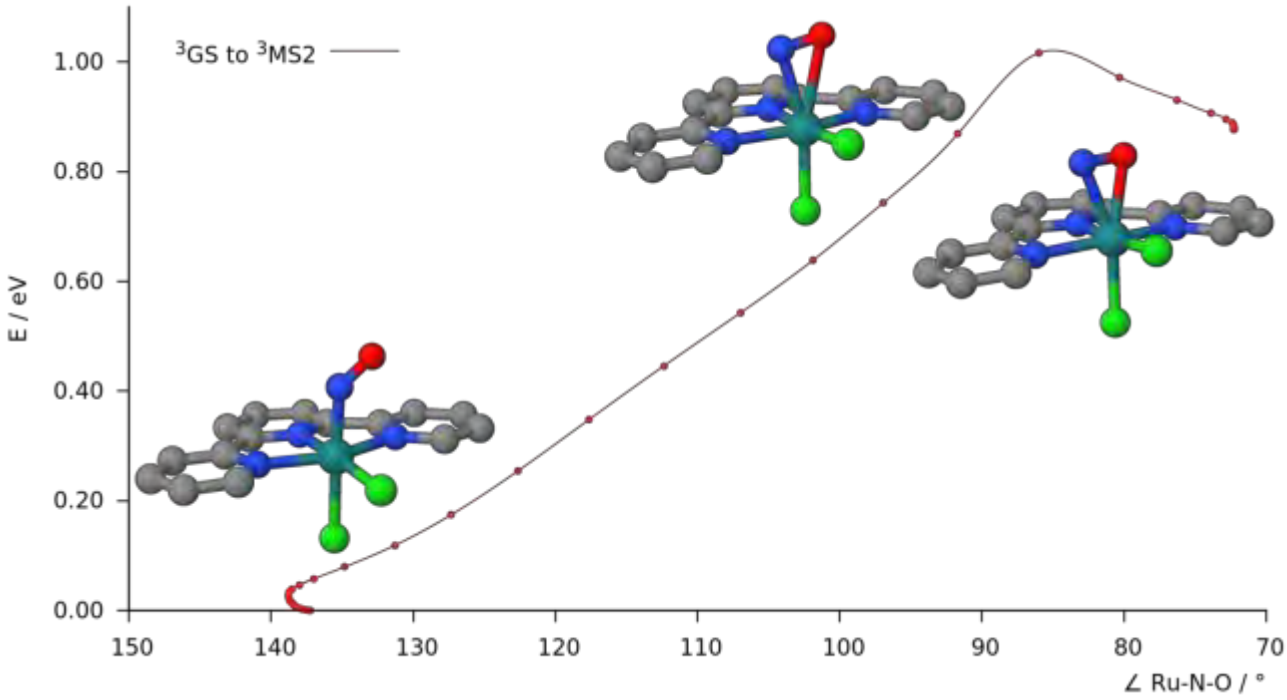

Figure AC12. Minimum Energy Path (MEP) between the triplets ^{3}**MS2** and ^{3}**MS1** of complex **3**, *cis*(Cl,Cl)-$[RuCl_2(NO)(terpy)]^+$, at the B3LYP-D3/**BS2** level of theory in vacuum.

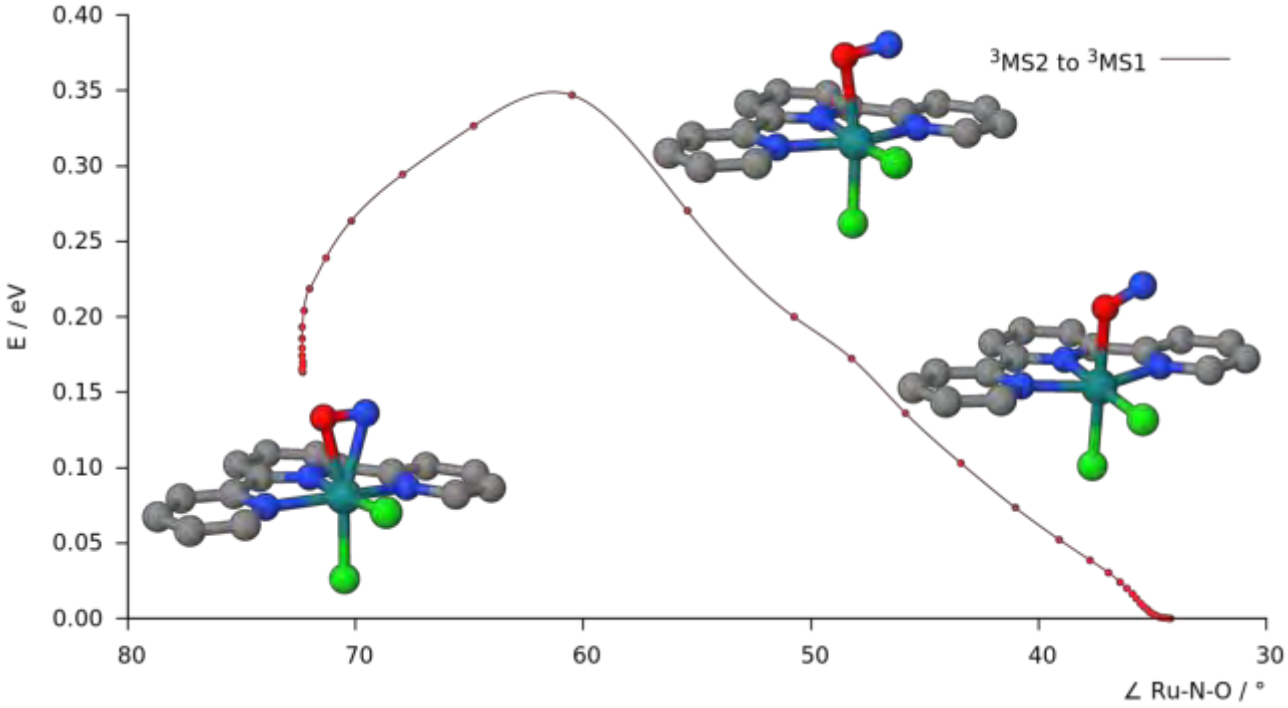

Figure AC13. Minimum Energy Path (MEP) between the **GS** and **MS2** isomers of complex **4**, *trans*(Cl,Cl)-$[RuCl_2(NO)(FT)]^+$, at the B3LYP-D3/**BS2** level of theory in vacuum.

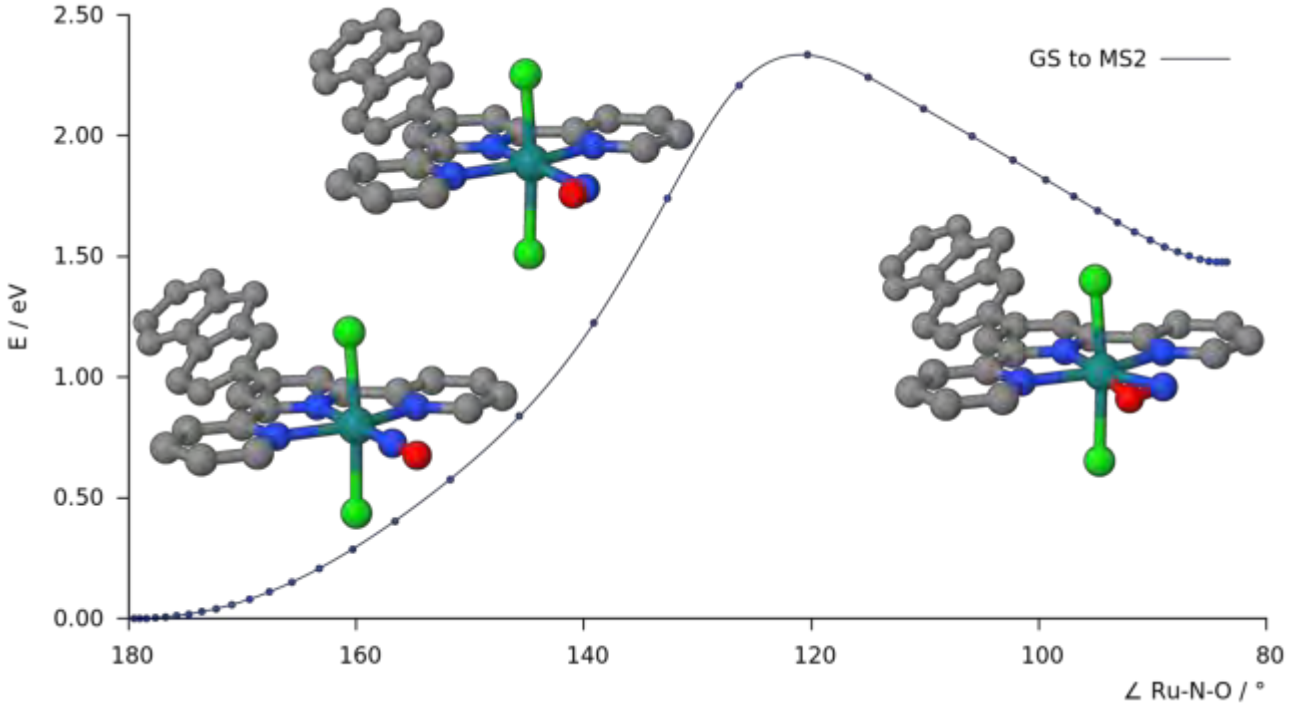

Figure AC14. Minimum Energy Path (MEP) between the **MS2** and **MSl** isomers of complex **4,** trans(Cl,Cl)-[RuCl2(NO)(FT)f, at the B3LYP-D3/BS21evel oftheory in vacuum.

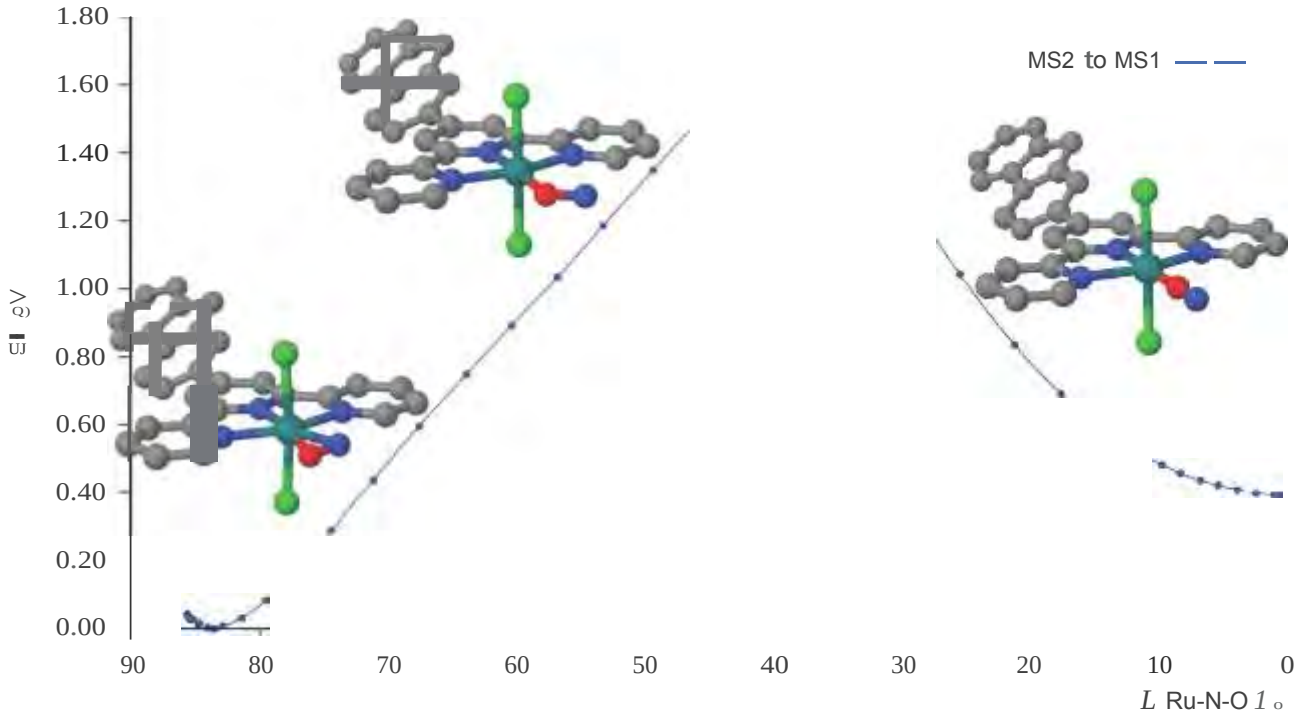

Figure AC15. Minimum Energy Path (MEP) between the triplets ^{3}**GS** and ^{3}**MS2** of complex **4**, *trans*(Cl,Cl)-$[RuCl_2(NO)(FT)]^{+}$, at the B3LYP-D3/**BS2** level of theory in vacuum.

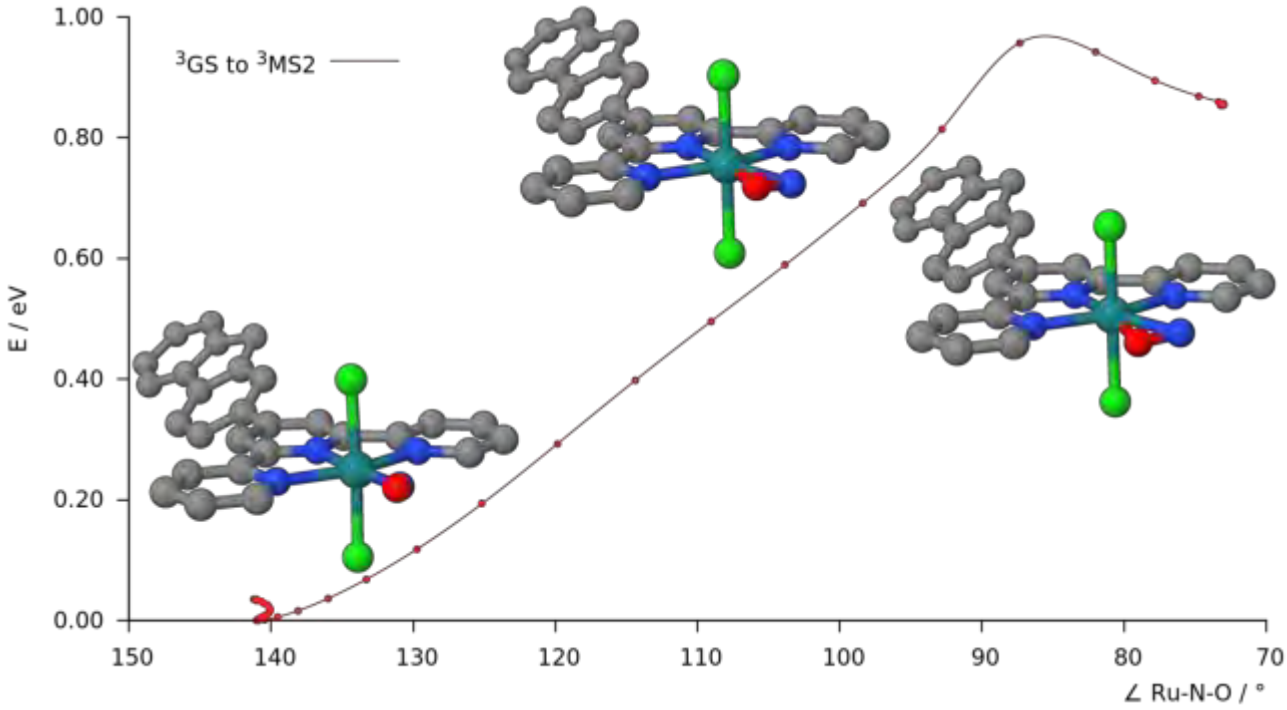

Figure AC16. Minimum Energy Path (MEP) between the triplets ^{3}**MS2** and ^{3}**MS1** of complex **4**, *trans*(Cl,Cl)-$[RuCl_2(NO)(FT)]^{+}$, at the B3LYP-D3/**BS2** level of theory in vacuum.

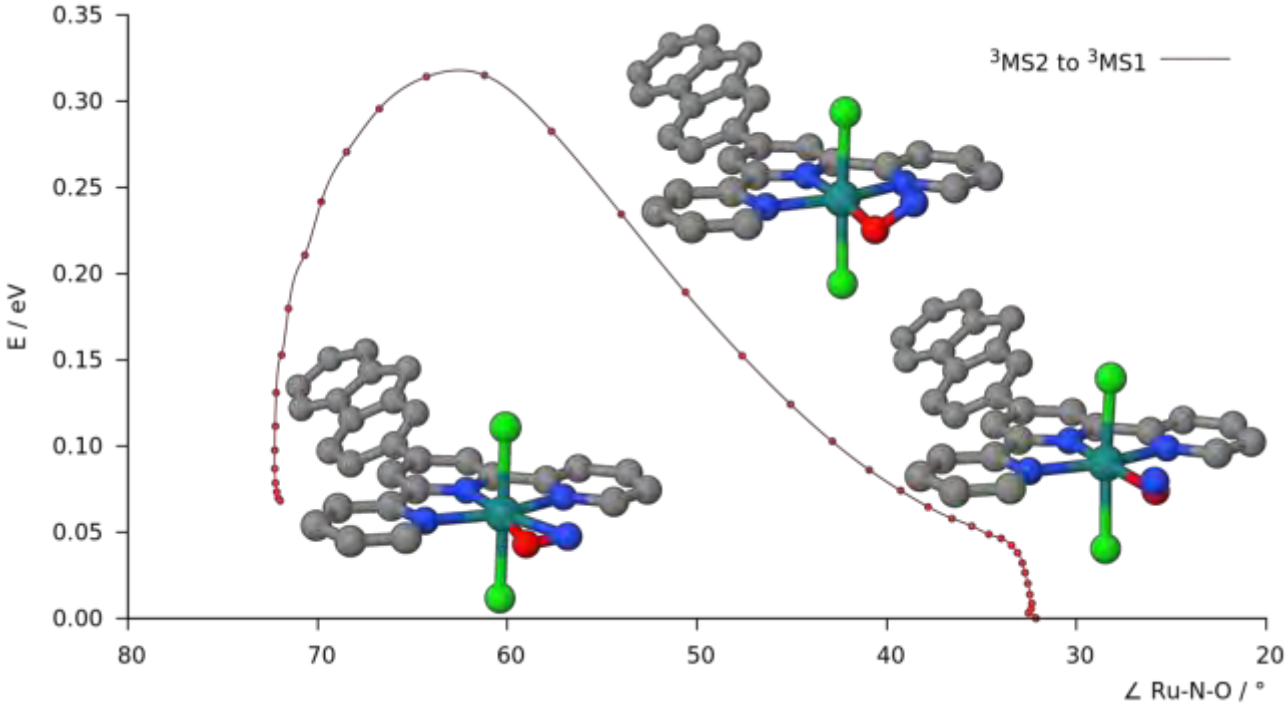

Figure AC17. Minimum Energy Path (MEP) between the **GS** and **MS2** isomers of complex **5**, *trans*(Cl,Cl)-$[RuCl_2(NO)(terpy)]^+$, at the B3LYP-D3/**BS2** level of theory in vacuum.

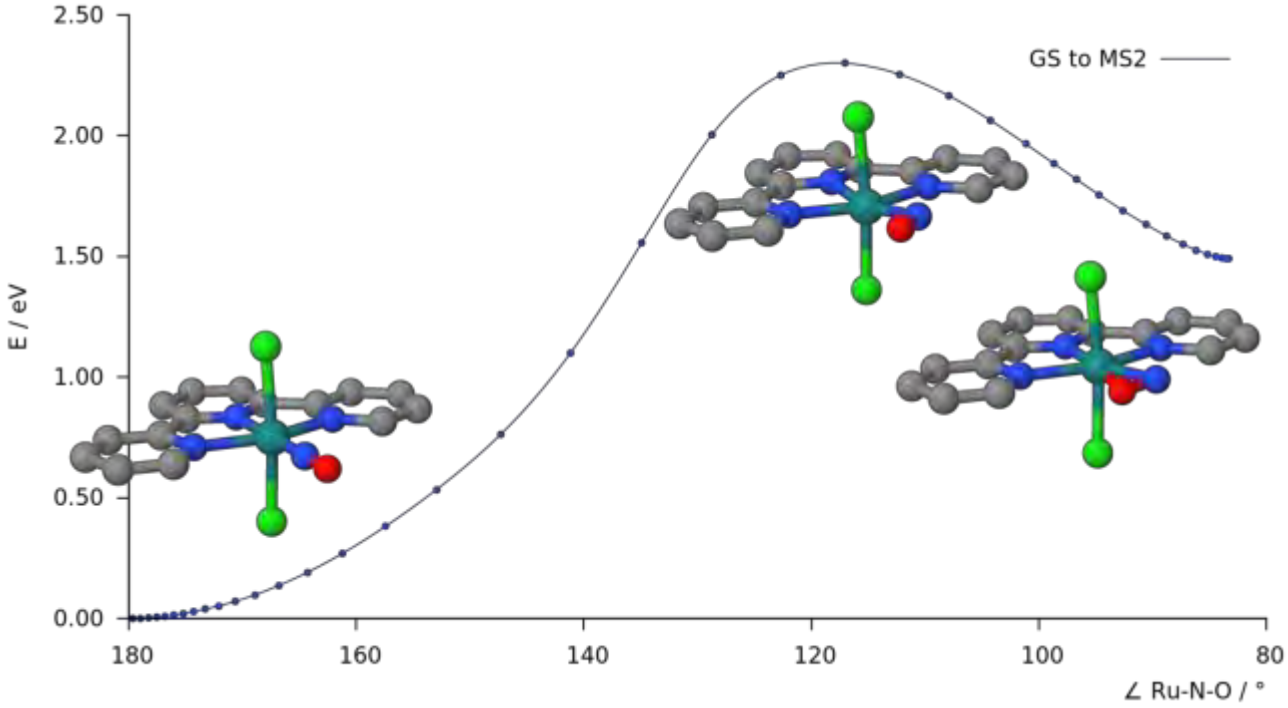

Figure AC18. Minimum Energy Path (MEP) between the **MS2** and **MSl** isomers of complex 5, trans(Cl,Cl)-[RuCl2(NO)(terpy)f, at the B3LYP-D3/BS2 level of theory in vacuum.

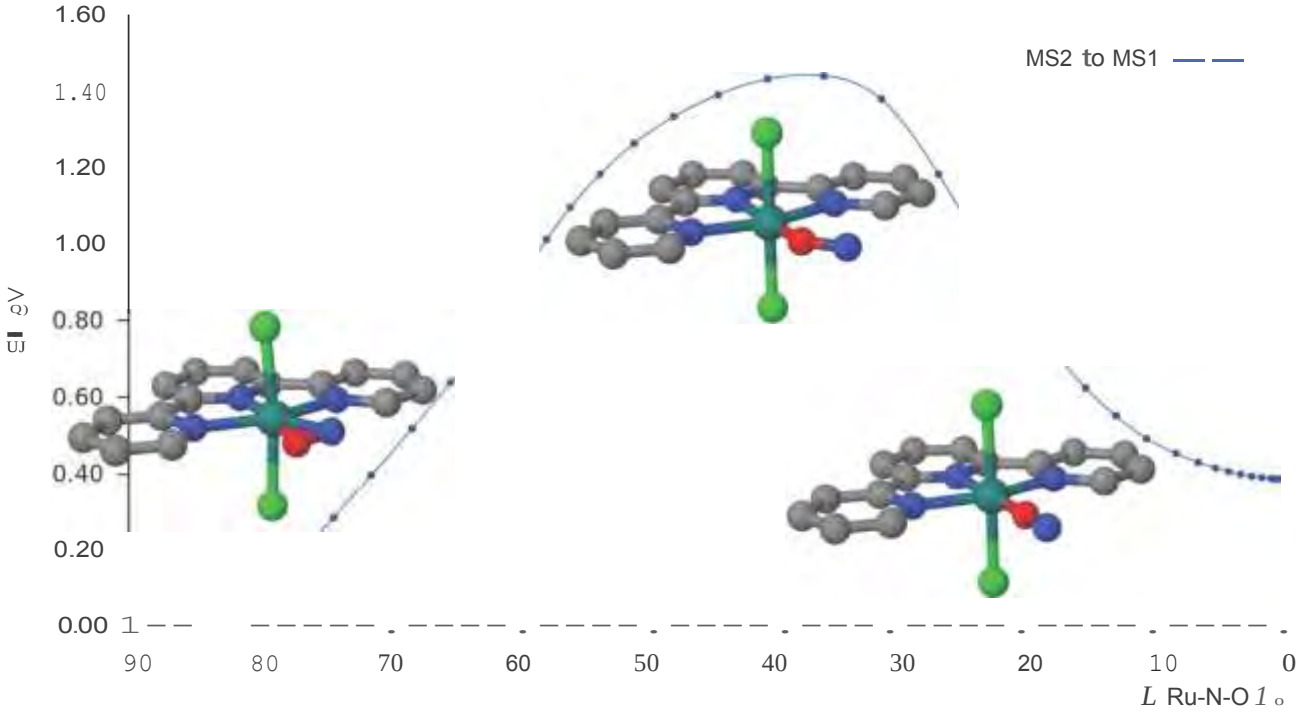

Figure AC19. Minimum Energy Path (MEP) between the triplets ^{3}**GS** and ^{3}**MS2** of complex **5**, *trans*(Cl,Cl)-$[RuCl_2(NO)(terpy)]^+$, at the B3LYP-D3/**BS2** level of theory in vacuum.

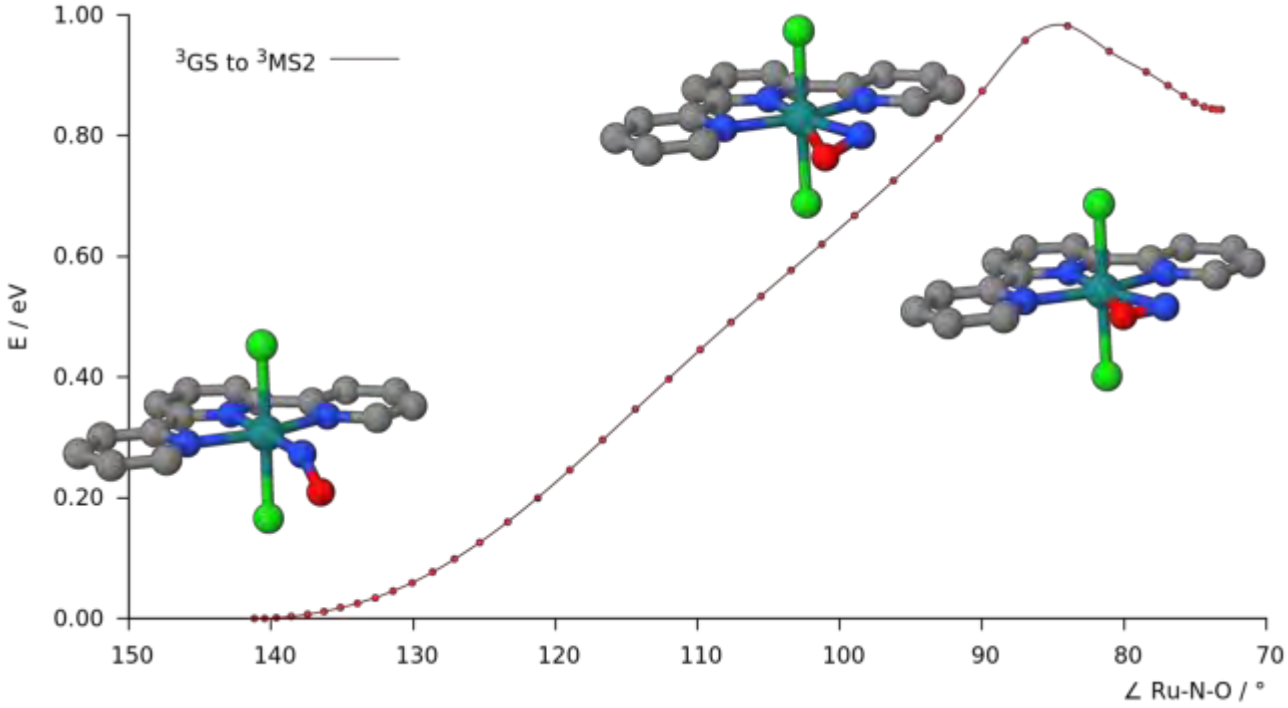

Figure AC20. Minimum Energy Path (MEP) between the triplets ^{3}**MS2** and ^{3}**MS1** of complex **5**, *trans*(Cl,Cl)-$[RuCl_2(NO)(terpy)]^+$, at the B3LYP-D3/**BS2** level of theory in vacuum.

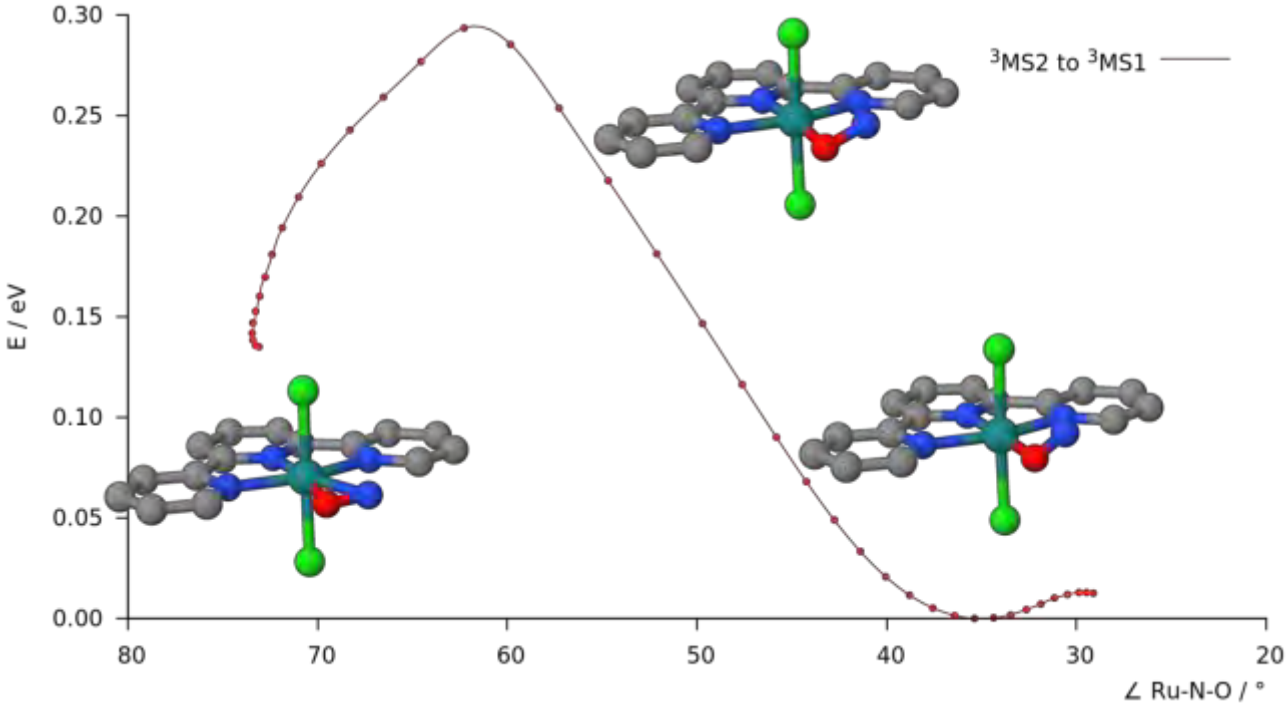

Figure AC21. Minimum Energy Path (MEP) for the dissociation of complex **1**, *trans*-$[RuCl(NO)(py)_4]^{2+}$, at the B3LYP-D3/**BS2** level of theory in vacuum.

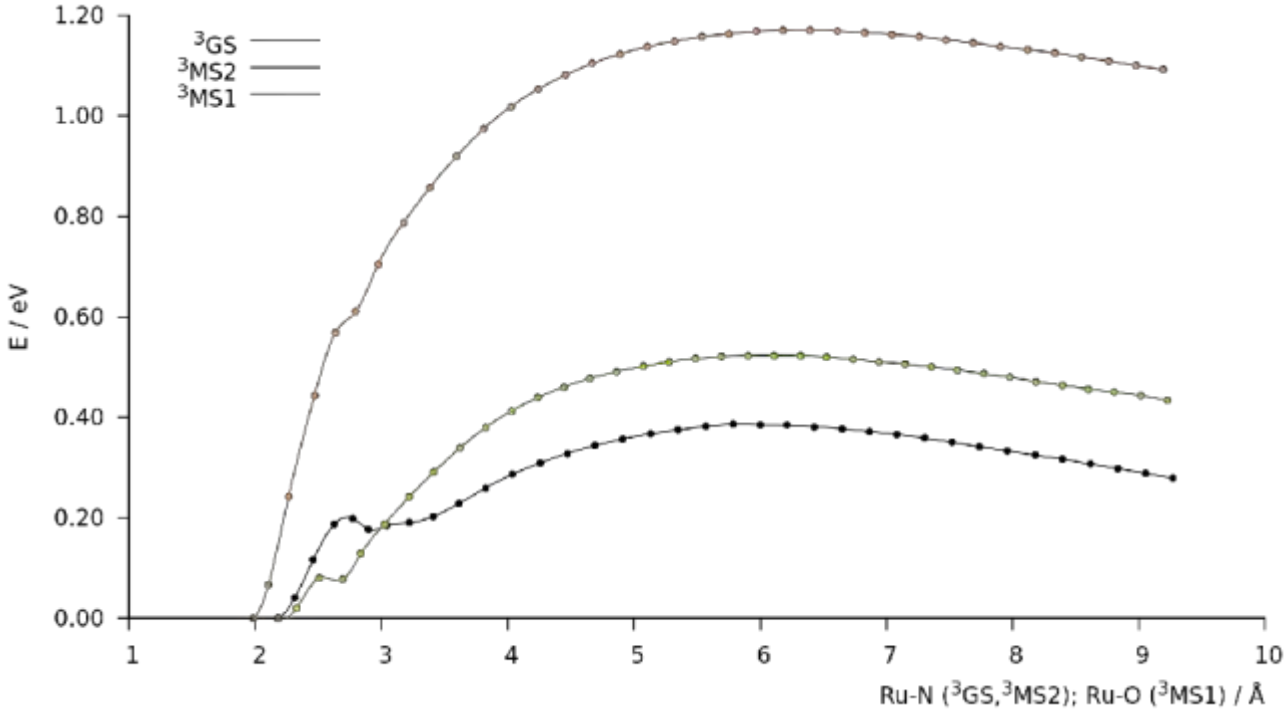

Figure AC22. Minimum Energy Path (MEP) for the dissociation of complex **2**, *cis*(Cl,Cl)-[$RuCl_2$(NO)(FT)]$^+$, at the B3LYP-D3/**BS2** level of theory in vacuum.

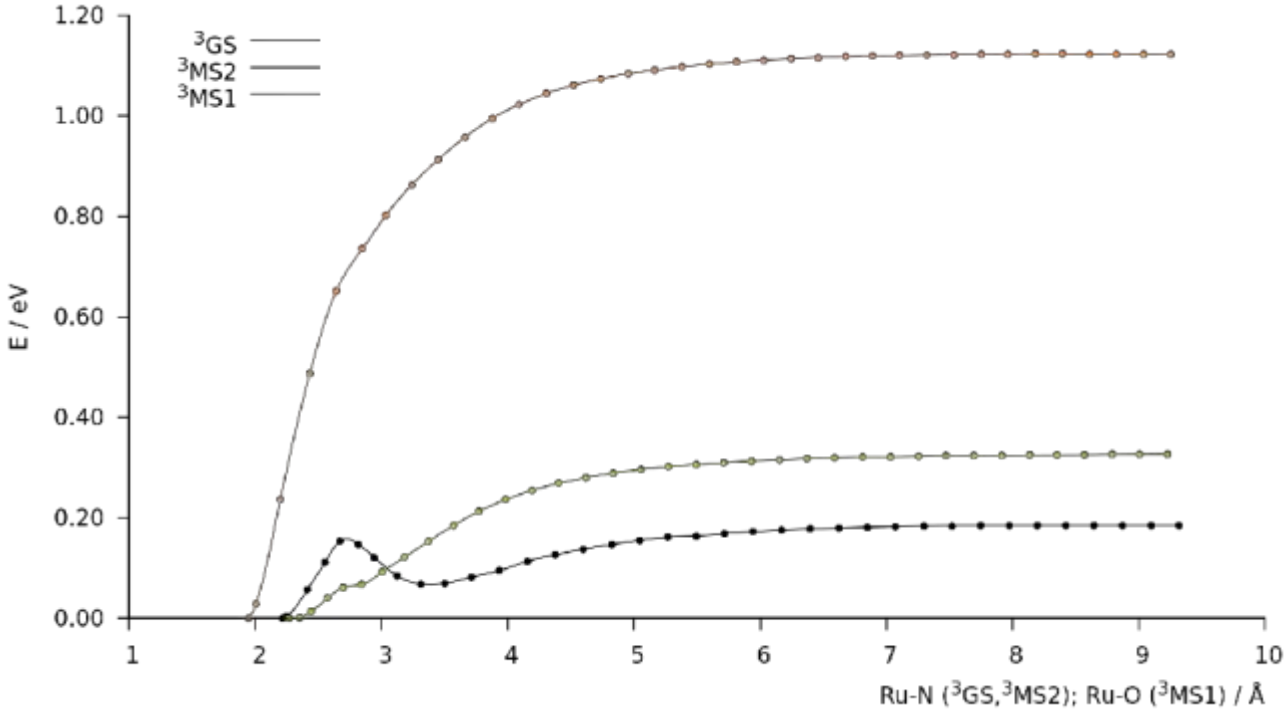

Figure AC23. Minimum Energy Path (MEP) for the dissociation of complex **3**, *cis*(Cl,Cl)-[$RuCl_2$(NO)(terpy)]$^+$, at the B3LYP-D3/**BS2** level of theory in vacuum.

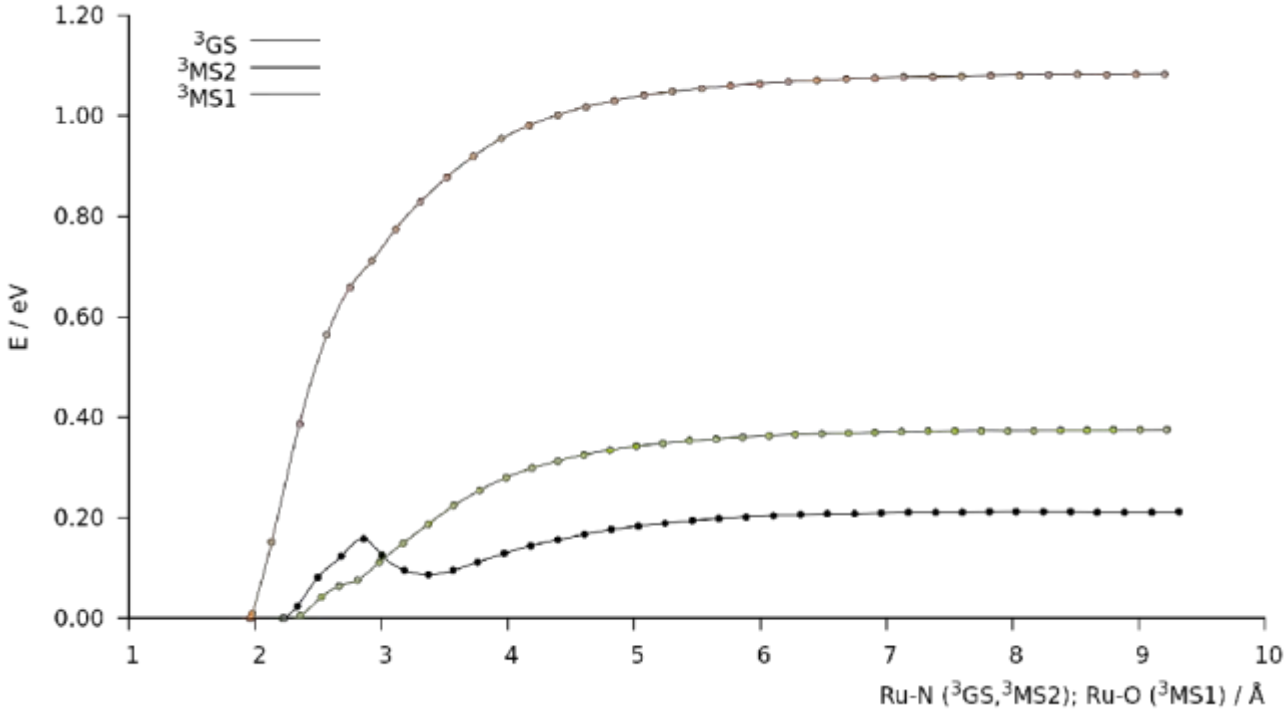

Figure AC24. Minimum Energy Path (MEP) for the dissociation of complex **4**, *trans*(Cl,Cl)-[$RuCl_2$(NO)(FT)]$^+$, at the B3LYP-D3/**BS2** level of theory in vacuum.

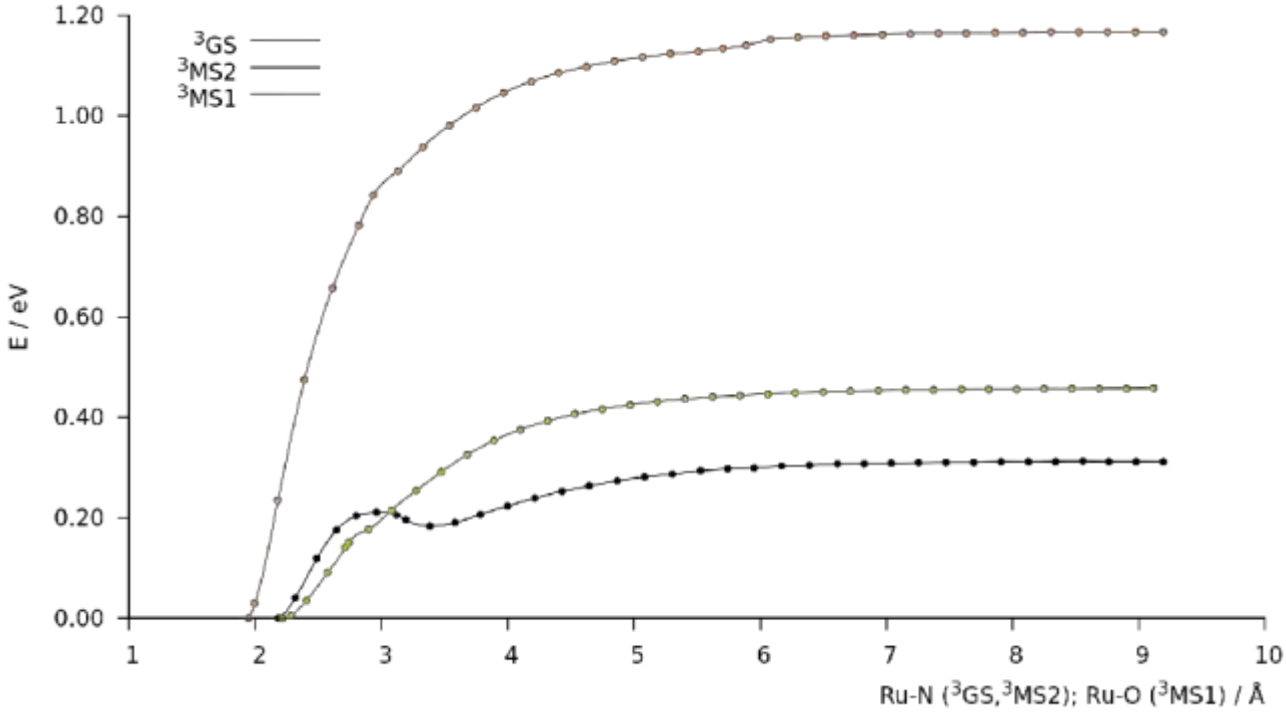

Figure AC25. Minimum Energy Path (MEP) for the dissociation of complex **5**, *trans*(Cl,Cl)-[$RuCl_2$(NO)(terpy)]$^+$, at the B3LYP-D3/**BS2** level of theory in vacuum.

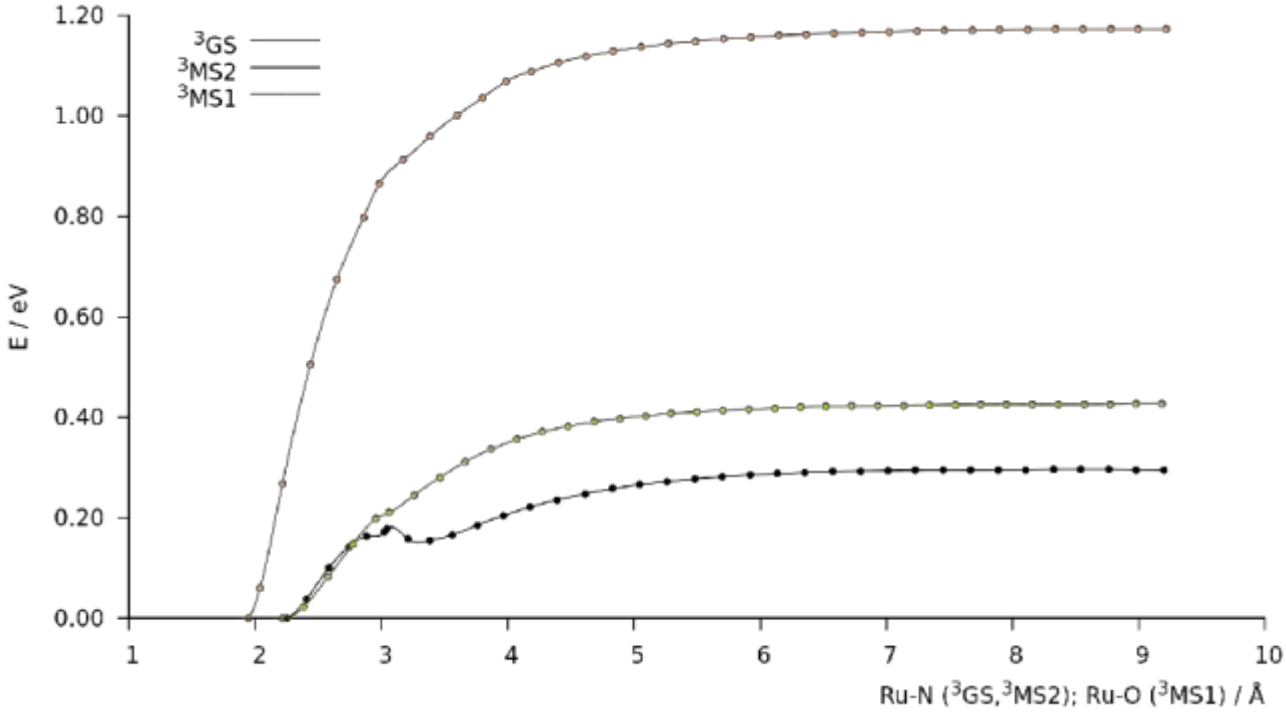

References

(1) Tomasi, J.; Mennucci, B.; Cammi, R. *Chem. Rev.* **2005**, *105* (8), 2999–3094.

(2) Frisch M. J., et al. *Gaussian 09, revision C.01*; Gaussian, Inc.: Wallingford, CT, 2010.

(3) Lee, C.; Yang, W.; Parr, R. G. *Phys. Rev. B* **1988**, *37* (2), 785.

(4) Becke, A. D. *J. Chem. Phys.* **1993**, *98* (7), 5648.

(5) Grimme, S.; Ehrlich, S.; Goerigk, L. *J. Comput. Chem.* **2011**, *32* (7), 1456–1465.

(6) Weigend, F.; Ahlrichs, R. *Phys. Chem. Chem. Phys.* **2005**, *7* (18), 3297–3305.

(7) Andrae, D.; Haeussermann, U.; Dolg, M.; Stoll, H.; Preuss, H. *Theor. Chim. Acta* **1990**, *77* (2), 123–141.

(8) E, W.; Ren, W.; Vanden-Eijnden, E. *J. Chem. Phys.* **2007**, *126* (16), 164103.

(9) Vanden-Eijnden, E.; Venturoli, M. *J. Chem. Phys.* **2009**, *130* (19), 194103.

(10) Schäfer, A.; Horn, H.; Ahlrichs, R. *J. Chem. Phys.* **1992**, *97* (4), 2571.

(11) Valiev, M.; Bylaska, E. J.; Govind, N.; Kowalski, K.; Straatsma, T. P.; Van Dam, H. J. J.; Wang, D.; Nieplocha, J.; Apra, E.; Windus, T. L.; de Jong, W. A. *Comput. Phys. Commun.* **2010**, *181* (9), 1477–1489.

(12) Grimme, S.; Antony, J.; Ehrlich, S.; Krieg, H. *J. Chem. Phys.* **2010**, *132* (15), 154104.

(13) Neese, F. *WIREs: Comput. Mol. Sci.* **2012**, *2* (1), 73–78.

(14) Sinnecker, S.; Rajendran, A.; Klamt, A.; Diedenhofen, M.; Neese, F. *J. Phys. Chem. A* **2006**, *110* (6), 2235–2245.

(15) Tao, J.; Perdew, J. P.; Staroverov, V. N.; Scuseria, G. E. *Phys. Rev. Lett.* **2003**, *91* (14), 146401.

(16) Becke, A. D. *Phys. Rev. A* **1988**, *38* (6), 3098–3100.

(17) Hirata, S.; Head-Gordon, M. *Chem. Phys. Lett.* **1999**, *314* (3–4), 291–299.

(18) Hirata, S.; Head-Gordon, M. *Chem. Phys. Lett.* **1999**, *302* (5–6), 375–382.

(19) Neese, F. *J. Comput. Chem.* **2003**, *24* (14), 1740–1747.

(20) Neese, F.; Wennmohs, F.; Hansen, A.; Becker, U. *Chem. Phys.* **2009**, *356* (1–3), 98–109.

(21) Martin, R. L. *J. Chem. Phys.* **2003**, *118* (11), 4775–4777.

Abstract

Over the last few decades, metal-nitrosyl complexes have gained an ever-growing interest among the pharmaceutical, chemical and material-science communities. This interest arises from their unique physicochemical properties, namely their response to light perturbation. Upon light irradiation, these compounds are able to release the nitric oxide radical, a signaling molecule in the vascular and other important physiological systems. It comes as no surprise that molecules with such properties have drawn the attention of the medical community for its potential use in photodynamic therapy treatment of several diseases such as cancer. This liability of nitric oxide can also be controlled with purely chemical redox reactions, with no electromagnetic perturbations. Reduction of the metal-nitrosyl moiety may trigger the cleavage of NO. Indeed, molecules that show charge transfer bands from a ligand to the metal-nitrosyl moiety in their UV-Vis absorption spectra afford photorelease quantum yields orders of magnitude larger than those who do not. This charge transfer may be considered as a M–NO reduction. Another important property shown by these metal-nitrosyl complexes is their extraordinary photochromic response to electromagnetic irradiation. In solid crystals, the changing color is due to a rearrangement of the NO ligand, going back and forth from the nitrosyl (N-bound) to the isonitrosyl (O-bound) forms. With the appropriate wavelength, the direction of the photoinduced linkage isomerization (forward and backwards) can be controlled. This feature is very appealing for the design of new high-capacity optical storage devices. One of the main goals of this PhD is to unravel the photochemical mechanisms behind both the photoisomerization and the photorelease phenomena of ruthenium-nitrosyl complexes. In order to shed some light into these processes, a full characterization of the electronic structures and potential energy surfaces of the ground and lowest excited states is required. Density Functional Theory calculations have proven to be suitable for the rationalization of the full photoinduced linkage isomerization mechanism of the *trans*-$[RuCl(NO)(py)_4]^{2+}$ molecule, a complex that yields one of the highest photoconversion rates (*ca*. 100%) observed among this family of complexes. The full characterization of the singlet ground state and of the lowest triplet excited state, as well as the identification of multiple crossings, allowed the establishment of the sequential two-photon absorption mechanism, involving a sideways-bonded metastable state. This predicted mechanistic picture has been confirmed by very recent experimental data. The proposed mechanism of the backwards reaction triggered by infrared or red irradiation is also consistent with the experimental data. A similar computational approach has been followed in the study of the

nitrosyl photorelease. In solution, the *trans*-$[RuCl(NO)(py)_4]^{2+}$ complex also shows photodissociation of NO, but in this case with low quantum yields. Assuming that photoisomerization and photorelease are competitive processes, both mechanisms have been studied for an ensemble of complexes in an attempt to rationalize which are the molecular features that would favor one mechanism over the other. Analyzing the results, it becomes clear that both processes are triggered by the same irradiation wavelengths, and that photoisomerization is a required process in the sequential photorelease of NO in ruthenium-nitrosyl complexes. Introducing appropriate ligands in the complex can enhance the photoinduced charge transfer to the Ru–NO, which favors the photorelease of NO in solution.

Résumé

Au cours des dernières années, l'intérêt pour les complexes métalliques à ligand nitrosyle n'a pas cessé de croître dans les communautés pharmaceutique, chimique et en science des matériaux. Cet intérêt s'explique par leurs uniques propriétés physico-chimiques, plus concrètement par leur réponse aux perturbations lumineuses. Sous irradiation, ces composés sont capables de libérer NO, molécule qui a un rôle important dans le système vasculaire, ainsi que dans d'autres systèmes physiologiques importants. Ce n'est donc pas surprenant que de telles molécules aient attiré l'attention de la communauté médicale par sa potentielle application dans le traitement par photothérapie dynamique de plusieurs maladies tel que le cancer. La libération d'oxyde nitrique peut aussi être contrôlée par des réactions redox sans aucune perturbation électromagnétique. La réduction de la partie M–NO peut déclencher le départ de NO. En effet, les molécules qui présentent des bandes de transfert de charge depuis un ligand vers la partie M–NO dans leurs spectres d'absorption UV-Vis ont des rendements quantiques de photolibération plus élevés que celles qui n'en présentent pas. Ces transferts de charge peuvent être considérés comme une réduction de la partie M–NO. Une autre propriété extraordinaire de ces complexes métalliques à ligand nitrosyle est leur réponse photochromique à l'irradiation électromagnétique. Dans un cristal, le changement de couleur est dû à un réarrangement du ligand NO entre sa forme nitrosyle (lié par l'azote) et sa forme isonitrosyle (lié par l'oxygène). Avec la longueur d'onde appropriée, le sens de la photoisomérisation d'enchainement (aller et retour) peut être contrôlé. Cette caractéristique est vraiment intéressante pour la conception des nouveaux dispositifs optiques de stockage massif. Un des objectifs fondamentaux de cette thèse concerne la modélisation des mécanismes de réactions qui décrivent les phénomènes de photoisomérisation et photolibération de NO dans les complexes de ruthénium à ligand nitrosyle. Pour éclaircir la nature de ces processus, une caractérisation complète des structures électroniques ainsi que des surfaces d'énergie potentielle de l'état fondamental et des états excités de plus basse énergie est nécessaire. Des calculs réalisés avec la Théorie de la Fonctionnelle de la Densité ont permis de rationaliser le mécanisme de photoisomérisation d'enchainement du *trans*-$[RuCl(NO)(py)_4]^{2+}$, un complexe qui permet d'obtenir un taux de photoconversion (*ca*. 100%) parmi les plus élevés dans cette famille de complexes. La caractérisation de l'état fondamental singulet et de l'état excité triplet de plus basse énergie ainsi que l'identification de plusieurs croisements ont permis d'établir un mécanisme séquentiel à deux photons, avec un intermédiaire métastable d'hapticité deux. Cette description mécanistique vient d'être

confirmée récemment par des observations expérimentales. Le mécanisme proposé pour la réaction de retour déclenchée par lumière rouge ou par l'infrarouge est également cohérent avec les observations expérimentales. Une approche similaire a été utilisée pour mener l'étude de la photolibération du ligand nitrosyle. En solution, le complexe *trans*-$[RuCl(NO)(py)_4]^{2+}$ présente aussi une photodissociation du NO, mais avec des faibles rendements quantiques. En supposant que la photoisomérisation et la photolibération sont des processus compétitifs, les deux mécanismes ont été étudiés pour un ensemble de complexes afin de rationaliser quelles sont les caractéristiques moléculaires qui favoriseraient un mécanisme au détriment de l'autre. Après analyse des résultats, il apparaît évident que les deux processus sont déclenchés à la même longueur d'onde d'irradiation, et que la photoisomérisation est nécessaire pour la photolibération séquentielle du NO de ces complexes. Avec des ligands appropriés, le transfert de charge vers la partie Ru−NO peut être accru, ce qui améliore la photolibération du NO en solution.